

Synthesis and Characterization of  
Antimicrobial Inhibitors of the  
"Macrophage Infectivity Potentiator" Protein  
and Fluorescent Probes



**Dissertation**

zur Erlangung des  
naturwissenschaftlichen Doktorgrades  
der Julius-Maximilians-Universität Würzburg

vorgelegt von  
Nicolas Julian Scheuplein  
aus Bad Neustadt an der Saale

Würzburg 2023





Eingereicht bei der Fakultät für Chemie und Pharmazie am:

\_\_\_\_\_

Gutachter der schriftlichen Arbeit:

1. Gutachter: \_\_\_\_\_

2. Gutachter: \_\_\_\_\_

Prüfer des öffentlichen Promotionskolloquiums:

1. Prüfer: \_\_\_\_\_

2. Prüfer: \_\_\_\_\_

3. Prüfer: \_\_\_\_\_

Datum des öffentlichen Promotionskolloquiums:

\_\_\_\_\_

Doktorurkunde ausgehändigt am:

\_\_\_\_\_



Die vorliegende Arbeit wurde am Institut für Pharmazie und Lebensmittelchemie der Bayerischen Julius-Maximilians-Universität Würzburg auf Anregung und unter der Anleitung von

**Frau Prof. Dr. Ulrike Holzgrabe**

angefertigt.

Ihr gilt mein besonderer Dank für die freundliche Aufnahme in den Arbeitskreis, das Anvertrauen der interessanten Forschungsthemen und die stetige Unterstützung während meiner Promotion. Zudem möchte ich ihr für das entgegengebrachte Vertrauen, den mir gewährten wissenschaftlichen Freiraum und ihre konstruktiven Ratschläge danken. Sie hat wesentlich dazu beigetragen, meine Fähigkeiten als Forscher zu entwickeln und zu festigen.

Ein besonderer Dank gebührt den Kooperationspartnern:

- Dr. Nicholas Harmer und Arbeitsgruppe von der *University of Exeter*, die Theresa und mich bei der Etablierung des Fluoreszenz-Polarisations-Assays unterstützten und bei der Auswertung sowie Interpretation der Daten wertvolle Hilfe leisteten.
- Dr. Mitali Sarkar-Tyson, Nicole Bzdyl und Arbeitsgruppe von der *University of Western-Australia*, die für die biologischen Testungen der Verbindungen verantwortlich waren.
- Prof. Dr. Ute Hellmich und Arbeitsgruppe für die NMR Untersuchungen der Mip Protein-Dynamik.
- Prof. Dr. Felix Hausch und Arbeitsgruppe für den guten Austausch im Mip-Projekt und die Messung der Bindung an humane FKBP.
- Allen weiteren Arbeitsgruppen aus dem iMip-Projekt.

Ein herzliches Dankeschön möchte ich meiner Kollegin Theresa Lohr aussprechen, mit der ich gemeinsam am Mip-Projekt forschte. Die Unterstützung, wissenschaftlichen Diskussionen und gegenseitige Motivation bei Rückschlägen waren von unschätzbarem Wert!

## Danksagungen

---

Mein Dank gilt auch den Praktikantinnen, die ich während meiner Promotion betreuen durfte und die mir tatkräftig zur Seite standen: Eva Schaller, Maria Lupp, Lea Schneider und Madeleine Bathon.

Weiterhin gilt mein Dank auch Dr. Curd Schollmeyer, Dr. Jens Schmitz, Dr. Ludwig Höllein, Lieselotte Möhler und Martina Wecklein-Weidinger, die bei technischen und organisatorischen Fragen stets eine hilfreiche Hand boten.

Danke an die Kolleginnen und Kollegen aus den anderen Arbeitskreisen im Institut, welche mich bei den unterschiedlichsten Experimenten unterstützten: Markus, Marcus, Max, Simon und allen anderen!

Ich möchte auch all meinen Labor- und Arbeitskolleginnen und -kollegen sowie den Assistentinnen und Assistenten des 2. Semesters für die exzellente Zusammenarbeit, die inspirierende Arbeitsatmosphäre, die gemeinsamen Kaffeepausen, die geselligen Abende und die unvergesslichen Ski- und Wanderausflüge danken: Adrian, Alex, Alena, Anja, Antonio, Cristian, Christine E., Christine H., Christiane, Daniela, Emilie, Florian, Jonas W., Jonas U., Joseph, Joshua, Klaus, Laura, Liana, Liling, Lukas, Markus, Michi, Mohamed, Nelson, Niclas, Nina, Patrick, Rasmus, Regina, Ruben, Sebastian, Sylvia, Theresa, Thomas und allen, die ich versehentlich vergessen habe!

Abschließend möchte ich meiner Familie, Laura und meinen Freunden meinen tiefsten Dank aussprechen, die mich während der vergangenen Jahre stets großartig unterstützt haben.

---

**"Nothing in life is to be feared, it is only to be understood.  
Now is the time to understand more, so that we may fear less."**

Marie Curie (1867 – 1934)

---

*Meinen Eltern, meinen Schwestern  
und meiner Freundin.*



---

**Table of Contents**

<b>ABBREVIATIONS</b> .....	<b>X</b>
<b>I INTRODUCTION</b> .....	<b>1</b>
1 Strategies for the Discovery and Development of New Drugs .....	1
2 Phases of Target-Based Drug Development.....	3
2.1 Target Identification .....	4
2.2 Target Validation and Assessment.....	7
2.3 Assay Development for Compound Screening and Hit Identification .....	9
2.4 Fluorescence Polarization Assay.....	10
2.5 Hit Identification .....	12
2.6 Lipinski's Rule of Five.....	13
2.7 Hit-to-Lead Phase .....	14
2.8 Lead Optimization Phase .....	16
3 Targeting Protein Folding: A Novel Approach for the Treatment of Pathogenic Bacteria.....	18
3.1 Abstract .....	19
3.2 Introduction.....	19
3.3 The Immunophilins, a Superfamily of Folding Enzymes .....	20
3.4 FK506 Binding Proteins in Bacteria.....	23
3.5 Development of Inhibitors to the Mip Protein in Gram-Negative Bacteria .....	28
3.6 Cyclophilins in Bacteria .....	44
3.7 Potential To Develop Inhibitors of Bacterial Cyclophilins.....	49
3.8 Parvulins.....	56
3.9 Parvulin Inhibitors .....	62
3.10 Concluding Remarks.....	70
3.11 References .....	74
<b>II AIMS</b> .....	<b>97</b>
<b>III RESULTS AND DISCUSSION</b> .....	<b>98</b>
1 Development of Biotin-Labeled Antileishmanial Compounds .....	98
1.1 Leishmaniasis .....	98
1.2 Antileishmanial Compounds Derived from Natural Extracts of <i>Valeriana Wallichii</i> .....	98
1.3 Biotinylated Probes for Target Deconvolution.....	99
1.4 Design and Synthesis of Biotinylated Probes 11 and 12.....	101
1.5 Design and Synthesis of Biotinylated Probe 22.....	103

## Table of Contents

1.6	General Experimental Procedures and Equipment.....	105
1.7	Synthesis of the Biotin-Labeled Antileishmanial Compounds 11 and 12.....	108
1.8	Synthesis of the Biotin-Labeled Antileishmanial Compound 22.....	115
2	Fluorescent probe for the identification of potent inhibitors of the macrophage infectivity potentiator (Mip) protein of <i>Burkholderia pseudomallei</i> .....	121
2.1	Abstract .....	122
2.2	Introduction.....	122
2.3	Results and Discussion .....	124
2.4	Conclusion .....	134
2.5	Methods .....	135
2.6	Author information.....	146
2.7	References .....	148
2.8	Supporting Information .....	154
3	Development of Fluorophore-Labeled Mip Inhibitors as FP Probes for Various Mip Proteins .....	165
3.1	Additional Information on FP Probe 30 .....	166
3.2	Variation of the Linker Length with FP Probe 31 .....	167
3.3	Development and Synthesis of Side Chain-Bearing FP Probe 32 .....	170
3.4	Development and Synthesis of Side Chain-Bearing FP Probe 29 .....	182
3.5	Experimental Part – FP Probes.....	186
4	Analysis of Structure–Activity-Relationships of Novel Inhibitors of the Macrophage Infectivity Potentiator (Mip) Proteins of <i>Neisseria meningitidis</i> , <i>Neisseria gonorrhoeae</i> , and <i>Burkholderia pseudomallei</i> .....	201
	Abstract .....	202
4.1	Introduction.....	202
4.2	Results and Discussion .....	207
4.3	Conclusion .....	221
4.4	Experimental Section .....	222
4.5	References .....	243
4.6	SUPPORTING INFORMATION - Analysis of Structure–Activity-Relationships of Novel Inhibitors of the Macrophage Infectivity Potentiator (Mip) Proteins of <i>Neisseria meningitidis</i> , <i>Neisseria gonorrhoeae</i> , and <i>Burkholderia pseudomallei</i> .....	252
<b>IV</b>	<b>GENERAL DISCUSSION.....</b>	<b>329</b>
	Evolution of Mip Inhibitors Derived from Rapamycin.....	329
	Side Chain Introduction Increases BpMip Binding Affinity and Enzymatic Inhibition.....	331
	Binding of Mip Inhibitors to Human FKBP.....	332
	Overview of SAR Findings from the Side Chain Paper .....	333

## Table of Contents

---

Confirmation of the FPA as Superior Screening Method for BpMip Inhibitors .....	334
A Comparative Analysis of Synthetic Routes for Stereochemically Pure Pipecolic Amide Mip Inhibitors .....	336
Stereochemistry and Chiral HPLC Analysis .....	338
Preparing for <i>in-vivo</i> Testing .....	338
Plasma Protein Binding (PPB) .....	339
Membrane Permeability .....	340
Broad Spectrum Screening .....	340
Testing the Anti-Virulence Hypothesis .....	341
Concluding Remarks .....	341
<b>V SUMMARY .....</b>	<b>342</b>
<b>VI ZUSAMMENFASSUNG .....</b>	<b>348</b>
<b>VII BIBLIOGRAPHY .....</b>	<b>354</b>
<b>VIII APPENDIX .....</b>	<b>377</b>
1 HPLC Purity Data .....	377
2 <sup>1</sup> H NMR Spectra .....	396
3 Authorship Statement .....	414
4 Compounds .....	418

## Abbreviations

Most abbreviations used in this PhD thesis are given within each paper. The following abbreviations are used throughout the rest of the thesis.

Abbreviation	Meaning
$^1\text{H}$ NMR	Proton Nuclear Magnetic Resonance
$^{13}\text{C}$ NMR	Carbon-13 Nuclear Magnetic Resonance
3D	Three-Dimensional
A	Anisotropy
ABPP	Activity-Based Protein Profiling
ACN	Acetonitrile
ADME	Absorption, Distribution, Metabolism, and Excretion
Alox N/UV254	Aluminum Oxide Sheets with UV254 Indicator
AMR	Antimicrobial Resistance
Boc	<i>tert</i> -Butyloxycarbonyl
BpMip	<i>Burkholderia pseudomallei</i> macrophage infectivity potentiator
bRo5	Beyond Rule of 5
CADD	Computer-Aided Drug Design

CCCP	Compound-Centric Chemical Proteomics
CL	Cutaneous Leishmaniasis
CL <sub>int</sub>	Intrinsic Clearance
CRC	Concentration-Response Curves
CRISPR-Cas9	Clustered Regularly Interspaced Short Palindromic Repeats and CRISPR-associated protein 9
CYP	Cytochrome P450
DALY	Disability-Adjusted Life Year
DCM	Dichloromethane
DCC	<i>N,N'</i> -Dicyclohexylcarbodiimide
DCM	Dichloromethane
DAD	Diode Array Detector
DMAP	4-Dimethylaminopyridine
DMPK	Drug Metabolism and Pharmacokinetics
DMSO	Dimethyl Sulfoxide
DMF	<i>N,N</i> -Dimethylformamide
DIPEA	<i>N,N</i> -Diisopropylethylamine
EA	Ethyl Acetate
EDC	1-Ethyl-3-(3-dimethylaminopropyl)carbodiimide
ELSD	Evaporative Light Scattering Detector
ESI	Electrospray Ionization

## Abbreviations

EtOH	Ethanol
FA	Formic Acid
FAM	Fluorescein Amidite
FP	Fluorescence Polarization
FPA	Fluorescence Polarization Assay
FK506	Tacrolimus
GPCR	G Protein-Coupled Receptor
GST	Glutathione S-Transferase
H2L	Hit-to-Lead
HBA	Hydrogen Bond Acceptor
HBD	Hydrogen Bond Donor
HDAC1	Histone Deacetylase I
HBTU	2-(1 <i>H</i> -benzotriazole-1-yl)- 1,1,3,3-tetramethyluronium hexafluorophosphate
HEK	Human Embryonic Kidney Cells
HTS	High-Throughput Screening
HPLC	High-Performance Liquid Chromatography
HRMS	High-Resolution Mass Spectrometry
ITC	Isothermal Titration Calorimetry
K <sub>D</sub>	Dissociation Constant
K <sub>M</sub>	Michaelis Constant
LC-MS/MS	Liquid Chromatography- Tandem Mass Spectrometry

LC-MS	Liquid Chromatography-Mass Spectrometry
LpMip	<i>Legionella pneumophila</i> macrophage infectivity potentiator
M	Molecular Weight
MCL	Mucocutaneous Leishmaniasis
MeOH	Methanol
MIC	Minimum Inhibitory Concentration
MBC	Minimum Bactericidal Concentration
Mip	Macrophage Infectivity Potentiator
MPLC	Medium Pressure Liquid Chromatography
MST	Microscale Thermophoresis
NIH	Mouse Embryonic Fibroblasts
NMM	<i>N</i> -Methylmorpholine
NMR	Nuclear Magnetic Resonance
PCR	Polymerase Chain Reaction
PD	Pharmacodynamics
PDB	Protein Data Bank
PEG	Polyethylene Glycol
Phe-Pro	Phenylalanine-Proline
PPIase	Peptidyl-Prolyl <i>Cis-Trans</i> Isomerase
PK	Pharmacokinetics

## Abbreviations

---

PSA	Polar Surface Area
Q <sup>3</sup>	Triple Quadrupole Mass Spectrometer
QTOF	Quadrupole Time-of-Flight Mass Spectrometer
RB	Rotatable Bonds
<i>R<sub>f</sub></i>	Retention Factor
RP-HPLC	Reverse Phase High-Performance Liquid Chromatography
SAR	Structure–Activity Relationship
SBDD	Structure-Based Drug Design
SiO <sub>2</sub>	Silicon Dioxide
SMILES	Simplified Molecular Input Line Entry System
SPR	Surface Plasmon Resonance
T	Temperature
TFA	Trifluoroacetic Acid
TLC	Thin Layer Chromatography
UV	Ultraviolet
$\Delta G$	Gibbs Free Energy
$\lambda$	Wavelength
$\sigma$	Standard Deviation

## I Introduction

### 1 Strategies for the Discovery and Development of New Drugs

The discovery and development of a new drug, from the initial idea to the launch of a marketable product, is an extremely difficult and often inefficient process that can take 12 to 15 years and cost more than \$1 billion.<sup>1</sup> Yet the need for first-in-class therapeutics with a novel and unique mechanism of action is enormous, especially in areas such as antibiotics. There, traditional forms of therapy are becoming increasingly ineffective, and resistance is raising the fear of a post-antibiotic era.<sup>2</sup> For 2019, Murray *et al.* estimate 4.95 million (3.62–6.57) deaths to be associated with bacterial, antimicrobial resistance (AMR) worldwide.<sup>3</sup>

Over the years, different strategies for the early stages of drug development have evolved, with two main concepts established in antimicrobial research and other therapeutic areas: phenotype-based drug discovery (PDD) and target-based drug discovery (TDD, cf. Figure 1).<sup>4, 5</sup> In the PDD approach, the target or mechanism of action is initially unknown.<sup>6, 7</sup> Target is a broad term that can be applied to a range of biological entities, which in turn can include proteins, genes or RNA.<sup>1</sup> PDD is characterized by screening small molecules or polypeptides in more complex systems such as cells, tissues, or organs based on existing pharmacology, assessing their effect on the phenotype - the observable characteristics of an organism. In contrast, TDD is hypothesis-driven, considered more systematic, and rational.<sup>8</sup> The concept of TDD begins with the determination of a target and subsequent identification of active molecules, primarily in reduced biological/biochemical assays that allow medium- to high-throughput screening (HTS).<sup>7, 9</sup>

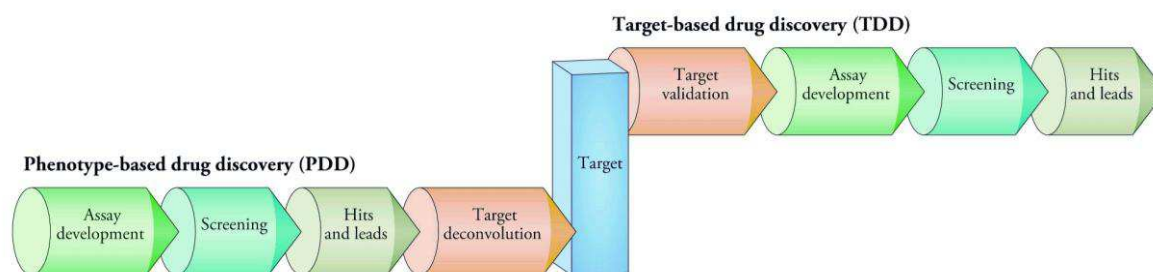


Figure 1. Schematic comparison between phenotype-based and target-based drug discovery (PDD and TDD). It illustrates the early phase of drug discovery, which focuses on identifying targets and lead molecules. In the phenotype-based approach, lead molecules are first obtained in a target-agnostic manner, followed by target deconvolution to identify the molecular targets underlying the observed phenotypic effects. In the target-based approach, molecular targets are identified and validated before lead discovery begins, followed by assays and screens to find a lead.<sup>10</sup>

Starting in the 1980s, advances in molecular biology and genomics led to the widespread replacement in the pharmaceutical industry of phenotypic screening with screens against defined targets associated with a disease.<sup>11</sup> Advances, particularly in cloning technology, enabled the isolation of pure proteins, which were then used to screen an extensive library of compounds using HTS.<sup>8</sup> This target-based approach was supported by structure-based drug design (SBDD), increasingly accurate crystal structures, enormous amounts of data, and the increasing use of artificial intelligence.<sup>12</sup> However, it is a matter of current debate which of the two approaches presented is more successful in discovering first-in-class molecules.<sup>5, 10, 11</sup>

Table 1. Advantages and disadvantages of phenotypic (PDD) and target-based drug discovery (TDD) approaches according to Kiriiri *et al.*<sup>8</sup>

Advantages	Disadvantages
<b>Phenotypic drug discovery (PDD)</b>	
Enables establishment of therapeutic relevance early in the drug discovery process	Difficulties in modelling some diseases
Does not require knowledge of the mechanism of action	Policy changes addressing animal rights
Enhances the chances of serendipitous discoveries	Does not enable the use of high-technology platforms and has a low screening capacity
The process closely simulates the typical physiological environment	Complicated analysis due to confounding factors
	Rational drug design is not applicable to this approach
<b>Target-based drug discovery (TDD)</b>	
Knowledge of the mechanism of action with benefits such as side effects associated with it	Intensive target validation is essential to ensure that the observed response is physiologically relevant in the natural environment
High chances of developing best-in-class molecules	Requires knowledge of the underlying mechanism of action <i>a priori</i>
Allows screening of vast chemical libraries; high screening capacity	Chances of serendipitous drug discovery are minimized
Allows utilization of high-technology platforms	In antibiotic research, it is essential to early test hit substances in assays against the living pathogen, e.g., to ensure cell penetration.
Knowledge of the target can help address species selectivity in anti-infective research	

In contrast to other fields, the target-agnostic usage of phenotypic screening has been particularly popular in antimicrobial drug discovery, given the simplicity and strong translational relevance of antimicrobial activity as an assay read-out.<sup>5</sup> It is applied in bioactivity-guided isolation of natural products from complex mixtures and libraries of crude extracts.<sup>13</sup>



In the past, natural products have been the most important source of antibiotic lead compounds. Considering the last 40 years, about 60% of all new chemical entities in the field of antibacterial agents were based on or derived from natural products.<sup>14</sup> In addition, biological screenings against living bacteria rather than single target proteins provide an early indication of fundamental characteristics such as the penetration of the active substance through the bacterial cell envelope. Indeed, the bacterial cell membrane can be a high hurdle for the discovery of new drugs, especially in Gram-negative bacteria that have an additional outer membrane.<sup>15</sup> This is also demonstrated by the fact that no new class of Gram-negative antibiotics has been launched on the market for over 50 years.<sup>16</sup> Nevertheless, retrospective identification and validation of the role of the molecular target(s) in the observed phenotypic responses in PDD, also known as target deconvolution, is essential. Knowledge of the drug target and the corresponding mechanism of action can greatly facilitate subsequent targeted optimization of pharmacological/pharmacodynamic properties through structure–activity relationship (SAR) studies. Additionally, target identification and validation can help address species selectivity in anti-infective research and, more generally, target-based side effects, which could reduce later-stage failures.<sup>5</sup> Certainly, the two strategies outlined have the potential to benefit from each other when used in a complementary manner. Too unilateral a focus on a target-based approach could result in minimizing the chances of serendipitous drug discovery or that observed responses in simplified biochemical assays may not be physiologically relevant in the natural environment.<sup>8</sup> Re-implementation of phenotypic assays in the early stages of target-based drug discovery can address these weaknesses and lead to minimizing costly attrition and developing first-in-class drugs faster and more efficiently.<sup>8</sup>

## 2 Phases of Target-Based Drug Development

Independent of the approach chosen, however, the principles and general methods of structure optimization on the way to a drug are quite similar. As mentioned before, initial phenotypic screenings are common in antimicrobial research. Still, the target-based approach is more widespread in a broader therapeutic field.<sup>17, 18</sup> Therefore, the order of steps in the following will be based on the TDD approach. On the path to a drug, numerous early phases of the drug discovery process have to be performed: From initial target identification and validation, assay development, compound screening, hit identification, hit-to-lead development, and lead optimization to the final selection of a candidate molecule for preclinical and clinical development (cf. Figure 2).<sup>1</sup>

In various steps of this overall process, it has proven helpful to possess labeled compounds that enable, for instance, target identification in chemical proteomics or lay the basis for the analysis of SAR as probes in compound screenings.<sup>19, 20</sup> In the following sections, the individual steps of the drug development process are outlined briefly, and examples are provided where labeled compounds are beneficial.

A detailed theoretical introduction to the topic of macrophage infectivity potentiator (Mip) proteins and respective small molecule inhibitors, which is the main focus of this thesis, is provided in the subsequent perspective "Targeting Protein Folding: A Novel Approach for the Treatment of Pathogenic Bacteria".<sup>21</sup>

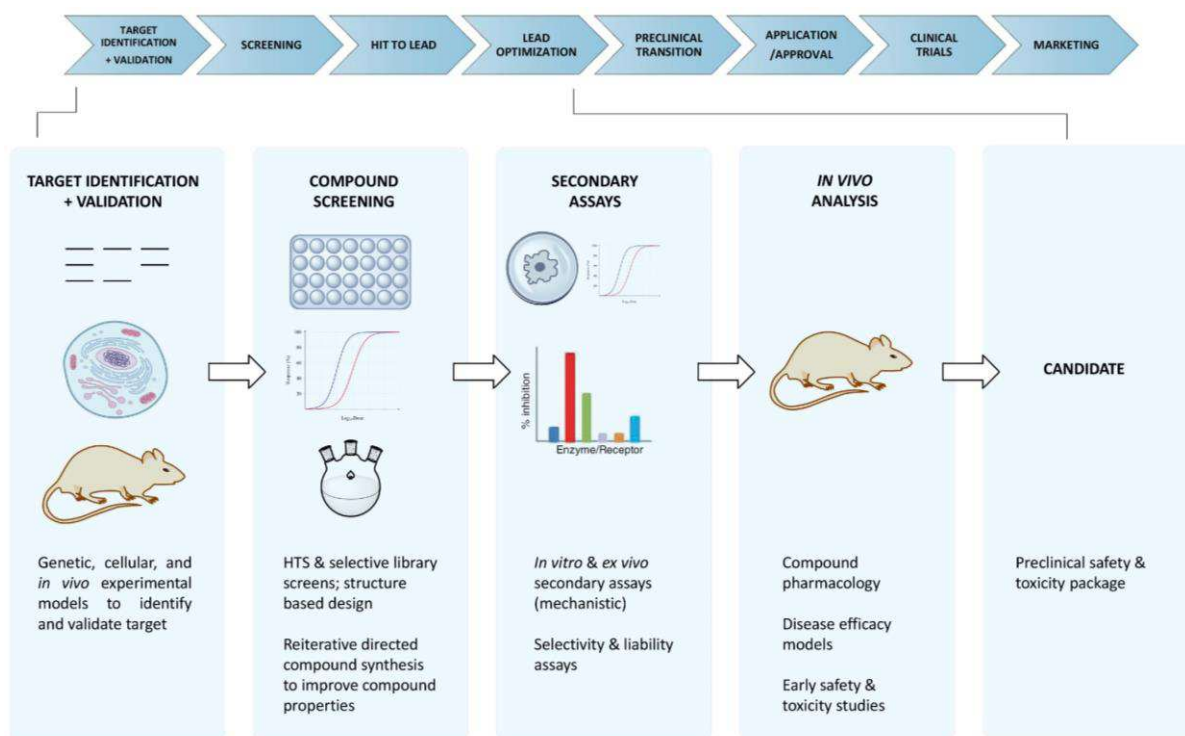


Figure 2. Overview of the early phases of drug development within the target-based drug discovery (TDD) approach, designed according to Hughes *et al.*<sup>1</sup> and Emmerich *et al.*<sup>5</sup>

## 2.1 Target Identification

Target identification and validation are the two initial steps in a TDD approach. Early knowledge of the target and the mechanism of action has several benefits (see Table 1), such as the potential to determine possible side effects associated with the target.<sup>19</sup> Especially in the case of anti-infectives, the search for new targets is an indispensable step in the fight against increasing AMR.<sup>13, 22</sup>

In their review of new approaches in antimicrobial drug development, Lakemeyer *et al.* describe the target classes addressed by known antibiotics, as well as microbial resistance mechanisms that undermine their mechanism of action (cf. Figure 3).<sup>22</sup>

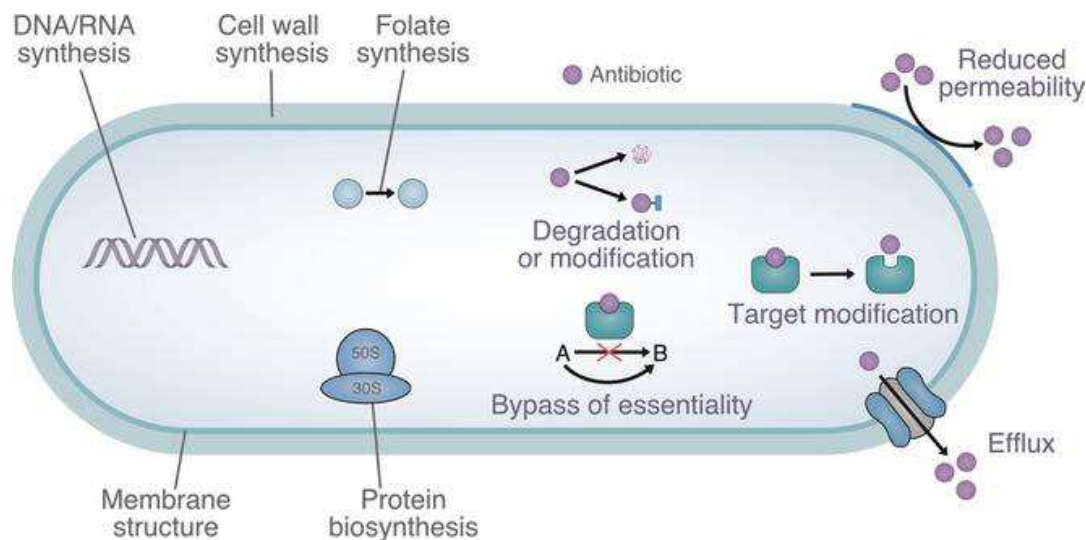


Figure 3. Schematic of a gram-negative bacterial cell. Target structures of known antibiotic classes and resistance mechanisms are shown. Reprinted with permission from M. Lakemeyer *et al.*, *Angew. Chem. Int. Ed.* 2018, 57, 14440. © 2018 Wiley-VCH Verlag GmbH & Co. KGaA, Weinheim.

Miethke *et al.* describe two main types of targets that should be considered in antibacterial research: molecular targets, which are vital for all stages of the bacterial life cycle ('essential targets'), and so-called 'non-essential targets'.<sup>13</sup> When targeting 'essential targets', clearance of the bacteria from the host is directly promoted. 'Non-essential targets', on the other hand, can be defined as bacterial structures that are not vital under standard growth conditions in the laboratory but become critical during host colonization and infection.<sup>13</sup> Several systematic methods for identifying the targets of (especially in antimicrobial research) often natural products, such as transcriptome-wide compound signature profiling, chemical genomics approaches, and yeast two-hybrid methods have been developed in recent decades.<sup>19, 22</sup>

For the identification of targets as well as for later validation at the proteomic level, a widely applicable approach named chemical proteomics has evolved from classical drug affinity chromatography.<sup>7, 23, 24</sup> It is an approach to fish and identify multiple protein targets of active small molecules, for which a suitable probe is first designed and synthesized, followed by target fishing and protein identification by mass spectrometric analysis.<sup>19</sup>

Based on their different workflows, they can be divided into activity-based protein profiling (ABPP) and compound-centric chemical proteomics (CCCP; cf. Figure 4A).

According to Cravatt *et al.*,<sup>25</sup> ABPP is based on developing active-site-directed covalent probes to interrogate specific subsets of enzymes in complex proteomes. Thus, ABPP can provide the basis for a quantitative readout of the functional state of each enzyme in the family. In ABPP, a probe consists of a drug-derived moiety capable of covalent binding to the active site of a target, a linker, and some kind of reporter unit. In CCCP, the drug molecule, which does not have to be a covalent binder, is designed to be immobilized on a matrix, e.g., magnetic or agarose beads.<sup>19</sup> A CCCP procedure was used by Schreiber *et al.* to identify an essential member of the FK506 (**1**)-binding proteins, FKBP12.<sup>26</sup> ABPP in particular, has been established in recent years, as it can overcome immobilization-induced activity impairment.<sup>25</sup> Here, probes are synthesized that retain the pharmacological activity of the parent molecules to ensure the accuracy of subsequent target identification and allow easy enrichment of the bound target proteins through a reporter unit.<sup>24</sup> The probes are then incubated with effector living cells, lysate, or tissue homogenates to allow them to fully bind their target proteins. After enrichment using chemical and biochemical techniques, the target proteins are determined through proteomics approaches. Figure 4B shows some of the most commonly used reporter tags for later enrichment: activity-based probes labeled with, e.g., biotin (**2**), which allows streptavidin (**3**)/avidin (**4**) pull down with respective beads; click chemistry probes with a, compared to biotin (**2**) much smaller, biorthogonal azide or alkyne group, which can be bound to beads by click reaction; and finally, photoaffinity probes, which can bind to proteins when exposed to specific wavelengths, often additionally equipped with click chemistry groups.<sup>19</sup> Compared to immobilized probes, activity-based probes (ABPs) can interact with proteins in the active proteome before enrichment and even penetrate the cell membrane to bind target proteins in living cells, which may reflect the actual drug-target interactions under physiological conditions in cells.<sup>19</sup> The ABPP concept was used, for example, to elucidate the mechanism of resveratrol (**5**), a natural product that shows anti-cancer activity in mouse melanoma cells.<sup>27</sup> Therefore, a probe with the structure of resveratrol (**5**) and a biotin (**2**) tag was used for subsequent enrichment with streptavidin (**3**) beads. Thus, using chemical proteomics, histone deacetylase I (HDAC1) was identified as a protein target of resveratrol (**5**) in mouse melanoma cells.

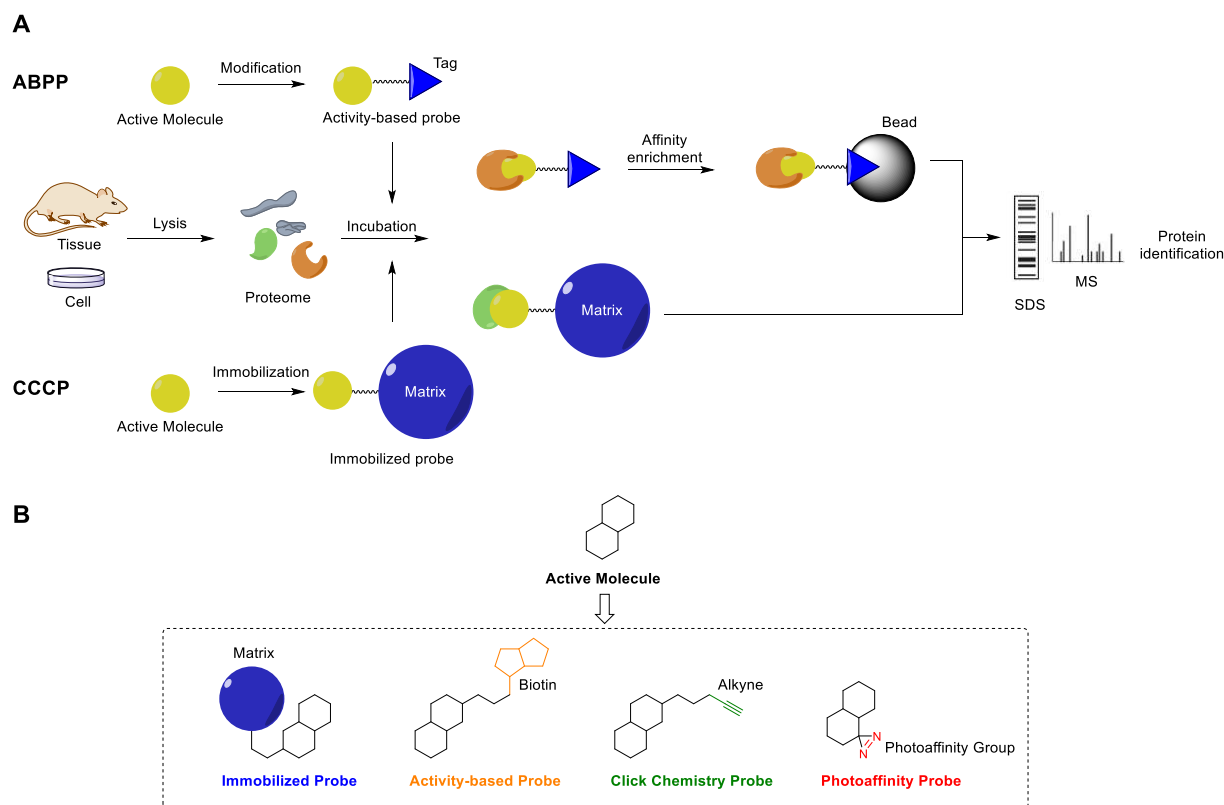


Figure 4A. Schematic illustration of the activity-based probe profiling (ABPP) and compound-centric chemical proteomics (CCCP). In the case of ABPP, a probe must first be designed from the covalently binding active molecule, a linker, and a reporter tag. The probe is then used for fishing the target proteins or structures out of a cell lysate. After affinity enrichment and work-up, the proteins/targets can be identified by mass spectrometry. In CCCP, the first step is to immobilize an active molecule using a matrix, which is incubated with cell lysate. Figure 4B. General molecular structures of the different types of chemical proteomics probes: Immobilized probes, activity-based probes labeled with, e.g., biotin (2), click chemistry probes with an azide or alkyne group, and photoaffinity probes that attach to proteins when exposed to specific wavelengths.<sup>19</sup>

## 2.2 Target Validation and Assessment

Once a new target is identified, various strategies are used to provide validation of the target. Target validation generally describes the technical evaluation of whether a target plays a key role in a disease process and whether pharmacologic modulation of the target might be effective in a defined patient population.<sup>28</sup> Importantly, insufficient early-stage drug target validation has been associated with costly clinical failures<sup>29</sup> and low drug approval rates.<sup>30</sup> The presented activity-based protein profiling (ABPP) is suitable for target identification and one of the numerous possibilities used for target validation.<sup>31</sup> Other methods may include surface plasmon resonance (SPR), microscale thermophoresis (MST), and isothermal titration calorimetry (ITC).<sup>19</sup> General principles of target validation are illuminated by Emmerich *et al.* in their practical guideline to what they call 'target assessment', a broader concept of target validation.<sup>5</sup>

The authors offer several sets of guiding questions for various areas of target validation, including antimicrobial research. Thus, they aim to promote early awareness among academic scientists of factors that make translational research more robust and efficient and to facilitate collaboration between academia and industry. First, the authors address the aspect of the 'druggability' of a target, which is commonly understood as the likelihood that a protein pocket can accommodate a drug-like ligand. Egner *et al.* further specify the term towards the likelihood of finding a selective small molecule that can bind with high affinity to a target and modify its activity.<sup>32, 33</sup> Druggability also includes considerations such as whether the type of target (e.g., GPCR, ion channel) has a history of success in drug development and whether there are known molecules that modulate the target.<sup>31</sup> In addition, there must be genetic confirmation of the role of the target, e.g., by gene knock-out in mice or small interfering RNA (siRNA).<sup>31</sup> In 2007, the *Nobel Prize in Physiology or Medicine* was awarded to the inventors of specific gene modification techniques and mouse embryonic stem cell technology that, when combined, enabled the creation of knockout mice.<sup>34</sup> Studies in these animals, which lack a specific gene or genes, are an essential basis for models of many human diseases and a commonly used tool for target validation.<sup>35, 36</sup> Other novel genetics-based methods, such as the CRISPR-Cas9 technology (*Nobel Prize in Chemistry 2020*), are also increasingly being used for target validation.<sup>37, 38</sup> Supported by these and other inventions, systematic genetic association testing of both human diseases and quantitative traits, along with the resulting insights into coincident associations between them, have gained importance in recent years.<sup>39</sup> It is a powerful approach to infer drug targetable candidates and to develop better *in vitro* assays to identify compounds that can therapeutically modulate them. With respect to microbial drug targets, Emmerich *et al.*<sup>5</sup> and Silver<sup>40</sup> add the following key considerations for druggability: (i) essentiality for microbial growth and survival; (ii) pharmacological tractability and accessibility; (iii) similarity to related mammalian proteins, enzymes, etc. in terms of drug safety; (iv) presence in important pathogens; (v) the potential for the development of resistance, especially if only one target is addressed; and (vi) the lack of target-based cross-resistance. Another key consideration in target assessment is whether assays for binding and/or function of the target are available - also referred to as its 'assayability'. This includes biochemical assays as well as animal models or secondary low-throughput assays representing the physiology and biology of the target modulation.<sup>31</sup> Emmerich *et al.* also address target assessment considerations that go beyond these scientific aspects.

These include legal and intellectual property issues, the extent of unmet medical needs in the potential patient populations expected to benefit from the new drug, and the commercial potential of the new drug if it is successfully brought to market.<sup>5</sup> Implementing these considerations early in academic drug development could facilitate collaboration with industrial institutions and minimize subsequent costly clinical attrition.<sup>5</sup>

### 2.3 Assay Development for Compound Screening and Hit Identification

Once the target has been validated, selecting and developing an appropriate screening method for hit identification and the subsequent lead discovery phase is necessary. Screening strategies range from *in vitro* formats such as biochemical screenings of large, commercially available substance libraries (from low throughput of fewer than 500 compounds per day to HTS with 10,000–100,000 compounds per day<sup>9</sup>) as well as NMR screening techniques to *in silico* strategies like structure-based virtual screening (SBVS).<sup>1</sup> To accelerate the identification of new chemicals, Miethke *et al.* recommend limiting the screening of already broadly characterized groups, such as compounds derived from secondary metabolite producers like the actinomycetes in antibacterial research.<sup>13</sup> Carefully designed and possibly even preselected (‘biased’) chemical libraries that enable screening of a suitable chemical space against the target(s) of interest, represent an important first step to start a reliable hit identification campaign.<sup>13</sup> In academia, as screening capacity is often smaller, focused, knowledge-based, and targeted screenings, often supported by SBVS, may assist. As one of the most promising techniques of computer-aided drug design (CADD), SBVS attempts to predict the best mode of interaction between two molecules to form a stable complex. This involves applying scoring functions to estimate the strength of non-covalent interactions between a ligand and a molecular target.<sup>41</sup> In this context, an indispensable prerequisite for using SBVS is the availability of a high-resolution 3D structure of the target protein, often obtained by X-ray crystal structures. Recently, the barrier to this requirement was substantially lowered when researchers from the AlphaFold project revealed the likely 3D structures of nearly all known proteins, more than 200 million from bacteria to humans, obtained solely by prediction from the amino acid sequences by artificial intelligence.<sup>42, 43</sup>

However, even though computational methods using artificial intelligence and big data have gained momentum in recent years, none of them can do without confirmation of the results in biological or biochemical *in vitro* assays to date. A variety of *in vitro* assay formats have been developed for screening compounds, with the choice of assay format depending primarily on the biology of the target protein and the infrastructure of the laboratory in which the compound is being tested. The nature of the target protein initially determines whether cell-based assays or simpler biochemical assays are used. Nevertheless, according to Hughes *et al.*,<sup>1</sup> there is a series of universal factors that need to be taken into account when selecting an assay format. First would be the pharmacological relevance of the assay. If available, studies should be performed with known ligands that are active at the target under investigation to determine whether the pharmacology of the assay can predict the disease state and to demonstrate that the assay is capable of identifying compounds with the desired potency and mechanism of action. Furthermore, the reproducibility of the assay should be ensured. In the context of a drug screening program, it is necessary that an assay is reproducible across different test plates, throughout many screening days, and over the duration of the entire drug discovery program. In addition, the quality of the assay should be ensured through validation and the development of quality control procedures, among other measures. Thus, as an example, the so-called Z-factor, which was established by Zhang *et al.*, is determined in the industry for plate-based HTS measurements.<sup>44</sup> It is a statistical parameter that takes into account not only the signal window in the assay, but also the variance around the high and low signals in the assay. While the Z-factor can have a value from 0 to 1, an assay is considered adequately robust for compound screening if it is above 0.4, at best above 0.6.<sup>1</sup>

### 2.4 Fluorescence Polarization Assay

The fluorescence polarization assay (FPA) is an easy and rapid technique that allows quantitative evaluation of enzyme-inhibitor interactions.<sup>45</sup> It is applicable in different stages of drug development, such as initial drug screening (from low- to high-throughput) or later optimization phases. The FPA uses plane-polarized light to measure the binding of a small fluorescent ligand, hereafter referred to as a probe, to a larger protein target. Using the polarization signal, the FPA detects changes in the effective molecular volume that determines molecular rotation in solution.<sup>20,</sup>



For this purpose, fluorescence polarization (FP) measures the light emitted from the probe in two planes (horizontal and vertical) after excitation with plane-polarized light in one of these planes. Using the intensities of the light detected in the parallel ( $I_{\parallel}$ ) and perpendicular ( $I_{\perp}$ ) planes with respect to the excitation light, the anisotropy  $A$  is consequently calculated:<sup>20</sup>

$$A = \frac{I_{\parallel} - I_{\perp}}{I_{\parallel} + 2I_{\perp}} \quad (1)$$

Other authors use the polarization  $P$  to define the relationship between the intensities of the detected light, whereas  $A$  is more arithmetically convenient.<sup>20</sup> Both  $A$  and  $P$  are dimensionless quantities.

$$P = \frac{I_{\parallel} - I_{\perp}}{I_{\parallel} + I_{\perp}} \quad (2)$$

The probe rotates rapidly in the solution. Upon excitation by plane-polarized light, its rapid tumbling due to its small molecular volume causes the emission of depolarized light and a low polarization (cf. Figure 5A). According to (1) and (2),  $A$  and  $P$  become 0 when  $I_{\parallel} = I_{\perp}$ . When the fluorescent probe in solution is bound to the larger target protein, it increases its effective volume and tumbles more slowly. Therefore, more emitted light remains polarized in the same plane as the excitation light, increasing polarization (cf. Figure 5B).<sup>20</sup> Thus, FP can be used to measure the binding of the probe to a larger macromolecule and in a subsequent competitive binding assay. There, the binding affinity of an additional ligand can be determined that displaces the probe from the probe-target complex, decreasing polarization (cf. Figure 5C).<sup>20</sup>

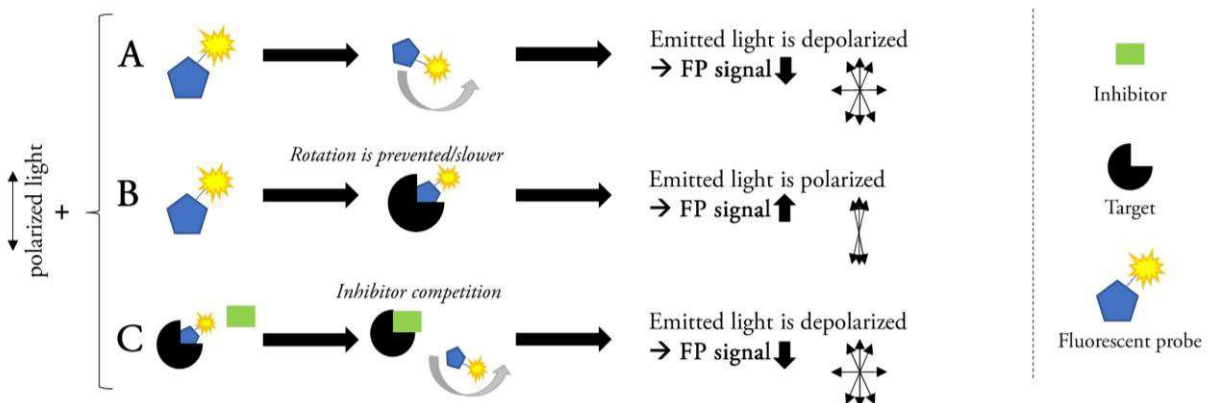


Figure 5. Principle of FP. A: Upon excitation by plane-polarized light its rapid tumbling in solution due to its small molecular volume causes emission of depolarized light and a low polarization. B: When bound to the larger target protein, the fluorescent probe increases its effective volume and tumbles more slowly, causing more emitted light to remain polarized in the same plane as the excitation light, increasing polarization. C: In a subsequent competitive binding assay, binding affinity of an additional ligand to the target can be measured by displacing the probe from the probe-target complex, decreasing polarization.<sup>47</sup>

In the design of such probes, the key factor is to consider the activity of the drug molecule. In other words, the incorporation of the fluorophore and the linker should not influence the binding of the active molecule.<sup>20</sup>

Further criteria to be addressed in the design of the fluorescent probe, as well as advantages over other assays, are highlighted in the subsequent publication.<sup>48</sup>

### 2.5 Hit Identification

According to Hughes *et al.*, a ‘hit’ molecule is a compound that exhibits the desired activity in a compound screening and whose activity is confirmed upon retesting.<sup>1</sup> The criteria for a hit molecule differ depending on the field of application, and continuous revision of these criteria is essential.<sup>18</sup> Within the hit identification phase, the properties of each cluster – a group of chemical analogs with a structural similarity that have shown activity in a screening – are investigated.<sup>9, 49</sup> This includes detecting rudimentary SAR across a set of compounds. That is, whether a series of compounds or clusters that share a particular moiety or chemical motif can be identified and whether adding different functional groups to that core structure leads to a different activity. Chemical synthesis considerations such as the ease of preparation, the potential suitability for parallel synthesis, and the ability to generate diversity from late intermediates have to be evaluated.<sup>1</sup> Beyond this, the drug-like nature of the chemical class needs to be studied in the context of chemical reactivity, stability, and solubility.<sup>31</sup> When the activity of each hit has been confirmed by repeated testing and obtaining concentration-response curves (CRC), the surviving hits are examined in a secondary assay for the chosen target, for example, in a more complex cell-based bioassay.<sup>1</sup> Miethke *et al.* recommend an early determination of minimum inhibitory concentrations (MIC) and minimum bactericidal concentrations (MBC) in antimicrobial research.<sup>13</sup> Subsequently, representative examples of each of the obtained miniseries are subjected to various *in vitro* assays to obtain early information concerning pharmacokinetic (PK) properties such as absorption, distribution, metabolism, and excretion (ADME) properties as well as selectivity issues of a compound series.<sup>31</sup> Here, *in silico* models and rule-of-thumbs such as Lipinski’s rule of 5 presented below can be helpful. In this way, the strengths and weaknesses of each series are revealed and a decision is made on the most promising series of agents to continue. Hit molecules at this stage typically possess potencies of 100 nM to 5 mM at the drug target.<sup>1</sup>

## 2.6 Lipinski's Rule of Five

For a drug to be effective, a potent molecule must reach its target in the body in sufficient concentration and remain there in a bioactive form long enough for the expected biological events to occur.<sup>50</sup> In modern drug development, the assessment ADME properties is increasingly performed earlier in the discovery process, at a stage when candidate compounds are numerous but access to physical samples is limited.<sup>50</sup> Lipinski's rule of 5 (Ro5) was one of the pioneering attempts to interpret the physicochemical properties of existing drugs to develop general rules for drug-likeness of molecules achieving sufficient cell permeability and oral bioavailability (cf. Figure 6).<sup>51</sup> According to the Ro5, a drug-like compound should have the following attributes: molecular weight of no more than 500 g/mol, a log P value of a maximum of 5 (describing its degree of hydrophobicity), no more than 5 hydrogen bond donors (HBD), and no more than 10 hydrogen bond acceptor (HBA) sites.<sup>51</sup> Veber *et al.* added two more conditions to consider: a polar surface area (PSA) of less than or equal to 140 Å<sup>2</sup> and no more than 10 rotatable bonds (RB), which are correlated with drug permeability and flexibility (cf. Figure 6).<sup>52</sup>

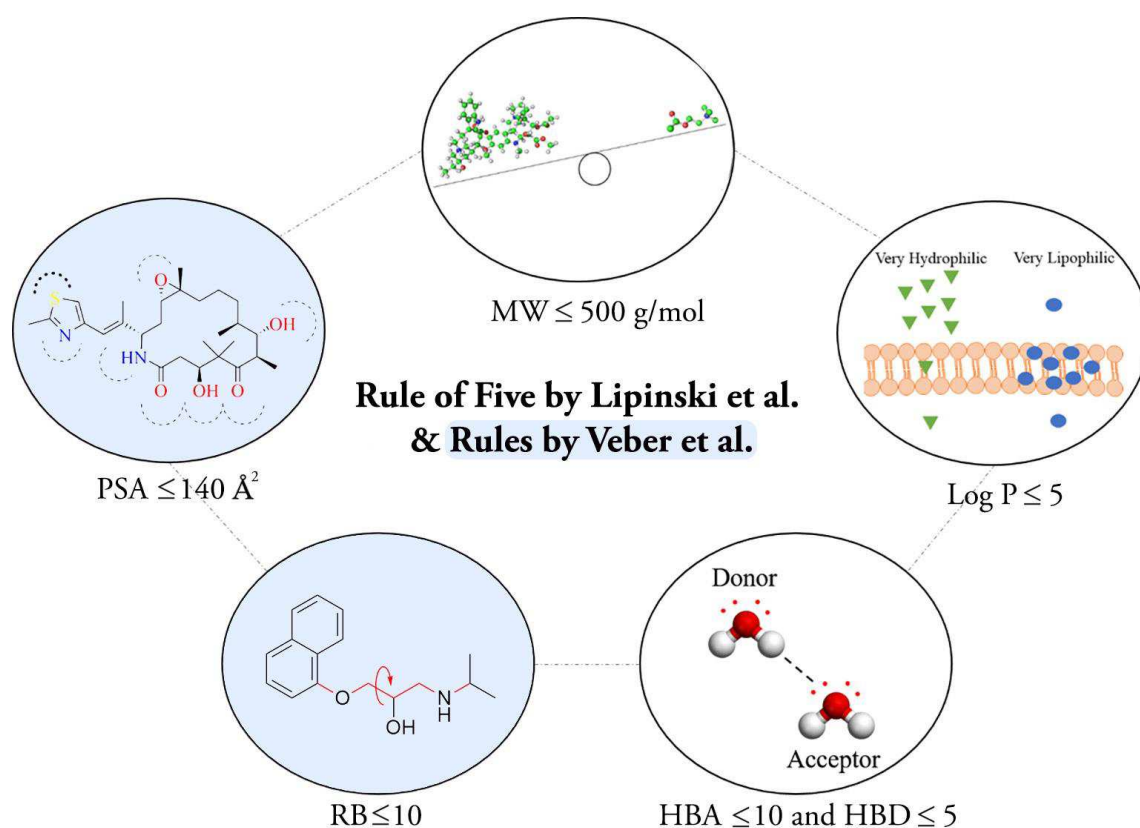


Figure 6. According to the Ro5, to be sufficiently orally bioavailable, a drug-like compound should have a molecular weight of no more than 500 g/mol, a log P value of a maximum of 5, no more than 5 hydrogen bond donors (HBD), and no more than 10 hydrogen bond acceptor (HBA) sites. Veber *et al.* added two more conditions to consider: a polar surface area (PSA) of less than or equal to 140 Å<sup>2</sup> and no more than 10 rotatable bonds (RB).<sup>52, 53</sup>

A rotatable bond in this concept is defined as any single non-ring bond, attached to a non-terminal, non-hydrogen atom. Amide C-N bonds are not counted because of their high barrier to rotation. Over the past two decades, this type of rules has been critically discussed and adapted.<sup>54</sup> Thus, studies have shown that some natural products break the Ro5, such as heavier macrolides and peptides.<sup>55</sup> In this oral druggable space beyond the rule of 5 (bRo5), properties like intramolecular hydrogen bonding and macrocyclization become more relevant.<sup>55</sup>

### 2.7 Hit-to-Lead Phase

During the Hit-to-Lead (H2L) phase, the focus is on optimizing a chemical hit series to improve any compound properties that may be an obstacle to further progression.<sup>18</sup> Strovel *et al.* define a chemical lead as a synthetically feasible, stable, and drug-like molecule active in primary and secondary assays with acceptable *specificity* and *selectivity* for the target.<sup>31</sup> Thus, it is now the goal to build confidence in the quality of a compound hit series and its associated data. Furthermore, data should be generated that will guide medicinal chemists to design and synthesize continuously improved derivatives in an iterative process of series expansion.<sup>56</sup> The challenge is to simultaneously optimize all properties necessary for the drug to be most effective and least toxic.<sup>13</sup> Two main types of criteria are usually covered: disease-specific criteria, which focus on affinity, efficacy (such as a low half-maximal inhibitory concentration (IC<sub>50</sub>) and MIC for anti-infectives), and selectivity; in addition, the compound-specific criteria, which focus mainly on the chemical scope of the compound and a risk assessment of drug metabolism and pharmacokinetics (DMPK) and physical properties adequate to examine their efficacy in any available *in vivo* models.<sup>1, 18</sup>

Depending on the profile, the H2L strategy and medicinal chemistry plan can vary between series. Intensive SAR investigations around each core compound structure are conducted. In-depth-SAR can be accelerated by structure-based drug design techniques using molecular modelling and techniques such as X-ray crystallography and NMR to develop the SAR faster and more focused.<sup>1</sup> A compound meeting basic criteria would be escalated into a further bank of assays. As such, a secondary pharmacology selectivity profile would be established. In antimicrobial research, this would include human orthologues and paralogues of the targeted enzyme or receptor, if known.<sup>18</sup>

Assessment of aqueous solubility, permeability, and metabolic stability is critical to evaluate the potential of an active molecule to enter a patient's circulation by injection or, more commonly, by oral ingestion and absorption in the digestive tract.<sup>57</sup>

*In vitro* measurements of metabolic stability using human or rodent liver microsomes should be conducted as they are generally a good predictor of metabolic stability *in vivo*.<sup>58</sup> Metabolic stability refers to the susceptibility of compounds to biotransformation and is usually expressed as the intrinsic clearance  $CL_{int}$ . *In vitro* clearance is determined by tracking the formation of metabolites or monitoring the depletion of substrates over time in subcellular liver fractions (like microsomes) or primary hepatocytes.<sup>59</sup> In the depletion method, the substrate is incubated in, e.g., liver microsomes at a low concentration level. Liver microsomes are particularly suitable when phase I metabolism is to be investigated, especially by cytochromes P450s (CYPs). The initial substrate concentration is maintained well below the Michaelis constant  $K_m$  of all enzymes involved, often 1  $\mu\text{mol/L}$ , and the substrate concentration is tracked over the time of incubation.<sup>60</sup>  $CL_{int}$  is estimated from the half-life obtained and scaled to a whole liver using standard scaling factors.<sup>60</sup> Primary hepatocytes offer the advantage of retaining all phase I and phase II metabolic enzymes (such as glucuronosyltransferase (UGT) or glutathione S-transferases (GST)) and the cofactors required for biotransformation as well as maintaining drug transport function.<sup>59, 61, 62</sup>

Typically, solubility in phosphate-buffered saline should be above 10  $\mu\text{M}$ , as a sufficient level of solubility is expected to avoid problematic formulations.<sup>18</sup> Acceptable lipophilicity should be achieved with LogP values of no more than 5, corresponding to the Ro5, or ideally less than 3.<sup>51</sup> Interestingly, during the H2L phase and later lead optimization, the molecular structures usually gain structural complexity.<sup>63</sup> The initial lead structures typically have lower molecular weight, lower number of rings and rotatable bonds, and lower hydrophobicity (lower cLogP) compared to the later drugs. Therefore, to price in a later increase in MW or lipophilicity in an effort to gain selectivity and affinity, chemical libraries should consider less complex structures in initial screenings.<sup>63</sup>

The Caco-2 permeability assay is an established method that measures the rate of flux of a compound across polarized Caco-2 cell monolayers to predict *in vivo* absorption of drugs.<sup>64</sup>

Compounds possessing good potency, *in vitro* metabolic stability, and reasonable aqueous solubility will be progressed for *in vivo* evaluation.

The following steps may include an assessment of *in vivo* pharmacokinetic (PK) properties in the mouse and rat, such as oral bioavailability.<sup>57</sup>

Detailed understanding of rat PK after *intravenous* and *per oral* dosing will allow the generation of key PK parameters such as bioavailability, clearance, the volume of distribution, and half-life, which can be used to assess compound limitations and design further analogs with improved properties.<sup>57</sup>

A variety of *in vitro* assays can be used as predictors of potential safety issues for the chemical series. These include the hERG safety assay<sup>65</sup> to evaluate potential cardiotoxicity and the Ames test<sup>66</sup> to identify chemical mutagens. Cell cytotoxicity and proliferation assays are generally used to determine whether test molecules affect cell proliferation or exhibit direct cytotoxic effects, e.g., on liver or kidney cells.<sup>67</sup>

If *in vitro* screening reveals a specific safety concern, it may be beneficial to run the assay early in the testing cascade and to prioritize compounds with improved properties.<sup>57</sup>

### 2.8 Lead Optimization Phase

The object of this final Lead Optimization Phase is to maintain favourable properties in lead compounds gained in the various *in vitro* and *in vivo* assays while improving deficiencies to ultimately identify a clinical candidate.<sup>1</sup> A selection of a few best candidates gained by in-depth SAR studies in the H2L phase is further optimized focusing on the major constraints. The required assays have already been addressed to a large extent in the H2L section. At this final stage of early drug development, further models of genotoxicity, such as the aforementioned Ames test<sup>66</sup>, and *in vivo* models, such as the Irwin test<sup>68</sup>, are focused. High-dose pharmacology, further pharmacokinetics/pharmacodynamics (PK/PD) studies for human dose prediction, dose linearity<sup>69</sup> and repeat dosing PK looking for drug-induced metabolism and metabolic profiling<sup>70</sup> all need to be carried out by the end of this stage.<sup>1</sup> Demonstration of efficacy in a relevant animal model and a rough estimation of a reasonable safety margin is often a prerequisite to attract investors for subsequent clinical trials.<sup>13</sup> Typically, 200,000 to 10<sup>6</sup> compounds are initially screened for each project in industry (in academia often less, but perhaps more rational), and hundreds of compounds are investigated during subsequent H2L and lead optimization programs to narrow down to one or two clinical candidate molecules.<sup>1</sup>

Only about 10% of small molecule projects in the industry make the transition to a clinical candidate due to failure at multiple stages. According to Hughes *et al.*, these failures can be due to the following reasons:<sup>1</sup> (i) inability to develop a reliable assay; (ii) no developable hits from compound screening; (iii) compounds do not behave as desired in secondary or native tissue assays; (iv) compounds are toxic *in vitro* or *in vivo*; (v) compounds have undesirable side effects that cannot be readily filtered out or separated from the mechanism of action at the target; (vi) inability to obtain a good PK/PD profile consistent with the dosing regimen required in humans; and (vii) inability to cross the blood-brain barrier for compounds whose target is in the central nervous system. During the subsequent clinical phase, only about 7% of the clinical candidates make it to the later approval stage (biologicals and other types included).<sup>30</sup>

Discussions are ongoing on how to increase the success rate, especially in the clinical phase, by "failing fast and cheap".<sup>1, 8, 71</sup> Some of these considerations relate to the design of clinical trials. However, some others relate to the early stages of drug discovery presented (some of which have already been mentioned<sup>5</sup>). Thus, carrying out more studies prior to clinical development, such as improved toxicology screens and a better understanding of the target as well as the disease being addressed – supported by academic-industry partnerships – might help to ensure that drug development is crowned with success.<sup>1, 5, 13</sup> And the need would undoubtedly be here.

---

*The bibliography for this chapter can be found at the end of this thesis (chapter VII).*

### 3 Targeting Protein Folding: A Novel Approach for the Treatment of Pathogenic Bacteria

Nicolas J. Scheuplein<sup>1\*</sup>, Nicole M. Bzdyl<sup>2\*</sup>, Emily A. Kibble<sup>2,3</sup>, Theresa Lohr<sup>1</sup>, Ulrike Holzgrabe<sup>1#</sup> and Mitali Sarkar-Tyson<sup>2#</sup>

<sup>1</sup> Institute of Pharmacy and Food Chemistry, University of Würzburg, Am Hubland, 97074 Würzburg, Germany

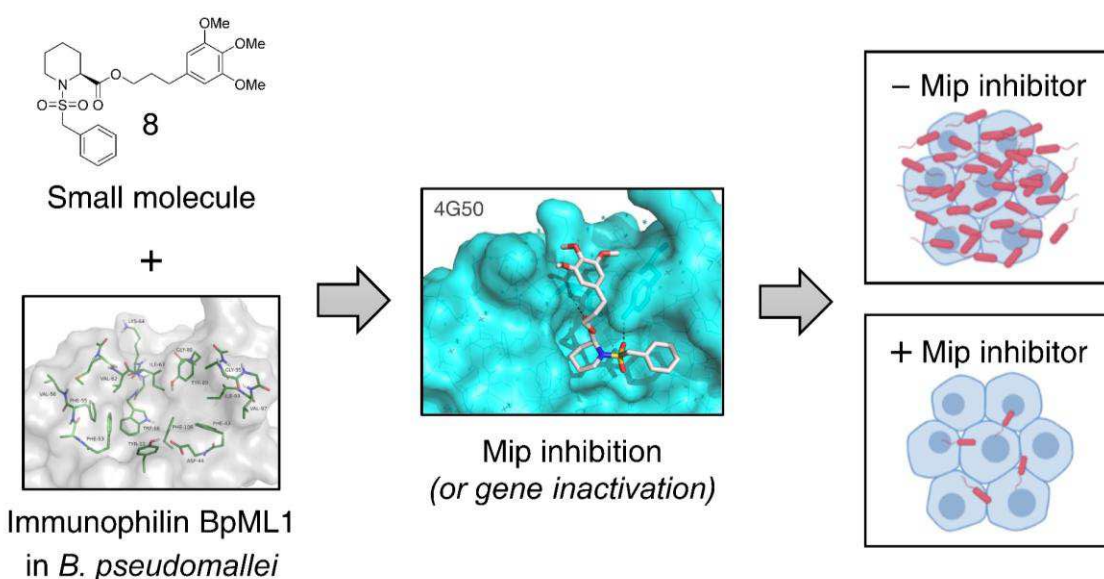
<sup>2</sup> Marshall Centre for Infectious Diseases Research and Training, School of Biomedical Sciences, University of Western Australia, 6009 Perth, Australia

<sup>3</sup> School of Veterinary and Life Sciences, Murdoch University, 6150 Murdoch, Australia.

\*Equal first authors. #Equal corresponding authors

*Reprinted with permission from Scheuplein, N. J.; Bzdyl, N. M.; Kibble, E. A.; Lohr, T.; Holzgrabe, U.; Sarkar-Tyson, M.; J. Med. Chem. 2020, 63 (22), 13355-13388. DOI: 10.1021/acs.jmedchem.0c00911. Copyright © 2020, American Chemical Society.*

#### Graphical Abstract



**Keywords:** Immunophilins, cyclophilin, FKBP, Parvulin, macrophage infectivity potentiator, PIN1, small molecular inhibitors, bacteria, virulence factor



### 3.1 Abstract

Infectious diseases are a major cause of morbidity and mortality worldwide, exacerbated by increasing antibiotic resistance in many bacterial species. The development of drugs with new modes of action is essential. A leading strategy is antivirulence, with the aim to target bacterial proteins that are important in disease causation and progression but do not affect growth, resulting in reduced selective pressure for resistance. Immunophilins, a superfamily of peptidyl-prolyl *cis-trans* isomerase (PPIase) enzymes have been shown to be important for virulence in a broad-spectrum of pathogenic bacteria. This Perspective will provide an overview of the recent advances made in understanding the role of each immunophilin family, cyclophilins, FK506 binding proteins (FKBPs), and parvulins in bacteria. Inhibitor design and medicinal chemistry strategies for development of novel drugs against bacterial FKBPs will be discussed. Furthermore, drugs against human cyclophilins and parvulins will be reviewed in their current indication as antiviral and anticancer therapies.

### 3.2 Introduction

Antibiotic resistance has been declared by the World Health Organization (WHO) as a serious threat to global public health, which requires immediate action. Antibiotic resistance in bacteria occurs over time due to genetic changes of a bacterium when challenged with antibiotics. This process is accelerated due to the misuse of antibiotics, and antibiotic resistant bacteria are now found in every country. It is predicted that without swift action, we will enter a “postantibiotic era”, where minor infections and injuries will be fatal once again. Currently, countries around the world are implicating antibiotic stewardship programs to improve the safe and appropriate use of antibiotics, with limited success.<sup>1</sup> It is, therefore, imperative to identify new methods of combating antibiotic resistance.

One such method is antivirulence therapy, which focuses on targeting virulence factors essential for infection of a host but not for growth in external environments. This method of combating pathogenic bacteria has gained momentum with antivirulence therapy possibly becoming an alternative treatment option for serious infections, as more bacterial species become resistant to available antibiotics.<sup>2</sup> Effectively disarming the virulence of a bacterium negates the evolutionary challenge to survive which can result in antibiotic resistance. The inhibition of bacterial virulence

may help existing antibiotics and the host's own natural immune response to efficiently eliminate infection, thereby presenting an attractive co-administered therapy option that would promote rapid clearance of bacteria. Targets for antivirulence therapy include factors involved in microbial attachment and invasion such as pilin, bacterial toxins, secretion systems, factors involved in biofilms, quorum sensing, and two-component systems.<sup>3</sup> For example, the anticancer drug 5-fluorouracil (**1**, Figure 1) has been shown to interfere with quorum sensing, preventing biofilm formation on catheters in large-scale clinical trials.<sup>4</sup> In *Pseudomonas aeruginosa*, synthetic halogenated furanone (**2**, Figure 1) has been shown to inhibit quorum sensing resulting in reduced biofilm and bacteremia in a pulmonary mouse model.<sup>5</sup> Small molecules, peptides, and monoclonal antibodies targeting the type III secretion systems of various bacteria are currently in various phases of development including preclinical studies.<sup>2, 6</sup> Although many antivirulence compounds have been developed in an organism specific manner, broad-spectrum therapeutics, inhibiting virulence targets which are common to multiple bacterial species is a highly attractive strategy for combatting multiple bacterial infections without the need for diagnostics. One such superfamily of proteins important for virulence in bacteria are the immunophilins; over the past 30 years they have been shown to be important for virulence in a number of pathogenic bacteria, leading to the development of novel inhibitors, some of which display broad-spectrum activity.

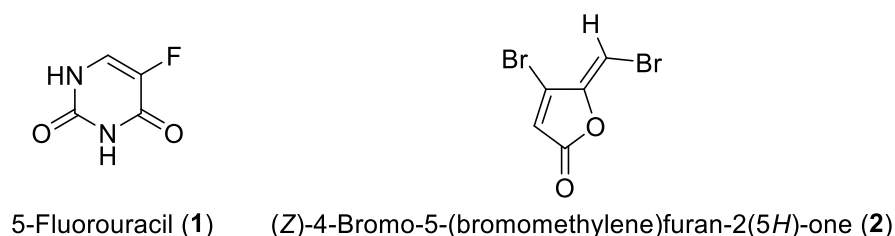


**Figure 1.** Structures of the anticancer drug 5-fluorouracil (**1**, left) which has been shown to prevent biofilm formation on catheters<sup>4</sup> and the halogenated furanone-derivative (**2**, right), which has been shown to interfere with quorum sensing and preventing biofilm formation in *P. aeruginosa*.<sup>5</sup>

### 3.3 The Immunophilins, a Superfamily of Folding Enzymes

The *cis-trans* isomerization of peptide bonds preceding a proline residue is known to be a rate-limiting reaction in the process of protein folding.<sup>7,8</sup> The immunophilin superfamily contains enzymes exhibiting peptidyl-prolyl *cis-trans* isomerase (PPIase) activity (EC 5.2.1.8), which enable catalysis of this inherently slow reaction, allowing the rate of protein folding to increase (Figure 2).<sup>9</sup> As well as protein assembly, PPIases also facilitate protein chaperone and cell-division activities.<sup>10</sup> This PPIase protein superfamily includes three subfamilies: the FK506 (**3**) binding proteins

(FKBPs), cyclophilins, and parvulins, which are all found in both eukaryotic and prokaryotic cells.

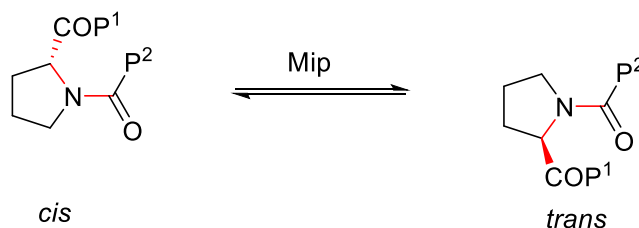


**Figure 2.** The PPIase activity of the immunophilins, such as the macrophage infectivity potentiator (Mip) protein, catalyzes the *cis*–*trans* isomerization of the peptide bonds preceding a proline residue in a polypeptide chain; P<sup>1</sup> = peptide chain 1 and P<sup>2</sup> = peptide chain 2. Due to steric hindrance, most amino acids have a strong energetic preference for the *trans* peptide bond conformation, but proline's unusual structure stabilizes the *cis* form so that both isomers are populated under biologically relevant conditions, allowing the correct folding of polypeptide chains into correctly structured proteins.

The FKBP family is named as such due to their ability to bind to, and be inhibited by, the immunosuppressive macrolide antibiotics FK506 (**3**) and rapamycin (**4**) (Figure 3). There are 18 known mammalian FKBP's to date, including the cytosolic FKBP12.<sup>11</sup> FKBP12 complexes with FK506, creating an FKBP-FK506 complex that binds calcineurin, an enzyme important for T-cell activation. FKBP12 also complexes with rapamycin, creating a FKBP-rapamycin complex that binds to the mammalian target of rapamycin (mTOR), a kinase important for cell growth and proliferation.<sup>12</sup> Murine cells lacking FKBP12 manifest cell cycle arrest in G1 phase.<sup>13</sup> In bacteria, the FKBP subfamily contains the macrophage infectivity potentiator (Mip) proteins and Mip-like (ML1) proteins, Trigger factor proteins, and sensitive to lysis D (SlyD) proteins. Trigger factor and SlyD have been examined enzymatically and structurally; however, the role of these proteins in bacterial virulence is limited. In comparison, Mip and ML1 proteins have been widely investigated in Gram-negative bacteria and shown to be integral to the virulence of a variety of species with deletion of these genes resulting in decreased bacterial survival in multiple pathogens, including *Legionella pneumophila* and *Burkholderia pseudomallei* in animal infection models.<sup>14,15</sup>

The cyclophilin subfamily is inhibited by cyclosporin A (CsA, **5**, Figure 4). Humans have seven major cyclophilins (Cyp), including cytosolic CypA, which binds to cyclosporin A, forming a complex that inhibits the phosphatase activity and biological function of calcineurin.<sup>16</sup> Other human cyclophilins can be found within the endoplasmic reticulum, mitochondria, and nucleus.<sup>17</sup> Murine cells lacking CypA were able to grow normally and able to differentiate into hematopoietic precursor cells *in vitro* which indicates that cyclophilins are not essential for cell viability.<sup>18</sup> The role of human cyclophilin A (hCypA) has been found to be essential for viral replication; for example,

drugs have been developed with strong antiviral properties against hepatitis C virus (HCV) and have shown promise in clinical trials.<sup>19</sup> Bacteria possess two cyclophilins, periplasmic/outer membrane PpiA and cytoplasmic PpiB. Bacterial cyclophilins have PPIase and chaperone activity and are involved in several biological processes, such as cellular signal transduction, adaptation to stress, control of pathogens virulence, and modulation of host immune response.<sup>20</sup>

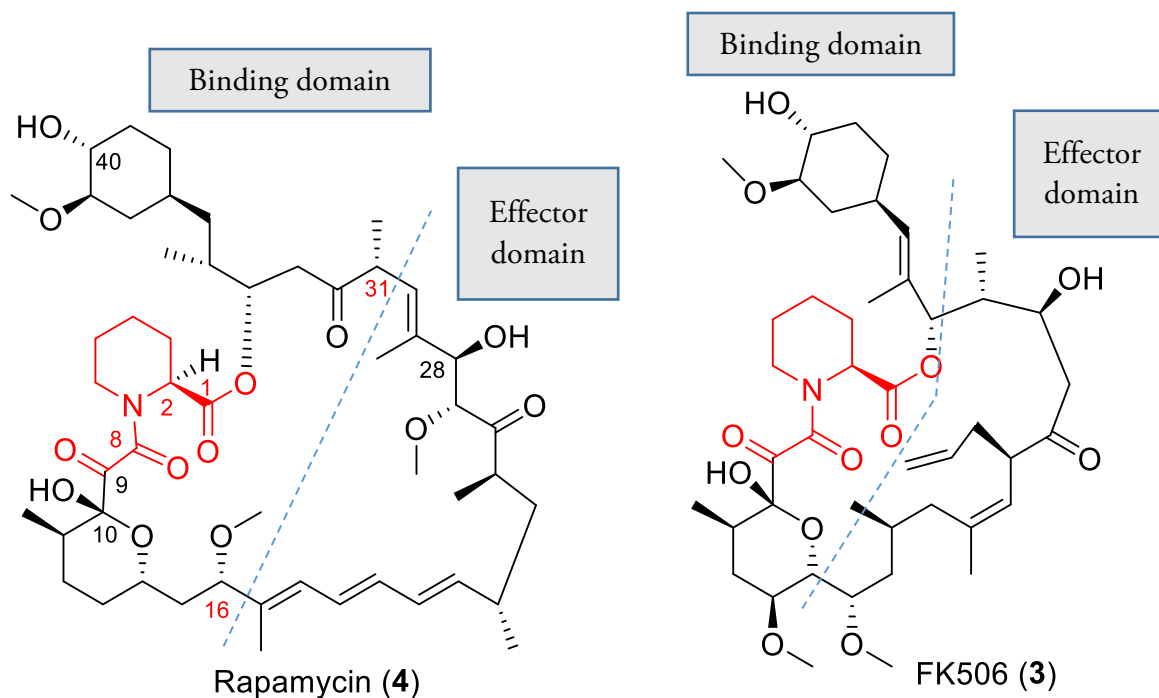


**Figure 3.** Structures of the natural products rapamycin (4) and FK506 (3). The common pipercoline substructure is marked red. Blue dashed lines show approximate limits of the binding domain, which depend on the respective FKBP and the effector domains, which interact with mTOR in the case of rapamycin or with calcineurin in the case of FK506. The numbers are indicating the atom number of the longest ring structure.

The parvulin subfamily is irreversibly inhibited by juglone (6, Figure 4).<sup>21</sup> Parvulin proteins include human PIN1, *Escherichia coli* Par10, and survival protein A (SurA).<sup>22</sup> Parvulins are the most recently discovered subfamily of the immunophilins and can range from 10 to 68 kDa in size, normally consisting of one parvulin domain with various N- and C-terminal extensions.<sup>23</sup> Eukaryotic PIN1 has been found to be involved in a variety of cellular functions, such as transcriptional regulation, mitotic cell control, and phosphorylation-dependent signal transduction pathways.<sup>24-28</sup> The important role of PIN1 in cellular functioning has stimulated interest in the development of drugs for anticancer therapies.<sup>29</sup> Prokaryotic parvulins have varied effects; in *E. coli* parvulins SurA and Ybau (also known as PpiD) are important for assembly of outer membrane proteins, with null mutations in both genes resulting in lethality.<sup>30</sup> In nitrogen assimilating bacteria

such as *Klebsiella pneumoniae* and *Azotobacter vinelandii*, the parvulin NifM ensures the activity of the nitrogenase reductase protein.<sup>31, 32</sup>

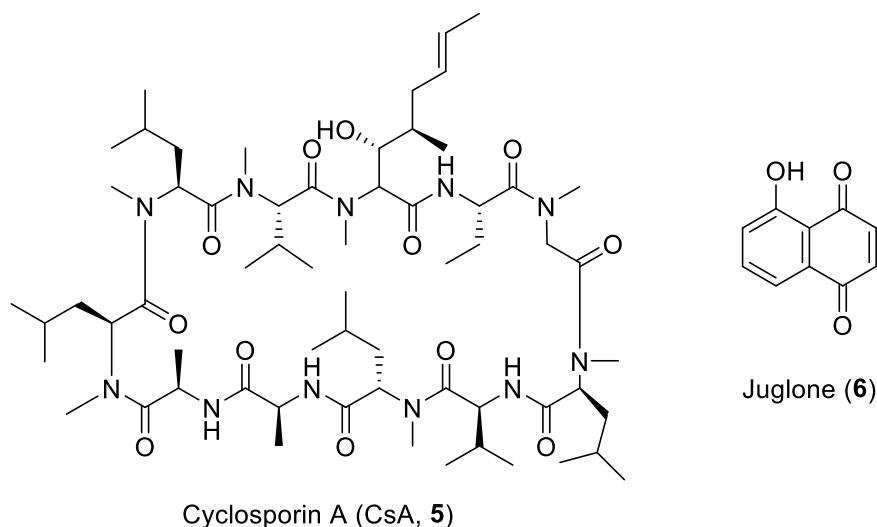


**Figure 4.** Chemical structures of the cognate inhibitor of cyclophilins, cyclosporin A (CsA) (5, left), and of parvulins, juglone (6, right).

This Perspective aims to provide an overview of each immunophilin subfamily and their role in bacterial virulence and pathogenesis, and a comprehensive review of the development of novel drugs against each subfamily along with structure–activity relationships and their efficacy against pathogenic bacteria. Currently, there are no drugs targeted to bacterial cyclophilins and parvulins; however there has been a number of drugs developed as antivirals and anticancer therapies which will be discussed in this review. The successes in anticancer and antiviral drug development pave the way for designing specific therapies that target bacterial cyclophilins and parvulins. It is clear from the literature that immunophilins, although representing promising antivirulence targets, are in the shadows of other virulence factors such as type 3 secretion systems and quorum sensing. This review highlights the advances in our knowledge of these enzymes in pathogenic bacteria and also the key strategies already undertaken to effectively target these enzymes with great potential to be broad-spectrum antivirulence therapeutics in our battle against antibiotic resistant bacteria.

### 3.4 FK506 Binding Proteins in Bacteria

As already mentioned, the FKBP subfamily comprises a group of distinct protein types: Mip and ML1 proteins, Trigger factor proteins, and SlyD proteins. Mip proteins are classically approximately 28 kDa in size, consisting of two distinct domains, an N-terminal dimerization domain linked to a domain containing the FKBP fold exhibiting PPIase activity. These proteins

are believed to form a homodimer on the outer membrane of the bacterial cell of approximately 60 kDa.<sup>33,34</sup> ML1 proteins possess the FKBP fold domain but lack the dimerization domain, resulting in an approximately 12-14 kDa protein with PPIase activity, believed to be located within the cytoplasm or periplasm of the bacterial cell.<sup>15</sup> Trigger factor proteins are approximately 48 kDa in size with three distinct domains. The N-terminal domain is homologous to parts of chaperone protein Hsp33 and is involved in ribosome docking of the protein.<sup>35</sup> The C-terminal domain is homologous to the chaperone protein SurA and has been shown to prevent protein aggregation. These two domains are linked by a central domain, containing the FKBP fold that exhibits PPIase activity.<sup>35</sup> SlyD proteins contain two domains: an N-terminal domain with the FKBP fold responsible for the PPIase activity of the protein, and an insert-in-flap (IF) domain, which has been shown to increase the rate of PPIase activity of the FKBP domain by 200-fold.<sup>36</sup> SlyD has also been shown to be involved in metal-dependent enzyme assembly. Thereby, SlyD displays both PPIase and chaperone activity and has been shown to be responsible for increasing solubility of aggregation-prone proteins in the *E. coli* cytoplasm.<sup>37</sup> Presence or absence of each of these proteins varies by bacterial species; for example, FkpA (a Mip protein homologue), Trigger factor, and SlyD have all been found to be present in *E. coli*, while *Mycoplasma genitalium* has been found to possess Trigger factor as its only folding isomerase protein.<sup>38</sup> Regardless, FKBP have been implicated in the virulence of many pathogenic bacteria, summarized in Table 1.

#### ***Role of FKBP in Gram-Positive Bacteria***

Investigation of FKBP is limited in Gram-positive bacteria. Specifically, only Trigger factor has been studied in bacterial species including *Bacillus subtilis*, *Streptococcus pyogenes*, and *Listeria monocytogenes*, resulting in various phenotypes (Table 1). In *B. subtilis* deletion of Trigger factor showed no effect on heat, osmotic, or oxidative stress, and only a double deletion in combination with a cyclophilin gene, *ppiB*, resulted in decreased growth under starvation conditions.<sup>39</sup> Trigger factor, known as RopA in *S. pyogenes*, has been found to be required for maturation and expression of the secreted cysteine proteinase (SCP).<sup>40</sup> Absence of Trigger factor results in impaired survival of *L. monocytogenes* in the presence of heat and ethanol stresses, and while no effect on intracellular survival was seen, the Trigger factor gene deletion strain did show reduced capacity to persist in the spleens and livers of infected mice.<sup>41</sup> These initial and promising results prove that more research is required to understand the role these FKBP may play in Gram-positive bacterial infections.

**Table 1.** Summary of the known functions of FKBP in bacteria.

Bacterial Species	Gene	Size (kDa); Cellular Location <sup>1,2</sup>	Phenotype	Ref
<b>Gram-positive</b>				
<i>Bacillus subtilis</i>	<i>Tig</i>	47; RB	- Double deletion with <i>ppiB</i> showed decreased growth under minimal conditions (double $\Delta tig \Delta ppiB$ mutant)	39
<i>Listeria monocytogenes</i>	<i>Tig</i>	48; RB	- Reduced persistence in spleens and livers of Swiss mice	41
<i>Streptococcus pyogenes</i>	<i>Tig</i>	47; RB	- Extracellular secretion of protease not present - <i>tig</i> required for maturation of protease polypeptide	40, 42
<b>Gram-negative</b>				
<i>Burkholderia pseudomallei</i>	<i>fbp</i>	11.9; PM	- Required for invasion and survival in J774A.1 macrophages - Decreased virulence in BALB/c mice - Decreased motility	15
	<i>BPSL0918</i>	16; CM	- Reduced replication in J774A.1 macrophages and HeLa cells - Decreased virulence in BALB/C mice - Increased beta-lactam susceptibility	43
<i>Neisseria meningitidis</i>	<i>mip</i>	28; OM	- Decreased survival in human whole blood - Decreased invasion of Detroit 562 cells upon treatment with Mip inhibitors	44-45
<i>Neisseria gonorrhoeae</i>	<i>mip</i>	30; OM	- Decreased intracellular survival in Raw 264.7 macrophages - 30% decrease in survival in neutrophils - Decreased growth rate over 6 hours	34
<i>Chlamydia trachomatis</i>	<i>mip</i>	27; ERB	- Inhibition with FK506/rapamycin increased infectivity for McCoy cells - Inhibition with Mip inhibitors results in decreased progeny infectivity	46-47
<i>Legionella pneumophila</i>	<i>mip</i>	25; OM	- Reduced capacity to invade U937 macrophages and explanted human macrophages - Decreased survival in <i>A. castellanii</i> and a guinea pig model of infection - Reduced growth at sub-optimal temperatures (17 °C and 44 °C) - FKBP domain needed for full virulence	14, 33, 48-50

Bacterial Species	Gene	Size (kDa); Cellular Location <sup>1,2</sup>	Phenotype	Ref
<i>Legionella longbeachae</i>	<i>mip</i>	24.7; OM	- Induced apoptosis of HL-60 cells but failed to multiply intracellularly - Unable to infect and multiply in <i>Acanthamoeba</i> model - Unable to cause death in an aerosolized Guinea pig model - No adverse symptoms in infected Guinea pigs seen	51-52
<i>Legionella micdadei</i>	<i>mip</i>	25.9; OM	- 24-fold decrease in bacteria in differentiated U937 cells 2 hours post-infection - 10-fold decrease in recovered bacteria after 24 hours in a <i>Hartmannella vermiformis</i> model of infection	53
<i>Escherichia coli</i>	<i>fkpA</i>	26; PM	- Highly active colicin M preparations were inactive against $\Delta fkpA$ - $\Delta fkpA$ stimulates transcription of the <i>degP</i> locus	54-57
	<i>tig</i>	48; RB	- No phenotype under tested conditions - $\Delta tig \Delta dnaK$ double knock-out is lethal	58-59
	<i>slyD</i>	21; CM	- Stabilized E protein, allowing for accumulation to levels to exert a lytic effect	60
<i>Salmonella enterica</i>	<i>slyD</i>	21; CM	- Attenuated colonization in 50% of chicks	61
<i>Salmonella enterica</i> serovar Enteritidis	<i>slyD</i>	21; CM	- No phenotype under tested conditions	62
<i>Salmonella enterica</i> serovar Typhimurium	<i>fkpA</i>	29; PM	- Decreased survival in Caco-2 epithelial and J774A.1 macrophage cells after 6 hours	63
<i>Aeromonas hydrophila</i>	<i>fkpA</i>	28.7; PM	- No attenuation of virulence seen	64
<i>Aggregatibacter actinomycetemcomitans</i>	<i>mip</i>	24; PM/IM <sup>3</sup>	- 4-fold decrease in bacteria after 6 hours of infection in HeLa cells	65

<sup>1</sup>Cellular location: RB, ribosome bound; CM, cytoplasm; PM, periplasm; OM, outer membrane; IM, inner membrane; ERB, elementary body bound and reticulate body bound.

<sup>2</sup>Protein size (kDa) and cellular location were ascertained from the associated references where possible, if not, UniProt, NCBI and the algorithm PSORTb were used to determine kDa and cellular location. <sup>3</sup>Unable to fully classify subcellular localization.



### *Role of FKBP's in Gram-Negative Bacteria*

Trigger factor has been investigated in *E. coli*, and while a single Trigger factor mutant showed no phenotype under tested conditions, a combination deletion with chaperone protein DnaK resulted in lethality to the organism.<sup>58, 59</sup> An *E. coli* SlyD mutant was found to stabilize the E lysis protein of bacteriophage  $\phi$ X174, allowing for accumulation to levels required to exert a lytic effect. E lysis protein contains five proline residues, which may explain the importance of the presence of SlyD in order for its full maturation.<sup>60</sup> A transposon insertion mutant of SlyD in *Salmonella enterica* serovar Typhimurium resulted in a 50% decrease in numbers of colonized chicks.<sup>61</sup> Clearly, a range of phenotypes are observed in the absence of the FKBP's Trigger factor and SlyD, and these proteins and their effects on bacterial functioning require further investigation.

The most well studied FKBP is the macrophage infectivity potentiator (Mip) protein and the closely related ML1 proteins. They have been implicated in the virulence of a variety of human bacterial pathogens including *L. pneumophila*, *B. pseudomallei*, *Neisseria meningitidis*, *Neisseria gonorrhoeae*, *S. enterica*, and *Chlamydia trachomatis*.<sup>14, 15, 33, 34, 37, 44, 46, 48, 50, 63</sup> Consistently, Mip and ML1 proteins have been found to have a pleiotropic effect on virulence across all of these bacterial species. Deletion of Mip in *L. pneumophila* was found to reduce invasion capability in U937 monocytic cells and explanted human macrophages, as well as reduced survival in both the amoebae, *Acanthamoeba castellanii*, and a guinea pig infection model, as well as reduced bacterial growth at suboptimal temperatures.<sup>14, 33, 48-50</sup> Similarly, in the closely related organism, *Legionella longbeachae* deletion of Mip results in reduced intracellular survival in the human leukemia cell line HL-60, a decreased invasive capability in *A. castellanii*, and the inability to cause lethal disease in an aerosolized guinea pig model.<sup>51, 52</sup> A mutant in *S. enterica* lacking FkpA (Mip homologue), resulted in decreased survival in Caco-2 intestinal epithelial cells as well as J774A.1 murine macrophages after 6 h.<sup>63</sup> Similarly, deletion of Mip in *Aggregatibacter actinomycetemcomitans*, resulted in a 4-fold reduction in survival after 6 h infection in HeLa cells.<sup>65</sup> The Mip-like gene (*ML1/fbp*) in *B. pseudomallei* was also shown to be important for intracellular survival with a Mip-deletion mutant showing reduced invasion and survival in both macrophage and epithelial cell lines and ultimately resulted in decreased virulence in the BALB/c mouse infection model.<sup>15</sup> In the pathogenic *Neisseria species*, deletion of the Mip gene has resulted in decreased survival of *N. gonorrhoeae* in macrophage cells and decreased survival of *N. meningitidis* in blood.<sup>34, 44</sup> While the exact mode of action of Mip proteins is still unknown, the homology between Mip and Mip-like

proteins in Gram-negative bacteria and its role in the virulence of these pathogens intracellularly make these attractive drug targets. This has led to the testing of small molecule inhibitors against the Mip and ML1 proteins of *L. pneumophila*, *B. pseudomallei*, *C. trachomatis*, *N. gonorrhoeae*, and *N. meningitidis*.<sup>66-68</sup> Pipecolic derived compounds inhibited enzymatic activity of the LpMip; however, this enzymatic reduction had no detrimental impact on the infectivity of inhibitor-treated bacteria.<sup>67</sup> Similarly, inhibitors were designed against *B. pseudomallei* Mip (BpML1), with these inhibitors demonstrating inhibition both enzymatically and in *in vitro* infection of macrophages.<sup>69</sup> The Mip inhibitor-treated *C. trachomatis*, *N. gonorrhoeae*, and *N. meningitidis* were also shown to be impaired in invasion and survival within host cells.<sup>68</sup> The implication of Mip and Mip-like proteins in the persistence and survival of a varied range of pathogenic bacteria within human host cells is quite clearly demonstrated and reinforced by the few studies that have tested and shown Mip to be required for virulence of bacteria *in vivo*.

While more investigation into the role of the FKBP's SlyD and Trigger factor in bacterial virulence is necessary, it is clear that a subset of FKBP's, the Mip and ML1 proteins, play an important role in the pathogenic potential of a wide variety of bacterial species. This group of evolutionarily distant organisms all utilize Mip and ML1 proteins in similar ways for virulence, with gene deletion mutants all exhibiting decreased survival in macrophages and animals. The conservation and homology between these proteins among pathogenic bacteria indicate the importance of Mip and ML1 proteins for bacterial function. While the precise folding partners of these proteins remain unknown, there is much data to prove the necessity of Mip and ML1 proteins in infectivity and survival within the host. The structural conservation suggests Mip and ML1 proteins are broad spectrum antivirulence drug targets, with already promising results.

### 3.5 Development of Inhibitors to the Mip Protein in Gram-Negative Bacteria

#### *Commercially Available FKBP Inhibitors and Their Complexes*

Rapamycin (**4**, sirolimus) and FK506 (**3**, tacrolimus) are commercially available drugs initially isolated from *Streptomyces hygroscopicus* and *Streptomyces tsukudaiensis*, respectively, and their chemical structures are shown in Figure 3.<sup>70, 71</sup> They are potent inhibitors of FKBP's including the bacterial Mip proteins; however they exhibit immunosuppressive activity. FKBP-FK506 complexes bind to calcineurin in cells which prevents the dephosphorylation of nuclear factor of activated T-cell (NF-AT) that is required for interleukin 2 (IL-2) gene expression and T-cell activation.<sup>72, 73</sup>

Rapamycin (**4**) also complexes with FKBP; however, the complex interacts with the mammalian target of rapamycin (mTOR) instead of calcineurin and induces immunosuppressant activity.<sup>74, 75</sup> The immunosuppressant activity of these compounds makes them unsuitable as antibacterial therapies; fortunately the domain responsible for the immunosuppressive effects is separate from the enzyme binding domain, a characteristic that has been exploited by several groups to design small molecule inhibitors lacking the immunosuppressive action.<sup>76, 77</sup> This has been shown to be a successful strategy, particularly with the use of rapamycin (**4**) as the basis for the design of small molecule inhibitors of bacterial Mip proteins.<sup>67, 69</sup>

### *Structure–Activity Relationships of the Rapamycin-FKBP12 Complex*

Alluded to above, the effector domains of rapamycin (**4**) and FK506 (**3**), which lead to immunosuppressant activity, are different from the PPIase binding domain. In both structures, the PPIase binding domain can essentially be traced back to the already mentioned pipercolic acid moiety. Depending on which FKBP is binding, the overlap extends approximately from C31 to C16 for rapamycin (**4**) and C14 to C26 for FK506 (**3**, Figure 3).<sup>78, 79</sup> Due to the homology between human FKBP12 and Mip, detailed analysis of FKBP12 using structure–activity relationship (SAR) with rapamycin (**4**) has significantly aided design of inhibitors to Mip proteins. However, differences in their binding modes have also helped toward design of tailor-made inhibitors for each target. There are two main interactions between rapamycin (**4**) and FKBP12, hydrophobic interactions with the piperidine (Tyr26, Phe46, Trp59, Phe99) and hydrogen bonds (a total of three) formed between the  $\alpha$ -ketoamide functions of rapamycin (**4**). Both subunits dive deep into FKBP12, while other parts of the rapamycin (**4**) structure attach rather superficially. The C9-carbonyl plugs into a specific small binding pocket of FKBP12, which is formed by the edges of Tyr26, Phe36, and Phe99 (Figure 5). As a consequence of the different spatial orientation in Mip compared to FKBP12 and the resulting lack of cavity, this hydrogen bond between the amide carbonyl cannot be formed. Therefore, the lead structure for Mip-inhibition needed modification. The tetrahydropyran ring of rapamycin (**4**) is involved in numerous interactions with FKBP12 (Phe36, Asp37, Ile90, Ile91), and the C10 hydroxyl forms a hydrogen bond with the Asp37 side chain, on the edge of the binding domain. At the other edge of the binding pocket the cyclohexyl ring interacts with FKBP12 (Gln53, Glu54, Val55, Ile56); additionally, a hydrogen bond occurs between the C40 OH group and the main-chain carbonyl of Gln53. Another hydrogen bond is

located between C28 OH, which is orientated toward FKBP12, and the Glu54 oxygen (Figure 5).<sup>79</sup>

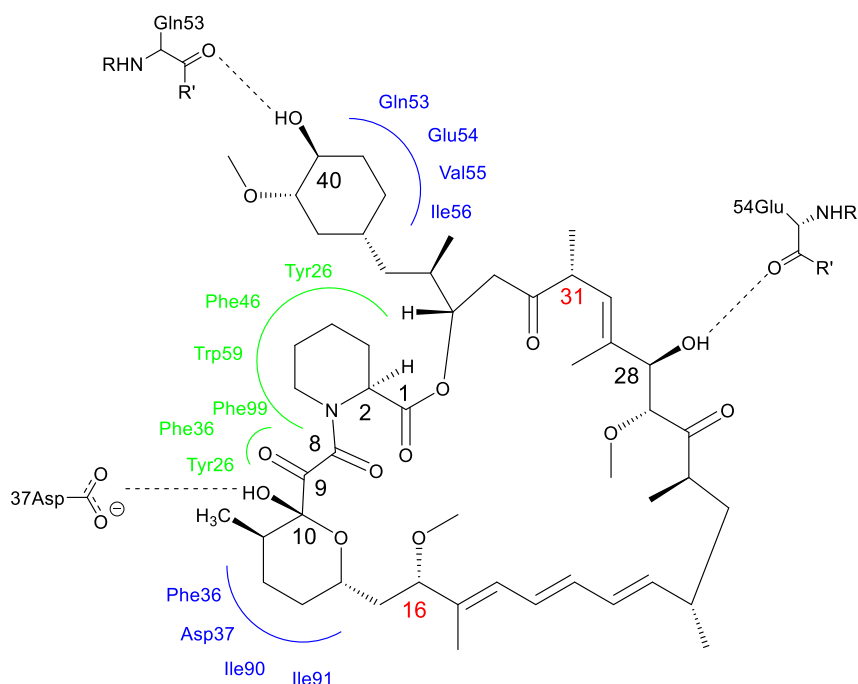


**Figure 5.** Detailed FKBP12 interactions with rapamycin (**4**), representative for other FKBP12s. Black dashed lines indicate hydrogen bonds. Green amino acids show points of contact deep in the binding pocket and blue amino acids on its surface.

### *Inhibitors of the Legionella pneumophila Mip Protein*

The first bacterial FKBP to be targeted for the development of potent inhibitors was the Mip protein from *Legionella pneumophila*.<sup>48</sup> The interactions between inhibitors and the *L. pneumophila* Mip (LpMip) protein were pivotal to design a lead structure for selective targeting, due to the binding pockets of FKBP12 and the LpMip having an almost identical amino acid sequence. Despite this similarity, the rapamycin–protein complexes show significant differences with respect to the orientation of rapamycin (**4**) in the binding pocket of both proteins. The Tyr109 of LpMip, projecting deep into the binding pocket, reduces its overall size in comparison to the FKBP12 pocket, resulting in different binding modes of the pipercoline moiety of rapamycin (**4**) with respect to the orientation of the aliphatic ring in the hydrophobic pocket, the conformation of the ester, and the hydrogen-bonding pattern of the carbonyl groups.<sup>67</sup>

### *Inhibitor Assay for $K_D$ and $IC_{50}$ Determination*

In order to evaluate the extent of Mip inhibition in *L. pneumophila*, an enzymatic PPIase assay was used to determine the  $K_D$  and  $IC_{50}$  of the inhibitors. In most cases, a protease-coupled enzymatic assay is suitable to quantify the inhibitory effect of the new compounds *in vitro*. In brief, a short *p*-nitroaniline labeled amino acid sequence is used as substrate, while  $\alpha$ -chymotrypsin serves as an

auxiliary protease, which only cleaves *trans*-linked Phe-Pro substrates. The conversion can be measured by absorption at 390 nm, owing to released *p*-nitroaniline. Initially, the absorption increases rapidly due to the 85% *trans*-proline that is in equilibrium in aqueous buffer (Figure 6). In the next phase of the reaction, the slow isomerization at room temperature leads to a moderate increase in absorption. In the presence of Mip, which catalyzes the isomerization from *cis* to *trans*, the absorption rises rapidly until the substrate is completely converted. An inhibitor screen can be performed by adding compounds to the assay, which prevents this catalytic isomerization and thus leads to reduced absorption values. This assay was first described by Fischer *et al.*,<sup>80</sup> but it is not appropriate for large scale screening, due to some drawbacks like high consumption of peptide and enzyme and its high susceptibility to temperature variation. In order to develop a medium throughput assay with improved robustness and higher reproducibility, Vivoli *et al.* optimized the assay conditions and created an improved version of PPIase assay.<sup>81</sup> This involved a temperature controlled plate reader which enabled semiautomated medium throughput assays increasing the number of samples to 84, a potentially 4-fold increase in the number of assays that can be run in a single day.

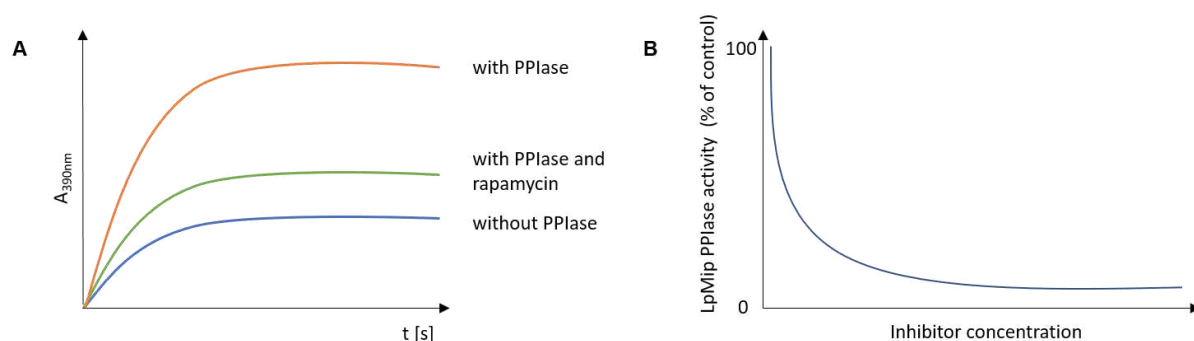


**Figure 6.** (A) Illustration of the absorption spectra during the protease-coupled reaction (with and without PPIase or rapamycin). Mip PPIase activity catalyzes the conversion from *cis* to *trans* of the substrate, and the absorption increases rapidly, while rapamycin, as a Mip inhibitor, prevents this effect. The reaction reaches equilibrium as all substrate is turned over to a *trans* state. (B) Residual activity curve of compounds. In the PPIase assay the catalytic efficiency of the unbound enzyme (without inhibitor) was assumed to be 100% of the enzyme activity, and all other efficiency values (with inhibitor) were compared. The residual activity of the enzyme could thus be maintained at different inhibitor concentrations, and therefore, the IC<sub>50</sub> value for each compound can be determined.

### Structure–Affinity Relationship of LpMip Inhibitors

Two pipercolic acid-type lead structures were identified and their binding affinity was compared to FKBP12 (Figure 7).

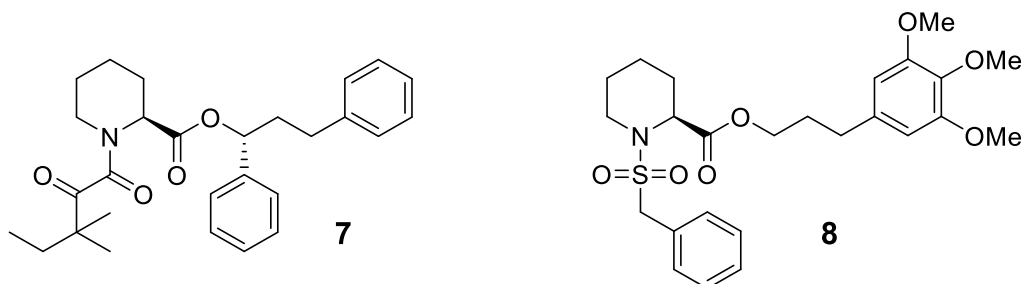


**Figure 7.** Starting point for investigations was two FKBP12 inhibitors that were tested for LpMip inhibition. Affinities of ligand 7 ( $K_i = 0.010 \mu\text{M}$ )<sup>82</sup> and ligand 8 ( $K_i = 0.230 \mu\text{M}$ ) to FKBP12 were described before.

Docking studies revealed comparable binding modes of the pipercoline groups of ligands 7 and 8 in FKBP12<sup>82</sup> but differences in LpMip. The binding of ligand 7 to LpMip is weak compared to ligand 8, which offers a very favorable hydrophobic interaction with the benzylsulfonamide group, which promises even better results than docking with FKBP12 (Figure 8). This effect can be explained by the less voluminous sulfonamide group of ligand 8 compared to the  $\alpha$ -ketoamide moiety of ligand 7, which is a better fit into the narrow binding pocket of Mip. Due to steric hindrance, larger ligands like the  $\alpha$ -ketoamide of compound 7 (Figure 7) lead to weak inhibition. On the basis of these data, a series of inhibitors were synthesized and tested for their ability to reduce the PPIase activity of LpMip.<sup>67</sup>

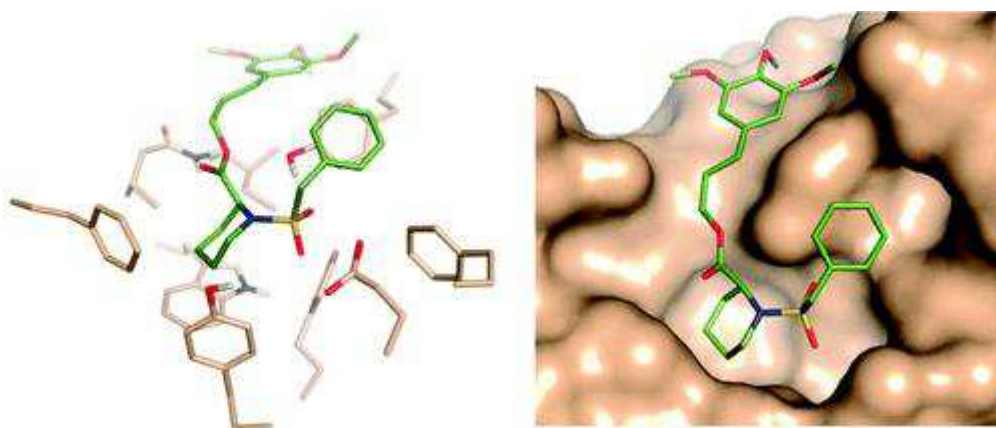


**Figure 8.** Top-binding mode of ligand 8 in LpMip justifies its selection as first lead structure. The pipercoline ring is placed deep in the active-site pocket, whereas the phenyl ring of the sulfonamide moiety occupies a subpocket and the trimethoxyphenyl moiety lies on the surface.<sup>67</sup> Reproduced with permission from *Journal of Medicinal Chemistry*, Juli *et al.*<sup>67</sup>

The comparison of phenyl ligand **9** and benzyl ligand **10** substituted sulfonamides (Figure 9) reveals a positive effect on binding affinity of the methylene group in LpMip, which was not observed with FKBP12. A meta substitution of the phenyl ring with nitro or amino groups substantially reduces the inhibitory effect; however, the nitro group is tolerated rather than the amino function.

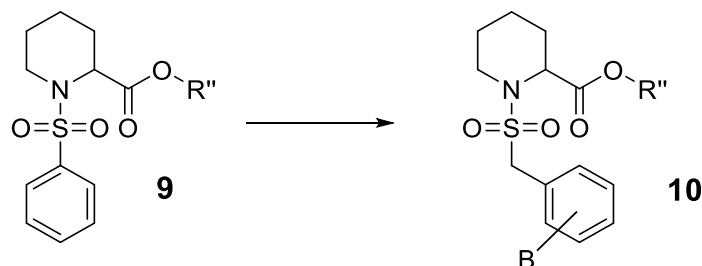


**Figure 9.** Comparison of the sulfonamide residue shows that the benzyl moiety in **10** is superior to phenyl (**9**) for Mip inhibition, and substitution B in meta position is possible and was also investigated.

For the R'' moiety, a large substituent attached to the ester seems to be crucial for a notable binding affinity to the LpMip (Figure 10). A small ethyl ester leads to a weak Mip inhibition but less so in FKBP12. A second aromatic ring ( $\alpha$ -position C), as it appears in ligand **7**, next to the carbonyl function has an unfavorable effect on the affinity to both proteins. Optimal results were achieved with a large propyltrimethoxyphenyl, ligand **11**, or -pyridine group, ligand **12** (Figure 10), which may result in greater water solubility while maintaining activity. Additionally, checking the activity of both enantiomers revealed the *S*-enantiomer to be clearly superior to the *R*-enantiomer, with the racemate hinting to a stereoselective effect and, thus, a specific binding. Taken together, the *S*-pipercoline sulfonamides is a promising lead structure for selective LpMip inhibition that may have broad-spectrum activity against other bacterial Mip proteins.<sup>67</sup>

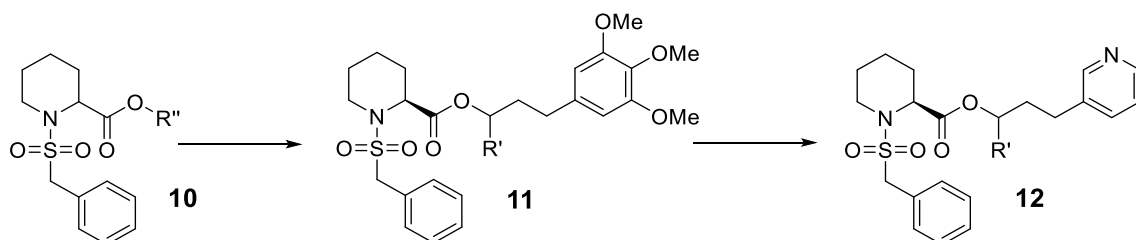


**Figure 10.** Optimization of the R'' residue showed that bulky trimethoxyphenyl (**11**) or pyridine rings (**12**) are moieties of choice in terms of Mip inhibition. Additionally, a pyridine residue promises an improved solubility of the compounds.

### Cycloheximide–Adamantane Hybrids

Cycloheximide (**13**),<sup>83</sup> and adamantane (**14**),<sup>84</sup> or hybrids of both,<sup>85</sup> constitute different classes of inhibitors, which also bind to the PPIase domain of the LpMip (Figure 11). Cycloheximide (**13**),

a natural product from *Streptomyces griseus*, was found in a screening campaign for nonimmunosuppressive FKBP inhibitors.<sup>83</sup> It represents an efficient inhibitor of eukaryotic protein synthesis, by inhibiting the activity of the peptidyl transferase on the 60S subunit of ribosomes, thus hindering successful translation. This unwanted effect can be prevented by N-substitution of the piperidine group. Structure–activity relationships in a series of synthesized cycloheximide derivatives with regard to cytotoxicity against eukaryotic cells is described by Christner *et al.*<sup>86</sup> An extensive analysis of BpML1 protein and its binding modes with cycloheximide compounds was carried out by Norville *et al.*<sup>87</sup> Interestingly, they discovered a conformation of cycloheximide N-ethylethanoate mimicking the conformation of a helical peptide, which was found in the crystal structure of BpML1 protein and is similar to human TGF (transforming growth factor) receptor, an activation modulator.<sup>87</sup>

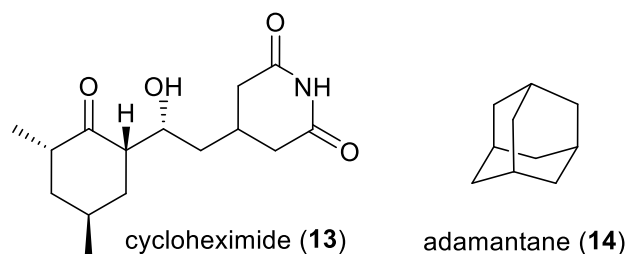


**Figure 11.** Hit compounds of the nonimmunosuppressive FKBP ligand screening: cycloheximide (**13**, left) and adamantane (**14**, right).

Adamantane (**14**), however, has been a hit of a custom-tailored computational prediction of the FKBP12-FK506 complex. Since, adamantane (**14**) and cycloheximide (**13**) target different areas of the active site of LpMip, the synthesis of various compounds consisting of both favorable hit characteristics seems to be a promising strategy in order to achieve a cumulative inhibitory effect. Adamantane (**14**) overlaps with the pipercolic acid area of FK506 (**3**), while cycloheximide (**13**) binds near the enzymatic cleft. Almost all tested inhibitors were far more efficient at inhibiting FKBP12 than LpMip as determined using the PPIase assay, except for the weakest compound **15** (Figure 12). The best inhibitor, a double methylated adamantane compound **16** surprisingly reduces the gap between LpMip and hFKBP12 binding affinity.<sup>85</sup>

Coupling of adamantane and cycloheximide results in 4 times lower  $IC_{50}$  values as seen with compound **15** compared to compounds **16–18** (Figure 12), in which the activity increased with nonpolar substitution on the adamantane backbone, such as methylation or ethylation in compounds **16–18**, while introduction of polar groups such as hydroxyl (compound **19**) was not



beneficial. All these trends of binding affinity associated with substitutions also hold true for FKBP12. However, despite some success against recombinant LpMip protein, the inhibitory effects could not be observed on *L. pneumophila* growth in liquid cultures containing compound or on bacterial replication rates during macrophage infection. Moreover, there was no difference between wild-type and isogenic Mip-deficient mutants of *L. pneumophila* indicating that these compounds exhibited off target effects.<sup>85</sup>

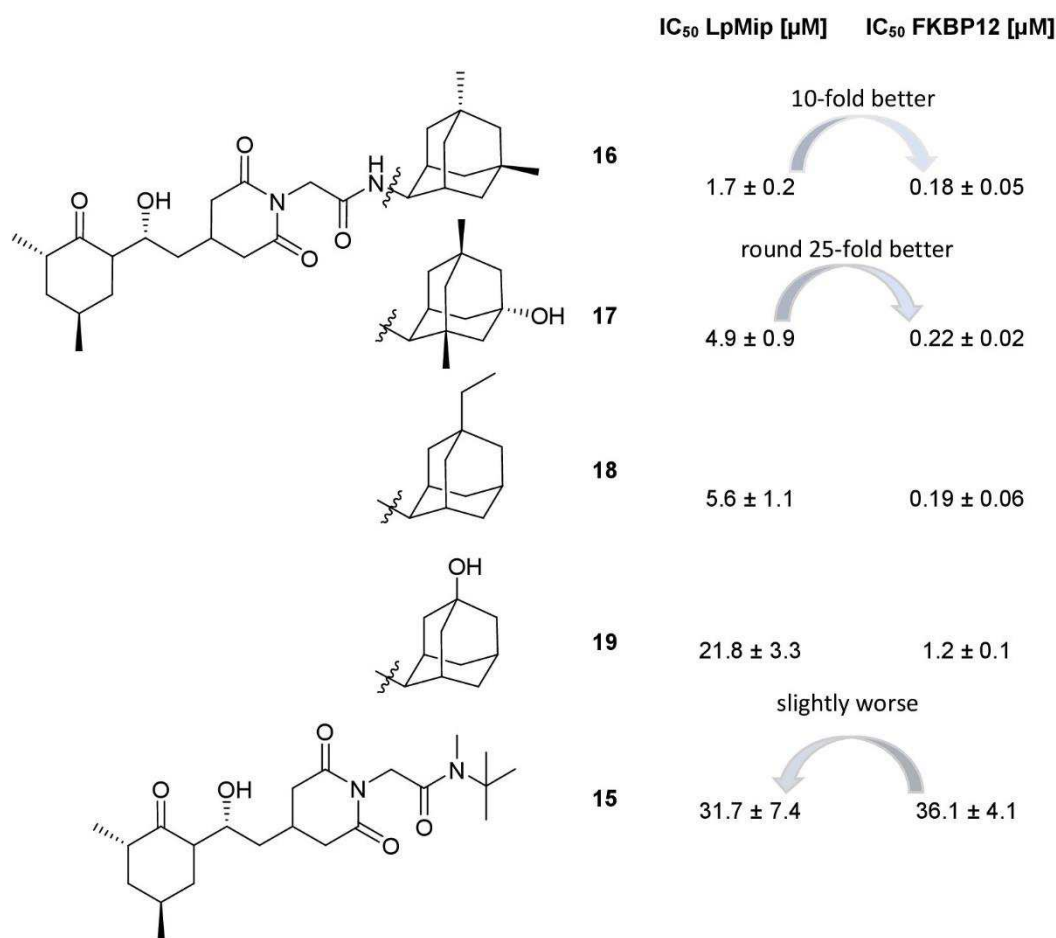


**Figure 12.** Several hybrids, highest to lowest activity. Hit compound **16** had 10-fold lower IC<sub>50</sub> values for LpMip than for FKBP12; the hydroxylation decreased the affinity especially for LpMip. The weakest compound **15** (tert-butyl instead of adamantane and N-methylation) significantly worsens the affinity, especially for FKBP12.

### *Inhibitors of B. pseudomallei Mip (BpML1)*

LpMip inhibitors was used as a starting point for the development of compounds toward BpML1,<sup>87</sup> with further optimization achieved through structural studies of BpML1 cocrystallized with rapamycin (**4**) and novel compounds **20–23** (Figure 13) by Begley *et al.* (Figure 14).<sup>66</sup>

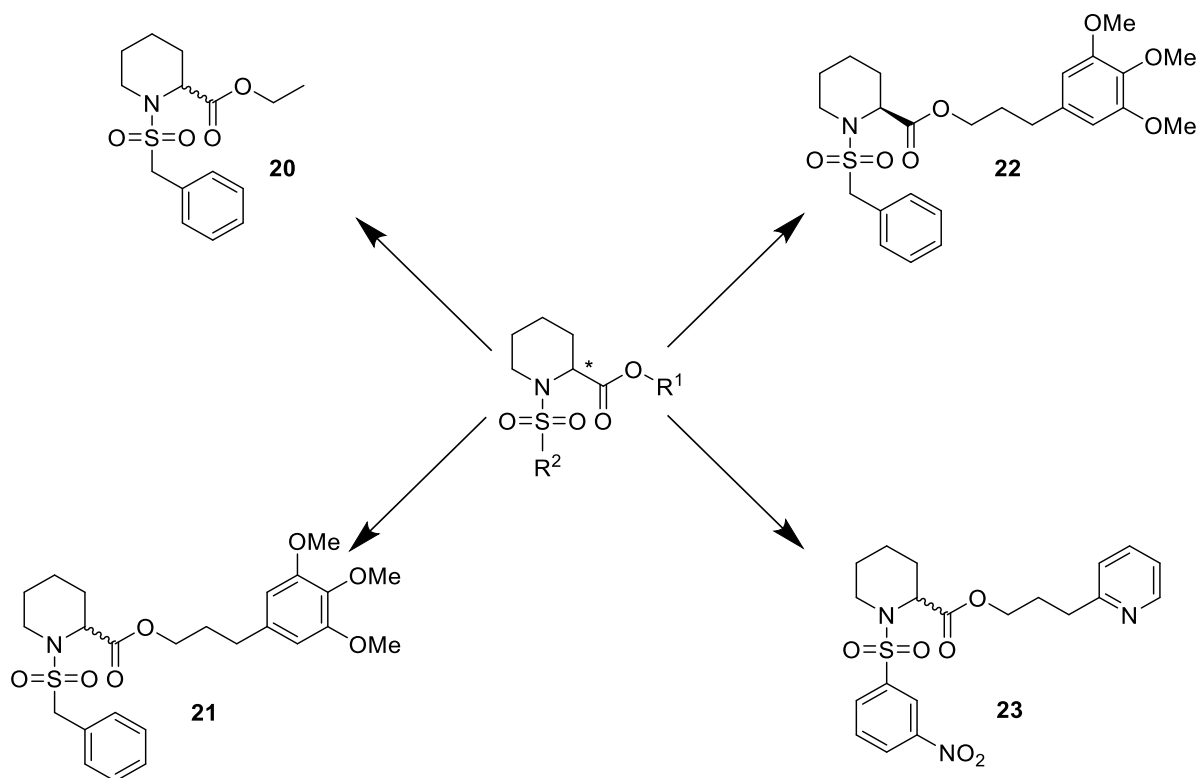


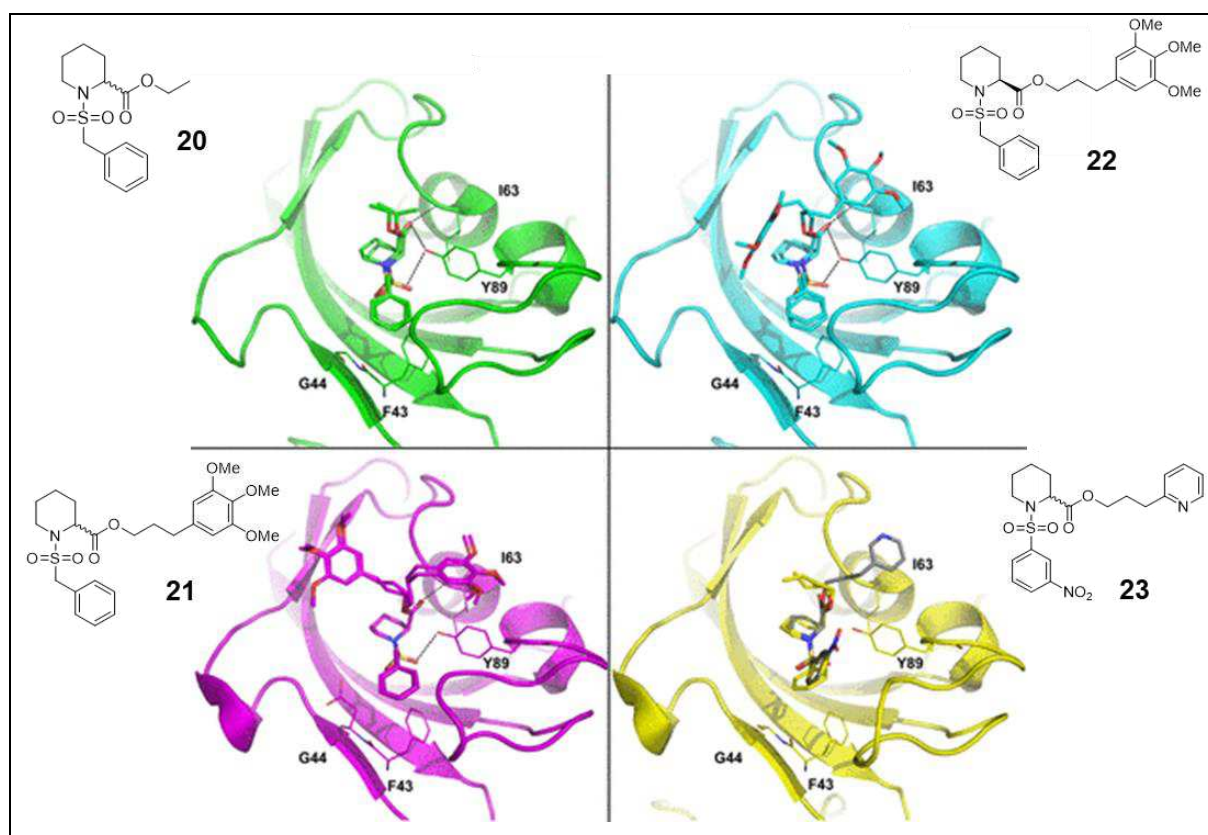
**Figure 13.** Cocrystallization trials with BpML1 were carried out with several piperolic acids. Compounds **20–23** delivered crystals with sufficient X-ray data for structure determination. Compound **22** represents the *S*-enantiomer of compound **21**, while all others were introduced as racemates.

In general, two to four different binding positions could be identified for each compound, with the largely conserved binding of the piperolic acid moiety across all four complexes. Compounds **20**, **21**, and **22** show a hydrogen bond between the sulfonyl oxygen and Y89; the carbonyl ester coordinates with the amide backbone of I63; the terminal phenyl ring forms a  $\pi$ -edge-stacking interaction with F43. The position of the trimethoxyphenyl residue appears to be more variable in the compound-BpML1 cocrystals, but the most common conformation overlaps the same binding pocket that occupies the methoxycyclohexanol substructure of rapamycin (**4**) and FK506 (**3**, Figure 15). The enantiospecific preference of the inhibitors was confirmed by docking studies, cocrystallization and associated X-ray data, NMR measurements, and PPIase assay, which generally led to a 4-fold higher binding affinity of the *S*-enantiomer compared to the racemate. As already mentioned, compounds **20–22** show similar binding poses (Figure 14), in contrast to compound **23**. First, the rotation of the carbonyl ester in compound **23** prevented any interaction with I63 within the crystal, compared with compounds **20–22**. Second, the uptake of the nitrobenzyl ring into the flexible outer loop A94 to I98, as observed for the benzyl residue of compounds **20–22**,

seems to be possible, but the positioning of the nitro group is unlikely for compound **23** due to the lack of the methylene moiety.<sup>66</sup>

The solution NMR characterization was carried out with <sup>15</sup>N-labeled, native BpML1, which was titrated with the pipercoline acid derivatives to calculate biophysical binding constants. The mean dissociation constants ( $K_D$ ) were calculated by using SOFAST-HMQC pulse sequence, based on the chemical shift perturbations (CSPs) of equally spaced amino acid residues around the binding site of BpML1. Compound **20**, which is lacking a large R<sup>1</sup> (Figure 13), showed the weakest affinity to BpML1, hence indicating a significant contribution of this region to enzyme inhibition. Nevertheless, the NMR analysis predicted similar affinity to the active site by compounds **22** and **23**; however the *in vitro* PPIase assays revealed enzymatic inhibition with compound **22**. Detailed structural information obtained by SOFAST-HMQC spectra showed a strong chemical shift for V62 and I63 and a weak shift for F53 confirming the hypothesis that the trimethoxyphenyl or pyridine moiety shares the same pocket as methoxycyclohexanol. The largest CSP occurred at I63, indicating a hydrogen bond with the carbonyl ester, and in contrast to rapamycin (**4**) and FK506 (**3**) generated unexpected shifts of the terminal aromatic ring of compounds **21–23**, which implies a new interaction area. Numerous other CSPs occurred for compound **23**, indicating a conformational change in solution, and the strong CSP for Y89 suggests interactions with the nitro group.

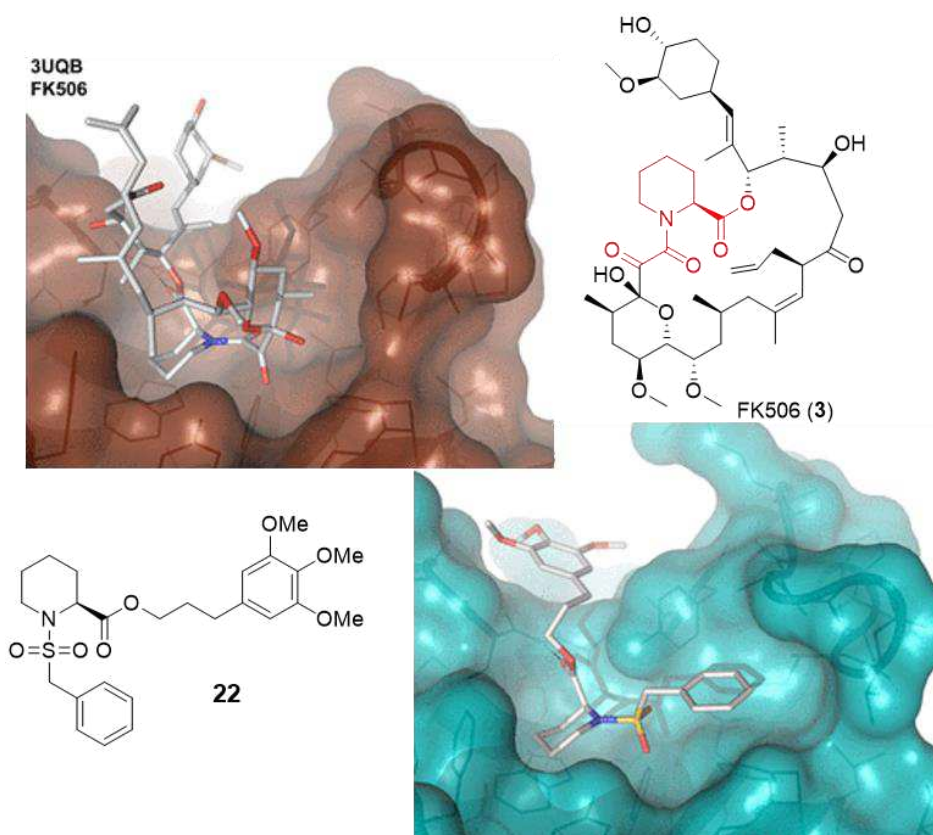
The lactate dehydrogenase (LDH)-release from murine macrophage J774A.1 cells was used to analyze the cytotoxicity caused by *B. pseudomallei* infection in the presence or absence of Mip inhibitors. Compounds **21–23** reduced the cytotoxicity by a magnitude of 30–40%, with no significant difference between the respective compounds, while compound **20** showed less activity compared to the other compounds. An inhibitor's cytotoxicity against J774A.1 cells themselves could not be determined for **20** and **23**, whereas **21** and **22** showed an effect less than 10%. This can be explained by their increased cell permeability due to increased lipophilicity. Compounds **20–23** are also active against recombinant Mip proteins from *Yersinia pestis* and *Francisella tularensis*.<sup>66</sup>



**Figure 14.** Structure ensemble for pipercolic acids binding to BpML1. Four crystallographic poses were observed for compound **21** (pink), while two poses each were obtained for compounds **20** (green), **22** (blue), and **23** (yellow). A full model complex for compound **23** is postulated (gray) and is based on NMR data and available space in the crystal structure. Non-carbon atoms for each compound are colored as follows: red, oxygen; blue, nitrogen; gold, sulfur.<sup>66</sup> Reproduced with permission from *Antimicrobial Agent and Chemotherapy*, Begley *et al.*, Volume 58, Issue 3, pp 1458–1467, Copyright 2014 American Society for Microbiology, DOI: 10.1128/aac.01875-13.<sup>66</sup>

Since a crystal structure of BpML1 bound to lead structure **21** was available and the binding mode was comparable with the postulated one obtained by docking studies for LpMip, a compound library starting from compound *S*-**21** was synthesized by Seufert *et al.*<sup>69</sup> The application of hot-spot analysis combined with docking studies and biological screenings revealed a high homogeneity for both binding pockets, except for the subpocket resulting in clear hot spot regions for hydrophobic substituents in para position of region R'' (Table 2). Due to less pronounced hot spots in LpMip, at best small hydrophobic substituents can be tolerated. Moreover, for an increased affinity toward BpML1, well-placed hydrogen bond donors are necessary to address carbonyl functions of Phe43 and Ala94. On the other hand, an increased affinity toward LpMip is even more pronounced because hydrogen bond donors can target the Phe65 and the Val114 as well as a suitable acceptor targets the NH of Gly116. Therefore, R' and R'' (Table 2) were selected as modification areas, and SARs were described for LpMip and BpML1. The exchange of the trimethoxyphenyl ring to

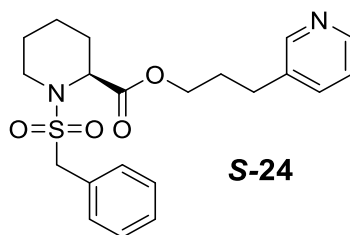
pyridine is desirable because of its nonspecific binding behavior to BpML1 as well as trimethoxyphenyl's high toxicity in macrophages and poor water solubility.<sup>69</sup>



**Figure 15.** Crystal structures of BpML1 bound to FK-506 (**3**, brown; PDB code 3UQB) and compound **22** (cyan; PDB code 4G50). The conformational change within the R92-I98 loop accommodates the terminal phenyl group of compound **22** (bottom), relative to the FK-506-bound structure (top). The R92 side chain is not modeled in the FK-506 structure (top) due to insufficient electron density.<sup>66</sup> Reproduced with permission from *Antimicrobial Agent and Chemotherapy*, Begley *et al.*, Volume 58, Issue 3, pp 1458–1467, Copyright 2014 American Society for Microbiology, DOI: 10.1128/aac.01875-13.<sup>66</sup>

An enantiospecific binding of compound **21** was observed for LpMip, as it was described by Holt *et al.* for FKBP's before.<sup>88</sup> In addition, previous docking studies showed an unfavorable distorted orientation of *R*-enantiomer in the binding pocket. As can be seen from Table 2 and expected from previous studies, compounds with an *S*-configuration always inhibit the PPIase more potently than the *R*-isomers. Thus, the next starting point of optimization was the new lead structure **S-24** (Figure 16). With regard to the modifications of the benzyl substitution (*R*'') especially compounds with a para halogen and nitro substitution show high levels of PPIase inhibition by a para-fluorine compound **S-25** for BpML1 ( $IC_{50}$  value of  $0.072 \pm 0.03 \mu\text{M}$ ) and para-chlorine **S-26** for LpMip ( $IC_{50}$  of  $2.4 \pm 0.1 \mu\text{M}$ ) compared to lead structure **S-24**. Meta substituted compounds, like meta-chlorine **S-30** or meta-nitro **S-31**, also inhibited well, whereas larger residues are not tolerated in

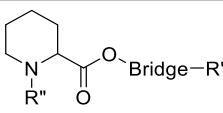
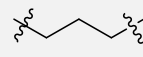
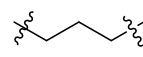
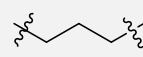
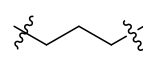
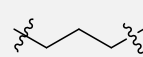
any position leading to significantly worse results. As a bridge between the pipercolic acid and the aromatic moiety, a second ester group **S-27**, an amide **S-28**, or an ether **S-29** was investigated. The diester inhibitors showed the highest activity, though the diester structure was prone to hydrolysis in buffer. Hence, it cannot be ruled out that the high inhibitory activity is due to active hydrolysis products. Replacement of the additional ester by an amide increases the stability but slightly decreases the activity.

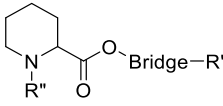
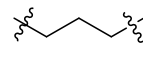
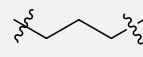
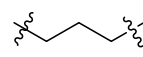
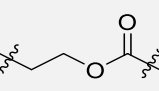
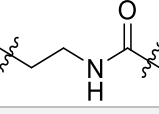
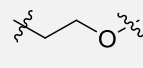


**Figure 16.** For BpML1 inhibition the new lead structure **S-24** could be identified and was a starting point for further optimization.<sup>69</sup>

Taken together, with the *S*-configuration of the carbon atom carrying the carboxylic group at the piperidine ring, a pyridine ring attached to an amide in the bridge section combines promising approaches in terms of activity, solubility, and stability for drug-like BpML1 inhibitors. The optimization of the benzyl area with para halogen substitution promotes affinity in BpML1 and LpMip.<sup>69</sup>

**Table 2.** Compounds derived from the primary lead structure **22** have spawned a new lead structure **S-24**.<sup>a</sup>

	R''	Bridge	R'	IC <sub>50</sub> value [μM] BpML1	IC <sub>50</sub> value [μM] LpMip
<b>21</b>	-SO <sub>2</sub> -CH <sub>2</sub> - C <sub>6</sub> H <sub>5</sub>		Trim	0.8 ± 0.1	9.0 ± 0.7
<b>S-21 = 22</b>	-SO <sub>2</sub> -CH <sub>2</sub> - C <sub>6</sub> H <sub>5</sub>		Trim	0.12 ± 0.09	6.0 ± 0.7
<b>R-21</b>	-SO <sub>2</sub> -CH <sub>2</sub> - C <sub>6</sub> H <sub>5</sub>		Trim	1.9 ± 0.3	12.8 ± 6.2
<b>S-24</b>	-SO <sub>2</sub> -CH <sub>2</sub> - C <sub>6</sub> H <sub>5</sub>		Pyr	0.69 ± 0.3	10.7 ± 1.8
<b>S-26</b>	-SO <sub>2</sub> -CH <sub>2</sub> - C <sub>6</sub> H <sub>5</sub> - <i>p</i> -Cl		Pyr	0.21 ± 0.08	2.4 ± 0.1

	R''	Bridge	R'	IC <sub>50</sub> value [μM] BpML1	IC <sub>50</sub> value [μM] LpMip
<b>S-30</b>	-SO <sub>2</sub> -CH <sub>2</sub> - C <sub>6</sub> H <sub>5</sub> - <i>m</i> -Cl		Pyr	0.23 ± 0.08	7.5 ± 1.0
<b>S-25</b>	-SO <sub>2</sub> -CH <sub>2</sub> - C <sub>6</sub> H <sub>5</sub> - <i>p</i> -F		Pyr	0.072 ± 0.03	5.7 ± 0.8
<b>S-31</b>	-SO <sub>2</sub> -CH <sub>2</sub> - C <sub>6</sub> H <sub>5</sub> - <i>m</i> - NO <sub>2</sub>		Pyr	0.48 ± 0.17	7.9 ± 1.2
<b>S-27</b>	-SO <sub>2</sub> -CH <sub>2</sub> - C <sub>6</sub> H <sub>5</sub>		Pyr	0.22 ± 0.08	2.6 ± 0.6
<b>S-28</b>	-SO <sub>2</sub> -CH <sub>2</sub> - C <sub>6</sub> H <sub>5</sub>		Pyr	0.42 ± 0.18	11.4 ± 1.7
<b>S-29</b>	-SO <sub>2</sub> -CH <sub>2</sub> - C <sub>6</sub> H <sub>5</sub>		Pyr	2.2 ± 0.4	7.7 ± 2.5

<sup>a</sup> Modifications were carried out in R'', R' and bridge section and IC<sub>50</sub> values determined for BpML1 and LpMip using the protease-coupled PPIase assay; with trim = trimethoxyphenyl and pyr = pyridine in region R'.

### Inhibition of *C. trachomatis*, *N. gonorrhoeae*, and *N. meningitidis* Mip Proteins

The Mip hit compound **21** (Figure 13) and a limited series of compounds having a meta- and para-nitro substitution at the benzylsulfonamide moiety were also screened against other Gram-negative pathogens to determine if these compounds had broad spectrum activity. The obtained IC<sub>50</sub> values from protease-coupled PPIase assay were compared to rapamycin (**4**).<sup>68</sup> The activity of *C. trachomatis* Mip protein (CtrMip) is inhibited by rapamycin (**4**) with an IC<sub>50</sub> value of 0.0079 ± 0.0006 μM.<sup>77</sup> The synthesized pipercoline acid derivatives were observed to be slightly less potent than rapamycin (**4**), with para-nitro compound **21P** showing 3.7-fold higher potency against CtrMip compared to the meta-nitro **21M** compound (Table 3). Interestingly, both the para-nitro (**21P**) and meta-nitro compound **21M** inhibitors were still highly effective when screened directly against the development cycle of *C. trachomatis* in HeLa cells. In brief, the lysates of infected cells containing chlamydial progeny were treated with inhibitor prior to infecting new cells. Next to no infectious progeny could be produced in the presence of rapamycin (**4**) or meta-nitro compound **21M** treated cells, whereas para-nitro **21P** reduced the infectivity levels by 50%.<sup>68</sup>

The neisserial Mip proteins NgMip and NmMip show 97% amino acid identity and leads to the

assumption of similar enzyme activity, hence NgMip recombinant protein was used as a representative of both species. Similar observations were made for NgMip in the PPIase assay as with CtrMip; however, the IC<sub>50</sub> values of the meta and para have a greater difference in potency (Table 3). Due to the different cellular habitats of *N. gonorrhoeae* and *N. meningitidis*, two survival assays were performed. In the presence of inhibitors the survival of *N. gonorrhoeae* was reduced in neutrophil granulocytes, with meta-nitro compound **21M** showing greater potency than para-nitro compound **21P**. The opposite was observed for survival of *N. meningitidis* in Detroit 562 pharyngeal epithelial cells, where the para-nitro compound **21P** demonstrated greater potency.<sup>68</sup> These results and previous observations made for LpMip<sup>89</sup> and BpML1<sup>43</sup> are strong indications that functions, other than the PPIase activity of Mips, are important for bacterial virulence and intracellular survival. In addition, NgMip-deletion mutants also responded to the inhibitors; thus, Mip-independent mechanisms may also be targeted by these inhibitors, and this needs to be investigated further.<sup>68</sup>

**Table 3.** IC<sub>50</sub> values of rapamycin and compounds **21M** and **21P** determined by the protease-coupled PPIase assay for CtrMip and NgMip.<sup>a</sup>

	IC <sub>50</sub> for CtrMip [μM]	IC <sub>50</sub> for NgMip [μM]
<b>Rapamycin (4)</b>	0.0079 ± 0.0006	0.0158 ± 0.0042
<i>meta</i> -NO <sub>2</sub> <b>21 (21M)</b>	0.241 ± 0.031	2.79 ± 0.78
<i>para</i> -NO <sub>2</sub> <b>21 (21P)</b>	0.0646 ± 0.011	0.0956 ± 0.022

<sup>a</sup> NgMip is a representative for both *Neisseria* species. Rapamycin (**4**) is still the most potent agent and **21P** seems to be superior to **21M** in this assay.

### Antibacterial Activity of Other Human FKBP Compounds

Beyond ligand-induced immunosuppression, human FKBP, like FKBP12, 12.6, 51 and 52, are involved in several physiological mechanisms.<sup>90, 91</sup> Many of them are of great therapeutic interest due to their role in calcium signaling, metabolic and psychiatric disorder, or chronic pain. In particular, S-C<sup>5</sup> substituted aza[4.3.1]bicyclic sulfonamides, which represent a group of promising human FKBP-inhibitors, were screened against pathogens such as *Candida albicans*, *Plasmodium falciparum*, *Chlamydia pneumonia*, *C. trachomatis*, and *L. pneumophila*. Compound **32**, a highly potent inhibitor of human FKBP12, FKBP51, and FKBP52, was the starting point for the analysis of the SAR and offers three regions for modifications (R<sup>1</sup>, R<sup>2</sup>, R<sup>3</sup>) (Figure 17).<sup>92</sup>



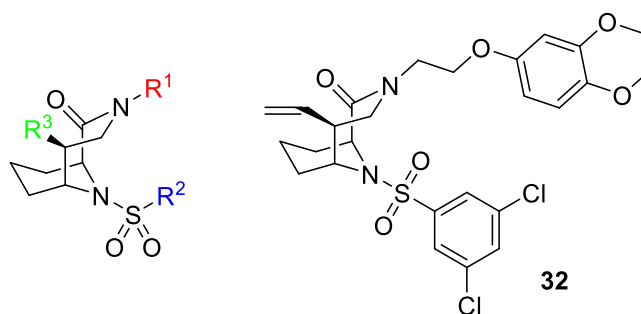


**Figure 17.** In a screening campaign potent human FKBP inhibitors were tested against several pathogens to find new hits for the respective microbial Mips. The common framework of this series of compounds offers three regions to modify ( $R^1$ ,  $R^2$ ,  $R^3$ ). Hit compound **32** for human FKBP inhibition was the starting point of microbial investigations.

The inhibitory activity decreased depending on the level of sequence homology to hFKBP12 in the following order: CaFKBP12 (*C. albicans*) > PffFKBP35 (*P. falciparum*) >> CpMip (*C. pneumonia*)  $\approx$  LpMip (*L. pneumophila*) > CtrMip (*C. trachomatis*). It was observed that almost all compounds inhibited hFKBPs far more efficiently than microbial Mip proteins, which diminishes the opportunity to develop selective Mip inhibitors without significant hFKBP inhibition. Nevertheless, Hausch *et al.* successfully synthesized specific microbial Mip inhibitors.<sup>92</sup> Initially, the second nitrogen of the bridged pipercolic acid moiety ( $R^1$ ) was widely substituted with alkyl ethers of different lengths, heterocycles, alkynes, nitriles, amines, short esters and others. Interestingly, the position of the ether is essential, and all other moieties do not influence the reduction of PPIase activity significantly. Removal of the ether group ( $R^1 = \text{H, Me, } -\text{CH}_2-\text{CH}$ ) marginally compromised the affinity but can be restored by introducing alternative hydrogen bond acceptors. Replacement of the 3-dimethoxy phenyl ether of **32** (Figure 17) with pyridine analogs (pyrazine, pyrimidine) is well tolerated because of similar hydrogen bond acceptor behavior, and therefore, a picolyl moiety was kept for further modifications in  $R^2$  and  $R^3$ . In contrast, phenyl or five-membered heterocycles instead of the pyridine led to lower Mip inhibition except for *Chlamydia* Mip, whose hit compound **33** contains a furanylmethyl moiety in  $R^1$  (Figure 18). Second, halogen substitutions in the meta position of the phenyl ring  $R^2$  increase the potency for Mip and FKBP-inhibition compared to unsubstituted analogs. Especially in the case of Mip, a nitrile moiety is advantageous. A pyrimidine ring enhanced affinity just for *C. albicans* Mip. Modifications in region  $R^3$ , e.g., a substitution of hydroxymethyl to methoxymethyl, have low influence on the affinity, but carbonyl groups decrease the affinity dramatically. Interestingly, all modification regions are independent of each other, apart from hydrogen bond acceptors in regions  $R^1$  and  $R^2$ , which might interact with the same hydrogen donor. Taking everything in

consideration, compound **34** combines many positive substructures for hFKBP and microbial Mips and can be regarded as a new lead structure. Modification of compound **34** led to the hit compound **35** for *P. falciparum* and *L. pneumophila*, which has high affinity even to multiresistant strains in the case of *P. falciparum* and shows a dose-dependent reduction of the proliferation of *L. pneumophila* in human THP-1-monocytes (Figure 18). For *C. trachomatis* the determined IC<sub>50</sub> value of compound **33** was even lower than the IC<sub>50</sub> of FK506 (**3**).<sup>92</sup>

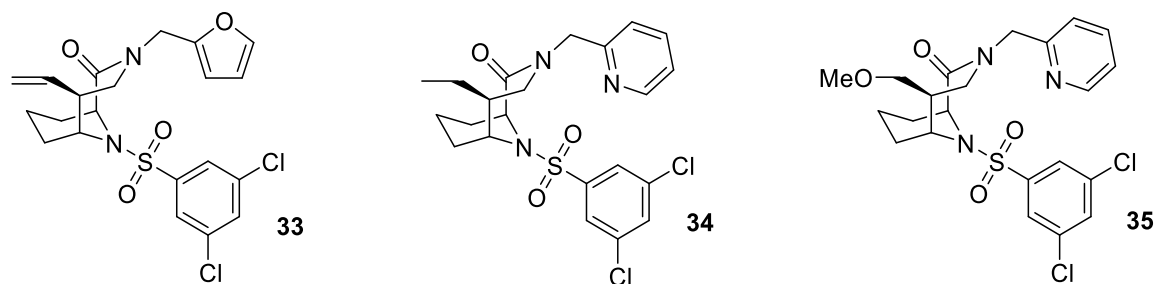


**Figure 18.** New hit compounds for microbial Mip inhibition were found by the screening of known human FKBP inhibitors. Compound **33** represents an exclusive inhibitor of the *Chlamydia* Mip protein, whereas compound **34** combines many advantageous structural elements for a broad spectrum of microbial Mip proteins and, with some modification, becomes a potent inhibitor of *Plasmodium* and *Legionella* Mip.

A multipronged approach to the design of inhibitors against the macrophage infectivity potentiator proteins has led to the development of compounds with relatively high levels of efficacy against these bacterial proteins. *In vitro* efficacy has been demonstrated for numerous generations of compounds across a multitude of bacterial species, many of which are antibiotic resistant. Moving forward, the broad-spectrum effects of these compounds would need to be demonstrated, as well as preclinical efficacy studies. The specificity of lead compounds to eukaryotic FKBP would also need to be investigated for any possible off target effects. To summarize, lead compounds demonstrating efficacy against multiple pathogenic bacteria have been successfully synthesized with exciting future prospects.

### 3.6 Cyclophilins in Bacteria

The first reports on the role of cyclophilins in *B. subtilis* and *E. coli* started in the early 1990s.<sup>93–95</sup> Since then, technology has drastically evolved and so has our understanding of the pleiotropic role of immunophilins within pathogenic bacteria. As previously mentioned, bacteria possess a maximum of two cyclophilins, unlike the human genome which encodes for 17 cyclophilin paralogues,<sup>96–97</sup> perhaps a reflection of the complexity of the organism and the number of PPIases required to function. In bacteria, cyclophilin A (PpiA) is located in the periplasm and outer

membrane in Gram-negative and Gram-positive bacteria, respectively. Also present is cyclophilin B (PpiB) which is located in the cytoplasm. Interestingly *PpiB* is present in all bacteria, unlike PpiA which has, in some instances, been completely lost, for example, in *Clostridioides difficile* and *B. subtilis*, indicating differences in the relative importance of *PpiB* and PpiA with the latter playing a less significant role.<sup>95, 98</sup> Gene deletion studies of either PpiA or *PpiB* in bacteria suggests pleiotropic functions of these cyclophilins in protein folding, stress response, motility, and virulence. As such, bacteria with gene deletions in either of these cyclophilins display an array of phenotypes ranging from indistinguishable to parental strains to complete attenuation in animal models clearly demonstrating the variable and, in some instances, essential roles of cyclophilins in the virulence of pathogenic bacterial species (summarized in Table 4).<sup>20</sup>

**Table 4.** Summary of the known functions of cyclophilins in bacteria.<sup>100</sup>

Bacterial Species	Gene	Size (kDa); Cellular Location <sup>1,2</sup>	Phenotype	Ref
<b>Gram-positive bacteria</b>				
<i>Bacillus subtilis</i>	<i>ppiB</i>	17.6; CM	- No phenotype under tested conditions - $\Delta$ <i>tig</i> $\Delta$ <i>ppiB</i> double mutant displayed decreased growth under minimal conditions	39, 94-95, 99
<i>Enterococcus faecalis</i>	<i>ef1534</i>	27.4; SX	- Decreased viability in saline - Grows better under oxidative stress and high levels of manganese - Increase sensitivity to ampicillin (52), but more resistant to DNA-associated antibiotics. - $\Delta$ <i>ef1534</i> attenuated in <i>Galleria mellonella</i> model - 2-log decrease in ability to colonize the kidney in a BALB/C mouse model	100-101
	<i>ef2898</i>	21.5; CM	- No phenotype under tested conditions	101
<i>Streptococcus mutans</i>	<i>ppiA</i>	28.6; SX	- More readily phagocytosed by differentiated THP-1 monocytes - Suppressed MARCO-dependent mediated phagocytosis	102
<i>Streptococcus pneumoniae</i>	<i>slrA</i>	29; SX	- Decreased ability to colonize the nasopharynx and airways of mice - Decreased ability to adhere to epithelial and endothelial cells	103

Bacterial Species	Gene	Size (kDa); Cellular Location <sup>1,2</sup>	Phenotype	Ref
<i>Streptococcus gordonii</i>	<i>ppiA</i>	29; SX	- 11-fold increase in phagocytic uptake in macrophages	104
<i>Staphylococcus aureus</i>	<i>ppiB</i>	21.6; CM	- Decreased nuclease activity and haemolysin activity - 14-fold decrease in bacterial number in BALB/C mice and decreased overall organ burdens - Decrease survival in RPMI2650 epithelial cells 48 hours post-infection - Reduced formation of $\alpha$ PSMs	105-107
<i>Clostridioides difficile</i>	<i>ppiB</i>	19; CM	- Decreased tolerance to cysteine - Increased toxin production leading to high levels of cytotoxicity of NIH-3T3 mouse fibroblast - Increased susceptibility to amoxicillin	98
<b>Gram-negative bacteria</b>				
<i>Burkholderia pseudomallei</i>	<i>ppiB</i>	17.9; CM	- Decrease intracellular counts in J774A.1 macrophages - Decreased MNGC formation - Increased susceptibility to oxidative stress and antibiotics - Decreased motility and biofilm - Avirulent in BALB/c mice - Proteomic imbalance	108
<i>Legionella pneumophila</i>	<i>Lcy</i>	18; CM	- Decreased growth at 16 degrees - Decreased intracellular survival in <i>Acanthamoeba castellanii</i> model of infection	50, 109-110
	<i>lpg1962</i>	20; PM	- No phenotype under tested conditions	50, 109
<i>Escherichia coli</i>	<i>rotA</i>	20.4; PM	- Increased biofilm (PPIase activity independent) - Increased swimming motility	111
	<i>ppiB</i>	18.2; CM	- Increased swarming and swimming motility - Increased biofilm production - Cellular filamentation	112-114
<i>Acinetobacter baylyi</i>	<i>rotA</i>	20; PM	- No phenotype under tested conditions	115
<i>Brucella abortus</i>	<i>BAB1_1118 (CypA)</i>	20.8; PM	- Decreased growth at 23 degrees and in the presence of environmental stresses	116

Bacterial Species	Gene	Size (kDa); Cellular Location <sup>1,2</sup>	Phenotype	Ref
	<i>BAB1_1117</i> ( <i>CypB</i> )	18.2; CM	- Unable to survive in HeLa epithelial - 10-fold decrease in bacterial load at 12 weeks post infection in a BALB/c mouse chronic model of infection	116

<sup>1</sup>Cellular location: CM, cytoplasm; PM, periplasm; SX, surface exposed.

<sup>2</sup>Protein size (kDa) and cellular location were ascertained from the associated references where possible; if not, UniProt, NCBI, and the algorithm PSORTb were used to determine kDa and cellular location.

### Role of Cyclophilins in Gram-Positive Bacteria

In Gram-positive bacteria, the commonly surface-exposed PpiA, also known as SlrA in the *Streptococcus* spp., have been shown to be important for internalization into mammalian cells. Both in *Streptococcus* mutans<sup>102</sup> and *Streptococcus gordonii*<sup>104</sup> slrA gene deletion mutants have increased internalization into phagocytic cells compared to wild-type; however, interestingly, no change in intracellular survival was observed. Using animal models of infection deletion of the PpiA homologues, slrA and Ef1534, in *Streptococcus pneumoniae* and *Enterococcus faecalis*, respectively, resulted in attenuation and increased animal survival demonstrating the importance of cyclophilin A in these species for virulence.<sup>101, 103</sup> Bhaduri *et al.* demonstrated that PpiA of *M. tuberculosis* was phylogenetically and structurally closer to human cyclophilin A rather than other prokaryotic cyclophilin A proteins.<sup>117</sup> Furthermore, *M. tuberculosis* PpiA contained a unique N terminal signal sequence “MADCDSVTNSP”, absent in nonpathogenic Mycobacterium species, and is vital for secretion of PpiA to interact with the host proteins. Further details of the interactome of secreted PpiA of Mycobacterium tuberculosis investigated using a bacterial two-hybrid system identified interactions with human lung proteins involved in iron storage, signal transduction, and immune response.<sup>117</sup> This is the first study that shows how pathogens have evolved to use their cyclophilins to their advantage, in this case to function as an effector mimic against the host cyclophilin A. Further studies like this are required to explore this interaction in detail and to understand how this ultimately impacts the virulence of certain pathogenic bacteria in host and animal infection models.

The cytoplasmic cyclophilins in Gram-positive bacteria have a more subtle effect on the cell. In *B. subtilis* deletion of the *ppiB* gene shows no discernible phenotype under any conditions tested.<sup>39, 94, 95, 99</sup> In contrast, deletion of the sole cyclophilin gene, *ppiB*, in *C. difficile* reduces cysteine tolerance and increases eukaryotic cell cytotoxicity associated with toxin production.<sup>98</sup> Reflecting the diverse roles of immunophilins, unlike in most studies to date, deletion of *ppiB* gene in *C. difficile* results in the strain causing increased toxicity in host cells rather than attenuation as observed in other pathogens, with further studies needed to establish if this is also the case in vivo. In *Staphylococcus aureus* *PpiB* is required for the efficient folding and secretion of secreted nuclease and hemolysin, both of which are important virulence factors for optimal infection. This was confirmed using the mouse infection model where the *S. aureus*Δ*ppiB* mutant was attenuated with decreased bacterial burdens in all studied organs.<sup>105–107</sup> These two pathogens indicate that cytoplasmic cyclophilins in Gram-positive bacteria play a role in either folding secreted virulence factors directly or regulating secretory pathways which pathogens utilize to invade host cells and cause disease; further research is required to determine the exact mechanisms behind this.

### Role of Cyclophilins in Gram-Negative Bacteria

In Gram-negative bacteria the periplasmic cyclophilins appear to play a lesser role in virulence compared to their cytoplasmic counterparts. In *S. aureus* and *Acinetobacter baylyi* deletion of their periplasmic cyclophilins, *Lpg1962* and *rotA*, respectively, resulted in no phenotype under the tested conditions.<sup>109, 115</sup> In *E. coli* deletion of the *ppiA* gene results in increased swimming motility and biofilm production; the latter was independent of its PPIase activity.<sup>111</sup> Meanwhile, in *Brucella abortus*, the causative agent of brucellosis, both cyclophilins CypA (*PpiA*) and CypB (*PpiB*) were essential for virulence with increased susceptibility to cellular stresses and decreased ability to cause chronic infection in hamsters shown. The reduction in virulence was restored when complementation studies were done with either cyclophilin indicating cyclophilins from *B. abortus* play a similar, interchangeable role.<sup>116</sup>

The cytoplasmic cyclophilin, *PpiB*, in *E. coli* is a negative modulator of biofilm production, swarming and swimming motilities with a *ppiB* gene deletion strain showing increased biofilm production and motility,<sup>114</sup> with modulation of swimming motility found to be independent of the PPIase activity of *PpiB*.<sup>112, 113</sup> *L. pneumophila* Lcy (*PpiB*) is important for tolerance to cold temperatures with the Δ*lcy* mutant strain displaying reduced growth at 16 °C. This mutant was

also attenuated in an *Acanthaeomba castellanii* model of infection.<sup>50, 109, 110</sup> Rasch *et al.* determined that Lcy and the FKBP, Mip, are able to partially compensate for the loss of the other protein, indicating that there is interplay between the different families of immunophilins within bacterial cells.<sup>50</sup>

One of the most exciting phenotypes seen was in the cytoplasmic cyclophilin B mutant in *B. pseudomallei*, *BpsΔppiB*, which was interestingly avirulent in the mouse model of infection. On closer examination, *PpiB* is critical for replication in macrophages and the formation of multinucleated giant cells, which is the main mechanism by which *B. pseudomallei* successfully spreads intracellularly. These results strongly suggest that the *ppiB* gene is essential for *B. pseudomallei* to cause disease in mice. To identify which pathways had been disrupted in *BpsΔppiB*, proteomic analysis was conducted and demonstrated proteome-wide disruptions of multiple virulence pathways including type 6 secretion systems, important for *B. pseudomallei* virulence.<sup>108</sup> Cyclophilins play a pleiotropic role in bacteria which is apparent with the vast array of phenotypes displayed in gene deletion studies. Instances of opposing phenotypes such as between *E. coli PpiB* and *B. pseudomallei PpiB*, where biofilm production and motility have an opposite effect upon deletion of *PpiB*, demonstrate that our knowledge of the function of cyclophilins in bacteria remains in its infancy. What is abundantly clear is that, although not always essential, cyclophilins maintain a balance within a cell and their loss leads to pathogenic bacteria being unable to cause infection to the same degree as wild-type strains.

### 3.7 Potential To Develop Inhibitors of Bacterial Cyclophilins

Targeting cyclophilins in bacteria has not been thoroughly investigated, probably due to the lack of information on the essentiality of these proteins and therefore their potential as therapeutic targets. A large amount of studies have been conducted to target human cyclophilin A as a novel antiviral. This work will be discussed here to stimulate research into adapting some of this technology for novel antibacterial studies. As shown with *PpiB* from *B. pseudomallei*, targeting this cyclophilin would be successful in disabling the bacterium from causing serious infection, a key strategy in our fight against multidrug resistant bacteria.

#### Overview of Human-Based Cyclophilin A Inhibitors for HCV/HBV Infections

The peptidic macrocycle cyclosporin A (CsA (5), Table 5), first isolated from broths of the insect-pathogenic fungus *Tolypocladium inflatum*,<sup>118</sup> binds strongly to cyclophilins.<sup>8, 80</sup> CsA (5) has non-

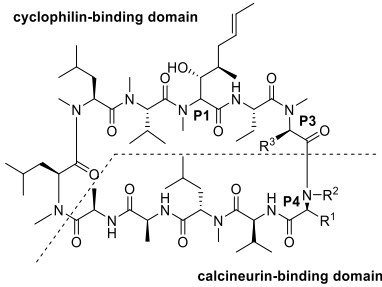
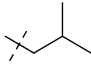
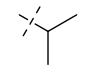
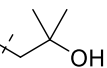
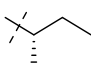
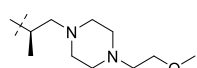
cytotoxic immunosuppressant activity *in vivo*, by reversibly inhibiting cytokine secretion from stimulated T-cells.<sup>119</sup> CsA (**5**) achieves this by simultaneously binding to the active site of cyclophilin A (hCypA) and interacting with the protein calcineurin, inhibiting its phosphatase activity.<sup>120</sup> However, dividing CsA (**5**) into separate cyclophilin and calcineurin binding domains is not entirely accurate (Table 5).<sup>121</sup> The large macrocycle is very flexible and bulky and even substitution at the P1-position can lead to decreased calcineurin binding, as this group extends from the cyclophilin binding interface to a region very near the calcineurin-binding region.<sup>122, 123</sup> Moreover, substitution at the P4-position can have an impact on cyclophilin binding.<sup>124</sup> So far, CsA (**5**) is the only approved drug that inhibits cyclophilins, but its immunosuppressive activity limits its clinical uses to transplantation and autoimmune diseases.<sup>125</sup> However, new natural cyclic peptides like NIM811 (**36**) have been discovered, which strongly inhibit hCypA but lack the ability to bind calcineurin, thereby lacking immunosuppressive properties (Table 5). Further studies with peptides such as NIM811 (**36**) have demonstrated that human cyclophilins are involved in diseases such as asthma, cancer, and even viral infections.<sup>126–128</sup>

Certain viruses rely heavily on host cyclophilins, as their genome does not encode all of the necessary proteins essential for their survival and replication in host cells.<sup>123</sup> Several cyclophilins are known to contribute to the life cycle of hepatitis C virus (HCV) with strong evidence that hCypA interacts with the viral NS5A protein to stimulate viral RNA replication.<sup>129</sup> In contrast to most direct-acting antiviral (DAA) drugs, significant resistance to cyclophilin inhibitors, so-called host-targeting antivirals (HTA), is rarely observed and cyclophilin inhibitors are effective across all HCV genotypes.<sup>129, 130</sup> For human immunodeficiency virus (HIV) and HCV, participation of cyclophilins in viral amplification has been well documented and the effectiveness of compound treatment in clinical trials has been proven.<sup>123</sup> Unfortunately for HIV, there are naturally occurring coat protein mutants that are resistant to treatment with cyclophilin inhibitors, restricting their use against HIV.<sup>131</sup> Lack of these natural coat proteins in HCV means that cyclophilin inhibitors are a very promising treatment option. Three compounds that have been studied in clinical trials, NIM811 (**36**), alisporivir (**37**), and SCY-635 (**38**), with each showing good therapeutic efficacy (Table 5).<sup>132, 133</sup> However, all cyclophilin inhibiting drug candidates faced obstacles that stopped their development.<sup>125</sup> The first nonimmunosuppressive cyclophilin inhibitor to enter clinical trials, alisporivir (**37**), was associated with hyperbilirubinemia, an increase in circulating levels of



conjugated and unconjugated bilirubin, in a subset of patients which was attributed to inhibition of transporters.<sup>134</sup> CsA (**5**), alisporivir (**37**), NIM811 (**36**), and the other early cyclosporin analogs are potent inhibitors of important endogenous biological transporters such as organic anion transporting polypeptide OATP1B1, multidrug-resistance-associated protein MRP2, and multidrug resistance protein MDR1.<sup>124, 132, 133</sup> Inhibition of these transporters can cause drug–drug interactions and interfere with the normal excretion of biomolecules,<sup>124</sup> which is critical, because addition of cyclophilin inhibitors such as alisporivir (**37**) or NIM811 (**36**) to pegylated IFN- $\alpha$  (PegIFN- $\alpha$ ) and ribavirin (RBV) can improve their efficacy in HCV therapy significantly.<sup>132, 134</sup> Sweeney *et al.* from Novartis have tried to address the transporter liability associated with alisporivir (**37**) and developed NIM258 (**39**, Table 5).<sup>124, 135</sup> The Novartis group showed that a methyl group at the P3 position improves Cyp binding affinity.<sup>135</sup> Moreover, a  $\beta$ -branched side chain at the P4 position also enhances Cyp binding affinity and decreases calcineurin interaction. More importantly, P4 substitution with hydrophilic, amine-containing analogs decreases transporter interactions and improves pharmaceutical properties.<sup>135</sup> Compared to alisporivir (**37**), NIM258 (**39**) has a better  $K_D = 1.2$  nM to hCypA (CsA (**5**),  $K_D = 2.2$  nM), a slightly better inhibition of replication of a subgenomic HCV replicon ( $EC_{50} = 40$   $\mu$ M, compared to CsA (**5**),  $EC_{50} = 46$  nM), and a decreased inhibition of OATP1B1 transporter activity ( $K_i = 6.1$   $\mu$ M, compared to CsA (**5**),  $K_i = 0.8$   $\mu$ M).<sup>124</sup> All in all, new cyclosporins have promising pharmacokinetic profiles in preclinical species, are not immunosuppressive *in vitro*, and have good potency in cellular antiviral assays.<sup>124</sup>

**Table 5.** Structures of cyclosporin A (CsA, **5**) and its nonimmunosuppressive analogs Alisporivir (**37**), SCY-635 (**38**), NIM811 (**36**), and NIM258 (**39**)

Cyclosporin core structure	Compound	R <sup>1</sup>	R <sup>2</sup>	R <sup>3</sup>
	CsA ( <b>5</b> )		CH <sub>3</sub>	H
	Alisporivir ( <b>37</b> )		CH <sub>2</sub> CH <sub>3</sub>	CH <sub>3</sub>
	SCY-635 ( <b>38</b> )		CH <sub>3</sub>	SCH <sub>2</sub> CH <sub>2</sub> N(CH <sub>3</sub> ) <sub>2</sub>
	NIM811 ( <b>36</b> )		CH <sub>3</sub>	H
	NIM258 ( <b>39</b> )		CH <sub>3</sub>	CH <sub>3</sub>

## Sanglifehrins

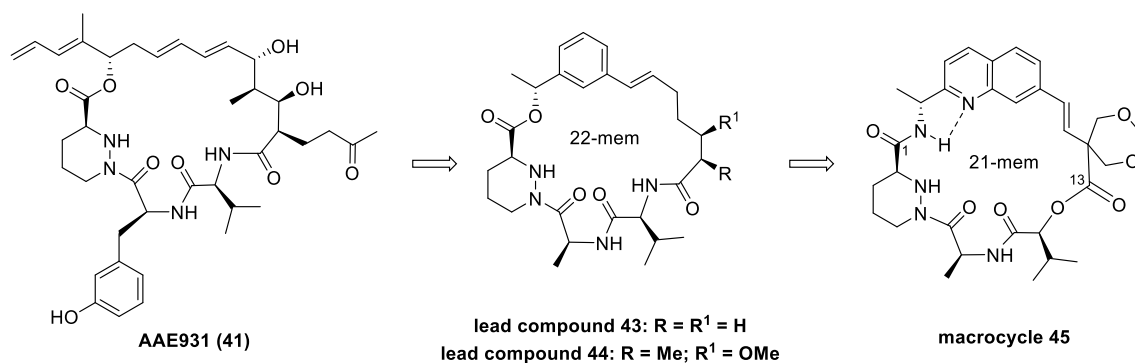
The sanglifehrins are another class of immunosuppressive macrocyclic natural products that bind to cyclophilins.<sup>123, 136</sup> Like the cyclosporins, sanglifehrin A (SfA, **40**, Table 6), the most abundant member of this class of molecules, binds to hCypA about 60 times stronger than CsA (**5**).<sup>123</sup> SfA (**40**) binds in the active site of cyclophilin A,<sup>137</sup> but immunosuppressive activity is not caused by calcineurin binding (Table 6).<sup>138</sup> Additionally, there is no inhibition of mTOR or of the purine/pyrimidine de novo synthesis.<sup>139</sup> The mechanism of immunosuppression seems to be connected to dendritic cell (DC) chemokine and migration inhibition but remains to be fully elucidated.<sup>123, 138</sup> Degradation studies on SfA (**40**) revealed that removal of the C24 polyketide side chain (corresponding to R<sup>1</sup> in Table 6) eliminated the immunosuppressive properties of the molecule while maintaining the nanomolar binding affinity to hCypA, -B, and -C.<sup>128, 136, 140</sup> One of these nonimmunosuppressive sanglifehrins, AAE931 (**41**, Table 6), showed potent anti-HCV activity in the replicon assay (IC<sub>50</sub> = 130 nM).<sup>140</sup>

Investigation of the X-ray crystal structure of a nonimmunosuppressive analog of AAE931 (**41**) complexed with hCypA revealed that the unique piperazic acid functionality occupies the same hydrophobic pocket as the Val11 of CsA (**5**), while some additional important hydrophobic interactions are maintained between hCypA and the valine group of the sanglifehrin analog.<sup>136</sup> Thus, this part of the ligand is also known as the recognition domain (Table 6).<sup>136</sup> The C13–C26 fragment, also known as the spacer domain, extends on the surface of the complex and plays a critical role in maintaining the molecule in the optimal three-dimensional conformation.<sup>136</sup> Researchers at Biotica converted the C26–C27 oxidative cleavage intermediate to the corresponding amides, which led to a series of compounds, termed sangamides, with potent antiviral activity.<sup>141, 142</sup> The sangamide NVP018 (**42**) is more potent against anti-HCV and anti-HIV cellular assays than alisporivir (**37**) and more importantly is only a weak inhibitor of OATP1B1 and OATP1B3. Unfortunately, NVP018 (**42**) seems to be still poorly orally bioavailable in mouse pharmacokinetic experiments.<sup>123</sup>

**Table 6.** Structures of Sangliferhin A (SfA, **40**) and the nonimmunosuppressive Sangliferhin analogs AAE931 (**41**) and NVP018 (**42**)

Sangliferhin core structure	Compound	R <sup>1</sup>	R <sup>2</sup>
<p>spacer domain</p> <p>cyclophilin binding, recognition domain</p>	Sangliferhin A (SfA, <b>40</b> )		H
	AAE931 ( <b>41</b> )		H
	NVP018 ( <b>42</b> )		F

In an earlier publication Mackman *et al.* described two initial leads **43** and **44** (Figure 19) derived from the sangliferhin A analog AAE931 (**41**), with potent hCypA inhibition and modest anti-HCV activity but poor pharmacokinetics.<sup>128</sup> In a more recent article, Mackman *et al.* reported the structure-guided optimization of the sangliferhin **44** to the highly orally bioavailable macrocycle **45**, which was performed in three steps.<sup>130</sup> First, the styrene moiety was replaced by isoquinoline and the size of the macrocycle was reduced to a 21-membered ring. These modifications improved binding affinity and anti-HCV replicon potency while lowering human plasma protein binding. In a second step, the C1 lactone and C13 lactam groups were switched and isoquinoline was changed to quinoline, which introduced an intramolecular hydrogen bond (Figure 19), resulting in significantly improved membrane permeability leading to high oral absorption. In a final step, modification of the C14 substituents to a spiro-1,3-dioxane lowered log *D*, reduced oxidative metabolism, and reduced pregnane X receptor (PXR) related drug–drug interactions.


**Figure 19.** Sangliferhin **41** derived Cyp A inhibiting macrocycles **43** and **44** were turned to the highly orally bioavailable macrocycle **45** by structure guided optimization by Mackman *et al.*<sup>130</sup>

This macrocycle **45** demonstrates potent CypA inhibition ( $K_D = 5$  nM), potent anti-HCV 2a activity ( $EC_{50} = 98$  nM), and high oral bioavailability in rats (100%) and dogs (55%).<sup>130</sup>

### *Small Molecule Cyclophilin Inhibitors.*

The existing macrocyclic inhibitors, derived from CsA (**5**) or Sfa (**40**), have disadvantages, which are related to their size, such as a high synthetic effort, poor cell permeability, and drug–drug interactions because of transporter inhibition.<sup>143</sup> Recent studies revealed that large, hydrophobic peptides are often OATP inhibitors.<sup>144</sup> To overcome these disadvantages, Guichou *et al.* focused on developing small molecule inhibitors.<sup>145–147</sup> Using a fragment-based drug design (FBDD) approach, in which over 34409 fragments were screened to fit into the CypD binding pocket, they identified two lead fragments in the initial step.<sup>147</sup> Superimposition of those fragments with the known structures of CsA (**5**) and Sfa (**40**) suggested that a urea moiety could be used as a linker between the two fragments because of one hydrogen bond with Gln63 and two with Asn102.<sup>143</sup> Further structure-based compound optimization included the introduction of a thiomethyl group, which increased binding affinity by establishing a transient contact with Arg55 Nε. Addition of a phenyl ring adjacent to the urea group and the carbonyl function stabilized the bioactive conformation by a  $\pi$ - $\pi$ -interaction between the two phenyl moieties and a 3-fold gain of anti-PPIase activity was achieved, resulting in hit compound **46** (Figure 20).<sup>143</sup> Overall, Guichou *et al.* was able to generate a new family of nonpeptidic, small-molecule cyclophilin inhibitors, unrelated to CsA (**5**) or Sfa (**40**), which potently inhibit hCypA, CypB, and CypD.<sup>143</sup> These small molecules have a potent PPIase inhibitory activity, antiviral activity against HCV, HIV, and coronaviruses *in vitro*, and druggable properties.<sup>143</sup>

Ni *et al.* also discovered potent small molecule hCypA inhibitors by using a *de novo* drug design approach.<sup>148</sup> Starting with a lead compound containing an acylurea motif ( $IC_{50} = 31.6 \pm 2.0$  nM, hCypA PPIase), further SAR studies resulted in nanomolar level hCypA inhibitors like compound **47** with a fluorene site and an ortho bisubstituted phenyl ring, connected with an acylurea-linker (Figure 20). Unfortunately, their compounds were only poorly soluble and gave variable results in the PPIase assays.<sup>145</sup> Furthermore, no crystallographic structure of the compounds complexed with cyclophilins could be obtained.<sup>143</sup> Shore *et al.* made use of the compounds of Guichou *et al.* as a starting point for further lead optimization targeting hCypD. They established that the *R*-stereoisomer at the proline ring is the preferred form for binding to hCypD (Figure 20).<sup>145</sup>

Substitutions between the urea and the carbonyl moiety seemed to mimic the (4*R*)-4-[(*E*)-2-butenyl]-4-methyl-L-threonine (Bmt) group of CsA (**5**), with an *S*-methionine showing the best affinity. By means of lead optimization, Shore *et al.* obtained a cyclophilin inhibitor **48** (Figure 20) with  $K_i = 99$  nM against hCypD, compared to CsA (**5**) with  $K_i = 8.2$  nM.<sup>145</sup> Up to now, all reported cyclophilin inhibitors are potent inhibitors of at least human cyclophilins A, B, and D.<sup>123</sup> Selective, small molecule inhibitors of cyclophilins would be an interesting tool for further studying cyclophilin biology.

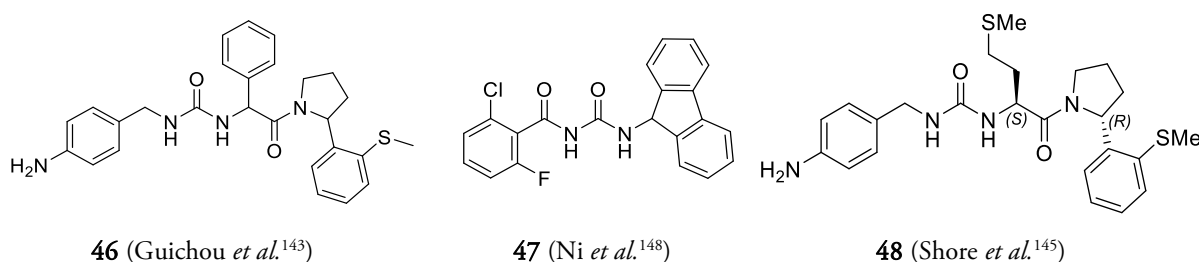


**Figure 20.** Structures of small molecule cyclophilin inhibitors **46**, **47**, and **48**.

### *Targeting Bacterial Cyclophilins.*

Development of inhibitors against bacterial cyclophilins would require a concerted effort. First, a screen of compounds that have been developed against human cyclophilins could be conducted to identify any lead structures. It is well-known that the bacterial cyclophilin *E. coli* RotA has a 500-fold greater resistance to CsA binding compared to hCypA which is attributed to the change of a highly conserved tryptophan residue in the enzyme active site to a phenylalanine.<sup>93</sup> The tryptophan residue is highly conserved in eukaryotic cyclophilins, and interestingly this tryptophan to phenylalanine change is widely distributed in bacterial cyclophilin sequences, a change that could be exploited to create compounds with increased efficacy and specificity to bacterial cyclophilins. Additionally, a fragment-based drug design (FBDD) approach could be adopted to develop compounds with bacterial cyclophilin inhibition in order to determine the best scaffold upon which to elaborate. Ideally a compound that can specifically bind to bacterial cyclophilins while having low affinity to hCyp's should be developed, but the use of cyclophilin inhibitors as HTA's indicates that low binding affinity to human cyclophilins could be tolerable to the human body upon administration.

### 3.8 Parvulins

Parvulins were formally identified in 1994 by Rahfeld *et al.*<sup>149</sup> and represent the most recent addition to the immunophilin superfamily, although it must be acknowledged that various parvulins had been studied by earlier groups but not based on their PPIase activity. Parvulins have been well researched in relation to their chaperone ability, with the role of individual parvulins difficult to determine at times due to many studies looking at genetic mutation strains containing multiple gene deletions, making it unclear as to the exact role of the parvulin protein.<sup>150, 151</sup> However, numerous studies have also investigated the role of individual parvulins in bacterial virulence, and these will be discussed here (Table 7).

**Table 7.** Summary of the known functions of parvulins in bacteria.

Bacterial Species	Gene	Size (kDa); Cellular Location <sup>1,2</sup>	Phenotype	Ref
<b>Gram-positive</b>				
<i>Staphylococcus aureus</i>	<i>prsA</i>	35.6; SX	<ul style="list-style-type: none"> <li>- Decreased secreted protease and phospholipase activity</li> <li>- Increased bacterial auto-aggregation</li> <li>- Increased adhesion rate to A549 epithelial cells</li> <li>- Increased susceptibility to cephalosporins</li> <li>- Increased susceptibility to oxacillin (49)</li> <li>- Decrease in PBP2A in the membrane fraction</li> </ul>	105, 107, 152-154
<i>Bacillus subtilis</i>	<i>prsA</i>	33; SX	<ul style="list-style-type: none"> <li>- Indispensable for viability in a high-level protein secreting strains of <i>B. subtilis</i>, and following protein depletion</li> <li>- Decreased mature <math>\alpha</math>-amylase, indicating a role, in post-translocation folding</li> <li>- Over-expression leads to over-secretion of exoproteins</li> <li>- Depleted proteins become filamentous prior to cell lysis</li> <li>- Required for folding of PBPs which allow for lateral cell wall growth</li> </ul>	155-161
<i>Enterococcus faecalis</i>	<i>ef0685</i>	37.4; SX	<ul style="list-style-type: none"> <li>- Increased sensitivity to osmotic stress</li> <li>- Increased susceptibility to ampicillin (52)</li> <li>- Attenuated in a <i>G. mallowella</i> model</li> <li>- Decreased cell cytotoxicity in Caco-2/T7 cells</li> </ul>	101

Bacterial Species	Gene	Size (kDa); Cellular Location <sup>1,2</sup>	Phenotype	Ref
<i>Listeria monocytogenes</i>	<i>prsA2</i>	32.7; SX	- Decreased bacterial burden in Swiss mice - Decreased invasion of J774A.1 macrophages - Reduced plaque size in L2 fibroblasts - Increased sensitivity to Penicillin G (53)	162-164
	<i>prsA1</i>	32.6; SX	- No phenotype under the tested conditions	162-163
<i>Streptococcus pneumoniae</i>	<i>ppmA</i>	34.4; SX	- Decreased colonising capacity in CD-1 mice - Increased uptake in human PMNs and J774A.1 macrophages	165
<b>Gram-negative</b>				
<i>Escherichia coli</i>	<i>ppiD</i>	69; IM	- Located at the periplasmic interface of the SecYEG translocon. - Induced under heat shock conditions (50°C), under transcriptional regulation of Cpx-R-Cps-A and $\sigma^{32}$ - Increased susceptibility to hydrophobic antibiotics and detergents - Differences in levels of OMPs.	30
	<i>surA</i>	47.3; PM	- Stark differences in OMPs - Longer doubling time at 30°C (60 min vs 45 min) - Increased susceptibility to Novobiocin (54) and detergents - UPEC strain UTI89 showed increased susceptibility to Novobiocin (54), decreased haemagglutination of guinea pig erythrocytes, decreased binding and invasion of 5637 human bladder epithelial cells. Decreased maturation of pilus usher, FimD at the outer membrane. Decreased piliation. - Decreased survival during stationary phase of growth	30, 56, 166-168
<i>Salmonella enterica</i> serovar Typhimurium	<i>surA</i>	47.3; PM	- Decreased adhesion and invasion of Hep-2 cells - 5 and 3.5-log increase in LD <sub>50</sub> orally and intravenously respectively in BALB/c mice - Decreased bacterial burden in all organs studied	169
<i>Shigella flexneri</i>	<i>surA</i>	47.3; PM	- Decreased plaque formation in Henle cells - Increased levels of IcsA on the surface	170
<i>Bordetella pertussis</i>	BP3561/ <i>par</i> 27	27; PM	- Slightly decreased growth rate	171
<i>Yersinia pseudotuberculosis</i>	<i>surA</i>	47.7; PM	- Irregular bacterial surface, leaky membranes - Decreased LPS assembly	172-173

Bacterial Species	Gene	Size (kDa); Cellular Location <sup>1,2</sup>	Phenotype	Ref
			- Increased susceptibility to vancomycin (51), bacitracin (55), bile salts and detergents - Avirulent in a BALB/c animal model (2-log decrease in ID <sub>50</sub> ) - 40-fold decrease adhesion to HeLa cells	
	<i>ppiD</i>	69.9; IM	- No discernible phenotype under tested conditions	173

<sup>1</sup>Cellular location: PM, periplasm; IM, inner membrane; SX, surface-exposed.

<sup>2</sup>Protein size (kDa) and cellular location were ascertained from the associated references where possible; if not, UnitProt, NCBI, and the algorithm PSORTb were used to determine kDa and cellular location.

### *Parvulins in Gram-Positive Bacteria*

*B. subtilis* utilizes the parvulin, PrsA, to fold post-translocated exoproteins into their correct formation,<sup>156–158, 161</sup> with deletion of the gene leading to decreased secretion of mature  $\alpha$ -amylase and the protease subtilisin.<sup>156</sup> *B. subtilis* PrsA mutants also display a decrease in secreted proteins as well as changes with cellular morphology resulting in filament formation prior to cell lysis.<sup>158, 160</sup> These results indicate that PrsA plays a pivotal role in controlling the folding and secretion of essential proteins in *B. subtilis*. This phenotype was found to be the result of PrsA folding penicillin binding proteins (PBPs) which in *B. subtilis* are responsible for lateral cell wall growth as a cell divides.<sup>155</sup> This lethality is independent of PPIase activity with complementation of enzymatically inactive PrsA capable of rescuing cell death.<sup>159</sup> Similarly in *S. aureus* a PrsA mutant was found to have decreased secreted protease and phospholipase activity.<sup>105, 107</sup> It also displayed an increased rate of autoaggregation and more readily adhered to A549 epithelial cells. Reports on attenuation of virulence are conflicting with Keogh *et al.*<sup>105</sup> seeing no attenuation in virulence in an abscess and systematic model of infection, while Lin *et al.* reported a substantial decrease in animal mortality in an intravenous model of infection with a *S. aureus prsA* mutant.<sup>154</sup> Additionally an increased susceptibility to cephalosporin antibiotics as well as oxacillin (49) and the glycopeptides teicoplanin (50) and vancomycin (51) was observed in the *S. aureus prsA* mutant (Figure 21).<sup>152, 153</sup> Membrane-bound levels of PBP2A were also significantly decreased,<sup>152</sup> explaining the increase in susceptibility and indicating that PrsA is involved in the folding of PBPs in *S. aureus* as well as in *B. subtilis*. Furthermore, in *S. aureus* PrsA expression is transcriptionally controlled by VraRS two-component system in response to cell-wall stress.<sup>153</sup>



In *S. pneumoniae* the parvulin PpmA, putative proteinase maturation protein A, is a surface associated lipoprotein important for pneumococcal colonization of the murine nasopharynx in CD-1 mice. The mutant was also more readily taken up by both human polymorphonuclear (PMNs) and murine macrophage cells, suggesting a role in immune evasion.<sup>165</sup> Sharing homology to *S. pneumoniae* PpmA is the protein Ef0685 from *E. faecalis* and is the only parvulin encoded by this bacteria.<sup>101</sup> Deletion of the *ef0685* gene in *E. faecalis* results in increased susceptibility to osmotic stress, with this susceptibility heightened when double mutations in both *ef0685* and the cyclophilin encoding gene *ef1534* were made. This double mutant was also more susceptible to ampicillin (**52**, Figure 21) and interestingly more resistant to quinolone-derived antibiotics.<sup>101</sup> In a *Galleria mellonella* model of infection, the *E. faecalis ef0685* gene deletion mutant was highly attenuated, with 90% larvae survival compared to ~15% of those infected with a wild-type strain surviving. Infection of Caco-2/T7 epithelial cells resulted in low levels of cell cytotoxicity indicating that the parvulin Ef0685 in *E. faecalis* is involved in cellular cytotoxicity.<sup>101</sup> Ef0685 was also found to be a protective antigen against *E. faecalis* infections in mice, indicating it is either secreted or present on the outer membrane and is potentially a vaccine candidate.<sup>174</sup>

*Listeria monocytogenes* encodes for two PrsA homologues, PrsA1 and PrsA2. Deletion of the *prsA2* gene in *L. monocytogenes* results in decreased invasion of murine macrophages, an 80% reduction in plaque size in L2 fibroblast cells, and decreased levels in secreted factors listeriolysin O (LLO) and a broad-specificity phospholipase (PC-PLC) both of which are important for virulence in *L. monocytogenes*. The *prsA2* gene is also important for establishing an infection *in vivo* with the mutant strain demonstrating a 5- and 6-log decrease in bacterial burden seen in the liver and spleens, respectively, of Swiss mice using an intravenous model of infection.<sup>163</sup> An increase in sensitivity to penicillin G (**53**) (Figure 21) was also observed in the PrsA2 mutant, indicating that PrsA2 was involved in PBP folding, as shown with several other parvulin proteins.<sup>164</sup> Interestingly, PrsA1 does not play a role in the virulence of *L. monocytogenes*.<sup>162-164</sup>

These studies demonstrate the importance of parvulins in the virulence of a number of pathogenic Gram-positive bacteria. As discussed, multiple bacteria use PrsA to fold PBPs during bacterial cell division, resulting in abhorrent cell shape and an increase in susceptibility to cell-wall attacking antibiotics.

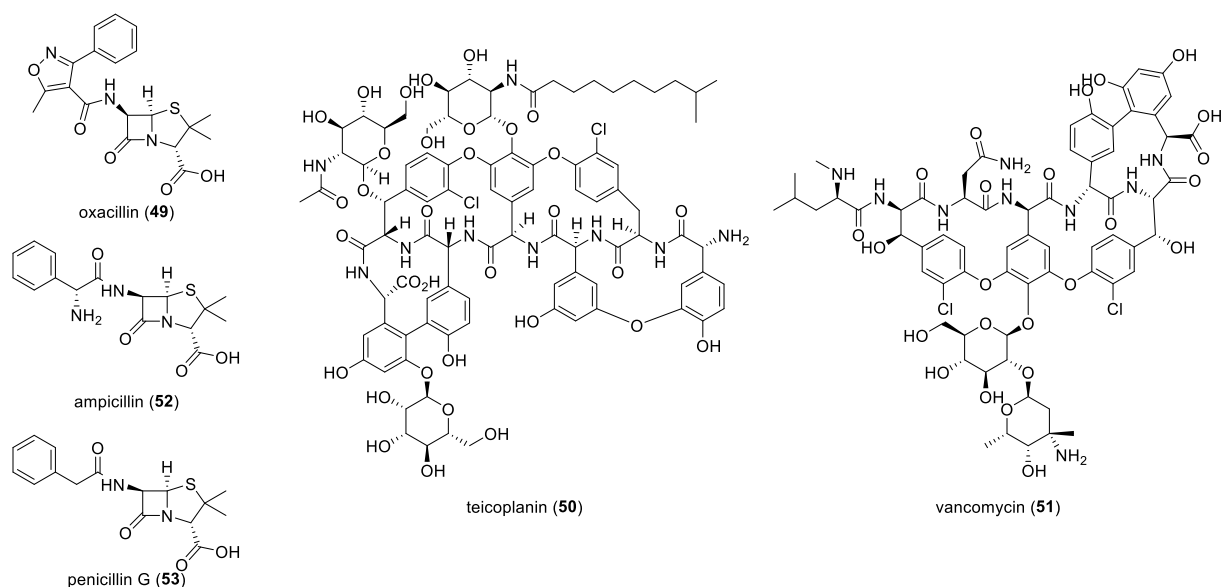


**Figure 21.** Structures of the antibiotics oxacillin (49) and the glycopeptides teicoplanin (50) and vancomycin (51) to which an increased susceptibility was observed in the *S. aureus prsA* mutant.<sup>152–153</sup> The antibiotic ampicillin (52) was also found to have an increased efficacy against *E. faecalis*  $\Delta$ ef0685 $\Delta$ ef1534.<sup>101</sup> The antibiotic, penicillin G (53), displayed increased efficacy in the PrsA2 mutant, indicating that PrsA2 was involved in PBP folding, thus mediating penicillin G resistance.<sup>164</sup>

### *Parvulins in Gram-Negative Bacteria*

*E. coli* is perhaps the most studied organism in the field of parvulin research, probably due to the ease of handling, manipulation, and availability of molecular tools and libraries such as the easily accessible Keio library.<sup>175</sup> Mutations in the *E. coli* parvulin gene *surA* have a slightly increased doubling time of 60 min at 30 °C (vs 45 min) and are also highly susceptible to novobiocin (54, Figure 22) and detergents, indicating membrane instability and a change in the composition of outer membrane proteins (OMP).<sup>30, 56</sup> Increased susceptibility to novobiocin (54) was also seen in a SurA mutant constructed in a uropathogenic strain of *E. coli*, UTI89. This pathogenic strain of *E. coli* also displayed a decrease in hemeagglutination of guinea pig erythrocytes as well as a reduction in binding and invasive ability against 5637 human bladder epithelial cells.<sup>168</sup> A quad mutant of *E. coli* with deletions in periplasmic cyclophilin, FKBP, and parvulins (*ppiA*, *fkpA*, *ppiD*, *surA*) displayed a diminished growth defect in media.<sup>166</sup> Compared to the *E. coli surA* mutant, the quad mutant strain had enhanced susceptibility to novobiocin (54), bacitracin (55, Figure 22), and vancomycin (51), indicating that there is a degree of overlap between the functions of all the periplasmic immunophilins.<sup>166</sup> SurA is also important for piliation in *E. coli* with electron microscopy showing that strains lacking SurA were much less piliated and there was a decrease in the outer membrane usher protein, FimD, expression.<sup>166</sup> Loss of SurA results in altered levels of

outer-membrane proteins with the  $\sigma^E$  factor cell envelope stress response being strongly induced.<sup>176, 177</sup> PpiD was identified as a parvulin in *E. coli* that has structural similarities to that of SurA. It is induced during heat shock and localizes to the periplasmic interface of the inner membrane, where it is anchored with a single transmembrane  $\alpha$ -helix.<sup>30</sup> Deletion of the *ppiD* gene in *E. coli* results in increased susceptibility to hydrophobic antibiotics such as novobiocin (**54**), as well as to detergents indicating that there was a loss of membrane integrity in the mutant strain. Interestingly, a double mutant strain of *ppiD* and *surA* could not be created, with the loss of both parvulins reportedly leading to synthetic lethality.<sup>30</sup> However a few years later, Justice *et al.* successfully constructed a double deletion mutant in the same MC4100 *E. coli* strain.<sup>166</sup> Membrane preparations show that in both the *ppiD*- and *surA*-mutant strains there is a change in outer membrane proteins (OMPs), indicating that both of these periplasmic parvulins play a role in either the chaperoning or folding of essential proteins which are directed to the outer membrane.<sup>30</sup> Due to the fact that many studies on *E. coli* parvulins have been conducted on K12 derivatives, which are common laboratory strains of *E. coli*, further investigation needs to be conducted on pathogenic strains, as done by Watt *et al.*,<sup>168</sup> to determine if the phenotypes seen correlate with infectious strains of the bacterium. Moving into pathogenic, disease-causing strains would also allow investigation into the roles of parvulins *in vivo* using animal models of infection.

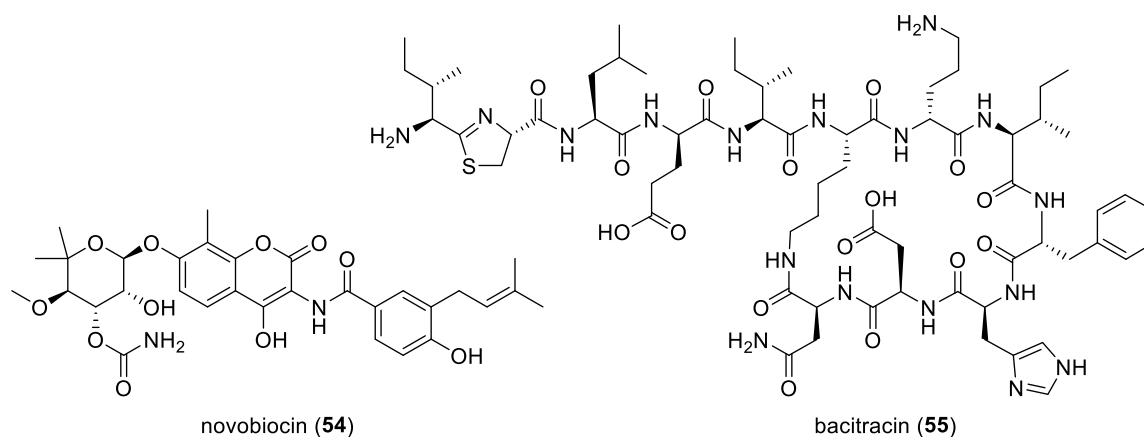


**Figure 22.** Structures of antimicrobials novobiocin (**54**) and bacitracin (**55**).

*Shigella flexneri* lacking *surA* displayed a reduced ability to produce plaques in Henle epithelial cells, as well as a decreased presentation of the outer membrane protein IcsA (VirG) on its surface.<sup>170</sup> The *Salmonella enterica* serovar Typhimurium *surA* mutant displayed decreased adhesive and invasive capability in human epithelial type 2 (HEp-2) cells and was highly attenuated when administered orally in BALB/c mouse infection model. Furthermore, mice

immunized with *S. enterica* serovar Typhimurium *surA* mutant were protected against subsequent infection with wild-type strains 10 weeks postexposure.<sup>169</sup> *Yersinia pseudotuberculosis* mutants of periplasmic PPIases displayed no individual discernible phenotypes apart from a *surA* mutant which had membrane leakiness and increased susceptibility to vancomycin (**51**), bacitracin (**55**), and bile salts, as well as detergents. The *Y. pseudotuberculosis surA* mutant displayed a 40-fold decrease in its ability to adhere to HeLa epithelial cells.<sup>172</sup> In the BALB/c mouse infection model, *Y. pseudotuberculosis surA* mutant was attenuated, demonstrating asymptomatic disease.<sup>173</sup>

Parvulin research in Gram-negatives has focused primarily on the chaperone roles of parvulins in the periplasm. Only a handful of studies have looked at the role of these proteins in bacterial virulence. As highlighted here, it is clear that parvulins are very important in virulence, and further research is required to elucidate their mechanisms of action. Despite this, they show promise as drug targets especially in important bacterial infections caused by pathogens such as UPEC, *Shigella flexneri* and *Salmonella* Typhimurium, bacteria that belong to the family *Enterobacteriaceae*, which are associated with increased global morbidity and mortality<sup>178, 179</sup> and have been labeled as a serious threat to human health by the Centers for Disease Control and Prevention (CDC).

### 3.9 Parvulin Inhibitors

As with the cyclophilins there is limited research published on inhibitors to bacterial parvulins. In contrast, the human parvulin, PIN1, is a very druggable and attractive target, as it has a well-defined active site and high substrate specificity with limited expression in normal tissues.<sup>180, 181</sup> In most human cancers, PIN1 is activated and its overexpression causes chromosome instability and tumorigenesis. PIN1 inhibition or knockout suppresses cancer cell growth *in vitro* and tumorigenesis in mice.<sup>180</sup> In contrast to FK506 (**3**) binding proteins and cyclophilins, the parvulin family of peptidyl-prolyl *cis-trans* isomerases cannot be inhibited by FK506 (**3**) or by cyclosporin A (CsA, **5**).<sup>21</sup> Therefore, the cancer promoting properties of human PIN1 and its druggability give this target great therapeutic potential. Drug discovery strategies against PIN1 will be summarized here, and their potential to target bacterial parvulins will be discussed.

PIN1 binds to phosphopeptides through a positively charged surface, which makes it unique among the PPIases. Therefore, PIN1 inhibitors must navigate this pocket feature by including highly

electronegative substituents, which is challenging as the same features often reduce membrane permeability.<sup>182</sup> 5-Hydroxy-1,4-naphthoquinone, commonly known as juglone (**6**, Figure 4), was the first discovered and most prominent irreversible parvulin inhibitor.<sup>21</sup> Juglone (**6**) covalently interacts with the catalytic domain of PIN1, more specifically with the cysteine residue in the catalytic center of the first discovered parvulin in *E. coli* parvulin Par10 (Cys69) and human hPIN1 (Cys113).<sup>183, 184</sup> However, juglone (**6**) has a relatively simple structure that affects its specificity.<sup>183</sup> In fact, juglone (**6**) has several off-target effects and manifests PIN1-independent activities as its 1,4-naphthoquinone moiety covalently modifies all accessible cytoplasmic cysteine residues available in a cell.<sup>181, 184, 185</sup> In one approach by Wildemann *et al.* a combinatorial cellulose-bound peptide library of 5-mer acetylated peptides containing nonproteinogenic amino acids surrounding a D-phosphothreonine residue was screened against the PPIase domain of PIN1 and bound hits were detected by Western blot.<sup>186</sup> With its *S*-pipecolate core, hit-compound **56** ( $K_i = 18$  nM; Figure 23) resembles a lot of known FKBP inhibitors. Switching the orientation of the phosphothreonine residue to the L-isomer resulted in a 30-fold loss in activity ( $K_i = 550$  nM), and removal of the phosphate group disrupted the interaction.

Crystallization of both stereoisomers (D- and L-form at  $C^*$ , Figure 23a) of compound **56** with PIN1 resulted in almost identical conformations, where the electronegative phosphate group was anchored in the phosphate recognition pocket of the PPIase domain and interacted with Lys63 and Arg69 (Figure 23b,c). While both PIN1 domains, the phosphorylation on Ser or Thr residue WW domain and the PPIase domain, are capable of binding to phosphorylated targets, inhibitor **56** specifically bound to PIN1's PPIase domain, leaving the WW domain untouched.<sup>187</sup> On basis of their structures, the reasons for the huge difference of the two stereoisomers in binding affinity were not obvious. Interestingly, the PIN1 active site bound to these peptides adopted a conformation that is very similar to FKBP12 bound to rapamycin (**4**), with both pipercolic rings having almost identical orientations (Figure 23d,e). Since rapamycin (**4**) has no measurable affinity for PIN1, the affinity of peptide **56** for PIN1 is likely to depend on the phosphate-binding surface.<sup>187</sup> Finally, an intramolecular hydrogen bond observed in the peptide **56**/PIN1 complex mimics the cyclic conformation of FK506 and rapamycin (Figure 23d). Thus, Wildemann *et al.* suggested that a cyclic peptide polyketide bridge, like that found in FK506 (**3**) and rapamycin (**4**) or a similar linkage, may significantly improve the binding affinity of structure-based PIN1 inhibitors.<sup>186, 187</sup>

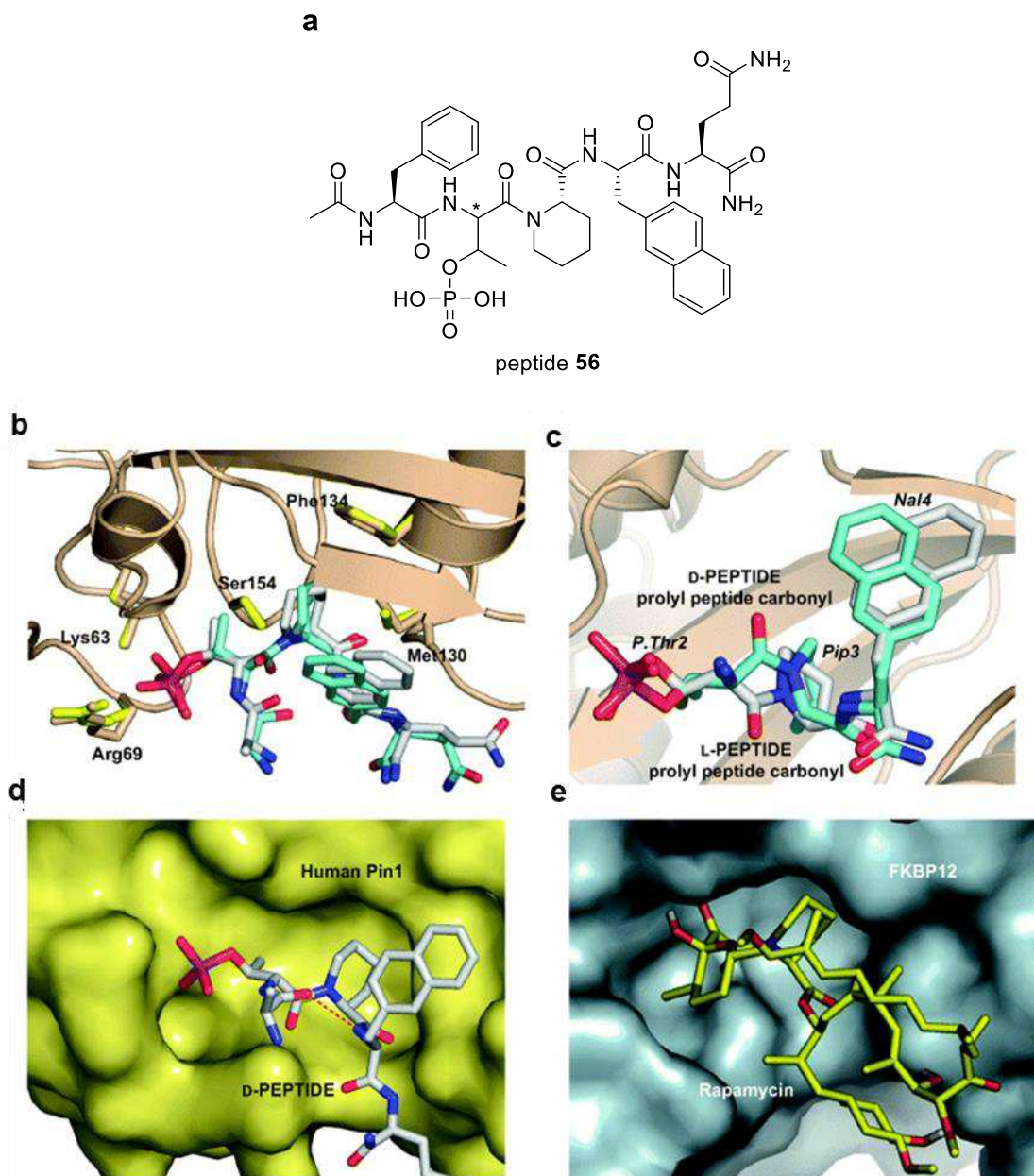


**Figure 23.** Peptide PIN1 inhibitor **56** by Wildemann *et al.*, which was discovered by screening a cellulose-bound peptide library of 5-mer acetylated peptides containing nonproteinogenic amino acids surrounding a D-phosphothreonine.<sup>186</sup> Shown is a comparison of the active sites of human PIN1 and FKBP complexes. (a) Chemical structure of peptide **56**. The D- and L-stereoisomers differ on the marked carbon atom C\*. (b) Comparative binding modes of the D- and L- stereoisomer of peptide **56** to human PIN1 shown as superimposed images. The D- and L-isomer-bound structures of PIN1 are identical to each other. The PIN1 amino acid side chains involved in peptide recognition are shown as half-colored bonds with carbon shown in brown for the D-isomer complex and yellow for the L-isomers complex. D- and L-isomer are depicted as half-colored bonds with carbon colored light gray for the D-isomer and cyan for the L-form. (c) A close-up view rendered in a slightly different orientation than panel a. (d) Surface of PIN1 complexed with the D-isomer of **56**. The intramolecular hydrogen bond (dashed red cylinders) between the carbonyl oxygen of Phe1 and the amide nitrogen of Nal4 defines a bound peptide conformation that closely resembles the conformation and binding mode of rapamycin bound to FKBP depicted in panel d (PDB code 1FKB). (e) Rendered 3D structure of the FKBP12/rapamycin complex. In PIN1, the Pip residue forms several hydrophobic interactions with Phe134 and Leu122 in the PIN1 active site. In the FKBP–rapamycin complex this interaction is spatially conserved with Phe46 and Trp59 in human FKBP12 sequestering the Pip moiety of rapamycin.<sup>187</sup> Reproduced with permission from *ACS Chemical Biology*, Zhang *et al.*<sup>187</sup>

To solve problems of the peptide PIN1 inhibitors for *in vivo* studies such as proteolytic degradation and poor permeability through the cell membrane, Liu *et al.* developed several cyclopeptide PIN1 inhibitors.<sup>188</sup> In addition, due to its reduced conformational freedom, cyclization can lead to a higher binding affinity and specificity than their linear peptide counterparts. Thus, the Liu group screened a library of cyclic peptides containing a tripeptide core with an electronegative amino acid, an isomerizable hydrophobic residue, and a general hydrophobic, aromatic, or positively charged residue.<sup>188</sup> Their hit compounds comprised a D-pThr-Pip-Nal (pThr: phosphothreonine) mark in the figure motif, with the flanking residues having only minimal effects on the binding affinity. These cyclic peptides were then rendered cell permeable either by attaching an octaarginine sequence to the side chain using a disulfide linker, which is reduced in the cytosol (compound **57**, Figure 24), or by direct incorporation of arginine residues into the cyclic peptide backbone (comparable to their later compound **58**, Figure 24). Even though their first cyclic peptides were relatively potent inhibitors of PIN1 *in vitro* with IC<sub>50</sub> values in the nanomolar range, they exhibited only a modest antiproliferative activity in cell culture, which indicated poor cell-permeability of the peptides. In subsequent SAR analysis and sequence optimization some structural features of peptides proved to be critical for high cellular entry efficiency such as peptide cyclization, the presence of both arginine and hydrophobic residues, and small ring sizes ( $\leq 9$  aa).<sup>189</sup> In this way, further work by Bedewy *et al.* was able to improve compound **57** to a small, cell-permeable and biologically active cycloheptapeptide **58** (see Figure 24).<sup>190</sup> It was suggested that these compounds enter cells by endocytosis and subsequently exit from the endosome into the cytosol by a vesicle budding and collapsing mechanism.<sup>190</sup>

To improve the cell permeability of their cyclic inhibitors, Lian *et al.* also explored a bicyclic system in which the cell-penetrating peptide (CPP) motif is placed in one ring whereas the target-binding sequence constitutes the other ring.<sup>191</sup> This cell-penetrating peptide efficiently escapes the endosome and “delivers” the target-binding peptide to the cytosol (comparable to later, non-phosphorylated compound **59**).<sup>191</sup> Treatment of cervical cancer HeLa cells with these compounds resulted in inhibited cell growth and increased stability of the PIN1 substrate, promyelocytic leukemia protein (PML). However, the phosphoamino moiety remains susceptible to hydrolysis by the nonspecific phosphatases in human serum and also contributes to a poor membrane permeability. Jiang *et al.* developed a cell-permeable and metabolically stable nonphosphorylated bicyclic peptide **59** (Figure 24).<sup>192</sup> Although removal of the phosphoamino group resulted in a

reduction in binding affinity *in vitro*, the improved cell permeability makes compound **59** a more potent PIN1 inhibitor for *in vivo* applications.<sup>192</sup> Thus, treatment of HeLa cells with inhibitor **59** resulted in dose-dependent inhibition of cell growth (45% inhibition after treatment for 3 days at 20  $\mu$ M inhibitor), whereas the impermeable predecessors had no effect. Peptides lacking the phosphate group were internalized by HeLa cells around 4-fold more efficiently than their phosphate-containing analogs. Presumably, the negative charged phosphate group interacted electrostatically with the positively charged CPP motif and reduced the cellular uptake efficiency of the latter.<sup>192</sup> Moreover, compound **59** inhibited the intracellular PIN1 activity in cultured mammalian cells but had little effect on other isomerases such as PIN4, FKBP12, or cyclophilin A.<sup>192</sup>

Although competitive assays suggest that compound **59** binds to the active site of PIN1, future structural studies will hopefully elucidate the exact binding, especially the important binding interactions independent of the phosphate-binding site.<sup>192</sup> Beyond this, Dougherty's review is worth mentioning, in which they discuss the challenges and tools in finding cell-penetrating peptides (CPPs).<sup>193</sup>

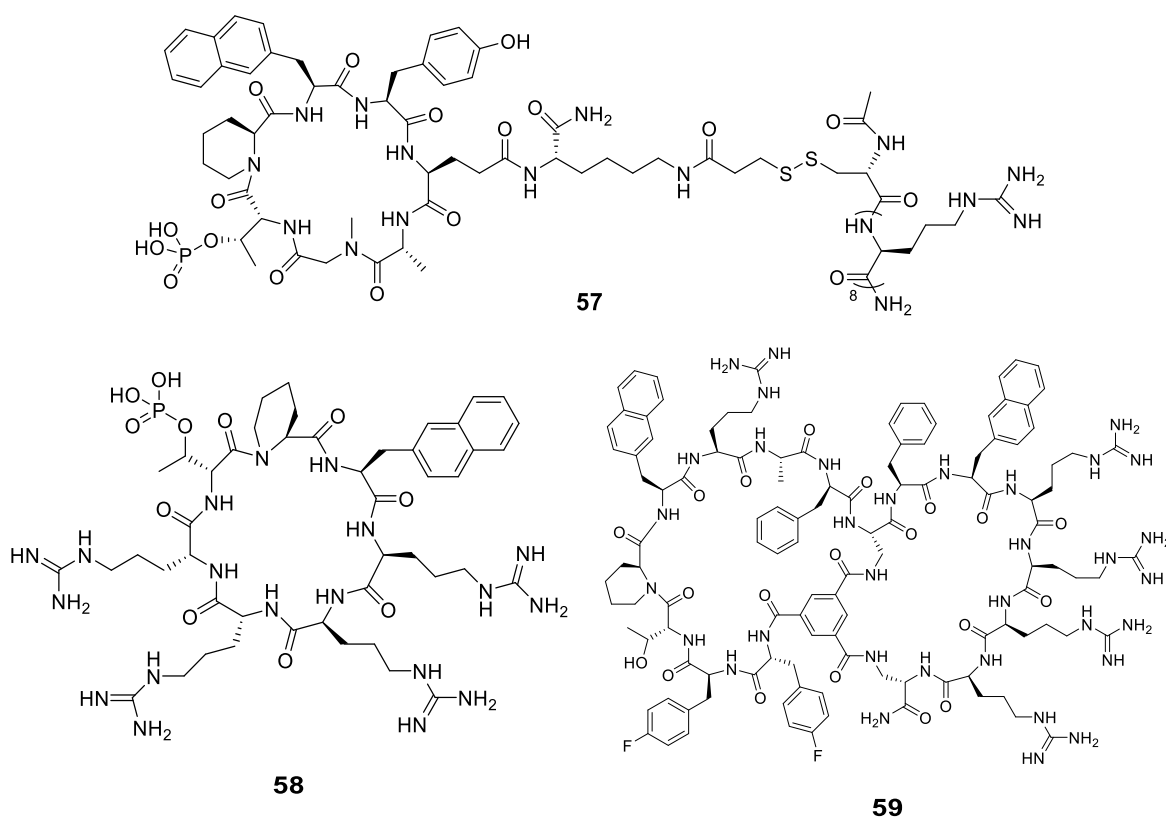


**Figure 24.** Top: First generation, cyclic peptide PIN1 inhibitor **57** by Bedewy *et al.*,<sup>190</sup> attached to an octaarginine sequence using a disulfide linker, which is reduced in the cytosol.<sup>188</sup> Left: Cell-permeable and biologically active cycloheptapeptide **58**.<sup>190</sup> Right: Cell-permeable and metabolically stable nonphosphorylated bicyclic peptide **59**.<sup>191</sup>



By structure-based rational design, a series of peptidomimetic inhibitors of PIN1 have been identified such as conformationally *cis*-locked phosphorylated peptide-mimetic inhibitors (e.g. compound **60**, Figure 25) by Wang *et al.* and Xu *et al.*<sup>194, 195</sup> Core structures of several small-molecule PIN1 inhibitors mostly contain a phosphate group like compound **61** (Figure 25) by Guo *et al.*<sup>196</sup> or their later inhibitors, where the phosphate was replaced by a carboxylate group.<sup>197</sup> Potter *et al.* developed PIN1 inhibiting  $\alpha$ -benzimidazolyl-substituted amino acids such as compound **62**,<sup>198, 199</sup> which address the phosphate-binding pocket of the PIN1 active site (Figure 25).<sup>180</sup> Although compound **62** has a low affinity in the nanomolar scale *in vitro*, it is inactive in cells like compounds **60** and **61** because the negatively charged phosphate or carboxylate moiety of these inhibitors makes them almost cell impermeable, which is a common problem in the development of new PIN1 inhibitors.<sup>181</sup>

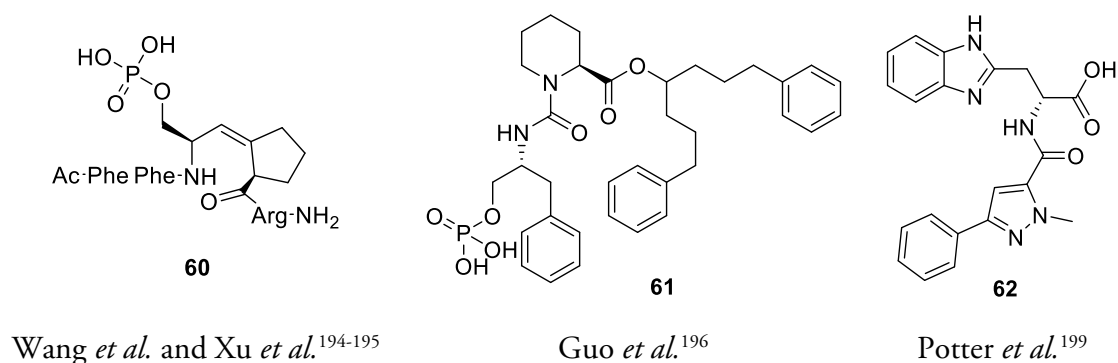


**Figure 25.** Small molecule, phosphate or carboxylate containing PIN1 inhibitors **60**, **61**, and **62**.

In 2003, Uchida *et al.* identified some tetraoxobenzophenanthroline compounds and other similar polycyclic derivatives that competitively blocked PIN1 PPIase activity to low micromolar IC<sub>50</sub> values *in vitro*. Among these, tetraoxobenzophenanthroline derivative PiB (**63**, Figure 26) showed the best IC<sub>50</sub> of 1.5  $\mu$ M, had the least nonspecific toxicity, and inhibited the growth of several cancer lines *in vitro*.<sup>200</sup> Since the low solubility of compound **63** in DMSO limited studies of its effectiveness as an anticancer agent, the Uchida group screened for more soluble compounds and identified dipentamethylene thiuram monosulfide (DTM, **64**, Figure 26) as an effective inhibitor of PIN1 PPIase activity.<sup>201</sup> However, DTM (**64**) did not show strong antifungal and/or anticancer activities, inhibiting proliferation of HCT116 colon carcinoma cells only with a half maximal effective concentration (EC<sub>50</sub>) of 10  $\mu$ M.<sup>201</sup>

Wei *et al.* identified the vitamin A derivative all-*trans* retinoic acid (ATRA, **65**, Figure 26), which had previously been used for the medical treatment of acne and acute promyelocytic leukemia (APL), as a PIN1 inhibitor by mechanism-based drug screening.<sup>202</sup> ATRA (**65**), also known as tretinoin, binds to the proline binding pocket in the catalytic center and inhibits PIN1 at a submicromolar range ( $K_D = 0.8 \mu\text{M}$ ).<sup>202</sup> The cyclohexene ring anchors into the proline binding pocket, with the alkene chain extending the carboxylic acid into the cationic phosphate binding region.<sup>202</sup> By inhibiting PIN1, ATRA (**65**) induces its degradation and thereby destabilizes its substrate, the fusion oncoprotein promyelocytic leukemia-retinoic acid receptor  $\alpha$  (PML-RAR- $\alpha$ ), allowing treatment of APL in cell and animal models and even in human patients.<sup>202</sup> However, regular ATRA (**65**) formulation has a very short half-life of only 45 min in humans, limiting its efficacy against solid tumors.<sup>203</sup> To overcome these limitations, biodegradable, nontoxic controlled release formulations of ATRA (**65**) with a longer half-life are under development.<sup>204</sup> Kozono *et al.* showed that PIN1 can be synergistically targeted by arsenic trioxide (ATO, **66**) and ATRA (**65**), which could be helpful in combating breast and other cancers.<sup>205</sup> ATO (**66**) inhibits and degrades PIN1 and suppresses its oncogenic function by noncovalent binding to PIN1's active site. While ATRA (**65**) inhibits PIN1 itself, it increases cellular ATO uptake by up-regulating aquaporin 9. A combination of ATO (**66**) and ATRA (**65**) cooperatively inhibits PIN1 to block numerous cancer-driving pathways and inhibits the growth of triple-negative breast cancer cells and tumor-initiating cells in cell and animal models.<sup>205</sup>

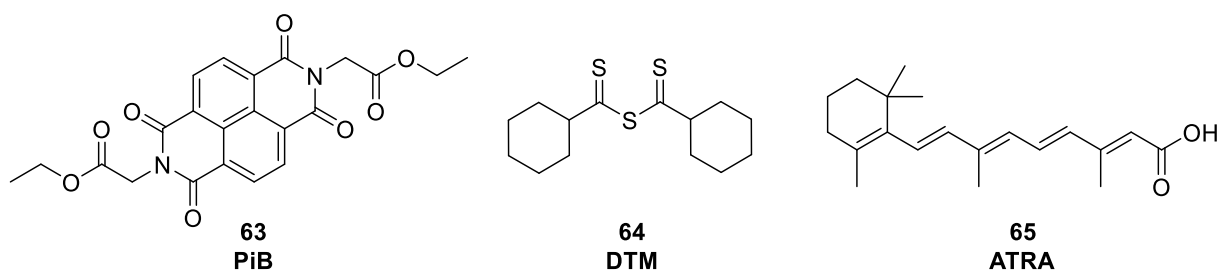


**Figure 26.** Structures of the small molecule PIN1 inhibitors PiB (**63**),<sup>200</sup> DTM (**64**),<sup>201</sup> and ATRA (**65**).<sup>202</sup> ATRA (**65**) is already being used for the medical treatment of acne and acute promyelocytic leukemia (APL).

The major flavonoid in green tea, epigallocatechin-3-gallate (EGCG, **67**, Figure 27), a heavily studied cancer chemopreventative, inactivates PIN1 by blocking the binding sites for pSer-Pro substrates within the PPIase and especially the WW-domain.<sup>206, 207</sup> In 2017, Campaner *et al.* developed the covalent PIN1 inhibitor KPT-6566 (**68A**, Figure 27).<sup>183</sup> It irreversibly blocks the active catalytic center of PIN1 by transferring its sulfanyl-acetate moiety to PIN1 Cys113, forming

a disulfide bridge to the cysteine residue and leading to the byproduct KPT-6566B (**68B**, Figure 27). This species, in turn, being released in the cellular compartment, interacts with different cellular molecules. Both structures contain a quinone-mimicking substructure with the potential to generate reactive oxygen species (ROS) like  $H_2O_2$  and induce oxidative stress response.<sup>208</sup> In addition, KPT-6566-B (**68B**) is a highly reactive electrophile that can interfere with different nucleophilic species in the cancer cells, in which PIN1 is overexpressed, causing DNA damage by forming DNA adducts and ultimately leading to cell death.<sup>209</sup> Campaner *et al.* observed a strong suppression of all tested cancer-related phenotypes depending on PIN1 function, namely proliferation, colony formation, invasion and cancer stem cells (CSC) maintenance, caused by the simultaneous impairment of several PIN1 targets. In contrast to juglone (**6**) or PiB (**63**), which also exert their effect through parvulin-14-inhibition, KPT-6566 (**68A**) is highly specific toward PIN1 and mainly ineffective in cells deprived of PIN1.<sup>183</sup>

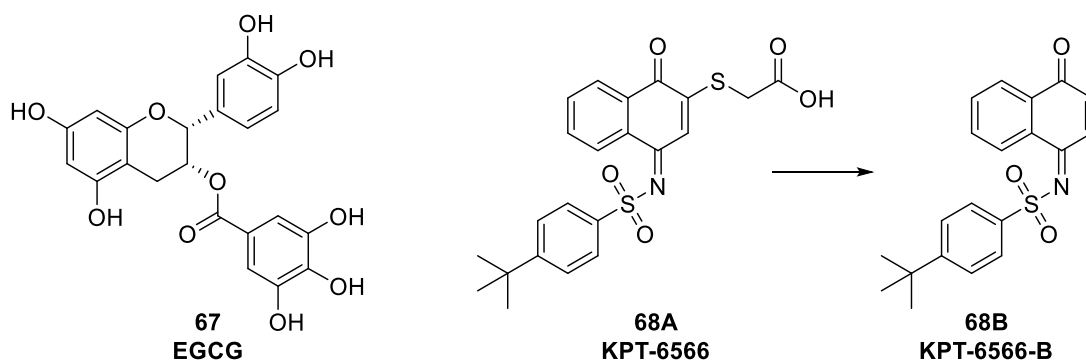


**Figure 27.** Structures of the small molecule PIN1 inhibitors EGCG (**67**) and KPT-6566 (**68A**) and its byproduct KPT-6566-B (**68B**).<sup>183, 206, 207</sup>

Although many PIN1 inhibiting molecules, mainly noncovalent inhibitors, have been discovered to date, none of them have reached clinical trials due to poor pharmacological performance in terms of potency, selectivity, solubility, cell permeability, and stability.<sup>183</sup> Furthermore, there are complications in terms of possible long-term side effects of PIN1 inhibition. Ho-Lee *et al.* demonstrated that PIN1 has an essential and conserved role in regulating telomeric repeat-binding factor 1 (TRF1) stability, telomere maintenance and aging, especially preventing neurodegeneration.<sup>210</sup> In PIN1<sup>-/-</sup> mice they noticed an accelerated telomere loss and a wide range of premature-aging phenotypes from which they concluded a pivotal role of PIN1 in preventing aging. Furthermore, Atchison *et al.* found that PIN1 regulates the timing of proliferation of primordial germ cells (PGCs) during mouse embryonic development. PGCs give rise to male and female germ cells to transmit the genome from generation to generation and defects in PGC

development often result in infertility. In fact, both the male and female PIN1<sup>-/-</sup> mice had profound fertility defects.<sup>211</sup> Results like those from Ho-Lee *et al.* and Atchison *et al.* suggest that PIN1 inhibition could have long-term side effects such as neurodegeneration, Alzheimer's disease, and infertility. However, on a positive note, short-term cancer treatment with PIN1 inhibitors could be free of these side effects, especially if the inhibitors cannot pass through the blood–brain barrier and blood–testis barrier.<sup>180</sup>

### *Targeting the Bacterial Parvulins*

As previously mentioned, there are limited studies on the effect of inhibitors on bacterial parvulins. Structural studies have indicated that the peptide binding region of *E. coli* SurA and PpiD adopts a homologous shape to that of PIN1,<sup>212</sup> although there is a range of reported catalytic activities due to slight variations in sequence. Similar to cyclophilins and cyclophilin inhibitors, a screen of to-date PIN1 inhibitors would need to be conducted to determine if any are capable of binding to and inhibiting PPIase and chaperone activity of bacterial parvulins. Cocrystal structures with any inhibitor hits would allow for a more targeted approach to optimizing compounds to allow for increased specificity to bacterial proteins rather than the human equivalents. If this approach was unsuccessful in identifying lead compounds, a structure-based drug design could be employed in order to find an initial scaffold upon which further generations of inhibitors could be designed. The evidence to date suggests that parvulins are heavily involved in bacterial membrane stability. They are therefore attractive antibacterial targets; inhibitors to bacterial parvulins potentially will destabilize and weaken bacteria, and when used in combination with current antibiotics, they may render them highly effective against antibiotic resistance bacteria.<sup>101, 162–164, 172</sup> However, caution needs to be taken with designing inhibitors, making sure there is no or very little binding to the human parvulin PIN1 to avoid adverse effects.

### **3.10 Concluding Remarks**

It is clear from this review that the immunophilin proteins in bacterial pathogens are an exciting, underexplored group of targets for drug discovery. Due to the pleiotropic roles immunophilins play in bacteria, multiple pathways can be targeted simultaneously with a single inhibitor. Pathways such as those involved in antimicrobial resistance, cell to cell spread, and stress responses are all important targets that would result in disarming the pathogen without the challenge of resistance

rising. Inhibitors to the macrophage infectivity potentiator (Mip) protein are a clear example of how effective inhibitors can be in ultimately reducing survival of multiple pathogens in many different cell infection models. The drug design strategy and medicinal chemistry used to develop Mip inhibitors are an example of how target specific action can be achieved, an important consideration in the development of drugs against immunophilins which are universal proteins throughout life. Furthermore, targeted development of inhibitors against the other two families of bacterial immunophilins is an exciting prospect. Cyclophilin B has been shown to play an essential role in *B. pseudomallei* virulence, while the parvulin, PrsA, has been shown to render antibiotic resistant bacteria sensitive to  $\beta$ -lactam-based antibiotics once more. These targets could prove to be just as druggable as Mip, and inhibitors could demonstrate increased efficacy in future studies. Furthermore, as discussed in detail, there are a large amount of novel inhibitors already available and that can be used as a basis to design target specific inhibitors. A key consideration in drug discovery is the ability to synthesize drugs with the appropriate pharmacology for successful clinical trials; in the case for immunophilins drugs there are several that meet these requirements and are used routinely for various medical treatments. It is feasible therefore to develop inhibitors that will act only on a specific immunophilin protein and use medicinal chemistry to generate drugs that are effective in clinical trials.

### **Author information**

#### **Corresponding Authors**

M.S-T.: email, [mitali.sarkar-tyson@uwa.edu.au](mailto:mitali.sarkar-tyson@uwa.edu.au)

U.H.: email, [ulrike.holzgrabe@uni-wuerzburg.de](mailto:ulrike.holzgrabe@uni-wuerzburg.de)

#### **ORCID**

Nicolas J. Scheuplein: 0000-0003-3261-7964

Nicole M. Bzdyl: 0000-0003-2204-1172

Ulrike Holzgrabe: 0000-0002-0364-7278

Mitali Sarkar-Tyson: 0000-0002-6764-8499

#### **Notes**

The authors declare no competing financial interest.

### Author Contributions

N.J.S. and N.M.B. are equal first authors, and U.H. and M.S.-T. are equal corresponding authors.

### Biographies

**Nicolas J. Scheuplein** is an organic chemist (M.Sc.) and currently a final year PhD student at the Julius-Maximilians-University of Würzburg (Germany) under the supervision of Prof. Dr. Ulrike Holzgrabe. Besides synthesizing fluorescent tool compounds to improve the testing of Mip inhibitors, he is focusing on the development of more drug-like Mip inhibitors. Before this, he has worked on the synthesis of molecules for selective immunotherapy in cancer treatment. In addition, he has contributed to the teaching and supervision of students and masters research students.

**Nicole M. Bzdyl** is a molecular microbiologist and currently a final year PhD student at the University of Western Australia (Australia) under the supervision of Dr Mitali Sarkar-Tyson focusing on understanding the roles of cyclophilins in the bacterium *Burkholderia pseudomallei*. In addition she has contributed to the teaching and supervision of multiple honors and masters research students.

**Emily A. Kibble** is a third year molecular microbiology PhD student at Murdoch University (Australia). She is supervised by Dr Geoff Coombs, as well as Dr Mitali Sarkar-Tyson and Dr Charlene Kahler at the University of Western Australia (Australia). Her PhD is focused on investigating the function of FK506 binding proteins in the human pathogen, *Neisseria meningitidis*.

**Theresa Lohr** is currently a PhD student at the Julius-Maximilians-University of Würzburg (Germany) under the supervision of Prof. Dr. Ulrike Holzgrabe. She is focusing on testing well-known inhibitors of the macrophage infectivity potentiator protein and synthesizing new tailor-made compounds for *Trypanosoma cruzi*. She will further analyze the possibility of using the hit compounds as drugs. In addition, she has contributed to the teaching and supervision of students and masters research students.

**Ulrike Holzgrabe** received her Chemistry diploma at Marburg University (1979), her Pharmacy approbation (1982), and her PhD in Pharmaceutical Chemistry at Kiel University (1983). After habilitation (1989) she became associate professor at Bonn University (1990-1999). She was a post-doc (1988) at Bath University, UK, a visiting professor at Erlangen University with Gasteiger

(1994), and the University of Illinois at Chicago with Hopfinger (1995). Since 1999, she holds a full professorship at Würzburg University (declining offers from Tübingen, Münster, Berlin). She served as vice-rector of Bonn University, as a president of the German Pharmaceutical Society and vicepresident of Würzburg University. She received the “Bayerischen Verdienstorden” (2019). Her main research interest is the development of antiinfectives. She is co-owner of Aamuthera, a company dealing with anticancer drugs.

**Mitali Sarkar-Tyson** is the Le Souef Research Fellow within the School of Biomedical Sciences at the University of Western Australia since 2016. Prior to that, she was a Principle Scientist at the Defence Science Technology Laboratory, United Kingdom for 13 years, and in this role she lead the medical countermeasures programme to identify and characterize novel bacterial targets for drug discovery. She has collaborated extensively with international groups to focus on the inhibition of immunophilin proteins in bacteria with Mip as the main target. At UWA, she has grown her research team to focus on understanding the molecular role of immunophilins in Gram-negative bacteria and developed screening methods of novel inhibitors in cell infection assays and animal models.

### **Acknowledgements**

This work was supported by the North Atlantic Treaty Organization (NATO), Brussels, Belgium, Grant SPS 984835, and the German Research Foundation (DFG, Bonn, Germany, Grant SFB 630) for the development of Mip inhibitors against *Legionella pneumophila* and *Burkholderia pseudomallei*, respectively, and The Federal Ministry of Education and Research for the development of Mip inhibitors against *Trypanosoma cruzi* given to U.H. This paper includes research that was supported by DMTC Limited (Australia). The authors have prepared this paper in accordance with the intellectual property rights granted to partners from the original DMTC project.

### **Abbreviations Used**

PPIase, peptidyl-prolyl *cis-trans* isomerase; MIP, macrophage infectivity potentiator; hCypA, human cyclophilin A; FKBP, FK506 binding protein; WHO, World Health Organization; ML1, Mip-like protein; SlyD, sensitive to lysis D; surA, survival protein A; CsA, cyclosporin A; Sfa, sangliferin A; kDa, kilodalton; NF-AT, nuclear factor of activated T-cell; mTOR, mammalian target of rapamycin; TGF, transforming growth factor; NMR, nuclear magnetic resonance; CSP,

chemical shift perturbation; LDH, lactose dehydrogenase; SAR, structure activity relationship;  $K_D$ , dissociation constant;  $IC_{50}$ , inhibitory concentration of 50%; DAA, direct-acting antiviral; HCV, hepatitis C virus; HIV, human immunodeficiency virus; HTA, host-targeting antiviral; FBDD, fragment-based drug design; CPP, cell-penetrating peptide; DMSO, dimethyl sulfoxide; DTM, dipentamethylene thiuram monosulfide; ROS, reactive oxygen species.

### 3.11 References

- (1) Bal, A. M.; Gould, I. M., Antibiotic Stewardship: Overcoming Implementation Barriers. *Curr. Opin. Infect. Dis.* **2011**, *24* (4), 357-362. DOI: 10.1097/QCO.0b013e3283483262
- (2) Rasko, D. A.; Sperandio, V., Anti-Virulence Strategies to Combat Bacteria-Mediated Disease. *Nat. Rev. Drug Discovery* **2010**, *9* (2), 117-128. DOI: 10.1038/nrd3013
- (3) Cegelski, L.; Marshall, G. R.; Eldridge, G. R.; Hultgren, S. J., The Biology and Future Prospects of Antivirulence Therapies. *Nat. Rev. Microbiol.* **2008**, *6* (1), 17-27. DOI: 10.1038/nrmicro1818
- (4) Walz, J. M.; Avelar, R. L.; Longtine, K. J.; Carter, K. L.; Mermel, L. A.; Heard, S. O.; Anti-Infective External Coating of Central Venous Catheters: a Randomized, Noninferiority Trial Comparing 5-Fluorouracil with Chlorhexidine/Silver Sulfadiazine in Preventing Catheter Colonization. *Crit. Care Med.* **2010**, *38* (11), 2095-2102. DOI: 10.1097/CCM.0b013e3181f265ba
- (5) Hentzer, M.; Givskov, M., Pharmacological Inhibition of Quorum Sensing for the Treatment of Chronic Bacterial Infections. *J. Clin. Invest.* **2003**, *112* (9), 1300-1307. DOI: 10.1172/JCI20074
- (6) Fasciano, A. C.; Shaban, L.; Meccas, J., Promises and Challenges of the Type Three Secretion System Injectisome as an Antivirulence Target. *EcoSal Plus.* **2019**, 261-276. DOI: 10.1128/ecosalplus.ESP-0032-2018
- (7) Brandts, J. F.; Halvorson, H. R.; Brennan, M., Consideration of the Possibility that the Slow Step in Protein Denaturation Reactions is due to *Cis-Trans* Isomerism of Proline Residues. *Biochemistry* **1975**, *14* (22), 4953-4963. DOI: 10.1021/bi00693a026
- (8) Lang, K.; Schmid, F. X.; Fischer, G., Catalysis of Protein Folding by Prolyl Isomerase. *Nature* **1987**, *329* (6136), 268-270. DOI: 10.1038/329268a0
- (9) Schiene-Fischer, C.; Yu, C., Receptor Accessory Folding Helper Enzymes: the Functional Role of Peptidyl Prolyl *Cis/Trans* Isomerases. *FEBS Lett.* **2001**, *495* (1-2), 1-6. DOI: 10.1016/S0014-5793(01)02326-2



- (10) Fischer, G.; Aumüller, T. Regulation of Peptide Bond *Cis/Trans* Isomerization by Enzyme Catalysis and its Implication in Physiological Processes. *Reviews of Physiology, Biochemistry and Pharmacology*; Springer; Berlin, 2003; pp 105-150. DOI: <https://doi.org/10.1007/s10254-003-0011-3>
- (11) Ghartey-Kwansah, G.; Li, Z.; Feng, R.; Wang, L.; Zhou, X.; Chen, F. Z.; Xu, M. M.; Jones, O.; Mu, Y.; Chen, S.; Bryant, J.; Isaacs, W. B.; Ma, J.; Xu, X., Comparative Analysis of FKBP Family Protein: Evaluation, Structure, and Function in Mammals and *Drosophila melanogaster*. *BMC Dev. Biol.* **2018**, *18* (1), 7. DOI: [10.1186/s12861-018-0167-3](https://doi.org/10.1186/s12861-018-0167-3)
- (12) Kolos, J. M.; Voll, A. M.; Bauder, M.; Hausch, F., FKBP Ligands - Where We Are and Where to Go? *Front. Pharmacol.* **2018**, *9*, 1425. DOI: <https://doi.org/10.3389/fphar.2018.01425>
- (13) Aghdasi, B.; Ye, K.; Resnick, A.; Huang, A.; Ha, H. C.; Guo, X.; Dawson, T. M.; Dawson, V. L.; Snyder, S. H., FKBP12, the 12-kDa FK506-Binding Protein, is a Physiologic Regulator of the Cell Cycle. *Proc. Natl. Acad. Sci. U.S.A.* **2001**, *98* (5), 2425-2430. DOI: [10.1073/pnas.041614198](https://doi.org/10.1073/pnas.041614198)
- (14) Köhler, R.; Fanghänel, J.; König, B.; Lüneberg, E.; Frosch, M.; Rahfeld, J.-U.; Hilgenfeld, R.; Fischer, G.; Hacker, J.; Steinert, M., Biochemical and Functional Analyses of the Mip Protein: Influence of the N-Terminal Half and of Peptidylprolyl Isomerase Activity on the Virulence of *Legionella pneumophila*. *Infect. Immun.* **2003**, *71* (8), 4389-4397. DOI: [10.1128/IAI.71.8.4389-4397.2003](https://doi.org/10.1128/IAI.71.8.4389-4397.2003)
- (15) Norville, I. H.; Harmer, N. J.; Harding, S. V.; Fischer, G.; Keith, K. E.; Brown, K. A.; Sarkar-Tyson, M.; Titball, R. W., A *Burkholderia pseudomallei* Macrophage Infectivity Potentiator-like Protein has Rapamycin-Inhibitible Peptidylprolyl Isomerase Activity and Pleiotropic Effects on Virulence. *Infect. Immun.* **2011**, *79* (11), 4299-4307. DOI: [10.1128/IAI.00134-11](https://doi.org/10.1128/IAI.00134-11)
- (16) Liu, J.; Farmer Jr, J. D.; Lane, W. S.; Friedman, J.; Weissman, I.; Schreiber, S. L., Calcineurin is a Common Target of Cyclophilin-Cyclosporin A and FKBP-FK506 Complexes. *Cell* **1991**, *66* (4), 807-815. DOI: [10.1016/0092-8674\(91\)90124-H](https://doi.org/10.1016/0092-8674(91)90124-H)
- (17) Wang, P.; Heitman, J., The Cyclophilins. *Genome Biol.* **2005**, *6* (7), 226. DOI: <https://doi.org/10.1186/gb-2005-6-7-226>
- (18) Colgan, J.; Asmal, M.; Luban, J., Isolation, Characterization and Targeted Disruption of Mouse Ppia: Cyclophilin A is not Essential for Mammalian Cell Viability. *Genomics* **2000**, *68* (2), 167-178. DOI: [10.1006/geno.2000.6295](https://doi.org/10.1006/geno.2000.6295)
- (19) Frausto, S. D.; Lee, E.; Tang, H., Cyclophilins as Modulators of Viral Replication. *Viruses* **2013**, *5* (7), 1684-1701. DOI: [10.3390/v5071684](https://doi.org/10.3390/v5071684)

- (20) Dimou, M.; Venieraki, A.; Katinakis, P., Microbial Cyclophilins: Specialized Functions in Virulence and Beyond. *World J. Microbiol. Biotechnol.* **2017**, *33* (9), 164. DOI: 10.1007/s11274-017-2330-6
- (21) Hennig, L.; Christner, C.; Kipping, M.; Schelbert, B.; Rucknagel, K. P.; Grabley, S.; Kullertz, G.; Fischer, G., Selective Inactivation of Parvulin-Like Peptidyl-Prolyl *Cis/Trans* Isomerases by Juglone. *Biochemistry* **1998**, *37* (17), 5953-5960. DOI: <https://doi.org/10.1021/bi973162p>
- (22) Uchida, T.; Fujimori, F.; Tradler, T.; Fischer, G.; Rahfeld, J.-U., Identification and Characterization of a 14 kDa Human Protein as a Novel Parvulin-Like Peptidyl Prolyl *Cis/Trans* Isomerase. *FEBS Lett.* **1999**, *446* (2-3), 278-282. DOI: 10.1016/S0014-5793(99)00239-2
- (23) Kühlewein, A.; Voll, G.; Hernandez Alvarez, B.; Kessler, H.; Fischer, G.; Rahfeld, J. U.; Gemmecker, G., Solution Structure of *Escherichia coli* Par10: The Prototypic Member of the Parvulin Family of Peptidyl-Prolyl *Cis/Trans* Isomerases. *Protein Sci.* **2004**, *13* (9), 2378-2387. DOI: 10.1110/ps.04756704
- (24) Arévalo-Rodríguez, M.; Cardenas, M. E.; Wu, X.; Hanes, S. D.; Heitman, J., Cyclophilin A and Ess1 Interact with and Regulate Silencing by the Sin3-Rpd3 Histone Deacetylase. *EMBO J.* **2000**, *19* (14), 3739-3749. DOI: 10.1093/emboj/19.14.3739
- (25) Wu, X.; Wilcox, C. B.; Devasahayam, G.; Hackett, R. L.; Arévalo-Rodríguez, M.; Cardenas, M. E.; Heitman, J.; Hanes, S. D., The Ess1 Prolyl Isomerase is Linked to Chromatin Remodeling Complexes and the General Transcription Machinery. *EMBO J.* **2000**, *19* (14), 3727-3738. DOI: 10.1093/emboj/19.14.3727
- (26) Lu, K. P.; Hanes, S. D.; Hunter, T., A Human Peptidyl-Prolyl Isomerase Essential for Regulation of Mitosis. *Nature* **1996**, *380* (6574), 544-547. DOI: 10.1038/380544a0
- (27) Winkler, K. E.; Swenson, K. I.; Kornbluth, S.; Means, A. R., Requirement of the Prolyl Isomerase Pin1 for the Replication Checkpoint. *Science* **2000**, *287* (5458), 1644-1647. DOI: 10.1126/science.287.5458.1644
- (28) Ryo, A.; Suizu, F.; Yoshida, Y.; Perrem, K.; Liou, Y.-C.; Wulf, G.; Rottapel, R.; Yamaoka, S.; Lu, K. P., Regulation of NF- $\kappa$ B Signaling by Pin1-Dependent Prolyl Isomerization and Ubiquitin-Mediated Proteolysis of p65/RelA. *Mol. Cell* **2003**, *12* (6), 1413-1426. DOI: 10.1016/S1097-2765(03)00490-8
- (29) Lu, K. P., Prolyl isomerase Pin1 as a Molecular Target for Cancer Diagnostics and Therapeutics. *Cancer Cell* **2003**, *4* (3), 175-180. DOI: 10.1016/S1535-6108(03)00218-6
- (30) Dartigalongue, C.; Raina, S., A New Heat-Shock Gene, *ppiD*, Encodes a Peptidyl-Prolyl Isomerase Required for Folding of Outer Membrane Proteins in *Escherichia coli*. *EMBO J.* **1998**, *17* (14), 3968-3980. DOI: 10.1093/emboj/17.14.3968

- (31) Howard, K. S.; McLean, P.; Hansen, F.; Lemley, P.; Koblan, K.; Orme-Johnson, W., *Klebsiella pneumoniae nifM* Gene Product is Required for Stabilization and Activation of Nitrogenase Iron Protein in *Escherichia coli*. *J. Biol. Chem.* **1986**, *261* (2), 772-778.
- (32) Kennedy, C.; Gamal, R.; Humphrey, R.; Ramos, J.; Brigle, K.; Dean, D., The *nifH*, *nifM* and *nifN* Genes of *Azotobacter vinelandii*: Characterisation by Tn5 Mutagenesis and Isolation from pLAFR1 Gene Banks. *Mol. Gen. Genet.* **1986**, *205* (2), 318-325. DOI: 10.1007/BF00430445
- (33) Helbig, J.; Lück, P.; Steinert, M.; Jacobs, E.; Witt, M., Immunolocalization of the Mip Protein of Intracellularly and Extracellularly Grown *Legionella pneumophila*. *Lett. Appl. Microbiol.* **2001**, *32* (2), 83-88. DOI: 10.1046/j.1472-765x.2001.00861.x
- (34) Leuzzi, R.; Serino, L.; Scarselli, M.; Savino, S.; Fontana, M. R.; Monaci, E.; Taddei, A.; Fischer, G.; Rappuoli, R.; Pizza, M., Ng-MIP, a Surface-Exposed Lipoprotein of *Neisseria gonorrhoeae*, has a Prolyl *Cis/Trans* Isomerase (PPIase) Activity and is Involved in Persistence in Macrophages. *Mol. Microbiol.* **2005**, *58* (3), 669-681. DOI: 10.1111/j.1365-2958.2005.04859.x
- (35) Hoffmann, A.; Bukau, B.; Kramer, G., Structure and Function of the Molecular Chaperone Trigger Factor. *Biochim. Biophys. Acta, Mol. Cell Res.* **2010**, *1803* (6), 650-661. DOI: <https://doi.org/10.1016/j.bbamcr.2010.01.017>
- (36) Knappe, T. A.; Eckert, B.; Schaarschmidt, P.; Scholz, C.; Schmid, F. X., Insertion of a Chaperone Domain Converts FKBP12 into a Powerful Catalyst of Protein Folding. *J. Mol. Biol.* **2007**, *368* (5), 1458-1468. DOI: 10.1016/j.jmb.2007.02.097
- (37) Wagner, S.; Baars, L.; Ytterberg, A. J.; Klussmeier, A.; Wagner, C. S.; Nord, O.; Nygren, P.-Å.; van Wijk, K. J.; de Gier, J.-W., Consequences of Membrane Protein Overexpression in *Escherichia coli*. *Mol. Cell. Proteomics* **2007**, *6* (9), 1527-1550. DOI: 10.1074/mcp.M600431-MCP200
- (38) Bang, H.; Pecht, A.; Raddatz, G.; Scior, T.; Solbach, W.; Brune, K.; Pahl, A., Prolyl Isomerases in a Minimal Cell: Catalysis of Protein Folding by Trigger Factor from *Mycoplasma genitalium*. *Eur. J. Biochem.* **2000**, *267* (11), 3270-3280. DOI: 10.1046/j.1432-1327.2000.01355.x
- (39) Göthel, S. F.; Scholz, C.; Schmid, F. X.; Marahiel, M. A., Cyclophilin and Trigger Factor from *Bacillus subtilis* Catalyze in Vitro Protein Folding and are Necessary for Viability under Starvation Conditions. *Biochemistry* **1998**, *37* (38), 13392-13399. DOI: 10.1021/bi981253w
- (40) Lyon, W. R.; Gibson, C. M.; Caparon, M. G., A Role for Trigger Factor and an Rgg-Like Regulator in the Transcription, Secretion and Processing of the Cysteine Proteinase of *Streptococcus pyogenes*. *EMBO J.* **1998**, *17* (21), 6263-6275. DOI: 10.1093/emboj/17.21.6263

- (41) Bigot, A.; Botton, E.; Dubail, I.; Charbit, A., A Homolog of *Bacillus subtilis* Trigger Factor in *Listeria monocytogenes* is Involved in Stress Tolerance and Bacterial Virulence. *Appl. Environ. Microbiol.* **2006**, *72* (10), 6623-6631. DOI: 10.1128/AEM.00624-06
- (42) Lyon, W. R.; Caparon, M. G., Trigger Factor-Mediated Prolyl Isomerization Influences Maturation of the *Streptococcus pyogenes* Cysteine Protease. *J. Bacteriol.* **2003**, *185* (12), 3661-3667. DOI: 10.1128/JB.185.12.3661-3667.2003
- (43) Norville, I. H.; Breitbach, K.; Eske-Pogodda, K.; Harmer, N. J.; Sarkar-Tyson, M.; Titball, R. W.; Steinmetz, I., A Novel FK-506-Binding-Like Protein that Lacks Peptidyl-Prolyl Isomerase Activity is Involved in Intracellular Infection and *In Vivo* Virulence of *Burkholderia pseudomallei*. *Microbiology* **2011**, *157* (9), 2629-2638. DOI: 10.1099/mic.0.049163-0
- (44) Echenique-Rivera, H.; Muzzi, A.; Del Tordello, E.; Seib, K. L.; Francois, P.; Rappuoli, R.; Pizza, M.; Serruto, D., Transcriptome Analysis of *Neisseria meningitidis* in Human Whole Blood and Mutagenesis Studies Identify Virulence Factors Involved in Blood Survival. *PLoS Pathogens* **2011**, *7* (5), e1002027. DOI: 10.1371/journal.ppat.1002027
- (45) Hung, M.-C.; Salim, O.; Williams, J. N.; Heckels, J. E.; Christodoulides, M., The *Neisseria meningitidis* Macrophage Infectivity Potentiator Protein Induces Cross-Strain Serum Bactericidal Activity and is a Potential Serogroup B Vaccine Candidate. *Infect. Immun.* **2011**, *79* (9), 3784-3791. DOI: 10.1128/IAI.05019-11
- (46) Lundemose, A. G.; Kay, J. E.; Pearce, J. H., *Chlamydia trachomatis* Mip-Like Protein has Peptidylprolyl *Cis/Trans* Isomerase Activity that is Inhibited by FK506 and Rapamycin and is Implicated in Initiation of Chlamydial Infection. *Mol. Microbiol.* **1993**, *7* (5), 777-783. DOI: 10.1111/j.1365-2958.1993.tb01168.x
- (47) Lundemose, A. G.; Rouch, D. A.; Birkelund, S.; Christiansen, G.; Pearce, J. H., *Chlamydia trachomatis* Mip-Like Protein. *Mol. Microbiol.* **1992**, *6* (17), 2539-2548. DOI: 10.1111/j.1365-2958.1992.tb01430.x
- (48) Cianciotto, N.; Eisenstein, B.; Mody, C.; Toews, G.; Engleberg, N., A *Legionella pneumophila* Gene Encoding a Species-Specific Surface Protein Potentiates Initiation of Intracellular infection. *Infect. Immun.* **1989**, *57* (4), 1255-1262. DOI: 10.1128/IAI.57.4.1255-1262.1989
- (49) Wagner, C.; Khan, A. S.; Kamphausen, T.; Schmausser, B.; Ünal, C.; Lorenz, U.; Fischer, G.; Hacker, J.; Steinert, M., Collagen Binding Protein Mip Enables *Legionella pneumophila* to Transmigrate Through a Barrier of NCI-H292 Lung Epithelial Cells and Extracellular Matrix. *Cell. Microbiol.* **2007**, *9* (2), 450-462. DOI: 10.1111/j.1462-5822.2006.00802.x

- (50) Rasch, J.; Unal, C. M.; Klages, A.; Karsli, U.; Heinsohn, N.; Brouwer, R.; Richter, M.; Dellmann, A.; Steinert, M., Peptidyl-Prolyl-*Cis/Trans*-Isomerases Mip and *PpiB* of *Legionella pneumophila* Contribute to Surface Translocation, Growth at Suboptimal Temperature, and Infection. *Infect. Immun.* **2019**, *87* (1), e00939-17. DOI: 10.1128/IAI.00939-17
- (51) Arakaki, N.; Higa, F.; Koide, M.; Tateyama, M.; Saito, A., Induction of Apoptosis of Human Macrophages *in Vitro* by *Legionella longbeachae* Through Activation of the Caspase Pathway. *J. Med. Microbiol.* **2002**, *51* (2), 159-168. DOI: 10.1099/0022-1317-51-2-159
- (52) Doyle, R. M.; Steele, T. W.; McLennan, A. M.; Parkinson, I. H.; Manning, P. A.; Heuzenroeder, M. W., Sequence Analysis of the *mip* Gene of the Soilborne Pathogen *Legionella longbeachae*. *Infect. Immun.* **1998**, *66* (4), 1492-1499. DOI: 10.1128/IAI.66.4.1492-1499.1998
- (53) O'Connell, W. A.; Bangsberg, J. M.; Cianciotto, N. P., Characterization of a *Legionella micdadei mip* Mutant. *Infect. Immun.* **1995**, *63* (8), 2840-2845. DOI: 10.1128/IAI.63.8.2840-2845.1995
- (54) Saul, F.; Arie, J.-P.; Vulliez-le Normand, B.; Kahn, R.; Betton, J.-M.; Bentley, G., Structural and Functional Studies of FkpA from *Escherichia coli*, a *Cis/Trans* Peptidyl-Prolyl Isomerase with Chaperone Activity. *J. Mol. Biol.* **2004**, *335* (2), 595-608. DOI: 10.1016/j.jmb.2003.10.056
- (55) Hullmann, J.; Patzer, S. I.; Römer, C.; Hantke, K.; Braun, V., Periplasmic Chaperone FkpA is Essential for Imported Colicin M Toxicity. *Mol. Microbiol.* **2008**, *69* (4), 926-937. DOI: 10.1111/j.1365-2958.2008.06327.x
- (56) Missiakas, D.; Betton, J. M.; Raina, S., New Components of Protein Folding in Extracytoplasmic Compartments of *Escherichia coli* SurA, FkpA and Skp/OmpH. *Mol. Microbiol.* **1996**, *21* (4), 871-884. DOI: 10.1046/j.1365-2958.1996.561412.x
- (57) Horne, S. M.; Young, K. D., *Escherichia coli* and Other Species of the Enterobacteriaceae Encode a Protein Similar to the Family of Mip-Like FK506-Binding Proteins. *Arch. Microbiol.* **1995**, *163* (5), 357-365. DOI: 10.1007/BF00404209
- (58) Deuerling, E.; Schulze-Specking, A.; Tomoyasu, T.; Mogk, A.; Bukau, B., Trigger Factor and DnaK Cooperate in Folding of Newly Synthesized Proteins. *Nature* **1999**, *400* (6745), 693-696. DOI: 10.1038/23301
- (59) Teter, S. A.; Houry, W. A.; Ang, D.; Tradler, T.; Rockabrand, D.; Fischer, G.; Blum, P.; Georgopoulos, C.; Hartl, F. U., Polypeptide Flux Through Bacterial Hsp70: DnaK Cooperates with Trigger Factor in Chaperoning Nascent Chains. *Cell* **1999**, *97* (6), 755-765. DOI: 10.1016/S0092-8674(00)80787-4

(60) Bernhardt, T. G.; Roof, W. D.; Young, R., The *Escherichia coli* FKBP-Type PPIase SlyD is Required for the Stabilization of the E Lysis Protein of Bacteriophage  $\phi$ X174. *Mol. Microbiol.* **2002**, *45* (1), 99-108. DOI: 10.1046/j.1365-2958.2002.02984.x

(61) Morgan, E.; Campbell, J. D.; Rowe, S. C.; Bispham, J.; Stevens, M. P.; Bowen, A. J.; Barrow, P. A.; Maskell, D. J.; Wallis, T. S., Identification of Host-Specific Colonization Factors of *Salmonella enterica* Serovar Typhimurium. *Mol. Microbiol.* **2004**, *54* (4), 994-1010. DOI: 10.1111/j.1365-2958.2004.04323.x

(62) Guo, R.; Zhu, S.; Jiao, Y.; An, S.; Xue, Y.; Fei, X.; Geng, S.; Pan, Z.; Jiao, X., Deletion-Mutant Construction, Prokaryotic Expression and Characterization of Peptidyl-Prolyl *Cis-Trans* Isomerase SlyD from *Salmonella enteritidis*. *Acta Microbiol. Sin.* **2016**, *56* (8), 1282-1290.

(63) Horne, S. M.; Kottom, T. J.; Nolan, L. K.; Young, K. D., Decreased Intracellular Survival of an FkpA Mutant of *Salmonella typhimurium* Copenhagen. *Infect. Immun.* **1997**, *65* (2), 806-810. DOI: 10.1128/IAI.65.2.806-810.1997

(64) Wong, C.; Heuzenroeder, M. W.; Quinn, D. M.; Flower, R., Cloning and Characterization of Two Immunophilin-Like Genes, *ilpA* and *fkpA*, on a Single 3.9-kilobase Fragment of *Aeromonas hydrophila* Genomic DNA. *J. Bacteriol.* **1997**, *179* (11), 3397-3403. DOI: 10.1128/JB.179.11.3397-3403.1997

(65) Maeda, T.; Maeda, H.; Yamabe, K.; Mineshiba, J.; Tanimoto, I.; Yamamoto, T.; Naruishi, K.; Koikeguchi, S.; Takashiba, S., Highly Expressed Genes in a Rough-Colony-Forming Phenotype of *Aggregatibacter actinomycetemcomitans*: Implication of a *mip*-Like Gene for the Invasion of Host Tissue. *FEMS Immunol. Med. Microbiol.* **2010**, *58* (2), 226-236. DOI: 10.1111/j.1574-695X.2009.00624.x

(66) Begley, D. W.; Fox, D.; Jenner, D.; Juli, C.; Pierce, P. G.; Abendroth, J.; Muruthi, M.; Safford, K.; Anderson, V.; Atkins, K.; Barnes, S. R.; Moen, S. O.; Raymond, A. C.; Stacy, R.; Myler, P. J.; Staker, B. L.; Harmer, N. J.; Norville, I. H.; Holzgrabe, U.; Sarkar-Tyson, M.; Edwards, T. E.; Lorimer, D. D., A Structural Biology Approach Enables the Development of Antimicrobials Targeting Bacterial Immunophilins. *Antimicrob. Agents Chemother.* **2014**, *58* (3), 1458-1467. DOI: 10.1128/AAC.01875-13

(67) Juli, C.; Sippel, M.; Jäger, J.; Thiele, A.; Weiwad, M.; Schweimer, K.; Rösch, P.; Steinert, M.; Sottriffer, C. A.; Holzgrabe, U., Pipecolic Acid Derivatives as Small-Molecule Inhibitors of the *Legionella* MIP Protein. *J. Med. Chem.* **2011**, *54* (1), 277-283. DOI: 10.1021/jm101156y

(68) Reimer, A.; Seufert, F.; Weiwad, M.; Ebert, J.; Bzdyl, N. M.; Kahler, C. M.; Sarkar-Tyson, M.; Holzgrabe, U.; Rudel, T.; Kozjak-Pavlovic, V., Inhibitors of Macrophage Infectivity Potentiator-Like PPIases Affect Neisserial and Chlamydial Pathogenicity. *Int. J. Antimicrob. Agents* **2016**, *48* (4), 401-408. DOI: 10.1016/j.ijantimicag.2016.06.020

- (69) Seufert, F.; Kuhn, M.; Hein, M.; Weiwad, M.; Vivoli, M.; Norville, I. H.; Sarkar-Tyson, M.; Marshall, L. E.; Schweimer, K.; Bruhn, H.; Rösch, P.; Harmer, N. J.; Sotriffer, C. A.; Holzgrabe, U., Development, Synthesis and Structure–Activity-Relationships of Inhibitors of the Macrophage Infectivity Potentiator (Mip) Proteins of *Legionella pneumophila* and *Burkholderia pseudomallei*. *Bioorg. Med. Chem.* **2016**, *24* (21), 5134-5147. DOI: 10.1016/j.bmc.2016.08.025
- (70) Swindells, D. N.; White, P. S.; Findlay, J. A., The X-ray Crystal Structure of Rapamycin, C51H79NO13. *Can. J. Chem.* **1978**, *56* (18), 2491-2492. DOI: 10.1139/v78-407
- (71) Tanaka, H.; Kuroda, A.; Marusawa, H.; Hatanaka, H.; Kino, T.; Goto, T.; Hashimoto, M.; Taga, T., Structure of FK506, a Novel Immunosuppressant Isolated from Streptomyces. *J. Am. Chem. Soc.* **1987**, *109* (16), 5031-5033. DOI: 10.1021/ja00250a050
- (72) Huai, Q.; Kim, H.-Y.; Liu, Y.; Zhao, Y.; Mondragon, A.; Liu, J. O.; Ke, H., Crystal Structure of Calcineurin-Cyclophilin-Cyclosporin Shows Common but Distinct Recognition of Immunophilin-Drug Complexes. *Proc. Natl. Acad. Sci. U.S.A.* **2002**, *99* (19), 12037-12042. DOI: <https://doi.org/10.1073/pnas.192206699>
- (73) Ke, H.; Huai, Q., Structures of Calcineurin and its Complexes with Immunophilin-Immunosuppressants. *Biochem. Biophys. Res. Commun.* **2003**, *311* (4), 1095-1102. DOI: 10.1016/S0006-291X(03)01537-7
- (74) Sharma, V. K.; Li, B.; Khanna, A.; Sehajpal, P. K.; Suthanthiran, M., Which Way for Drug-Mediated Immunosuppression? *Curr. Opin. Immunol.* **1994**, *6* (5), 784-790. DOI: 10.1016/0952-7915(94)90085-X
- (75) Kang, C. B.; Hong, Y.; Dhe-Paganon, S.; Yoon, H. S., FKBP Family Proteins: Immunophilins with Versatile Biological Functions. *Neurosignals* **2008**, *16* (4), 318-325. DOI: 10.1159/000123041
- (76) Bierer, B. E.; Somers, P. K.; Wandless, T. J.; Burakoff, S. J.; Schreiber, S. L., Probing Immunosuppressant Action with a Nonnatural Immunophilin Ligand. *Science* **1990**, *250* (4980), 556-559. DOI: 10.1126/science.1700475
- (77) Schreiber, S. L., Chemistry and Biology of the Immunophilins and their Immunosuppressive Ligands. *Science* **1991**, *251* (4991), 283-287. DOI: 10.1126/science.1702904
- (78) Choi, J.; Chen, J.; Schreiber, S. L.; Clardy, J., Structure of the FKBP12-Rapamycin Complex Interacting with Binding Domain of Human FRAP. *Science* **1996**, *273* (5272), 239-242. DOI: 10.1126/science.273.5272.239

- (79) Van Duyne, G. D.; Standaert, R. F.; Karplus, P. A.; Schreiber, S. L.; Clardy, J., Atomic Structures of the Human Immunophilin FKBP-12 Complexes with FK506 and Rapamycin. *J. Mol. Biol.* **1993**, *229* (1), 105-124. DOI: 10.1006/jmbi.1993.1012
- (80) Fischer, G.; Bang, H.; Mech, C., Determination of Enzymatic Catalysis for the *Cis-Trans*-Isomerization of Peptide Binding in Proline-Containing Peptides. *Biomed. Biochim. Acta* **1984**, *43*, 1101-1111.
- (81) Vivoli, M.; Renou, J.; Chevalier, A.; Norville, I. H.; Diaz, S.; Juli, C.; Atkins, H.; Holzgrabe, U.; Renard, P.-Y.; Sarkar-Tyson, M.; Harmer, N. J., A Miniaturized Peptidyl-Prolyl Isomerase Enzyme Assay. *Anal. Biochem.* **2017**, *536*, 59-68. DOI: 10.1016/j.ab.2017.08.004
- (82) Holt, D. A.; Luengo, J. I.; Yamashita, D. S.; Oh, H. J.; Konialian, A. L.; Yen, H. K.; Rozamus, L. W.; Brandt, M.; Bossard, M. J.; Levy, M. A.; Eggleston, D. S.; Liang, J.; Schultz, W.; Stout, T. J.; Clardy, J., Design, Synthesis and Kinetic Evaluation of High-Affinity FKBP Ligands and the X-Ray Crystal Structures of Their Complexes with FKBP12. *J. Am. Chem. Soc.* **1993**, *115*, 9925-9938. DOI: 10.1021/ja00075a008
- (83) Ünal, C. M.; Steinert, M., Microbial Peptidyl-Prolyl *Cis/Trans* Isomerases (PPIases): Virulence Factors and Potential Alternative Drug Targets. *Microbiol. Mol. Biol. Rev.* **2014**, *78* (3), 544-571. DOI: 10.1128/MMBR.00015-14
- (84) Babine, R. E.; Bleckman, T.; Kissinger, C.; Showalter, R.; Pelletier, L.; Lewis, C.; Tucker, K.; Moomaw, E.; Parge, H.; Villafranca, J. E., Design, Synthesis and X-Ray Crystallographic Studies of Novel FKBP-12 Ligands. *Bioorg. Med. Chem. Lett.* **1995**, *5* (15), 1719-1724. DOI: 10.1016/0960-894X(95)00290-A
- (85) Rasch, J.; Theuerkorn, M.; Ünal, C.; Heinsohn, N.; Tran, S.; Fischer, G.; Weiwad, M.; Steinert, M., Novel Cycloheximide Derivatives Targeting the Moonlighting Protein Mip Exhibit Specific Antimicrobial Activity Against *Legionella pneumophila*. *Front. Bioeng. Biotech.* **2015**, *3*, 41. DOI: 10.3389/fbioe.2015.00041
- (86) Christner, C.; Wyrwa, R.; Marsch, S.; Küllertz, G.; Thiericke, R.; Grabley, S.; Schumann, D.; Fischer, G., Synthesis and Cytotoxic Evaluation of Cycloheximide Derivatives as Potential Inhibitors of FKBP12 with Neuroregenerative Properties. *J. Med. Chem.* **1999**, *42* (18), 3615-3622. DOI: 10.1021/jm991038t
- (87) Norville, I. H.; O'Shea, K.; Sarkar-Tyson, M.; Zheng, S.; Titball, R. W.; Varani, G.; Harmer, N. J., The Structure of a *Burkholderia pseudomallei* Immunophilin-Inhibitor Complex Reveals New Approaches to Antimicrobial Development. *Biochem. J.* **2011**, *437* (3), 413-422. DOI: 10.1042/BJ20110345



- (88) Holt, D. A.; Konialian-Beck, A. L.; Oh, H.-J.; Yen, H.-K.; Rozamus, L. W.; Krog, A. J.; Erhard, K. F.; Ortiz, E.; Levy, M. A.; Brandt, M.; Bossard, M. J.; Luengo, J. I., Structure-Activity Studies of Synthetic FKBP Ligands as Peptidyl-Prolyl Isomerase Inhibitors. *Bioorg. Med. Chem. Lett.* **1994**, *4* (2), 315-320. DOI: 10.1016/S0960-894X(01)80135-9
- (89) Wintermeyer, E.; Ludwig, B.; Steinert, M.; Schmidt, B.; Fischer, G.; Hacker, J., Influence of Site Specifically Altered Mip Proteins on Intracellular Survival of *Legionella pneumophila* in Eukaryotic Cells. *Infect. Immun.* **1995**, *63* (12), 4576-4583. DOI: 10.1128/IAI.63.12.4576-4583.1995
- (90) Marks, A. R., Cellular Functions of Immunophilins. *Physiol. Rev.* **1996**, *76* (3), 631-649. DOI: 10.1152/physrev.1996.76.3.631
- (91) Kolos, J. M.; Voll, A. M.; Bauder, M.; Hausch, F., FKBP Ligands - Where We Are and Where to Go? *Front. Pharmacol.* **2018**, *9* (1425). DOI: <https://doi.org/10.3389/fphar.2018.01425>
- (92) Pomplun, S.; Sippel, C.; Hähle, A.; Tay, D.; Shima, K.; Klages, A.; Unal, C. M.; Rieß, B.; Toh, H. T.; Hansen, G.; Yoon, H. S.; Bracher, A.; Preiser, P.; Rupp, J.; Steinert, M.; Hausch, F., Chemogenomic Profiling of Human and Microbial FK506-Binding Proteins. *J. Med. Chem.* **2018**, *61* (8), 3660-3673. DOI: 10.1021/acs.jmedchem.8b00137
- (93) Liu, J.; Chen, C. M.; Walsh, C. T., Human and *Escherichia coli* Cyclophilins: Sensitivity to Inhibition by the Immunosuppressant Cyclosporin A Correlates with a Specific Tryptophan Residue. *Biochemistry* **1991**, *30* (9), 2306-2310. DOI: 10.1021/bi00223a003
- (94) Herrler, M.; Bang, H.; Brune, K.; Fischer, G.; Marahiel, M. A., Peptidyl-Prolyl *Cis-Trans* Isomerase from *Bacillus subtilis*. A Prokaryotic Enzyme that is Highly Sensitive to Cyclosporin A. *FEBS Lett.* **1992**, *309* (3), 231-234. DOI: 10.1016/0014-5793(92)80779-G
- (95) Herrler, M.; Bang, H.; Marahiel, M. A., Cloning and Characterization of *ppiB*, a *Bacillus subtilis* Gene which Encodes a Cyclosporine A-Sensitive Peptidyl-Prolyl *Cis-Trans* Isomerase. *Mol. Microbiol.* **1994**, *11* (6), 1073-1083. DOI: 10.1111/j.1365-2958.1994.tb00384.x
- (96) Galat, A., Compression of Large Sets of Sequence Data Reveals Fine Diversification of Functional Profiles in Multigene Families of Proteins: A Study for Peptidyl-Prolyl *Cis/Trans* Isomerases (PPIase). *Biomolecules* **2019**, *9* (2), 59. DOI: 10.3390/biom9020059
- (97) Davis, T. L.; Walker, J. R.; Campagna-Slater, V.; Finerty Jr, P. J.; Paramanathan, R.; Bernstein, G.; MacKenzie, F.; Tempel, W.; Ouyang, H.; Lee, W. H.; Eisenmesser, E. Z.; Dhe-Paganon, S., Structural and Biochemical Characterization of the Human Cyclophilin Family of Peptidyl-Prolyl Isomerases. *PLoS Biol.* **2010**, *8* (7), e1000439. DOI: 10.1371/journal.pbio.1000439

- (98) Ünal, C. M.; Karagöz, M. S.; Berges, M.; Priebe, C.; de Acuña, J. M. B.; Wissing, J.; Jänsch, L.; Jahn, D.; Steinert, M., Pleiotropic *Clostridioides difficile* Cyclophilin PpiB Controls Cysteine-Tolerance, Toxin Production, the Central Metabolism and Multiple Stress Responses. *Front. Pharmacol.* **2019**, *10*, 340. DOI: 10.3389/fphar.2019.00340
- (99) Achenbach, T. V.; Göthel, S. F.; Marahiel, M. A., Histidine 109 in Peptidyl-Prolyl *Cis-Trans* Isomerase of *Bacillus subtilis* Plays an Important Role in Catalysis and in Cyclosporin A Binding. *FEMS Microbiol. Lett.* **1997**, *154* (1), 139-144. DOI: 10.1111/j.1574-6968.1997.tb12635.x
- (100) Reffuveille, F.; Leneveu, C.; Chevalier, S.; Auffray, Y.; Rincé, A., Lipoproteins of *Enterococcus faecalis*: Bioinformatic Identification, Expression Analysis and Relation to Virulence. *Microbiology* **2011**, *157* (11), 3001-3013. DOI: 10.1099/mic.0.053314-0
- (101) Reffuveille, F.; Connil, N.; Sanguinetti, M.; Posteraro, B.; Chevalier, S.; Auffray, Y.; Rince, A., Involvement of Peptidylprolyl *Cis/Trans* Isomerases in *Enterococcus faecalis* Virulence. *Infect. Immun.* **2012**, *80* (5), 1728-1735. DOI: 10.1128/IAI.06251-11
- (102) Mukouhara, T.; Arimoto, T.; Cho, K.; Yamamoto, M.; Igarashi, T., Surface Lipoprotein PpiA of *Streptococcus mutans* Suppresses Scavenger Receptor MARCO-Dependent Phagocytosis by Macrophages. *Infect. Immun.* **2011**, *79* (12), 4933-4940. DOI: 10.1128/IAI.05693-11
- (103) Hermans, P. W.; Adrian, P. V.; Albert, C.; Estevão, S.; Hoogenboezem, T.; Luijendijk, I. H.; Kamphausen, T.; Hammerschmidt, S., The Streptococcal Lipoprotein Rotamase A (SlrA) is a Functional Peptidyl-Prolyl Isomerase Involved in Pneumococcal Colonization. *J. Biol. Chem.* **2006**, *281* (2), 968-976. DOI: 10.1074/jbc.M510014200
- (104) Cho, K.; Arimoto, T.; Igarashi, T.; Yamamoto, M., Involvement of Lipoprotein PpiA of *Streptococcus gordonii* in Evasion of Phagocytosis by Macrophages. *Mol. Oral Microbiol.* **2013**, *28* (5), 379-391. DOI: 10.1111/omi.12031
- (105) Keogh, R. A.; Zapf, R. L.; Trzeciak, E.; Null, G. G.; Wiemels, R. E.; Carroll, R. K., Novel Regulation of Alpha-Toxin and the Phenol-Soluble Modulins by Peptidyl-Prolyl *Cis/Trans* Isomerase Enzymes in *Staphylococcus aureus*. *Toxins* **2019**, *11* (6), 343. DOI: 10.3390/toxins11060343
- (106) Keogh, R. A.; Zapf, R. L.; Wiemels, R. E.; Wittekind, M. A.; Carroll, R. K., The Intracellular Cyclophilin PpiB Contributes to the Virulence of *Staphylococcus aureus* Independently of its Peptidyl-Prolyl *Cis/Trans* Isomerase Activity. *Infect. Immun.* **2018**, *86* (11), e00379-18. DOI: 10.1128/IAI.00379-18
- (107) Wiemels, R. E.; Cech, S. M.; Meyer, N. M.; Burke, C. A.; Weiss, A.; Parks, A. R.; Shaw, L. N.; Carroll, R. K., An Intracellular Peptidyl-Prolyl *Cis/Trans* Isomerase is Required for Folding and Activity of

the *Staphylococcus aureus* Secreted Virulence Factor Nuclease. *J. Bacteriol.* **2017**, *199* (1), e00453-16. DOI: 10.1128/JB.00453-16

(108) Bzdyl, N. M.; Scott, N. E.; Norville, I. H.; Scott, A. E.; Atkins, T.; Pang, S.; Sarovich, D. S.; Coombs, G.; Inglis, T. J. J.; Kahler, C. M.; Sarkar-Tyson, M., Peptidyl-Prolyl Isomerase *ppiB* Is Essential for Proteome Homeostasis and Virulence in *Burkholderia pseudomallei*. *Infect. Immun.* **2019**, *87* (10), e00528-19. DOI: 10.1128/IAI.00528-19

(109) Söderberg, M. A.; Cianciotto, N. P., A *Legionella pneumophila* Peptidyl-Prolyl *Cis-Trans* Isomerase Present in Culture Supernatants is Necessary for Optimal Growth at Low Temperatures. *Appl. Environ. Microbiol.* **2008**, *74* (5), 1634-1638. DOI: 10.1128/AEM.02512-07

(110) Schmidt, B.; Tradler, T.; Rahfeld, J. U.; Ludwig, B.; Jain, B.; Mann, K.; Rücknagel, K. P.; Janowski, B.; Schierhorn, A.; Küllertz, G.; Hacker, J.; Fischer, G., A Cyclophilin-Like Peptidyl-Prolyl *Cis/Trans* Isomerase from *Legionella pneumophila*-Characterization, Molecular Cloning and Overexpression. *Mol. Microbiol.* **1996**, *21* (6), 1147-1160. DOI: 10.1046/j.1365-2958.1996.00061.x

(111) Skagia, A.; Vezyri, E.; Grados, K.; Venieraki, A.; Karpusas, M.; Katinakis, P.; Dimou, M., Structure-Function Analysis of the Periplasmic *Escherichia coli* Cyclophilin PpiA in Relation to Biofilm Formation. *J. Mol. Microbiol. Biotechnol.* **2017**, *27* (4), 228-236. DOI: 10.1159/000478858

(112) Skagia, A.; Vezyri, E.; Sigala, M.; Kokkinou, A.; Karpusas, M.; Venieraki, A.; Katinakis, P.; Dimou, M., Structural and Functional Analysis of Cyclophilin *PpiB* Mutants Supports an *In Vivo* Function not Limited to Prolyl Isomerization Activity. *Genes Cells* **2017**, *22* (1), 32-44. DOI: 10.1111/gtc.12452

(113) Skagia, A.; Zografou, C.; Venieraki, A.; Fasseas, C.; Katinakis, P.; Dimou, M., Functional Analysis of the Cyclophilin *PpiB* Role in Bacterial Cell Division. *Genes Cells* **2017**, *22* (9), 810-824. DOI: 10.1111/gtc.12514

(114) Skagia, A.; Zografou, C.; Vezyri, E.; Venieraki, A.; Katinakis, P.; Dimou, M., Cyclophilin *PpiB* is Involved in Motility and Biofilm Formation Via its Functional Association with Certain Proteins. *Genes Cells* **2016**, *21* (8), 833-851. DOI: 10.1111/gtc.12383

(115) Kok, R. G.; Christoffels, V. M.; Vosman, B.; Hellingwerf, K. J., A Gene of *Acinetobacter calcoaceticus* BD413 Encodes a Periplasmic Peptidyl-Prolyl *Cis-Trans* Isomerase of the Cyclophilin Sub-Class that is not Essential for Growth. *Biochim. Biophys. Acta, Gene Struct. Expression* **1994**, *1219* (3), 601-606. DOI: 10.1016/0167-4781(94)90218-6

- (116) Roset, M. S.; Garcia Fernandez, L.; DelVecchio, V. G.; Briones, G., Intracellularly Induced Cyclophilins Play an Important Role in Stress Adaptation and Virulence of *Brucella abortus*. *Infect. Immun.* **2013**, *81* (2), 521-530. DOI: 10.1128/IAI.01125-12
- (117) Bhaduri, A.; Misra, R.; Maji, A.; Bhetaria, P. J.; Mishra, S.; Arora, G.; Singh, L. K.; Dhasmana, N.; Dubey, N.; Viridi, J. S.; Singh, Y., *Mycobacterium tuberculosis* Cyclophilin A Uses Novel Signal Sequence for Secretion and Mimics Eukaryotic Cyclophilins for Interaction with Host Protein Repertoire. *PLoS One* **2014**, *9* (2), e88090. DOI: <https://doi.org/10.1371/journal.pone.0088090>
- (118) Colombo, D.; Ammirati, E., Cyclosporine in Transplantation—A History of Converging Timelines. *J. Biol. Regul. Homeostatic Agents* **2011**, *25*, 493-504.
- (119) Matsuda, S.; Koyasu, S., Mechanisms of Action of Cyclosporine. *Immunopharmacology* **2000**, *47* (2-3), 119-125. DOI: 10.1016/S0162-3109(00)00192-2
- (120) Schreiber, S. L.; Crabtree, G. R., The Mechanism of Action of Cyclosporin A and FK506. *Immunol. Today* **1992**, *13* (4), 136-142. DOI: 10.1016/0167-5699(92)90111-J
- (121) Paeshuyse, J.; Kaul, A.; De Clercq, E.; Rosenwirth, B.; Dumont, J. M.; Scalfaro, P.; Bartenschlager, R.; Neyts, J., The Non-Immunosuppressive Cyclosporin DEBIO-025 is a Potent Inhibitor of Hepatitis C Virus Replication In Vitro. *Hepatology* **2006**, *43* (4), 761-770. DOI: 10.1002/hep.21102
- (122) Quesniaux, V. F.; Schreier, M. H.; Wenger, R. M.; Hiestand, P. C.; Harding, M. W.; Van Regenmortel, M. H., Cyclophilin Binds to the Region of Cyclosporine Involved in its Immunosuppressive Activity. *Eur. J. Immunol.* **1987**, *17* (9), 1359-1365. DOI: 10.1002/eji.1830170921
- (123) Sweeney, Z. K.; Fu, J.; Wiedmann, B., From Chemical Tools to Clinical Medicines: Nonimmunosuppressive Cyclophilin Inhibitors Derived from the Cyclosporin and Sanglifehrin Scaffolds. *J. Med. Chem.* **2014**, *57* (17), 7145-7159. DOI: 10.1021/jm500223x
- (124) Fu, J.; Tjandra, M.; Becker, C.; Bednarczyk, D.; Capparelli, M.; Elling, R.; Hanna, I.; Fujimoto, R.; Furegati, M.; Karur, S.; Kasprzyk, T.; Knapp, M.; Leung, K.; Li, X.; Lu, P.; Mergo, W.; Miault, C.; Ng, S.; Parker, D.; Peng, Y.; Roggo, S.; Rivkin, A.; Simmons, R. L.; Wang, M.; Wiedmann, B.; Weiss, A. H.; Xiao, L.; Xie, L.; Xu, W.; Yifru, A.; Yang, S.; Zhou, B.; Sweeney, Z. K., Potent Nonimmunosuppressive Cyclophilin Inhibitors with Improved Pharmaceutical Properties and Decreased Transporter Inhibition. *J. Med. Chem.* **2014**, *57* (20), 8503-8516. DOI: 10.1021/jm500862r
- (125) Kuo, J.; Bobardt, M.; Chatterji, U.; Mayo, P. R.; Trepanier, D. J.; Foster, R. T.; Gallay, P.; Ure, D. R., A Pan-Cyclophilin Inhibitor, CRV431, Decreases Fibrosis and Tumor Development in Chronic Liver Disease Models. *J. Pharmacol. Exp. Ther.* **2019**, *371* (2), 231-241. DOI: 10.1124/jpet.119.261099

(126) Rosenwirth, B.; Billich, A.; Datema, R.; Donatsch, P.; Hammerschmid, F.; Harrison, R.; Hiestand, P.; Jaksche, H.; Mayer, P.; Peichl, P., Inhibition of Human Immunodeficiency Virus Type 1 Replication by SDZ NIM 811, a Nonimmunosuppressive Cyclosporine Analog. *Antimicrob. Agents Chemother.* **1994**, *38* (8), 1763-1772. DOI: 10.1128/AAC.38.8.1763

(127) Traber, R.; Kobel, H.; Loosli, H. R.; Senn, H.; Rosenwirth, B.; Lawen, A., [Melle<sup>4</sup>]Cyclosporin, a Novel Natural Cyclosporin with Anti-HIV Activity: Structural Elucidation, Biosynthesis and Biological Properties. *Antiviral Chem. Chemother.* **1994**, *5* (5), 331-339. DOI: 10.1177/095632029400500507

(128) Steadman, V. A.; Pettit, S. B.; Poullennec, K. G.; Lazarides, L.; Keats, A. J.; Dean, D. K.; Stanway, S. J.; Austin, C. A.; Sanvoisin, J. A.; Watt, G. M.; Fliri, H. G.; Licican, A. C.; Jin, D.; Wong, M. H.; Leavitt, S. A.; Lee, Y. J.; Tian, Y.; Frey, C. R.; Appleby, T. C.; Schmitz, U.; Jansa, P.; Mackman, R. L.; Schultz, B. E., Discovery of Potent Cyclophilin Inhibitors Based on the Structural Simplification of Sanglifehrins. *J. Med. Chem.* **2017**, *60* (3), 1000-1017. DOI: 10.1021/acs.jmedchem.6b01329

(129) Gallay, P. A.; Lin, K., Profile of Alisporivir and its Potential in the Treatment of Hepatitis C. *Drug Des. Dev. Ther.* **2013**, *7*, 105-115. DOI: 10.2147/DDDT.S30946

(130) Mackman, R. L.; Steadman, V. A.; Dean, D. K.; Jansa, P.; Poullennec, K. G.; Appleby, T.; Austin, C.; Blakemore, C. A.; Cai, R.; Cannizzaro, C.; Chin, G.; Chiva, J. C.; Dunbar, N. A.; Fliri, H.; Highton, A. J.; Hui, H.; Ji, M.; Jin, H.; Karki, K.; Keats, A. J.; Lazarides, L.; Lee, Y. J.; Licican, A.; Mish, M.; Murray, B.; Pettit, S. B.; Pyun, P.; Sangi, M.; Santos, R.; Sanvoisin, J.; Schmitz, U.; Schrier, A.; Siegel, D.; Sperandio, D.; Stepan, G.; Tian, Y.; Watt, G. M.; Yang, H.; Schultz, B. E., Discovery of a Potent and Orally Bioavailable Cyclophilin Inhibitor Derived from the Sanglifehrins Macrocyclic Core. *J. Med. Chem.* **2018**, *61* (21), 9473-9499. DOI: 10.1021/acs.jmedchem.8b00802

(131) Chatterji, U.; Bobardt, M. D.; Stanfield, R.; Ptak, R. G.; Pallansch, L. A.; Ward, P. A.; Jones, M. J.; Stoddart, C. A.; Scalfaro, P.; Dumont, J. M.; Besseghir, K.; Rosenwirth, B.; Gallay, P. A., Naturally Occurring Capsid Substitutions Render HIV-1 Cyclophilin A Independent in Human Cells and TRIM-Cyclophilin-Resistant in Owl Monkey Cells. *J. Biol. Chem.* **2005**, *280* (48), 40293-40300. DOI: 10.1074/jbc.M506314200

(132) Lawitz, E.; Godofsky, E.; Rouzier, R.; Marbury, T.; Nguyen, T.; Ke, J.; Huang, M.; Praestgaard, J.; Serra, D.; Evans, T. G., Safety, Pharmacokinetics, and Antiviral Activity of the Cyclophilin Inhibitor NIM811 Alone or in Combination with Pegylated Interferon in HCV-Infected Patients Receiving 14 Days of Therapy. *Antiviral Res.* **2011**, *89* (3), 238-245. DOI: 10.1016/j.antiviral.2011.01.003

- (133) Hopkins, S.; Gally, P., Cyclophilin Inhibitors: an Emerging Class of Therapeutics for the Treatment of Chronic Hepatitis C Infection. *Viruses* **2012**, *4* (11), 2558-2577. DOI: 10.3390/v4112558
- (134) Flisiak, R.; Jaroszewicz, J.; Flisiak, I.; Lapinski, T., Update on Alisporivir in Treatment of Viral Hepatitis C. *Expert Opin. Invest. Drugs* **2012**, *21* (3), 375-382. DOI: 10.1517/13543784.2012.658641
- (135) Fu, J.; Becker, C.; Cao, L.; Capparelli, M.; Denay, R.; Fujimoto, R.; Gai, Y.; Gao, Z.; Guenat, C.; Karur, S.; Kim, H.; Li, W.; Li, X.; Li, W.; Lochmann, T.; Lu, A.; Lu, P.; Luneau, A.; Meier, N.; Mergo, W.; Ng, S.; Parker, D.; Peng, Y.; Riss, B.; Rivkin, A.; Roggo, S.; Schroeder, H.; Schuerch, F.; Simmons, R. L.; Sun, F.; Sweeney, Z. K.; Tjandra, M.; Wang, M.; Wang, R.; Weiss, A. H.; Wenger, N.; Wu, Q.; Xiong, X.; Xu, S.; Xu, W.; Yifru, A.; Zhao, J.; Zhou, J.; Zurcher, C.; Gallou, F., Development of a Cyclosporin A Derivative with Excellent Anti-Hepatitis C Virus Potency. *Bioorg. Med. Chem.* **2018**, *26* (4), 957-969. DOI: 10.1016/j.bmc.2017.09.008
- (136) Sedrani, R.; Kallen, J.; Martin Cabrejas, L. M.; Papageorgiou, C. D.; Senia, F.; Rohrbach, S.; Wagner, D.; Thai, B.; Jutzi Eme, A. M.; France, J.; Oberer, L.; Rihs, G.; Zenke, G.; Wagner, J., Sanglifohrin-Cyclophilin Interaction: Degradation Work, Synthetic Macrocyclic Analogs, X-Ray Crystal Structure, and Binding Data. *J. Am. Chem. Soc.* **2003**, *125* (13), 3849-3859. DOI: 10.1021/ja021327y
- (137) Kallen, J.; Sedrani, R.; Zenke, G.; Wagner, J., Structure of Human Cyclophilin A in Complex with the Novel Immunosuppressant Sanglifohrin A at 1.6 Å Resolution. *J. Biol. Chem.* **2005**, *280* (23), 21965-21971. DOI: 10.1074/jbc.M501623200
- (138) Immecke, S. N.; Baal, N.; Wilhelm, J.; Bechtel, J.; Knoche, A.; Bein, G.; Hackstein, H., The Cyclophilin-Binding Agent Sanglifohrin A is a Dendritic Cell Chemokine and Migration Inhibitor. *PLoS One* **2011**, *6* (3), e18406. DOI: 10.1371/journal.pone.0018406
- (139) Zenke, G.; Strittmatter, U.; Fuchs, S.; Quesniaux, V. F.; Brinkmann, V.; Schuler, W.; Zurini, M.; Enz, A.; Billich, A.; Sanglier, J. J.; Fehr, T., Sanglifohrin A, a Novel Cyclophilin-Binding Compound Showing Immunosuppressive Activity with a New Mechanism of Action. *J. Immunol.* **2001**, *166* (12), 7165-7171. DOI: 10.1371/journal.pone.0018406
- (140) Gaither, L. A.; Borawski, J.; Anderson, L. J.; Balabanis, K. A.; Devay, P.; Joberty, G.; Rau, C.; Schirle, M.; Bouwmeester, T.; Mickanin, C.; Zhao, S.; Vickers, C.; Lee, L.; Deng, G.; Baryza, J.; Fujimoto, R. A.; Lin, K.; Compton, T.; Wiedmann, B., Multiple Cyclophilins Involved in Different Cellular Pathways Mediate HCV Replication. *Virology* **2010**, *397* (1), 43-55. DOI: 10.1016/j.virol.2009.10.043
- (141) Gregory, M. A.; Bobardt, M.; Obeid, S.; Chatterji, U.; Coates, N. J.; Foster, T.; Gally, P.; Leyssen, P.; Moss, S. J.; Neyts, J.; Nur-e-Alam, M.; Paeshuyse, J.; Pirae, M.; Suthar, D.; Warneck, T.; Zhang, M. Q.; Wilkinson, B., Preclinical Characterization of Naturally Occurring Polyketide Cyclophilin Inhibitors

from the Sanglifehrin Family. *Antimicrob. Agents Chemother.* **2011**, *55* (5), 1975-1981. DOI: 10.1128/AAC.01627-10

(142) Moss, S. J.; Bobardt, M.; Leyssen, P.; Coates, N.; Chatterji, U.; Dejian, X.; Foster, T.; Liu, J.; Nure-Alam, M.; Suthar, D.; Yongsheng, C.; Warneck, T.; Zhang, M.-Q.; Neyts, J.; Gallay, P.; Wilkinson, B.; Gregory, M. A., Sangamides, a New Class of Cyclophilin-Inhibiting Host-Targeted Antivirals for Treatment of HCV Infection. *MedChemComm* **2012**, *3* (8), 944-949. DOI: 10.1039/C1MD00227A

(143) Ahmed-Belkacem, A.; Colliandre, L.; Ahnou, N.; Nevers, Q.; Gelin, M.; Bessin, Y.; Brillet, R.; Cala, O.; Douguet, D.; Bourguet, W.; Krimm, I.; Pawlowsky, J. M.; Guichou, J. F., Fragment-Based Discovery of a New Family of Non-Peptidic Small-Molecule Cyclophilin Inhibitors with Potent Antiviral Activities. *Nat. Commun.* **2016**, *7*, 12777. DOI: 10.1038/ncomms12777

(144) Karlgren, M.; Ahlin, G.; Bergstrom, C. A.; Svensson, R.; Palm, J.; Artursson, P., *In Vitro* and *In Silico* Strategies to Identify OATP1B1 Inhibitors and Predict Clinical Drug-Drug Interactions. *Pharm. Res.* **2012**, *29* (2), 411-426. DOI: 10.1007/s11095-011-0564-9

(145) Shore, E. R.; Awais, M.; Kershaw, N. M.; Gibson, R. R.; Pandalaneni, S.; Latawiec, D.; Wen, L.; Javed, M. A.; Criddle, D. N.; Berry, N.; O'Neill, P. M.; Lian, L. Y.; Sutton, R., Small Molecule Inhibitors of Cyclophilin D To Protect Mitochondrial Function as a Potential Treatment for Acute Pancreatitis. *J. Med. Chem.* **2016**, *59* (6), 2596-2611. DOI: 10.1021/acs.jmedchem.5b01801

(146) Dunsmore, C. J.; Malone, K. J.; Bailey, K. R.; Wear, M. A.; Florance, H.; Shirran, S.; Barran, P. E.; Page, A. P.; Walkinshaw, M. D.; Turner, N. J., Design and Synthesis of Conformationally Constrained Cyclophilin Inhibitors Showing a Cyclosporin-A Phenotype in *C. elegans*. *ChemBioChem.* **2011**, *12* (5), 802-810. DOI: 10.1002/cbic.201000413

(147) Guichou, J. F.; Viaud, J.; Mettling, C.; Subra, G.; Lin, Y. L.; Chavanieu, A., Structure-Based Design, Synthesis, and Biological Evaluation of Novel Inhibitors of Human Cyclophilin A. *J. Med. Chem.* **2006**, *49* (3), 900-910. DOI: 10.1021/jm050716a

(148) Ni, S.; Yuan, Y.; Huang, J.; Mao, X.; Lv, M.; Zhu, J.; Shen, X.; Pei, J.; Lai, L.; Jiang, H.; Li, J., Discovering Potent Small Molecule Inhibitors of Cyclophilin A Using *De Novo* Drug Design Approach. *J. Med. Chem.* **2009**, *52* (17), 5295-5298. DOI: 10.1021/jm9008295

(149) Rahfeld, J.-U.; Rücknagel, K. P.; Schelbert, B.; Ludwig, B.; Hacker, J.; Mann, K.; Fischer, G., Confirmation of the Existence of a Third Family Among Peptidyl-Prolyl *Cis/Trans* Isomerases. Amino Acid Sequence and Recombinant Production of Parvulin. *FEBS Lett.* **1994**, *352* (2), 180-184. DOI: 10.1016/0014-5793(94)00932-5

- (150) Matern, Y.; Barion, B.; Behrens-Kneip, S., PpiD is a Player in the Network of Periplasmic Chaperones in *Escherichia coli*. *BMC Microbiol.* **2010**, *10* (1), 251. DOI: 10.1186/1471-2180-10-251
- (151) Volokhina, E. B.; Grijpstra, J.; Stork, M.; Schilders, I.; Tommassen, J.; Bos, M. P., Role of the Periplasmic Chaperones Skp, SurA, and DegQ in Outer Membrane Protein Biogenesis in *Neisseria meningitidis*. *J. Bacteriol.* **2011**, *193* (7), 1612-1621. DOI: 10.1128/JB.00532-10
- (152) Jousselin, A.; Manzano, C.; Biette, A.; Reed, P.; Pinho, M. G.; Rosato, A. E.; Kelley, W. L.; Renzoni, A., The *Staphylococcus aureus* Chaperone PrsA is a New Auxiliary Factor of Oxacillin Resistance Affecting Penicillin-Binding Protein 2A. *Antimicrob. Agents Chemother.* **2016**, *60* (3), 1656-1666. DOI: 10.1128/AAC.02333-15
- (153) Jousselin, A.; Renzoni, A.; Andrey, D. O.; Monod, A.; Lew, D. P.; Kelley, W. L., The Posttranslocational Chaperone Lipoprotein PrsA is Involved in Both Glycopeptide and Oxacillin Resistance in *Staphylococcus aureus*. *Antimicrob. Agents Chemother.* **2012**, *56* (7), 3629-3640. DOI: 10.1128/AAC.06264-11
- (154) Lin, M. H.; Li, C. C.; Shu, J. C.; Chu, H. W.; Liu, C. C.; Wu, C. C., Exoproteome Profiling Reveals the Involvement of the Foldase PrsA in the Cell Surface Properties and Pathogenesis of *Staphylococcus aureus*. *Proteomics* **2018**, *18* (5-6), 1700195. DOI: 10.1002/pmic.201700195
- (155) Hyyryläinen, H. L.; Marciniak, B. C.; Dahncke, K.; Pietiäinen, M.; Courtin, P.; Vitikainen, M.; Seppala, R.; Otto, A.; Becher, D.; Chapot-Chartier, M. P.; Kuipers, O. P.; Kontinen, V. P., Penicillin-Binding Protein Folding is Dependent on the PrsA Peptidyl-Prolyl *Cis-Trans* Isomerase in *Bacillus subtilis*. *Mol. Microbiol.* **2010**, *77* (1), 108-127. DOI: 10.1111/j.1365-2958.2010.07188.x
- (156) Jacobs, M.; Andersen, J. B.; Kontinen, V.; Sarvas, M., *Bacillus subtilis* PrsA is Required *In Vivo* as an Extracytoplasmic Chaperone for Secretion of Active Enzymes Synthesized Either With or Without Pro-Sequences. *Mol. Microbiol.* **1993**, *8* (5), 957-966. DOI: 10.1111/j.1365-2958.2010.07188.x
- (157) Kontinen, V.; Saris, P.; Sarvas, M., A Gene (*prsA*) of *Bacillus subtilis* Involved in a Novel, Late Stage of Protein Export. *Mol. Microbiol.* **1991**, *5* (5), 1273-1283. DOI: 10.1111/j.1365-2958.1991.tb01901.x
- (158) Kontinen, V. P.; Sarvas, M., The PrsA Lipoprotein is Essential for Protein Secretion in *Bacillus subtilis* and Sets a Limit for High-Level Secretion. *Mol. Microbiol.* **1993**, *8* (4), 727-737. DOI: 10.1111/j.1365-2958.1993.tb01616.x
- (159) Vitikainen, M.; Lappalainen, I.; Seppala, R.; Antelmann, H.; Boer, H.; Taira, S.; Savilahti, H.; Hecker, M.; Vihinen, M.; Sarvas, M.; Kontinen, V. P., Structure-Function Analysis of PrsA Reveals Roles



for the Parvulin-Like and Flanking N-and C-Terminal Domains in Protein Folding and Secretion in *Bacillus subtilis*. *J. Biol. Chem.* **2004**, *279* (18), 19302-19314. DOI: 10.1074/jbc.M400861200

(160) Vitikainen, M.; Pummi, T.; Airaksinen, U.; Wahlström, E.; Wu, H.; Sarvas, M.; Kontinen, V. P., Quantitation of the Capacity of the Secretion Apparatus and Requirement for PrsA in Growth and Secretion of  $\alpha$ -Amylase in *Bacillus subtilis*. *J. Bacteriol.* **2001**, *183* (6), 1881-1890. DOI: 10.1128/JB.183.6.1881-1890.2001

(161) Kontinen, V. P.; Sarvas, M., Mutants of *Bacillus subtilis* Defective in Protein Export. *Microbiology* **1988**, *134* (8), 2333-2344. DOI: 10.1099/00221287-134-8-2333

(162) Alonzo, F.; Freitag, N. E., *Listeria monocytogenes* PrsA2 is Required for Virulence Factor Secretion and Bacterial Viability Within the Host Cell Cytosol. *Infect. Immun.* **2010**, *78* (11), 4944-4957. DOI: 10.1128/IAI.00532-10

(163) Alonzo, F.; Port, G. C.; Cao, M.; Freitag, N. E., The Posttranslocation Chaperone PrsA2 Contributes to Multiple Facets of *Listeria monocytogenes* Pathogenesis. *Infect. Immun.* **2009**, *77* (7), 2612-2623. DOI: 10.1128/IAI.00280-09

(164) Alonzo III, F.; Xayarath, B.; Whisstock, J. C.; Freitag, N. E., Functional Analysis of the *Listeria monocytogenes* Secretion Chaperone PrsA2 and its Multiple Contributions to Bacterial Virulence. *Mol. Microbiol.* **2011**, *80* (6), 1530-1548. DOI: 10.1111/j.1365-2958.2011.07665.x

(165) Cron, L. E.; Bootsma, H. J.; Noske, N.; Burghout, P.; Hammerschmidt, S.; Hermans, P. W., Surface-Associated Lipoprotein PpmA of *Streptococcus pneumoniae* is Involved in Colonization in a Strain-Specific Manner. *Microbiology* **2009**, *155*, 2401–2410. DOI: 10.1099/mic.0.026765-0

(166) Justice, S. S.; Hunstad, D. A.; Harper, J. R.; Duguay, A. R.; Pinkner, J. S.; Bann, J.; Frieden, C.; Silhavy, T. J.; Hultgren, S. J., Periplasmic Peptidyl Prolyl *Cis-Trans* Isomerases are not Essential for Viability, but SurA is Required for Pilus Biogenesis in *Escherichia coli*. *J. Bacteriol.* **2005**, *187* (22), 7680-7686. DOI: 10.1128/JB.187.22.7680-7686.2005

(167) Tormo, A.; Almiron, M.; Kolter, R., *surA*, an *Escherichia coli* Gene Essential for Survival in Stationary Phase. *J. Bacteriol.* **1990**, *172* (8), 4339-4347. DOI: 10.1128/JB.172.8.4339-4347.1990

(168) Watts, K. M.; Hunstad, D. A., Components of SurA Required for Outer Membrane Biogenesis in Uropathogenic *Escherichia coli*. *PLoS One* **2008**, *3* (10), e3359. DOI: 10.1371/journal.pone.0003359

(169) Sydenham, M.; Douce, G.; Bowe, F.; Ahmed, S.; Chatfield, S.; Dougan, G., *Salmonella enterica* Serovar Typhimurium SurA Mutants are Attenuated and Effective Live Oral Vaccines. *Infect. Immun.* **2000**, *68* (3), 1109-1115. DOI: 10.1128/IAI.68.3.1109-1115.2000

(170) Purdy, G. E.; Fisher, C. R.; Payne, S. M., IcsA Surface Presentation in *Shigella flexneri* Requires the Periplasmic Chaperones DegP, Skp, and SurA. *J. Bacteriol.* **2007**, *189* (15), 5566-5573. DOI: 10.1128/JB.00483-07

(171) Hodak, H.; Wohlkönig, A.; Smet-Nocca, C.; Drobecq, H.; Wieruszeski, J.-M.; Sénéchal, M.; Landrieu, I.; Locht, C.; Jamin, M.; Jacob-Dubuisson, F., The Peptidyl-Prolyl Isomerase and Chaperone Par27 of *Bordetella pertussis* as the Prototype for a New Group of Parvulins. *J. Mol. Biol.* **2008**, *376* (2), 414-426. DOI: 10.1016/j.jmb.2007.10.088

(172) Obi, I. R.; Francis, M. S., Demarcating SurA Activities Required for Outer Membrane Targeting of *Yersinia pseudotuberculosis* Adhesins. *Infect. Immun.* **2013**, *81* (7), 2296-2308. DOI: 10.1128/IAI.01208-12

(173) Obi, I. R.; Nordfelth, R.; Francis, M. S., Varying Dependency of Periplasmic Peptidyl-Prolyl *Cis-Trans* Isomerases in Promoting *Yersinia pseudotuberculosis* Stress Tolerance and Pathogenicity. *Biochem. J.* **2011**, *439* (2), 321-332. DOI: 10.1042/BJ20110767

(174) Kazemian, H.; Pourmand, M. R.; Siadat, S. D.; Mahdavi, M.; Yazdi, M. H.; Majelan, P. A.; Afshar, D.; Yaseri, M.; Davari, M.; Getso, M. I., Molecular Cloning and Immunogenicity Evaluation of PpiC, GeLE, and VS87\_01105 Proteins of *Enterococcus faecalis* as Vaccine Candidates. *Iran. Biomed. J.* **2019**, *23* (5), 343-353. DOI: 10.29252/jbj.23.5.6

(175) Baba, T.; Ara, T.; Hasegawa, M.; Takai, Y.; Okumura, Y.; Baba, M.; Datsenko, K. A.; Tomita, M.; Wanner, B. L.; Mori, H., Construction of *Escherichia coli* K-12 In-Frame, Single-Gene Knockout Mutants: the Keio Collection. *Mol. Sys. Biol.* **2006**, *2* (1), 2006.0008. DOI: 10.1038/msb4100050

(176) Sklar, J. G.; Wu, T.; Kahne, D.; Silhavy, T. J., Defining the Roles of the Periplasmic Chaperones SurA, Skp, and DegP in *Escherichia coli*. *Genes Dev.* **2007**, *21* (19), 2473-2484. DOI: 10.1101/gad.1581007

(177) Vertommen, D.; Ruiz, N.; Leverrier, P.; Silhavy, T. J.; Collet, J. F., Characterization of the Role of the *Escherichia coli* Periplasmic Chaperone SurA using Differential Proteomics. *Proteomics* **2009**, *9* (9), 2432-2443. DOI: 10.1002/pmic.200800794

(178) Rodríguez-Baño, J.; Alcalá, J. C.; Cisneros, J. M.; Grill, F.; Oliver, A.; Horcajada, J. P.; Tórtola, T.; Mirelis, B.; Navarro, G.; Cuenca, M.; Esteve, M.; Peña, C.; Llanos, A. C.; Cantón, R.; Pascual, A., Community Infections Caused by Extended-Spectrum  $\beta$ -Lactamase-Producing *Escherichia coli*. *Arch. Intern. Med.* **2008**, *168* (17), 1897-1902. DOI: 10.1001/archinte.168.17.1897

(179) Rottier, W. C.; Ammerlaan, H. S.; Bonten, M. J., Effects of Confounders and Intermediates on the Association of Bacteraemia Caused by Extended-Spectrum  $\beta$ -Lactamase-Producing Enterobacteriaceae and

Patient Outcome: a Meta-Analysis. *J. Antimicrob. Chemother.* **2012**, *67* (6), 1311-1320. DOI: 10.1093/jac/dks065

(180) Zhou, X. Z.; Lu, K. P., The Isomerase PIN1 Controls Numerous Cancer-Driving Pathways and is a Unique Drug Target. *Nat. Rev. Cancer* **2016**, *16* (7), 463-478. DOI: 10.1038/nrc.2016.49

(181) Moore, J. D.; Potter, A., Pin1 Inhibitors: Pitfalls, Progress and Cellular Pharmacology. *Bioorg. Med. Chem. Lett.* **2013**, *23* (15), 4283-4291. DOI: 10.1016/j.bmcl.2013.05.088

(182) Dunyak, B. M.; Gestwicki, J. E., Peptidyl-Proline Isomerases (PPIases): Targets for Natural Products and Natural Product-Inspired Compounds. *J. Med. Chem.* **2016**, *59* (21), 9622-9644. DOI: 10.1021/acs.jmedchem.6b00411

(183) Campaner, E.; Rustighi, A.; Zannini, A.; Cristiani, A.; Piazza, S.; Ciani, Y.; Kalid, O.; Golan, G.; Baloglu, E.; Shacham, S.; Valsasina, B.; Cucchi, U.; Pippione, A. C.; Lolli, M. L.; Giabbai, B.; Storici, P.; Carloni, P.; Rossetti, G.; Benvenuti, F.; Bello, E.; D'Incalci, M.; Cappuzzello, E.; Rosato, A.; Del Sal, G., A Covalent PIN1 Inhibitor Selectively Targets Cancer Cells by a Dual Mechanism of Action. *Nat. Commun.* **2017**, *8*, 15772. DOI: 10.1038/ncomms15772

(184) Matena, A.; Rehic, E.; Honig, D.; Kamba, B.; Bayer, P., Structure and Function of the Human Parvulins Pin1 and Par14/17. *Biol. Chem.* **2018**, *399* (2), 101-125. DOI: 10.1515/hsz-2017-0137

(185) Fila, C.; Metz, C.; van der Sluijs, P., Juglone Inactivates Cysteine-Rich Proteins Required for Progression Through Mitosis. *J. Biol. Chem.* **2008**, *283* (31), 21714-21724. DOI: 10.1074/jbc.M710264200

(186) Wildemann, D.; Erdmann, F.; Alvarez, B. H.; Stoller, G.; Zhou, X. Z.; Fanghanel, J.; Schutkowski, M.; Lu, K. P.; Fischer, G., Nanomolar Inhibitors of the Peptidyl Prolyl *Cis/Trans* Isomerase Pin1 from Combinatorial Peptide Libraries. *J. Med. Chem.* **2006**, *49* (7), 2147-2150. DOI: 10.1021/jm060036n

(187) Zhang, Y.; Daum, S.; Wildemann, D.; Zhou, X. Z.; Verdecia, M. A.; Bowman, M. E.; Lucke, C.; Hunter, T.; Lu, K. P.; Fischer, G.; Noel, J. P., Structural Basis for High-Affinity Peptide Inhibition of Human Pin1. *ACS Chem. Biol.* **2007**, *2* (5), 320-328. DOI: 10.1021/cb7000044

(188) Liu, T.; Liu, Y.; Kao, H. Y.; Pei, D., Membrane Permeable Cyclic Peptidyl Inhibitors Against Human Peptidyl-Prolyl Isomerase Pin1. *J. Med. Chem.* **2010**, *53* (6), 2494-2501. DOI: 10.1021/jm901778v

(189) Qian, Z.; Liu, T.; Liu, Y. Y.; Briesewitz, R.; Barrios, A. M.; Jhiang, S. M.; Pei, D., Efficient Delivery of Cyclic Peptides into Mammalian Cells with Short Sequence Motifs. *ACS Chem. Biol.* **2013**, *8* (2), 423-431. DOI: 10.1021/cb3005275

- (190) Bedewy, W.; Liao, H.; Abou-Taleb, N. A.; Hammad, S. F.; Nasr, T.; Pei, D., Generation of a Cell-Permeable Cycloheptapeptidyl Inhibitor Against the Peptidyl-Prolyl Isomerase Pin1. *Org. Biomol. Chem.* **2017**, *15* (21), 4540-4543. DOI: 10.1039/C7OB00430C
- (191) Lian, W.; Jiang, B.; Qian, Z.; Pei, D., Cell-Permeable Bicyclic Peptide Inhibitors Against Intracellular Proteins. *J. Am. Chem. Soc.* **2014**, *136* (28), 9830-9833. DOI: 10.1021/ja503710n
- (192) Jiang, B.; Pei, D., A Selective, Cell-Permeable Nonphosphorylated Bicyclic Peptidyl Inhibitor Against Peptidyl-Prolyl Isomerase Pin1. *J. Med. Chem.* **2015**, *58* (15), 6306-6312. DOI: 10.1021/acs.jmedchem.5b00411
- (193) Dougherty, P. G.; Sahni, A.; Pei, D., Understanding Cell Penetration of Cyclic Peptides. *Chem. Rev.* **2019**, *119* (17), 10241-10287. DOI: 10.1021/acs.chemrev.9b00008
- (194) Wang, X. J.; Xu, B.; Mullins, A. B.; Neiler, F. K.; Etkorn, F. A., Conformationally Locked Isostere of PhosphoSer-Cis-Pro Inhibits Pin1 23-fold Better than PhosphoSer-Trans-Pro Isostere. *J. Am. Chem. Soc.* **2004**, *126* (47), 15533-15542. DOI: 10.1021/ja046396m
- (195) Xu, G. G.; Etkorn, F. A., Pin1 as an Anticancer Drug Target. *Drug News Perspect.* **2009**, *22* (7), 399-407. DOI: 10.1358/dnp.2009.22.7.1414594
- (196) Guo, C.; Hou, X.; Dong, L.; Dagostino, E.; Greasley, S.; Ferre, R.; Marakovits, J.; Johnson, M. C.; Matthews, D.; Mroczkowski, B.; Parge, H.; Vanarsdale, T.; Popoff, I.; Piraino, J.; Margosiak, S.; Thomson, J.; Los, G.; Murray, B. W., Structure-Based Design of Novel Human Pin1 Inhibitors (I). *Bioorg. Med. Chem. Lett.* **2009**, *19* (19), 5613-5616. DOI: 10.1016/j.bmcl.2009.08.034
- (197) Dong, L.; Marakovits, J.; Hou, X.; Guo, C.; Greasley, S.; Dagostino, E.; Ferre, R.; Johnson, M. C.; Kraynov, E.; Thomson, J.; Pathak, V.; Murray, B. W., Structure-Based Design of Novel Human Pin1 Inhibitors (II). *Bioorg. Med. Chem. Lett.* **2010**, *20* (7), 2210-2214. DOI: 10.1016/j.bmcl.2010.02.033
- (198) Potter, A.; Oldfield, V.; Nunns, C.; Fromont, C.; Ray, S.; Northfield, C. J.; Bryant, C. J.; Scrace, S. F.; Robinson, D.; Matossova, N.; Baker, L.; Dokurno, P.; Surgenor, A. E.; Davis, B.; Richardson, C. M.; Murray, J. B.; Moore, J. D., Discovery of Cell-Active Phenyl-Imidazole Pin1 Inhibitors by Structure-Guided Fragment Evolution. *Bioorg. Med. Chem. Lett.* **2010**, *20* (22), 6483-6488. DOI: 10.1016/j.bmcl.2010.09.063
- (199) Potter, A. J.; Ray, S.; Gueritz, L.; Nunns, C. L.; Bryant, C. J.; Scrace, S. F.; Matossova, N.; Baker, L.; Dokurno, P.; Robinson, D. A.; Surgenor, A. E.; Davis, B.; Murray, J. B.; Richardson, C. M.; Moore, J. D., Structure-Guided Design of Alpha-Amino Acid-Derived Pin1 Inhibitors. *Bioorg. Med. Chem. Lett.* **2010**, *20* (2), 586-590. DOI: 10.1016/j.bmcl.2009.11.090

- (200) Uchida, T.; Takamiya, M.; Takahashi, M.; Miyashita, H.; Ikeda, H.; Terada, T.; Matsuo, Y.; Shirouzu, M.; Yokoyama, S.; Fujimori, F.; Hunter, T., Pin1 and Par14 Peptidyl Prolyl Isomerase Inhibitors Block Cell Proliferation. *Chem. Biol.* **2003**, *10* (1), 15-24. DOI: 10.1016/S1074-5521(02)00310-1
- (201) Tatara, Y.; Lin, Y. C.; Bamba, Y.; Mori, T.; Uchida, T., Dipentamethylene Thiuram Monosulfide is a Novel Inhibitor of Pin1. *Biochem. Biophys. Res. Commun.* **2009**, *384* (3), 394-398. DOI: 10.1016/j.bbrc.2009.04.144
- (202) Wei, S.; Kozono, S.; Kats, L.; Nechama, M.; Li, W.; Guarnerio, J.; Luo, M.; You, M. H.; Yao, Y.; Kondo, A.; Hu, H.; Bozkurt, G.; Moerke, N. J.; Cao, S.; Reschke, M.; Chen, C. H.; Rego, E. M.; Lo-Coco, F.; Cantley, L. C.; Lee, T. H.; Wu, H.; Zhang, Y.; Pandolfi, P. P.; Zhou, X. Z.; Lu, K. P., Active Pin1 is a Key Target of All-Trans Retinoic Acid in Acute Promyelocytic Leukemia and Breast Cancer. *Nat. Med.* **2015**, *21* (5), 457-466. DOI: 10.1038/nm.3839
- (203) Smith, M. A.; Adamson, P. C.; Balis, F. M.; Feusner, J.; Aronson, L.; Murphy, R. F.; Horowitz, M. E.; Reaman, G.; Hammond, G. D.; Fenton, R. M.; Phase I and Pharmacokinetic Evaluation of All-Trans-Retinoic Acid in Pediatric Patients with Cancer. *J. Clin. Oncol.* **1992**, *10* (11), 1666-1673. DOI: 10.1200/JCO.1992.10.11.1666
- (204) Yang, D.; Luo, W.; Wang, J.; Zheng, M.; Liao, X. H.; Zhang, N.; Lu, W.; Wang, L.; Chen, A. Z.; Wu, W. G.; Liu, H.; Wang, S. B.; Zhou, X. Z.; Lu, K. P., A Novel Controlled Release Formulation of the Pin1 Inhibitor ATRA to Improve Liver Cancer Therapy by Simultaneously Blocking Multiple Cancer Pathways. *J. Controlled Release* **2018**, *269*, 405-422. DOI: 10.1016/j.jconrel.2017.11.031
- (205) Kozono, S.; Lin, Y. M.; Seo, H. S.; Pinch, B.; Lian, X.; Qiu, C.; Herbert, M. K.; Chen, C. H.; Tan, L.; Gao, Z. J.; Masefski, W.; Doctor, Z. M.; Jackson, B. P.; Chen, Y.; Dhe-Paganon, S.; Lu, K. P.; Zhou, X. Z., Arsenic Targets Pin1 and Cooperates with Retinoic Acid to Inhibit Cancer-Driving Pathways and Tumor-Initiating Cells. *Nat. Commun.* **2018**, *9* (1), 3069. DOI: 10.1038/s41467-018-05402-2
- (206) Urusova, D. V.; Shim, J. H.; Kim, D. J.; Jung, S. K.; Zykova, T. A.; Carper, A.; Bode, A. M.; Dong, Z., Epigallocatechin-Gallate Suppresses Tumorigenesis by Directly Targeting Pin1. *Cancer Prev. Res.* **2011**, *4* (9), 1366-1377. DOI: 10.1158/1940-6207.CAPR-11-0301
- (207) Xi, L.; Wang, Y.; He, Q.; Zhang, Q.; Du, L., Interaction Between Pin1 and its Natural Product Inhibitor Epigallocatechin-3-Gallate by Spectroscopy and Molecular Dynamics Simulations. *Spectrochim. Acta, Part A* **2016**, *169*, 134-143. DOI: 10.1016/j.saa.2016.06.036
- (208) Kilgore, J. A.; Du, X.; Melito, L.; Wei, S.; Wang, C.; Chin, H. G.; Posner, B.; Pradhan, S.; Ready, J. M.; Williams, N. S., Identification of DNMT1 Selective Antagonists Using a Novel Scintillation Proximity Assay. *J. Biol. Chem.* **2013**, *288* (27), 19673-19684. DOI: 10.1074/jbc.M112.443895

(209) Balam Muñoz, B.; Albores, A., DNA Damage Caused by Polycyclic Aromatic Hydrocarbons: Mechanisms and Markers, Selected Topics in DNA Repair. In *Selected Topics in DNA Repair*; Chen, C. C., Ed.; IntechOpen, 2011; pp 125-144. DOI: 10.5772/22527

(210) Lee, T. H.; Tun-Kyi, A.; Shi, R.; Lim, J.; Soohoo, C.; Finn, G.; Balastik, M.; Pastorino, L.; Wulf, G.; Zhou, X. Z.; Lu, K. P., Essential role of Pin1 in the regulation of TRF1 Stability and Telomere Maintenance. *Nat. Cell Biol.* **2009**, *11* (1), 97-105. DOI: 10.1038/ncb1818

(211) Atchison, F. W.; Capel, B.; Means, A. R., Pin1 Regulates the Timing of Mammalian Primordial Germ Cell Proliferation. *Development* **2003**, *130* (15), 3579-3586. DOI: 10.1242/dev.00584

(212) Weininger, U.; Jakob, R. P.; Kovermann, M.; Balbach, J.; Schmid, F. X., The Prolyl Isomerase Domain of PpiD from *Escherichia coli* Shows a Parvulin Fold but is Devoid of Catalytic Activity. *Protein Sci.* **2010**, *19* (1), 6-18. DOI: 10.1002/pro.277

## II Aims

The overall goal of this study was to advance the development of innovative anti-infectives that address the macrophage infectivity potentiator (Mip) protein, a promising antivirulence factor.<sup>72</sup>

In this regard, it was aimed to design and synthesize fluorescent probes that would allow robust and efficient screening for potential Mip inhibitors of various pathogens using a fluorescence polarization assay (FPA).<sup>20</sup> This would overcome the limitations of the protease-coupled PPIase assay previously used,<sup>73</sup> such as the need for low temperatures and lack of robustness.

Second, novel Mip inhibitors with a pipercolic acid backbone should be synthesized with improved affinity and enzymatic inhibition for a broad spectrum of pathogens, including *Burkholderia pseudomallei* and *Neisseria meningitidis*. For this purpose, the backbone of Mip inhibitors was aimed to be equipped with different side chains along with testing the stereochemical influence on binding (cf. Figure 7).

The metabolism of Mip inhibitors by human liver microsomes was to be studied to identify active metabolites and improve the metabolic stability of the compounds. This would involve the use of mass spectrometry methods to analyze metabolic transformations and subsequently modify inhibitor structures accordingly.

As a side project, synthesis of biotinylated antileishmanial compounds derived from the rhizomes of *Valeriana wallichii*<sup>74</sup> was expected to enable the identification of targets for a more targeted, structure-based drug development.

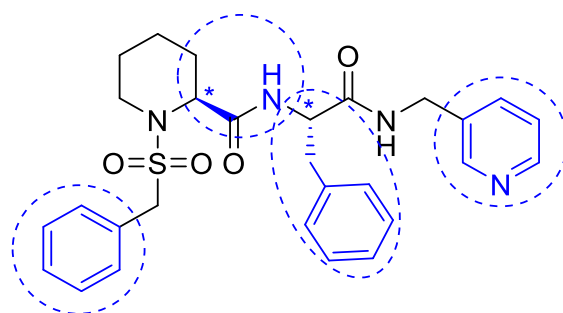


Figure 7. Molecular structure of the side chain bearing Mip inhibitor **S,S-10a**. The potential variation areas are highlighted in blue. In addition, the highlighted side chain as well as the pyridine moiety represent potential sites for attachment of a linker-fluorophore moiety to obtain an FP probe.

### III Results and Discussion

#### 1 Development of Biotin-Labeled Antileishmanial Compounds

*The bibliography for this chapter can be found at the end of this thesis (chapter VII).*

##### 1.1 Leishmaniasis

*Leishmania* is a vector-borne, obligate intracellular protozoan parasite of the *Trypanosomatidae* family, comprising various subspecies. It causes three main clinical manifestations of leishmaniasis disease: visceral leishmaniasis (VL), cutaneous leishmaniasis (CL), and mucocutaneous leishmaniasis (MCL).<sup>75, 76</sup> Leishmaniasis belongs to the neglected tropical diseases (NTDs) and infects the world's poorest populations in over 90 countries.<sup>75</sup> As of 2019, it is estimated that between 498,000 and 862,000 new cases of all forms of leishmaniasis occur each year, resulting in up to 18,700 deaths and up to 1.6 million 'disability-adjusted life years' (DALYs) lost.<sup>77</sup> The insect vector is the female sand fly of the genus *Phlebotomus* or *Lutzomyia*, depending on the location.<sup>76</sup>

##### 1.2 Antileishmanial Compounds Derived from Natural Extracts of *Valeriana Wallichii*

Jan Glaser performed bioactivity-guided fractionation of a chloroform extract from pulverized rhizomes of *Valeriana wallichii* known to have *in vitro* antileishmanial activity against *Leishmania major* promastigotes. With this, their active antileishmanial compounds were to be isolated and identified.<sup>74, 78</sup>

This approach corresponds to that of PDD presented in the introduction (see chapter I\_1). Briefly, PDD starts with target-agnostic phenotypic screenings and explores the active molecules' target in a later step called target-deconvolution. Thus, in addition to thirteen compounds already described in the literature as ingredients of various *Valeriana* species or other plants, four compounds were isolated from *V. wallichii* for the first time. Although valtrate-type iridoids were found to be the primary source of antileishmanial activity of the extract, these compounds were unstable in solution. Furthermore, they exhibited cytotoxicity against *J774.1* murine macrophages, rendering them unsuitable for further investigation. Another ingredient of the extract, bornyl caffeate (**6**, cf. Figure 8) and its derivatives, which were synthesized afterward, on the other hand, were found to have leishmanicidal properties while showing lower cytotoxicity compared to the iridoids. Therefore, this structure was used as a scaffold for the synthesis of a compound library to establish SAR.<sup>74, 79</sup>



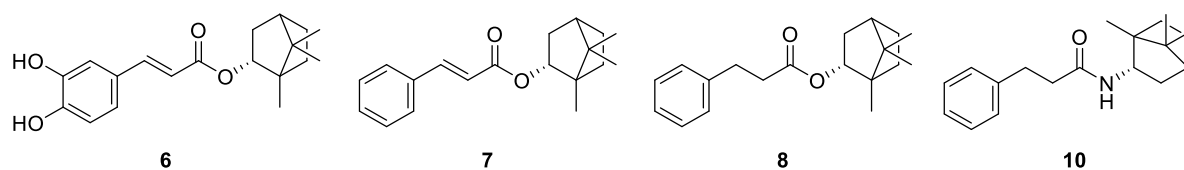


**Figure 8.** Molecular structures of bornyl caffeate (**6**), found as a component of *Valeriana Wallichii* extract, and its synthesized derivatives, (-)-bornyl cinnamate (**7**), (-)-bornyl 3-phenylpropanoate (**8**, *JGBE044*), and (*R*)-(+)-bornyl 3-phenylpropanamide (**10**, *JGBEN051*).<sup>74,78</sup> The compounds studied by J. Glaser exhibited antileishmanial activity *in vitro* against *L. donovani* and *L. major*.<sup>74</sup> Lead **8** also showed *in vivo* activity in *L. major*-infected BALB/c mice.<sup>80</sup> Amide derivative **10** demonstrated *in vivo* activity in BALB/c mice infected with *L. donovani*.<sup>78</sup>

Since the catechol moiety and the  $\alpha,\beta$ -unsaturated carbonyl moiety of bornyl caffeate **6** contributed significantly to the cytotoxicity of similar compounds and proved unnecessary for antileishmanial activity, these structural features were omitted. The cinnamic acid bornyl ester derivative (-)-bornyl cinnamate (**7**, cf. Figure 8) and the saturated analog (-)-bornyl 3-phenylpropanoate (**8**, *JGBE044*) exhibited antileishmanial activity *in vitro* against *L. donovani* ( $IC_{50}$  = 15.6  $\mu$ M for **7** and > 100  $\mu$ M for **8**) and against *L. major* ( $IC_{50}$  (promastigotes) = 39.6  $\mu$ M for **7** and 50.2  $\mu$ M for **8**).<sup>74-79</sup> Borneol (**9**) proved itself to be the most effective substituent together with other bulky or sterically demanding alcohols, e.g., thymol, menthol, or adamantol. Thus, similar compounds of the established compound library bearing different bulky substituents also proved effective antischistosomal agents for *Schistosoma mansoni* (*San Francisco*) *in vitro*.<sup>81</sup>

Lead **8** demonstrated promising activity in *L. major*-infected BALB/c mice *in vivo*.<sup>80</sup>

Amide derivative **10** (*JGBEN051*, cf. Figure 8) demonstrated a 34% reduction in parasite load *in vivo* in BALB/c mice infected with *L. donovani* after administration of the compound at 1 mg/kg/day for five days using intraperitoneal injection.<sup>78</sup>

### 1.3 Biotinylated Probes for Target Deconvolution

Although the found structures can be considered potential leads for developing new antileishmanial therapeutic approaches, knowledge of the biological target is essential for further development. As described in the introduction of this thesis (see chapter I\_2.1), learning about the target can help to achieve species-selectivity, reduce mechanism-connected side effects, and turn drug development more rational. Hence, this project aimed to identify possible targets of the found caffeic acid analogs in the parasites using compound-centric chemical proteomics (CCCP, see page 7). In recent years, an increasing number of researchers have begun to screen the target proteins of natural products

using chemical proteomics approaches that can provide a wide range of protein targets of active small molecules. Chemical proteomics experiments for target identification/deconvolution typically consist of two key steps: (1) designing and synthesizing chemical probes and (2) fishing and identifying the target(s).<sup>19</sup> In designing a chemical proteomics probe for the antileishmanial and antischistosomal compounds studied, biotin (**2**) was chosen as a reporter unit. This would later allow biotin (**2**)-streptavidin (**3**) affinity chromatography and coupled nanoLC-MS/MS analysis (nanoscale liquid chromatography coupled to tandem mass spectrometry analysis). Affinity chromatography is an established method for the purification of proteins and their complexes, but also the investigation of ligand-target interactions.<sup>82, 83</sup>

In somewhat more detail, the process would start with the design and synthesis of a probe consisting of the found lead compounds covalently linked to (+)-biotin (**2**). Afterward, the biotinylated ligand is applied to streptavidin (**3**) beads for immobilization, which are incubated with the cell lysate of the pathogens for protein enrichment. The bound proteins are then eluted using a streptavidin matrix, separated with SDS-Page, and subsequently characterized. By using quantitative mass spectrometry and comparing it with the control without biotinylated ligands, it is then possible to find potential binding partners of the substances.<sup>19</sup>

The binding of biotin (**2**), also known as vitamin B7 or vitamin H, to the 60 kDa homotetramer streptavidin (**3**), purified from the bacterium *Streptomyces avidinii*, is one of the strongest non-covalent interactions known in nature.<sup>84, 85</sup> One protein binds four molecules of biotin (**2**) with very high affinity, exhibiting a  $K_D$  of  $\approx 10^{-14}$  mol/L.<sup>87</sup> Besides that, the resistance of the streptavidin (**3**)-biotin (**2**) complex to organic solvents, denaturants, detergents, proteolytic enzymes, and various temperatures has further contributed to the popularity of this system.<sup>84, 86</sup> Biotin (**2**) has been used in affinity chromatography for decades and also in more recent chemical proteomics approaches such as ABPP (cf. chapter I\_2.1).<sup>25, 84, 87</sup>

However, since the target (or targets) and the exact binding mode of the active compounds are not yet known, probes were designed featuring different attachment points for the linker (cf. Figure 9). Therefore, probes were developed containing the linkage point with the linker-reporter unit on the phenyl ring and a probe bearing it on the opposite side. A biotinylated probe of the antileishmanial amide derivative **10** was also prepared to ensure chemical stability (cf. Figure 9). The high chemical stability (and poor reactivity) of amides is well understood by the strength of the resonance-stabilized amide C-N bond.<sup>88</sup>

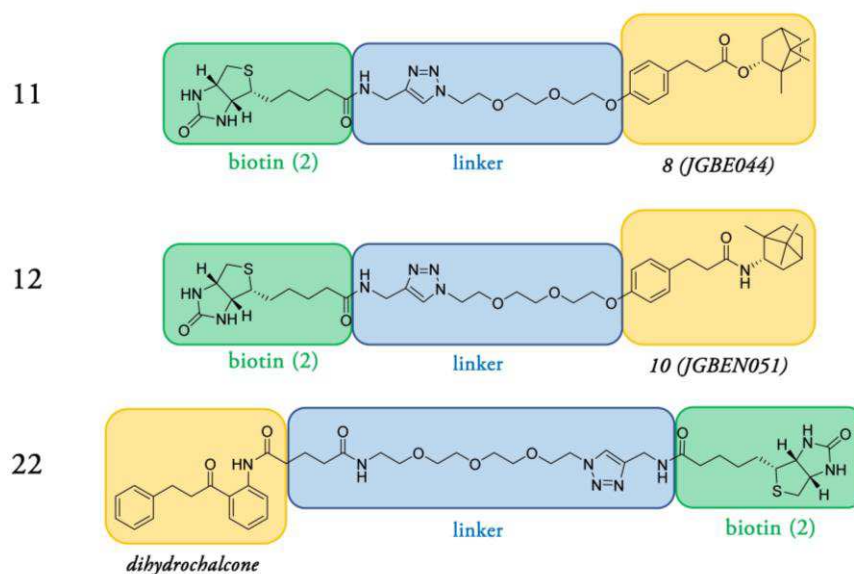


Figure 9. Overview of the synthesized biotin (**2**)-labeled probes of antileishmanial compounds. Green: reporter unit/biotin (**2**), blue: PEG-linker, orange: antileishmanial compound. The orientation of compound **22** is presented inversely to illustrate that the attachment point, in contrast to the other probes, is situated on the opposing side of the inhibitor moiety.

#### 1.4 Design and Synthesis of Biotinylated Probes 11 and 12

In the design of the biotinylated probes, biotin (**2**) and the drug moiety were mainly determined. Still, the type of the linker and its attachment point were to be chosen. Hence, a short polyethylene glycol (PEG) chain was selected to ensure good water solubility (cf. Scheme 1). Short PEG chains of different lengths are often used in chemical proteomics as a linker between the active molecule and the reporter unit, primarily because of their excellent solubility properties compared to alkyl chains.<sup>19, 89, 90</sup>

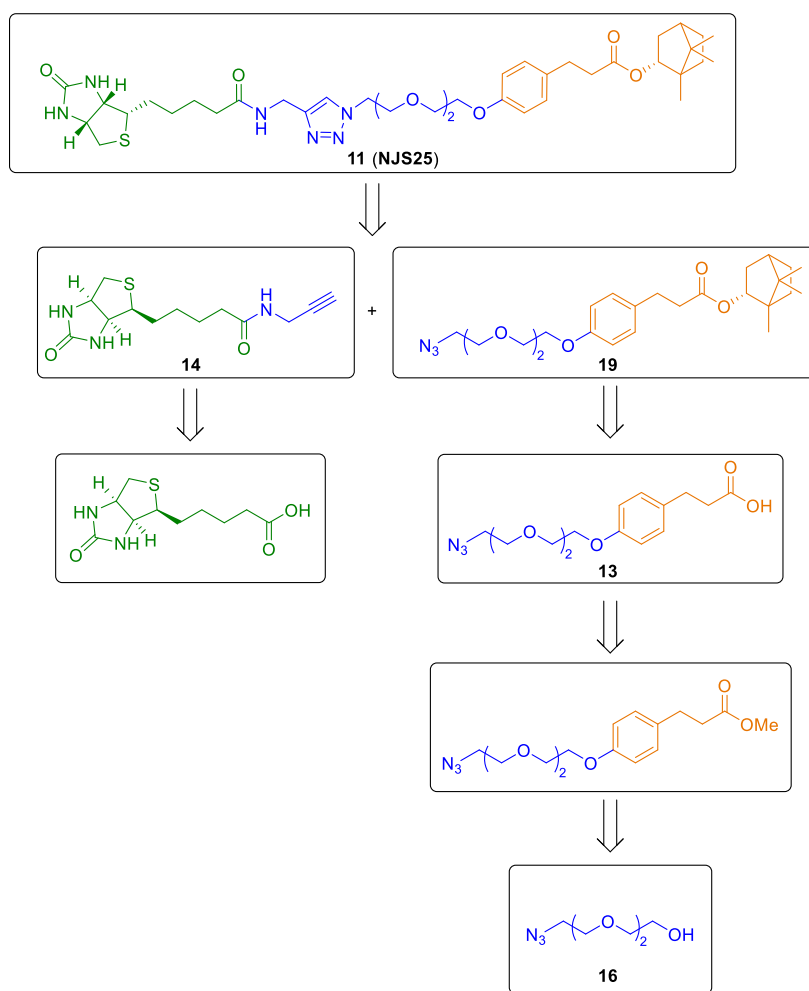
The attachment of the linker in *para* position of the active compound's benzene ring was selected to ensure the maximum possible distance of the linker from the remaining part of the active molecule. With this, the potential influence of the linker on the binding of the compound moiety to the target was to be minimized.

The Cu-catalyzed 'click reaction' and its logical precursors were chosen for their orthogonality towards esterifications and amidations (cf. Scheme 1). Moreover, if necessary, the azide intermediate could be easily functionalized with (commercially available) reporter groups other than biotin (**2**). Only recently, the inventors of click chemistry were awarded the *Nobel Prize in Chemistry*.<sup>91</sup> This type of synthesis has made its way into a wide range of chemical and biological applications, primarily as it can be carried out under mild conditions with (bio)orthogonal

precursors and nearly no by-products.<sup>91</sup>

The late formation of the borneol ester bond allows a late variation in case other bulky residues should be tested, which were also investigated by J. Glaser.<sup>78</sup> In addition, a photo-reactive group could be added to this position if an ABPP concept was to be tested.<sup>19, 25</sup>

Scheme 1. Retrosynthetic approach for the synthesis of **11**. Green: reporter unit/biotin (**2**), blue: PEG-linker, orange: antileishmanial compound.



The probes **11** (*NJS25*) and **12** (*NJS28*) were each prepared in six steps (see Scheme 2). Variation of the borneol (**9**) residue took place using the shared intermediate **13**. Biotin alkyne **14** was to be used to synthesize all aimed probes.

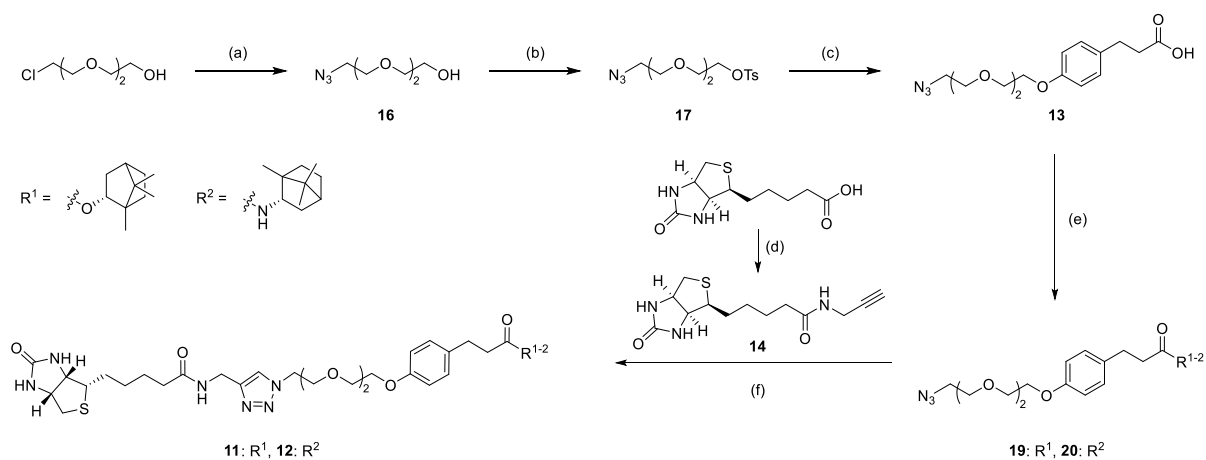
Starting with 2-(2-(2-chloroethoxy)ethoxy)ethan-1-ol (**15**), the azide group was introduced in an  $S_N2$  reaction using sodium azide, giving **16**. After transforming the alcohol group into the better tosylate leaving group of **17**, the ether bond connecting the PEG<sub>2</sub>-linker and the aromatic of methyl 3-(4-hydroxyphenyl)propanoate (**18**) was established using potassium carbonate. The methoxy ester protecting group was removed by basic saponification using lithium hydroxide to give the

shared intermediate **13**. Based on this shared precursor, borneol ester **19** and borneol amide **20** were synthesized separately. In the case of the ester **19**, **13** was reacted with (–)-borneol (**9**), DCC, and DMAP in a Steglich esterification. To obtain the amide analog **20**, **13** was amide-coupled with *R*-(+)-bornylamine (**21**), using DCC and HOBT. Biotin alkyne **14** was prepared by amide-coupling (+)-biotin (**2**) with propargylamine using EDC·HCl and HOBT according to P. Nagl.<sup>92</sup>

In the final step, the azide derivatives **19** and **20** were each ‘clicked’ with biotin alkyne **14** to give the final compounds **11** and **12**. The applied Cu-catalyzed click reaction was catalyzed by addition of the catalyst tris(benzyltriazolylmethyl)amine (TBTA). The TBTA ligand promotes catalysis presumably by stabilizing the copper(I)-oxidation state while allowing the catalytic cycle of the CuAAC reaction to propagate.<sup>93</sup> The overall yield for probe **11** was 4%, respectively 6% for **12**.

Application of the probes in target fishing is still pending to date. The developed probes may, however, serve as valuable tools to elucidate the target(s) of antileishmanial and antischistosomal compounds derived from *Valeriana wallichii* using chemical proteomics in the future.

Scheme 2. Synthesis of biotinylated probes **11** and **12**.



**Reagents and conditions:** (a)  $\text{NaN}_3$ , DMF, 85 °C, 6 h, > 99%; (b) TsCl, DIPEA, DCM, 0 °C  $\rightarrow$  rt, 1 d, 77%; (c) i) methyl 3-(4-hydroxyphenyl)propanoate (**18**),  $\text{K}_2\text{CO}_3$ , DMF, rt (16 h), 65 °C (9 h), 35%, ii) LiOH, THF/MeOH/ $\text{H}_2\text{O}$  = 3:1:1, rt, 4 d, > 99%; (d) propargylamine, EDC·HCl, HOBT, DMF 0 °C  $\rightarrow$  rt, 1 d, 73%; (e) esterification: (–)-borneol, DCC, DMAP, DCM, rt, 1 d, 43%; amidation: (*R*)-(+)-bornylamine (**21**), DCC, HOBT, DCM, rt, 1 d, 45%; (f) sodium ascorbate,  $\text{CuSO}_4 \cdot 5 \text{H}_2\text{O}$ , TBTA, DMF, rt, 2 d, 54% (**11**), 75% (**12**). Overall yield of **11** synthesis: 4%, overall yield for **12**: 6%.

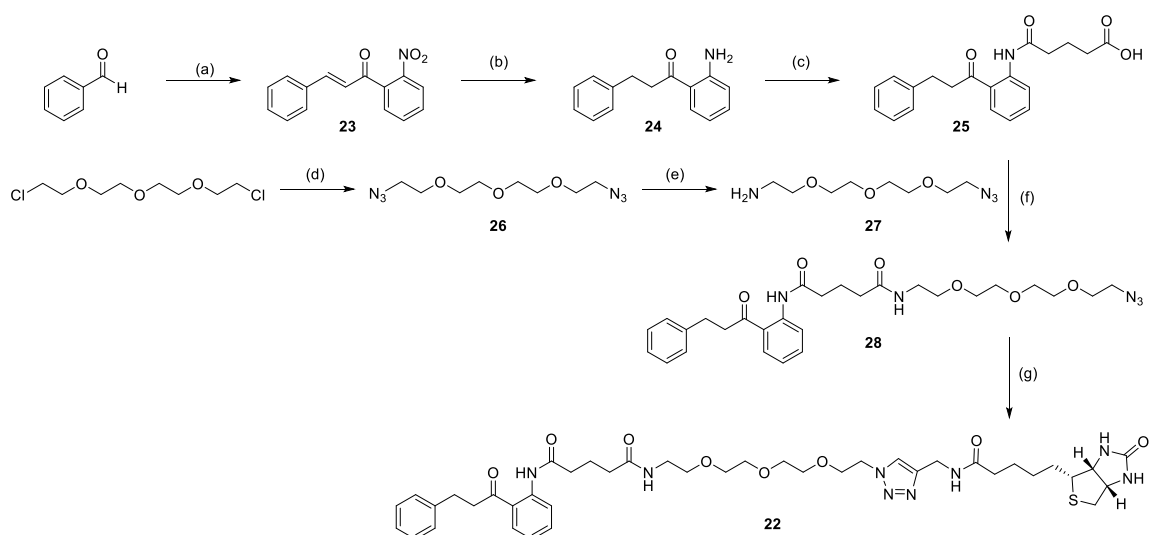
### 1.5 Design and Synthesis of Biotinylated Probe 22

Since the target(s) and binding mode(s) were not yet known, a further probe was to be developed possessing the point of linker attachment at the site of the active substances' bulky residues. If the probes **11** and **12** would be sterically hindered from binding to the target by their linker, probe **22**

(cf. Scheme 3) could potentially serve as an alternative. J. Glaser also tested aromatic residues at this position, which exhibited activity against *L. major* promastigotes and *L. donovani* promastigotes.<sup>74</sup> Thus, a dihydrochalcone backbone was chosen to ensure synthetic feasibility. In addition, thereby, the ester was substituted with a ketone, increasing stability.

In the first step, benzaldehyde and 2'-nitroacetophenone were coupled in a basic aldol condensation reaction to give chalcone **23** (cf. Scheme 3). Subsequently, the double bond and the nitro group were reduced under a hydrogen atmosphere of 1 atm and palladium catalysis to give dihydrochalcone **24**. The amide bond was established by reaction of the primary amino group of **24** with glutaric anhydride under ring opening to provide carboxylic acid **25**. The PEG<sub>3</sub> linker was synthesized starting with bis[2-(2-chloroethoxy)ethyl]ether in an S<sub>N</sub>2 reaction with sodium azide. One azide group of PEG-diazidotriethylene glycol (**26**) was then selectively reduced in a Staudinger reaction with equimolar amounts of **26** and triphenylphosphane. Carboxylic acid **25** and PEG<sub>3</sub>-linker **27** were amide-coupled using DCC and HOBT. In the final step, the azide derivative **28** and biotin alkyne **14** were coupled in a click reaction to give probe **22**. The overall yield for **22** was 3%. Probe **22** may prove a useful additional tool for target deconvolution of the studied antileishmanial and antischistosomal compounds if **11** and **12** do not exhibit the desired binding to the target(s).

**Scheme 3.** Synthesis scheme for biotinylated probe **22**.



**Reagents and conditions:** (a) 2'-nitroacetophenone, NaOH, MeOH/H<sub>2</sub>O (16:1), rt, 4 h, 96%; (b) Pd/C, THF, H<sub>2</sub> (1 atm), rt, 6 h, 46%; (c) glutaric anhydride, DCM, rt, 4 d, 50%; (d) NaN<sub>3</sub>, DMF, 80 °C, 18 h, 92%; (e) PPh<sub>3</sub>, dil. HCl, Et<sub>2</sub>O, 2 d, 74%; (f) HOBT, DCC, DCM, rt, 1 d, 50%; (g) biotin alkyne **14**, sodium ascorbate, CuSO<sub>4</sub> · 5H<sub>2</sub>O, TBTA, DMF, rt, 3 d, 37%. Overall yield: 3%.

## 1.6 General Experimental Procedures and Equipment

The general experimental procedures and equipment used in this study have been previously described in detail in the submitted manuscript of [Scheuplein, N. J.; Bzdyl, N. M.; Lohr, T.; Kibble, E. A.; Hasenkopf, A.; Sarkar-Tyson, M.; Holzgrabe, Ulrike. *Analysis of Structure–Activity–Relationships of Novel Inhibitors of the Macrophage Infectivity Potentiator (Mip) Proteins of Neisseria meningitidis, Neisseria gonorrhoeae, and Burkholderia pseudomallei. unpublished results 2023*]. The article is given in subchapter III\_4. The following four sites closely follow the published article, with modifications and extensions as appropriate for this study. All credit for the original methodology and equipment is attributed to the authors of the cited article.

**General.** Reagents used for the synthesis were obtained from *Alfa Aesar* (Ward Hill, USA), *Merck* (Darmstadt, Germany), *Avantor* (Darmstadt, Germany), *TCI Deutschland GmbH* (Eschborn, Germany), *Fisher Scientific* (Schwerte, Germany), and *ABCR* (Karlsruhe, Germany). The purchased chemicals were used without further purification. Dry solvents for organic synthesis were produced and stored according to general procedures.<sup>94</sup> All syntheses were performed under an argon or nitrogen protective atmosphere using Schlenk technique.

**Flash chromatography.** For purification by medium pressure liquid chromatography (MPLC, flash chromatography), a *puriFlash<sup>®</sup>430* system from *Interchim* (Montluçon, France) with an integrated UV diode array detector (DAD) covering a scanning range of 200 – 600 nm was used. Non-UV-active compounds were detected using a *Flash-ELSD* (evaporative light scattering detector) version 2011 from *Interchim* (Montluçon, France). The following pre-packed columns were used: *Chromabond Flash*, type: RS15 C18 ec, 16 g from *Macherey-Nagel* (Düren, Germany); *puriFlash*, type: SI-Std (IR-50SI), 12 g and 25 g from *Interchim* (Montluçon, France); and *FlashPure EcoFlex*, type: alumina neutral, 24 g from *Büchi Labortechnik AG* (Flawil, Switzerland). One of the following methods was typically used: SiO<sub>2</sub>, A: PE, B: EA, gradient: 0→100% B; SiO<sub>2</sub>, A: DCM, B: MeOH, gradient: 0→30% B; RP 18, A: H<sub>2</sub>O + 1% FA, B: MeOH + 1% FA, gradient: 5→100% B.

For each specific compound and its corresponding flash chromatography method, only the initial and final percentages of the gradient are provided, in addition to the stationary and mobile phases. The detailed procedure for each compound can be described as follows:

- 0 – 5 min: Isocratic elution with the initial composition of mobile phase A and B
- 5 – 45 min: Gradient elution transitioning from the initial to the final ratio of mobile phase A and B
- 45 – 50 min: Isocratic elution with the final composition of mobile phase A and B

**Gravity-driven column chromatography.** For gravity-driven column chromatography, silica gel 60 (0.063–0.200 nm) purchased from *Merck* (Darmstadt, Germany) or basic aloxide 90 (0.050–0.200 nm) purchased from *Macherey-Nagel* (Düren, Germany) were used. The column packing was carried out ‘wet’. One of the following isocratic methods was typically used: SiO<sub>2</sub>, PE/EA = 3:1; SiO<sub>2</sub>, DCM/MeOH = 20:1; aloxide basic III, DCM/MeOH = 20:1.

**HPLC.** Purity analysis was carried out using an HPLC system from *Shimadzu Scientific instruments* (Kyoto, Japan). Mobile phase A was Milli-Q®-water with 0.1% formic acid (FA) added, while mobile phase B was MeOH with 0.1% FA. The gradient started with 5% of mobile phase B and the ratio of mobile phase B was increased to 100% over 8 min and held for 4 min. For re-equilibration, the mobile phase B ratio was reduced from 100% to 5% in another 4 min. Subsequently, the column was flushed with 5% B for 2 min. The flow rate was set to 1.0 mL/min. The injection volume was 20 µL. The UV signal at 254 nm was chosen for detection, the oven temperature was rt.

**Infrared Spectroscopy (IR).** IR spectra were recorded on a *Jasco-FT-IR-6100* system (*Jasco Deutschland GmbH*, Groß-Umstadt, Germany) in combination with a diamond ATR accessory. The wave numbers of characteristic absorption bands are given in [cm<sup>-1</sup>]. The intensities of the IR bands are abbreviated as follows: vs = very strong, s = strong, m = medium, and w = weak, br = broad.

**Mass spectrometry.** Electrospray ionization (ESI) mass spectra were measured with a *Shimadzu LCMS-2020* (*Shimadzu Scientific instruments*, Kyoto, Japan) in positive ion mode. Data are reported as mass-to-charge ratio (m/z) of the respective positively charged molecular ions.



**Melting points.** To determine melting points, an MP70 melting point system (*Mettler-Toledo GmbH*, Gießen, Germany) was used.

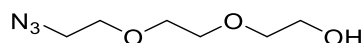
**Nuclear Magnetic Resonance Spectroscopy.**  $^1\text{H}$  (400.132 MHz) and  $^{13}\text{C}$  (100.613 MHz) NMR spectra were recorded on a Bruker AV 400 instrument (*Bruker Biospin*, Ettlingen, Germany) at a temperature of 300 K. The residual  $^1\text{H}$ -solvent signal (containing one less deuterium atom than the perdeuterated solvent) was used as an internal standard for  $^1\text{H}$  spectra. For  $^{13}\text{C}$  spectra, the solvent signals resulting from the  $^{13}\text{C}$  atoms in natural abundance in the perdeuterated solvent were used for calibration.  $\text{ACN-}d_3$ :  $^1\text{H}$ : 1.94 ppm,  $^{13}\text{C}$ : 1.32 ppm, 118.26 ppm;  $\text{CDCl}_3$ :  $^1\text{H}$ : 7.26 ppm,  $^{13}\text{C}$ : 77.16 ppm;  $\text{CD}_3\text{OD}$ :  $^1\text{H}$ : 3.31 ppm,  $^{13}\text{C}$ : 49.00 ppm;  $\text{DMSO-}d_6$ :  $^1\text{H}$ : 2.50 ppm,  $^{13}\text{C}$ : 39.52 ppm.<sup>95</sup> Abbreviations for multiplicity are: s, singlet; d, doublet; t, triplet; m, multiplet; br, broad; dd, doublet of doublets; ddd, doublet of doublets of doublets. MestReNova<sup>®</sup> (version 6.0.2-5475) software (*Mestrelab Research S.L.*, Santiago de Compostela, Spain) or Topspin<sup>®</sup> (version 3.2-pl7) software (*Bruker Biospin*, Ettlingen, Germany) was applied for processing of NMR spectra.

**Purity.** All purities of the compounds were verified by HPLC. All final compounds synthesized had purities above 95%.

**Solvents.** Dry solvents for organic synthesis were produced and stored according to general procedures.<sup>94</sup> Tetrahydrofuran (THF) was pre-dried over KOH and distilled over sodium. Dichloromethane (DCM) was dried over  $\text{CaCl}_2$  and then distilled.

**TLC.** Thin layer chromatography (TLC) was performed on pre-coated silica gel glass plates SIL G-25 or aluminum sheets coated with aluminum oxide ALUGRAM Alox N/UV254 from *Macherey-Nagel* (Düren, Germany). Spots were evidenced by quenching at 254 nm or intrinsic fluorescence at 365 nm. Staining reagents such as bromocresol green, *p*-anisaldehyde, ninhydrin, Dragendorff reagent, etc., were prepared according to the literature.<sup>96</sup>

## 1.7 Synthesis of the Biotin-Labeled Antileishmanial Compounds 11 and 12

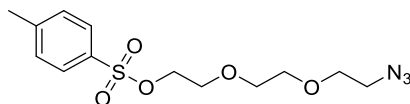
1.7.1 2-(2-(2-Azidoethoxy)ethoxy)ethan-1-ol (16; *NJS19*)

**Chemical Formula:** C<sub>6</sub>H<sub>13</sub>N<sub>3</sub>O<sub>3</sub>, **Molecular Weight:** 175.19 g/mol.

**16** was synthesized according to a modified protocol by *Gavrilyuk et al.*,<sup>97</sup> using 5.03 g of 2-(2-(2-chloroethoxy)ethoxy)ethan-1-ol (**15**; 29.8 mmol) and sodium azide (7.76 g, 119.3 mmol) in dry DMF (60 mL). After heating the mixture under reflux for 6 h, the reaction was allowed to cool to rt and stirred for another 16 h. The reaction was quenched with water (60 mL) and extracted with diethyl ether (3 · 40 mL). After separation of the phases, the solvent of the combined organic phases was removed *in vacuo*. The crude product was obtained as a colorless oil in a yield of 99% (5.22 g, 29.8 mmol, Lit.:<sup>97</sup> 89%).

**TLC:** R<sub>f</sub> = 0.28 (SiO<sub>2</sub>, PE/EtOAc = 2:3).

*The recorded spectra agree with the literature.*<sup>98, 99</sup>

1.7.2 2-(2-(2-Azidoethoxy)ethoxy)ethyl 4-methylbenzenesulfonate (17; *NJS20*)

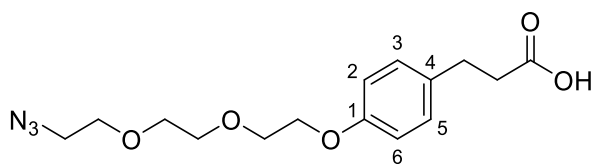
**Chemical Formula:** C<sub>13</sub>H<sub>19</sub>N<sub>3</sub>O<sub>5</sub>S, **Molecular Weight:** 329.37 g/mol.

**17** was synthesized analogous to *Hawkins et al.*<sup>100</sup>, using 4.90 g of **16** (28.0 mmol), *p*-toluenesulfonyl chloride (6.40 g, 33.6 mmol), and triethylamine (7.75 ml, 5.66 mg, 55.9 mmol) in dry DCM (50 mL). After stirring at rt for 1 d, the reaction mixture was worked up according to the literature.<sup>100</sup> Subsequent flash chromatography (SiO<sub>2</sub>, A: PE, B: <sup>i</sup>PrOH, gradient: 0 → 30% B) afforded **17** as a yellowish oil in a yield of 77% (7.13 g, 28.0 mmol; Lit.: 99%).

**TLC:** R<sub>f</sub> = 0.66 (SiO<sub>2</sub>, PE/<sup>i</sup>PrOH = 2:1).

*The recorded spectra agree with the literature.*<sup>99, 101</sup>

## 1.7.3 3-(4-(2-(2-(2-Azidoethoxy)ethoxy)ethoxy)phenyl)propanoic acid (13)



**Chemical Formula:** C<sub>15</sub>H<sub>21</sub>N<sub>3</sub>O<sub>5</sub>, **Molecular Weight:** 323.35 g/mol.

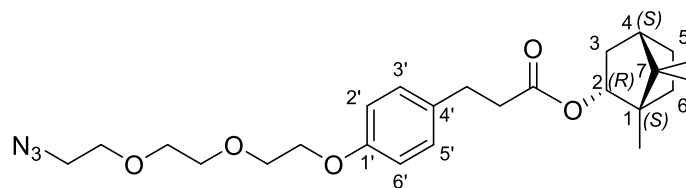
After stirring potassium carbonate (2.57 g, 18.6 mmol) and methyl 3-(4-hydroxyphenyl)propanoate (**18**; 2.02 g, 11.0 mmol) in dry DMF (50 mL) for 90 min at rt, **17** (2.78 g, 8.44 mmol) was added under ice cooling. The reaction was subsequently heated to 65°C and stirred for 10 h. The reaction mixture was allowed to cool to rt, solids were removed by filtration, and the solvent was removed *in vacuo*. After addition of water (30 mL), the mixture was extracted with DCM (150 mL), and the DCM phase was washed with water (2 × 30 mL). After separation of the phases, the organic solvent was again removed *in vacuo*, and the intermediate product was obtained as a slightly yellowish oil in a yield of 40% (1.00 g, 2.97 mmol). Subsequently, the intermediate product (900 mg, 2.67 mmol) was treated with a solution of lithium hydroxide (192 mg, 8.00 mmol) in a mixture of THF, MeOH, and water (30 mL/10 mL/10 mL) at rt. After stirring for 1 d, the organic solvents were removed *in vacuo*, and the aqueous phase was acidified with diluted hydrochloric acid (1 M, pH ≈ 0–1, 50 mL). The mixture was extracted with chloroform (3 · 100 mL) and washed with water (2 · 25 mL). The phases were separated, and the solvent of the combined organic phases was removed *in vacuo*. **13** was obtained quantitatively as a yellowish oily solid (860 mg, 2.67 mmol).

**TLC:** R<sub>f</sub> = 0.50 (SiO<sub>2</sub>, DCM/MeOH = 15:1)

**IR (ATR,  $\tilde{\nu}_{max}$  [cm<sup>-1</sup>]):** 3300–2500 (br), 3028 (w), 2921 (m), 2103 (s), 1697 (s), 1513 (s), 835 (m), 816 (m).

**<sup>1</sup>H NMR (CDCl<sub>3</sub>):** δ = 7.13–7.08 (m, 2H, CH-3,5), 6.87–6.82 (m, 2H, CH-2,6), 4.13–4.09 (m, 2H, PhOCH<sub>2</sub>), 3.87–3.83 (m, 2H, OCH<sub>2</sub>), 3.75–3.71 (m, 2H, OCH<sub>2</sub>), 3.70–3.66 (m, 4H, OCH<sub>2</sub>), 3.38 (t, <sup>3</sup>J = 5.1 Hz, 2H, CH<sub>2</sub>N<sub>3</sub>), 2.89 (t, <sup>3</sup>J = 7.7 Hz, 2H, PhCH<sub>2</sub>CH<sub>2</sub>COOH), 2.63 (t, <sup>3</sup>J = 7.7 Hz, PhCH<sub>2</sub>CH<sub>2</sub>COOH) ppm.

**<sup>13</sup>C NMR (CDCl<sub>3</sub>):** δ = 178.4 (1C, COOH), 157.5 (1C, C-1), 132.7 (1C, C-4), 129.3 (2C, CH-3,5), 114.9 (2C, CH-2,6), 71.0 (1C, OCH<sub>2</sub>), 70.9 (1C, OCH<sub>2</sub>), 70.2 (1C, OCH<sub>2</sub>), 70.0 (1C, OCH<sub>2</sub>), 67.6 (1C, PhOCH<sub>2</sub>), 50.8 (1C, CH<sub>2</sub>N<sub>3</sub>), 35.9 (1C, PhCH<sub>2</sub>CH<sub>2</sub>COOH), 29.9 (1C, PhCH<sub>2</sub>CH<sub>2</sub>COOH) ppm.

1.7.4 (1*S*,2*R*,4*S*)-1,7,7-Trimethylbicyclo[2.2.1]heptan-2-yl 3-(4-(2-(2-(2-azidoethoxy)ethoxy)ethoxy)phenyl)propanoate (**19**; *NJS24*)

**Chemical Formula:** C<sub>25</sub>H<sub>37</sub>N<sub>3</sub>O<sub>5</sub>, **Molecular Weight:** 459.59 g/mol.

**19** was synthesized according to general procedure A, using 275 mg of **13** (835 μmol), DMAP (163 mg, 1.34 mmol), DCC (190 mg, 919 μmol), and (–)-borneol (159 mg, 1.00 mmol) in dry DCM (40 mL). After stirring at rt for 1 d, the reaction was worked up according to the general procedure. The crude oily product was purified by flash chromatography (run 1: SiO<sub>2</sub>, 80 g, A: DCM, B: MeOH, gradient: 0→10% B; run 2: RP 18, 16 g, A: H<sub>2</sub>O, B: MeOH, gradient: 5→100% B). **19** was obtained as a colorless oil in a yield of 43% (165 mg, 359 μmol).

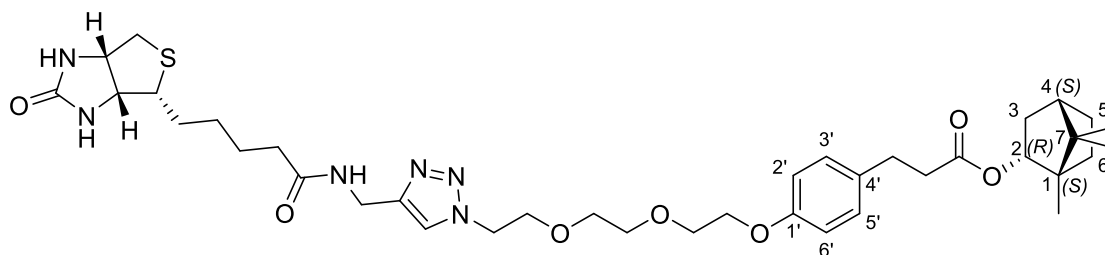
**TLC:** R<sub>f</sub> = 0.78 (SiO<sub>2</sub>, PE/EA = 1:2)

**IR (ATR,  $\tilde{\nu}_{max}$  [cm<sup>-1</sup>]):** 3030 (w), 2952 (s), 2925 (s), 2871 (s), 2099 (s), 1727 (vs), 1511 (vs), 1244 (vs), 1138 (vs), 1112 (vs), 824 (m).

**<sup>1</sup>H NMR (CDCl<sub>3</sub>):** δ = 7.11 (d, <sup>3</sup>J = 8.7 Hz, 2H, CH-3', 5'), 6.84 (d, <sup>3</sup>J = 8.7 Hz, 2H, CH-2', 6'), 4.86 (ddd, <sup>3</sup>J = 10.0, 3.4 Hz, <sup>4</sup>J = 2.2 Hz, 1H, CH-2), 4.10 (t, <sup>3</sup>J = 4.7 Hz, 2H, C-1'OCH<sub>2</sub>), 3.85 (t, <sup>3</sup>J = 4.7 Hz, 2H, C-1'OCH<sub>2</sub>CH<sub>2</sub>), 3.76–3.66 (m, 6H, OCH<sub>2</sub>), 3.38 (t, <sup>3</sup>J = 5.1 Hz, 2H, CH<sub>2</sub>N<sub>3</sub>), 2.90 (t, dd, <sup>3</sup>J = 8.2, 7.2 Hz, 2H, C-4'CH<sub>2</sub>CH<sub>2</sub>), 2.61 (dd, <sup>3</sup>J = 8.2, 7.2 Hz, 2H, C-4'CH<sub>2</sub>CH<sub>2</sub>), 2.37–2.27 (m, 1H, CH<sub>2</sub>-3), 1.92–1.84 (m, 1H, CH<sub>2</sub>-5), 1.77–1.66 (m, 1H, CH<sub>2</sub>-6), 1.67–1.61 (m, 1H, CH-4), 1.33–1.22 (m, 1H, CH<sub>2</sub>-5), 1.21–1.13 (m, 1H, CH<sub>2</sub>-6), 0.91–0.86 (m, 1H, CH<sub>2</sub>-3), 0.89 (s, 3H, C-7CH<sub>3</sub>), 0.86 (s, 3H, C-7CH<sub>3</sub>), 0.78 (s, 3H, C-1CH<sub>3</sub>) ppm.

**<sup>13</sup>C NMR (CDCl<sub>3</sub>):** δ = 173.4 (1C, COO), 157.4 (1C, C-1'), 133.0 (1C, C-4'), 129.3 (2C, CH-3', 5'), 114.8 (2C, CH-2', 6'), 80.0 (1C, CH-2), 71.0 (1C, OCH<sub>2</sub>), 70.9 (1C, OCH<sub>2</sub>), 70.2 (1C, OCH<sub>2</sub>), 70.0 (1C, OCH<sub>2</sub>), 67.6 (1C, C-1'OCH<sub>2</sub>), 50.8 (1C, OCH<sub>2</sub>CH<sub>2</sub>N<sub>3</sub>), 48.9 (1C, C-7), 47.9 (1C, C-1), 45.0 (1C, C-4), 36.9 (1C, CH<sub>2</sub>-3), 36.5 (1C, C-4'CH<sub>2</sub>CH<sub>2</sub>), 30.4 (1C, C-4'CH<sub>2</sub>CH<sub>2</sub>), 28.1 (1C, CH<sub>2</sub>-6), 27.2 (1C, CH<sub>2</sub>-5), 19.8 (1C, C-7CH<sub>3</sub>), 19.0 (1C, C-7CH<sub>3</sub>), 13.6 (1C, C-1CH<sub>3</sub>) ppm.

1.7.5 (2*R*)-1,7,7-Trimethylbicyclo[2.2.1]heptan-2-yl 3-(4-(2-(2-(2-(4-((5-((3*aR*,4*R*,6*aS*)-2-oxohexahydro-1*H*-thieno[3,4-*d*]imidazol-4-yl)pentanamido)methyl)-1*H*-1,2,3-triazol-1-yl)ethoxy)ethoxy)ethoxy)phenyl)propanoate (11; NJS25)



**Chemical Formula:** C<sub>38</sub>H<sub>56</sub>N<sub>6</sub>O<sub>7</sub>S, **Molecular Weight:** 740.96 g/mol.

Analogous to Donnelly *et al.*,<sup>93</sup> to a solution of **19** (150 mg, 326 μmol) in dry DMF (15 mL), was added sodium ascorbate (12.3 mg, 62.0 μmol), copper(II) sulfate pentahydrate (4.9 mg, 19.6 μmol), tris((1-benzyl-4-triazolyl)methyl)amine (TBTA, 12.1 mg 22.8 μmol), and biotin propargylamide (**14**; 91.8 mg, 326 μmol) at rt and stirred for 3 d. Subsequently, the copper ions were removed using the ion exchanger Amberlite IRC-718 (4.0 g) for 90 min at rt. After removing the ion exchanger by filtration, the solvent was removed *in vacuo*. The crude oily product was purified by flash chromatography (RP 18, A: H<sub>2</sub>O, B: MeOH, gradient: 5→100% B) to give **11** as a white solid in a yield of 54% (130 mg, 175 μmol).

**TLC:** R<sub>f</sub> = 0.26 (SiO<sub>2</sub>, DCM/MeOH = 8:1)

**Melting Point:** 115 °C

**IR (ATR,  $\tilde{\nu}_{max}$  [cm<sup>-1</sup>]):** 3281 (br s), 3080 (m), 2952 (s), 2925 (s), 2872 (s), 1730 (m), 1692 (vs), 1654 (s), 1511 (s), 1244 (s), 821 (m).

**Purity (HPLC):** >95%

**<sup>1</sup>H NMR (CD<sub>3</sub>CN):** δ = 7.70 (s, 1H, CH<sub>triazole</sub>), 7.13 (d, <sup>3</sup>J = 8.6 Hz, 2H, CH-3', 5'), 6.94 (br s, 1H, NH<sub>amide</sub>), 6.83 (d, <sup>3</sup>J = 8.6 Hz, 2H, CH-2', 6'), 5.47 (br s, 1H, NH<sub>biotin</sub>), 5.19 (br s, 1H, NH<sub>biotin</sub>), 4.84–4.77 (m, 1H, CH-2), 4.46 (t, <sup>3</sup>J = 5.2 Hz, 2H, N<sub>triazole</sub>CH<sub>2</sub>CH<sub>2</sub>O), 4.42–4.37 (m, 1H, HNCH<sub>biotin</sub>), 4.35 (d, <sup>3</sup>J = 5.8 Hz, 2H, NHCH<sub>2</sub>C<sub>triazole</sub>), 4.24–4.19 (m, 1H, HNCH<sub>biotin</sub>), 4.07–4.01 (m, 2H, C-1'OCH<sub>2</sub>), 3.83 (t, <sup>3</sup>J = 5.2 Hz, 2H, N<sub>triazole</sub>CH<sub>2</sub>CH<sub>2</sub>O), 3.74–3.69 (m, 2H, OCH<sub>2</sub>CH<sub>2</sub>OC-1'), 3.60–3.54 (m, 4H, OCH<sub>2</sub>), 3.16–3.10 (m, 1H, SCH<sub>biotin</sub>H<sub>2</sub>), 2.90–2.82 (m, 3H, C-4'CH<sub>2</sub>CH<sub>2</sub>, SC<sub>biotin</sub>H<sub>2</sub>), 2.63 (d, 1H, <sup>2</sup>J = 13.0 Hz, SC<sub>biotin</sub>H<sub>2</sub>), 2.59 (t, <sup>3</sup>J = 7.5 Hz, 2H, C-4'CH<sub>2</sub>CH<sub>2</sub>), 2.31–2.27 (m, 1H, CH<sub>2</sub>-3), 2.14 (t, <sup>3</sup>J = 7.3 Hz, 2H, CH<sub>2</sub>CONH), 1.92–1.84 (m, 1H, CH<sub>2</sub>-5), 1.78–1.47 (m, 6H, CH<sub>2</sub>CH<sub>2</sub>CH<sub>2</sub>CH<sub>2</sub>CONH, CH-4, CH<sub>2</sub>-6),

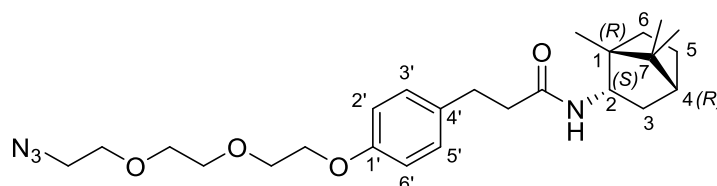
1.41–1.24 (m, 3H, CH<sub>2</sub>CH<sub>2</sub>CH<sub>2</sub>CONH, CH<sub>2</sub>-5), 1.21–1.13 (m, 1H, CH<sub>2</sub>-6), 0.89 (s, 3H, C-7CH<sub>3</sub>), 0.86 (s, 3H, C-7CH<sub>3</sub>), 0.84 (d, <sup>3</sup>J = 3.4 Hz, 1H, CH<sub>2</sub>-3), 0.77 (s, 3H, C-1CH<sub>3</sub>) ppm.

<sup>13</sup>C NMR (CD<sub>3</sub>CN): δ = 173.9 (1C, COO), 173.8 (1C, CONH), 164.1 (1C, CO<sub>biotin</sub>), 158.3 (1C, C-1'), 146.2 (1C, CH<sub>2</sub>CCH<sub>triazole</sub>), 134.1 (1C, C-4'), 130.4 (2C, CH-3', 5'), 123.9 (1C, CH<sub>triazole</sub>), 115.5 (2C, CH-2', 6'), 80.4 (1C, CH-2), 71.2 (1C, OCH<sub>2</sub>), 71.1 (1C, OCH<sub>2</sub>), 70.4 (1C, CH<sub>2</sub>CH<sub>2</sub>OC-1'), 70.1 (1C, N<sub>triazole</sub>CH<sub>2</sub>CH<sub>2</sub>O), 68.4 (1C, C-1'OCH<sub>2</sub>), 62.4 (1C, HNCH<sub>biotin</sub>), 60.9 (1C, HNCH<sub>biotin</sub>), 56.3 (1C, SCH<sub>biotin</sub>), 50.9 (1C, N<sub>triazole</sub>CH<sub>2</sub>CH<sub>2</sub>O), 49.5 (1C, C-7), 48.6 (1C, C-1), 45.8 (1C, C-4), 41.2 (1C, SC<sub>biotin</sub>H<sub>2</sub>), 37.4 (1C, CH<sub>2</sub>-3), 36.8 (1C, C-4'CH<sub>2</sub>CH<sub>2</sub>), 36.2 (1C, CH<sub>2</sub>CONH), 35.5 (1C, NHCH<sub>2</sub>C<sub>triazole</sub>), 30.8 (1C, C-4'CH<sub>2</sub>CH<sub>2</sub>), 29.03 (1C, SCHCH<sub>2</sub> biotin), 28.98 (1C, CH<sub>2</sub>-6), 28.6 (1C, CH<sub>2</sub>-5), 27.8 (1C, CH<sub>2</sub> biotin), 26.3 (1C, CH<sub>2</sub> biotin), 20.0 (1C, C-7CH<sub>3</sub>), 19.1 (1C, C-7CH<sub>3</sub>), 13.8 (1C, C-1CH<sub>3</sub>) ppm.

LC/MS (m/z): 741.30 [M+H]<sup>+</sup>.

*Biotin propargylamide (14)* was prepared according to P. Nagl.<sup>92, 99</sup>

#### 1.7.6 3-(4-(2-(2-(2-Azidoethoxy)ethoxy)ethoxy)phenyl)-N-((1S,2R,4S)-1,7,7-trimethylbicyclo[2.2.1]heptan-2-yl)propanamide (20; NJS26)



**Chemical Formula:** C<sub>25</sub>H<sub>38</sub>N<sub>4</sub>O<sub>4</sub>, **Molecular Weight:** 458.60 g/mol.

**20** was synthesized according to general procedure A, using 230 mg of **13** (711 μmol), (*R*)-(+)-bornylamine (**21**; 109 mg, 711 μmol), HOBt (154 mg, 1.14 mmol), and DCC (161 mg, 782 μmol) in dry DCM (35 mL). After stirring at rt for 1d, the reaction was worked up according to the general procedure. The crude oily product was purified by flash chromatography (run 1: SiO<sub>2</sub>, 80 g, A: DCM, B: MeOH, gradient, 3→20% B; run 2: RP 18, 25 g, A: H<sub>2</sub>O, B: MeOH, gradient: 30→100% B) to obtain **20** as a white oily solid in a yield of 45% (147 mg, 321 μmol).

TLC: R<sub>f</sub> = 0.65 (DCM/MeOH = 19:1)

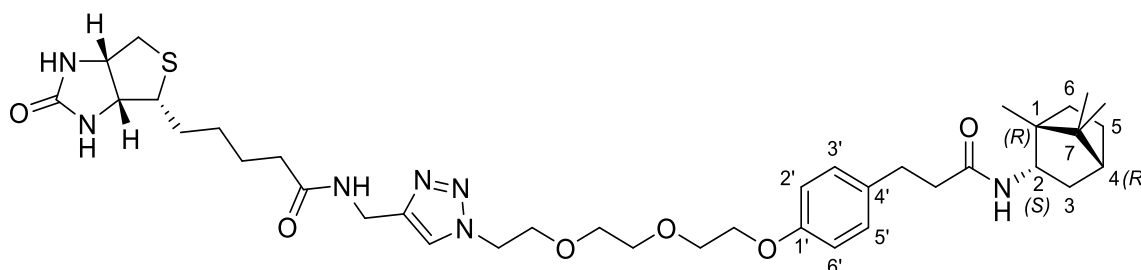
IR (ATR,  $\tilde{\nu}_{max}$  [cm<sup>-1</sup>]): 3306 (m), 3033 (w), 2950 (s), 2925 (s), 2874 (s), 2098 (s), 1638 (vs), 1542 (s), 1510 (vs), 1243 (vs), 1117 (vs), 822 (m).

<sup>1</sup>H NMR (CDCl<sub>3</sub>): δ = 7.12 (d, <sup>3</sup>J = 8.6 Hz, 2H, CH-3', 5'), 6.84 (d, <sup>3</sup>J = 8.6 Hz, 2H, CH-2', 6'),

5.32 (d,  $^3J = 8.4$  Hz, 1H, *NH*), 4.23–4.15 (m, 1H, *CH*-2), 4.12–4.08 (m, 2H, C-1'*OCH*<sub>2</sub>), 3.87–3.83 (m, 2H, C-1'*OCH*<sub>2</sub>*CH*<sub>2</sub>), 3.75–3.66 (m, 6H, *OCH*<sub>2</sub>), 3.38 (t,  $^3J = 5.1$  Hz, 2H, *CH*<sub>2</sub>*N*<sub>3</sub>), 2.90 (t,  $^3J = 7.4$  Hz, 2H, C-4'*CH*<sub>2</sub>*CH*<sub>2</sub>), 2.47 (t,  $^3J = 7.4$  Hz, 2H, C-4'*CH*<sub>2</sub>*CH*<sub>2</sub>), 2.34–2.24 (m, 1H, *CH*<sub>2</sub>-3), 1.76–1.66 (m, 1H, *CH*<sub>2</sub>-6), 1.61 (t,  $^3J = 4.5$  Hz, 1H, *CH*-4), 1.33–1.18 (m, 2H, *CH*<sub>2</sub>-5), 1.09–1.01 (m, 1H, *CH*<sub>2</sub>-6), 0.91 (s, 3H, C-7-*CH*<sub>3</sub>), 0.84 (s, 3H, C-7-*CH*<sub>3</sub>), 0.73 (s, 3H, C-1-*CH*<sub>3</sub>), 0.63 (dd,  $^2J = 13.4$ ,  $^3J = 4.5$  Hz, 1H, *CH*<sub>2</sub>-3) ppm.

<sup>13</sup>C NMR (CDCl<sub>3</sub>):  $\delta = 172.3$  (1C, CONH), 157.4 (1C, C-1'), 133.3 (1C, C-4'), 129.5 (2C, *CH*-3', 5'), 114.9 (2C, *CH*-2', 6'), 71.0 (1C, *OCH*<sub>2</sub>), 70.9 (1C, *OCH*<sub>2</sub>), 70.2 (1C, *OCH*<sub>2</sub>), 70.0 (1C, *OCH*<sub>2</sub>), 67.7 (1C, C-1'*OCH*<sub>2</sub>), 53.8 (1C, *CH*-2), 50.8 (1C, *OCH*<sub>2</sub>*CH*<sub>2</sub>*N*<sub>3</sub>), 49.4 (1C, C-1), 48.2 (1C, C-7), 45.0 (1C, C-4), 39.1 (1C, C-4'*CH*<sub>2</sub>*CH*<sub>2</sub>), 37.8 (1C, *CH*<sub>2</sub>-3), 31.2 (1C, C-4'*CH*<sub>2</sub>*CH*<sub>2</sub>), 28.4 (1C, *CH*<sub>2</sub>-6), 28.0 (1C, *CH*<sub>2</sub>-5), 19.9 (1C, C-7*CH*<sub>3</sub>), 18.8 (1C, C-7*CH*<sub>3</sub>), 13.7 (1C, C-1*CH*<sub>3</sub>) ppm.

1.7.7 *N*-((1-(2-(2-(2-(4-(3-Oxo-3-(((2*S*)-1,7,7-trimethylbicyclo[2.2.1]heptan-2-yl)-amino)propyl)phenoxy)ethoxy)ethoxy)ethyl)-1*H*-1,2,3-triazol-4-yl)methyl)-5-(((3*aR*,4*R*,6*aS*)-2-oxohexahydro-1*H*-thieno[3,4-*d*]imidazol-4-yl)pentanamide (12; NJS28)



Chemical Formula: C<sub>38</sub>H<sub>57</sub>N<sub>7</sub>O<sub>6</sub>S, Molecular Weight: 739.98 g/mol.

Analogous to Donnelly *et al.*,<sup>93</sup> to a solution of **20** (110 mg, 240  $\mu$ mol) in dry DMF (15 mL), sodium ascorbate (9.0 mg, 45.6  $\mu$ mol), copper(II) sulfate pentahydrate (4 mg, 14.4  $\mu$ mol), TBTA (9.0 mg, 16.8  $\mu$ mol), and biotin propargylamide (**14**; 68 mg, 240  $\mu$ mol) were added at rt and stirred for 3 d. Subsequently, the copper ions were removed using the ion exchanger Amberlite IRC-718 (5.0 g) for 90 min at rt. After removing the ion exchanger by filtration, the solvent was removed *in vacuo*. The crude oily product was purified by flash chromatography (RP 18, A: H<sub>2</sub>O, B: MeOH, gradient: 5  $\rightarrow$  100% B) to give **12** as a white solid in a yield of 73% (130 mg, 176  $\mu$ mol).

**TLC:**  $R_f = 0.25$  (SiO<sub>2</sub>, DCM/MeOH = 8:1)  
**Melting Point:** 97 °C  
**Purity (HPLC):** 95.7%,  $t_R = 10.1$  min  
**IR (ATR,  $\tilde{\nu}_{max}$  [cm<sup>-1</sup>]):** 3287 (br, m), 3071 (w), 2921 (s), 2872 (m), 1696 (s), 1638 (s), 1540 (s), 1510 (s), 822 (w).

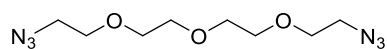
**<sup>1</sup>H NMR (CD<sub>3</sub>CN):**  $\delta = 7.71$  (s, 1H, CH<sub>triazole</sub>), 7.13 (d, <sup>3</sup>J = 8.5 Hz, 2H, CH-3', 5'), 7.02 (br s, 1H, C<sub>triazole</sub>CH<sub>2</sub>NHCO), 6.82 (d, <sup>3</sup>J = 8.5 Hz, 2H, CH-2', 6'), 6.45–6.38 (m, 1H, CONHCH-2), 5.43 (br s, 1H, NH<sub>biotin</sub>), 5.20 (br s, 1H, NH<sub>biotin</sub>), 4.46 (t, <sup>3</sup>J = 5.2 Hz, 2H, N<sub>triazole</sub>CH<sub>2</sub>CH<sub>2</sub>O), 4.43–4.38 (m, 1H, CH<sub>biotin</sub>), 4.34 (d, <sup>3</sup>J = 5.8 Hz, 2H, NHCH<sub>2</sub>C<sub>triazole</sub>), 4.24–4.19 (m, 1H, CH<sub>biotin</sub>), 4.15–4.07 (m, 1H, CH-2), 4.06–4.02 (m, 2H, CH<sub>2</sub>OC-1'), 3.83 (t, <sup>3</sup>J = 5.2 Hz, 2H, N<sub>triazole</sub>CH<sub>2</sub>CH<sub>2</sub>O), 3.74–3.69 (m, 2H, OCH<sub>2</sub>CH<sub>2</sub>OC-1'), 3.60–3.54 (m, 4H, CH<sub>2</sub>OCH<sub>2</sub>CH<sub>2</sub>OCH<sub>2</sub>), 3.16–3.10 (m, 1H, SCH<sub>biotin</sub>), 2.87 (dd, <sup>2</sup>J = 12.7, <sup>3</sup>J = 5.0 Hz, 1H, SC<sub>biotin</sub>H<sub>2</sub>), 2.81 (t, <sup>3</sup>J = 7.6 Hz, 2H, C-4'CH<sub>2</sub>CH<sub>2</sub>), 2.63 (d, 1H, <sup>2</sup>J = 12.7 Hz, SC<sub>biotin</sub>H<sub>2</sub>), 2.47–2.41 (m, 2H, C-4'CH<sub>2</sub>CH<sub>2</sub>), 2.19–2.15 (m, 1H, CH<sub>2</sub>-3), 2.15 (t, <sup>3</sup>J = 7.4 Hz, 2H, C<sub>biotin</sub>H<sub>2</sub>CONH), 1.73–1.45 (m, 7H, CH<sub>2</sub> biotin CH<sub>2</sub>CH<sub>2</sub>CH<sub>2</sub> biotin CONH, CH-4, CH<sub>2</sub>-5, CH<sub>2</sub>-6), 1.41–1.20 (m, 4H, CH<sub>2</sub>CH<sub>2</sub> biotin CH<sub>2</sub>CH<sub>2</sub>CONH, CH<sub>2</sub>-5, CH<sub>2</sub>-6), 0.91 (s, 3H, C-7CH<sub>3</sub>), 0.84 (s, 3H, C-7CH<sub>3</sub>), 0.79–0.73 (m, 1H, CH<sub>2</sub>-3), 0.67 (s, 3H, C-1CH<sub>3</sub>) ppm.

**<sup>13</sup>C NMR (CD<sub>3</sub>CN):**  $\delta = 173.9$  (1C, CONH), 173.2 (1C, CONH), 164.0 (1C, NHCO<sub>biotin</sub>NH), 158.0 (1C, C-1'), 146.0 (1C, C<sub>triazole</sub>CH), 134.5 (1C, C-4'), 130.3 (2C, CH-3', 5'), 123.9 (1C, CCH<sub>triazole</sub>N), 115.3 (2C, CH-2', 6'), 71.03 (1C, N<sub>triazole</sub>CH<sub>2</sub>CH<sub>2</sub>OCH<sub>2</sub>CH<sub>2</sub>), 70.98 (1C, N<sub>triazole</sub>CH<sub>2</sub>CH<sub>2</sub>OCH<sub>2</sub>CH<sub>2</sub>), 70.2 (1C, CH<sub>2</sub>CH<sub>2</sub>OC-1'), 69.9 (s, N<sub>triazole</sub>CH<sub>2</sub>CH<sub>2</sub>O), 68.3 (1C, C-1'OCH<sub>2</sub>), 62.3 (1C, HNCH<sub>biotin</sub>), 60.8 (1C, HNCH<sub>biotin</sub>), 56.2 (1C, SCH<sub>biotin</sub>), 54.3 (1C, CH-2), 50.8 (1C, N<sub>triazole</sub>CH<sub>2</sub>CH<sub>2</sub>O), 50.1 (1C, C-7), 48.8 (1C, C-1), 45.8 (1C, C-4), 41.0 (1C, SCH<sub>2</sub> biotin), 38.8 (1C, C-4'CH<sub>2</sub>CH<sub>2</sub>), 37.1 (1C, CH<sub>2</sub>-3), 36.1 (1C, CH<sub>2</sub> biotin CONH), 35.3 (1C, NHCH<sub>2</sub>C<sub>triazole</sub>), 31.7 (1C, C-4'CH<sub>2</sub>CH<sub>2</sub>), 28.92 (1C, SCHCH<sub>2</sub> biotin), 28.85 (1C, CH<sub>2</sub>-6), 28.6 (1C, CH<sub>2</sub>-5), 28.4 (1C, CH<sub>2</sub> biotin CH<sub>2</sub>CH<sub>2</sub>CONH), 26.2 (1C, CH<sub>2</sub>CH<sub>2</sub> biotin CH<sub>2</sub>CONH), 20.0 (1C, C-7CH<sub>3</sub>), 18.8 (1C, C-7CH<sub>3</sub>), 14.0 (1C, C-1CH<sub>3</sub>) ppm.

**LC/MS (m/z):** 740.20 [M+H]<sup>+</sup>, 370.70 [M+2H]<sup>2+</sup>.



## 1.8 Synthesis of the Biotin-Labeled Antileishmanial Compound 22

1.8.1 1-Azido-2-(2-(2-(2-azidoethoxy)ethoxy)ethoxy)ethane (26; *NJS32*)

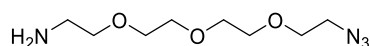
**Chemical Formula:** C<sub>8</sub>H<sub>16</sub>N<sub>6</sub>O<sub>3</sub>, **Molecular Weight:** 244.26 g/mol.

**26** was synthesized according to Risseuw *et al.*<sup>102</sup>, using bis[2-(2-chloroethoxy)ethyl]ether (5.30 g, 22.9 mmol) and sodium azide (5.96 g, 92.0 mmol) in dry dimethylformamide (100 mL). The reaction mixture was stirred at 80 °C for 18 h, whereas the reaction solution turned bluish after a few minutes. The reaction was completed for 2 d at rt. The solvent was removed *in vacuo*, the residue was taken up in diethyl ether (100 mL), and the suspension was filtered. The residue was washed with diethyl ether and ethyl acetate (100 mL each). The filtrate was washed with water (3 · 50 mL), the phases were separated, and the organic solvent was removed *in vacuo*. The product was obtained as a slightly yellowish oil in a yield of 92% (5.14 g, 21.0 mmol, Lit.:<sup>102</sup> 98%).

**TLC:** R<sub>f</sub> = 0.79 (SiO<sub>2</sub>, PE/<sup>i</sup>PrOH = 2:1).

**IR (ATR,  $\tilde{\nu}_{max}$  [cm<sup>-1</sup>]):** 2866 (s), 2091 (s), 1441 (m), 1345 (m), 1283 (s), 1116 (s), 934 (m), 851 (m), 645 (w).

*The analytical data are in agreement with the literature.*<sup>102</sup>

1.8.2 2-(2-(2-(2-Azidoethoxy)ethoxy)ethoxy)ethan-1-amine (27; *NJS34*)

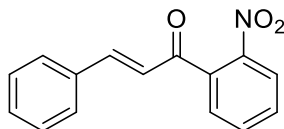
**Chemical Formula:** C<sub>8</sub>H<sub>18</sub>N<sub>4</sub>O<sub>3</sub>, **Molecular Weight:** 218.26 g/mol.

**27** was synthesized analogous to Risseuw *et al.*,<sup>102</sup> using 5.00 g of **26** (20.5 mmol) in a mixture of diethyl ether (80 mL) and diluted hydrochloric acid (0.7 M, 80 mL). To this solution was slowly added a solution of triphenylphosphane (5.40 g, 20.5 mmol) in 50 mL diethyl ether at rt, and the reaction mixture was stirred at rt for 2 d. The phases were separated, and the acidic aqueous phase was washed with diethyl ether (3 × 100 mL). The phases were again separated, and the aqueous phase was adjusted to pH 11 with aqueous sodium hydroxide solution (3 M) under cooling and extracted with DCM (3 × 100 mL). The phases were separated and the solvent of the combined organic phases was removed *in vacuo*. **27** was obtained as a colorless oil in a yield of 74% (3.31 g 15.2 mmol, Lit.:<sup>102</sup> 88%).

**TLC:**  $R_f = 0.68$  ( $\text{SiO}_2$ , PE/ $i$ PrOH = 6:1).

*The analytical data are in agreement with Goncalves et al. and Risseuw et al.*<sup>102, 103</sup>

### 1.8.3 (*E*)-1-(2-Nitrophenyl)-3-phenylprop-2-en-1-one (**23**; *NJS27*)



**Chemical Formula:**  $\text{C}_{15}\text{H}_{11}\text{NO}_3$ , **Molecular Weight:** 253.26 g/mol.

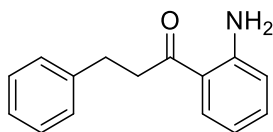
According to a protocol by Sun *et al.*,<sup>104</sup> to a solution of sodium hydroxide (1.26 g, 31.5 mmol) in a methanol/water mixture (85 mL, 16:1) was added 2'-nitroacetophenone (4.00 g, 24.2 mmol) at rt. After 5 min, benzaldehyde (2.83 g, 26.6 mmol) was added to the reaction mixture, forming a beige precipitate after 5 min. After 4 h, 50 mL of a saturated aqueous  $\text{NH}_4\text{Cl}$  solution was added to the reaction mixture, the precipitate was filtered off and washed with water (2 · 20 mL) and with cold methanol (10 mL). Residual solvent was removed *in vacuo* and **23** was obtained as a light beige solid in a yield of 96% (5.87 g, 23.3 mmol, Lit.:<sup>105</sup> 95%).

**TLC:**  $R_f = 0.66$  ( $\text{SiO}_2$ , DCM, *p*-anisaldehyde)

**Melting point:** 125 °C (Lit.:<sup>105</sup> 125–127 °C)

*The recorded spectra are in agreement with those of Kirubavathy et al.*<sup>106</sup> and Bunce *et al.*<sup>105</sup>

### 1.8.4 1-(2-Aminophenyl)-3-phenylpropan-1-one (**24**; *NJS29*)



**Chemical Formula:**  $\text{C}_{15}\text{H}_{15}\text{NO}$ , **Molecular Weight:** 225.29 g/mol.

Analogous to Bradshaw *et al.*,<sup>107</sup> to a suspension of palladium on charcoal (600 mg, 10-wt%, 0.56 mmol) in THF (50 mL) was added (*E*)-1-(2-nitrophenyl)-3-phenylprop-2-en-1-one (4.00 g, 15.8 mmol) at rt under argon atmosphere. The reaction was purged with hydrogen three times using a balloon, and the reaction mixture was stirred for 6 h at rt and standard pressure. The catalyst was filtered off over celite and washed with THF (50 mL) and acetone (50 mL). The solvent of the filtrate was removed *in vacuo*, and the crude oily product was purified by column chromatography ( $\text{SiO}_2$ , PE/ $\text{Et}_2\text{O}$ / $\text{NEt}_3$  = 66:33:1) to give **24** as a yellow solid in a yield of 46% (1.63 g, 7.24 mmol,

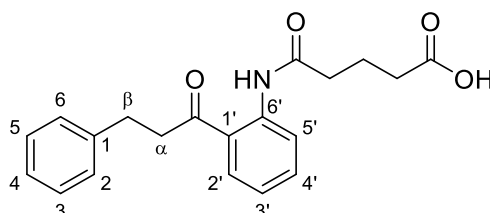
Lit.:<sup>105</sup> 50%).

**TLC:**  $R_f = 0.56$  (SiO<sub>2</sub>, PE/iPrOH = 3:1, *p*-anisaldehyde)

**Melting point:** 73 °C (Lit.:<sup>108</sup> 74 – 76 °C)

*The recorded spectra are in agreement with Brunce et al.*<sup>105</sup>

### 1.8.5 5-Oxo-5-((2-(3-phenylpropanoyl)phenyl)amino)pentanoic acid (**25**; *NJS33*)



**Chemical Formula:** C<sub>20</sub>H<sub>21</sub>NO<sub>4</sub>, **Molecular Weight:** 339.39 g/mol.

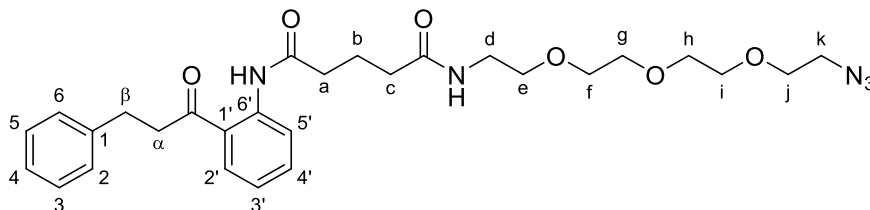
**24** (800 mg, 3.55 mmol) and glutaric anhydride (608 mg, 5.33 mmol) were dissolved in dry DCM (60 mL) at rt and stirred for 4 d, monitored by LC/MS. The solvent was removed *in vacuo*, and the crude oily product was purified by flash chromatography (run 1: SiO<sub>2</sub>, A: DCM, B: MeOH, gradient: 0→30% B; run 2: RP 18, A: H<sub>2</sub>O, B: MeOH, gradient: 5→100% B). **25** was obtained as a slightly yellowish-beige solid in a yield of 50% (600 mg, 1.77 mmol).

**TLC:**  $R_f = 0.86$  (SiO<sub>2</sub>, DCM/MeOH = 4:1, bromocresol green)

**IR (ATR,  $\tilde{\nu}_{max}$  [cm<sup>-1</sup>]):** 3033 (s), 3200 – 2700 (br s), 2917 (s), 1716 (s), 1692 (s), 1651 (s), 764 (s); 712 (s), 690 (s).

**<sup>1</sup>H NMR (CDCl<sub>3</sub>):**  $\delta = 11.74$  (br s, 1H, NH), 8.74 (dd, <sup>3</sup>*J* = 8.5, <sup>4</sup>*J* = 1.3 Hz, 1H, CH-2'), 7.90 (dd, <sup>3</sup>*J* = 8.5, <sup>4</sup>*J* = 1.3 Hz, 1H, CH-5'), 7.57–7.51 7.54 (ddd, <sup>3</sup>*J* = 8.5, 7.4 Hz, <sup>4</sup>*J* = 1.5 Hz, 1H, CH-4'), 7.33–7.28 (2H, m, CH-3,5), 7.25–7.21 (m, 3H, CH-2,4,6), 7.09 (ddd, <sup>3</sup>*J* = 8.5, 7.4 Hz, <sup>4</sup>*J* = 1.2 Hz, 1H, CH-3'), 3.36 (t, <sup>3</sup>*J* = 7.7 Hz, 2H, CH<sub>2</sub>- $\alpha$ ), 3.05 (t, <sup>3</sup>*J* = 7.7 Hz, 2H, CH<sub>2</sub>- $\beta$ ), 2.55 (t, <sup>3</sup>*J* = 7.3 Hz, 2H, HNC(=O)CH<sub>2</sub>), 2.51 (t, <sup>3</sup>*J* = 7.3 Hz, 2H, CH<sub>2</sub>COOH), 2.10 (p, <sup>3</sup>*J* = 7.3 Hz, 2H, COCH<sub>2</sub>CH<sub>2</sub>CH<sub>2</sub>CO) ppm.

**<sup>13</sup>C NMR (CDCl<sub>3</sub>):**  $\delta = 203.9$  (1C, COC-1'), 178.3 (1C, COOH), 171.7 (1C, HNCO), 141.0 (1C, C-6'), 140.9 (1C, C-1), 135.2 (1C, CH-4'), 130.8 (1C, CH-5'), 128.8 (2C, CH-3,5), 128.5 (2C, CH-2,6), 126.5 (1C, CH-4), 122.6 (1C, CH-3'), 121.7 (1C, C-1'), 121.2 (1C, CH-2'), 41.9 (1C, CH<sub>2</sub>- $\alpha$ ), 37.4 (1C, NHCOCH<sub>2</sub>), 33.1 (1C, CH<sub>2</sub>COOH), 30.5 (1C, CH<sub>2</sub>- $\beta$ ), 20.4 (1C, CH<sub>2</sub>CH<sub>2</sub>CH<sub>2</sub>) ppm.

1.8.6 *N'*-(2-(2-(2-(2-Azidoethoxy)ethoxy)ethoxy)ethyl)-*N*'-(2-(3-phenylpropanoyl)phenyl)glutaramide (**28**; *NJS35*)

**Chemical Formula:** C<sub>28</sub>H<sub>37</sub>N<sub>5</sub>O<sub>6</sub>, **Molecular Weight:** 539.63 g/mol.

**28** was synthesized according to general procedure A, using 150 mg of **25** (0.44 mmol), 2-(2-(2-azidoethoxy)ethoxy)ethan-1-amine (118 mg, 0.49 mmol), *N,N'*-dicyclohexylcarbodiimide (100 mg, 0.49 mmol), and HOBt (108 mg, 0.71 mmol) in dry DCM (40 mL). After stirring for 1 d at rt, the reaction was worked up according to the general procedure. The crude oily product was purified by flash chromatography (SiO<sub>2</sub>, A: CyH, B: EtOAc/iPrOH = 95:5, gradient: 0→100% B). **28** was obtained as a colorless oil in a yield of 50% (120 mg, 0.44 mmol).

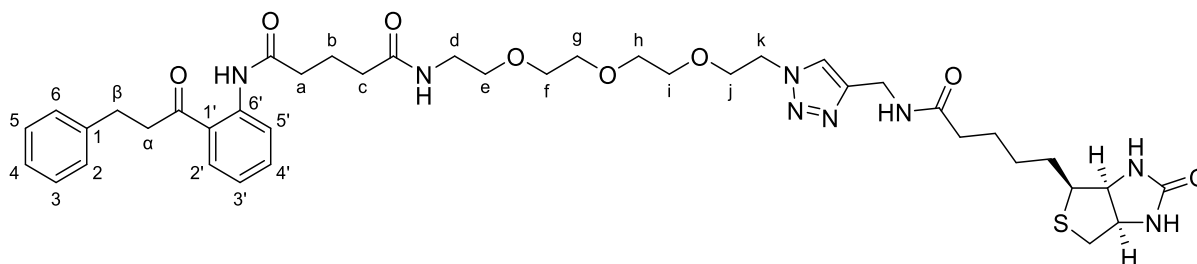
**TLC:**  $R_f = 0.58$  (SiO<sub>2</sub>, DCM/MeOH = 9:1)

**IR (ATR,  $\tilde{\nu}_{max}$  [cm<sup>-1</sup>]):** 3320 (br), 3060 (w), 2933 (s), 2867 (s), 2105 (m), 1651 (s), 1583 (s), 1520 (s), 1126 (br, m), 755 (w), 701 (w), 659 (w).

**<sup>1</sup>H NMR (CDCl<sub>3</sub>):**  $\delta = 11.68$  (s, 1H, *phenyl-NH*), 8.71 (dd, <sup>3</sup>*J* = 8.3, <sup>4</sup>*J* = 1.2 Hz, 1H, *CH-2'*), 7.89 (dd, <sup>3</sup>*J* = 8.3, <sup>4</sup>*J* = 1.2 Hz, 1H, *CH-5'*), 7.53 (ddd, <sup>3</sup>*J* = 8.3, 7.4, <sup>4</sup>*J* = 1.2 Hz, 1H, *CH-4'*), 7.33–7.27 (m, 2H, *CH-3,5*), 7.25–7.18 (m, 3H, *CH-2,4,6*), 7.08 (ddd, <sup>3</sup>*J* = 8.3, 7.4, <sup>4</sup>*J* = 1.2 Hz, 1H, *CH-3'*), 6.39 (br, *NHCH<sub>2</sub>-d*, 1H), 3.68–3.60 (m, 10H, *CH<sub>2</sub>-f,g,h,i,j*), 3.58–3.53 (m, 2H, *CH<sub>2</sub>-e*), 3.49–3.43 (m, 2H, *CH<sub>2</sub>-d*), 3.39–3.32 (m, 4H, *CH<sub>2</sub>- $\alpha$ , CH<sub>2</sub>-k*), 3.07–3.01 (m, 2H, *CH<sub>2</sub>- $\beta$* ), 2.51 (t, <sup>3</sup>*J* = 7.2 Hz, 2H, *CH<sub>2</sub>-a*), 2.32 (t, <sup>3</sup>*J* = 7.2 Hz, 2H, *CH<sub>2</sub>-c*), 2.09 (p, <sup>3</sup>*J* = 7.2 Hz, 2H, *CH<sub>2</sub>-b*) ppm.

**<sup>13</sup>C NMR (CDCl<sub>3</sub>):**  $\delta = 203.8$  (1C, C1'*CO*), 172.5 (1C, *CONH*), 172.0 (1C, *phenyl-NHCO*), 141.0 (1C, *C-1*), 140.9 (1C, *C-6'*), 135.0 (1C, *CH-4'*), 130.7 (1C, *CH-5'*), 128.7 (2C, *CH-2,6*), 128.5 (2C, *CH-3,5*), 126.4 (1C, *CH-4*), 122.5 (1C, *CH-3'*), 121.8 (1C, *CH-2'*), 121.1 (1C, *C-1'*), 70.8 (1C, *OCH<sub>2</sub>*), 70.73 (1C, *OCH<sub>2</sub>*), 70.67 (1C, *OCH<sub>2</sub>*), 70.4 (1C, *OCH<sub>2</sub>*), 70.1 (1C, *OCH<sub>2</sub>*), 70.0 (1C, *OCH<sub>2</sub>-e*), 50.8 (1C, *CH<sub>2</sub>-kN<sub>3</sub>*), 41.8 (1C, *CH<sub>2</sub>- $\alpha$* ), 39.4 (1C, *CH<sub>2</sub>-d*), 37.5 (1C, *CH<sub>2</sub>-a*), 35.6 (1C, *CH<sub>2</sub>-c*), 30.4 (1C, *CH<sub>2</sub>- $\beta$* ), 21.6 (1C, *CH<sub>2</sub>-b*) ppm.

1.8.7 *N*<sup>1</sup>-(2-(2-(2-(2-(4-((5-((3*aS*,4*S*,6*aR*)-2-oxohexahydro-1*H*-thieno[3,4-*d*]imidazol-4-yl)pentanamido)methyl)-1*H*-1,2,3-triazol-1-yl)ethoxy)ethoxy)ethyl)-*N*<sup>5</sup>-(2-(3-phenylpropanoyl)phenyl)glutaramide (22, *NJS36*)



**Chemical Formula:** C<sub>41</sub>H<sub>56</sub>N<sub>8</sub>O<sub>8</sub>S, **Molecular Weight:** 821.01 g/mol.

Analogous to Donnelly *et al.*,<sup>93</sup> to a solution of **28** (90 mg, 170 μmol) in DMF (15 ml), biotinpropargylamide (47 mg, 170 μmol), TBTA (6.2 mg, 12 μmol), sodium ascorbate (12 mg, 61 μmol), and copper(II) sulfate pentahydrate (4.5 mg, 18 μmol) were added at rt. After stirring for 7 d, the copper ions were removed by treating the mixture with activated ion-exchanger Amberlite IRC-718 (4.00 g) at rt for 18 h. The ion exchanger was removed by filtration, the solvent was removed *in vacuo* and the crude oily product was purified by flash column chromatography (run 1: RP 18, 16 g, A: H<sub>2</sub>O, B: MeOH, 5→100% B; run 2: SiO<sub>2</sub>, 40 g, A: DCM, B: MeOH, gradient: 0→20% B) to obtain **22** in a yield of 37% (50 mg, 61 μmol).

**TLC:** R<sub>f</sub> = 0.25 (SiO<sub>2</sub>, DCM/MeOH = 9:1)

**Purity (HPLC):** 99.7% , t<sub>R</sub> = 9.9 min.

**IR (ATR,  $\tilde{\nu}_{max}$  [cm<sup>-1</sup>]):** 3275 (br), 3079 (w), 3065 (w), 2923 (m), 2856 (m), 1697 (s), 1638 (s), 1523 (s), 1449 (s), 1100 (br s), 752 (m), 728 (m), 696 (m).

**<sup>1</sup>H NMR (CD<sub>3</sub>CN):** 11.46 (s, 1H, CO⋯HNC-6'), 8.61 (dd, <sup>3</sup>J = 8.3, <sup>4</sup>J = 1.3 Hz, 1H, CH-2'), 8.03 (dd, <sup>3</sup>J = 8.3, <sup>4</sup>J = 1.3 Hz, 1H, CH-5'), 7.71 (s, 1H, triazole-CH), 7.56 (ddd, <sup>3</sup>J = 8.3, 7.4, <sup>4</sup>J = 1.3 Hz, 1H, CH-4'), 7.32–7.25 (m, 4H, CH-2,3,5,6), 7.23–7.17 (m, 1H, CH-4), 7.14 (ddd, <sup>3</sup>J = 8.3, 7.4, <sup>4</sup>J = 1.3 Hz, 1H, CH-3'), 7.01–6.95 (br s, 1H, CONH), 6.78–6.70 (br s, 1H, CONH), 5.33 (s, 1H, biotin-NHCONH), 5.07 (s, 1H, biotin-NHCONH), 4.47–4.43 (m, 2H, CH<sub>2</sub>-k), 4.42–4.39 (m, 1H, biotin-CHNHCO), 4.38–4.35 (m, 2H, biotin-CH<sub>2</sub>NHCO), 4.23–4.18 (m, 1H, biotin-CHNHCO), 3.84–3.78 (m, 2H, CH<sub>2</sub>-j), 3.55–3.45 (m, 10H, OCH<sub>2</sub>-e,f,g,h,i), 3.39 (t, <sup>3</sup>J = 7.6 Hz, 2H, CH<sub>2</sub>-α), 3.32–3.27 (m, 2H, CH<sub>2</sub>-d), 3.15–3.09 (m, 1H, biotin-CHS), 3.03–2.97 (m, 2H, CH<sub>2</sub>-β), 2.86 (dd, <sup>2</sup>J = 12.7, <sup>3</sup>J = 5.0 Hz, 1H, biotin-CH<sub>2</sub>S), 2.63 (d, <sup>2</sup>J = 12.7 Hz, 1H, biotin-CH<sub>2</sub>S), 2.42 (t, <sup>3</sup>J = 7.4 Hz, 2H, CH<sub>2</sub>-a), 2.23–2.13 (m, 4H, CH<sub>2</sub>-c, biotin-CH<sub>2</sub>CONH),

1.93–1.88 (m, 2H,  $\text{CH}_2\text{-b}$ ), 1.70–1.47 (m, 4H, *biotin-CHCH<sub>2</sub>CH<sub>2</sub>CH<sub>2</sub>*), 1.40–1.33 (m, 2H, *biotin-CHCH<sub>2</sub>CH<sub>2</sub>CH<sub>2</sub>*) ppm.

$^{13}\text{C}$  NMR ( $\text{CD}_3\text{CN}$ ):  $\delta$  = 205.4 (1C,  $\text{C1}'\text{CO}$ ), 173.8 (1C, *biotin-CONH*), 173.3 (1C,  $\text{CONHCH}_2\text{-d}$ ), 172.8 (1C,  $\text{COCH}_2\text{-a}$ ), 163.9 (1C, *biotin-NHCONH*), 146.2 (1C, *triazole-C<sub>quaternary</sub>*), 142.3 (1C,  $\text{C-1}$ ), 141.5 (1C,  $\text{C-6}'$ ), 135.5 (1C,  $\text{CH-4}'$ ), 132.2 (1C,  $\text{CH-5}'$ ), 129.46 (2C,  $\text{CH-2,6}$ ), 129.44 (2C,  $\text{CH-3,5}$ ), 127.1 (1C,  $\text{CH-4}$ ), 124.0 (1C, *triazole-CH*), 123.4 (1C,  $\text{CH-3}'$ ), 121.4 (1C,  $\text{CH-2}'$ ), 71.1 (2C,  $\text{OCH}_2$ ), 71.0 (1C,  $\text{OCH}_2$ ), 70.9 (1C,  $\text{OCH}_2$ ), 70.4 (1C,  $\text{OCH}_2$ ), 70.0 (1C,  $\text{OCH}_2\text{-j}$ ), 62.4 (1C, *biotin-CHNHCO*), 60.8 (1C, *biotin-CHNHCO*), 56.3 (1C, *biotin-CHS*), 50.9 (1C,  $\text{CH}_2\text{-k}$ ), 42.4 (1C,  $\text{CH}_2\text{-}\alpha$ ), 41.2 (1C, *biotin-CH<sub>2</sub>S*), 39.9 (1C,  $\text{CH}_2\text{-d}$ ), 38.2 (1C,  $\text{CH}_2\text{-a}$ ), 36.2 (1C, *biotin-CH<sub>2</sub>CO*), 35.8 (1C,  $\text{CH}_2\text{-c}$ ), 35.5 (1C, *biotin-CH<sub>2</sub>NHCO*), 31.0 (1C,  $\text{CH}_2\text{-}\beta$ ), 29.03 (1C, *biotin-CH<sub>2</sub>CH<sub>2</sub>CH<sub>2</sub>CHS*), 29.00 (1C, *biotin-CH<sub>2</sub>CH<sub>2</sub>CH<sub>2</sub>CHS*), 26.3 (1C, *biotin-CH<sub>2</sub>CH<sub>2</sub>CH<sub>2</sub>CHS*), 22.3 (1C,  $\text{CH}_2\text{-b}$ ) ppm.

LC/MS ( $m/z$ ): 411.20  $[\text{M}+2\text{H}]^{2+}$ , 821.20  $[\text{M}+\text{H}]^+$ , 843.20  $[\text{M}+\text{Na}]^+$ .

## 2 Fluorescent probe for the identification of potent inhibitors of the macrophage infectivity potentiator (Mip) protein of *Burkholderia pseudomallei*

Nicolas Julian Scheuplein<sup>1‡</sup>, Theresa Lohr<sup>1‡</sup>, Mirella Vivoli Vega<sup>2‡</sup>, Dyan Ankrett<sup>2</sup>, Florian Seufert<sup>1</sup>, Lukas Kirchner<sup>1</sup>, Nicholas J. Harmer<sup>2\*</sup>, Ulrike Holzgrave<sup>1\*</sup>

<sup>1</sup> Institute of Pharmacy and Food Chemistry, University of Würzburg, Am Hubland, 97074 Würzburg, Germany

<sup>2</sup> Living Systems Institute, Stocker Road, Exeter, EX4 4QD, U.K.

<sup>‡</sup> Present address: School of Biochemistry, University of Bristol, Bristol BS8 1TD, U.K.

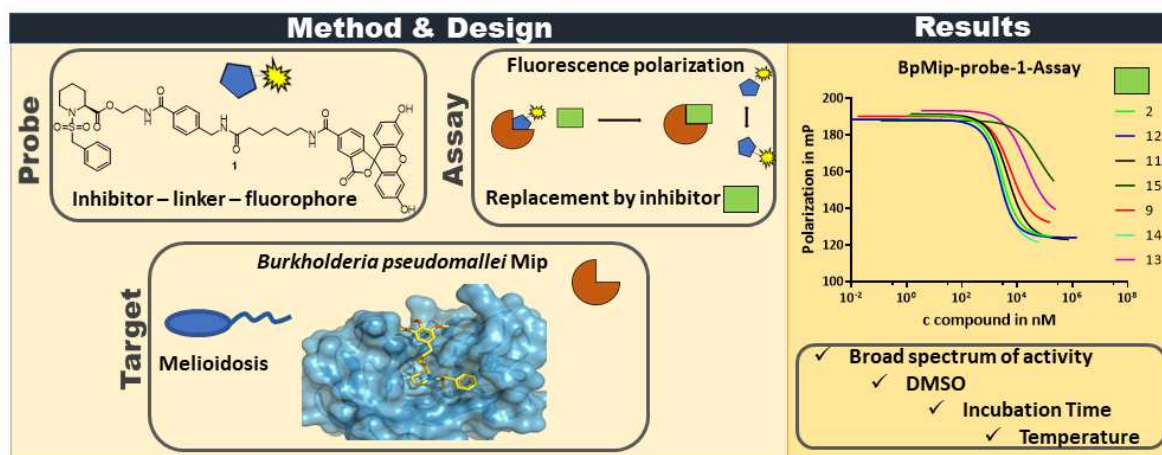
<sup>‡</sup> equal first authors

\* equal corresponding authors

*This is an open access article licensed under a Creative Commons Attribution 4.0 International License (CC BY 4.0), <https://creativecommons.org/licenses/by/4.0/>. © 2023, Scheuplein, N. J.; Lohr, T.; Vivoli Vega, M.; Ankrett, D.; Seufert, F.; Kirchner, L.; et al. Fluorescent probe for the identification of potent inhibitors of the macrophage infectivity potentiator (Mip) protein of *Burkholderia pseudomallei*. *SLAS Discov.* 2023.*

*<https://doi.org/10.1016/j.slasd.2023.03.004>. Published by Elsevier Inc. on behalf of Society for Laboratory Automation and Screening.*

### Graphical Abstract



**Keywords:** PPIase, Fluorescence polarization, Anisotropy, High throughput screening, *Burkholderia pseudomallei* Mip, Mip inhibitor

## 2.1 Abstract

The macrophage infectivity potentiator (Mip) protein belongs to the immunophilin superfamily. This class of enzymes catalyzes the interconversion between the *cis* and *trans* configuration of proline-containing peptide bonds. Mip has been shown to be important for the virulence of a wide range of pathogenic microorganisms, including the Gram-negative bacterium *Burkholderia pseudomallei*. Small molecules derived from the natural product rapamycin, lacking its immunosuppression-inducing moiety, inhibit Mip's peptidyl-prolyl *cis-trans* isomerase (PPIase) activity and lead to a reduction in pathogen load *in vitro*. Here, a fluorescence polarization assay (FPA) to enable the screening and effective development of BpMip inhibitors was established. A fluorescent probe was prepared, derived from previous pipercolic scaffold Mip inhibitors labeled with fluorescein. This probe showed moderate affinity for BpMip and enabled a highly robust FPA suitable for screening large compound libraries with medium- to high-throughput (Z factor ~ 0.89) to identify potent new inhibitors. The FPA results are consistent with data from the protease-coupled PPIase assay. Analysis of the temperature dependence of the probe's binding highlighted that BpMip's ligand binding is driven by enthalpic rather than entropic effects. This has considerable consequences for the use of low-temperature kinetic assays.

**Keywords:** PPIase, fluorescence polarization, anisotropy, high throughput screening, *Burkholderia pseudomallei* Mip, Mip inhibitor.

## 2.2 Introduction

The macrophage infectivity potentiator (Mip) protein has emerged as a promising new anti-virulence target in the effort to find new treatments for bacteria that display either intrinsic or acquired resistance to antimicrobials.<sup>1-4</sup> Mip proteins are found across Gram-negative bacteria and in some unicellular parasites. They have been associated with virulence in proteobacteria (e.g. *Legionella*,<sup>5</sup> *Burkholderia*,<sup>2</sup> *Klebsiella*,<sup>3</sup> and *Neisseria*<sup>6</sup>), other Gram-negative pathogens such as *Chlamydia*<sup>7, 8</sup>, and eukaryotic pathogens (trypanosoma<sup>9</sup> and leishmania<sup>3</sup>). Mips consist of a highly conserved FKBP type pre-prolyl peptide isomerase (peptidyl-prolyl isomerase, PPIase) domain, and



in most cases one of two dimerization/chaperone domains. The PPIase domain has the greatest contribution to virulence, and can be inhibited by small molecules, leading to a decrease in pathogen load *in vitro*.<sup>4</sup> One such targetable pathogen is *Burkholderia pseudomallei*, the causative agent of melioidosis.<sup>10</sup> This potentially life-threatening infection causes an estimated global burden of 84.3 per 100 000 people or 4.6 million disability-adjusted life years per year.<sup>11</sup> *B. pseudomallei* is a Gram-negative betaproteobacterium containing two Mip paralogues. Of these, only the 11.9 kDa BpMip protein (consisting of only a PPIase domain) is relevant to virulence.<sup>2, 12</sup> BpMip shows 40% sequence identity to the *Legionella pneumophila* Mip,<sup>13, 14</sup> with almost identical active sites.<sup>2</sup>

For the targeted development of new inhibitors, rapid and robust measurement of binding affinity is crucial. In the past, Mip inhibitors designed by Juli *et al.*<sup>15, 16</sup> and Seufert *et al.*<sup>17, 18</sup> have been screened using a protease-coupled PPIase assay established by Fischer *et al.*<sup>19</sup> Briefly, a short amino acid sequence labeled with *p*-nitroaniline is used as a substrate, while  $\alpha$ -chymotrypsin serves as an auxiliary protease that cleaves only trans-linked Phe-Pro substrates. The conversion can be measured by absorbance at around 390 nm, which is due to the released *p*-nitroaniline.<sup>19</sup> This assay has some disadvantages as it has to be carried out at low temperatures, making it time-consuming and requiring dedicated equipment.<sup>20, 21</sup> Whilst the PPIase assay directly measures the desired effect of proposed inhibitors, it is highly challenging to use for high-throughput screening (HTS).

A fluorescence polarization (FP) assay could be a potent alternative for HTS. FP uses plane-polarized light to measure the binding of a small fluorescent ligand to a larger protein, detecting the change in the effective molecular volume.<sup>22, 23</sup> The FP assay (FPA) has significant advantages compared to other assays used to study enzyme-ligand interactions for studying the Mip-ligand interaction.<sup>24</sup> It does not require separation of bound and free ligand, allowing ligand binding to be quantified without disturbing the equilibrium. This makes it suitable for measuring interactions with low affinity and rapid dissociation rates, such as the Mip-ligand interaction.<sup>23</sup> FP avoids the use of radioactivity, is non-destructive, and can resolve thermodynamic parameters such as  $\Delta H^\circ$  and  $\Delta S^\circ$ , requiring less protein than an isothermal titration calorimetry measurement.<sup>23</sup> A key advantage for Mips is that FP can operate across temperatures where the sample protein is folded. This avoids the need to use low temperatures (as in the PPIase enzyme assay<sup>19, 20</sup>), and can readily measure activity at 37 °C, the relevant physiological conditions for human pathogens. Protein-ligand interactions can be highly temperature dependent, and lower temperature determinations can be misleading. Once established, the FPA can be performed in 384 or even 1536 well format

with moderate read times, allowing for medium- or even high-throughput screening. Kozany *et al.* described the application of an FPA for the high-throughput screening of human FKBP that show strong structural similarity to the microbial Mip PPIase domain.<sup>25</sup> Pomplun *et al.* used a refined FPA to screen compounds against microbial Mips, such as *Neisseria meningitidis* Mip (NmMip).<sup>26</sup> However, the binding affinity of the tracer molecule previously used is very high (low nanomolar). This makes differentiation of weaker BpMip inhibitors in the competition assay more challenging. For initial screening aiming at obtaining compounds with a  $K_D$  of 1–10  $\mu$ M, a tracer molecule binding in the low micromolar range would be a useful alternative. Furthermore, no application toward BpMip has been described to date.

Here, we describe the design of a fluorescent probe with a low micromolar affinity for the PPIase domain of the BpMip protein. We used this to establish a highly robust FPA suitable for medium to high throughput screening of large compound libraries to identify potent new inhibitors. We demonstrate the use of the assay to prioritize example compounds from our optimization pipeline for Mip inhibitors. This assay will facilitate and accelerate the search for new BpMip inhibitors and thus new therapeutic options against melioidosis and other microbial diseases caused by Mip-bearing pathogens. The analysis of the temperature dependence of the binding of the probe demonstrated that binding of this compound series is driven by enthalpic rather than entropic effects. Nevertheless, the temperature dependence is considerable. This has important consequences for the use of kinetic assays at low temperatures, as the compound affinity is expected to increase as the temperature lowers. The FPA presented here, which is performed at room temperature and could operate at 37 °C, should therefore provide more valid and realistic results than the cooled protease-coupled PPIase assay.

## 2.3 Results and Discussion

### 2.3.1 Design of Tracer Molecule 1

Key steps in probe design include the selection of a ligand to be labeled, as well as a suitable attachment point for a linker of appropriate length and a suitable fluorophore. These must not result in a significant loss of binding affinity due to steric hindrance.<sup>27</sup> The functionalized 5-carboxyfluorescein derivative was chosen as a fluorophore as it has similar properties to the parent compound fluorescein (**Figure 1**). Fluorescein, being used in immunofluorescence microscopy<sup>28</sup> and various biochemical applications,<sup>29, 30</sup> has excellent fluorescence properties for FP application,

such as a high fluorescence quantum yield  $\Phi = 0.92 \pm 0.02$  of the dianion form and a relatively long fluorescence lifetime of approximately 4 ns.<sup>31</sup> A similar fluorophore was used successfully in FP assays by Hausch *et al.* and Banaszynski *et al.* to screen potential FKBP ligands.<sup>25, 32</sup> The absorption maximum  $\lambda_{\max}$  for fluorescein lies at approximately 485 nm, sufficiently high to avoid autofluorescence of the sample, and its emission maximum  $\lambda_{\text{em}}$  is about 520 nm.<sup>33, 34</sup> The coupling of the fluorescent dye to the ligand should be rigid enough so that the fluorophore cannot rotate independently of the status of the ligand, arguing against linkers that are too long.<sup>34</sup> A chain that is too short, on the other hand, can sterically hinder the binding of the inhibitor to the Mip protein. Banaszynski *et al.* showed that direct fluorescein labeling of rapamycin to the alcohol group of C40 significantly reduced binding to FKBP12 ( $K_D = 10$  mM).<sup>32</sup> By varying the linker length of their FP tracer for the screening of the related FKBP51 binding ligands, Hausch *et al.* found that a fluorescein-labeled tracer linked to rapamycin via glycine did not work for FKBP51, while a hexyl-glycine linker consisting of a total of eleven atoms proved to be suitable.<sup>25</sup> The small molecule FP tracer later used, being much smaller than rapamycin, worked successfully with a shorter chain length of only five atoms.<sup>25</sup> Based on the similarity of the binding pocket of human FKBP and microbial Mips, a hexyl linker with a total length of ten atoms was selected (**Figure 1**).

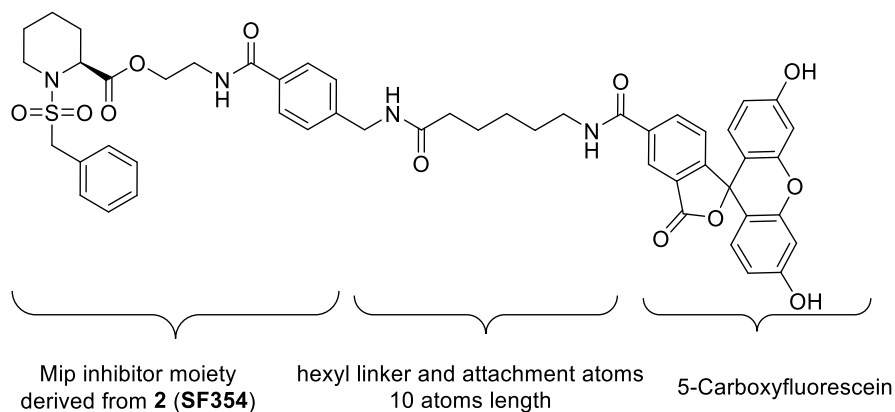


**Figure 1:** Chemical structure of the designed FP tracer molecule **1**, consisting of a mip inhibitor moiety derived from **2**, a hexyl linker and attachment atoms with a total length of 10 atoms, and the fluorophore 5-carboxyfluorescein.

The crystal structures of BpMip bound to compound **2** (SF354, PDB ID 5V8T; **Figure 2A**)<sup>3</sup> and **3** (CJ168, PDB ID 4G50; **Figure 2B**)<sup>16</sup> highlight a likely point to introduce the linker without interfering in compound binding to BpMip. The pipercolic ring of both Mip inhibitors is located deep in the active site pocket, and the phenyl ring of the sulfonamide moiety occupies a sub-pocket, ruling out these parts of the molecule as a linkage point (**Figure 2**). However, the trimethoxyphenyl

group in the case of **3** and the ether-substituted benzene ring in the case of **2** are located rather superficially on the protein surface, rendering this part of the inhibitors an interesting linkage point (**Figure 2**). Indeed, this group changes location in crystal structures with different protein packing, indicating that the interactions with Mip are weak.<sup>3</sup> The lead structure **2** has a  $K_i$  (PP1ase) of  $0.98 \pm 0.29 \mu\text{M}$ , despite carrying rather bulky ether groups that are well tolerated at this position.<sup>18</sup> Consequently, the attachment point for the linker was chosen in the *para* position on this benzene ring. The backbone of **2** was used for the Mip inhibitor moiety of the tracer, leaving out the ether groups at the benzene ring to prevent interactions with the fluorophore or the linker and to improve synthetic accessibility.

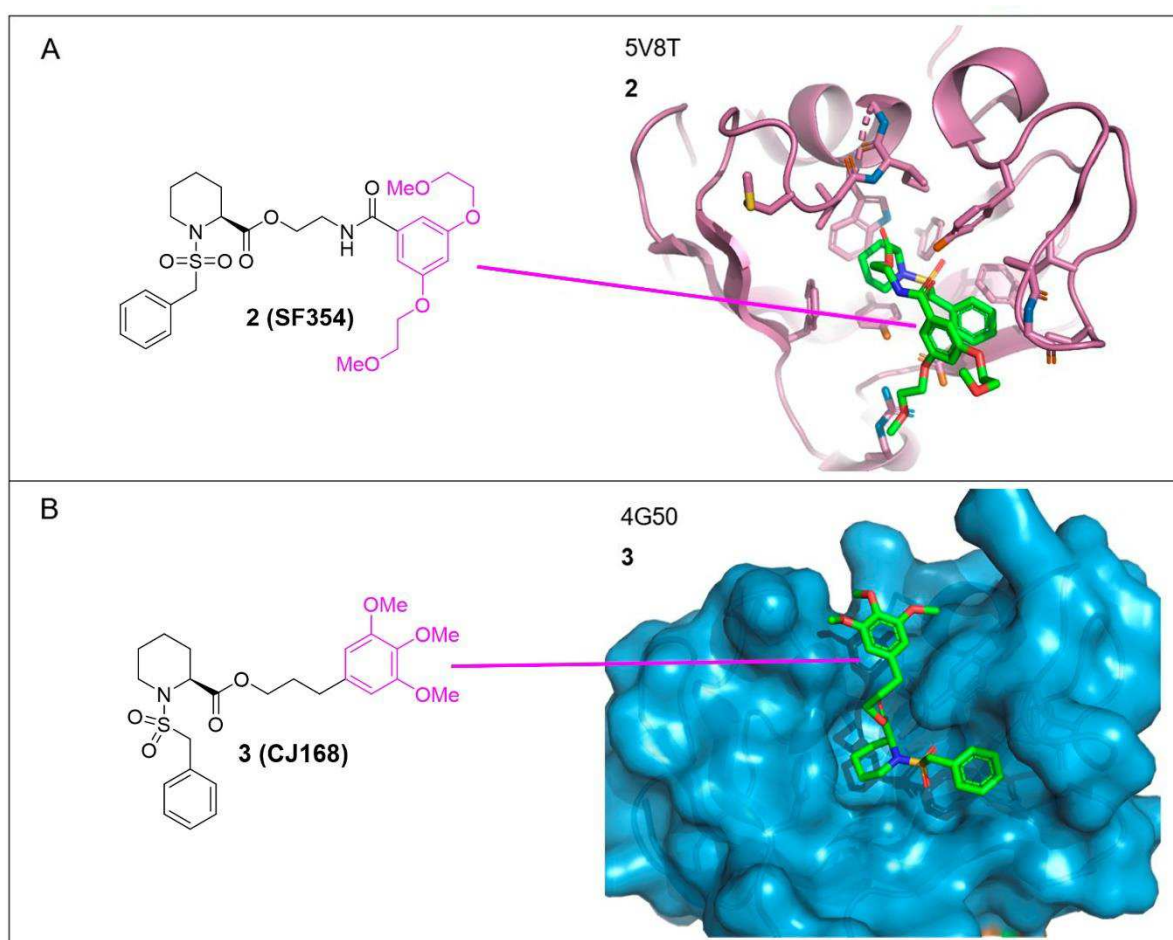


**Figure 2:** Chemical structures of the Mip inhibitors **2** (**Fig. 2A**) and **3** (**Fig. 2B**) and their corresponding co-crystal structures with BpMip; PDB ID 5V8T for **2** and PDB ID 4G50 for **3**. The part of the molecule that was subsequently chosen as position for linker attachment is marked in pink in the chemical structure. As can be seen from the crystal structures, in each case, the piperoline ring is located deep in the active site pocket and the phenyl ring of the sulfonamide moiety occupies a sub-pocket, whereas the ether-substituted benzene moiety (for **2**) and the trimethoxyphenyl moiety (for **3**) are located on the protein surface. This part of the molecule constitutes a suitable area for the attachment of the linker without affecting binding to Mip. Non-carbon atoms are colored as follows: red, oxygen; blue, nitrogen; yellow, sulfur.

## 2.3.2 Synthesis of Tracer 1

The primary amino group of 4-(aminomethyl)benzoic acid was Cbz-protected (to give **4**) and the acid function amide-coupled with ethanolamine using EDC-HCl and HOBT (**Figure 3**). **5** was then esterified with *N*-Boc-(*S*)-pipercolic acid under Steglich conditions using DCC and catalytic amounts of DMAP. Subsequently, the Boc protecting group of **6** was cleaved with TFA, and the resulting amine **7** was coupled with phenylmethanesulfonyl chloride to give sulfonamide **8**. The Cbz protecting group was removed hydrogenolytically under Pd catalysis to obtain the primary amine **9**. The fluorophore linker moiety **10** was prepared by the reaction of 5-carboxyfluorescein with 6-methoxy-6-oxohexane-1-amium chloride, the coupling reagent HBTU and NEt<sub>3</sub> in DMF followed by saponification of the methoxy ester with aqueous LiOH solution. In the final step, **9** was amide-coupled with **10** using HBTU and DIPEA to give tracer molecule **1**.

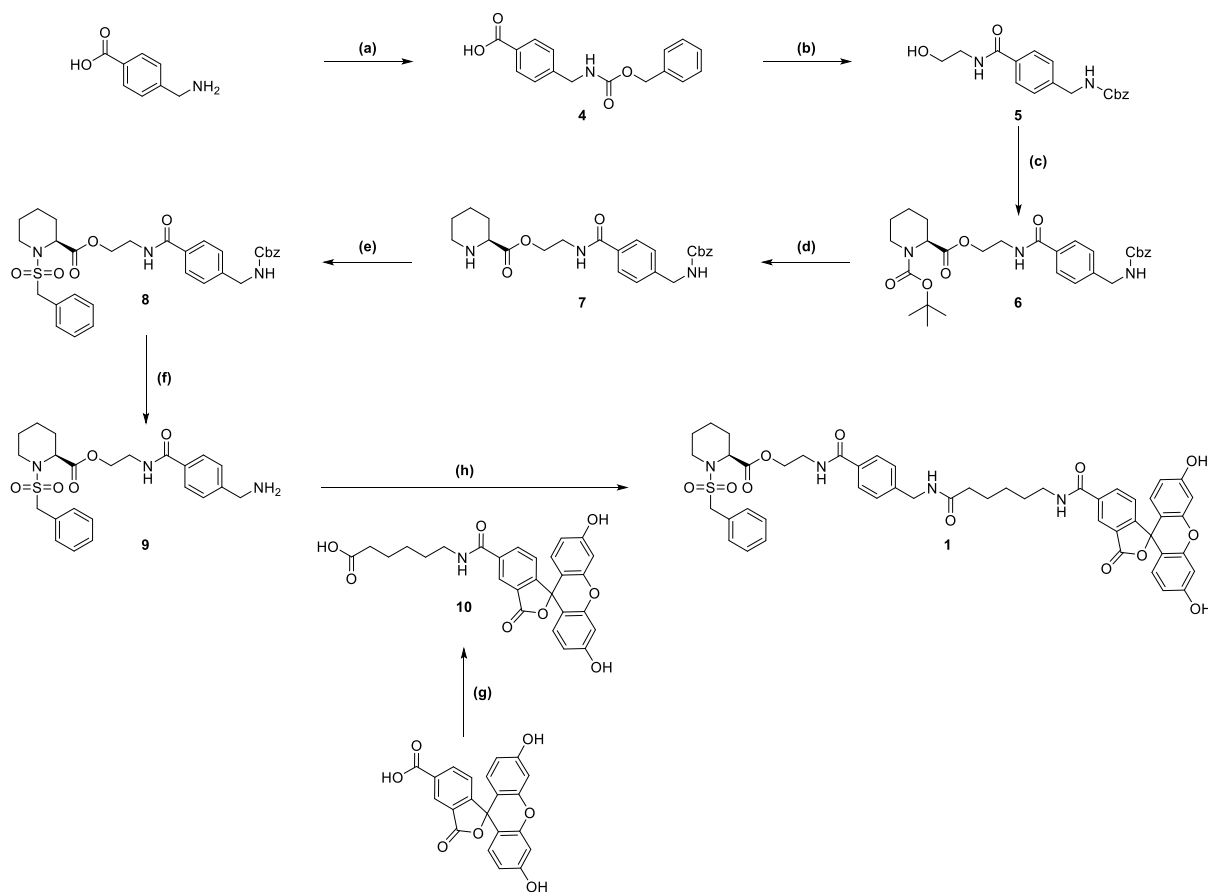


**Figure 3:** Synthesis pathway of the fluorescent probe **1** and the intermediate product **8**. Reagents and conditions: (a) Cbz-Cl, NaHCO<sub>3</sub>, water/THF (1:1), 1 d, rt, 99%; (b) ethanolamine, EDC-HCl, HOBT, DCM, rt, 1 d, 87%; (c) *S*-*N*-Boc-pipercolic acid, DCC, DMAP, DCM/DMF (3:1), rt, 4 h, 48%; (d) TFA, DCM, rt, 2.5 h, 93%; (e) NEt<sub>3</sub>, DCM, phenylmethanesulfonyl chloride, rt, 3 d, 44%; (f) Pd/C (10 wt%), H<sub>2</sub> (10 bar), acetic acid, MeOH, rt, 2 d, 13%; (g) i) HBTU, 6-methoxy-6-oxohexane-1-amium chloride, NEt<sub>3</sub>, DMF, rt, 18 h, ii) LiOH, water, rt, 1 d, 33%; (h) HBTU, DIPEA, fluorescein-5-hexanoic acid, DCM/DMF (2:1), rt, 1 d, 44%.

### 2.3.3 FP Assay Validation with BpMip and Probe 1 and Thermodynamic Study of the Influence of Temperature on $K_D$

To establish the FP assay, the optimal concentration of tracer molecule **1** was determined by using different tracer concentrations when titrating the active site of BpMip.

To prove that fluorescence polarization is a concentration-independent parameter, **1** was subjected to a sensitivity test. By measuring a dilution series of the tracer molecule, we found that the tracer exhibits a stable polarization signal at concentrations ranging from 50 nM to 0.5 nM (**Figure 4A**).

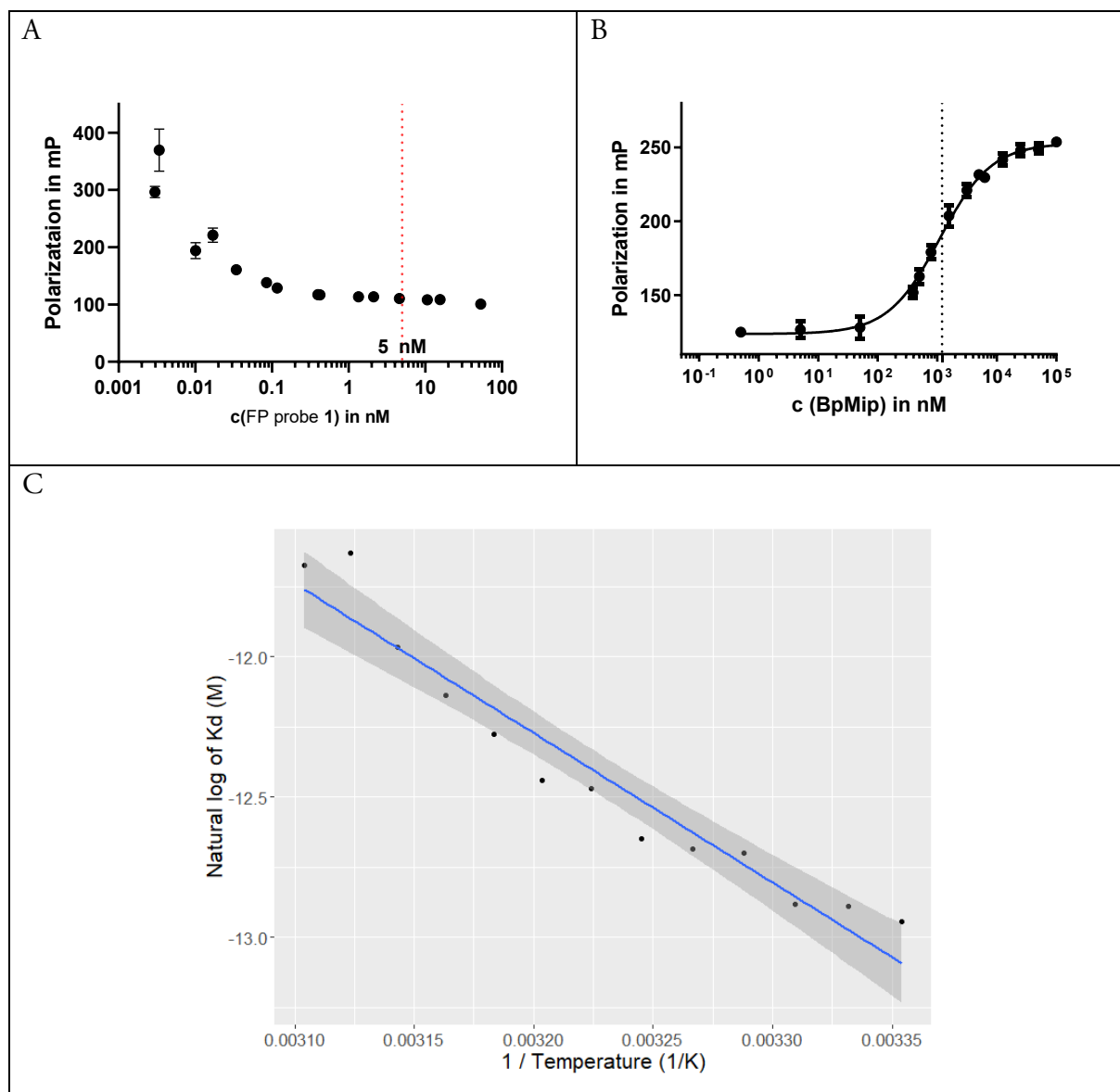


**Figure 4:** **A:** Stable, concentration-independent polarization was demonstrated in a sensitivity test by measuring a dilution series of the tracer molecule **1** for a range from 0.5 nM to 50 nM. **B:** An exemplary FP equilibrium saturation binding curve of BpMip and probe **1** at a concentration of 5 nM at 25 °C. Error bars represent standard error, with data points showing the mean of three scans of each well. A triple repetition resulted in a  $K_D$  of  $1200 \pm 120$  nM (dashed line). Triplicate is shown in the SI. **C:** Affinity was tested across a range of temperatures from 25 °C to 55 °C. The interaction showed a linear van't Hoff plot, suggesting that the heat capacity of the protein is unaffected by temperature. Thus, the enthalpy ( $\Delta H^\circ$ ) and entropy ( $\Delta S^\circ$ ) were determined to be  $-44 \pm 3$  kJ mol<sup>-1</sup> and  $-39 \pm 11$  J mol<sup>-1</sup>, respectively. Upper images were generated using GraphPad Prism v8.0.1; **Figure 4C** was generated using R v. 4.2.1.

A concentration of 5 nM **1** gave strong fluorescence and reproducible results and was used for all further experiments. We firstly determined the affinity of **1** for purified BpMip (**Figure 4B**). At 25 °C, the affinity was  $1200 \pm 120$  nM, which met our criteria for the intended affinity for BpMip. Based on this binding curve, a protein concentration of 2  $\mu$ M was chosen for further experiments. Reviews of FP recommend using a concentration showing 50-80% of the plateau FP change, and a substantial polarization range.<sup>35, 36</sup> A concentration of 2  $\mu$ M provided high sensitivity to the competitor and offered a dynamic range of 70 mP, sufficient for precise calculations. We used a value giving slightly greater than a 50% response to account for the reduced affinity in the presence of DMSO. BpMip can be readily produced in sufficient quantities.<sup>37</sup>

We then tested the affinity across a range of temperatures from 25 °C to 55 °C. The interaction showed a linear van't Hoff plot (**Figure 4C**), suggesting that the heat capacity of the protein is unaffected by temperature. From the van't Hoff plot, the enthalpy ( $DH^\circ$ ) and entropy ( $DS^\circ$ ) were calculated as  $-44 \pm 3$  kJ mol<sup>-1</sup> and  $-39 \pm 11$  J mol<sup>-1</sup>, respectively.<sup>23</sup> Due to the negative entropic element, the  $K_D$  increased with temperature. Screening at higher temperatures would require greater concentrations of BpMip, compromising the economy and sensitivity of the experiment. This indicates that the compound would be most useful at 20–25 °C, depending on the capabilities of the instrument. All further experiments were performed at room temperature with 2  $\mu$ M BpMip. A time-dependent equilibrium study was performed to investigate the stability of the enzyme-ligand complex formed. The formation occurred within the first few minutes and was stable for at least three hours (**Figure 5A**). No significant difference was observed in the  $K_D$  between the first measurement a few minutes after setup to the last one after three hours.

Many screening compounds are only soluble in a carrier such as DMSO. DMSO is a common and bio-tolerated solvent for experimental compounds. However, it is well documented to affect protein-ligand binding.<sup>38</sup> Therefore, the effects of DMSO on the Mip-1 complex were investigated in a DMSO tolerance assay.<sup>38</sup> An active site titration was performed in the presence of a defined DMSO concentration, and the change in binding capacity of the tracer was determined using the  $K_D$  value (**Figure 5B**). DMSO showed a clear effect on BpMip's affinity for the fluorescent ligand. For higher DMSO concentrations, the minimum significance ratio ( $MSR = 10^{2\sqrt{2}}$ ) of the  $K_D$  values relative to 0% DMSO was calculated.<sup>39</sup> Using the common criterion of an MSR of less than 3, there was a significant difference at 10% (v/v) DMSO. Although the MSR for DMSO concentrations of 5% or lower is less than 3, and so do not meet the test of a significant difference,

the apparent  $K_D$  value already doubles at 1% (v/v) DMSO. To maintain a sufficient signal-to-noise ratio and maximum precision in the competition assay, an expedient DMSO limit was set at  $\leq 1\%$  for the further experiments. This could be implemented because all inhibitors were sufficiently soluble in 1% (v/v) DMSO at the final assay concentration and is consistent with most HTS compounds.<sup>40</sup> **1** therefore satisfied our criteria as a useful tracer for moderate BpMip inhibitors and a good complement to the already known FKBP and Mip tracers.<sup>25, 26</sup>

The assay was further validated by determining the binding affinity of probe **1** for BpMip using the gold standard isothermal titration calorimetry (ITC). The ITC experiment was performed in 3% (v/v) DMSO. The determined  $K_D$  of  $5.50 \pm 0.03$  mM (**Figure 5C**, Supplementary Figure 3) shows good agreement with the FP assay ( $K_D = 3.63$  mM at 3% DMSO). Furthermore, ITC determined the stoichiometry of the probe for BpMip as  $1.10 \pm 0.03$ , confirming that BpMip has only one binding site for probe **1**, and that the BpMip sample has good integrity and is at the determined concentration.

Finally, the specificity of the assay was investigated. The mixture of BpMip and labeled probe **1** was titrated against the unlabeled probe **8**, to demonstrate that FP decreases to a minimum with increasing concentration of competitor.<sup>35</sup> The similar  $K_D$  values of the two molecules show that labeling has no significant effect on Mip binding, confirming the approach of determining the attachment point from the crystal structures (**Figure 2**).

The suitability for medium or upscaling to high throughput screening (HTS) is reflected by the Z-factor<sup>41</sup>:  $Z = 1 - \frac{(3\sigma^+ + 3\sigma^-)}{|\mu^+ - \mu^-|}$ , where the mean values and standard deviations for the negative and positive controls are indicated by  $\mu^-$ ,  $\sigma^-$  and  $\mu^+$ ,  $\sigma^+$ , respectively. The triplicate investigation of 12 samples each resulted in a Z-factor of 0.89 (Supplementary information). This result of well over 0.5 even guarantees suitability for HTS.



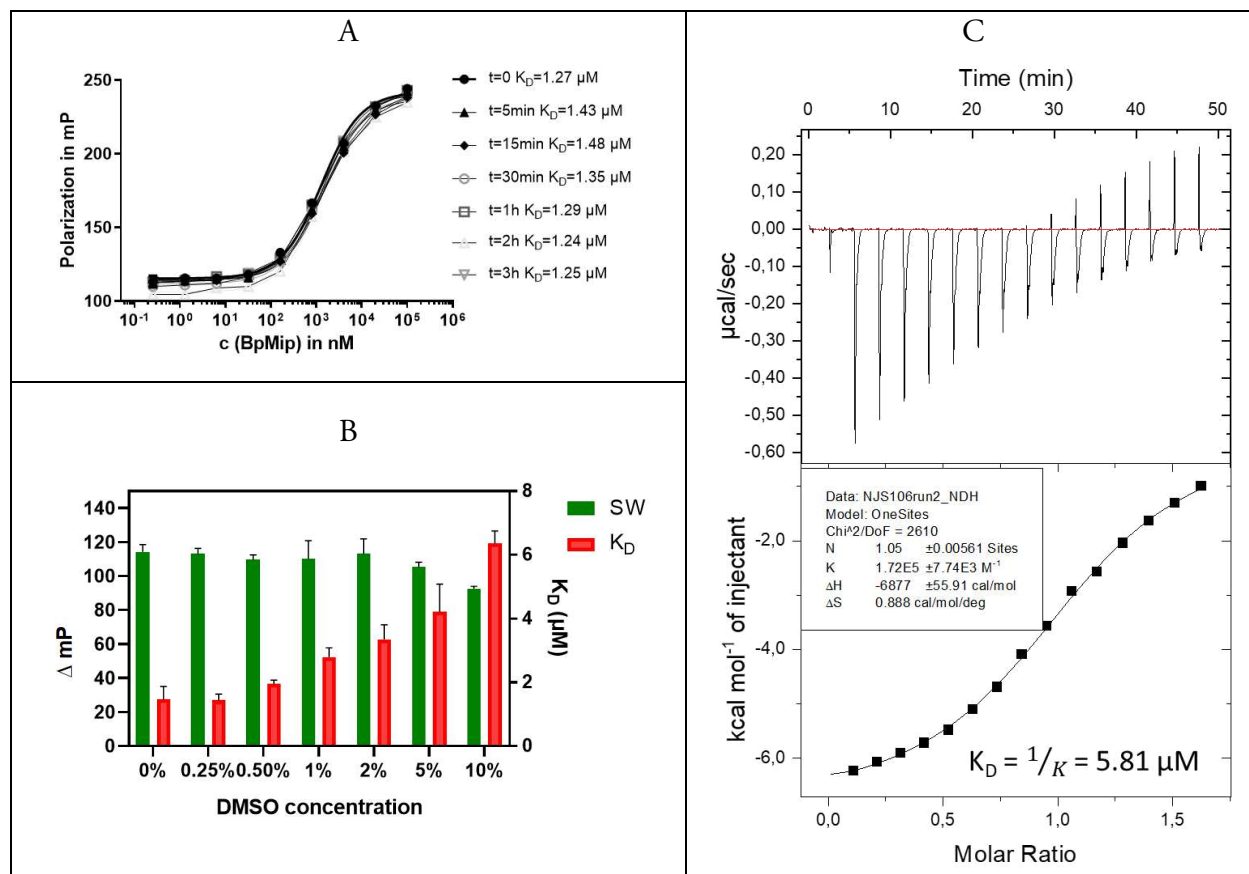
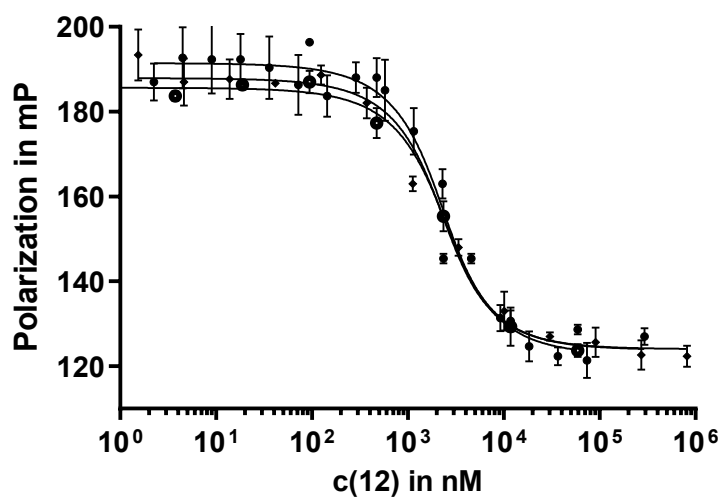


**Figure 5: Validation of the FP experiment.** **A:** Time-dependent equilibrium study. Fluorescence polarization was measured at timepoints from 5 minutes to three hours after experiment setup. The results are within error of each other, indicating that the enzyme-substrate complex is formed in the first few minutes after setup and was stable for at least three hours. **B:** In a DMSO tolerance assay, an active site titration was performed in the presence of a defined DMSO concentration and the change in binding capacity of the tracer was determined using the  $K_D$  value and the signal window (SW), calculated from a duplicate at least. For higher DMSO concentrations, the MSR of the  $K_D$  values relative to 0% DMSO was calculated (SI). If the common criterion of an MSR of less than 3 is used, a significant deviation is obtained at 10% DMSO. GraphPad Prism 8.0.1 was used for calculation and graphical representation. **C:** The binding affinity of probe 1 was verified using isothermal titration calorimetry. Three independent experiments were performed, injecting probe 1 into a solution of BpMip. An exemplary ITC plot is shown, giving a stoichiometric ratio of  $N = 1.05 \pm 0.006$  and a  $K_D$  of  $5.81 \pm 0.26 \mu\text{M}$  at 3% DMSO.

#### 2.3.4 Competitive Displacement Assay for The Screening of BpMip Inhibitors

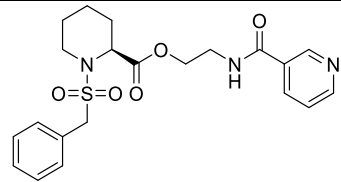
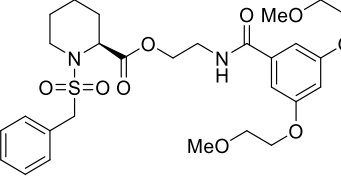
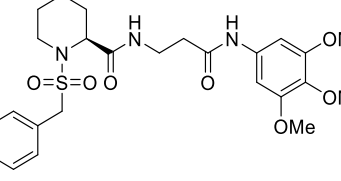
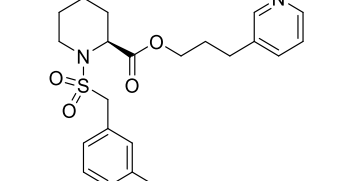
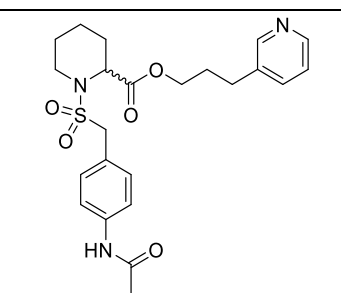
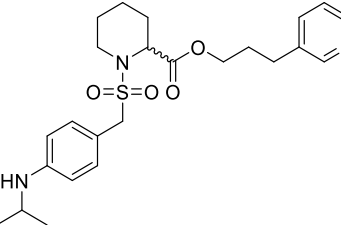
Based on their broad range of  $K_i$  values in the previously used PPIase assay, six inhibitors were selected to be tested in the developed competitive displacement FP assay (Table 1). In the following, using the probe 1, it was possible to distinguish between moderately strong inhibitors, such as 11 (SF235, see Table 1), and strong inhibitors, such as 12 (SF339, see Table 1 and Fig. 6). The trends from the previously used kinetic enzyme assay are congruent with the results obtained in the FP assay (Table 1 and Supplementary data). Minor differences can be explained by the fact that the FP assay measures affinity to the binding pocket, whereas the enzyme assay measures the effect on enzyme activity. In addition, the assays are performed at different temperatures.

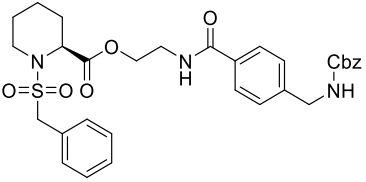
The determined  $K_D$  of **8** was  $2.36 \pm 0.27 \mu\text{M}$ , which is close to that of probe **1**. Since **8** corresponds to the inhibitor moiety of probe **1** except for the Cbz protecting group, it can be concluded that fluorescein labeling in probe **1** has no significant effect on protein binding. Using the established FP competition assay, we were able to screen out enzymatically ineffective inhibitors such as the racemic compound **13** ( $K_D = 10.64 \mu\text{M}$ , see **Table 1**).



**Figure 6:** Exemplary dose-response curve from competition assay performed with **12**. The triplicate measurement was performed on three different days with three different dilution series. **1** was used in a final concentration of 5 nM, BpMip at 2  $\mu\text{M}$  and **12** in a range of 60  $\mu\text{M}$  – 1 nM. GraphPad Prism 8.0.1 was used for calculation and graphical representation.

**Table 1:** Chemical structures of the Mip inhibitors examined and their respective  $K_i$  values determined by the established FP assay compared with the protease-coupled PPIase assay.<sup>20</sup> More detail is provided in supplementary information.

Inhibitor	Structure	$K_i$ [ $\mu\text{M}$ ], <i>FP</i>	$K_i$ [ $\mu\text{M}$ ], <i>PPIase</i>
11		$1.79 \pm 0.33$	$0.29 \pm 0.06$
2		$1.15 \pm 0.74$	$0.98 \pm 0.29$
12		$0.46 \pm 0.01$	$0.45 \pm 0.09$
14		$0.65 \pm 0.08$	$0.18 \pm 0.01$
13		$10.64 \pm 0.53$	$21.0 \pm 8.0$
15		$15.10 \pm 5.10$	$4.50 \pm 1.70$

Inhibitor	Structure	$K_i$ [ $\mu\text{M}$ ], <i>FP</i>	$K_i$ [ $\mu\text{M}$ ], <i>PPIase</i>
8		$2.36 \pm 0.27$	<i>Not determined</i>

## 2.4 Conclusion

In this study, an FPA has been established to enable the screening and effective development of BpMip inhibitors. A fluorescent probe derived from previous pipercolic scaffold Mip inhibitors was labeled with fluorescein. This probe showed moderate affinity for the PPIase domain of the BpMip protein and enabled a highly robust FPA suitable for screening large compound libraries with medium to high throughput ( $Z \sim 0.89$ ) to identify potent new inhibitors. A moderate  $K_D$  of 2.0  $\mu\text{M}$  renders **1** a useful tracer for moderate BpMip inhibitors and a good complement to the previously reported FKBP and Mip tracers.<sup>25, 26</sup>

The developed FPA has several advantages: it is very fast to perform, robust, can be easily parallelized, and the data processing is straightforward. Unlike SPR, this assay shows that the small molecule binds at the protein site of interest through competitive binding. The assay is suitable for both HTS and detailed hit analysis. Any new small molecule can be tested without derivatization or isotopic labeling. Limitations include that binding affinity does not provide concrete information on enzymatic activity, and that the assay's detection limit of  $\sim 200$ -400 nM may be insufficient for some applications.

The results obtained with the FPA are in line with the findings of the frequently used protease-coupled PPIase assay. Analysis of the temperature dependence of the probe's binding highlighted that BpMip's ligand binding is driven by enthalpic rather than entropic effects.

The assay presented here may contribute to the development of novel therapeutics against melioidosis and other microbial diseases.

## 2.5 Methods

**Chemicals.** Reagents used for the synthesis in this work were obtained from *Alfa Aesar* (Ward Hill, USA), *Merck* (Darmstadt, Germany), *Avantor* (Darmstadt, Germany), *TCI Deutschland GmbH* (Eschborn, Germany), *Fisher Scientific* (Schwerte, Germany), and *ABCR* (Karlsruhe, Germany). The purchased chemicals were used without further purification. Dry solvents for organic synthesis were produced and stored according to general procedures.<sup>42</sup>

**Gravity-driven column chromatography.** For gravity-driven column chromatography, silica gel 60 (0.063 – 0.200 nm) purchased from *Merck* (Darmstadt, Germany) was used.

**Flash chromatography.** For purification by medium pressure liquid chromatography (MPLC, flash chromatography), a *puriFlash*<sup>®</sup>430 system from *Interchim* (Montluçon, France) with an integrated UV diode array detector (DAD) with a scanning range of 200 – 600 nm was used. Non-UV-active compounds were detected using a *Flash-ELSD* (evaporative light scattering detector) version 2011 from *Interchim* (Montluçon, France). The following pre-packed columns were used: *Chromabond Flash*, type: RS15 C18 ec, 16 g from *Macherey-Nagel* (Düren, Germany) and *puriFlash*, type: SI-Std (IR-50SI), 12 g and 25 g from *Interchim* (Montluçon, France).

**HPLC.** Purity analysis was carried out using an HPLC (high performance liquid chromatography) system from *Shimadzu Scientific instruments* (Kyoto, Japan). Mobile phase A was Milli-Q<sup>®</sup>-water with 0.1% formic acid (FA) added, while mobile phase B was MeOH with 0.1% FA. The gradient started with 5% of mobile phase B and the ratio of mobile phase B was increased to 100% over 8 min and held for 4 min. For re-equilibration, the mobile phase B ratio was reduced from 100% to 5% in another 4 min. Subsequently, the column was flushed with 5% B for 2 min. The flow rate was set to 1.0 mL/min. The injection volume was 20 µL. The UV signal at 254 nm was chosen for detection, with the oven set to room temperature.

**TLC.** Thin layer chromatography (TLC) was performed on pre-coated silica gel glass plates SIL G-25 (*Macherey-Nagel*, Düren, Germany). Spots were evidenced by quenching at 254 nm or intrinsic fluorescence at 365 nm.

**High-Resolution Mass Spectrometry (HRMS)** was performed using an *Agilent* Infinity II LC-system (Waldbronn, Germany) consisting of a quaternary pump, a thermostatted autosampler and a thermostatted column compartment, coupled to a *Sciex* X500R QTOF mass spectrometer (Concord, Ontario, Canada) equipped with a Turbo V<sup>TM</sup> Ion Source (ESI). Automatic calibration

of the mass spectrometer was performed using the provided tuning solution for ESI (*Sciex*, Concord, Ontario, Canada). Mobile phase A was a mixture of water and 0.1% FA, while mobile phase B was acetonitrile with 0.1% FA. An isocratic elution of 50% B with a stop time of 1.5 min was used. The flow rate was set to 1 mL/min and the injection volume was 10  $\mu$ L. The parameters for the HRMS experiment were optimized by flow-injection using positive polarity (Gas1: 50 psi, Gas2: 50 psi, Curtain gas: 25 psi, Ionspray voltage: 5500 V, Temperature: 500  $^{\circ}$ C, Declustering potential: 70 +/- 10 V, Collision energy: 10 V).

**Infrared Spectroscopy (IR).** IR spectra were recorded on a Jasco-FT-IR-6100 system (*Jasco Deutschland GmbH*, Groß-Umstadt, Germany) in combination with a diamond ATR accessory. The wave numbers of characteristic absorption bands are given in [ $\text{cm}^{-1}$ ] and categorized according to their strength (vs = very strong, s = strong, m = medium, w = weak, br = broad).

**Nuclear Magnetic Resonance Spectroscopy.**  $^1\text{H}$  (400.132 MHz) and  $^{13}\text{C}$  (100.613 MHz) NMR spectra were recorded on a Bruker AV 400 instrument (*Bruker Biospin*, Ettlingen, Germany) at a temperature of 300 K. The signal of the respective deuterated solvent was used as internal standard ( $\text{CDCl}_3$ :  $^1\text{H}$ : 7.26 ppm,  $^{13}\text{C}$ : 77.16 ppm;  $\text{CD}_3\text{OD}$ :  $^1\text{H}$ : 3.31 ppm,  $^{13}\text{C}$ : 49.00 ppm;  $\text{DMSO-d}_6$ :  $^1\text{H}$ : 2.50 ppm,  $^{13}\text{C}$ : 39.52 ppm).<sup>43</sup> Abbreviations for multiplicity are: s, singlet; d, doublet; t, triplet; m, multiplet; br, broad; dd, doublet of doublets; ddd, doublet of doublets of doublets. MestReNova<sup>®</sup> (version 6.0.2-5475) software (*Mestrelab Research S.L.*, Santiago de Compostela, Spain) was applied for processing of NMR spectra.

**Melting points.** To determine melting points, an MP70 melting point system (*Mettler-Toledo GmbH*, Gießen, Germany) was used. The results are not corrected.

**Synthesis of the investigated Mip inhibitors.** The selected inhibitors **11**, **15**, **14**, and **2** and the corresponding synthesis have been described by Seufert *et al.*<sup>18</sup> **13** was synthesized using precursor 3-(pyridin-3-yl)propyl (*R, S*)-1-((4-aminobenzyl)sulfonyl) piperidine-2-carboxylate, described in the same publication. The synthesis of **12** has been described by Iwasaki *et al.*<sup>3</sup> **8** is an intermediate of tracer **1** synthesis and is described there. All compounds used had a purity >95% according to HPLC. Purity data are shown in the SI.

**Synthesis of 3-(Pyridin-3-yl)propyl (*R/S*)-1-((4-acetamidobenzyl)sulfonyl)piperidine-2-carboxylate (**13**).** Following a modified procedure by Baer *et al.*,<sup>44</sup> to a solution of 3-(pyridin-3-yl)propyl (*R, S*)-1-((4-aminobenzyl)sulfonyl)piperidine-2-carboxylate (100 mg, 240  $\mu$ mol) in dry DCM (20 mL) were added acetic anhydride (23  $\mu$ L, 240  $\mu$ mol) and  $\text{NEt}_3$  (66  $\mu$ L, 479  $\mu$ mol) under

ice cooling. After completion of the reaction monitored by TLC (SiO<sub>2</sub>, petroleum ether (PE)/EA 1:10), the reaction mixture was loaded directly onto silica gel and purified by flash chromatography (SiO<sub>2</sub>, A: PE, B: EA, gradient: 50% → 100% B). **13** was obtained as a yellowish oil in a yield of 91% (100 mg, 281 μmol).  $R_f = 0.10$  (SiO<sub>2</sub>, PE/EA 1:10), IR (ATR,  $\tilde{\nu}_{max}$  [cm<sup>-1</sup>]): 3308 (w), 3038 (w), 2940 (w), 2859 (w), 1733 (m), 1672 (m), 1534 (m), 1513 (m), 1371 (m), 1325 (m), 1176 (m), 1127 (s), 843 (m). <sup>1</sup>H NMR (CDCl<sub>3</sub>):  $\delta = 8.50 - 8.42$  (m, 2H), 7.69 (s, 1H), 7.56 – 7.47 (m, 3H), 7.42 – 7.33 (m, 2H), 7.25 – 7.20 (m, 1H), 4.50 (d, 1H, <sup>3</sup>J = 4.6 Hz), 4.25 – 4.10 (m, 4H), 3.49 – 3.42 (m, 1H), 3.17 (ddd, 1H, <sup>2</sup>J = 12.8 Hz, <sup>3</sup>J = 12.8, 2.9 Hz), 2.72 (t, 2H, <sup>3</sup>J = 7.8 Hz), 2.17 – 2.07 (m, 4H), 2.03 – 1.93 (m, 2H), 1.73 – 1.55 (m, 3H), 1.50 – 1.35 (m, 1H), 1.29 – 1.12 (m, 1H) ppm. <sup>13</sup>C NMR (CDCl<sub>3</sub>):  $\delta = 171.4, 168.7, 149.7, 147.5, 138.7, 136.3, 136.0, 131.4$  (2C), 124.4, 123.5, 119.6 (2C), 64.2, 58.3, 56.0, 43.4, 29.8, 29.1, 27.8, 24.9, 24.4, 20.3 ppm. Purity (HPLC): 99.4%. HRMS (m/z) C<sub>23</sub>H<sub>29</sub>N<sub>3</sub>O<sub>5</sub>S, (M+H)<sup>+</sup>, calculated 460.19007, found 460.18955, error: 1.1 ppm.

### 2.5.1 Synthesis of tracer 1

**Synthesis of 4-(((Benzyloxy)carbonyl)amino)methyl)benzoic acid (4).** **4** was synthesized according to a protocol by Lameijer *et al.*,<sup>45</sup> using 11.0 g of 4-aminomethylbenzoic acid (72.8 mmol), sodium hydrogen carbonate (7.34 g, 87.3 mmol) and benzyl chloroformate (12.4 mL, 87.3 mmol) in a mixture of THF and water (1:1; 200 mL). **4** was obtained quantitatively as a white powder (20.8 g, 72.8 mmol, > 99%; Lit.:<sup>45</sup> 83%).  $R_f = 0.46$  (DCM/MeOH 9:1), IR (ATR,  $\tilde{\nu}_{max}$  [cm<sup>-1</sup>]): 3340 (s), 3062 (w), 3034 (w), 2927 (m), 1683 (s), 1602 (s), 1550 (s), 1529 (s), 855 (w), 803 (w), 774 (m), mp: 320 °C under decomposition. <sup>1</sup>H NMR (CD<sub>3</sub>OD):  $\delta = 7.95 - 7.87$  (m, 2H), 7.39 – 7.15 (m, 7H), 5.11 (s, 2H), 4.34 (s, 2H) ppm. <sup>13</sup>C NMR (CD<sub>3</sub>OD):  $\delta = 173.8, 159.1, 143.6, 138.0, 135.5, 130.5$  (2C), 129.4 (2C), 129.0, 128.7 (2C), 127.7 (2C), 67.6, 45.2 ppm. The recorded spectra are in agreement with the literature.<sup>45</sup>

**Synthesis of Benzyl (4-((2-hydroxyethyl)carbamoyl)benzyl)carbamate (5).** To a solution of **4** (7000 mg, 24.5 mmol) in dry DCM (150 mL), HOBt (3315 mg, 24.5 mmol) and EDC · HCl (4703 mg, 24.5 mmol) were added under ice cooling and allowed to stir for 15 min. Subsequently, 2-aminoethan-1-ol (2.35 mL, 39.2 mmol) was added to the solution under ice cooling. The reaction was allowed to warm to rt and stirred for 2 d, monitored by TLC (SiO<sub>2</sub>, DCM/MeOH 10:1). The solvent was removed under reduced pressure, the crude oily product was loaded directly

onto silica gel and purified by flash chromatography (SiO<sub>2</sub>, A: DCM, B: MeOH, gradient: 0 → 25% B). **5** was obtained as a white solid in a yield of 87% (7.00 g, 21.3 mmol).  $R_f = 0.47$  (SiO<sub>2</sub>, DCM/MeOH 10:1), mp: 165 °C, IR (ATR,  $\tilde{\nu}_{max}$  [cm<sup>-1</sup>]): 3383 (s), 3142 (s) 2922 (s), 1692 (s), 1656 (s), 1592 (s), 1270 (s), 834 (s), 776 (s), 710 (s). <sup>1</sup>H NMR (DMSO-d<sub>6</sub>):  $\delta = 8.36$  (t, <sup>3</sup>J = 5.6 Hz, 1H), 7.86 (t, <sup>3</sup>J = 6.1 Hz, 1H), 7.83 – 7.75 (m, 2H), 7.41 – 7.28 (m, 7H), 5.05 (br s, 2H), 4.70 (t, <sup>3</sup>J = 5.6 Hz, 1H), 4.25 (d, <sup>3</sup>J = 6.1 Hz, 2H), 3.50 (dt, <sup>3</sup>J = 6.1, 5.9 Hz, 1H), 3.35 – 3.29 (m, 2H) ppm. <sup>13</sup>C NMR (DMSO-d<sub>6</sub>):  $\delta = 166.1, 156.4, 142.8, 137.1, 133.1, 128.4$  (2C), 127.8, 127.7, 127.2 (2C), 126.7 (2C), 65.4, 59.8, 43.6, 42.1 ppm.

**Synthesis of 2-(2-(4-(((Benzyloxy)carbonyl)amino)methyl)benzamido)ethyl)-1-(tert-butyl)-(S)-piperidine-1,2-dicarboxylate (6).** To a solution of (S)-1-(tert-butoxycarbonyl)piperidine-2-carboxylic acid (5.00 g, 21.8 mmol) in a mixture of dry DCM (150 mL) and dry DMF (50 mL), catalytic amounts of DMAP (500 mg, 4.09 mmol) and an excess of EDC · HCl (3.00 g, 15.7 mmol) were added under ice cooling and allowed to stir for 15 min. **5** (4.30 g, 13.1 mmol) was added to the solution under ice cooling, the reaction was allowed to warm to rt and stirred for 1 d, monitored by TLC (SiO<sub>2</sub>, DCM/MeOH 20:1). The solvent was removed *in vacuo*, the residue suspended in DCM and the mixture filtered. The solvent of the filtrate was removed *in vacuo*. The crude oily product was loaded directly onto silica gel and purified by column chromatography (SiO<sub>2</sub>, PE/EA 1:1, followed by PE/EA/MeOH 1:0.9:0.1). After subsequent purification by flash chromatography (SiO<sub>2</sub>, A: PE, B: EA, gradient: 0 → 50% B, ELSD), **6** was obtained as a colorless oily solid in a yield of 48% (3400 mg, 6.30 mmol).  $R_f = 0.17$  (SiO<sub>2</sub>, DCM/MeOH 20:1), IR (ATR,  $\tilde{\nu}_{max}$  [cm<sup>-1</sup>]): 3321 (m), 2932 (m), 1694 (s), 1643 (s), 1535 (s), 1245 (s), 1155 (s) 870 (w), 753 (w), 738 (w). <sup>1</sup>H NMR (CDCl<sub>3</sub>):  $\delta = 7.84 - 7.74$  (m, 2H), 7.40 – 7.28 (m, 7H), 5.18 – 5.09 (m, 3H), 4.78 (br s, 1H), 4.50 – 4.20 (m, 4H), 4.02 – 3.52 (m, 3H), 3.06 – 2.70 (m, 2H), 2.24 – 2.14 (m, 1H), 1.76 – 1.55 (m, 4H), 1.41 (br s, 9H), 1.31 – 1.11 (m, 1H) ppm. <sup>13</sup>C NMR (CDCl<sub>3</sub>):  $\delta = 172.5, 167.1, 156.7, 156.6, 142.5$  (br s, 1C), 136.5, 133.4, 128.7 (br s, 2C), 128.4 (br s, 1C), 128.3 (br s, 2C), 127.64 (br s, 2C), 127.59 (br s, 2C), 80.4, 67.2, 64.0, 54.5 (br s, 1C), 44.9, 42.7 & 39.3 (br s, 1C, *rotamers*), 38.8, 28.5 (s, 3C), 26.6, 24.7, 20.8 ppm.

**Synthesis of 2-(4-(((Benzyloxy)carbonyl)amino)methyl)benzamido)ethyl (S)-piperidine-2-carboxylate (7).** To a solution of **6** (2700 mg, 5.00 mmol) in dry DCM (25 mL) was slowly added 5.00 mL of TFA (65.0 mmol) at rt and the mixture was stirred for 2.5 h, monitored by TLC (SiO<sub>2</sub>, DCM/MeOH 20:0.5). Subsequently, the reaction mixture was washed with aqueous saturated



NaHCO<sub>3</sub> solution (3 · 20 mL) and with water (3 · 20 mL). The phases were separated, the organic phase was dried over sodium sulphate and filtrated. After removal of the organic solvent *in vacuo*, **7** was obtained as a white oily solid in a yield of 93% (2043 mg, 4.65 mmol).  $R_f = 0.23$  (SiO<sub>2</sub>, DCM/MeOH 20:0.5), IR (ATR,  $\tilde{\nu}_{max}$  [cm<sup>-1</sup>]): 3331 (s), 3033 (w), 2930 (m), 1738 (w), 1686 (s), 1636 (s), 1534 (s), 1202 (m), 848 (w), 746 (w). <sup>1</sup>H NMR (CDCl<sub>3</sub>):  $\delta = 7.74 - 7.68$  (m, 2H), 7.39 – 7.27 (m, 7H), 6.79 (br s, 1H), 5.34 (br s, 1H), 5.13 (s, 2H), 4.40 (br d, <sup>3</sup>J = 5.9 Hz, 2H), 4.32 (t, <sup>3</sup>J = 5.2 Hz, 2H), 3.74 – 3.67 (m, 2H), 3.38 (dd, <sup>3</sup>J = 9.9, 3.1 Hz, 1H), 3.10 – 3.03 (m, 1H), 2.68 – 2.60 (m, 1H), 2.29 (br s, 1H), 1.99 – 1.92 (m, 1H), 1.81 – 1.74 (m, 1H), 1.60 – 1.40 (m, 4H) ppm. <sup>13</sup>C NMR (CDCl<sub>3</sub>):  $\delta = 174.0, 167.4, 156.6, 142.4$  (br s, 1C), 136.5, 133.4, 128.7 (br s, 2C), 128.33 (br s, 1C), 128.27 (br s, 2C), 127.6 (br s, 2C), 127.5 (br s, 2C), 67.1, 63.8, 58.8 (br s, 1C), 45.8, 44.8, 39.6, 29.4, 25.8, 24.1 ppm.

**Synthesis of 2-(4-(((Benzyloxy)carbonyl)amino)methyl)benzamido)ethyl (S)-1-(benzylsulfonyl)piperidine-2-carboxylate (8).** To a solution of **7** (2350 mg, 5.35 mmol) in dry DCM (50 mL), NEt<sub>3</sub> (1.94 mL, 13.9 mmol) and phenylmethanesulfonyl chloride (1175 mg, 6.04 mmol) were added under ice cooling. The solution was immediately allowed to warm to rt and stirred for 3 d, monitored by TLC (SiO<sub>2</sub>, PE/EA 1:3). Subsequently, the mixture was washed with diluted acetic acid (0.1 M, 50 mL) and saturated ammonium chloride solution (30 mL). The phases were separated, the organic solvent was removed *in vacuo*, and the crude oily product was purified by flash chromatography (Run 1: SiO<sub>2</sub>, A: DCM, B: MeOH, gradient: 0% → 30% B; Run 2: SiO<sub>2</sub>, A: CyH, B: EA, gradient: 0% → 100% B). **8** was obtained as white oily solid in a yield of 44% (1400 mg, 2.36 mmol).  $R_f = 0.68$  (SiO<sub>2</sub>, PE/EA 1:3), IR (ATR,  $\tilde{\nu}_{max}$  [cm<sup>-1</sup>]): 3346 (br m), 2946 (m), 1704 (s), 1644 (s), 1534 (s), 1505 (s), 1321 (s), 847 (w), 824 (w), 781 (w). <sup>1</sup>H NMR (CDCl<sub>3</sub>):  $\delta = 7.84 - 7.79$  (m, 2H), 7.42 – 7.28 (m, 12H), 7.13 (t, <sup>3</sup>J = 5.4 Hz, 1H), 5.19 – 5.11 (m, 3H), 4.49 – 4.41 (m, 3H), 4.27 – 4.16 (m, 4H), 3.83 – 3.68 (m, 2H), 3.33 (d, <sup>2</sup>J = 12.8 Hz, 1H), 3.08 (ddd, <sup>2</sup>J = 12.8, <sup>3</sup>J = 12.8, 2.7 Hz, 1H), 2.13 (br d, <sup>2</sup>J = 13.4 Hz, 1H), 1.70 – 1.54 (m, 2H), 1.48 – 1.28 (m, 2H), 1.19 – 1.08 (m, 1H) ppm. <sup>13</sup>C NMR (CDCl<sub>3</sub>):  $\delta = 171.4, 167.2, 156.6, 142.1, 136.5, 133.3, 131.0$  (2C), 129.2, 129.0, 128.8 (2C), 128.7 (2C), 128.4, 128.3 (2C), 127.8 (2C), 127.5 (2C), 67.1, 64.9, 59.2, 56.7, 44.9, 44.2, 38.9, 27.2, 24.8, 20.2 ppm. Purity (HPLC): 95.1%. HRMS (m/z) C<sub>31</sub>H<sub>35</sub>N<sub>3</sub>O<sub>7</sub>S, (M+H)<sup>+</sup>, calculated 594.22685, found 594.22775, error: 1.5 ppm.

**Synthesis of 2-(4-(Aminomethyl)benzamido)ethyl (S)-1-(benzylsulfonyl)piperidine-2-carboxylate (9).** To a solution of **8** (450 mg, 758  $\mu\text{mol}$ ) in methanol (15 mL) and acetic acid (1 mL, 1 mol/L), catalytic amounts of palladium on charcoal (10 wt-%, 84 mg, 79  $\mu\text{mol}$ ) were added at rt under an Argon atmosphere. The reaction mixture was then stirred for 1 d at rt under a hydrogen pressure of 10 bar. Subsequently, the catalyst was removed over celite, which was then extracted with methanol (50 mL). The solvent was removed *in vacuo*. The residue was diluted with DCM (50 mL) and washed with saturated sodium hydrogen carbonate solution (2 · 20 mL). After separation of the phases, the solvent of the organic phase was removed *in vacuo*, and the crude oily product was purified by flash chromatography (SiO<sub>2</sub>, A: DCM, B: MeOH, gradient: 0% → 20% B). **9** was obtained as a slightly yellowish solid in a yield of 13% (45 mg, 99  $\mu\text{mol}$ ).  $R_f = 0.11$  (SiO<sub>2</sub>, DCM/MeOH 9:1), mp: 85 °C, IR (ATR,  $\tilde{\nu}_{\text{max}}$  [cm<sup>-1</sup>]): 3310 (br m), 2932 (m), 2857 (m), 1733 (s), 1637 (s), 1539 (s), 1498 (s), 1320 (s), 845 (w), 782 (w). <sup>1</sup>H NMR (CDCl<sub>3</sub>, protonated form of **9**):  $\delta = 7.85 - 7.80$  (m, 2H), 7.44 – 7.34 (m, 7H), 7.16 (t, <sup>3</sup>J = 5.7 Hz, 1H), 4.47 – 4.40 (m, 1H), 4.30 – 4.19 (m, 4H), 3.93 (br s, 2H), 3.83 – 3.70 (m, 2H), 3.33 (br d, <sup>2</sup>J = 12.7 Hz, 1H), 3.08 (ddd, <sup>2</sup>J = 12.7, <sup>3</sup>J = 12.7, 2.7 Hz, 1H), 2.26 (br s, 3 H), 2.12 (br d, <sup>2</sup>J = 13.3 Hz, 1H), 1.65 – 1.55 (m, 2H), 1.50 – 1.10 (m, 3H) ppm. <sup>13</sup>C NMR (CDCl<sub>3</sub>, protonated form of **9**):  $\delta = 171.5, 167.4, 145.7, 132.9, 131.0$  (2C), 129.2, 128.9, 128.8 (2C), 127.7 (2C), 127.4 (2C), 64.9, 59.2, 56.7, 46.0, 44.1, 38.9, 27.3, 24.8, 20.2 ppm.

**Synthesis of 6-(3',6'-Dihydroxy-3-oxo-3H-spiro[isobenzofuran-1,9'-xanthene]-5-carboxamido)hexanoic acid (10).** To a mixture of 5-carboxyfluorescein (495 mg, 1.25 mmol), 6-methoxy-6-oxohexane-1-aminium chloride (204 mg, 1.12 mmol), and NEt<sub>3</sub> (0.36 mL, 2.62 mmol) in dry DMF (20 mL), HBTU (507 mg, 1.34 mmol) was added at rt and stirred overnight. After removal of DMF *in vacuo*, the crude oily product obtained was treated with a solution of lithium hydroxide (0.4 M, 31.2 mL, 12.5 mmol) at rt for 1 d. The pH was then adjusted to 5 with diluted hydrochloric acid (10 mL, 1 M) under ice cooling. The solvent was removed *in vacuo*, the mixture was directly loaded onto silica gel, and the crude oily product was purified by flash chromatography (SiO<sub>2</sub>, A: DCM + 0.5% FA, B: MeOH + 0.5% FA, gradient: 0% → 10% B). **10** was obtained as an orange solid in a yield of 33% (180 mg, 368  $\mu\text{mol}$ ).  $R_f = 0.28$  (SiO<sub>2</sub>, CHCl<sub>3</sub>/MeOH 9:1 + 1% FA; 365 nm), mp: 262 °C (under decomposition), IR (ATR,  $\tilde{\nu}_{\text{max}}$  [cm<sup>-1</sup>]): 3043 (m), 2936 (m), 1707 (m), 1666 (m), 1577 (vs), 1530 (vs), 1455 (vs), 1295 (vs), 850 (m), 760 (m). <sup>1</sup>H NMR (CD<sub>3</sub>OD):  $\delta = 8.41$  (br s, 1H), 8.19 (dd, <sup>3</sup>J = 8.0, <sup>4</sup>J = 1.5 Hz, 1H), 7.29

(d,  $^3J = 8.0$  Hz, 1H), 6.69 (d,  $^4J = 2.3$  Hz, 2H), 6.59 (d,  $^3J = 8.7$  Hz, 2H), 6.53 (dd,  $^3J = 8.7$ ,  $^4J = 2.3$  Hz, 2H), 3.44 (t,  $^3J = 7.2$  Hz, 2H), 2.33 (t,  $^3J = 7.2$  Hz, 2H), 1.74 – 1.63 (m, 4H), 1.51 – 1.41 (m, 2H) ppm.  $^{13}\text{C}$  NMR ( $\text{CD}_3\text{OD}$ ):  $\delta = 177.5$ , 170.6, 168.4, 161.4 (br s, 2C), 156.6, 154.0 (2C), 138.1, 135.5, 130.1 (2C), 128.7, 125.7, 124.7, 113.7 (2C), 110.9 (2C), 103.6 (2C), 82.3, 41.1, 34.8, 30.1, 27.6, 25.8 ppm. The molecule is known in the literature,<sup>46</sup> but no synthesis or analytical data have been reported to date.

**Synthesis of 2-(4-((6-(3',6'-Dihydroxy-3-oxo-3H-spiro[isobenzofuran-1,9'-xanthene]-5-carboxamido)hexanamido)methyl)benzamido)ethyl (S)-1-(benzylsulfonyl)piperidine-2-carboxylate (1).** To a solution of **10** (32 mg, 65  $\mu\text{mol}$ ) in a mixture of dry DCM (10 mL) and DMF (5 mL), HBTU (33 mg, 88  $\mu\text{mol}$ ) and DIPEA (100  $\mu\text{L}$ , 570  $\mu\text{mol}$ ) were added under ice cooling and allowed to stir for 15 min. Subsequently, compound **9** (30 mg, 65  $\mu\text{mol}$ ) was added to the solution under ice cooling, the reaction was allowed to warm to rt and stirred for 1 d, monitored by TLC ( $\text{SiO}_2$ , DCM/MeOH 10:1 + 1% FA). Saturated ammonium chloride solution (10 mL) was added, the solvent was removed *in vacuo*, and the crude oily product was directly loaded onto silica gel. After purification by flash chromatography (Run 1:  $\text{SiO}_2$ , A: DCM, B: MeOH, gradient: 0  $\rightarrow$  20% B; Run 2: RP 18, A:  $\text{H}_2\text{O}$  + 0.1% FA, B: ACN + 0.1% FA, gradient: 5%  $\rightarrow$  40% B), **1** was obtained as a yellow solid in a yield of 44% (27 mg, 29  $\mu\text{mol}$ ).  $R_f = 0.40$  ( $\text{SiO}_2$ , DCM/MeOH 10:1 + 1% FA, 365 nm), mp: 160  $^\circ\text{C}$ , IR (ATR,  $\tilde{\nu}_{\text{max}}$  [ $\text{cm}^{-1}$ ]): 3341 (br, s), 3080 (br, s), 2941 (s), 1740 (s), 1704 (s), 1636 (vs), 1613 (vs), 1319 (s), 1109 (vs), 847 (m), 740 (m).  $^1\text{H}$  NMR ( $\text{CD}_3\text{OD}$ ):  $\delta = 8.42$  (br s, 1H), 8.17 (dd,  $^3J = 8.0$ ,  $^4J = 1.5$  Hz, 1H), 7.79 – 7.75 (m, 2H), 7.42 – 7.37 (m, 2H), 7.36 – 7.31 (m, 5H), 7.28 (d,  $^3J = 8.0$  Hz, 1H), 6.69 (d,  $^4J = 2.3$  Hz, 2H), 6.60 (d,  $^3J = 8.7$  Hz, 2H), 6.53 (dd,  $^3J = 8.7$ ,  $^4J = 2.3$  Hz, 2H), 4.44 – 4.38 (m, 3H), 4.38 – 4.33 (m, 2H), 4.33 – 4.30 (m, 2H), 3.73 – 3.61 (m, 2H), 3.46 – 3.36 (m, 3H), 3.14 (ddd,  $^2J = 12.8$ ,  $^3J = 12.8$ , 2.8 Hz, 1H), 2.30 (t,  $^3J = 7.3$  Hz, 2H), 2.14 – 2.07 (m, 1H), 1.77 – 1.64 (m, 4H), 1.60 – 1.32 (m, 6H), 1.24 – 1.15 (m, 1H) ppm.  $^{13}\text{C}$  NMR ( $\text{CD}_3\text{OD}$ ):  $\delta = 176.1$ , 172.8, 170.6, 170.0, 168.4, 161.3 (2C), 154.3 (2C), 144.3, 138.0, 135.2, 134.2, 132.2 (2C), 131.0, 130.3 (2C), 129.50–129.45 (m, 3C), 128.65–128.57 (m, 6C), 125.9, 125.0, 114.0 (2C), 111.1 (2C), 103.6 (2C), 82.0, 64.8, 59.4, 57.3, 44.6, 43.7, 41.0, 40.0, 36.9, 30.1, 28.5, 27.6, 26.6, 26.0, 21.2 ppm. Purity (HPLC): 95.4%. HRMS ( $m/z$ )  $\text{C}_{50}\text{H}_{50}\text{N}_4\text{O}_{12}\text{S}$ , ( $\text{M}+\text{H}$ ) $^+$ , calculated 931.32187, found 931.32079, error: 1.2 ppm.

### 2.5.2 Protease-Coupled PPIase Assay

BpMip was transformed into BL21(DE3) cells and expressed and prepared as described.<sup>37</sup> **13** was tested in the protease-coupled PPIase assay according to a protocol by Vivoli *et al.* analogous to the other inhibitors studied.<sup>20</sup> The protease-coupled PPIase assay data for inhibitors **11**, **15**, **14**, and **2** were reported by Seufert *et al.*,<sup>18</sup> PPIase data of **12** by Iwasaki *et al.*<sup>3</sup>

### 2.5.3 FP Assay Validation with BpMip and Probe 1, Thermodynamic Study of the Influence of Temperature on $K_D$ , and ITC measurement

BpMip was codon-optimized using an in-house script (available at <https://github.com/njharmer/CodonOptimise>) and the synthesized gene cloned into the pNIC28-Bsa4 vector (<https://www.addgene.org/26103/>) by Twist Bioscience. The BpMip-1 interaction was measured following the methods of Rossi and Taylor.<sup>23</sup> 5 nM **1** was mixed with 15 concentrations of BpMip (200 nM to 12 nM in two-fold dilutions), or a buffer blank, in a buffer of 35 mM Hepes pH 7.8 in a 384 well black walled plate (Corning #3820) in a total volume of 40  $\mu$ L. In the same plate, the same concentrations of BpMip in buffer alone, and with 5 nM **1** and 300 nM **11** were prepared to control for BpMip fluorescence and non-specific binding of **1** to BpMip. All samples were prepared in duplicate. Samples were incubated in the dark with mild shaking for 15 minutes, centrifuged at 300  $g$  for two minutes, and incubated at 25 °C for 20 minutes. Fluorescence anisotropy was measured using a Clariostar plate reader (BMG Labtech, Ortenberg, Germany) with excitation at 488 nm and emission at 518 nm. Gain optimization was performed using the manufacturer's recommendations. For measurements at different temperatures, the samples were incubated at the relevant temperature for 20 minutes before reading. A script was used to automate incubation and reading for samples and is available as a supplementary file. The raw parallel and perpendicular measurements were corrected for BpMip autofluorescence by subtracting the values of the paired BpMip only wells. Fluorescence anisotropy was calculated using equation 1:

$$A = \frac{(I_{\parallel} - I_{\perp})}{(I_{\parallel} + 2I_{\perp})} \quad [1]$$

Where  $I_{\parallel}$  and  $I_{\perp}$  are the parallel and perpendicular intensities respectively.

Anisotropy due to non-specific binding was calculated at each protein concentration using equation 2:

$$A_{NS} = (A_I - A_D) * \left(1 - \frac{A_M - A_D}{A_{DR} - A_D}\right) \quad [2]$$

Where  $A_{NS}$  is the non-specific anisotropy,  $A_M$  is the measured protein-1 anisotropy at this concentration,  $A_I$  is the measured protein-1 anisotropy in the presence of excess **1** at the relevant concentration,  $A_D$  is the anisotropy of **1** alone, and  $A_{DR}$  is the BpMip-1 anisotropy at saturating BpMip.  $A_{NS}$  was subtracted from  $A_M$  at each concentration to give the final specific anisotropy  $A_s$ . The  $A_s$  values were fitted to the four-parameter ligand saturation equation (3):

$$A_s = lower + (upper - lower) \left( \frac{[BpMip]^h}{([BpMip]^h + EC_{50}^h)} \right) \quad [3]$$

Where  $EC_{50}$  is the concentration of BpMip required to achieve a 50% effect, upper and lower are fully bound and unbound anisotropy of **1**, and  $h$  is the hill coefficient. As the  $EC_{50}$  is well in excess of the **1** concentration,  $EC_{50}$  is equivalent to  $K_D$  within error.

The van't Hoff plot was calculated by plotting the natural logarithm of  $K_D$  against the inverse of temperature (in Kelvin) and fitting a straight line with linear regression:

$$\ln K_D = \frac{\Delta H^\circ}{RT} + c \quad [4]$$

Where  $R$  is the gas constant (8.314 J K<sup>-1</sup> mol<sup>-1</sup>). From the gradient of the line,  $\Delta H^\circ$  can be calculated. This then allows  $\Delta S^\circ$  to be calculated:

$$\Delta G^\circ = RT \ln K_D \quad [5]$$

$$\Delta G^\circ = \Delta H^\circ - T\Delta S^\circ \quad [6]$$

All calculations were performed in *R*. A script for performing these calculations is available as a supplementary file.

The determination of the G-factor was performed using the protocol provided by *Berthold Technologies* (Bad Wildbad, Germany) and resulted in a value of 1.15 for the instrument used.

FP was measured for the sensitivity study at 15 concentrations of **1** (0.005 nM to 50 nM) diluted in HEPES buffer (HEPES 20 mM, TritonX-100 0.002%, KCl 13.4 mM, pH 8).

For active site titration, tracer molecule **1** was mixed in equal parts to a final concentration of 5 nM with at least 8 concentrations of BpMip (100 μM to 0.05 nM, in different steps of dilution).

For all experiments, the final volume in the 384 black, flat-bottom, non-binding well plates (*Greiner Bio-One*, Kremsmünster, Austria, #781900) was 60 μL. Incubation was performed for 30 min at room temperature in the dark, followed by measuring the FP value (Mithras LB 940, *Berthold Technologies*, Bad Wildbad, Germany) three times each well. The  $K_D$  value was calculated with GraphPad Prism 8.0.1 from Dotmatics (Boston, Massachusetts, USA) using the equation

given by Wang *et al.*<sup>47</sup>

$$\Delta F = \frac{A/[L]_t}{2} \left\{ ([P]_t + [L]_t + K_D - \sqrt{([P]_t + [L]_t + K_D)^2 - 4[P]_t[L]_t})} \right\}$$

Fitting parameter:

$\Delta F$  = change in FP signal

A = FP amplitude, constant

$L_t$  = total concentration of the ligand (tracer)

$P_t$  = total concentration protein

$K_D$  = dissociation constant

For the kinetics test, where the  $K_D$  value was determined over a period of 3 hours (0 min, 5 min, 15 min, 30 min, 1 h, 2 h and 3 h), the same procedure was followed as for active site titration. The experiment was carried out in duplicate and the incubation time of 30 min was maintained for all further experiments.

To examine the influence of DMSO, a mixture of a specific concentration of DMSO (0%, 0.5%, 1%, 2% and 4%) in HEPES buffer and the probe **1** (10 nM) was used in a total of 30  $\mu$ L. After adding to 30  $\mu$ L of BpMip (4  $\mu$ M), resulting in a final concentration of 5 nM for **1**, 2  $\mu$ M for BpMip and 0%, 0.25%, 0.5%, 1%, and 2% DMSO, respectively, and a total volume of 60  $\mu$ L, FP was measured.

Negative control for Z-factor determination was therefore the same mixture as mentioned above with a final DMSO concentration of 0.5%, which is the maximum of FP. For the minimum, the most potent inhibitor **12** in this series was chosen, diluted from DMSO stock to a final concentration of 150  $\mu$ M of **12** and 0.5% DMSO (see SI).

The ITC measurement was performed by MicroCal iTC200 (*Danaher Corporation*, Washington, D.C., USA, formerly: **GE HealthCare**, Chicago, Illinois, USA). For this purpose, a stock solution of **1** was prepared at a concentration of 600  $\mu$ M. Whereby the final DMSO concentration was 3%. Therefore, the measurement cell was filled with a 60 micromolar BpMip solution in HEPES buffer, which also contained 3% DMSO. After three measurements, the  $K_D$  value was  $5.50 \pm 0.03$   $\mu$ M. The FP assay gave a  $K_D$  of 3.6  $\mu$ M for this DMSO concentration. Data were calculated using

Origin 7 (*OriginLab Corporation*, Northampton, Massachusetts, USA).

#### 2.5.4 Competitive Displacement Assay for The Screening of BpMip Inhibitors

To determine inhibitor  $K_i$ , stock DMSO solutions of each compound (approximately 25 mM) were prepared and then diluted with HEPES buffer in various dilution patterns (1:10; 1:5, 1:3). All competition assays were carried out as triplicates.

In the well, 15  $\mu\text{L}$  inhibitor dilution (final concentrations from 50  $\mu\text{M}$  to 2 nM) was mixed with 15  $\mu\text{L}$  tracer (20 nM) as well as 30  $\mu\text{L}$  BpMip (4  $\mu\text{M}$ ) to again obtain a final concentration of 5 nM 1 and 2  $\mu\text{M}$  BpMip. To ensure the quality of the Mip protein before each measurement, a positive control consisting of BpMip (2  $\mu\text{M}$ ), probe 1 (20 nM), and buffer (in place of the competitor) was measured for each run. The constant binding affinity of the protein to the ligand is indicated by reaching the upper plateau of the mP values. This was interpreted as demonstrating the integrity of the Mip protein for that experiment.

Fitting parameter for the competition assay, according to Wang *et al.*<sup>48</sup>:

$$\Delta F = \frac{A\{2\sqrt{a^2 - 3b} \cos(\theta/3) - a\}}{3K_A + \{2\sqrt{a^2 - 3b} \cos(\theta/3) - a\}} + F_0$$

$$a = K_A + K_B + A_0 + B_0 - P_0$$

$$b = K_B * (A_0 - P_0) + K_A * (B_0 - P_0) + K_A * K_B$$

$$c = -K_A * K_B * P_0$$

$$\theta = \arccos\left(\frac{-2*a^3 + 9*a*b - 27*c}{2*\sqrt{(a-3b)^3}}\right)$$

$$Y = \text{Ampl} * \frac{2*\sqrt{(a-3b)}*\cos(\theta/3) - a}{3*K_A + (2*\sqrt{(a-3b)}*\cos(\theta/3) - a)} + \text{Back}$$

$K_A$  =  $K_D$  of the tracer (ligand A)

$K_B$  =  $K_i$  of the inhibitor (ligand B)

$B_0$  = free inhibitor concentration

$A_0$  = free tracer concentration

$P_0$  = free protein concentration

$F_0$  = FP signal minimum

*Data were collected on two different instruments at the Universities of Würzburg and Exeter, giving similar results.*

## 2.6 Author information

### Corresponding Authors

N.J.H.: email, [N.J.Harmer@exeter.ac.uk](mailto:N.J.Harmer@exeter.ac.uk)

U.H.: email, [ulrike.holzgrabe@uni-wuerzburg.de](mailto:ulrike.holzgrabe@uni-wuerzburg.de)

### ORCID

Nicolas J. Scheuplein: 0000-0003-3261-7964

Theresa Lohr: 0000-0001-6473-0983

Mirella Vivoli Vega: 0000-0002-1148-5651

Nicholas J. Harmer: 0000-0002-4073-0505

Ulrike Holzgrabe: 0000-0002-0364-7278

### Author Contributions

‡ N.J.S. and T.L. are equal first authors, and U.H. and N.J.H. are equal corresponding authors.

N.J.S.: Formal analysis, Investigation, Writing – original draft, review & editing. T.L.: Formal analysis, Investigation, Methodology, Writing – original draft, review & editing. M.V.V.: Investigation, Methodology. F.S.: Investigation, Methodology. D.A.: Investigation. L.K.: Investigation. N.J.H: Conceptualization, Formal analysis, Funding acquisition, Investigation, Supervision, Validation, Writing – review & editing. U.H.: Conceptualization, Funding acquisition, Project Administration, Supervision, Validation, Writing – review & editing.

### Declaration of Competing Interest

The authors declare that they have no known competing financial interests or personal relationships that could have appeared to influence the work reported in this paper.

### Acknowledgments

Thanks are due to Ute Hellmich for providing purified BpMip. Felix Hausch is thanked for supporting data analysis with GraphPad. This work was supported by the North Atlantic Treaty Organization (NATO), Brussels, Belgium grant SPS 984835, and the German Research Foundation (DFG, Bonn, Germany; grant SFB 630) for the development of Mip inhibitors against *Legionella pneumophila* and *Burkholderia pseudomallei*, respectively, and The Federal Ministry of



Education and Research (Germany, Berlin, project number 16GW0212 “iMIP”) for the development of Mip inhibitors against *Trypanosoma cruzi* given to UH. This paper includes research that was supported by DMTC Limited (Australia, project number 10.44 “pharmaceutical development of antivirulence compounds against bio-warfare pathogens”), BBSRC grant BB/N001591/1, and UKRI CoA funds. The authors have prepared this paper in accordance with the intellectual property rights granted to partners from the original DMTC project.

### Abbreviations used

ATR, attenuated total reflectance; Boc, *tert*-butyloxycarbonyl; BpMip, *Burkholderia pseudomallei* Mip; C18, octyldecylsilane; Cbz, benzyl chloroformate; DAD, diode array detection; DCC, *N,N'*-dicyclohexylcarbodiimide; DCM, dichloromethane; DIPEA, *N,N*-diisopropylethylamine; DMAP, 4-dimethylaminopyridine; DMF, dimethylformamide; DMSO, dimethyl sulfoxide; EA, ethyl acetate; EDC-HCl, 1-ethyl-3-(3-dimethylaminopropyl)carbodiimide hydrochloride; ELSD, evaporative light scattering detector; FA, formic acid; FKBP, FK506 binding proteins; FP, fluorescence polarization; FPA, fluorescence polarization assay; HBTU, hexafluorophosphate benzotriazole tetramethyl uronium; HOBT, 1-hydroxybenzotriazole; HPLC, high performance liquid chromatography; HRMS, high-resolution mass spectrometry; HTS, high-throughput screening; IC<sub>50</sub>, inhibitory concentration of 50%; IR, infrared; *K<sub>D</sub>*, dissociation constant; *K<sub>i</sub>*, inhibition constant;  $\lambda_{\max}$ , lambda max, wavelength at which a substance has its strongest photon absorption; Mip, macrophage infectivity potentiator; mP, millipolarization; NEt<sub>3</sub>, triethylamine; NMR, nuclear magnetic resonance; PDB ID, Protein Data Bank Identification; PE, petroleum ether; PPIase, peptidyl-prolyl *cis-trans* isomerase; rt, room temperature; SAR, structure–activity relationships; TFA, trifluoroacetic acid; TLC, thin layer chromatography;

### Supplementary Material

Supplementary data include NMR spectra and purity data of the tested compounds. The HRMS method and detailed *K<sub>D</sub>* data are also provided. Further data and figures for assay validation and all replications with SEM of the competition assay are shown.

Supplementary material associated with this article can be found, in the online version, at [doi:10.1016/j.slasd.2023.03.004](https://doi.org/10.1016/j.slasd.2023.03.004).

## 2.7 References

1. Kohler, R.; Fanghanel, J.; Konig, B.; Luneberg, E.; Frosch, M.; Rahfeld, J. U.; *et al.* Biochemical and functional analyses of the Mip protein: influence of the N-terminal half and of peptidylprolyl isomerase activity on the virulence of *Legionella pneumophila*. *Infect. Immun.* **2003**, *71* (8), 4389–97. DOI: 10.1128/IAI.71.8.4389-4397.2003.
2. Norville, I. H.; Harmer, N. J.; Harding, S. V.; Fischer, G.; Keith, K. E.; Brown, K. A.; *et al.* A *Burkholderia pseudomallei* macrophage infectivity potentiator-like protein has rapamycin-inhibitable peptidylprolyl isomerase activity and pleiotropic effects on virulence. *Infect. Immun.* **2011**, *79* (11), 4299–307. DOI: 10.1128/IAI.00134-11.
3. Iwasaki, J.; Lorimer, D. D.; Vivoli-Vega, M.; Kibble, E. A.; Peacock, C. S.; Abendroth, J.; *et al.* Broad-spectrum in vitro activity of macrophage infectivity potentiator inhibitors against Gram-negative bacteria and *Leishmania major*. *J. Antimicrob. Chemother.* **2022**, *77*, 1625–1634. DOI: 10.1093/jac/dkac065.
4. Scheuplein, N. J.; Bzdyl, N. M.; Kibble, E. A.; Lohr, T.; Holzgrabe, U.; Sarkar-Tyson, M. Targeting Protein Folding: A Novel Approach for the Treatment of Pathogenic Bacteria. *J. Med. Chem.* **2020**, *63* (22), 13355–88. DOI: 10.1021/acs.jmedchem.0c00911.
5. Rasch, J.; Unal, C. M.; Klages, A.; Karsli, U.; Heinsohn, N.; Brouwer, R.; *et al.* Peptidyl-Prolyl-cis/trans-Isomerases Mip and PpiB of *Legionella pneumophila* Contribute to Surface Translocation, Growth at Suboptimal Temperature, and Infection. *Infect. Immun.* **2019**, *87* (1): e00939-17. DOI: 10.1128/IAI.00939-17.
6. Leuzzi, R.; Serino, L.; Scarselli, M.; Savino, S.; Fontana, M. R.; Monaci, E.; *et al.* Ng-MIP, a surface-exposed lipoprotein of *Neisseria gonorrhoeae*, has a peptidyl-prolyl cis/trans isomerase (PPIase) activity and is involved in persistence in macrophages. *Mol. Microbiol.* **2005**, *58* (3), 669–81. DOI: 10.1111/j.1365-2958.2005.04859.x.
7. Lundemose, A. G.; Kay, J. E.; Pearce, J. H. *Chlamydia trachomatis* Mip-like protein has peptidylprolyl cis/trans isomerase activity that is inhibited by FK506 and rapamycin and is implicated in initiation of chlamydial infection. *Mol. Microbiol.* **1993**, *7* (5), 777–83. DOI: 10.1111/j.1365-2958.1993.tb01168.x.

8. Unal, C. M.; Steinert, M. FKBP in bacterial infections. *Biochim. Biophys. Acta* **2015**, *1850* (10), 2096–102. DOI: 10.1016/j.bbagen.2014.12.018.
9. Moro, A.; Ruiz-Cabello, F.; Fernandez-Cano, A.; Stock, R. P.; Gonzalez, A. Secretion by *Trypanosoma cruzi* of a peptidyl-prolyl cis-trans isomerase involved in cell infection. *EMBO J.* **1995**, *14* (11), 2483–90. DOI: 10.1002/j.1460-2075.1995.tb07245.x.
10. Wiersinga, W. J.; Virk, H. S.; Torres, A. G.; Currie, B. J.; Peacock, S. J.; Dance, D. A. B.; *et al.* Melioidosis. *Nat. Rev. Dis. Primers* **2018**, *4*, 17107. DOI: 10.1038/nrdp.2017.107.
11. Birnie, E.; Virk, H. S.; Savelkoel, J.; Spijker, R.; Bertherat, E.; Dance, D. A. B.; *et al.* Global burden of melioidosis in 2015: a systematic review and data synthesis. *Lancet Infect. Dis.* **2019**, *19* (8), 892–902. DOI: 10.1016/s1473-3099(19)30157-4.
12. Norville, I. H.; Breitbach, K.; Eske-Pogodda, K.; Harmer, N. J.; Sarkar-Tyson, M.; Titball, R. W.; *et al.* A novel FK-506-binding-like protein that lacks peptidyl-prolyl isomerase activity is involved in intracellular infection and in vivo virulence of *Burkholderia pseudomallei*. *Microbiology (Reading)* **2011**, *157* (Pt 9), 2629–38. DOI: 10.1099/mic.0.049163-0.
13. Norville, I. H.; O'Shea, K.; Sarkar-Tyson, M.; Zheng, S.; Titball, R. W.; Varani, G.; *et al.* The structure of a *Burkholderia pseudomallei* immunophilin–inhibitor complex reveals new approaches to antimicrobial development. *Biochem. J.* **2011**, *437* (3), 413–22.
14. Ceymann, A.; Horstmann, M.; Ehses, P.; Schweimer, K.; Paschke, A. K.; Steinert, M.; *et al.* Solution structure of the *Legionella pneumophila* Mip-rapamycin complex. *BMC Struct. Biol.* **2008**, *8*, 17. DOI: 10.1186/1472-6807-8-17.
15. Juli, C.; Sippel, M.; Jäger, J.; Thiele, A.; Weiwad, M.; Schweimer, K.; *et al.* Pipecolic acid derivatives as small-molecule inhibitors of the *Legionella* MIP protein. *J. Med. Chem.* **2011**, *54* (1), 277–83. DOI: 10.1021/jm101156y.
16. Begley, D. W.; Fox, D., 3rd; Jenner, D.; Juli, C.; Pierce, P. G.; Abendroth, J.; *et al.* A structural biology approach enables the development of antimicrobials targeting bacterial immunophilins. *Antimicrob. Agents Chemother.* **2014**, *58* (3), 1458–67. DOI: 10.1128/AAC.01875-13.

17. Reimer, A.; Seufert, F.; Weiwad, M.; Ebert, J.; Bzdyl, N. M.; Kahler, C. M.; *et al.* Inhibitors of macrophage infectivity potentiator-like PPIases affect neisserial and chlamydial pathogenicity. *Int. J. Antimicrob. Agents* **2016**, *48* (4), 401–8. DOI: 10.1016/j.ijantimicag.2016.06.020.
18. Seufert, F.; Kuhn, M.; Hein, M.; Weiwad, M.; Vivoli, M.; Norville, I. H.; *et al.* Development, synthesis and structure-activity-relationships of inhibitors of the macrophage infectivity potentiator (Mip) proteins of *Legionella pneumophila* and *Burkholderia pseudomallei*. *Bioorg. Med. Chem.* **2016**, *24* (21), 5134–47. DOI: 10.1016/j.bmc.2016.08.025.
19. Fischer, G.; Bang, H.; Mech, C. Detection of enzyme catalysis for cis-trans-isomerization of peptide bonds using proline-containing peptides. *Biomed. Biochim. Acta* **1984**, *43* (10), 1101–11.
20. Vivoli, M.; Renou, J.; Chevalier, A.; Norville, I. H.; Diaz, S.; Juli, C.; *et al.* A miniaturized peptidyl-prolyl isomerase enzyme assay. *Anal. Biochem.* **2017**, *536*, 59–68. DOI: 10.1016/j.ab.2017.08.004.
21. Mori, T.; Itami, S.; Yanagi, T.; Tatara, Y.; Takamiya, M.; Uchida, T. Use of a real-time fluorescence monitoring system for high-throughput screening for prolyl isomerase inhibitors. *J. Biomol. Screen.* **2009**, *14* (4), 419–24. DOI: 10.1177/1087057109333979.
22. Owicki, J. C. Fluorescence polarization and anisotropy in high throughput screening: perspectives and primer. *J. Biomol. Screen.* **2000**, *5* (5), 297–306. DOI: 10.1177/108705710000500501.
23. Rossi, A. M.; Taylor, C. W. Analysis of protein-ligand interactions by fluorescence polarization. *Nat. Protoc.* **2011**, *6* (3), 365–87. DOI: 10.1038/nprot.2011.305.
24. Jameson, D. M.; Ross, J. A. Fluorescence polarization/anisotropy in diagnostics and imaging. *Chem. Rev.* **2010**, *110* (5), 2685–708. DOI: 10.1021/cr900267p.
25. Kozany, C.; Marz, A.; Kress, C.; Hausch, F. Fluorescent probes to characterise FK506-binding proteins. *ChemBioChem* **2009**, *10* (8), 1402–10. DOI: 10.1002/cbic.200800806.
26. Pomplun, S.; Sippel, C.; Hahle, A.; Tay, D.; Shima, K.; Klages, A.; *et al.* Chemogenomic Profiling of Human and Microbial FK506-Binding Proteins. *J. Med. Chem.* **2018**, *61* (8), 3660–73. DOI: 10.1021/acs.jmedchem.8b00137.

27. Paulson, C. N.; Guan, X.; Ayoub, A. M.; Chan, A.; Karim, R. M.; Pomerantz, W. C. K.; *et al.* Design, Synthesis, and Characterization of a Fluorescence Polarization Pan-BET Bromodomain Probe. *ACS Med. Chem. Lett.* **2018**, *9* (12), 1223–9. DOI: 10.1021/acsmchemlett.8b00380.
28. Coons, A. H.; Kaplan, M. H. Localization of antigen in tissue cells; improvements in a method for the detection of antigen by means of fluorescent antibody. *J. Exp. Med.* **1950**, *91* (1), 1–13. DOI: 10.1084/jem.91.1.1.
29. Kitano, K.; Schwartz, D. M.; Zhou, H.; Gilpin, S. E.; Wojtkiewicz, G. R.; Ren, X.; *et al.* Bioengineering of functional human induced pluripotent stem cell-derived intestinal grafts. *Nat. Commun.* **2017**, *8* (1), 765. DOI: 10.1038/s41467-017-00779-y.
30. Grimm, J. B.; Heckman, L. M.; Lavis, L. D. The chemistry of small-molecule fluorogenic probes. *Prog. Mol. Biol. Transl. Sci.* **2013**, *113*, 1–34. DOI: 10.1016/B978-0-12-386932-6.00001-6.
31. Magde, D.; Wong, R.; Seybold, P. G. Fluorescence Quantum Yields and Their Relation to Lifetimes of Rhodamine 6G and Fluorescein in Nine Solvents: Improved Absolute Standards for Quantum Yields. *Photochem. Photobiol.* **2007**, *75* (4), 327–34. DOI: 10.1562/0031-8655(2002)0750327fqyatr2.0.Co2.
32. Banaszynski, L. A.; Liu, C. W.; Wandless, T. J. Characterization of the FKBP center dot rapamycin, FRB ternary complex (vol 127, pg 4715, 2005). *J. Am. Chem. Soc.* **2006**, *128* (49), 15928. DOI: 10.1021/ja0699788.
33. de Lorimier, R. M.; Smith, J. J.; Dwyer, M. A.; Looger, L. L.; Sali, K. M.; Paavola, C. D.; *et al.* Construction of a fluorescent biosensor family. *Protein Sci.* **2002**, *11* (11), 2655–75. DOI: 10.1110/ps.021860.
34. Rinke, A.; Lavogina, D.; Kopanchuk, S. Assays with Detection of Fluorescence Anisotropy: Challenges and Possibilities for Characterizing Ligand Binding to GPCRs. *Trends Pharmacol. Sci.* **2018**, *39* (2), 187–99. DOI: 10.1016/j.tips.2017.10.004.
35. Moerke, N. J. Fluorescence Polarization (FP) Assays for Monitoring Peptide-Protein or Nucleic Acid-Protein Binding. *Curr. Protoc. Chem. Biol.* **2009**, *1* (1), 1–15. DOI: 10.1002/9780470559277.ch090102.

36. Huang, X.; Aulabaugh, A. Application of Fluorescence Polarization in HTS Assays. *Methods Mol. Biol.* **2016**, *1439*, 115-30. DOI: 10.1007/978-1-4939-3673-1\_7.
37. Norville, I. H.; O'Shea, K.; Sarkar-Tyson, M.; Zheng, S.; Titball, R. W.; Varani, G.; *et al.* The structure of a Burkholderia pseudomallei immunophilin-inhibitor complex reveals new approaches to antimicrobial development. *Biochem. J.* **2011**, *437* (3), 413–22. DOI: 10.1042/BJ20110345.
38. Tjernberg, A.; Markova, N.; Griffiths, W. J.; Hallen, D. DMSO-related effects in protein characterization. *J. Biomol. Screen.* **2006**, *11* (2), 131–7. DOI: 10.1177/1087057105284218.
39. Eastwood, B. J.; Farnen, M. W.; Iversen, P. W.; Craft, T. J.; Smallwood, J. K.; Garbison, K. E.; *et al.* The minimum significant ratio: a statistical parameter to characterize the reproducibility of potency estimates from concentration-response assays and estimation by replicate-experiment studies. *J. Biomol. Screen.* **2006**, *11* (3), 253-61. DOI: 10.1177/1087057105285611.
40. Wildey, M. J.; Haunso, A.; Tudor, M.; Webb, M.; Connick, J. H. Chapter five - high-throughput screening. In *Annual reports in medicinal chemistry*, Goodnow, R. A. Ed.; Vol. 50, 149-195; Academic Press, **2017**.
41. Zhang, J. H.; Chung, T. D.; Oldenburg, K. R. A Simple Statistical Parameter for Use in Evaluation and Validation of High Throughput Screening Assays. *J. Biomol. Screen.* **1999**, *4* (2), 67–73. DOI: 10.1177/108705719900400206.
42. S. Hünig, P. K., G. Märkl, J. Sauer. *Arbeitsmethoden in der organischen Chemie*; Berlin: Lehmanns Verlag, 2006.
43. Fulmer, G. R.; Miller, A. J. M.; Sherden, N. H.; Gottlieb, H. E.; Nudelman, A.; Stoltz, B. M.; *et al.* NMR Chemical Shifts of Trace Impurities: Common Laboratory Solvents, Organics, and Gases in Deuterated Solvents Relevant to the Organometallic Chemist. *Organometallics* **2010**, *29* (9), 2176–9. DOI: 10.1021/om100106e.
44. Baer, T.; Beckers, T.; Gekeler, V.; Gimmnich, P.; Joshi, H.; Joshi, U.; *et al.*, inventors; 4SC AG, GE, assignee. Novel Tetrahydrofusedpyridines as histone deacetylase inhibitors. International patent, International publication number WO2009037001A4. 2009 Mar 26.
45. Lameijer, L. N.; Ernst, D.; Hopkins, S. L.; Meijer, M. S.; Askes, S. H. C.; Le Devedec, S. E.; *et al.* A Red-Light-Activated Ruthenium-Caged NAMPT Inhibitor Remains Phototoxic in

Hypoxic Cancer Cells. *Angew. Chem. Int. Ed. Engl.* **2017**, *56* (38), 11549–53. DOI: 10.1002/anie.201703890.

46. Beutel, B. A.; Dandliker, P. J.; Hale, S. P.; Murcko, M. A.; Boczek, E.; Mittasch, M.; *et al.*, inventors; Dewpoint Therapeutics, Inc., USA, assignee. Methods of characterizing condensate-associated characteristics of compounds and uses thereof. International Patent, international publication number WO2020163795A1, 2020 Aug 13.

47. Wang, Z.-X.; Ravi Kumar, N.; Srivastava, D. K. A novel spectroscopic titration method for determining the dissociation constant and stoichiometry of protein-ligand complex. *Anal. Biochem.* **1992**, *206* (2), 376–81. DOI: 10.1016/0003-2697(92)90381-g.

48. Wang, Z.-X. An exact mathematical expression for describing competitive binding of two different ligands to a protein molecule. *FEBS Lett.* **1995**, *360* (2), 111–4. DOI: 10.1016/0014-5793(95)00062-e.

## 2.8 Supporting Information

### Fluorescent probe for the identification of potent inhibitors of the macrophage infectivity potentiator (Mip) protein of *Burkholderia pseudomallei*

Nicolas Julian Scheuplein<sup>1‡</sup>, Theresa Lohr<sup>1‡</sup>, Mirella Vivoli Vega<sup>2</sup>, Dyan Ankrett<sup>2</sup>, Florian Seufert<sup>1</sup>, Lukas Kirchner<sup>1</sup>, Nicholas J. Harmer<sup>2\*</sup>, Ulrike Holzgrabe<sup>1\*</sup>

<sup>1</sup> Institute of Pharmacy and Food Chemistry, University of Würzburg, Am Hubland, 97074 Würzburg, Germany

<sup>2</sup> Living Systems Institute, Stocker Road, Exeter, EX4 4QD, U.K.

<sup>‡</sup>Present address: School of Biochemistry, University of Bristol, Bristol BS8 1TD, U.K.

<sup>‡</sup> equal first authors

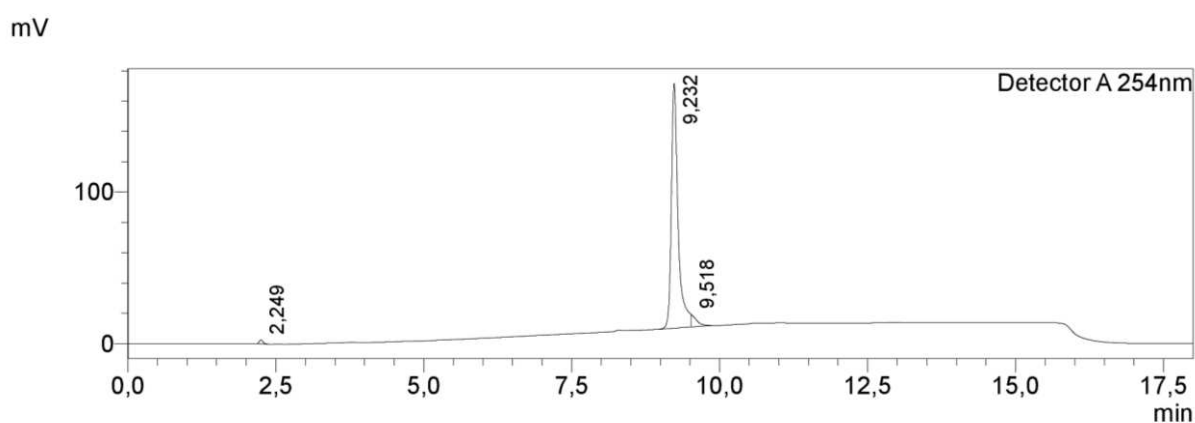
\* equal corresponding authors

#### 2.8.1 HPLC Chromatograms

8

$t_R = 9.23$  min

Purity: 95.1%



Peak#	Ret. Time	Area	Area%
1	2,249	11772	0,880
2	9,232	1273226	95,136
3	9,518	53318	3,984
Total		1338315	100,000

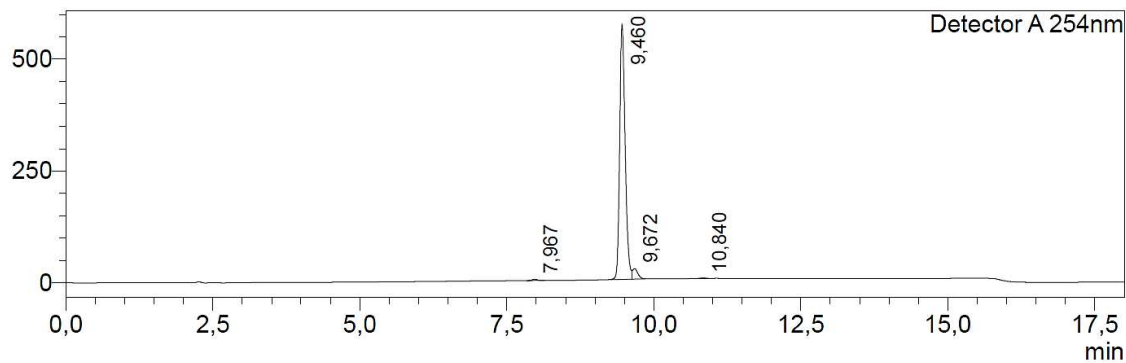


**1 (NJS106)**

$t_R = 9.46$  min

Purity: 95.4%

mV



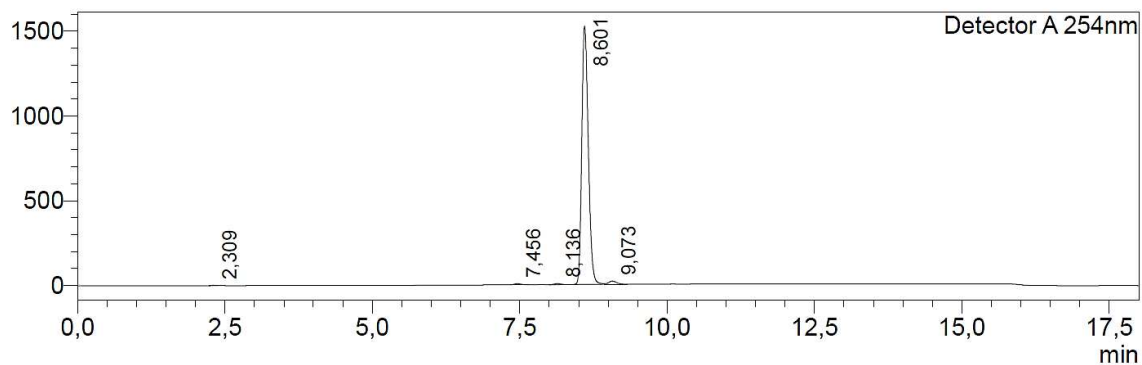
Peak#	Ret. Time	Area	Area%
1	7.967	17251	0.443
2	9.460	3716998	95.407
3	9.672	152478	3.914
4	10.840	9206	0.236
Total		3895934	100.000

**11**

$t_R = 8.60$  min

Purity: 97.7%

mV

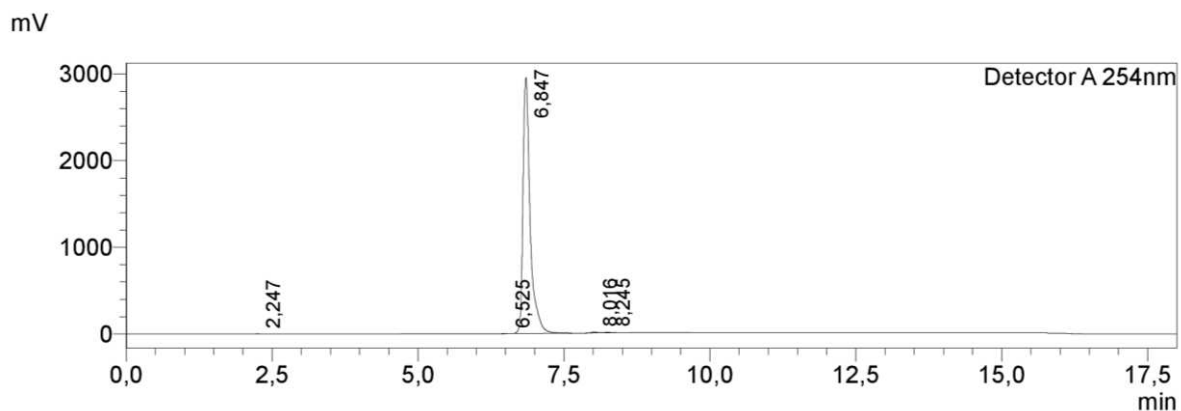


Peak#	Ret. Time	Area	Area%
1	2.309	9329	0.077
2	7.456	47420	0.392
3	8.136	47084	0.389
4	8.601	11822969	97.668
5	9.073	178457	1.474
Total		12105258	100.000

13

$t_R = 6.85$  min

Purity: 99.4%

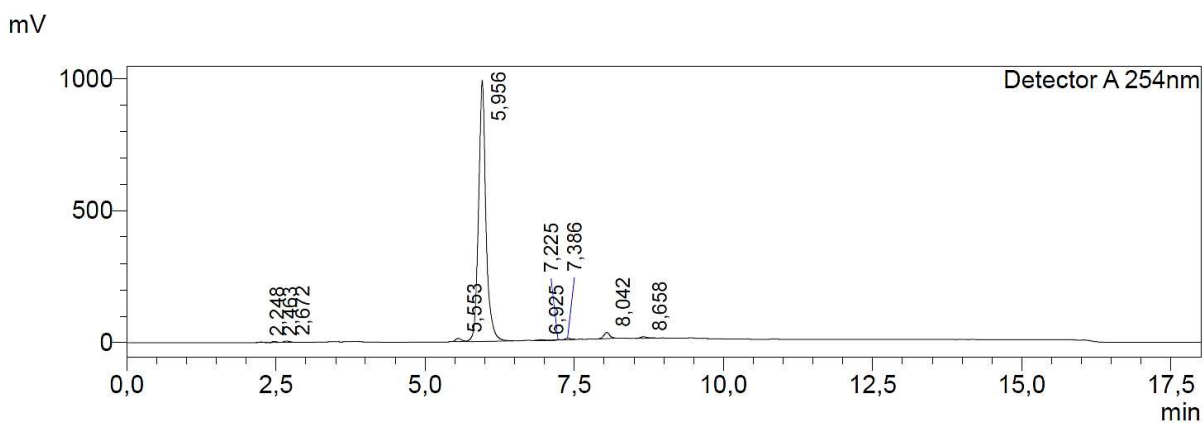


Peak#	Ret. Time	Area	Area%
1	2,247	11081	0,043
2	6,525	9475	0,037
3	6,847	25436609	99,374
4	8,016	80086	0,313
5	8,245	59630	0,233
Total		25596880	100,000

15

$t_R = 5.96$  min

Purity: 95.1%



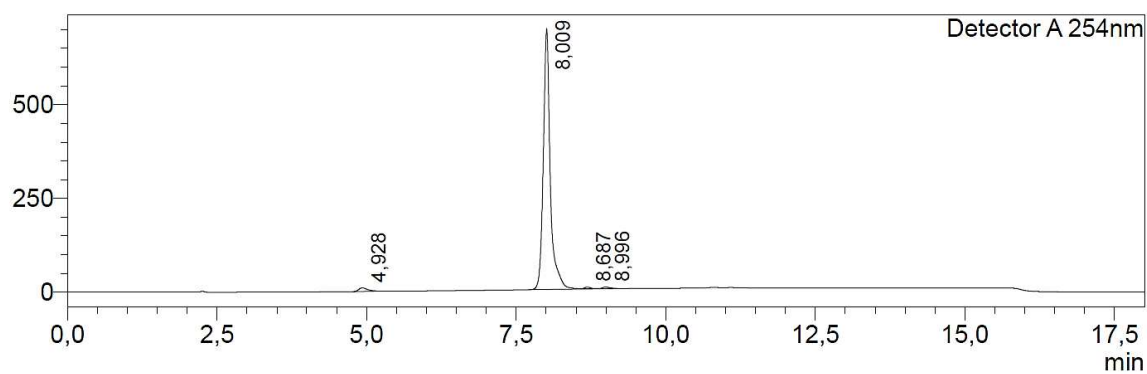
Peak#	Ret. Time	Area	Area%
1	2,248	11208	0,125
2	2,463	25972	0,289
3	2,672	37121	0,414
4	5,553	93413	1,041
5	5,956	8531455	95,059
6	6,925	17922	0,200
7	7,225	14262	0,159
8	7,386	37316	0,416
9	8,042	157762	1,758
10	8,658	48460	0,540
Total		8974891	100,000

14

$t_R = 8.01$  min

Purity: 97.3%

mV



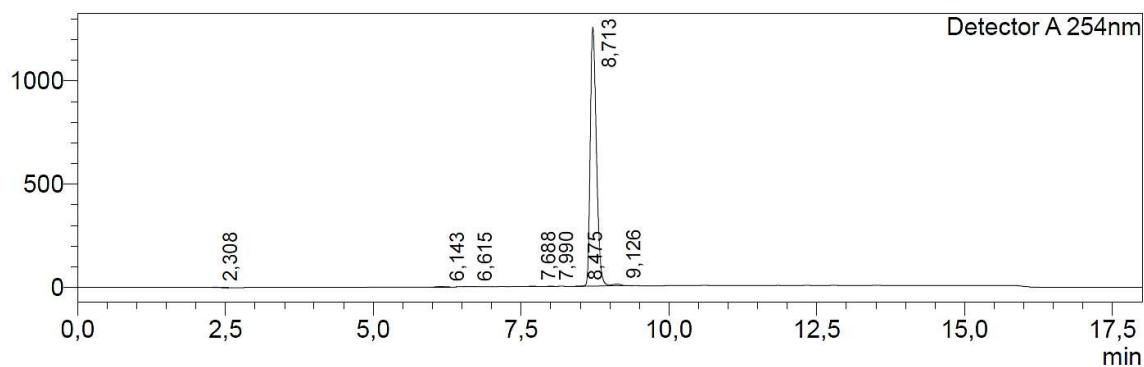
Peak#	Ret. Time	Area	Area%
1	4,928	99300	1,712
2	8,009	5644505	97,290
3	8,687	24663	0,425
4	8,996	33273	0,574
Total		5801741	100,000

12

$t_R = 8.71$  min

purity: 98.2%

mV



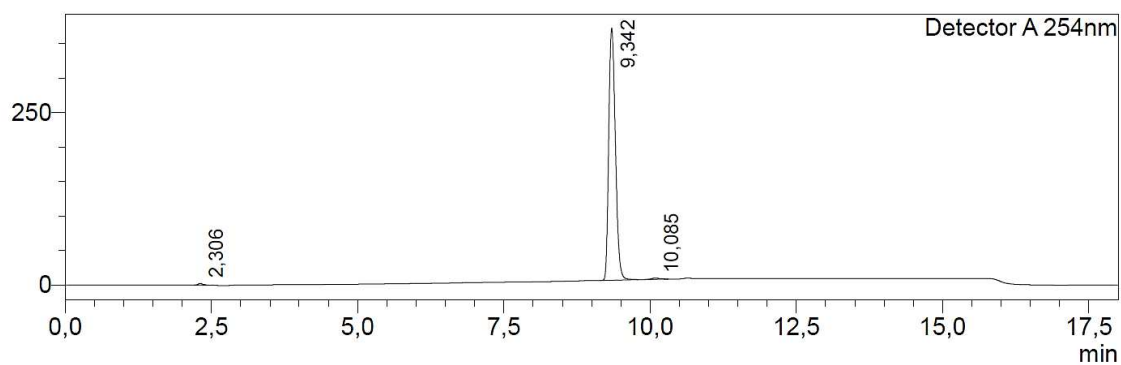
Peak#	Ret. Time	Area	Area%
1	2,308	18883	0,205
2	6,143	19462	0,212
3	6,615	6545	0,071
4	7,688	13458	0,146
5	7,990	6286	0,068
6	8,475	3549	0,039
7	8,713	9028042	98,188
8	9,126	98422	1,070
Total		9194647	100,000

2

$t_R = 9.34$  min

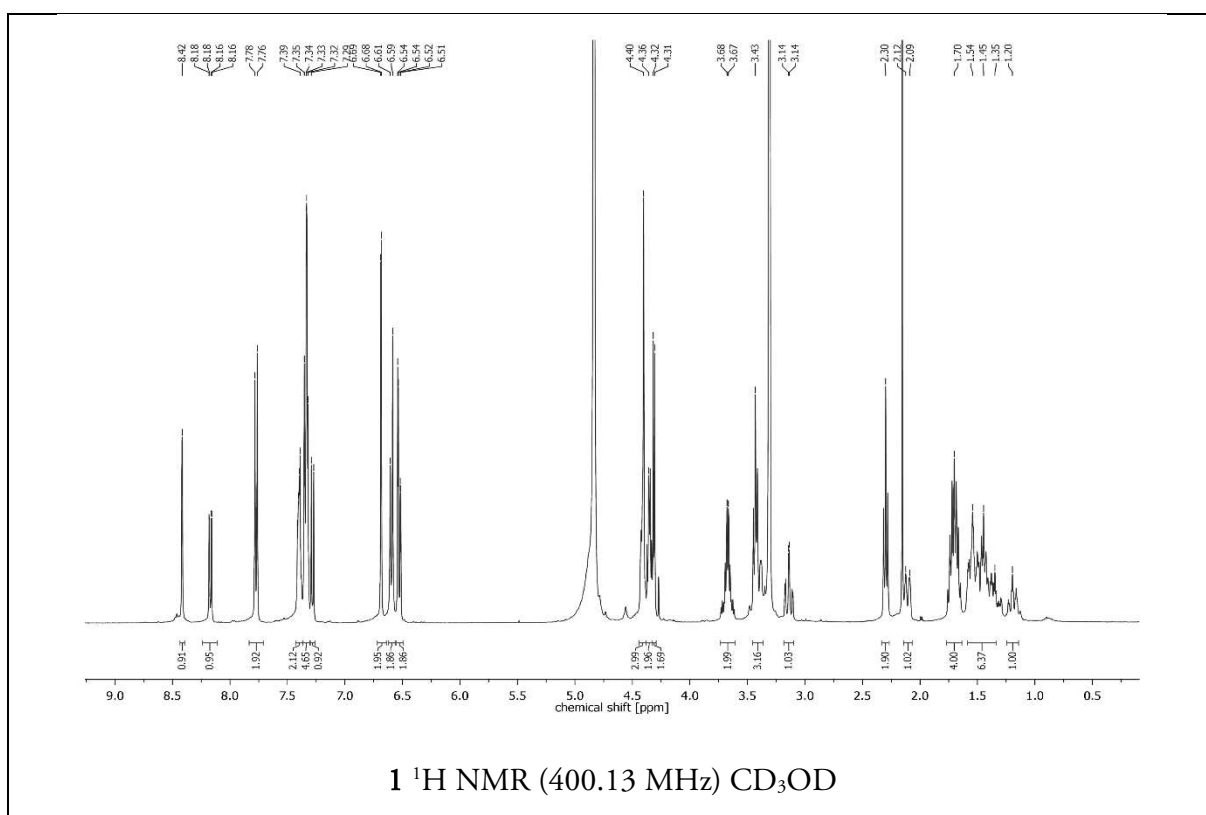
purity: 99.0%

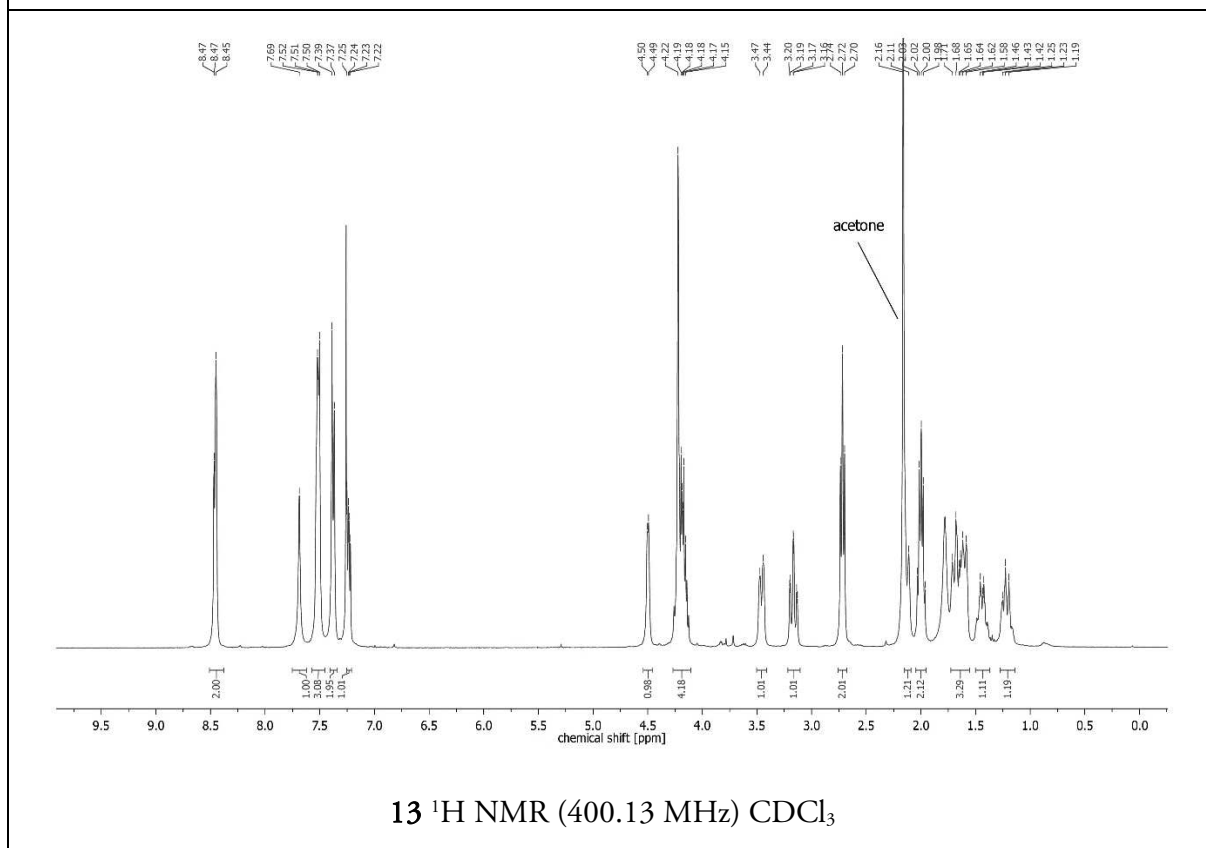
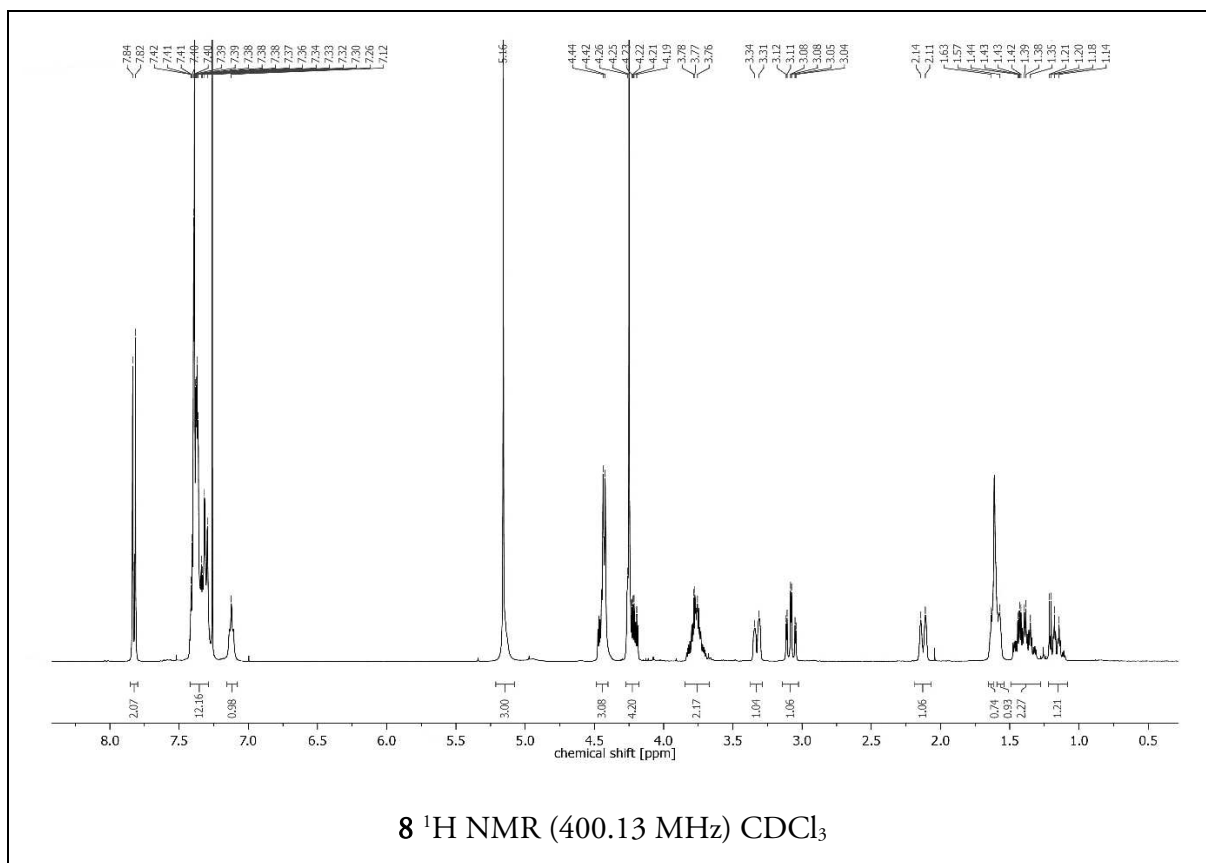
mV



Peak#	Ret. Time	Area	Area%
1	2,306	12787	0,437
2	9,342	2892442	98,957
3	10,085	17686	0,605
Total		2922915	100,000

### 2.8.2 $^1\text{H}$ NMR spectra





## 2.8.3 FP Binding Assay with BpMip and Probe 1

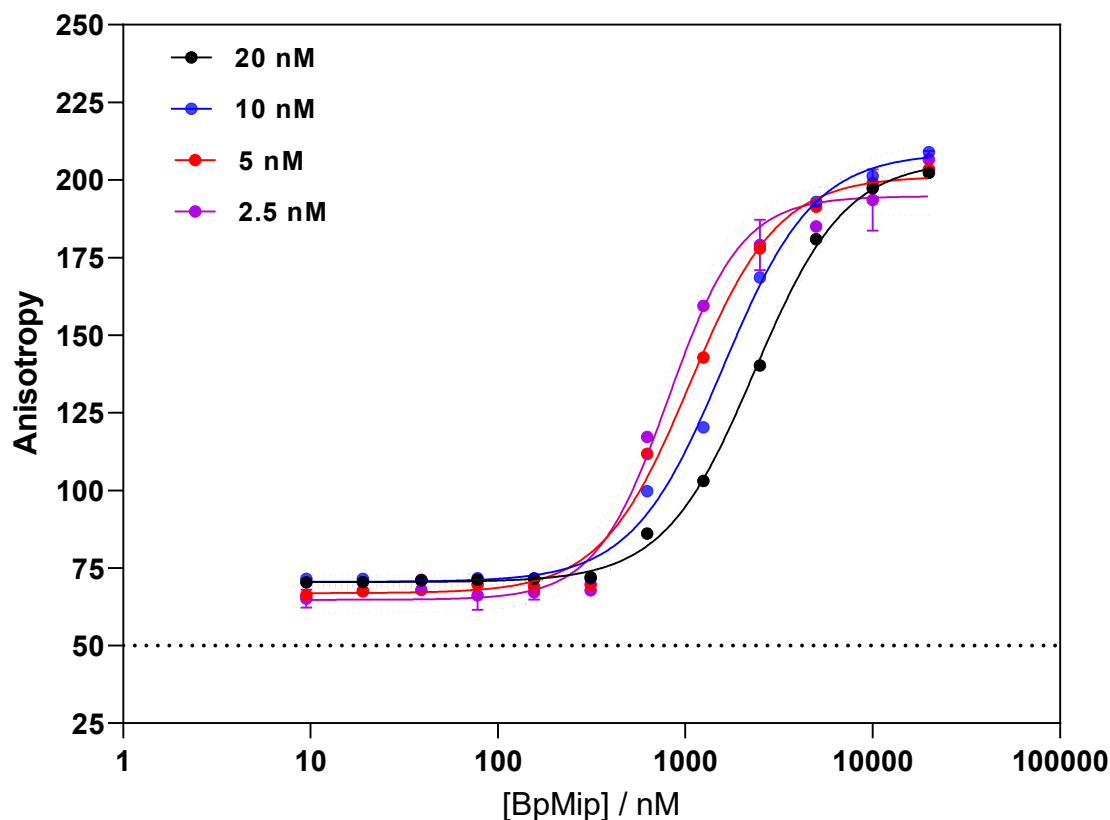


**Figure 1: Optimization of probe concentration.** Anisotropy of probe 1 was tested at varying concentrations of BpMip for four candidate probe concentrations. Each concentration provided a good fit. The error in the fit is slightly higher for 2.5 nM compared to other concentrations. 5 nM probe 1 was selected as providing an accurate readout for minimal compound. Error bars show the standard error of three experimental replicates; in most cases error bars are too small to show.

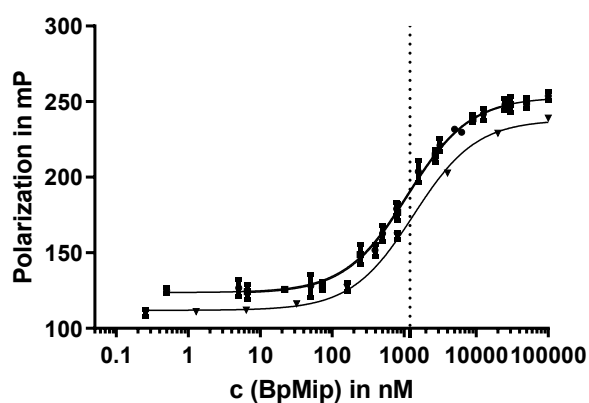


**Figure 2: Triplicate FP equilibrium saturation binding** curve of BpMip and probe 1 at a concentration of 5 nM at 25 °C. Error bars represent standard error, with data points showing the mean of three scans of each well. A triple repetition resulted in a  $K_D$  of  $1200 \pm 120$  nM (dashed line).

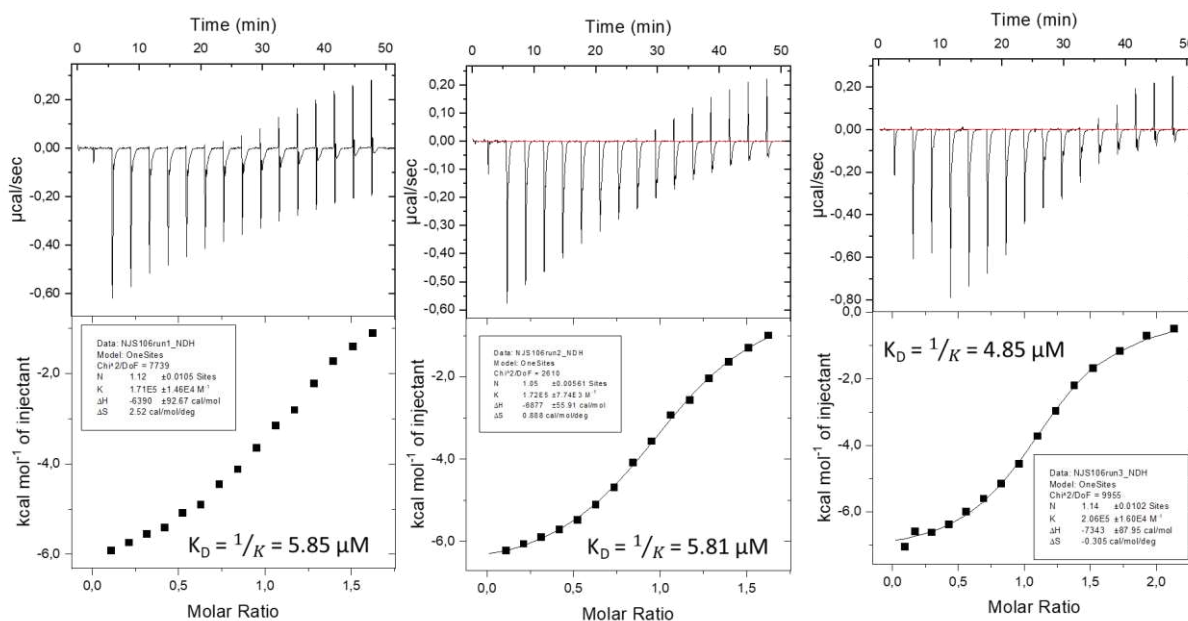


**Figure 3: Triplicate ITC binding curve** probe 1 (stock solution 600  $\mu\text{M}$ ) and BpMip (60  $\mu\text{M}$ ), containing 3 % (v/v) DMSO each. A triple repetition resulted in a  $K_D$  of  $5.50 \pm 0.03 \mu\text{M}$ , resulting in a high agreement with the FP assay, which revealed a  $K_D$  value of 3.63  $\mu\text{M}$ .

Table 1:  $K_D$  value and signal window at the respective DMSO concentration. The MSR was calculated relative to 0% DMSO, resulting in a significant deviation at 10%, although it should be noted that at 5% DMSO the MSR limit of 3 is also almost reached.

DMSO conc.	0%	0.25%	0.50%	1%	2%	5%	10%
Mean $K_D$ value ( $\mu\text{M}$ )	1.47	1.44	1.95	2.80	3.35	4.22	6.36
SEM	0.29	0.14	0.08	0.20	0.33	0.50	0.23
MSR				2.43	2.69	2.99	3.61
Mean SW (mP)	114.33	113.00	109.67	110.00	113.00	105.33	92.67
SEM	3.00	2.33	2.00	7.67	6.33	1.63	0.82

## 2.8.4 Establishment of the FP competitive assay and assay parameter evaluation

 Table 2: All  $K_i$  value measurements in detail, shown with mean and standard error of the mean (SEM). All data are given in  $\mu\text{M}$ . The upper and lower parts of the table were collected on different instruments with different BpMip preparations to illustrate the general applicability of probe 1.

repetition	$K_i$ 8	SEM (8)	$K_i$ 11	SEM (11)	$K_i$ 13	SEM (13)	$K_i$ 15	SEM (15)	$K_i$ 14	SEM (14)	$K_i$ 12	SEM (12)	$K_i$ 2	SEM (2)
n=1	2.06	0.27	1.67	0.18	11.25	1.09	17.15	3.48	0.67	0.13	0.47	0.09	0.54	0.10
n=2	2.58	7.37	2.16	0.35	10.34	1.12	19.55	15.27	0.72	0.13	0.46	0.10	1.58	0.35
n=3	2.43	0.50	1.54	0.24	10.33	1.37	8.61	5.01	0.57	0.17	0.45	0.11	0.92	0.15
n=4							11.12	8.61					1.32	0.22
Mean/SD	2.36	0.27	1.79	0.33	10.64	0.53	15.10	5.10	0.65	0.08	0.46	0.01	1.09	0.46
SEM	0.15		0.19		0.31		2.55		0.04		0.01		0.23	
n=1			2.69	0.18	9.74	1.37	nd		0.82	0.13	0.85	0.11	0.85	0.07
n=2			3.53	0.35	11.99	1.87	nd		0.78	0.13	0.63	0.06	1.75	0.20
n=3			2.98	0.24	8.30	2.56	nd		0.26	0.17	0.68	0.10		
n=4														
Mean/SD			3.07	0.43	7.52	5.90			0.93	0.11	0.72	0.12	1.30	0.64
SEM			0.25		3.41				0.06		0.07		0.45	

Determination of the dynamic range, signal-to-noise-ratio (S/N ratio), signal-to-background-ratio (S/B ratio), signal window value (SW) and Z'-factor

**Dynamic range:** mP value positive control – mP value negative (displaced) control = 67 mP

**S/N ratio:** signal to noise ratio should > 10 (Kim et al. <sup>1</sup>)

$$\text{S/N ratio} = \text{Diff}/(\text{SD}_{\text{n}}^2 + \text{SD}_{\text{p}}^2)^{0.5} = (\text{mP value positive control} - \text{mP value free tracer})/(\text{SD}_{\text{free}}^2 + \text{SD}_{\text{pos}}^2)^{0.5} = 13.55$$

**S/B ratio:** (> 3, Chen et al. <sup>2</sup>)

$$\text{S/B ratio} = \text{Mean positive control} / \text{mean negative, displaced control} = 1.57$$

The S/B ratio does not consider the SD; for a better estimation see Z'-factor.

**SW value:** ( $\geq 2$ , Assay Guidance Manual<sup>3</sup>)

$$\text{SW} = \frac{\left(\mu^- - \frac{3 \cdot \sigma^-}{\sqrt{n}}\right) - \left(\mu^+ + \frac{3 \cdot \sigma^+}{\sqrt{n}}\right)}{\mu^- / \sqrt{n}}$$

$$\text{SW} = 31.32$$



Table 3: Raw data for Z'-factor calculation (n=3)

	$\mu^-$	$\sigma^-$	$\mu^+$	$\sigma^+$	Z
n=1	180.8718	1.9396	118.7222	0.3977	0.8872
n=2	189.1026	1.8764	118.8056	0.6467	0.8923
n=3	192.1795	1.9608	121.1111	0.7116	0.8872
Mean					<b>0.89</b>
SEM					<b>0.00</b>

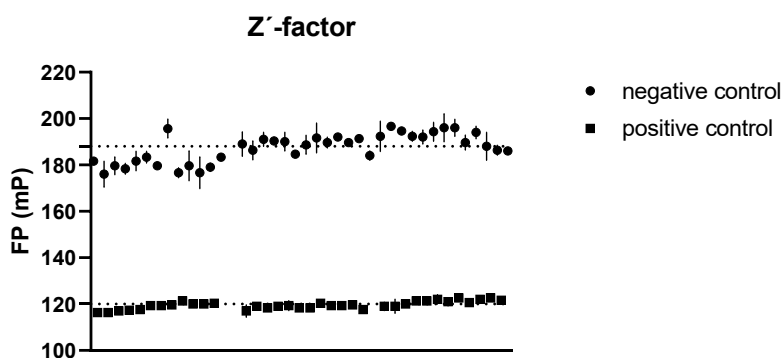


**Figure 4:** Measurement of the Z-factor was performed three times, each time on different days, with the maximum (negative control) using a 0.5% DMSO solution and the minimum (positive control) using a strong inhibitor **12**.

### 2.8.5 HRMS Equipment and Method

LC-System: *Agilent* (Waldbronn, Germany) Infinity II

Equipment: Binary Pump *Agilent* G7120A

Multisampler (thermostatted) *Agilent* G7167B

Column compartment (thermostatted) *Agilent* G7116B

No column was used

Method: Solvent A: Water + 0.1% FA

Solvent B: ACN + 0.1% FA

Elution: isocratic (50% B)

Flow: 1 mL/min

Injection: 10  $\mu$ L

Stoptime: 1.5 min

MS-System: Sciex (Concord, Ontario, Canada) X500R QTOF  
Equipment: Turbo VTM Ion Source (ESI)  
Method: Curtain gas: 25 psi  
Ion source gas 1: 50 psi  
Ion source gas 2: 50 psi  
Temperature: 500°C  
Polarity: positive  
Ionspray voltage: 5500 V  
Declustering potential: 70 +/- 10 V  
Collision energy: 10 V (no fragmentation)  
Stop time: 1.5 min

### 2.8.6 References

1. Kim, J.; Felts, S.; Llauger, L.; He, H.; Huezo, H.; Rosen, N.; et al. Development of a fluorescence polarization assay for the molecular chaperone Hsp90. *J. Biomol. Screen.* **2004**, *9* (5), 375-81. DOI: 10.1177/1087057104265995 From NLM Medline.
2. Chen, Y.; Tang, H. High-throughput screening assays to identify small molecules preventing photoreceptor degeneration caused by the rhodopsin P23H mutation. *Methods Mol. Biol.* **2015**, *1271*, 369-90. DOI: 10.1007/978-1-4939-2330-4\_24 From NLM Medline.
3. Iversen, P. W.; Beck, B.; Chen, Y.-F.; Dere, W.; Devanarayan, V.; Eastwood, B. J.; et al. HTS assay validation. In *Assay guidance manual*; 2012.

### 3 Development of Fluorophore-Labeled Mip Inhibitors as FP Probes for Various Mip Proteins

*The bibliography for this chapter can be found at the end of this thesis (chapter VII).*

In the past, the initial screening of new Mip inhibitors was mainly performed using a protease-coupled PPIase assay developed by Vivoli *et al.*<sup>73</sup> However, this assay suffers from some limitations, which are further discussed in chapter III\_2, such as nonphysiological temperatures of 4–8 °C and the lack of robustness.

Hence, an FPA for rapid and robust screening of novel BpMip inhibitors was to be developed. For this purpose, a series of fluorescent ligands was designed and synthesized here.

Therefore, we could rely on previous SAR studies<sup>93, 94</sup> and crystal structures.<sup>109</sup> In addition, the research of Banaszynski *et al.*<sup>110</sup> and Kozany *et al.*<sup>111</sup>, who synthesized rapamycin-derived FP probes for human FKBP, provided valuable information on the design of a Mip-adapted FP probe.

The development and successful application of FP probe **30** (*NJS106*; *tracer 1*) for the screening of BpMip inhibitors are described in detail in chapter III\_2.<sup>48</sup> Since the Mip binding pocket is highly conserved across a variety of species, the next goal was to investigate the suitability of the probe for the Mip proteins of *L. pneumophila* and *T. cruzi* (see chapter III\_3.1).<sup>21</sup>

The potential influence of the linker between the inhibitor moiety and the fluorophore on binding was investigated using FP probe **31** (cf. chapter III\_3.2).

The intensified focus on TcMip inhibitors and more potent BpMip inhibitors requiring a high-affinity tracer led to the development of **32** and **29** (see chapters III\_3.3 and III\_3.4).

Implementation of the synthesized probes in an FP experiment was kindly performed by Theresa Lohr.

### 3.1 Additional Information on FP Probe 30

**30** (*NJS106*; *tracer 1* in chapter III\_2) was developed as an FP probe for BpMip and also tested against the Mip proteins of other pathogens. Details on the probe's design and  $K_D$  determination with BpMip using an FPA are given in chapter III\_2. There, among other things, determination of an ideal attachment site and the appropriate linker length are discussed. Other Mip proteins were tested analogously to BpMip.

Briefly, **30** consists of an inhibitor moiety derived from lead compounds **33** (*SF354*), a linker comprising ten atoms, and fluorescein as a fluorophore (see Figure 10).

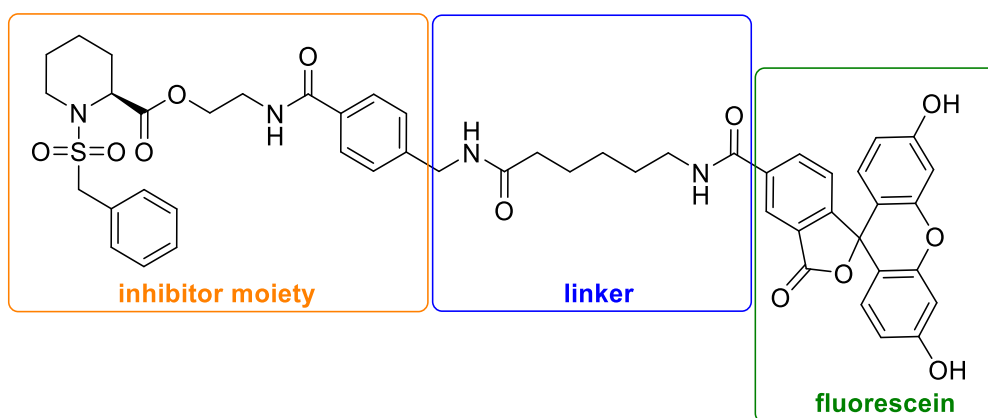


Figure 10. Molecular structure of FP probe **30**.

To test the suitability of **30** as a probe for the structurally related Mip proteins of *L. pneumophila* (LpMip) and *T. cruzi* (TcMip), respective FP binding assays were performed with **30**. As a result, the obtained  $K_D$ s with these Mips show that binding is only weakly pronounced (Table 2). For LpMip, a  $K_D$  of  $7.40 \pm 7.15 \mu\text{M}$  and for TcMip, a  $K_D$  of  $8.1 \pm 0.0 \mu\text{M}$  was determined. In the case of LpMip and especially TcMip, binding was insufficient and did not reach the upper plateau usually reached at high protein concentrations, making the obtained  $K_D$  value highly uncertain (cf. Figure 13 for the same effect with **31**). The weak binding renders **30** an unsuitable tracer for these two Mip proteins.

For BpMip, on the other hand, the  $K_D$  value of  $1.20 \mu\text{M}$  is in an excellent range to be displaced by medium-strength inhibitors such as **33** (*SF354*; see chapter III\_2). Even in the presence of 0.5% DMSO, **30** is well-balanced with a  $K_D$  of  $2.0 \mu\text{M}$ .

Table 2:  $K_D$  values of FP probe **30** for different Mip proteins. Data are given as mean  $\pm$  SD.

	TcMip	LpMip	BpMip
$K_D$	$8.1 \pm 0.0 \mu\text{M}^*$ $n=1$	$7.37 \pm 1.15 \mu\text{M}^*$ $n=1$	$1.20 \pm 0.12 \mu\text{M}$ $n=3$
Additional Details	*Upper plateau not reached (similar to Figure 13)	*Upper plateau not reached (similar to Figure 13)	0.5% DMSO-adjusted: $2.0 \pm 0.0 \mu\text{M}$

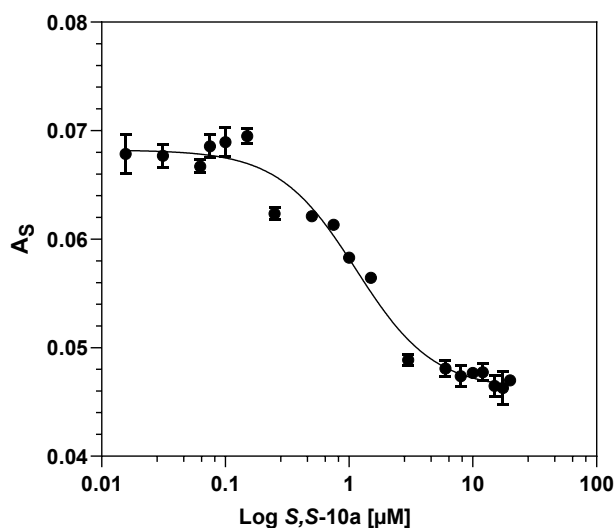


Figure 11. Dose-response curve of measured anisotropy as a function of inhibitor concentration of **S,S-10a** in the presence of **30** and BpMip. From this, the specific binding of **S,S-10a** to BpMip can be calculated (mean  $\pm$  SD,  $n = 3$ , measured by *Nicholas Harmer, University of Exeter, UK*).

### 3.2 Variation of the Linker Length with FP Probe **31**

#### 3.2.1 Starting Point

With probe **31**, the potential influence of the linker length on probe–protein binding was to be investigated. Therefore, the linker length of **31** was shortened from ten to four atoms (cf. Figure 12). Thus, a possible free rotation of a too-long linker in solution, also known as “propeller effect”, which might lead to a weakening of the FP signal, was to be prevented.<sup>112</sup> Ideally, this would result in a more pronounced difference in polarization for the bound tracer compared to the free probe. In addition, an amide was introduced at the C2 position of the pipercolic acid to increase chemical stability. While **30** showed no evidence of a lack of chemical stability, this was observed for some ester-bearing Mip inhibitors.

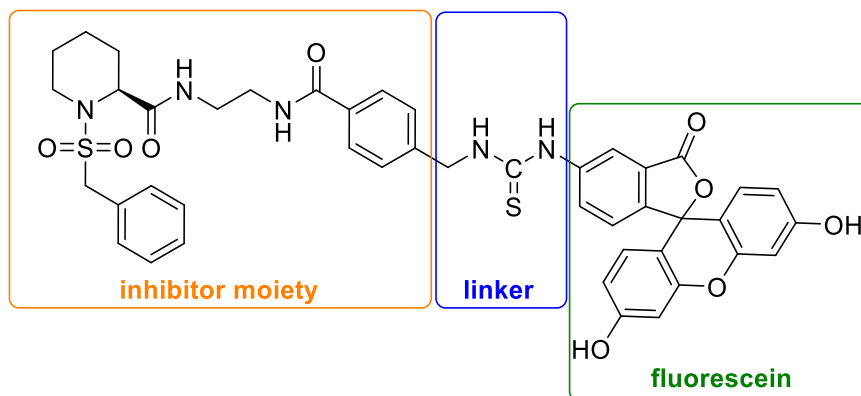
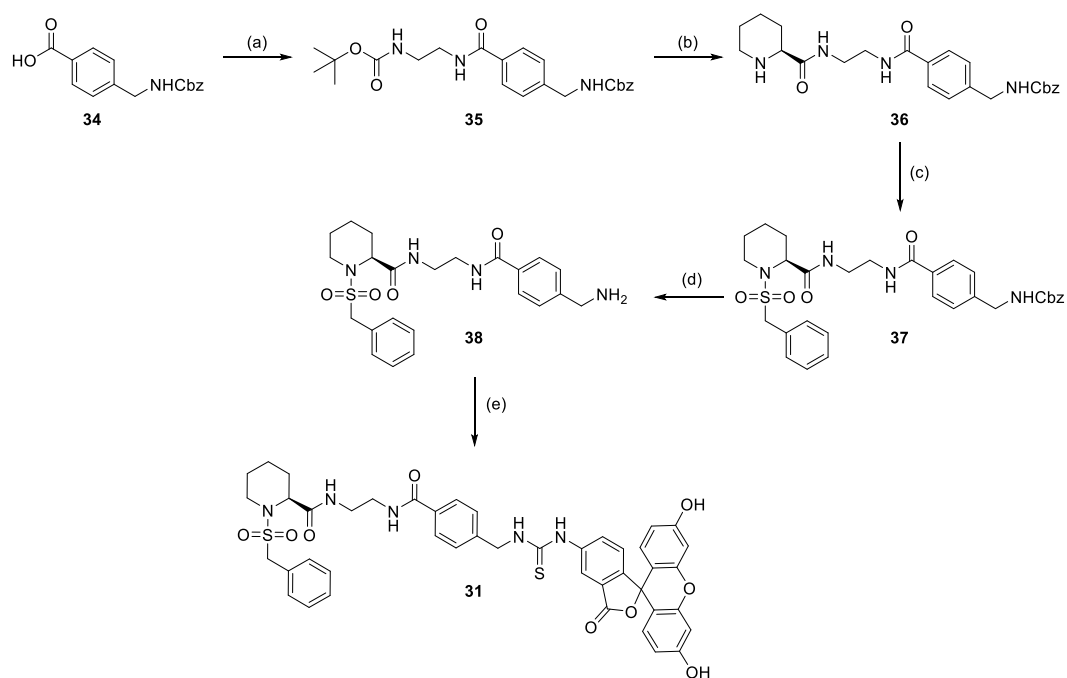


Figure 12. Molecular structure of FP probe 31.

### 3.2.2 Synthesis of Probe 31

The synthetic pathway of **31** (cf. Scheme 4) is largely analogous to that of **30** (see chapter III\_2) and is conducted in seven steps.

Deviating from the synthesis of **30**, **34** was, in the first step, amide-coupled to *N*-Boc-1,2-diaminoethane instead of ethanolamine, using EDC·HCl, HOBT, and DIPEA. After cleavage of the Boc-protecting group of **35** with an excess of TFA, the free amine was amide-coupled to (*S*)-*N*-Boc-piperidine-2-carboxylate using the same coupling reagents. Boc deprotection with TFA gave amine **36**. Subsequently, sulfonamide **37** was synthesized using phenylmethanesulfonyl chloride and DIPEA. Next, the Cbz protecting group of **37** was cleaved in a hydrogen bromide solution in acetic acid. Mechanistically, the Cbz protecting group decomposes into benzyl bromide and CO<sub>2</sub> during this process. Only 15% conversion was achieved due to difficulties in workup and column chromatography, presumably because of the retention behavior of the primary aliphatic amine. Finally, the primary amino group of **38** was coupled to fluorescein isothiocyanate (FITC), forming a thiourea bond between the inhibitor scaffold and fluorescein to give probe **31** in an overall yield of 2%.

Scheme 4: Synthetic route of FP probe **31**.

**Reagents and conditions:** (a) *N*-Boc-1,2-diaminoethane, EDC·HCl, DIPEA, HOBT, DCM, rt, 2 d, 84%; (b) i) TFA, DCM, rt, 3 h, 87%; ii) (*S*)-*N*-Boc-piperidine-2-carboxylate, EDC·HCl, HOBT, DCM, rt, 18 h, 91%; iii) TFA, DCM, 2 h, rt, 86%; (c) phenylmethanesulfonyl chloride, DIPEA, CHCl<sub>3</sub>, rt, 3 d, 83%; (d) HBr (32% in CH<sub>3</sub>COOH), DCM, 0 °C → rt, 3 h, 16%; (e) fluorescein isothiocyanate, DCM/THF = 3:2, NEt<sub>3</sub>, rt, 20 h, 27%. Overall yield: 2%.

### 3.2.3 FP Binding Assay of Probe **31** with the Mips of Various Pathogens

The influence of the linker length on protein binding and the suitability of **31** as an FP probe for the Mips of various pathogens were tested in respective FP binding assays. Dose-response curves were recorded (cf. Figure 13), and the  $K_D$  values were determined (cf. Table 3).

As a result, **31** performed significantly worse as an FP probe compared to its predecessor **30**. A clearer difference in polarization for the bound tracer compared to the free probe was not observed. On the contrary, ideal binding curves could not be obtained for TcMip, since weak binding prevented reaching the upper plateau at high protein concentrations (cf. Figure 13).

Since the replacement of the pipercolic ester by an amide led to only a slight change in binding affinity in the case of other Mip inhibitors (see chapter III\_4.2), it can be concluded that the difficulties of this probe are due to the altered chain length. Thus, a chain length of four atoms seems to be too short and presumably causes unfavorable interactions of the fluorophore with the protein's binding pocket.

All in all, **30** proved the more reliable FP probe, providing robust and reproducible measurements in the FPA with BpMip.

Table 3.  $K_D$  values of FP probe **31** with the Mip proteins of *Trypanosoma cruzi*, *Legionella pneumophila*, and *Burkholderia pseudomallei*. For some Mip proteins (\*) the binding curve does not reach the upper plateau, leading to high uncertainty and significant standard deviations. Data are shown as mean  $\pm$  SD. ND = not determined.

	TcMip	LpMip	BpMip
$K_D$	$26.8 \pm 6.7 \mu\text{M}^*$ $n = 3$	ND	$3.8 \pm 0.5 \mu\text{M}$ $n = 2$

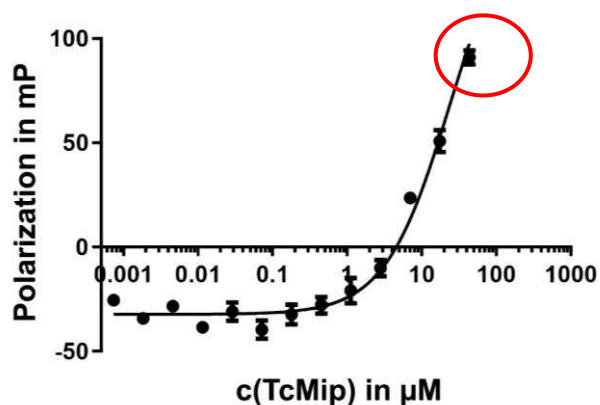


Figure 13. Dose-response curve of FP tracer **31** with TcMip. The upper plateau at high concentrations is not reached (highlighted in red), complicating evaluation. Data are shown as mean  $\pm$  SD,  $n = 3$ .

### 3.3 Development and Synthesis of Side Chain-Bearing FP Probe **32**

#### 3.3.1 Starting Point

The BpMip-FP probes developed so far exhibited insufficient  $K_D$  values for TcMip and LpMip. However, the studies on TcMip represented the next milestone. In addition, better binding to BpMip was desirable to allow the probe to compete with new, more potent inhibitors. Preliminary FP competition experiments with TcMip using the weak-binding probe **30** showed promising results for side chain-bearing inhibitors such as **S,S-10a** (cf. Scheme 5), suggesting binding to TcMip could also benefit from a side chain.

Therefore, a new FP probe **32** (*NJS205*) carrying an additional side chain was developed in collaboration with Theresa Lohr (cf. Scheme 5). Preliminary tests with **30** also indicated that a core structure similar to **39** (*CJ168*; cf. Scheme 5) containing a 1,2,3-trimethoxy-5-propylbenzene moiety might be advantageous for TcMip ligands.

The core structure of FP probe **40** (cf. Scheme 5), which was used by Kozany *et al.* for the inhibitor-screening against human FK506-binding proteins such as FKBP12 and FKBP51, offered additional input for potential FP probes with a side chain.<sup>111</sup> FP probe **40**, unlike **39**, carries a



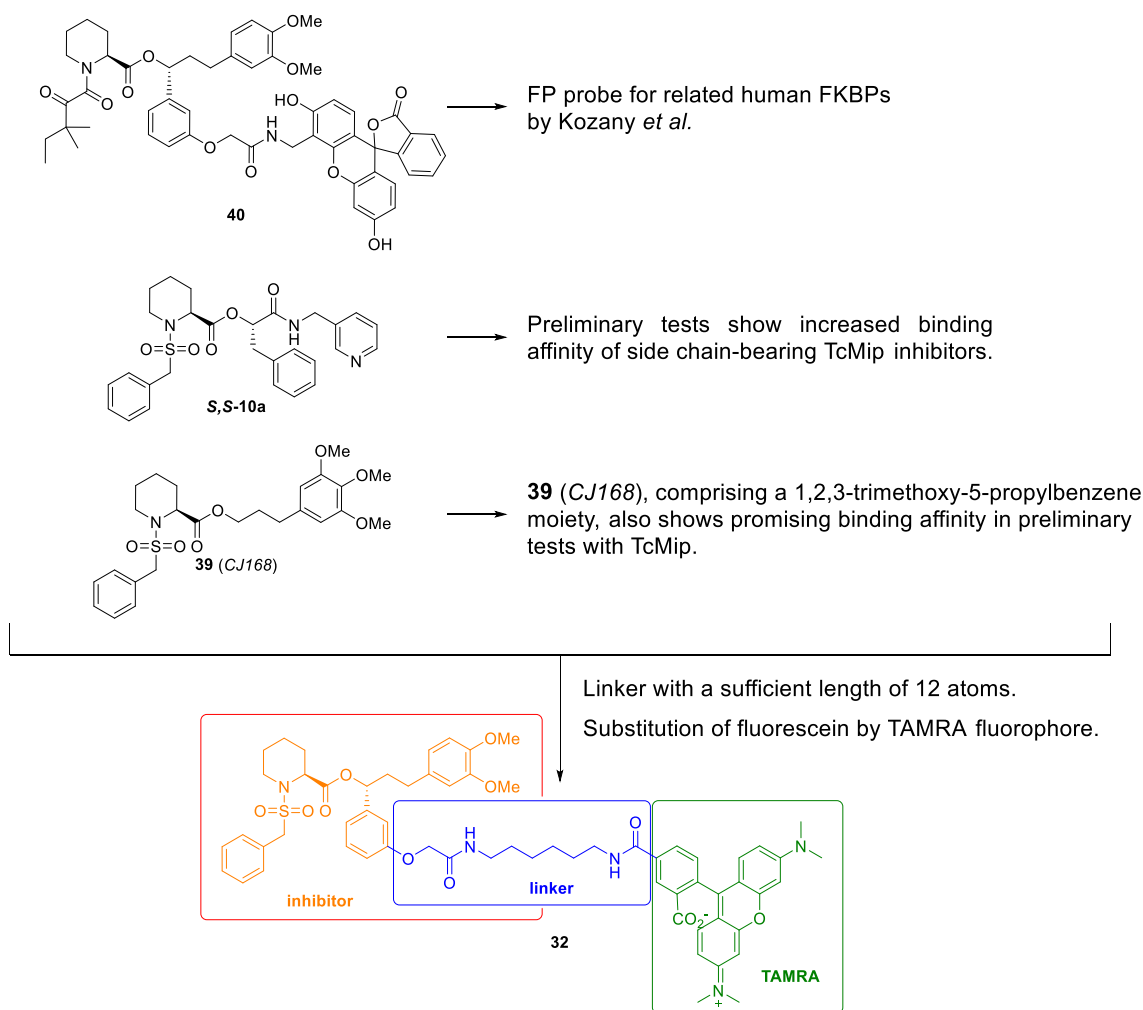
highly similar 1,2-dimethoxy-4-propylbenzene moiety, which should also be well tolerated. The dicarbonyl moiety of FP probe **40** (cf. Scheme 5) was replaced by the well-established phenylmethanesulfonamide moiety (as in **39**).

Next, the linker type and linkage point had to be considered. Alkyl linkers of about ten atoms in length, as in **30**, had been shown to be suitable for a BpMip-FP probe. In contrast, in the case of probe **31**, a linker length of only four atoms was found to be too short for BpMip and TcMip, probably leading to steric hindrance in protein binding. Hausch *et al.* found that a fluorescein-labeled probe linked to rapamycin via glycine did not work for the related FKBP51 protein, whereas a hexyl-glycine linker consisting of a total of eleven atoms proved suitable. Given the relative similarity of the PPIase domains of human FKBP5 and TcMip,<sup>113</sup> a comparable linker length of twelve atoms was used for probe **32**.

The attachment point at the side chain moiety (cf. Scheme 5) was chosen based on crystal structures of co-crystallized Mip inhibitors with the related BpMip protein. Begley *et al.*<sup>109</sup> and Iwasaki *et al.*<sup>114</sup> demonstrated that **41** (*SF235*) and **33** (*SF354*) establish polar contacts between the amide nitrogen of Ile63 and the pipercolic carbonyl ester of the respective inhibitor and between the hydroxyl group of Tyr89 and one of the sulfonyl oxygens. In addition, the terminal phenyl ring of the sulfonamide moiety participates in a  $\pi$ -edge stacking interaction with Phe43.<sup>114</sup> The successful introduction of the linker at the side chain in the case of **40** by Kozany *et al.* supported this decision.<sup>111</sup>

The fluorophore was changed to 5-carboxytetramethylrhodamine (5-TAMRA) as it is known to show a weaker dependence of fluorescence on the pH compared to fluorescein.<sup>115</sup> In addition, the TAMRA fluorophore has the advantages of a pH-insensitive quantum yield, excellent photostability, visible light excitation, and chemical stability under physiological conditions.<sup>116</sup> Furthermore, it should be investigated whether a more significant difference in polarization of the bound and the unbound state could be achieved with it. In addition, optical filters suitable for TAMRA's excitation and emission properties were installed in the available fluorometer. TAMRA is efficiently excited by the 543 nm spectral line of the green He-Ne laser (lit.: 540–547 nm)<sup>115, 117, 118</sup>, which is increasingly used for analytical instrumentation.<sup>118</sup> Fluorescence emission lies in the range of 565–573 nm.<sup>115, 117, 118</sup>

Scheme 5. Design of an optimized FP probe **32** (*NJS205*), suitable for TcMip and more potent BpMip inhibitors. It was derived from lead compounds **39** and **S,S-10a**. Additional information was obtained from FP probe **40**, which was used for human FKBP by Kozany *et al.*<sup>111, 119</sup>

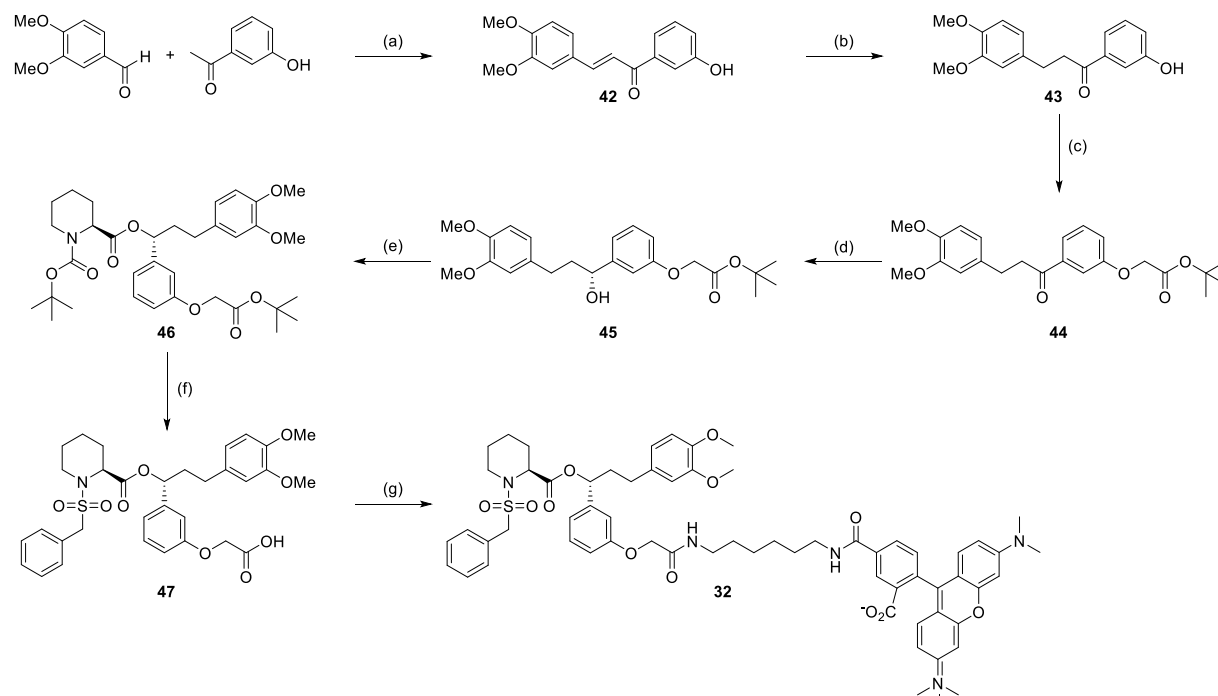


### 3.3.2 Synthetic Route for **32**

The development of a synthetic route for **32** (cf. Scheme 6) was inspired by the synthesis of related FKBP ligands by Jørgensen *et al.*<sup>120</sup> as well as by the synthesis of probe **40** developed by Keenan *et al.*<sup>121</sup> and Kozany *et al.*<sup>111</sup> However, modifications in the reaction conditions, catalysts, and coupling reagents were necessary.

In the first step, chalcone **42** was obtained in a basic aldol condensation of 3,4-dimethoxybenzaldehyde and 3'-hydroxyacetophenone. The following hydrogenation of the  $\alpha, \beta$ -unsaturated ketone was first carried out in the absence of  $\text{Ph}_2\text{S}$ , resulting in a complete hydrogenation of the enone towards an aliphatic propyl analog. The addition of 0.015 equivalents of the catalyst poison  $\text{Ph}_2\text{S}$ , according to a protocol by Mori *et al.*, was necessary to selectively

obtain dihydrochalcone **43**.<sup>122</sup> In the next step, the phenolic alcohol group of the dihydrochalcone **43** was deprotonated with potassium carbonate and reacted in an S<sub>N</sub>2 reaction with *tert*-butyl bromoacetate to give the ether bond in **44**. Since the reduction of ketone **44** to the alcohol **45** was to be enantioselective, a Corey-Bakshi-Shibata (CBS) reduction was carried out using the (*S*)-CBS catalyst and BH<sub>3</sub>·SMe<sub>2</sub> as a stoichiometric reduction reagent. The CBS reduction and its mechanism are further discussed in chapter III\_3.3.3.1. Next, alcohol **45** was coupled with *N*-Boc-(*S*)-pipercolic acid in a Steglich esterification using DIC as a coupling reagent and DMAP as an auxiliary base to give **46**. After clarification of the stereochemical purity of **46** (see chapter III\_3.3.4), the Boc protecting group and the *tert*-butyl protecting group were removed with TFA. Subsequently, the piperidine amino group was reacted with phenylmethanesulfonyl chloride in the presence of NMM to afford Mip inhibitor **47**. Amide coupling of **47** and 5-((6-aminohexyl)carbamoyl)-TAMRA using HBTU and DIPEA afforded probe **32**. The overall yield was 17%. The following chapters discuss the challenges of different synthesis steps and the respective approaches to address them.

Scheme 6. Synthetic route of FP probe **32**.

**Reagents and conditions:** (a) KOH, H<sub>2</sub>O/MeOH, rt, 18 h, 84%; (b) H<sub>2</sub>, Pd/C, Ph<sub>2</sub>S (0.01 equiv), MeOH, rt, 19 h, > 99%; (c) *tert*-butyl bromoacetate, K<sub>2</sub>CO<sub>3</sub>, DMF, rt, 1 d, 90%; (d) CBS-cat., BH<sub>3</sub>·SMe<sub>2</sub>, THF, 0 °C → rt, 3 d, 88%; (e) *N*-Boc-(*S*)-pipercolic acid, DIC, DMAP, DCM, 0 °C → rt, 4 h, 85%; (f) i) TFA, DCM, 0 °C → rt, 1 d, 89%; ii) phenylmethanesulfonyl chloride, NMM, DCM, rt, 2 d, 52%; (g) 5-((6-aminohexyl)carbamoyl)-TAMRA, HBTU, DIPEA, DCM, rt, 18 h, 64%. Overall yield: 17%.

### 3.3.3 CBS Reduction

Reaction conditions for the CBS reduction of **44** to **45** had to be tuned to enhance stereoselectivity (see chapter III\_3.3.3.2). The mechanism is briefly explained in the following sub-chapter.

#### 3.3.3.1 Mechanism of the Corey-Bakshi-Shibata Reduction of Prochiral Ketones

The Corey-Bakshi-Shibata (CBS) reduction is a very effective method for the asymmetric reduction of prochiral ketones<sup>123</sup> to alcohols, commonly featuring high yields and excellent selectivities.<sup>124</sup>

The oxazaborolidine catalyst, which is synthesized from a proline-derived amino alcohol, is known as CBS reagent according to its developers, although further reference should be made to Itsuno *et al.*<sup>125</sup> <sup>126</sup> Figure 14 illustrates some of the key steps in a CBS reduction: The active reducing agent is generated by complexation of the Lewis-acid borane with the Lewis-basic nitrogen of the catalyst (cf. Figure 14A).<sup>127</sup> Only catalytic amounts of about 10% of the catalyst are needed as borane is only reactive enough to reduce ketones when it is complexed with the Lewis basic nitrogen atom. The rest of the borane ‘waits’ until a molecule of the catalyst is released.<sup>127</sup>

CBS reductions provide the highest yields and stereochemical purities when the two substituents of the prochiral ketone ( $R^{\text{Small}} = R^{\text{S}}$  and  $R^{\text{Large}} = R^{\text{L}}$ ) are sterically well differentiated, such as phenyl ring and methyl group in acetophenone (cf. Figure 14B). Coordination between the Lewis acidic ring boron of the CBS catalyst and the carbonyl oxygen activates the ketone toward reduction (cf. Figure 14C). Then, the ketone is sufficiently electrophilic to be reduced by the relatively weak hydride source. Intramolecular hydride transfer from the borane coordinated to the ring nitrogen occurs via a six-membered ring-shaped, chair-like transition state (TS, cf. Figure 14C).<sup>128</sup> Enantioselectivity arises from this chair-like TS, in which the controlling steric interaction is exerted by the methyl substituent at the ring boron. The primary isomer results from the preferred TS in which the large substituent ( $R^{\text{L}}$ ) lies pseudoequatorial, thus avoiding the 1,3-diaxial interaction with the methyl group.<sup>129</sup> The CBS reagent is today considered one of the best asymmetric reducing agents.<sup>127</sup>

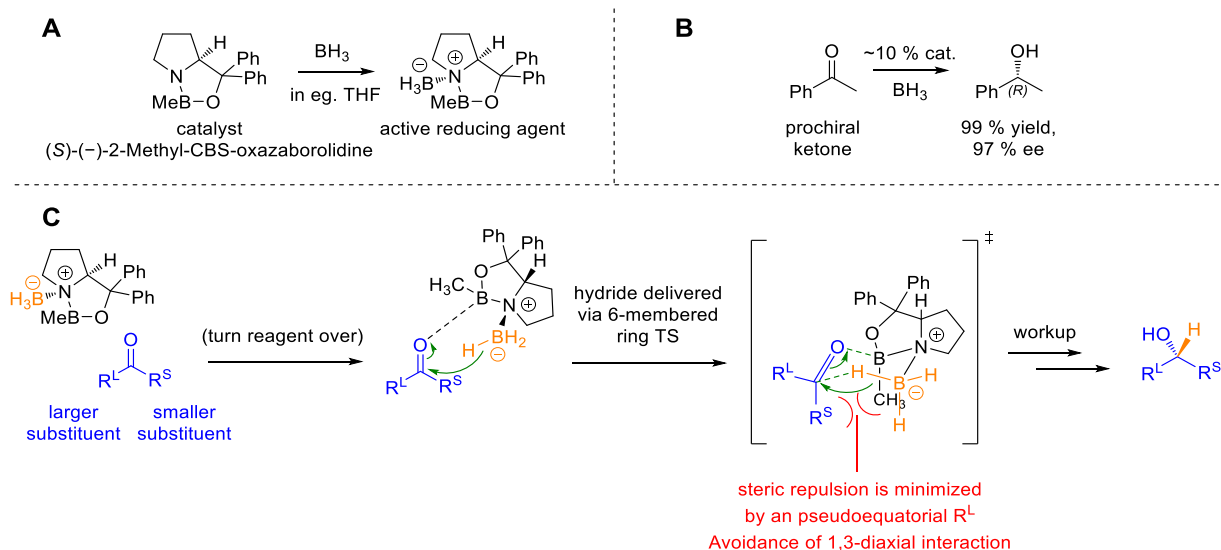


Figure 14. **A:** The active reducing agent is generated by coordination of the Lewis-acid  $\text{BH}_3$  to the Lewis-basic nitrogen of the CBS catalyst. **B:** Yields and enantiomeric purities are maximized when the prochiral ketone's substituents are sterically well differentiated, such as phenyl and methyl in acetophenone. **C:** Favoring of one stereo-isomer is mainly based on minimizing the steric repulsion in the chair-like TS between the boron's methyl group and the ketone's larger substituent  $\text{R}^L$ , which consequently occupies the pseudoequatorial position.<sup>127</sup> Other driving forces for stereo-selectivity, like London dispersion forces, have been discussed recently.<sup>124</sup>

The presented CBS catalyst has a tremendous substrate range, and related analogs have been developed for further substrates, differing, e.g., in the substitution at the boron atom.<sup>130</sup>

Interestingly, although the CBS reduction has been a well-known reaction used for several years, diverse aspects of the mechanism of catalysis necessary for developing new catalysts are still under discussion. One of the aspects is whether the six-membered TS is more boat-like or chair-like.<sup>124</sup> Eschmann *et al.* recently used DFT methods to calculate that the CBS reduction of acetophenone proceeds via a chair-like TS.<sup>124</sup> The postulated driving force for enantioselectivity – steric effects – is not always sufficient to predict the expected product for some ketones. According to Eschmann *et al.*, factors such as London dispersion forces must also be taken into account.<sup>124</sup> London dispersion forces, which are part of the van der Waals forces, are weak attractive forces between polar or nonpolar molecules and atoms, which originate from the spontaneous polarization of a molecule/atom and thereby induced dipoles in neighboring molecules/atoms.<sup>131</sup>

Although the debate over whether the CBS reduction TS favors a chair-like or a boat-like arrangement is still ongoing, it has been shown that both conformers of the transition structure are close in energy and impose similar steric requirements on the substrate.<sup>130</sup>

### 3.3.3.2 Variation of Reaction Conditions of the CBS Reduction and Verification via Chiral HPLC

HPLC analysis with an amylose-modified chiral column (*Lux® i-Amylose-1* from *phenomenex*, Torrance, USA) was performed as a control of the stereochemistry of **45** after the CBS reduction. The developed HPLC method is shown in Table 4. For comparison, a racemic non-stereo-selective reduction of **44** with NaBH<sub>4</sub> was carried out to give the racemic mixture **45rac**.<sup>132</sup> Analysis by HPLC confirmed that the alcohol **45rac** had an enantiomeric ratio *R/S* of 50:50. Analysis of a first attempt to synthesize the enantiomerically pure alcohol **45** gave an enantiomeric ratio (*er*) of 87/13 (Figure 15). Hence, different reaction conditions in terms of catalyst equivalents, reaction time, and temperature were tested. The tested conditions and the resulting enantiomeric ratios are shown in Table 5.

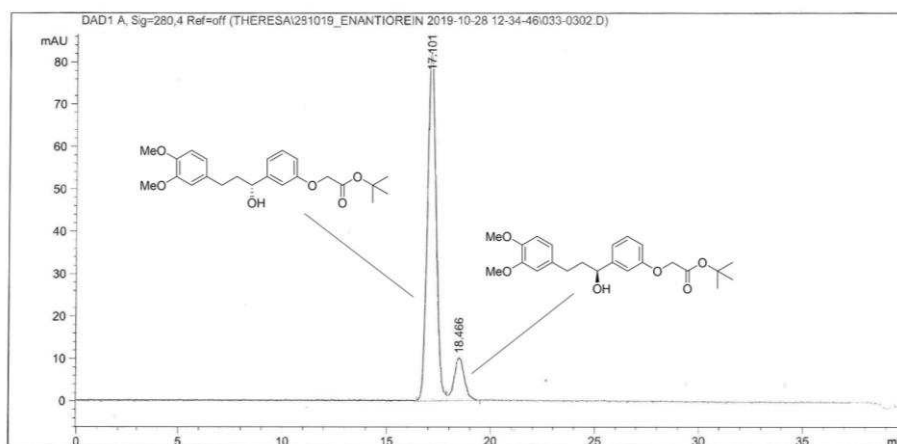


Figure 15. HPLC chromatogram of the obtained mixture of **45** enantiomers of synthesis variant No. 1 with a resulting *R:S* enantiomeric ratio calculated from the peak area of 87/13.

Table 4. HPLC method parameters to evaluate stereochemical purity after CBS reduction.

HPLC Conditions	
Column	Lux® i-Amylose-1, 5 µm, 250 · 4.6 mm, Phenomenex
Eluent	Water + 0.1% FA (A), ACN + 0.1% FA (B)
DAD wavelength	280 nm
Method	Isocratic, 55% A
Flow rate	1 mL/min
Column Oven	Not controlled
Injection volume	5 µL
Duration	40 min

Table 5. Overview of the different reaction conditions for enantioselective reduction of **44** and the *R/S* enantiomeric ratios obtained.

Synthesis variant	CBS-catalyst equivalents	Reaction time (h)	Reaction temperature	Yield (%)	<i>R : S</i> enantiomeric ratio
1	0.1	18	Rt	88	87:13
2	0.5	3	-5 – 0 °C	87	89:11
3	0.6	4	Rt	78	99:1
4	1	2	Rt	88	100:0

Varying the reaction conditions indicated that the amount of catalyst used was the most significant influence on the enantiomeric ratio. Thus, the enantiomeric ratio improved significantly with more catalyst equivalents being used. An ideal cost-benefit factor was found with 0.6 equivalents of catalyst and an *R : S* enantiomeric ratio of 99:1. Consequently, 0.6 equivalents of the CBS catalyst were used in subsequent, larger-scale approaches. Reaction time (2–18 h) and temperature (-5°C to rt), on the other hand, didn't show a significant influence on the yield or enantiomeric ratio.

### 3.3.4 Analysis of Stereochemical Purity of **46** in a Variable Temperature NMR Experiment

As the NMR spectrum of compound **46** showed an unexpected doubling of signals indicative of either diastereomers or rotamers (cf. Figure 16), a variable temperature (VT) NMR experiment was performed.<sup>133</sup>

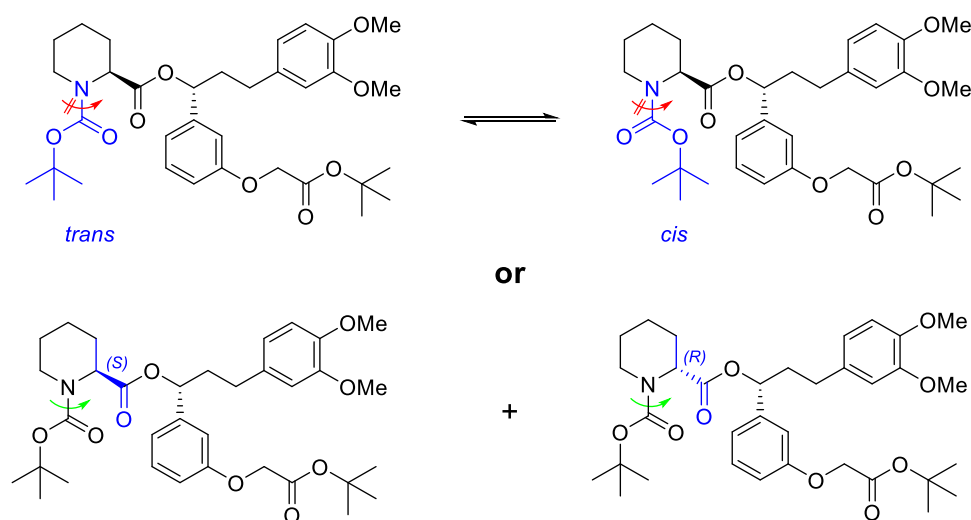
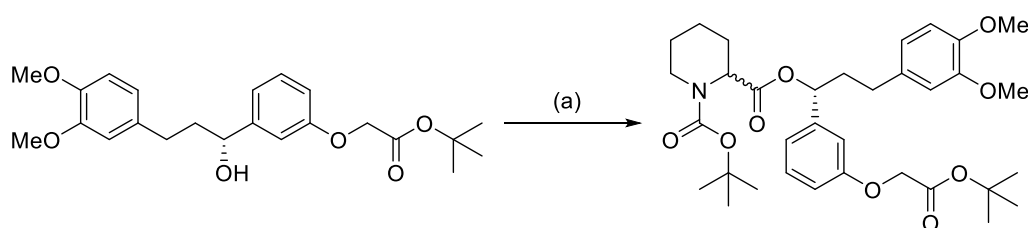


Figure 16. Doubling of <sup>1</sup>H NMR signals was investigated in a VT NMR experiment to distinguish whether this effect was due to rotamers (upper line) or diastereomers (line below).

If, in such an experiment, the split signals would converge with increasing temperature, it can be assumed that the splitting is due to a rotational barrier ( $\Delta G^\ddagger$ ) of the C–N bond of the Boc carbamate.<sup>134, 135</sup> Conversely, if the signals remain split at higher temperatures, the presence of diastereomers is more likely.

The existence of diastereomers would be possible if too high pH values were reached during esterification or workup, which is known to lead to epimerization at the C2 position of the piperidine ring. To allow comparison of the data, **46rac** was synthesized by coupling the alcohol **45** with racemic *N*-Boc pipercolic acid (Scheme 7).



Scheme 7. **45** was coupled with racemic *N*-Boc pipercolic acid as a reference for the VT NMR experiment of **46**. **Reagents and conditions:** (a) EDC, DMAP, DCM abs., rt, 21 h, 36%.

In the VT NMR experiment performed with **46**, coalescence of the proton signals at the stereocenter of the pipercolic acid was observed at higher temperatures (cf. Figure 17), suggesting the presence of rotamers. Due to increasing exchange rate by increasing temperature, the signals of the exchanging species broaden and migrate towards each other until they merge at the coalescence temperature  $T_c$  to an average signal, which narrows at further increasing temperatures.

By using the modified Eyring equation (1), the rotation barrier can be calculated.<sup>134</sup> The estimated coalescence temperature  $T_c$  is used in conjunction with the difference in chemical shift ( $\delta_A - \delta_B$ ) in the low-temperature spectra ( $\Delta\nu$  in Hz).

The modified Eyring equation provides a reasonable estimate of  $\Delta G^\ddagger$ . The derivation of this equation from the Eyring equation can be found in Günther *et al.*<sup>136</sup>

$$\Delta G^\ddagger = RT_c \left[ 22.96 + \ln \left( \frac{T_c}{\Delta\nu} \right) \right] \text{ (J mol}^{-1}\text{)}$$

$\Delta G^\ddagger$  = energy barrier (Jmol)

R = 8.314 JK<sup>-1</sup>mol<sup>-1</sup>

$T_c$  = coalescence temperature (K)

$\Delta\nu$  = difference in chemical shifts  $\delta_A - \delta_B$  (Hz)

1 Joule  $\approx$  0.239 cal



With a difference in chemical shifts  $\Delta\nu$  of around 27.5 Hz and an estimated coalescence temperature  $T_c$  of 312 K, the rotation barrier  $\Delta G^\ddagger$  was calculated to be 65.9 kJ/mol, respectively 15.7 kcal/mol. This is in the known range for rotation barriers in carbamates.<sup>137</sup>

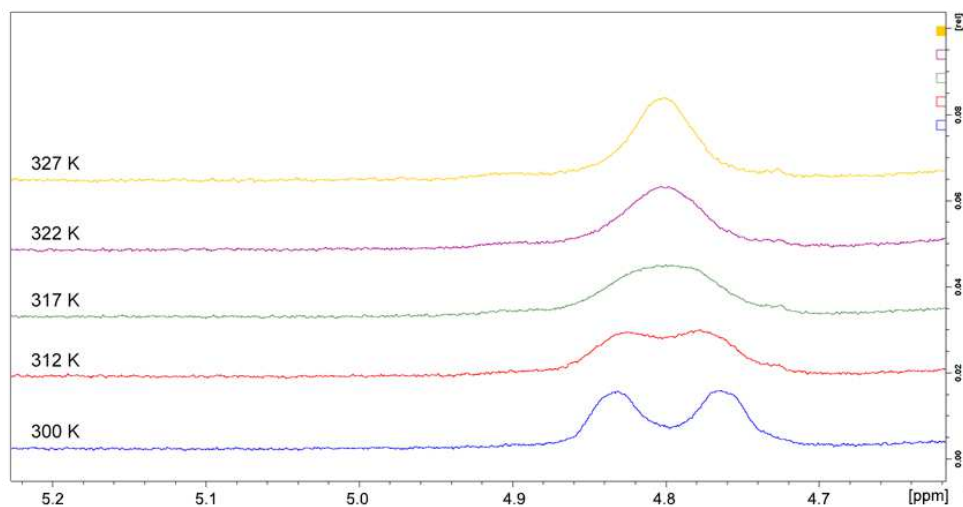


Figure 17. Excerpt from the  $^1\text{H}$  spectra taken in a VT NMR experiment of compound **46**. Temperatures from 300 K to 327 K were used. The signal(s) can be assigned to the proton at the C2 stereocenter of the pipercolic acid. Coalescence of the split signals can be seen at  $T_c \approx 312$  K, indicating the existence of rotamers.  $\text{CD}_3\text{CN}$  was used as a solvent and the shown range is from 4.6 to 5.2 ppm.

A similar VT experiment was performed with the synthesized diastereomeric mixture **46rac**.

Compared to the earlier VT experiment, here the signals at 4.76 ppm and 4.84 ppm converge to one broad signal at 4.80 ppm, while others remain separated (4.80 ppm and 4.90 ppm), indicating the coexistence of rotamers and diastereomers (see Figure 18).

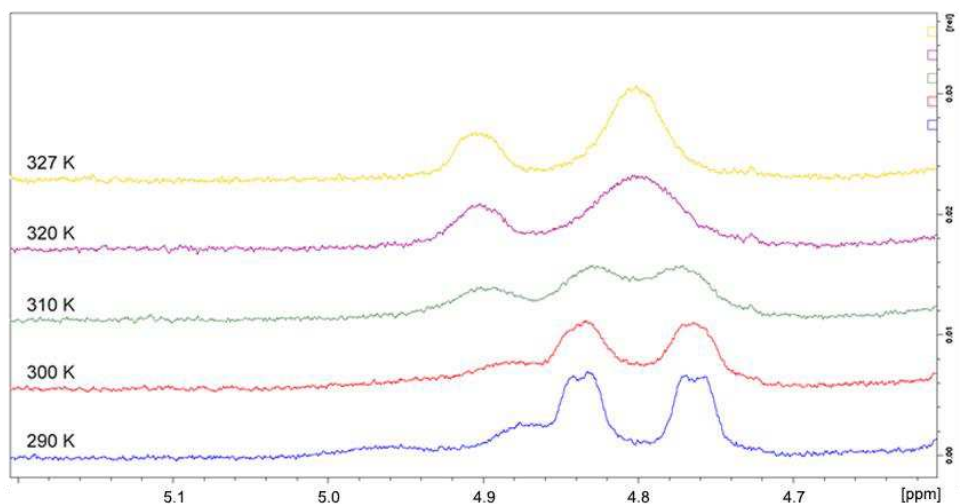


Figure 18. Excerpt from the VT NMR spectrum of compound **46rac** at different temperatures, showing the proton signal of the C2 stereocenter of the pipercolic acid. While some signals converge, others remain separated, indicating the presence of rotamers and diastereomers. Coalescence of the signals at  $\delta = 4.76$  ppm and 4.84 ppm can be seen near 310 K.

The signals of the diastereomers remain separated even at a higher temperature of 327 K. The coalescence of the rotamers' signals can be seen again near 310 K.

In conclusion, the results of the VT NMR experiments showed that the doubling of signals in the  $^1\text{H}$  NMR spectrum of **46** was due to the Boc carbamate rotation barrier of around 15.7 kcal/mol and that no mixture of diastereomers was present. Consequently, **46** was further used in the next steps.

### 3.3.5 FP Binding Assay of Probe **32** with the Mips of Various Pathogens

Analogous to the previous FP probes, **32** was tested in an FP binding assay with the Mip proteins of various pathogens (cf. Table 6).

Table 6:  $K_D$  values of FP tracer **32** for the Mip proteins of various pathogens. Data are shown as mean  $\pm$  SD. Due to the unstable FP signal, robust replicates could not be performed.

	TcMip	LpMip	BpMip
$K_D$	$271 \pm 148$ nM $n=3$	$12.9 \pm 5.8$ $\mu\text{M}$ $n=1$	$67 \pm 52$ nM $n=2$

**32** showed strong binding to TcMip of  $K_D = 271 \pm 148$  nM supporting the hypothesis of enhanced affinity by the addition of a side chain (cf. Figure 19). Furthermore, binding to BpMip was also improved compared to FP probes **30** and **31** to a  $K_D$  of  $67 \pm 52$  nM.

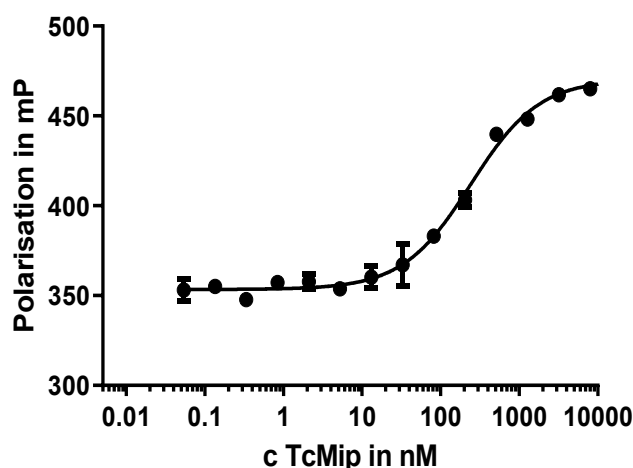


Figure 19. FP binding curve of probe **32** with TcMip. Data are shown as mean  $\pm$  SD,  $n = 3$ .

However, the FP signal strongly fluctuated throughout performing the assay, and data was not always reproducible. Thus, it was not possible to perform three repetitions in each case. Three possible explanations were suggested for this, which could also apply together.

- 1) **Instability of the pipecolic ester.** In flash chromatography purification using RP-modified columns, the ester was not as stable as expected, especially when TFA or FA was added, probably due to acid-catalyzed ester cleavage. Thus, the purification of **32** was more challenging. In-depth stability studies in the buffer medium used in the FPA were not possible due to lack of substance, but this property remains questionable.
- 2) **Impurities of the starting material.** Since purification of **32** was challenging, LC/MS measurements of the starting material were carried out to gain information on possible contaminants. This revealed that the TAMRA fluorophore starting material exhibited an insufficient purity of only some 90%. Contamination with dimethyl- and trimethyl-substituted rhodamine fluorophore was detected. Since these were also coupled to Mip inhibitor **47**, **32** was contaminated with the dimethyl- and trimethyl-substituted analogs. The highly similar retention behavior complicated purification of the probe and significantly lowered the yield.
- 3) **Aggregation and fluorescence-quenching due to lack of solubility.** The solubility of **32** in a broad spectrum of solvents is very low, as could be seen when dissolving it for the FPA (DMSO/water mixtures) or NMR measurements (CD<sub>3</sub>OD, CDCl<sub>3</sub>, etc.). Upon dissolving in the DMSO-buffer mixture, required to perform FPA, slight turbidity showed precipitation of the tracer, also causing inaccuracy in the dilution steps.

TMR dyes such as TAMRA and tetramethylrhodamine 5-isothiocyanate (TRITC) are relatively hydrophobic compared to their fluorescein counterparts FAM and FITC.<sup>118</sup> As a result, they have a tendency to aggregate in aqueous solutions under conditions where the labeling density is sufficient to permit dye–dye interactions.<sup>118</sup> A further consequence of these interactions is fluorescence self-quenching, which reduces the fluorescence output of the conjugate.<sup>118</sup> Since the probe was only soluble in pure DMSO, the DMSO concentration in the FPA was relatively high, which most likely affected the experiment. Details of how DMSO can influence the FP experiment are provided in chapter III \_2.

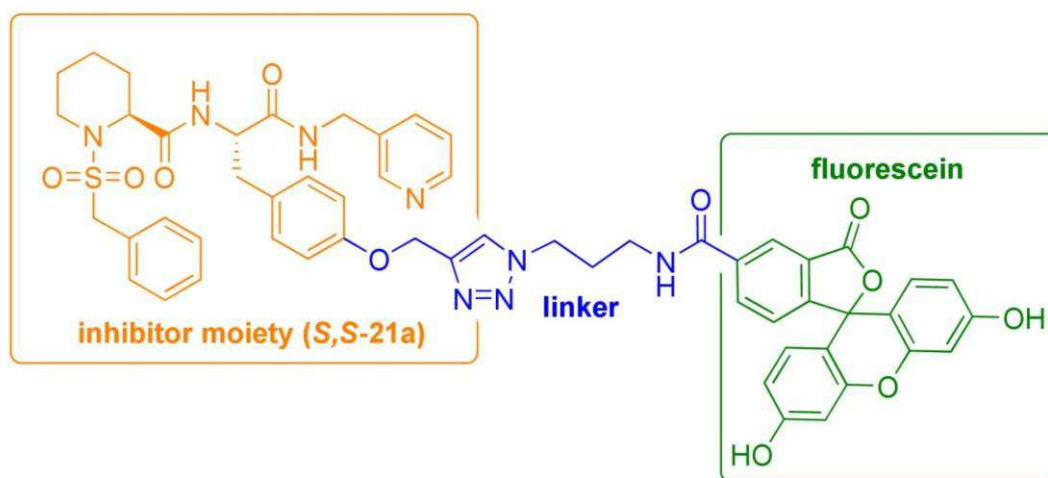
All in all, **32** has demonstrated that an additional side chain seems to be a viable option to obtain

a potent TcMip FP probe. Also, testing of more affine BpMip inhibitors could be feasible with a tracer of this type. However, a variety of problems with **32**, especially its low solubility, made it necessary to optimize the FP probe.

### 3.4 Development and Synthesis of Side Chain-Bearing FP Probe **29**

#### 3.4.1 Starting Point

The synthesis of probe **29** (*NJS254*, cf. Scheme 8) is described in chapter III\_4. Thus, this probe is discussed somewhat more briefly in the following sections to provide additional details.



Scheme 8. Chemical structure of probe **29**.

Probe **32** had demonstrated that attachment of an additional side chain could provide improved binding to TcMip compared to **30**. However, the solubility had to be increased compared to **32** and TAMRA had to be replaced by another fluorophore to avoid possible aggregation. Consequently, fluorescein was reinstated as a fluorophore due to its superior water solubility and successful application in **30** (cf. Scheme 8).

Attachment of the linker to the inhibitor's side chain had provided promising results with FP probe **32** and was therefore chosen here as well.

To further increase the solubility of the probe, the methoxy-substituted benzene ring of **32** was replaced with the well-known pyridine moiety. Thus, the inhibitor moiety corresponds to **S,S-21a** (cf. Scheme 8), which showed promising binding to TcMip in preliminary experiments and ensures good comparability to the tested inhibitors and specificity.

As in the case of **30**, ten atoms were chosen as the linker length.

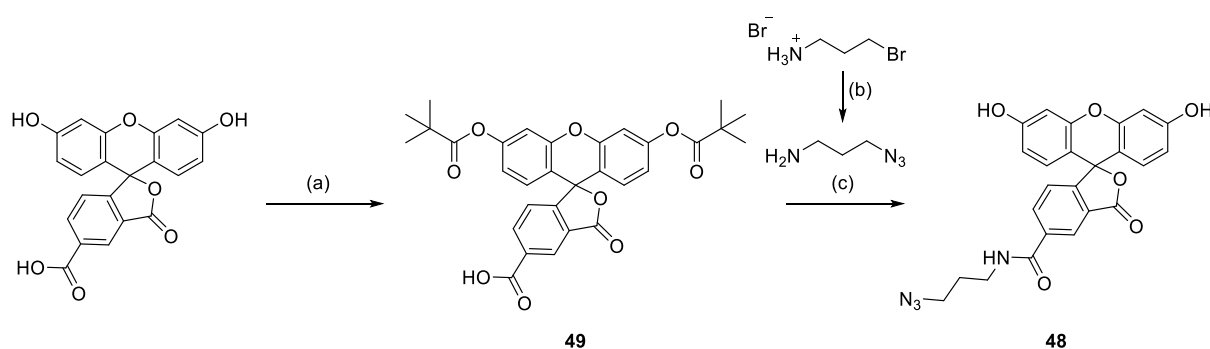
The ester was replaced with the amide to provide chemical stability, which was considered potentially problematic with **32**. Further aspects, such as stereochemically less demanding synthetic steps, were also to be taken into account.

### 3.4.2 Synthetic Route

**29** was synthesized in ten steps, including the synthesis of the fluorophore-linker moiety.

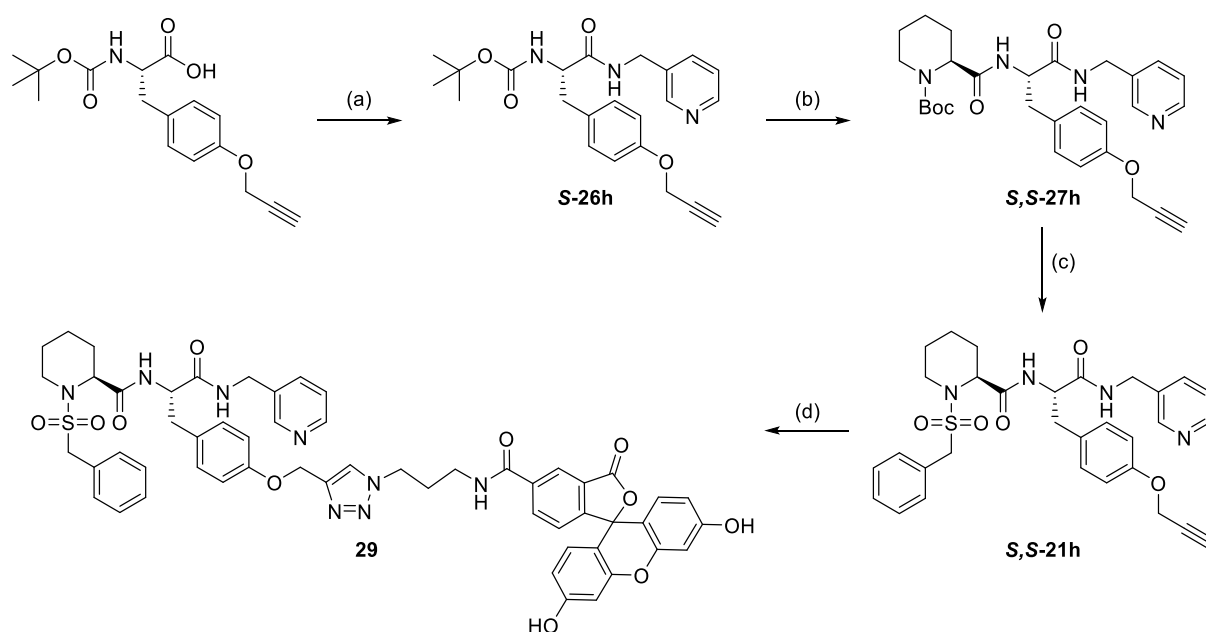
The latter, *N*-(3-azidopropyl)-fluorescein-5-carboxamide (**48**), was synthesized in four steps according to Oeberg *et al.*<sup>138</sup> and Farzan *et al.*<sup>139</sup> (cf. Scheme 9). For this purpose, first, the alcohol groups of fluorescein were protected as pivalic esters by treating the starting material with pivaloyl anhydride under reflux. The linker was prepared from 3-bromopropane-1-aminium bromide with sodium azide to afford the volatile 3-azidopropane-1-amine, which had to be coupled directly to **49** using HBTU and DIPEA. The fluorophore-linker-unit **48** was obtained by cleavage of the pivalic ester protecting group with 25% aqueous ammonia.

Scheme 9. Synthetic route of FAM azide **48**.



**Reagents and conditions:** (a) pivaloyl anhydride, 170 °C, 4 h, 36%; (b) 3-bromopropane-1-aminium bromide, sodium azide, H<sub>2</sub>O, reflux, 6 h, (c) i) HBTU, DIPEA, rt, 3 d, 73%, ii) 25% aqueous ammonia, THF, rt, 19 h, >99%.

To obtain the alkyne-bearing Mip inhibitor **S,S-21h**, (*S*)-2-(Boc-amino)-3-(4-(prop-2-yn-1-yloxy)phenyl)propanoic acid was first coupled to 3-picolylamine with HBTU and DIPEA to give the amide **S-26h** (cf. Scheme 10). After cleavage of the Boc-protecting group with TFA, the intermediate was again amide coupled to *N*-Boc-(*S*)-pipercolic acid with HBTU and DIPEA to give **S,S-27h**. After cleaving the Boc-protecting group with TFA, the *N*-sulfonamide was formed using phenylmethanesulfonyl chloride to give the alkyne-bearing inhibitor **S,S-21h**. In the final step, the azide functionalized fluorescein derivative **48** and **S,S-21h** were coupled in a click reaction under TBTA-catalysis to form probe **29**. The overall yield for **29** was 28%.

Scheme 10. Synthetic route of FP probe **29**.

**Reagents and conditions:** (a) 3-picolylamine, HBTU, DIPEA, DCM, rt, 5 d, 78%; (b) i) TFA, DCM, rt, ii) *N*-Boc-(*S*)-pipercolic acid, HBTU, DIPEA DCM, rt, 2 d, 98%; (c) i) TFA, DCM, rt, 1 d, ii) phenylmethanesulfonyl chloride, NMM, DCM, rt, 5 d, 48%; (d) *N*-(3-azidopropyl)-fluorescein-5-carboxamide, sodium ascorbate,  $\text{CuSO}_4 \cdot 5 \text{H}_2\text{O}$ , TBTA, ACN/DCM/EtOH (10:4:1), 9d, rt, 77%. Overall yield: 28%.

### 3.4.3 FP Binding Assay of Probe **29** with Mip Proteins of Various Pathogens

FP binding assays were performed with FP probe **29** using a variety of Mip proteins (see Table 7). The procedure and assay conditions of the FPA with BpMip established with Theresa Lohr can be found in chapter III\_4. The final concentration of the fluorescent probe was 2.5 nM. FPAs with TcMip and LpMip were performed analogously.

As a result, a  $K_D$  of  $815 \pm 8$  nM was measured for TcMip, and a  $K_D$  of  $1461 \pm 5$  nM for LpMip. This falls within the range of pipercoline-derived side chain-bearing Mip inhibitors previously tested with the [4.3.1]-aza-bicyclic sulfonamide tracer **50** (*MTQ238*) from the Hausch group.<sup>140</sup> Moreover, unlike FP probe **32**, **29** displayed a stable FP signal and sufficient solubility in DMSO and DMSO/buffer mixtures. Therefore, **29** proved to be a suitable probe for robust FPAs of TcMip- and LpMip-inhibitors.

For BpMip, a  $K_D$  of  $63 \pm 10$  nM was determined. This turned out to be within the potency of the inhibitors investigated and thus allows precise determination of activities even with minimal structural differences (cf. chapter III\_4).

In the competitive binding assay for the determination of  $K_i$  values of various inhibitors, a probe

concentration of 2.5 nM and a protein concentration of 250 nM BpMip (in the well) was chosen. Compared with FP probe **50** (*MTQ238*), which exhibits a  $K_D$  of about 1 nM for BpMip, the  $K_D$  of **29** is in a more balanced range for the piperazine-derived Mip inhibitors. This also applies to the other Mip proteins studied. Thus, too high concentrations of the inhibitors in the FPA, which can lead to precipitation, are avoided.

With **29**, an FP probe was designed and synthesized, which features a balanced  $K_D$  value for all tested Mip proteins, TcMip, LpMip, and BpMip. Moreover, **29** provides a stable FP signal and is relatively facile to synthesize. Consequently, **29** was successfully used to establish the FP assays for the investigated Mip proteins and to screen the piperazine-derived Mip inhibitors in respective competitive binding assays (cf. BpMip-screening in chapter III\_4.2).

Table 7:  $K_D$  values of the FP tracer **29** for different Mip proteins. Data are shown as mean  $\pm$  SD,  $n \geq 3$ .

	TcMip	LpMip	BpMip
$K_D$	815 $\pm$ 8 nM	1461 $\pm$ 5 nM	63 $\pm$ 10 nM

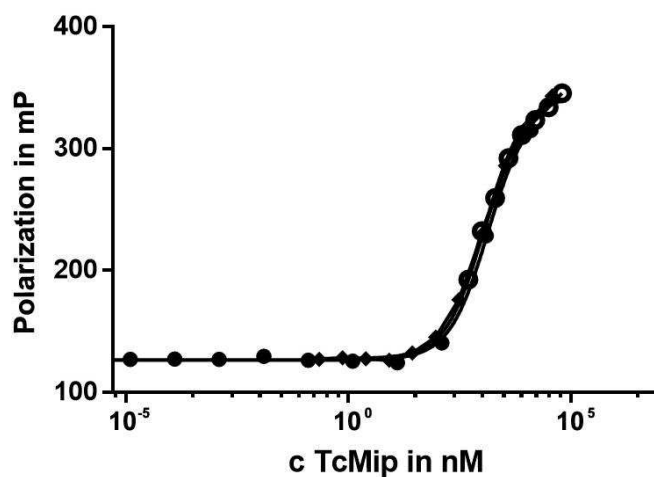


Figure 20. FP binding curve of probe **29** with TcMip. Data are shown as mean  $\pm$  SD,  $n = 3$ .

### 3.5 Experimental Part – FP Probes

General experimental procedures (NMR, IR, etc.) and equipment are described in subchapter III\_1.6.

#### HPLC for the Analysis of Stereo Chemical Purity.

For analytical HPLC, an *Agilent 1100* series HPLC system with degasser (G1322A), binary pump (G1312A), sample changer (G1313A), DAD detector (G1315B), and column oven (G1316A) was used. The Agilent-Chemstation software by *Agilent* (Böblingen, Germany) was used to analyze the data. As a stationary phase, the chiral HPLC column *Lux® i-Amylose-1* (5  $\mu\text{m}$ , 250 · 4.6 mm) from *Phenomenex* (Torrance, California, US) was used. Mobile phase A was Milli-Q®-water, while mobile phase B was acetonitrile. An isocratic method of 50% B was chosen with a duration of 25 min. The flow rate was set to 1.0 mL/min. The injection volume was 5  $\mu\text{L}$  (of a 1 mg/mL solution in acetonitrile). The UV signal at 254 nm was chosen for detection, the oven temperature was 30 °C.

**High-Resolution Mass Spectrometry.** High-resolution mass spectrometry (HRMS) was performed using an *Agilent* Infinity II LC-system (Waldbronn, Germany) consisting of a quaternary pump, a thermostatted autosampler, and a thermostatted column compartment, coupled to a *Sciex* X500R QTOF mass spectrometer (Concord, Ontario, Canada) equipped with a Turbo V™ Ion Source (ESI). Automatic calibration of the mass spectrometer was performed using the provided tuning solution for ESI (*Sciex*, Concord, Ontario, Canada). Mobile phase A was a mixture of water and 0.1% formic acid (FA), while mobile phase B was acetonitrile containing 0.1% FA. An isocratic elution of 50% B with a stop time of 1.5 min was used. The flow rate was set to 1 mL/min, and the injection volume was 10  $\mu\text{L}$ . The parameters for the HRMS experiment were optimized by flow-injection using positive polarity (Gas1: 50 psi, Gas2: 50 psi, Curtain gas: 25 psi, Ionspray voltage: 5500 V, Temperature: 500 °C, Declustering potential: 70 +/- 10 V, Collision energy: 10 V). The mass accuracy is given as an error in ppm and was calculated adapted from Lermyte<sup>141</sup>:  $\text{mass error (ppm)} = (|(m/z)_{\text{found}} - (m/z)_{\text{calculated}}| \times 1\,000\,000) / (m/z)_{\text{calculated}}$ .



**General Procedures.**

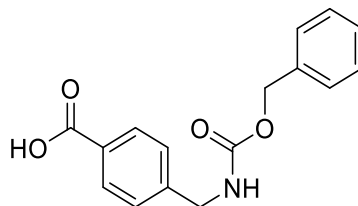
*The following procedures A – C have been reported in Scheuplein et al.<sup>142</sup>*

**General procedure A.** Esterification and amidation was carried out according to Seufert *et al.*<sup>52</sup> First, the corresponding carboxylic acid (1 equiv) was dissolved in dry DCM (30–40 mL per 1 mmol limiting reactant). In the case of esterifications, EDC·HCl (1.2 equiv) and DMAP (0.2–1 equiv) was added under ice cooling. In the case of amidations was added under ice cooling an auxiliary base (DIPEA, NMM or NEt<sub>3</sub>; 1–4 equiv) and either a combination of EDC·HCl (1.2 equiv) and HOBt (0.2–1 equiv) or HBTU alone (1.2–2 equiv). After stirring for 15 min, the corresponding amine or alcohol (1–1.2 equiv) was added to the solution under ice cooling. The reaction was allowed to warm up to rt and stirred until completion, monitored by TLC. The mixture was then washed several times with saturated ammonium chloride solution, brine, and water (2 × 50 mL per step). After separation of the phases, the combined organic phases were dried over Na<sub>2</sub>SO<sub>4</sub> and filtered. The organic solvent was removed *in vacuo*, and the crude product was purified by column chromatography or flash chromatography.

**General procedure B.** According to Seufert *et al.*,<sup>52</sup> the Boc-protection group was cleaved at rt using an excess of TFA (2–10 mL) in dry DCM (10–20 mL). After completion, monitored by TLC (usually around 24 h), the reaction was neutralized with a sat. NaHCO<sub>3</sub> solution and extracted with DCM (3 × 50 mL). After separation of the phases, the combined organic layers were dried over Na<sub>2</sub>SO<sub>4</sub>, filtered, and the solvent was removed *in vacuo* to give the crude product, which was used in the next step without further purification.

**General procedure C.** According to Seufert *et al.*,<sup>52</sup> to a solution of the piperidine-derivative (1 equiv) in dry DCM (20 mL per 1 mmol limiting reactant), *N*-methylmorpholine (NMM) (1.5–3 equiv) or DIPEA (1.5–3 equiv) and the corresponding sulfonyl chloride (phenylmethanesulfonyl chloride or (4-fluorophenyl)methanesulfonyl chloride) (1 equiv) were added and stirred at rt. After the reaction was completed according to TLC monitoring, the organic layer was washed consecutively with 2M HCl (50 mL), water (50 mL), and sat. NaHCO<sub>3</sub> solution (50 mL). The phases were separated, and the organic phase was dried over Na<sub>2</sub>SO<sub>4</sub>. The desiccant was filtered off, the solvent was removed *in vacuo*, and the product was purified using column chromatography or flash chromatography.

## 3.5.1 Synthesis of FP Probe 31

3.5.1.1 4-(((Benzyloxy)carbonyl)amino)methyl)benzoic acid (**34**, *NJS57*)

**Chemical Formula:** C<sub>16</sub>H<sub>15</sub>NO<sub>4</sub>, **Molecular Weight:** 285.30 g/mol.

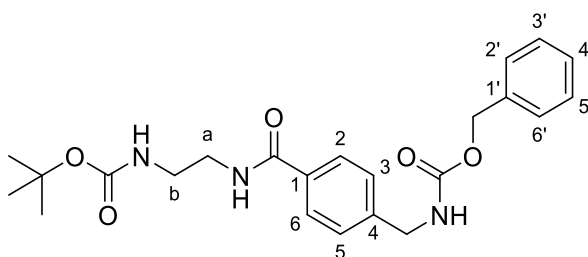
**34** was synthesized according to a protocol by Lameijer *et al.*,<sup>143</sup> using 11.0 g of 4-aminomethylbenzoic acid (72.8 mmol), sodium hydrogen carbonate (7.34 g, 87.3 mmol) and benzyl chloroformate (12.4 mL, 87.3 mmol) in a mixture of THF and water (1:1; 200 mL). **34** was obtained quantitatively as a white powder (20.8 g, 72.8 mmol, Lit.:<sup>143</sup> 83%).

**TLC:** R<sub>f</sub> = 0.46 (SiO<sub>2</sub>, DCM/MeOH 9:1, bromocresol green)

**IR (ATR,  $\tilde{\nu}_{max}$  [cm<sup>-1</sup>]):** 3340 (s), 3062 (w), 3034 (w), 2927 (m), 1683 (s), 1602 (s), 1550 (s), 1529 (s), 855 (w), 803 (w), 774 (m).

**Melting point:** 320 °C under decomposition

*The compound has already been synthesized and characterized by Lameijer et al.<sup>143</sup> The recorded spectra are in agreement with the literature.<sup>143</sup>*

3.5.1.2 Benzyl (4-((2-((*tert*-butoxycarbonyl)amino)ethyl)carbamoyl)benzyl)carbamate (**35**, *NJS117*)

**Chemical Formula:** C<sub>23</sub>H<sub>29</sub>N<sub>3</sub>O<sub>5</sub>, **Molecular Weight:** 427.50 g/mol.

Following general procedure A, **34** (2.14 g, 7.49 mmol) was treated with EDC·HCl (2.15 g, 11.2 mmol), DIPEA (2.6 ml, 15.0 mmol), HOBT (1.01 g, 7.49 mmol), and *N*-Boc-1,2-diaminoethane (1.20 g, 7.49 mmol) in dry DCM (100 mL). After stirring at rt for 2 d, the reaction was worked up according to the general procedure. Subsequently, the crude oily product was purified

by column chromatography (SiO<sub>2</sub>, DCM/MeOH = 100:0 for ~5 column volumes, then 10:1) to give **35** as a white solid in a yield of 84% (2.7 g, 6.32 mmol).

**TLC:**  $R_f = 0.36$  (SiO<sub>2</sub>, DCM/MeOH = 20:1)

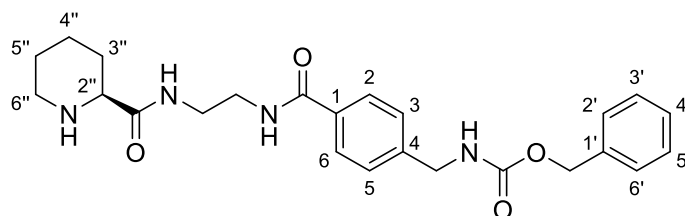
**Melting Point:** 139 °C

**IR (ATR,  $\tilde{\nu}_{max}$  [cm<sup>-1</sup>]):** 3304 (m), 3062 (w), 2981 (w), 2950 (w), 1690 (s), 1638 (s), 1534 (s), 846 (w), 781 (w), 750 (w), 715 (w), 684 (w).

**<sup>1</sup>H NMR (CDCl<sub>3</sub>):**  $\delta = 7.76$  (d,  $^3J = 8.0$  Hz, 2H, *CH*-2,6), 7.39–7.27 (m, 7H, *CH*-3,5,2'-6'), 7.23 (br, 1H, C-1CONH), 5.23 (br, 1H, *Cbz-NH*), 5.14 (s, 2H, *CH*<sub>2</sub>C-1'), 5.04 (br, 1H, *Boc-NH*), 4.41 (d,  $^3J = 5.9$  Hz, 2H, C-4*CH*<sub>2</sub>NH), 3.53 (dt,  $^3J = 10.7, 5.3$  Hz, 2H, *CH*<sub>2</sub>-a), 3.38 (dt,  $^3J = 10.7, 5.3$  Hz, 2H, *CH*<sub>2</sub>-b), 1.42 (s, 9H, C(*CH*<sub>3</sub>)<sub>3</sub>) ppm.

**<sup>13</sup>C NMR (CDCl<sub>3</sub>):**  $\delta = 167.6$  (1C, COC-1), 157.7 (1C, *Boc-CO*), 156.6 (1C, *Cbz-CO*), 142.2 (1C, C-4), 136.5 (1C, C-1'), 133.5 (1C, C-1), 128.7 (2C, *CH*-3,5), 128.4 (1C, C-4'), 128.3 (2C, *CH*-2,6), 127.6 (s, 4C, *CH*-2',3',5',6'), 80.2 (1C, C(*CH*<sub>3</sub>)<sub>3</sub>), 67.2 (1C, *CH*<sub>2</sub>C-1'), 44.9 (1C, C-4*CH*<sub>2</sub>NH), 42.3 (1C, *CH*<sub>2</sub>-a), 40.1 (1C, *CH*<sub>2</sub>-b), 28.5 (3C, C(*CH*<sub>3</sub>)<sub>3</sub>) ppm.

### 3.5.1.3 Benzyl (*S*)-(4-((2-(piperidine-2-carboxamido)ethyl)carbamoyl)benzyl)carbamate (**36**; *NJS120*)



**Chemical Formula:** C<sub>24</sub>H<sub>30</sub>N<sub>4</sub>O<sub>4</sub>, **Molecular Weight:** 438.53 g/mol.

**35** (2680 mg, 6.27 mmol) was deprotected according to general procedure B, using 5.3 mL of TFA (69.0 mmol) in dry DCM (70 mL). After stirring at rt for 3 h and workup according to the general procedure, the crude intermediate product was obtained as a white oily solid in a yield of 87% (1.79 g, 5.45 mmol). The intermediate product (1700 mg, 5.19 mmol) was further reacted according to general procedure A using 1.55 g (*S*)-*N*-Boc-piperidine-2-carboxylate (6.75 mmol), EDC·HCl (1.59 g, 8.31 mmol), HOBt (636 mg, 4.15 mmol), and DIPEA (1.81 mL, 10.4 mmol) in dry DCM (120 mL). After stirring at rt for 18 h and workup according to the general procedure, the crude oily product was purified by column chromatography (SiO<sub>2</sub>, DCM/MeOH = 20:1) to

give the intermediate product ( $R_f = 0.42$  (SiO<sub>2</sub>, DCM/MeOH = 15:1) in a yield of 91% (2.53 g, 4.70 mmol). Subsequently, the intermediate product (2400 mg, 4.46 mmol) was Boc-protected according to general procedure B using 3.1 mL TFA (40.1 mmol) in dry DCM (10 mL). After stirring at rt for 2 h, the reaction was ended by addition of saturated sodium hydrogen carbonate solution (30 mL). After workup according to the general procedure, **36** was obtained as a white solid in a yield of 86% (1688 mg, 4.46 mmol).

**TLC:**  $R_f = 0.20$  (SiO<sub>2</sub>, DCM/MeOH = 20:0.5)

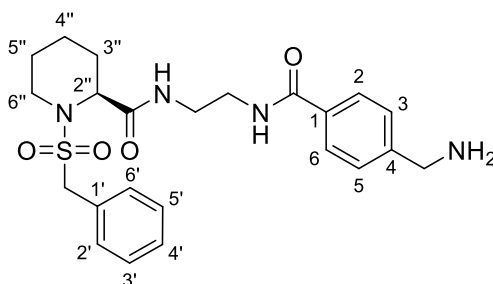
**Melting Point:** 164 °C.

**IR (ATR,  $\tilde{\nu}_{max}$  [cm<sup>-1</sup>]):** 3317 (s), 3293 (s), 3064 (w), 2926 (m), 1685 (s), 1636 (s), 1537 (s), 846 (m), 750 (w), 715 (m), 687 (m).

**<sup>1</sup>H NMR (CD<sub>3</sub>OD):**  $\delta = 7.77$  (d,  $^3J = 8.2$  Hz, 2H, CH-2,6), 7.41–7.15 (m, 7H, CH-3,5, 2'-6'), 5.10 (s, 2H, CH<sub>2</sub>C-1'), 4.35 (s, 2H, CH<sub>2</sub>C-4), 3.52–3.39 (m, 4H, NHCH<sub>2</sub>CH<sub>2</sub>NH), 3.16 (dd,  $^3J = 10.3$ , 2.8 Hz, 1H, CH-2''), 3.04 (br d,  $^2J = 12.2$  Hz, 1H, CH<sub>2</sub>-6''), 2.61 (ddd,  $^2J = 12.2$  Hz,  $^3J = 12.2$ , 2.8 Hz, 1H, CH<sub>2</sub>-6''), 1.86–1.77 (m, 2H, CH<sub>2</sub>-3'',4''), 1.61–1.34 (m, 4H, CH<sub>2</sub>-3'',4'',5'') ppm.

**<sup>13</sup>C NMR (CD<sub>3</sub>OD):**  $\delta = 176.4$  (1C, C-2''CONH), 170.3 (1C, NHCOC-1), 159.0 (1C, NHCOC-1), 144.7 (1C, C-4), 138.4 (1C, C-1'), 134.3 (1C, C-1), 129.5 (2C, CH-3',5'), 129.0 (1C, CH-4'), 128.8 (2C, CH-2,6), 128.5 (2C, CH-2',6'), 128.2 (2C, CH-3,5), 67.6 (1C, CH<sub>2</sub>C-1'), 61.1 (1C, CH-2''), 46.5 (1C, CH<sub>2</sub>-6''), 45.1 (1C, C-4CH<sub>2</sub>), 40.8 (1C, NHCH<sub>2</sub>CH<sub>2</sub>NH), 39.9 (1C, NHCH<sub>2</sub>CH<sub>2</sub>NH), 31.0 (1C, CH<sub>2</sub>-3''), 26.7 (1C, CH<sub>2</sub>-5''), 25.1 (1C, CH<sub>2</sub>-4'') ppm.

#### 3.5.1.4 (S)-N-(2-(4-(Aminomethyl)benzamido)ethyl)-1-(benzylsulfonyl)piperidine-2-carboxamide (**38**; NJS126)



**Chemical Formula:** C<sub>23</sub>H<sub>30</sub>N<sub>4</sub>O<sub>4</sub>S, **Molecular Weight:** 458.58 g/mol.

The sulfonamide was established following general procedure C, using **36** (1650 mg, 3.76 mmol),

phenylmethanesulfonyl chloride (1.10 g, 5.64 mmol), and DIPEA (1.97 mL, 11.29 mmol) in dry chloroform (70 mL). After stirring at rt for 3 d, TLC control indicated complete conversion of the starting material to the targeted product ( $R_f$  (*intermediate product*) = 0.40 (SiO<sub>2</sub>, DCM/MeOH = 15:1). The crude oily product was directly loaded onto silica gel and purified by flash chromatography (SiO<sub>2</sub>, A: DCM, B: MeOH, gradient: 0→20% B). The Cbz-protected intermediate **37** was obtained as a white oily solid in a yield of 83% (1.84 g, 3.11 mmol). Analogous to Mori *et al.*,<sup>144</sup> to a solution of **37** (204 mg, 0.34 mmol) in dry DCM (3 mL) was added hydrogen bromide (32% solution in acetic acid, 0.92 mL, 5.16 mmol) under ice cooling. After 2 h, the ice bath was removed, and the reaction was stirred at rt for 1 h. The reaction was terminated by the addition of NEt<sub>3</sub> (1.5 mL). An additional 50 mL of DCM was added, the mixture was filtered, and the solvent of the filtrate was removed *in vacuo*. After subsequent purification by column chromatography (aloxide basic, CHCl<sub>3</sub>/MeOH = 20:1), **38** was obtained as a colorless oily solid in a yield of 16% (25 mg, 0.06 mmol).

**TLC:**  $R_f$  = 0.11 (aloxide neutral, DCM/MeOH = 9:1)

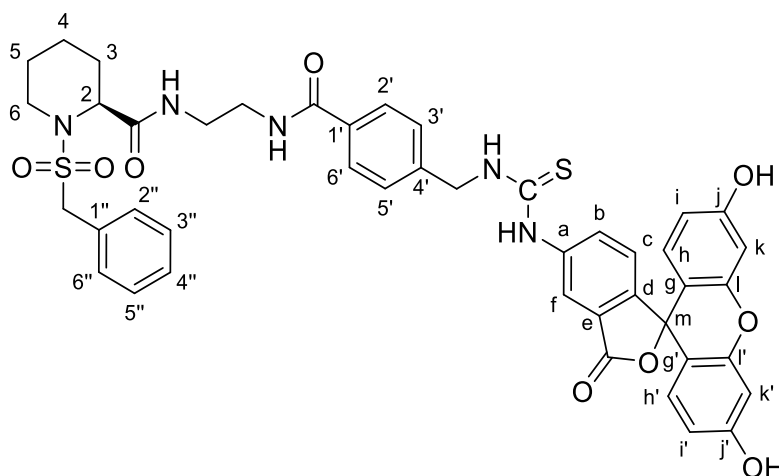
**IR (ATR,  $\tilde{\nu}_{max}$  [cm<sup>-1</sup>]):** 3298 (br, m), 3061 (w), 2921 (s), 2854 (m), 1636 (s), 1533 (s), 1365 (m), 1318 (br, s), 1183 (m), 1126 (s), 853 (w), 784 (w), 736 (w), 698 (w).

**<sup>1</sup>H NMR (CDCl<sub>3</sub>):**  $\delta$  = 7.77 (d, 2H, <sup>3</sup>J = 8.1 Hz, CH-2,6), 7.45–7.39 (m, 5H, CH-2'-6'), 7.34 (d, 2H, <sup>3</sup>J = 8.1 Hz, CH-3,5), 7.07 (m, 1H, NH), 6.68 (m, 1H, NH), 4.32 (s, 2H, SO<sub>2</sub>CH<sub>2</sub>), 4.27–4.26 (m, 1H, CH-2''), 3.90 (s, 2H, CH<sub>2</sub>NH<sub>2</sub>), 3.58–3.33 (m, 5H, CH<sub>2</sub>-6'', CONHCH<sub>2</sub>CH<sub>2</sub>), 3.00–2.93 (m, 1H, CH<sub>2</sub>-6), 2.24–2.17 (m, 1H, CH<sub>2</sub>-3''), 1.58–1.25 (m, 7H, NH<sub>2</sub>, CH<sub>2</sub>-3'', 4'', 5'') ppm.

**<sup>13</sup>C NMR (CDCl<sub>3</sub>):**  $\delta$  = 171.8 (1C, *pip*-CONH), 167.8 (1C, C-1CONH), 147.0 (1C, CH-1), 132.6 (1C, CH-4), 130.8 (2C, CH-2',6'), 129.1 (2C, CH-3',5'), 129.0 (C-4'), 127.5 (2C, CH-2,6), 127.2 (2C, CH-3,5), 58.6 (1C, SO<sub>2</sub>CH<sub>2</sub>), 56.2 (1C, CH-2''), 46.2 (1C, CH<sub>2</sub>NH<sub>2</sub>), 44.0 (1C, CH<sub>2</sub>-6''), 41.2 (1C, C-1CONHCH<sub>2</sub>), 40.0 (1C, C-2''CONHCH<sub>2</sub>), 26.1 (1C, CH<sub>2</sub>-3''), 24.5 (1C, CH<sub>2</sub>-5''), 19.9 (1C, CH<sub>2</sub>-4'') ppm.

**LC/MS (m/z):** 459.10 [M+H]<sup>+</sup>.

3.5.1.5 (S)-1-(Benzylsulfonyl)-N-(2-(4-((3-(3',6'-dihydroxy-3-oxo-3H-spiro[isobenzofuran-1,9'-xanthen]-5-yl)thioureido)methyl)benzamido)ethyl)-piperidine-2-carboxamide (31; *NJS166*)



**Chemical Formula:** C<sub>44</sub>H<sub>41</sub>N<sub>5</sub>O<sub>9</sub>S<sub>2</sub>, **Molecular Weight:** 847.96 g/mol.

Analogous to Carta *et al.*,<sup>145</sup> **38** (50 mg, 0.11 mmol) was reacted with fluorescein isothiocyanate (47 mg, 0.12 mmol) in a mixture of dry DCM (3 mL), dry THF (2 mL) and triethylamine (15  $\mu$ L, 0.11 mmol) under ice cooling. The reaction was allowed to warm to rt and stirred for 20 h. The crude oily product was directly loaded onto silica gel and purified by flash chromatography (run 1: SiO<sub>2</sub>, A: CHCl<sub>3</sub>, B: MeOH, gradient: 0 $\rightarrow$ 20% B; run 2: RP 18, A: H<sub>2</sub>O + 0.1% FA, B: MeOH + 0.1% FA, gradient: 5 $\rightarrow$ 100% B). **31** was obtained as a yellow solid in a yield of 27% (25 mg, 0.03 mmol).

**TLC:**  $R_f$  = 0.58 (SiO<sub>2</sub>, DCM/MeOH = 5:1)

**Melting Point:** 183 °C.

**Purity (HPLC):** 95.9,  $t_R$  = 9.30 min.

**IR (ATR,  $\nu_{max}$  [cm<sup>-1</sup>]):** 3310 (w), 3060 (w), 2360 (s), 2342 (s), 1735 (w), 1640 (m), 1608 (m), 1539 (m), 1455 (m), 1370 (m), 1316 (m), 1177 (m), 1110 (m), 845 (w), 745 (w), 700 (w).

**<sup>1</sup>H NMR (CD<sub>3</sub>OD):**  $\delta$  = 8.18 (s, 1H, *fluorescein-CH-f*), 7.81 (d,  $^3J$  = 8.3 Hz, 2H, *inhibitor-CH-2',6'*), 7.77 (dd,  $^3J$  = 8.3,  $^4J$  = 2.0 Hz, 1H, *fluorescein-CH-b*), 7.46 (d,  $^3J$  = 8.3 Hz, 2H, *inhibitor-CH-3',5'*), 7.43–7.41 (m, 2H, *inhibitor-CH-2'',6''*), 7.37–7.33 (m, 3H, *inhibitor-CH-3''-5''*), 7.15 (d,  $^3J$  = 8.3 Hz, 1H, *fluorescein-CH-c*), 6.67–6.65 (m, 4H, *fluorescein-CH-h,h',k,k'*), 6.53 (dd,  $^3J$  = 8.7,  $^4J$  = 2.4 Hz, 2H, *fluorescein-CH-i,i'*), 4.91 (s, 2H, CH<sub>2</sub>NHC=S), 4.39–4.29 (m, 3H,

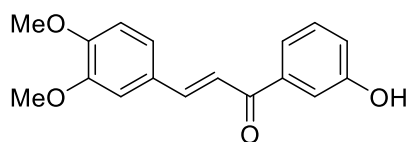
*pip-CH*-2, SO<sub>2</sub>CH<sub>2</sub>), 3.56–3.35 (m, 6H, *inhibitor-NHCH*<sub>2</sub>CH<sub>2</sub>NH, *pip-CH*<sub>2</sub>-6), 2.05 (d, 1H, *pip-CH*<sub>2</sub>-3), 1.60–1.29 (m, 5H, *pip-CH*<sub>2</sub>-3,4,5) ppm.

<sup>13</sup>C NMR (CD<sub>3</sub>OD): δ = 183.3 (1C, CS), 173.9 (1C, *pip-CONH*), 171.1 (1C, *fluorescein-CO*), 170.2 (1C, *inhibitor-C-1'*CONH), 161.7 (br 2C, *fluorescein-C-j,j'*), 154.2 (2C, *fluorescein-C-l,l'*), 142.4 (1C, *inhibitor-C-1''*), 134.3 (1C, *fluorescein-C-a*), 132.3 (1C, *inhibitor-C-1'*), 132.2 (3C, *fluorescein-CH-b*, *inhibitor-CH-2''*,6''), 131.0 (1C, *inhibitor-CH-4''*), 130.3 (1C, *inhibitor-CH-4'*), 129.5 (s, 4C, *inhibitor-CH-3''*,5'', *fluorescein-C-d,e*), 128.7 (s, 4C, *inhibitor-CH-2'*,6', *fluorescein-CH-h,h'*), 128.6 (2C, *inhibitor-CH-3'*,5'), 125.84 (1C, *fluorescein-CH-c*), 125.77 (1C, *fluorescein-CH-f*), 113.7 (2C, *fluorescein-CH-i,i'*), 111.5 (2C, *fluorescein-CH-g,g'*), 103.5 (2C, *fluorescein-CH-k,k'*), 82.6 (1C, *fluorescein-C-m*), 59.0 (1C, SO<sub>2</sub>CH<sub>2</sub>), 57.5 (1C, *pip-CH*-2), 48.4 (1C, CH<sub>2</sub>NHCS), 44.7 (1C, *pip-CH*<sub>2</sub>-6), 40.8 (1C, *inhibitor-CH*<sub>2</sub>NHCOC-1'), 40.2 (1C, *pip-CH*-2CONHCH<sub>2</sub>), 28.4 (1C, *pip-CH*<sub>2</sub>-3), 25.7 (1C, *pip-CH*<sub>2</sub>-5), 20.8 (1C, *pip-CH*<sub>2</sub>-4) ppm.

LC/MS (m/z): 848.15 [M+H]<sup>+</sup>, 424.75 [M+2H]<sup>2+</sup>.

### 3.5.2 Synthesis of FP probe 32

#### 3.5.2.1 (*E*)-3-(3,4-Dimethoxyphenyl)-1-(3-hydroxyphenyl)prop-2-en-1-one (42; *NJS134*)



**Chemical Formula:** C<sub>17</sub>H<sub>16</sub>O<sub>4</sub>, **Molecular Weight:** 284.31 g/mol.

**42** was synthesized according to a protocol by Jorgensen *et al.*,<sup>120</sup> using 2060 mg of 3,4-dimethoxyphenylbenzaldehyde (12.3 mmol) and 3'-hydroxyacetophenone (1593 mg, 11.5 mmol) in a mixture of methanol (10 mL) and an aqueous solution of potassium hydroxide (3.0 M, 15 mL). After stirring at rt for 1 d, the reaction was worked up according to the literature procedure and purified by column chromatography (SiO<sub>2</sub>, PE/EA = 3:2 + 3% FA) to obtain the product as a yellow solid in a yield of 84% (2750 mg, 9.67 mmol; Lit.:<sup>120</sup> 86%).

**TLC:** R<sub>f</sub> = 0.29 (SiO<sub>2</sub>, PE/EA = 3:2 + 3%FA)

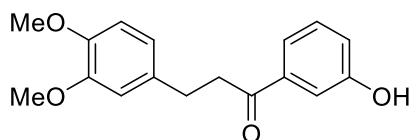
**Melting Point:** 139–142°C (Lit.:<sup>120</sup> 140–142 °C)

**IR (ATR, ν<sub>max</sub> [cm<sup>-1</sup>]):** 3437 (s), 3062 (w), 3011 (w), 2938 (w), 2835 (w), 1659 (s),

1574 (vs), 1509 (vs), 903 (w), 884 (w), 838 (w), 824 (w), 783 (w).

**42** has been reported by Keenan *et al.*<sup>121</sup> and Jorgensen *et al.*<sup>120</sup> The analytical data are in agreement with the literature.<sup>120</sup> No IR spectrum has been reported yet.

### 3.5.2.2 3-(3,4-Dimethoxyphenyl)-1-(3-hydroxyphenyl)propan-1-one (**43**; NJS136)



**Chemical Formula:** C<sub>17</sub>H<sub>18</sub>O<sub>4</sub>, **Molecular Weight:** 286.33 g/mol.

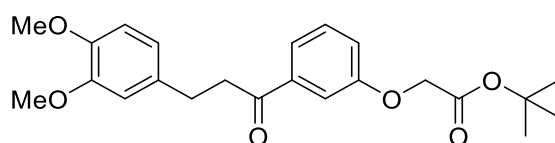
**43** was synthesized analogous to Mori *et al.*,<sup>122</sup> using 230 mg of **42** (809 μmol), catalytic amounts of diphenyl sulfide (2.3 mg, 2.0 μL, 12.1 μmol), and palladium/carbon catalyst (10-wt%, 30 mg) in methanol (5 mL). After suspending the starting material at rt under an argon atmosphere, the reaction mixture was purged with a hydrogen balloon three times and stirred at rt for 19 h, monitored by TLC. The catalyst was removed by filtration over celite, and the filter cake was washed with hot methanol (2 · 40 mL). The solvent of the filtrate was removed *in vacuo*, and the crude product was obtained quantitatively as a white solid (232 mg, 809 μmol, Lit.:<sup>120</sup> 68%).

**TLC:** R<sub>f</sub> = 0.53 (SiO<sub>2</sub>, PE/EA = 1:1)

**Melting point:** 118–121 °C (Lit.:<sup>120</sup> 119–121 °C)

The product has been reported by Keenan *et al.*<sup>121</sup> and Jorgensen *et al.*<sup>120</sup> The analytical data are in agreement with the literature.<sup>120</sup>

### 3.5.2.3 *tert*-Butyl 2-(3-(3-(3,4-dimethoxyphenyl)propanoyl)phenoxy)acetate (**44**; NJS148)



**Chemical Formula:** C<sub>23</sub>H<sub>28</sub>O<sub>6</sub>, **Molecular Weight:** 400.47 g/mol

**44** was synthesized according to Keenan *et al.*,<sup>121</sup> using 412 mg of **43** (1.44 mmol), potassium carbonate (418 mg, 3.02 mmol), and *tert*-butyl 2-bromoacetate (266 μL, 351 mg, 1.80 mmol) in acetone (10 mL). After 22 h of stirring at rt, the solid components of the reaction mixture were removed by filtration, and the crude oily product was purified by column chromatography (SiO<sub>2</sub>, PE/EA = 2:1). **44** was obtained as a yellowish oily solid in a yield of 90% (520 mg, 1.30 mmol).

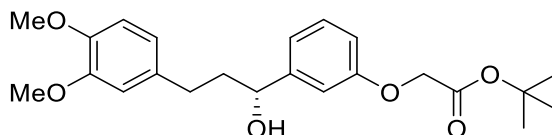


TLC:  $R_f = 0.37$  (SiO<sub>2</sub>, PE/EA = 3:1 + 1% FA)

IR (ATR,  $\nu_{\max}$  [cm<sup>-1</sup>]): 3315 (br m), 3062 (w), 3032 (w), 1701 (s), 1645 (s), 1454 (s), 886 (w), 840 (w), 825 (w), 780 (w).

*The analytical data are in agreement with Keenan et al.<sup>121</sup> No IR spectrum has been reported yet.*

3.5.2.4 *tert*-Butyl (*R*)-2-(3-(3-(3,4-dimethoxyphenyl)-1-hydroxypropyl)phenoxy)acetate  
(**45**; NJS154)



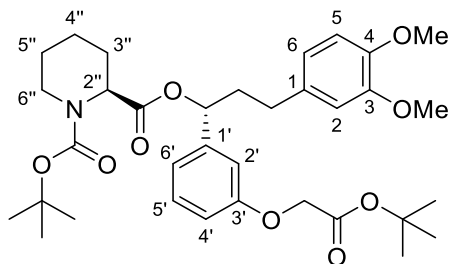
Chemical Formula: C<sub>23</sub>H<sub>30</sub>O<sub>6</sub>, Molecular Weight: 402.49 g/mol.

**45** was synthesized analogous to Jørgensen *et al.*,<sup>120</sup> using (*S*)-2-methyl-CBS-oxazaborolidine (1 M solution in THF, 0.53 mL, 0.53 mmol), BH<sub>3</sub> · SMe<sub>2</sub> (0.10 mL, 1.07 mmol), and **44** (214 mg, 0.53 mmol) in dry THF (10 mL). After stirring at rt for 3 h, the reaction was terminated by adding methanol (2 mL), water (5 mL), and 0.1 M hydrochloric acid (10 mL). The aqueous phase was extracted with DCM (3 · 40 mL), and the combined organic phases were washed with water. After separation of the phases, the organic solvent was removed *in vacuo* and the product was purified by column chromatography (SiO<sub>2</sub>, PE/EA 3:2 + 1% FA). **45** was obtained as a colorless oil in a yield of 88% (189 mg, 0.47 mmol, Lit.<sup>121</sup> 82%).

TLC:  $R_f = 0.39$  (SiO<sub>2</sub>, PE/EtOAc = 3:2 + 1% FA)

*The analytical data are in agreement with Keenan et al.<sup>121</sup>*

3.5.2.5 2-((*R*)-1-(3-(2-(*tert*-Butoxy)-2-oxoethoxy)phenyl)-3-(3,4-dimethoxyphenyl)-propyl) 1-(*tert*-butyl) (*S*)-piperidine-1,2-dicarboxylate (**46**; *NJS160*)



Chemical Formula:  $C_{34}H_{47}NO_9$ , Molecular Weight: 613.75 g/mol.

Analogous to Jørgensen *et al.*,<sup>120</sup> to a solution of **46** (1.93 g, 4.80 mmol) in dry DCM (30 mL) was added *N*-Boc-(*S*)-pipercolic acid (1.21 g, 5.28 mmol), DMAP (0.67 g, 5.28 mmol), and DIC (1.17 g, 9.59 mmol) under ice cooling. After 1 h, the reaction was allowed to warm to rt and stirred for an additional 4 h. The reaction mixture was washed with water (4 · 80 mL) and brine (80 mL), the phases were separated, and the solvent was removed *in vacuo*. Subsequent flash chromatography (SiO<sub>2</sub>, A: cyclohexane, B: EA, gradient: 0 → 100% B) afforded **46** as a colorless oil in a yield of 85% (2.52 g, 4.10 mmol).

TLC:  $R_f = 0.54$  (SiO<sub>2</sub>, PE/EA = 3:2 + 1% FA)

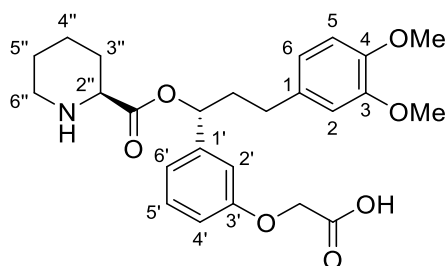
IR (ATR,  $\nu_{\max}$  [cm<sup>-1</sup>]): 3060 (w), 2974 (m), 2935 (m), 1735 (m), 1692 (s), 1516 (m), 1242 (m), 1147 (s), 870 (w), 848 (w), 774 (w).

<sup>1</sup>H NMR (CDCl<sub>3</sub>):  $\delta = 7.25$  (t, <sup>3</sup>*J* = 7.6 Hz, 1H, CH-5'), 6.95 (d, <sup>3</sup>*J* = 7.6 Hz, 1H, CH-6'), 6.88 (br s, 1H, CH-2), 6.83–6.75 (m, 2H, CH-6, 4'), 6.67–6.65 (m, 2H, CH-5, 2'), 5.76 (t, <sup>3</sup>*J* = 6.5 Hz, 1H, C-2''COOCH), 4.95 & 4.75 (br s, 1H, CH-2'', rotamers), 4.50 (br s, 2H, OCH<sub>2</sub>COO*t*Bu), 4.04–3.92 (m, 1H, CH<sub>2</sub>-6''), 3.86 (s, 3H, OCH<sub>3</sub>), 3.85 (s, 3H, OCH<sub>3</sub>), 3.00–2.80 (m, 1H, CH<sub>2</sub>-6''), 2.65–2.47 (m, 2H, CHCH<sub>2</sub>CH<sub>2</sub>C-1), 2.29–2.15 (m, 2H, COOCHCH<sub>2</sub>, CH<sub>2</sub>-3''), 2.10–1.97 (m, 1H, COOCHCH<sub>2</sub>), 1.72–1.12 (m, 23H, CH<sub>2</sub>-3'', 4'', 5'', *t*Bu-CH<sub>3</sub>) ppm.

<sup>13</sup>C NMR (CDCl<sub>3</sub>):  $\delta = 171.5$  (1C, C-2''COO), 168.0 (1C, CH<sub>2</sub>-COO*t*Bu), 158.2 (1C, C-3'), 149.0 (1C, C-3), 147.5 (1C, C-4), 142.0 (br 1C, C-1'), 133.6 (br 1C, C-1), 129.8 (1C, CH-5'), 120.3 (1C, CH-5), 119.9 (1C, CH-6'), 114.2 (br 1C, CH-6), 113.2 (br 1C, CH-2), 111.9 (br 1C, CH-4'), 111.5 (1C, CH-2'), 82.5 (1C, CH<sub>2</sub>COOC(CH<sub>3</sub>)<sub>3</sub>), 80.0 (br 1C, NCOOC(CH<sub>3</sub>)<sub>3</sub>), 76.0 (br 1C, pip-COOCH), 65.9 (1C, OCH<sub>2</sub>COO*t*Bu), 56.1 (1C, OCH<sub>3</sub>), 56.0 (1C, OCH<sub>3</sub>),

55.1 & 54.0 (br 1C, CH-2''), 42.3 & 41.2 (br 1C, CH<sub>2</sub>-6''), 38.1 (br 1C, COOCHCH<sub>2</sub>), 31.4 (br 1C, CHCH<sub>2</sub>CH<sub>2</sub>C<sub>q</sub>), 28.6–28.3 (m, 3C, *t*Bu-CH<sub>3</sub>, rotamers), 28.2 (3C, *t*Bu-CH<sub>3</sub>), 27.0 (br 1C, CH<sub>2</sub>-3''), 24.7 (br 1C, CH<sub>2</sub>-5''), 20.8 (br 1C, CH<sub>2</sub>-4'') ppm.

**3.5.2.6 2-(3-((*R*)-3-(3,4-Dimethoxyphenyl)-1-(((*S*)-piperidine-2-carbonyloxy)propyl)-phenoxy)acetic acid (51; NJS168)**



**Chemical Formula: C<sub>25</sub>H<sub>31</sub>NO<sub>7</sub>, Molecular Weight: 457.52 g/mol.**

According to general procedure B, **51** was synthesized using 2.10 g of **46** (3.42 mmol) and 2.64 mL of TFA (34.22 mmol) in dry DCM (22 mL). Deviating from the general procedure, saturated sodium hydrogen carbonate solution (10 mL) was added after 1 d. After separation of the phases, the aqueous phase was extracted with DCM (3 · 50 mL), the combined organic phases were washed with water (3 · 100 mL) and the organic solvent was removed *in vacuo*. After purification by column chromatography (SiO<sub>2</sub>, DCM/MeOH = 6:1 + 1% FA), **51** was obtained as a yellow oil in a yield of 89% (1.39 g, 3.04 mmol).

**TLC:** R<sub>f</sub> = 0.37 (SiO<sub>2</sub>, DCM/MeOH = 6:1 + 1% FA)

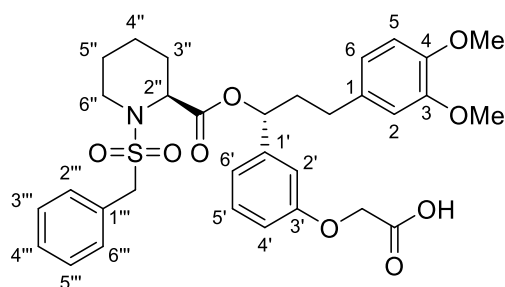
**IR (ATR, ν<sub>max</sub> [cm<sup>-1</sup>]):** 3300–2400 (br, m), 3020 (m), 2940 (m), 2841 (m), 1739 (vs), 1667 (vs), 1182 (s), 1136 (s), 854 (w), 796 (m), 766 (w).

**<sup>1</sup>H NMR (CD<sub>3</sub>OD):** δ = 7.29 (t, <sup>3</sup>J = 8.0 Hz, 1H, CH-5'), 6.99–6.94 (m, 2H, CH-2, 6'), 6.89 (dd, <sup>3</sup>J = 8.0 Hz, <sup>4</sup>J = 2.1 Hz, 1H, CH-4'), 6.86 (d, <sup>3</sup>J = 8.2 Hz, 1H, CH-6), 6.77 (d, <sup>4</sup>J = 2.1 Hz, 1H, CH-2'), 6.71 (dd, <sup>3</sup>J = 8.2 Hz, <sup>4</sup>J = 1.8 Hz, 1H, CH-5), 5.78 (dd, <sup>3</sup>J = 7.7, 5.9 Hz, 1H, COOCH), 4.64 (s, 2H, OCH<sub>2</sub>COOH), 4.04 (dd, <sup>3</sup>J = 11.5, 3.3 Hz, 1H, CH-2''), 3.81 (s, 3H, OCH<sub>3</sub>), 3.79 (s, 3H, OCH<sub>3</sub>), 3.39 (br d, <sup>2</sup>J = 12.3 Hz, 1H, CH<sub>2</sub>-6''), 3.01 (ddd, <sup>2</sup>J = 12.3, <sup>3</sup>J = 12.3, 3.3 Hz, 1H, CH<sub>2</sub>-6''), 2.66–2.52 (m, 2H, CH<sub>2</sub>C-1), 2.39–2.25 (m, 2H, COOCHCH<sub>2</sub>, CH<sub>2</sub>-3''), 2.19–2.10 (m, 1H, COOCHCH<sub>2</sub>), 1.95–1.66 (m, 5H, CH<sub>2</sub>-3'', 4'', 5'') ppm.

**<sup>13</sup>C NMR (CD<sub>3</sub>OD):** δ = 173.1 (1C, COOH), 169.4 (1C, C-2''COO), 159.8 (1C, C-3'), 150.5 (1C, methoxy-COMe), 149.0 (1C, methoxy-COMe), 142.4 (1C, C-1'), 135.0 (1C, C-1), 130.8

(1C, CH-5'), 121.7 (1C, CH-5), 120.7 (1C, CH-6'), 115.4 (1C, CH-4'), 114.2 (1C, CH-6), 113.6 (1C, CH-2), 113.3 (1C, CH-2'), 79.2 (1C, COOCH), 66.2 (1C, OCH<sub>2</sub>COOH), 58.1 (1C, CH-2''), 56.6 (1C, OCH<sub>3</sub>), 56.5 (1C, OCH<sub>3</sub>), 45.1 (1C, CH<sub>2</sub>-6''), 38.7 (1C, COOCHCH<sub>2</sub>CH<sub>2</sub>), 32.2 (1C, CH<sub>2</sub>C-1), 27.3 (1C, CH<sub>2</sub>-3''), 22.8 (br 2C, CH<sub>2</sub>-4'', 5'') ppm.

**3.5.2.7 2-(3-((R)-1-(((S)-1-(Benzylsulfonyl)piperidine-2-carbonyloxy)-3-(3,4-dimethoxyphenyl)propyl)phenoxy)acetic acid (47; NJS175)**



**Chemical Formula: C<sub>32</sub>H<sub>37</sub>NO<sub>9</sub>S, Molecular Weight: 611.71 g/mol.**

Following general procedure C, to a solution of **51** (90 mg, 0.20 mmol) in dry DCM (3 mL), phenylmethanesulfonyl chloride (41 mg, 0.22 mmol) and *N*-methylmorpholine (76  $\mu$ L, 0.69 mmol) were added under ice cooling. The reaction mixture was immediately allowed to warm to rt and stirred for 2 d. Subsequently, the reaction mixture was washed with dilute hydrochloric acid (15 mL, 1 M), H<sub>2</sub>O (2 · 15 mL) and brine (15 mL). After separation of the phases, the solvent of the organic layer was removed *in vacuo*. Subsequent purification by column chromatography (SiO<sub>2</sub>, DCM/MeOH = 20:1 + 1% FA) afforded **47** as a white oily solid in a yield of 52% (63 mg, 0.10 mmol).

**TLC:**  $R_f$  = 0.63 (SiO<sub>2</sub>, DCM/MeOH = 15:1 + 1% FA)

**IR (ATR,  $\nu_{\max}$  [cm<sup>-1</sup>]):** 3060 (w), 2937 (m), 2858 (w), 1734 (m), 1515 (m), 1454 (m), 1335 (s), 1237 (m), 1177 (s), 1028 (m), 967 (w), 783 (w), 699 (w).

**Purity (HPLC):** 96.6%,  $t_R$  = 10.29 min

**<sup>1</sup>H NMR (CD<sub>3</sub>OD):**  $\delta$  = 7.43–7.32 (m, 5H, CH-2'''–6'''), 7.27 (t, <sup>3</sup>*J* = 8.0 Hz, 1H, CH-5'), 6.99–6.93 (m, 2H, CH-2',6'), 6.90–6.86 (m, 1H, CH-4'), 6.84 (d, <sup>3</sup>*J* = 8.1 Hz, 1H, CH-5), 6.80 (d, <sup>4</sup>*J* = 1.7 Hz, 1H, CH-2), 6.71 (dd, <sup>3</sup>*J* = 8.1, <sup>4</sup>*J* = 1.7 Hz, 1H, CH-6), 5.73 (dd, <sup>3</sup>*J* = 8.3, 4.9 Hz, 1H, COOCHC-1'), 4.64 (s, 2H, OCH<sub>2</sub>COOH), 4.40–4.36 (m, 1H, CH-2''), 4.35–4.22 (m, 2H, SOCH<sub>2</sub>), 3.80–3.76 (m, 6H, OCH<sub>3</sub>), 3.50–3.43 (m, 1H, CH<sub>2</sub>-6''), 3.23 (ddd, <sup>2</sup>*J* = 12.8, <sup>3</sup>*J* = 12.8,

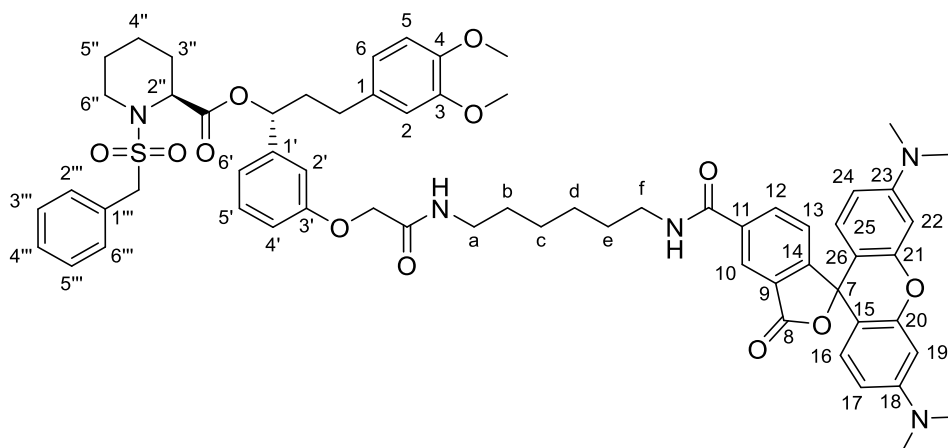
2.7 Hz, 1H,  $\text{CH}_2\text{-6''}$ ), 2.71–2.55 (m, 2H,  $\text{CH}_2\text{C-1}$ ), 2.30–2.18 (m, 1H,  $\text{COOCHCH}_2$ ), 2.16–1.99 (m, 2H,  $\text{CH}_2\text{-3''}$ ,  $\text{COOCHCH}_2$ ), 1.69–1.51 (m, 3H,  $\text{CH}_2\text{-3''}, 4'', 5''$ ), 1.48–1.35 (m, 1H,  $\text{CH}_2\text{-5''}$ ), 1.23–1.08 (m, 1H,  $\text{CH}_2\text{-4''}$ ) ppm.

$^{13}\text{C}$  NMR ( $\text{CD}_3\text{OD}$ ):  $\delta$  = 172.8 (1C,  $\text{COOH}$ ), 172.5 (1C,  $\text{C-2''COO}$ ), 159.7 (1C,  $\text{C-3'}$ ), 150.4 (1C,  $\text{C-3}$ ), 148.8 (1C,  $\text{C-4}$ ), 143.3 (1C,  $\text{C-1'}$ ), 135.5 (1C,  $\text{C-1}$ ), 132.2 (2C,  $\text{CH-2''}, 6''$ ), 131.1 (1C,  $\text{C-1''}$ ), 130.7 (1C,  $\text{CH-5'}$ ), 129.53 (1C,  $\text{CH-4''}$ ), 129.47 (2C,  $\text{CH-3''}, 5''$ ), 121.7 (1C,  $\text{CH-6}$ ), 120.7 (1C,  $\text{CH-6'}$ ), 115.6 (1C,  $\text{CH-4'}$ ), 113.76 (1C,  $\text{CH-2'}$ ), 113.68 (1C,  $\text{CH-2}$ ), 113.3 (1C,  $\text{CH-5}$ ), 77.9 (1C,  $\text{COOCH}$ ), 66.0 (1C,  $\text{CH}_2\text{COOH}$ ), 59.4 (1C,  $\text{SO}_2\text{CH}_2$ ), 57.5 (1C,  $\text{CH-2''}$ ), 56.6 (1C, *methoxy-OCH*<sub>3</sub>), 56.4 (1C, *methoxy-OCH*<sub>3</sub>), 44.7 (1C,  $\text{CH}_2\text{-6''}$ ), 39.4 (1C,  $\text{COOCHCH}_2$ ), 32.2 (1C,  $\text{CH}_2\text{C-1}$ ), 28.6 (1C,  $\text{CH}_2\text{-3''}$ ), 25.9 (1C,  $\text{CH}_2\text{-5''}$ ), 21.2 (1C,  $\text{CH}_2\text{-4''}$ ) ppm.

LC/MS (m/z): 634.20  $[\text{M}+\text{Na}]^+$ , 652.10  $[\text{M}+\text{K}]^+$ , 328.95  $[\text{M}+2\text{Na}]^{2+}$ .

HRMS (m/z):  $\text{C}_{32}\text{H}_{37}\text{NNaO}_9\text{S}$ ,  $[\text{M}+\text{Na}]^+$ , calc.: 634.20812, found: 634.20755, error: 0.9.

3.5.2.8 5-((6-(2-(3-((*R*)-1-(((*S*)-1-(benzylsulfonyl)piperidine-2-carbonyloxy)-3-(3,4-dimethoxyphenyl)propyl)phenoxy)acetamido)hexyl)carbamoyl)-2-(6-(dimethylamino)-3-(dimethyliminio)-3*H*-xanthen-9-yl)benzoate (32; *NJS205*)



Chemical Formula:  $\text{C}_{63}\text{H}_{71}\text{N}_5\text{O}_{12}\text{S}$ , Molecular Weight: 1122.34 g/mol.

32 was synthesized following general procedure A, using 25 mg of 5-((6-ammoniohexyl)carbamoyl)-2-(6-(dimethylamino)-3-(dimethyliminio)-3*H*-xanthen-9-yl)benzoate chloride (44  $\mu\text{mol}$ ), 47 (30 mg, 49  $\mu\text{mol}$ ), DIPEA (15  $\mu\text{mol}$ , 88  $\mu\text{mol}$ ), and HBTU (20 mg, 53  $\mu\text{mol}$ ) in a mixture of dry DMF and dry DCM (20 mL, 1:1). After workup according

to the general procedure the crude oily product was purified by column chromatography (SiO<sub>2</sub>, CHCl<sub>3</sub>/MeOH = 9:1 for ~5 column volumes, then 5:1). **32** was obtained as a violet oily solid in a yield of 64% (32 mg, 29 μmol).

*Cave: Further tries to purify 32 via an RP-flash method showed instability in aqueous medium.*

**TLC:** R<sub>f</sub> = 0.42 (SiO<sub>2</sub>, DCM/MeOH = 8:1, fluorescent (365 nm))

**Purity:** 97.8%, t<sub>R</sub> = 9.75 min

**IR (ATR, ν<sub>max</sub> [cm<sup>-1</sup>]):** 3073 (w), 2923 (s), 1738 (m), 1648 (s), 1595 (s), 1336 (s), 1259 (s), 1187 (s), 1028 (m), 799 (w), 732 (w), 699 (w).

**<sup>1</sup>H NMR (CDCl<sub>3</sub>):** δ = 8.48–8.42 (m, 1H, CH-10), 8.20 (dd, <sup>3</sup>J = 7.9, <sup>4</sup>J = 1.2 Hz, 1H, CH-12), 7.42–7.27 (m, 6H, CH-5', 2'''–6'''), 7.20–7.17 (m, 1H, CH-13, *partially hidden by residual CHCl<sub>3</sub>*), 6.99–6.93 (m, 3H, CH-2',6', NH), 6.90–6.82 (m, 2H, CH-4', NH), 6.80–6.76 (m, 1H, CH-5), 6.73–6.62 (m, 4H, CH-2,6,16,25), 6.52–6.48 (m, 2H, CH-19,22), 6.44–6.40 (m, 2H, CH-17,24), 5.80–5.75 (m, 1H, COOCHC-1'), 4.59–4.50 (m, 3H, CH-2'', C-3'OCH<sub>2</sub>), 4.21–4.10 (m, 2H, SOCH<sub>2</sub>), 3.84 (s, 6H, OCH<sub>3</sub>), 3.50–3.43 (m, 3H, CH<sub>2</sub>-6'',a,f), 3.38–3.30 (m, 2H, CH<sub>2</sub>-a,f), 3.27–3.17 (m, 1H, CH<sub>2</sub>-6''), 3.05–2.86 (m, 12H, rhodamine-N(CH<sub>3</sub>)<sub>2</sub>), 2.68–2.52 (m, 2H, CH<sub>2</sub>C-1), 2.30–2.18 (m, 2H, COOCHCH<sub>2</sub>), 2.10–1.99 (m, 1H, CH<sub>2</sub>-3''), 1.70–1.50 (m, 7H, CH<sub>2</sub>-3'',4'',5'',b,e), 1.50–1.30 (m, 5H, CH<sub>2</sub>-5'',c,d), 1.24–1.10 (m, 1H, CH<sub>2</sub>-4'') ppm.

**<sup>13</sup>C NMR (CDCl<sub>3</sub>):** δ = 172.6 (1C, HNCOC-11), 171.7 (1C, C-2''COO), 170.5 (1C, C<sub>q</sub>-8), 166.3 (1C, CONHCH<sub>2</sub>-a), 157.9 (1C, C<sub>quaternary</sub>-3'), 155.0 (2C, C<sub>quaternary</sub>-20,21), 152.6 (2C, C<sub>quaternary</sub>-18,23), 149.4 (2C, C<sub>quaternary</sub>-3,4), 146.8 (1C, C<sub>quaternary</sub>-14), 143.0 (1C, C<sub>quaternary</sub>-1'), 141.9 (1C, CH-12), 134.4 (1C, C<sub>quaternary</sub>-1), 133.4–127.0 (m, 13C, CH-9,10,11,13, 16, 25, 5', 1'''–6'''), 120.3 (2C, CH-6',6), 113.7 (1C, CH-4'), 113.9 (1C, CH-2'), 111.5 (1C, CH-2), 111.1 (1C, CH-5), 109.5 (2C, CH-17,24), 108.3 (2C, C<sub>quaternary</sub>-15, 26), 98.4 (2C, CH-19,22), 87.1 (1C, C<sub>quaternary</sub>-7), 77.4 (1C, COOCHC-1'), 67.4 (1C, C-3'OCH<sub>2</sub>), 58.4 (1C, SOCH<sub>2</sub>), 56.0 (1C, *pip*-CH-2), 55.8 (2C, OCH<sub>3</sub>), 43.6 (1C, CH<sub>2</sub>-6''), 40.5 (m, 5C, rhodamine-N(CH<sub>3</sub>)<sub>2</sub>, CH<sub>2</sub>-a), 38.4 (1C, OCHCH<sub>2</sub>), 38.0 (1C, CH<sub>2</sub>-f), 31.4 (1C, CH<sub>2</sub>C-1), 30.2 (1C, CH<sub>2</sub>-b), 29.9 (1C, CH<sub>2</sub>-e), 27.9 (1C, CH<sub>2</sub>-3''), 27.3 (1C, CH<sub>2</sub>-d), 26.1 (1C, CH<sub>2</sub>-c), 25.0 (1C, CH<sub>2</sub>-5''), 22.8 (1C, CH<sub>2</sub>-4'') ppm.

**LC/MS (m/z):** 420.25 [M+3H]<sup>3+</sup>, 561.85 [M+2H]<sup>2+</sup>

**HRMS (m/z):** C<sub>63</sub>H<sub>71</sub>N<sub>5</sub>O<sub>12</sub>S, [M+H]<sup>+</sup>, calc.: 1122.48927, found: 1122.48741  
error: 1.7

#### 4 Analysis of Structure–Activity–Relationships of Novel Inhibitors of the Macrophage Infectivity Potentiator (Mip) Proteins of *Neisseria meningitidis*, *Neisseria gonorrhoeae*, and *Burkholderia pseudomallei*

Nicolas J. Scheuplein<sup>1‡</sup>, Nicole M. Bzdyl<sup>2</sup>, Theresa Lohr<sup>1</sup>, Emily A. Kibble<sup>2,3</sup>, Anja Hasenkopf<sup>1</sup>, Mitali Sarkar-Tyson<sup>2\*</sup>, Ulrike Holzgrabe<sup>1\*</sup>

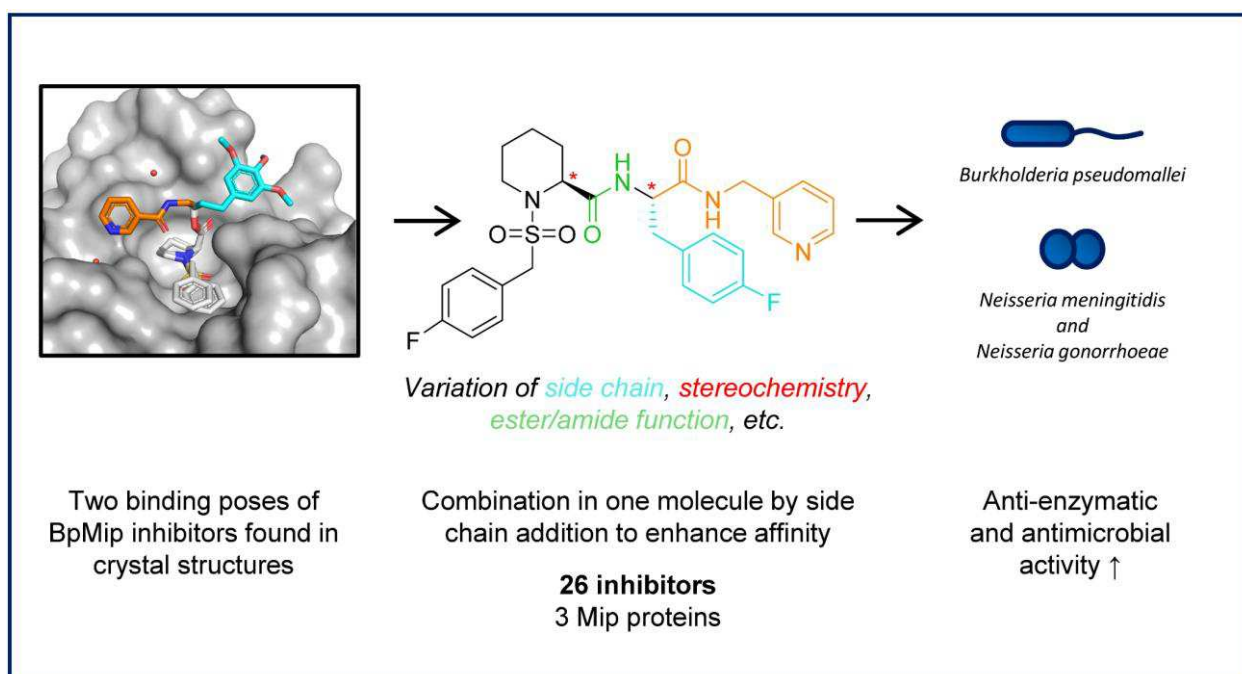
<sup>1</sup> Institute of Pharmacy and Food Chemistry, University of Würzburg, Am Hubland, 97074 Würzburg, Germany

<sup>2</sup> Marshall Centre for Infectious Diseases Research and Training, School of Biomedical Sciences, University of Western Australia, 6009, Perth, Australia

<sup>3</sup> DMTC Limited, Level 1, 620 High Street, Kew VIC 3101, Australia

‡ first author

\* equal corresponding authors



**Keywords:** Macrophage infectivity potentiator protein; Mip inhibitor; antimicrobial resistance; anti-virulence therapy; PPIase; *Neisseria meningitidis*; *Neisseria gonorrhoeae*; *Burkholderia pseudomallei*; Structure–activity–relationships;

## Abstract

The Macrophage infectivity potentiator (Mip) protein is a promising target for developing new drugs to combat antimicrobial resistance. New rapamycin-derived Mip inhibitors have been designed that may be able to combine two binding modes to inhibit the Mip protein of *Burkholderia pseudomallei* (BpMip). These novel compounds are characterized by an additional substituent in the middle chain linking the lateral pyridine to the pipercoline moiety, constituting different stereoisomers. These compounds demonstrated high affinity for the BpMip protein in the nanomolar range, high anti-enzymatic activity, and ultimately resulted in significantly reduced cytotoxicity of *B. pseudomallei* in macrophages. They also displayed strong anti-enzymatic activity against the Mip proteins of *Neisseria meningitidis* and *N. gonorrhoeae* and substantially improved the ability of macrophages to kill the bacteria. Hence, the new Mip inhibitors are promising, non-cytotoxic candidates for further testing against a broad spectrum of pathogens and infectious diseases.

### 4.1 Introduction

Due to increasing antimicrobial resistance (AMR), the treatment of infections, especially those caused by Gram-negative bacteria, is becoming a major challenge, and concerns are growing that we are heading towards or already finding ourselves in a post-antibiotic era.<sup>1,2</sup> In the indispensable search for new antibacterial strategies, the development of anti-virulence therapies (AVs) that aim to inhibit virulence factors to fight infections, has gained momentum.<sup>3-5</sup> By targeting virulence factors that are not essential for bacterial survival, it is believed that the selection pressure for the emergence of resistance in the pathogen and microbiome is reduced, thereby avoiding the development of AMR to anti-infective agents.<sup>5</sup> The macrophage infectivity potentiator (Mip) protein and the closely related Mip-like (ML1) proteins are FK506 binding proteins (FKBPs) and are virulence factors that have been identified as promising drug targets.<sup>6-8</sup> They exhibit peptidyl-prolyl *cis-trans* isomerase (PPIase) activity, resulting in isomerization of peptide bonds preceding a proline residue, a process required for correct protein folding.<sup>9</sup> Mip proteins are typically 24 to 30 kDa in size and consist of two distinct domains, an *N*-terminal dimerization domain linked to a domain containing the highly conserved FKBP fold, which bears the PPIase activity.<sup>10</sup> It is believed that these proteins form a homodimer at the outer membrane of the bacterial cell.<sup>11, 12</sup>



ML1 proteins feature the FKBP folding domain but not a dimerization domain, resulting in a protein of about 12–14 kDa with PPIase activity, located in the cytoplasm or periplasm of the bacterial cell.<sup>13</sup> Mip and ML1 proteins have been demonstrated to have a significant impact on virulence for a broad spectrum of bacterial species.<sup>10</sup> First discovered in *Legionella pneumophila*, deletion of Mip resulted in reduced invasion ability in monocytic U937 cells and human alveolar macrophages, as well as reduced bacterial growth at sub-optimal temperatures.<sup>14,15</sup> LpMip-deletion also resulted in reduced survival *in vivo*, in the amoebae, *Acanthamoeba castellanii*,<sup>16</sup> and the guinea pig infection model.<sup>16,17</sup>

*Burkholderia pseudomallei* is a highly pathogenic Gram-negative bacterium and the causative agent of melioidosis, a potentially life-threatening infection with estimated 165,000 cases and 89,000 deaths per year worldwide.<sup>18</sup> The pathogen shows resistance to several groups of antibiotics due to characteristics such as its lipopolysaccharide structure, porin proteins, efflux pumps, expression of various beta-lactamases, and biofilm formation.<sup>19-21</sup> Norville *et al.* identified two Mip paralogues (BpML1 = BpMip and BPSL0918) in the genome of *B. pseudomallei* strain K96243.<sup>13,22</sup> Interestingly, BPSL0918 did not show any PPIase activity; however, deletion of the gene has serious implications for the intracellular survival of the pathogen in a mouse infection model.<sup>22</sup> The PPIase domain of the 11.9 kDa BpMip protein shows high homology to that of LpMip and exhibits PPIase activity.<sup>23,24</sup> Deletion of the *mip* gene in *B. pseudomallei* results in numerous negative effects on virulence mechanisms, ultimately resulting in reduced invasion and survival in macrophage and epithelial cells, as well as attenuation in the BALB/c mouse infection model.<sup>13</sup>

Mip proteins are also abundant in the outer membrane of *Neisseria meningitidis*, an obligate human Gram-negative diplococcus.<sup>25</sup> Though *N. meningitidis* is part of the normal nasopharyngeal microbiome in many healthy individuals it causes significant morbidity and mortality from meningitis and septicaemia in susceptible patients.<sup>26-28</sup> Even with antimicrobial therapies, the overall mortality rate for invasive meningococcal disease (IMD) remains high, between 10 and 15%.<sup>29</sup> In recent years, in addition to the known resistance to sulfonamides, repeated outbreaks with ciprofloxacin (1, see Figure 1)-resistant variants have been observed.<sup>30,31</sup> *N. meningitidis* encodes two Mip proteins, the 29 kDa NmMip (NEIS1487) with a putative dimerization leader sequence and the smaller, 110-amino acid NEIS0004.<sup>25,32</sup> The *NEIS1487* gene is highly up-regulated in human whole blood upon infection and deletion of the gene results in reduced survival

in the blood.<sup>33</sup> The NmMip protein is being investigated as a potential meningococcal serogroup B vaccine antigen that showed using recombinant truncated NmMip proteins that exhibited cross-reactivity for other *Neisseria* subtypes like *N. gonorrhoeae*.<sup>25, 34, 35</sup>

The closely related Gram-negative diplococcus *N. gonorrhoeae* expresses the highly conserved and surface-exposed Mip protein NgMip of 30 kDa.<sup>12, 35</sup> *N. gonorrhoeae* causes one of the most prevalent sexually transmitted infections (STI), gonorrhoea, with an estimated 87 million cases among persons aged 15–49 years worldwide in 2016.<sup>36-38</sup> In recent years, AMR has emerged against the last remaining effective drugs, the extended-spectrum cephalosporins (ESCs) cefixime (**2**) and ceftriaxone (**3**), as well as azithromycin (**4**), earning *N. gonorrhoeae* the status of a superbug that might become untreatable in the near future.<sup>39, 40</sup> NgMip shows high homology towards other pathogens' Mip, especially NmMip with an identity of 97% of the C-terminal PPIase domain.<sup>12, 25, 41</sup> Deletion of the NgMip gene also results in decreased survival of *N. gonorrhoeae* in macrophage cells.<sup>12</sup>

Macrophages play a crucial role in the innate immune response to microorganisms. Recent information suggests that gonococcus can hijack the host response by mechanisms that involve the control of macrophage activity.<sup>42</sup> The pathogen can further avoid elimination by the host immune system through a variety of mechanisms, including manipulation of phagocytosis, modulation of the oxidative burst, defense against toxic neutrophil products, and extension of neutrophil lifespan.<sup>5</sup>

FKBPs form stable complexes with the immunosuppressive natural products FK506 (tacrolimus, **5**)<sup>43, 44</sup> and rapamycin (sirolimus, **6**),<sup>45, 46</sup> with both drugs showing low nanomolar binding affinity and PPIase inhibition of Mips from a wide range of microbial species.<sup>24, 47</sup> The human FKBP12 complex formed with these drugs successively interacts with calcineurin<sup>48</sup> and mTOR<sup>49, 50</sup>, respectively, inducing immunosuppressant activity.

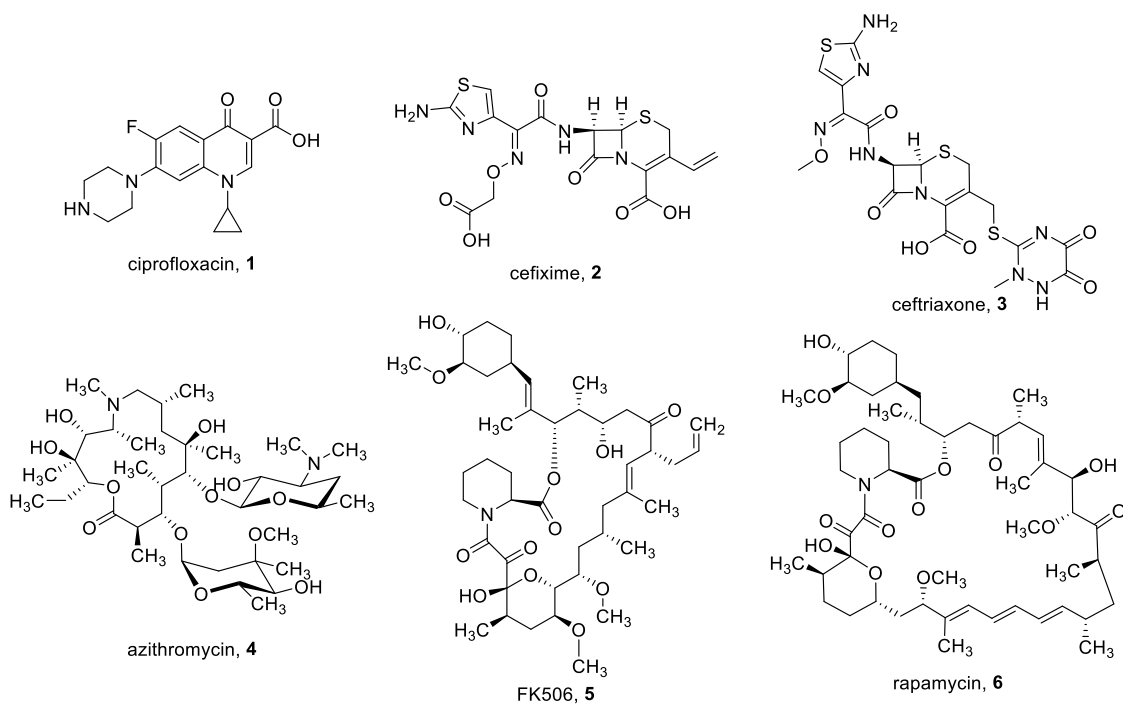


**Figure 1.** Structural formula of antibiotics 1–4 to which resistance has recently been reported in the species studied and the FKBP ligands FK506 (5) and rapamycin (6).

While these molecules are unsuitable for treating infectious diseases, they have shown that Mips are druggable, rendering these proteins attractive targets for new inhibitors. Derived from rapamycin with its FKBP-affine binding domain and the effector domain, which is required to interact with mTOR, early Mip inhibitors lacking the effector domain part were developed by Juli *et al.* (e.g., lead compound 7 (Figure 2B)).<sup>6</sup> In this manner, it was possible to develop inhibitors that bind to LpMip<sup>6</sup> and BpMip<sup>7</sup> without inducing an immunosuppressive effect.<sup>7</sup> NMR-HSQC experiments confirmed that the developed compounds bind to the same hydrophobic binding pocket as rapamycin.<sup>6</sup> Furthermore, the pipecolic acid derivatives were able to reduce the cytotoxic effects in macrophage cells induced by *B. pseudomallei*.<sup>7</sup>

The druggability of microbial Mip proteins with rapamycin-derived small molecules was again confirmed by Pomplun *et al.*<sup>51</sup> using structurally related compounds with an (*S*)-*C*<sup>5</sup>-substituted [4.3.1]-aza-amide bicyclic scaffold (see general structure 8, Figure 2C). These compounds demonstrated anti-infective activity *in vitro* against *Plasmodium falciparum*, *L. pneumophila*, *Chlamydia pneumoniae*, and *C. trachomatis*.<sup>51</sup>

Seufert *et al.* performed structure–activity relationship (SAR) studies for *B. pseudomallei* and *L. pneumophila* Mip, establishing a library of small molecule Mip inhibitors in the nanomolar range

and improved drug-likeness (such as lead compound **9**, **Figure 2B**).<sup>52</sup>

Reimer *et al.*<sup>53</sup> identified similar Mip inhibitors effective against the pathogens *C. trachomatis*, *N. gonorrhoeae*, and *N. meningitidis*, as the high degree of conservation of Mip proteins constitutes a good prerequisite for successful screening across multiple pathogens. The lead structures were able to inhibit the PPIase activity of recombinant gonococcal NgMip and led to reduced intracellular survival of *N. gonorrhoeae* in polymorphonuclear neutrophils (PMNs). Recently, using co-crystallography experiments with recombinant *B. pseudomallei* Mip (BpMip) protein and Mip inhibitors, biochemical analysis, and computational modeling, Iwasaki *et al.* were able to expand the spectrum of pathogens that can be treated with the lead structures identified (including compound **9** (**Figure 2B**)).<sup>8</sup> Thus, the lead compounds strongly inhibited the PPIase activity of Mip proteins from *N. meningitidis*, *Klebsiella pneumoniae*, and *Leishmania major* and significantly reduced the intracellular burden of these pathogens *in vitro*.

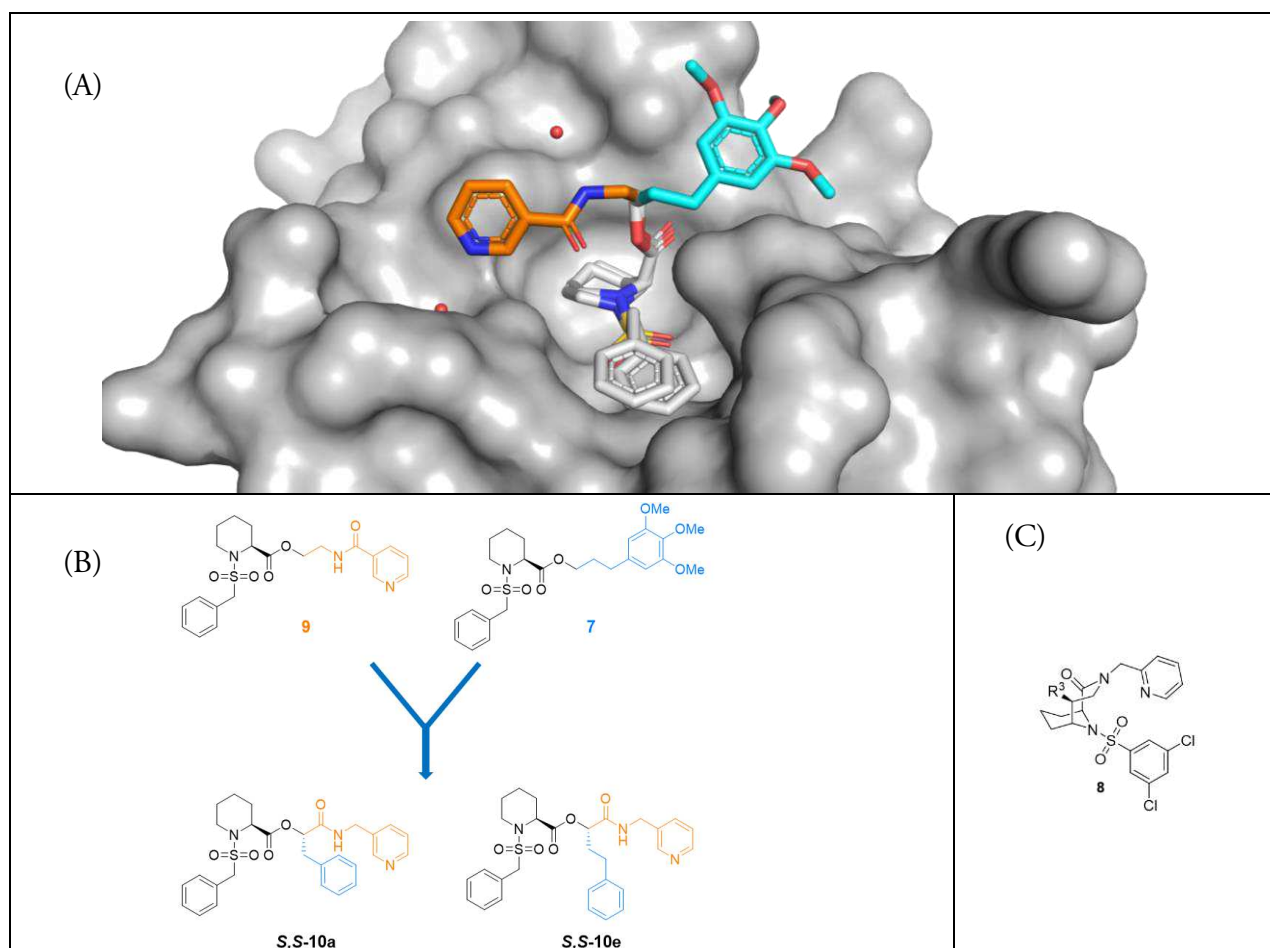


**Figure 2.** (A) Superimposed crystal structures of BpMip co-crystallized with lead structures<sup>6, 52</sup> **7** (PDB ID: 4G50)<sup>7</sup> and **9** (PDB ID: 6O4A)<sup>8</sup>. The trimethoxy benzene moiety of **7** occupies a different position than the pyridine ring of **9**. (B) By combining the two molecules, i.e., adding an additional side chain, both binding positions should be occupied by one molecule, such as *S,S*-**10a** and *S,S*-**10e**, thereby increasing the binding affinity. (C) General lead structure **8** by Pomplun *et al.*, targeting human FKBP and microbial Mips.<sup>51</sup>

In previous studies, a methyl group was introduced next to the ester moiety of piperidine-2-carboxylate to improve chemical stability, showing a slight preference for the *S*-configuration of the methyl group, but still no major gain in anti-PPIase activity.<sup>52</sup>

Analysis of the different crystal structures of BpMip co-crystallized with **7** (PDB ID: 4G50) and **9** (PDB ID: 6O4A) reveals that the trimethoxy benzene group of **7** occupies a different position from the pyridine ring of **9** (**Figure 2A**).<sup>7,8</sup> By combining the two molecules, that is, adding an additional side chain, both binding positions should be occupied by one molecule, such as *S,S*-**10a** and *S,S*-**10e** (cf. **Figure 2B**), thus increasing the binding affinity (**Figure 2B**).

This work establishes a library of pipercolic acid derivatives with additional side chain and improved affinity to various Mip proteins. Synthesis of the different stereoisomers and evaluation of the compounds in enzymatic and Fluorescence Polarization assays (FPA) against BpMip, as well as the application in a cell-based assay, resulted in Mip inhibitors with increased anti-PPIase activity and strong reduction of *B. pseudomallei*-induced cytotoxicity in macrophages. Subsequent extension to the Mip proteins of *N. meningitidis* also demonstrated a strong broad-spectrum effect of the novel compounds in the enzymatic assay and subsequent cell-based assay in macrophages, also against the related *N. gonorrhoeae*.

## 4.2 Results and Discussion

### Library Development and Chemistry

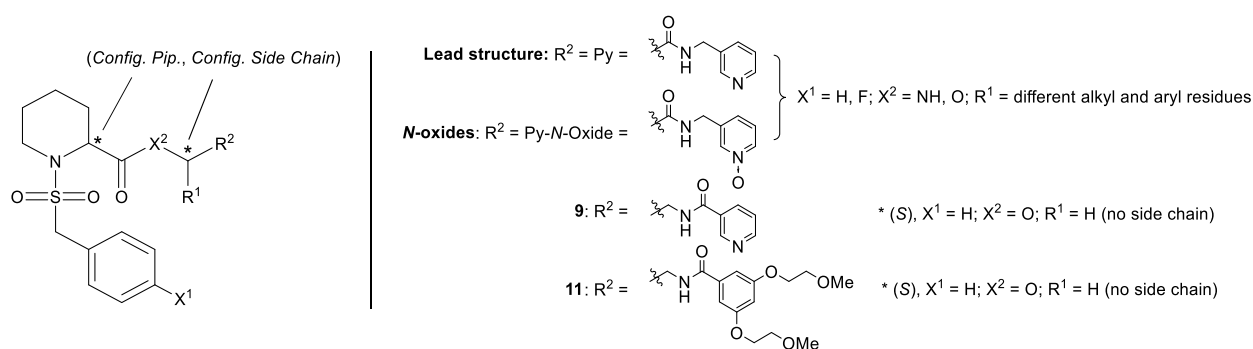
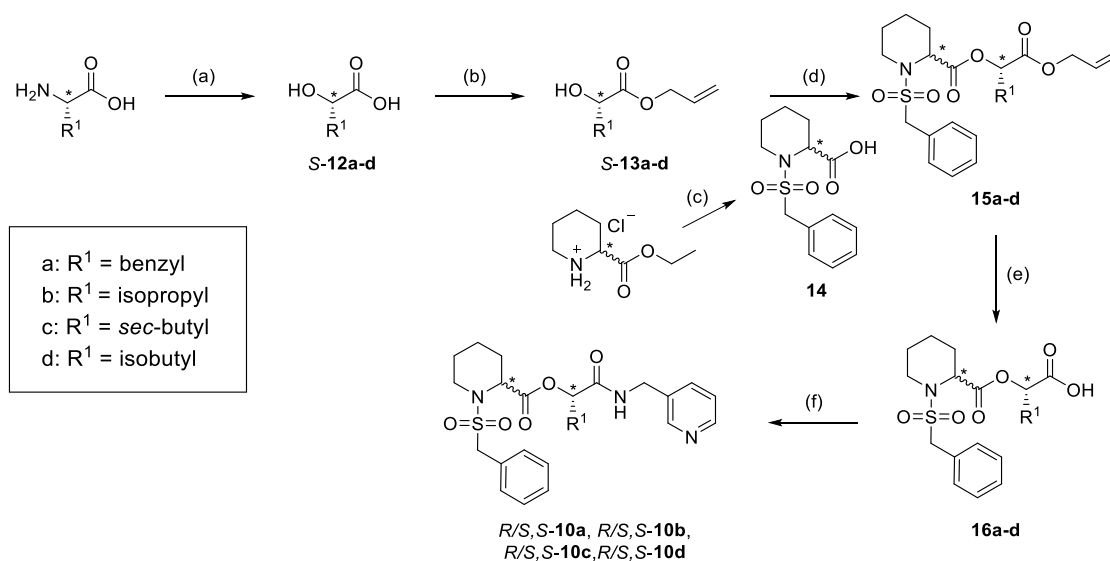


**Figure 3.** The general structure of the developed library of Mip inhibitors bearing an additional side chain and the former lead structures **9** and **11**. All compounds synthesized, including their explicit side chains, are shown in **Table 1**.

By inserting an additional side chain, another stereo center is established. The first objective was to develop a library of pipercolic acid ester derivatives ( $X^2 = \text{O}$ , **Figure 3**) with a variety of additional side chains ( $R^1$ ) and different stereochemical orientations at the two stereocenters (\**config. pip.* and

*\*config. side chain, Figure 3*) to test the respective influence on the binding affinity to BpMip as measured by FPA.<sup>54</sup> The pyridine moiety ( $R^2 = \text{Py}$ , **Figure 3**) was kept constant in this series, as this subgroup provided promising properties in terms of solubility, cytotoxicity, and affinity towards BpMip.<sup>6,52</sup> As a residue at the sulfonamide unit, a benzyl ( $X^1 = \text{H}$ ) and a *para*-fluorobenzyl ( $X^1 = \text{F}$ , **Figure 3**) moiety had turned out to be advantageous for PPIase-inhibition against BpMip.<sup>52</sup> *Para*-fluorine-substitution here and at the side chain were intended to block enzymatic metabolism such as CYP-mediated hydroxylation. Thus, these derivatives should be used to test the effect of substitution on anti-PPIase activity and activity in the cell-based assay. The amide position at the pyridine residue was changed compared to the lead compound **9** (**Figure 2**) for reasons of synthetic feasibility so that the side chain could be introduced by amino acids. This allows for inexpensive reagents and easy preparation of the compounds by amidation and esterification reactions under mild conditions without affecting the stereo-information.

### Synthesis of *R/S* Pipcolic Ester Diastereomeric Mixtures



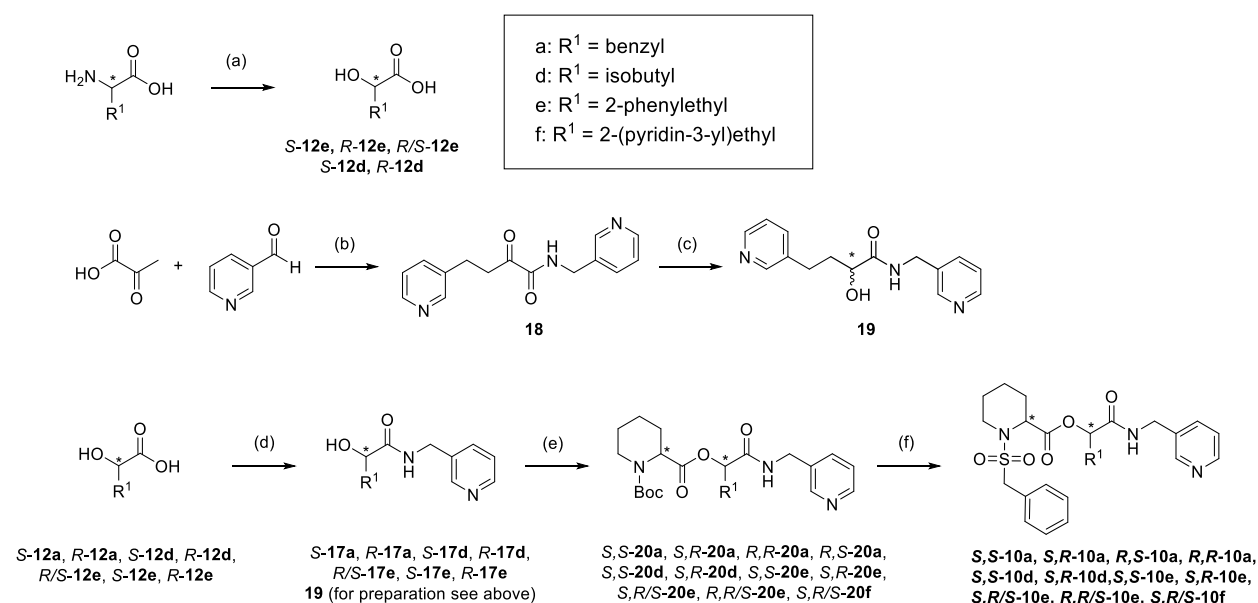
**Scheme 1.** Synthesis scheme for the *R/S* mixed pipcolic ester derivatives *R/S,S-10a*, *R/S,S-10b*, *R/S,S-10c*, and *R/S,S-10d*.

Reagents and conditions: (a)  $\text{NaNO}_2$ ,  $\text{H}_2\text{SO}_4$  (1 M),  $\text{H}_2\text{O}$ ,  $0^\circ\text{C} \rightarrow \text{rt}$ ; (b)  $\text{K}_2\text{CO}_3$ , allyl bromide, DMF, rt; (c) i)  $\text{NaHCO}_3$ , DCM, rt ii)  $\text{BnSO}_2\text{Cl}$ , NMM, DCM,  $0^\circ\text{C}$ , iii)  $\text{LiOH}$  (1 M), DCM, rt; (d) EDC·HCl, DMAP, DCM,  $0^\circ\text{C} \rightarrow \text{rt}$ ; (e)  $\text{Pd}(\text{PPh}_3)_4$ , morpholine, THF,  $0^\circ\text{C} \rightarrow \text{rt}$ ; (f) 3-picolyamine, EDC·HCl, HOBT, DCM,  $0^\circ\text{C} \rightarrow \text{rt}$ .

To test different aliphatic and aromatic substituents as side chains, the diastereomeric mixtures *R/S,S-10a–d* were synthesized (**Scheme 1**). The substances were also intended to be used as a reference for stereochemically pure compounds to test whether the preference for the

*S*-configuration at the C2 position of the pipercolic acid observed by Seufert *et al.*<sup>52</sup> also applies in the presence of an additional side chain. In addition, they should be used to see if the diastereomers can be analytically distinguished from each other. L-phenylalanine, L-valine, L-leucine, and L-isoleucine, respectively, were reacted with NaNO<sub>2</sub>/H<sub>2</sub>SO<sub>4</sub> via diazonium salt in a Sandmeyer-type reaction to convert the amino function to a hydroxyl group. The carboxylic group of the  $\alpha$ -hydroxy acids **12a–d** was then protected using allyl bromide and K<sub>2</sub>CO<sub>3</sub> to give **13a–d**. Subsequently, the ester was formed under Steglich conditions by linking the amides and racemic (*R/S*)-1-(benzylsulfonyl)piperidine-2-carboxylate (**14**) with DMAP and NMM. The allyl protecting group of **15a–d** was cleaved under palladium catalysis with Pd(PPh<sub>3</sub>)<sub>4</sub> and morpholine, resulting in **16a–d**. In a final step, 3-picolylamine was attached to the carboxylic acid by amide coupling using EDC·HCl and HOBT to give *R/S,S*-**10a–d**.

### Synthesis of the Pipercolic Ester Derivatives with a Specific Stereo-Information at the Pipercolic Acid C2 Position



**Scheme 2.** Synthesis scheme of the pipercolic ester derivatives, which allows the preparation of the explicit stereoisomers.

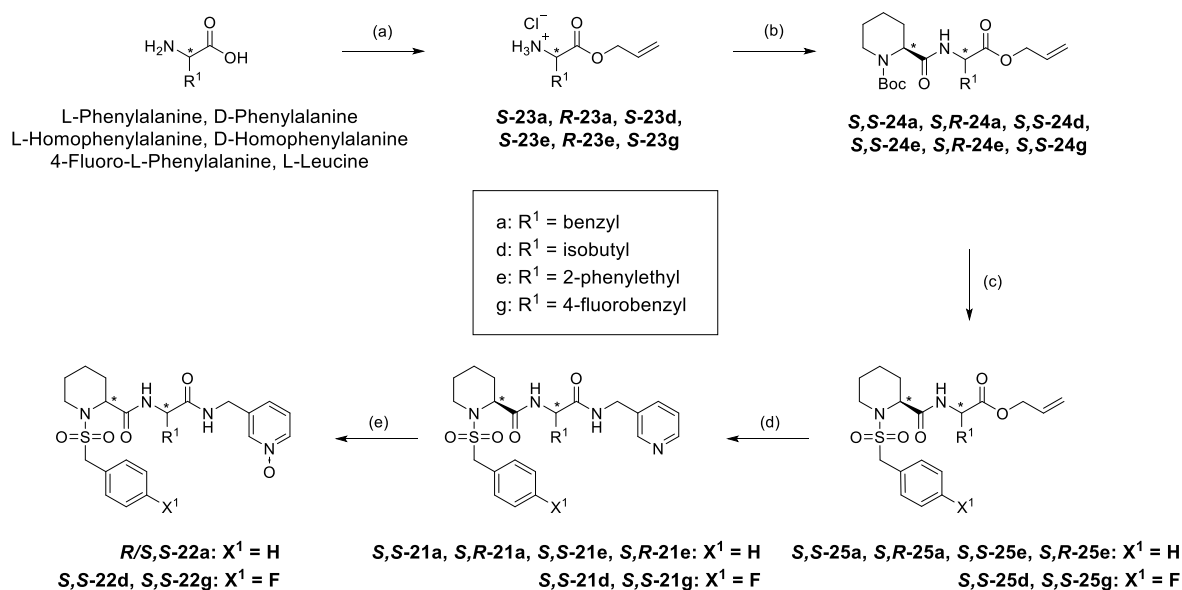
Reagents and conditions: (a) NaNO<sub>2</sub>, H<sub>2</sub>SO<sub>4</sub> (2M), 0 °C; (b) i) KOH, MeOH, 40°C, ii) 10% Pd/C, H<sub>2</sub> (15 bar), MW 400W, isopropanol, iii) EDC·HCl, HOBT, 3-picolylamine, DCM, 0 °C → rt; (c) NaBH<sub>4</sub>, MeOH, 0°C; (d) 3-picolylamine, EDC·HCl, HOBT, DCM, 0 °C → rt; (e) (*S*)-Boc-pipercolic acid **or** (*R*)-Boc-pipercolic acid, EDC·HCl, DMAP, DCM, 0°C → rt; (f) i) trifluoroacetic acid (TFA), DCM, 0°C → rt, 2 h, ii) BnSO<sub>2</sub>Cl, NMM, DCM, rt.

The following synthetic pathway was developed to obtain pipercolic ester derivatives with a defined configuration at the C2 position of the piperidine ring and the possibility of a defined configuration

at the side chain when the respective amino acid was used (**Scheme 2**). Since *R/S,S*-**10b** and *R/S,S*-**10c** (**Scheme 1**) exhibited only weak inhibition of BpMip in the FPA, these side chain moieties were omitted. The basic hydrolysis used in the preparation of racemic **14** was left out in the following synthetic routes to obtain the distinct stereoisomers, as it was known to lead to racemization. In addition, care was taken during synthesis and workup not to use too basic conditions once the pipercolic acid moiety was introduced. To ensure the correct stereochemistry, pure isomers were used as starting material, and synthetic procedures were chosen, which are known for the retention of stereochemistry. When the pure stereoisomers were synthesized, as from the introduction of the second stereo center, differentiation of diastereomers via <sup>1</sup>H NMR became possible and was carried out. The absence of diastereomers in the prepared pure stereoisomers in NMR, as evidenced by a single data set, also suggests the absence of enantiomers due to potential racemization.

The synthetic route started with conversion of the enantiomers of homophenylalanine and leucine into the respective  $\alpha$ -hydroxy acids **12d** and **12e**. For amide formation, the  $\alpha$ -hydroxy acids were then converted with 3-picolylamine, EDC·HCl, and HOBT to give **17**. Deviating from this, for the preparation of *S,R/S*-**10f**, **18** was obtained by aldol condensation, subsequent hydrogenation of the double bond to give **19**, amide coupling with 3-picolylamine, and a non-stereoselective reduction of the keto group at the  $\alpha$ -position of the amide to the alcohol with NaBH<sub>4</sub>. Next, the ester was formed under Steglich-conditions linking the amide intermediates with the Boc-protected (*S*)- or (*R*)-pipercolic acid to achieve the respective stereoisomers **20**. Finally, cleavage of the Boc-group with TFA and a S<sub>N</sub>2 reaction of the piperidine-nitrogen with phenylmethanesulfonyl chloride lead to the inhibitors *S,S*-**10a**, *S,R*-**10a**, *R,S*-**10a**, *R,R*-**10a**, *S,R/S*-**10e**, *R,R/S*-**10e**, *S,S*-**10e**, *S,R*-**10e**, *S,R/S*-**10f**, *S,S*-**10d**, and *S,R*-**10d**.



Synthesis of the (*S*)-Pipelicolic Amide Stereochemically Pure DerivativesScheme 3. Synthesis scheme for the (*S*)-pipelicolic acid amide derivatives as stereochemically pure compounds.

Reagents and conditions: (a) allyl alcohol, SOCl<sub>2</sub>, 0 °C → 60 °C; (b) *N*-Boc-(*S*)-pipelicolic acid, EDC·HCl + HOBT or HBTU, DIPEA, DCM, 0 °C → rt; (c) i) TFA, DCM, 0 °C → rt, ii) phenylmethanesulfonyl chloride or (4-fluorophenyl)methanesulfonyl chloride, NMM, DCM, 0 °C → rt; (d) i) Pd(PPh<sub>3</sub>)<sub>4</sub>, morpholine, THF, 0 °C → rt, ii) 3-picolylamine, EDC·HCl + HOBT or HBTU, DIPEA, DCM, 0 °C → rt; (e) *m*-CPBA, EtOAc, rt.

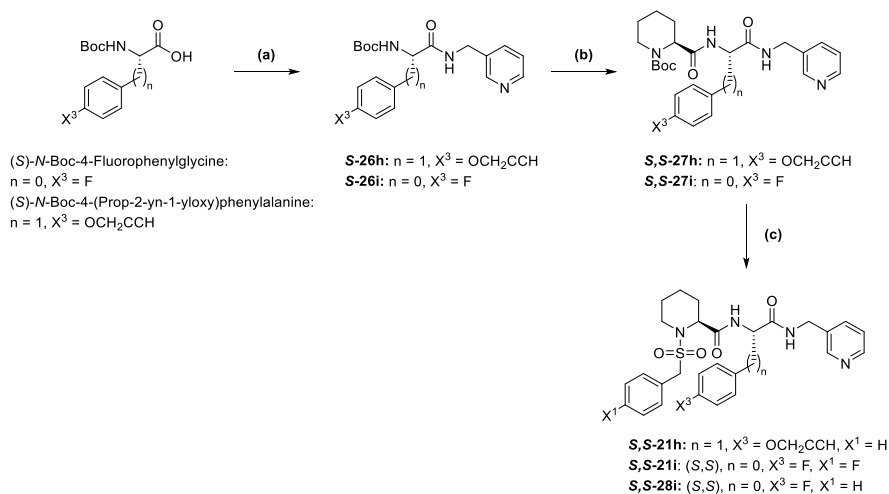
Due to the generally higher chemical and metabolic stability of amides (X<sup>2</sup> = NH, **Figure 3**) compared to ester compounds (X<sup>2</sup> = O), the stereochemically pure amides *S,S*-**21a**, *S,R*-**21a**, *S,S*-**21e**, *S,R*-**21e**, *S,S*-**21g**, and *S,S*-**21d** were also prepared via a synthetic route that allows late variation of the pyridine moiety (cf. Scheme 3). The *N*-oxides *R/S,S*-**22a**, *S,S*-**22g**, and *S,S*-**22d** were prepared by oxidation of the respective inhibitor with *meta*-chloroperoxybenzoic acid (*m*-CPBA) in EtOAc. At this point, the superiority of the *S*-configuration at the pipelicolic acid was evident for compounds with a side chain. Thus, only the configuration at the side chain was subsequently varied.

As mentioned above, a fluorine substituent in the *para* position of the sulfonamide benzene ring (*S,S*-**21d**), as well as on the aromatic side chain (*S,S*-**21g**) was intended to block enzymatic metabolization, and the compatibility of this substitution should therefore be tested.

The synthesis route started with the O-protection of different amino acids by using thionyl chloride and allyl alcohol to give the allyl esters **23**. After amidation with Boc-protected *S*-pipelicolic acid, the Boc-protection group of the amides **24** was cleaved with TFA. The *N*-sulfonamides **25** were formed using the respective sulfonyl chloride and NMM, and the allyl function was again cleaved

under palladium catalysis. The stereochemically pure amides *S,S*-21a, *S,R*-21a, *S,S*-21e, *S,R*-21e, *S,S*-21d, and *S,S*-21g were obtained by amidation with 3-picolylamine.

### Synthesis of *S*-Pipelicolic Amide Derivatives via an Alternative Pathway for Late Variation of the Sulfonamide Moiety



**Scheme 4.** Synthesis scheme of an alternative pathway for stereochemically pure *S*-pipelicolic amide derivatives *S,S*-21h, *S,S*-21i, and *S,S*-28i that allows a late variation of the sulfonamide moiety.

Reagents and conditions: (a) 3-picolylamine, HBTU, DIPEA, DCM, 0°C → rt; (b) i) TFA, rt; ii) *N*-Boc-(*S*)-pipelicolic acid, HBTU, DIPEA, DCM, 0°C → rt; (c) i) TFA, rt; ii) phenylmethanesulfonyl chloride or (4-fluorophenyl)methanesulfonyl chloride, NMM or DIPEA, DCM, 0°C → rt.

To allow a late variation of the sulfonamide moiety, an alternative synthesis pathway was established for the stereochemically pure pipelicolic amide derivatives (**Scheme 4**). Replacing the allyl protecting group with the Boc group has the additional advantage of being toxicologically safe, which would also be important in a prospective scale-up. The Boc-protected amino acids (*S*)-*N*-Boc-4-(prop-2-yn-1-yloxy)phenylalanine and (*S*)-*N*-Boc-4-fluorophenylglycine, respectively, were amide coupled to 3-picolylamine with HBTU and DIPEA to give the amides *S*-26h and *S*-26i. After cleavage of the Boc-protection group with TFA, the compounds were again amide coupled to the Boc-protected *S*-pipelicolic acid with HBTU and DIPEA to give *S,S*-27h and *S,S*-27i. After cleaving the Boc-protection group again with TFA, the *N*-sulfonamides were formed with the respective sulfonyl chloride derivative to give *S,S*-21h, *S,S*-21i, and *S,S*-28i.

## Initial Screening of BpMip Inhibitors by Fluorescence Polarization and Subsequent Investigation of Inhibition of PPIase Activity

For initial screening, a newly developed FPA was used, whose development was recently submitted, under minor modifications.<sup>55</sup> The results of the FPA and the protease-coupled BpMip-PPIase assay, measuring the remaining PPIase activity at an inhibitor concentration of 400 nM, proved largely congruent (cf. **Table 1**), with only few deviations, such as *R/S,S-10b* and *R/S,S-10c*.

The introduction of an additional side chain appears to have a considerable enhancing effect on the inhibition of BpMip PPIase activity and on the binding affinity (c.f. **9** with a  $K_{i, FPA}$  of 4000 nM and *S,S-10a* with a  $K_{i, FPA}$  of 122 nM). By adding a side chain, the  $K_i$  can decrease from a micromolar to a two-digit nanomolar range (cf.  $K_{i, FP}(S,S-21i) = 17$  nM). Here, the correct configuration at both stereo centers is essential for the binding affinity and enzymatic inhibition of BpMip. The reported superiority of a *S*-configuration at the C2 position of the pipercolic acid for anti-PPIase activity remains valid when an additional side chain is inserted.<sup>52</sup> A comparison of all four stereoisomers of **10a** demonstrates clearly that a *S*-configuration at both stereocenters (*S,S-10a*) is the preferred configuration. This observation is confirmed for all other comparisons of stereoisomers with varying degrees of manifestation (cf. *S,S-10d*, *S,S-10e*, and *S,S-21e*). Enzymatic activity of BpMip can be almost entirely prevented (up to 96%) with compounds such as *S,S-21d* and *S,S-21h*.

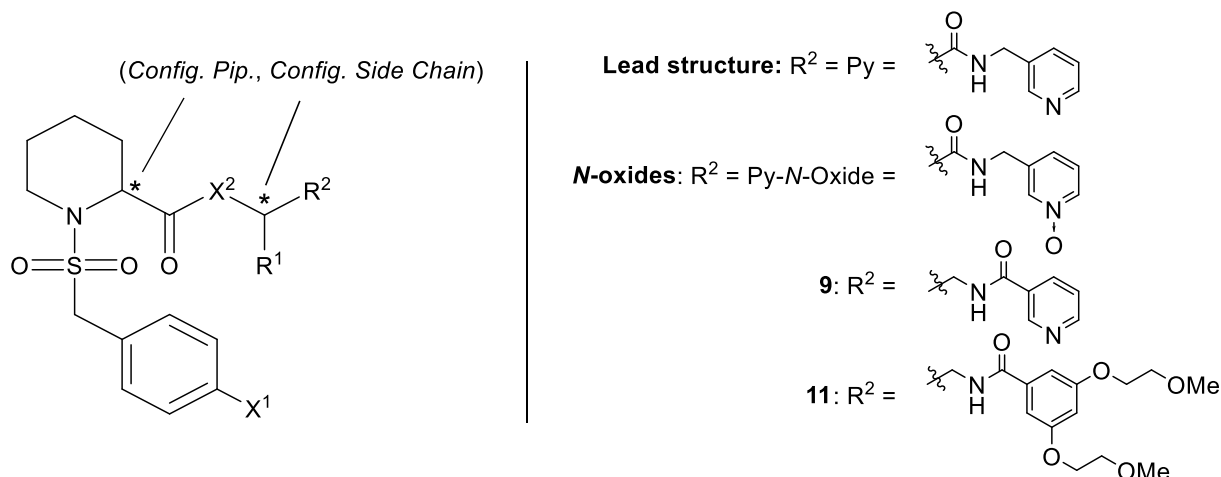
Replacement of piperidine-2-carboxylate ( $X^2 = O$ , **Figure 3**) by an amide ( $X^2 = NH$ ) seems to be well tolerated (cf. *S,S-10e* and *S,S-21e*). Benefits such as chemical or metabolic stability could speak for the use of amides instead of esters, and an affinity loss-free exchange supports this approach. Both aromatic and alkyl residues in the side chain ( $R^1$ ) work as possible substituents.

The reported advantageous effect on the enzymatic inhibitory activity of a *para*-fluorine substitution on the benzene ring ( $X^1 = F$ ) connected to the sulfonamide,<sup>52</sup> was confirmed in the FPA, although only weakly pronounced (cf. *S,S-28i* and *S,S-21i*). *Para*-fluorination of both benzene rings (as in *S,S-21g*) also shows slightly better inhibition than the non-fluorinated derivative (*S,S-21a*). This and the possible increased metabolic stability argue for the introduction of a *para*-fluoro substituent.

The importance of the pyridine moiety becomes evident when replacing it with an allyl group (*S,S-25g*), resulting in a drastic loss of affinity. Thus, this derivative was not investigated further *in vitro*.

Oxidation of the pyridine moiety to the *N*-oxide results in a significant loss of affinity (cf. *S,S*-21d vs. *S,S*-22d and *S,S*-21g vs. *S,S*-22g), but considerations such as highly increased solubility could argue for such replacement in future development towards druglike compounds (see SI).

**Table 1.** General structure and overview of the synthesized Mip inhibitors and their results in the FPA and protease-coupled enzymatic assay. *ND* = not determined. *NB* = no binding.



Inhibitor	Config. Pip. *	X <sup>1</sup>	X <sup>2</sup>	Side Chain Code	Side Chain R <sup>1</sup>	Config Side Chain *	R <sup>2</sup>	FPA K <sub>i</sub> [nM], BpMip, n = 3	BpMip %remaining activity at 400 nM inh., n = 3	NmMip %remaining activity at 400 nM inh., n = 3	NEIS0004 %remaining activity at 400 nM inh., n = 3
<b>9</b>	<i>S</i>	H	O	<b>Xxx</b>	Xxx	Xxx	See above	3959.7	50.3	52.2	61.9
<b>11</b>	<i>S</i>	H	O	<b>Xxx</b>	Xxx	Xxx	See above	1055.2	52.3	85.0	88.9
<i>R/S,S</i> -10a	<i>R/S</i>	H	O	<b>A</b>		<i>S</i>	Py	48.8	15.9	14.0	6.9
<i>S,R</i> -10a	<i>S</i>	H	O	<b>A</b>		<i>R</i>	Py	41115.5	151.1	51.1	106.0
<i>S,S</i> -10a	<i>S</i>	H	O	<b>A</b>		<i>S</i>	Py	122.1	7.0	10.0	6.7
<i>R,R</i> -10a	<i>R</i>	H	O	<b>A</b>		<i>R</i>	Py	NB	154.6	51.3	107.5
<i>R,S</i> -10a	<i>R</i>	H	O	<b>A</b>		<i>S</i>	Py	42421.0	146.8	27.2	122.4
<i>S,S</i> -21a	<i>S</i>	H	NH	<b>A</b>		<i>S</i>	Py	34.7	23.7	27.3	8.5
<i>S,R</i> -21a	<i>S</i>	H	NH	<b>A</b>		<i>R</i>	Py	625.6	21.5	87.9	45.4
<i>R/S,S</i> -22a	<i>R/S</i>	H	NH	<b>A</b>	<i>S</i>	Py- <i>N</i> -Oxide	4450.7	51.9	66.7	45.5	
<i>R/S,S</i> -10b	<i>R/S</i>	H	O	<b>B</b>		<i>S</i>	Py	1084.1	13.9	25.2	10.9
<i>R/S,S</i> -10c	<i>R/S</i>	H	O	<b>C</b>		<i>R/S</i>	Py	3131.4	16.8	73.3	9.4
<i>R/S,S</i> -10d	<i>R/S</i>	H	O	<b>D</b>		<i>S</i>	Py	15.8	17.4	22.1	3.4
<i>S,R</i> -10d	<i>S</i>	H	O	<b>d</b>		<i>R</i>	Py	2520.5	ND	ND	ND
<i>S,S</i> -10d	<i>S</i>	H	O	<b>d</b>		<i>S</i>	Py	60.5	4.8	35.6	3.8
<i>S,S</i> -21d	<i>S</i>	F	NH	<b>d</b>		<i>S</i>	Py	45.6	5.8	23.6	4.2
<i>S,S</i> -22d	<i>S</i>	F	NH	<b>d</b>		<i>S</i>	Py- <i>N</i> -Oxide	148.0	21.0	44.4	23.8

Inhibitor	Config. Pip. *	X <sup>1</sup>	X <sup>2</sup>	Side Chain Code	Side Chain R <sup>1</sup>	Config Side Chain *	R <sup>2</sup>	FPA K <sub>i</sub> [nM], BpMip, n = 3	BpMip %remaining activity at 400 nM inh., n = 3	NmMip %remaining activity at 400 nM inh., n = 3	NEIS0004 %remaining activity at 400 nM inh., n = 3
<i>S,R/S-10e</i>	<i>S</i>	H	O	<b>e</b>		<i>R/S</i>	Py	207.0	28.7	47.0	8.4
<i>R,R/S-10e</i>	<i>R</i>	H	O	<b>e</b>		<i>R/S</i>	Py	NB	139.6	93.7	119.2
<i>S,S-10e</i>	<i>S</i>	H	O	<b>e</b>		<i>S</i>	Py	15.3	14.8	54.0	11.1
<i>S,R-10e</i>	<i>S</i>	H	O	<b>e</b>		<i>R</i>	Py	3381.3	100.6	83.5	70.0
<i>S,S-21e</i>	<i>S</i>	H	NH	<b>e</b>		<i>S</i>	Py	10.5	17.6	44.8	12.9
<i>S,R-21e</i>	<i>S</i>	H	NH	<b>e</b>		<i>R</i>	Py	320.0	23.4	83.7	39.9
<i>S,R/S-10f</i>	<i>S</i>	H	O	<b>f</b>		<i>R/S</i>	Py	4155.0	32.6	82.0	32.8
<i>S,S-21g</i>	<i>S</i>	F	NH	<b>g</b>		<i>S</i>	Py	18.8	12.5	11.5	37.2
<i>S,S-22g</i>	<i>S</i>	F	NH	<b>g</b>		<i>S</i>	Py- <i>N</i> -Oxide	1312.9	40.9	49.4	24.0
<i>S,S-25g</i>	<i>S</i>	F	NH	<b>g</b>		<i>S</i>		NB	ND	ND	ND
<i>S,S-21h</i>	<i>S</i>	H	NH	<b>h</b>		<i>S</i>	Py	34.3	4.4	12.3	4.9
<i>S,S-28i</i>	<i>S</i>	H	NH	<b>i</b>		<i>S</i>	Py	73.2	11.3	63.5	27.2
<i>S,S-21i</i>	<i>S</i>	F	NH	<b>i</b>		<i>S</i>	Py	17.0	13.5	43.3	30.6

## Mip Inhibitors Reduce *B. pseudomallei*-Induced Cytotoxicity in RAW264.7 Murine Macrophages

*B. pseudomallei* is an intracellular pathogen that replicates within macrophages.<sup>56</sup> Infection of macrophages with *B. pseudomallei* leads to a high level of cell death 24 h after infection, which can be measured by the release of lactose dehydrogenase (LDH).<sup>13</sup> Deletion of Mip from *B. pseudomallei* has been shown to result in less severe infection, especially a decrease in cytotoxicity in macrophages.<sup>7, 13</sup>

Pre-treatment followed by further 24 h treatment of *B. pseudomallei* with new, side chain bearing inhibitors, such as *S,R-21a* results in up to a 70% reduction in cytotoxicity of RAW264.7 macrophage cells compared to the DMSO-only control (see **Table 2**, cf. also *S,R/S-10f*, *R/S,S-22a*, *S,S-21i*, and *S,S-21d*). This reduction is significantly higher than the levels observed for previous generations of Mip inhibitors, which agrees well with the results obtained in the FPA and PPIase assay (cf. < 40% reduction with **7** in J774A.1 macrophages,<sup>7</sup> resp. < 32% reduction with **9** and **11** in RAW264.7 macrophages, cf. **Table 2**).

Interestingly, the correlation between the stereochemistry of the inhibitors' side chain and their

effect in the cell-based assay is not quite as clear compared to the FPA screening (cf. *S,R*-**10a** vs. *S,S*-**10a** and *S,R*-**21a** vs. *S,S*-**21a**). While at the side chain, an *R*-configuration is sometimes even advantageous (cf. *S,R*-**21a** vs. *S,S*-**21a**), the *S*-configuration at the piperidine unit remains superior at all times. Based on crystal structures, it is evident that the piperidine moiety dives deeper into the binding pocket (cf. **Figure 2A**). Iwasaki *et al.* had observed a tight binding conformation of the piperidic acid backbone of lead compounds **9** and **11** to BpMip in co-crystallization studies.<sup>8</sup> This binding was mainly characterized by polar contacts between the amide nitrogen of Ile63 and the carbonyl ester of the inhibitors and between the hydroxyl group of Tyr89 and one of the sulfonyl oxygens. In addition, they observed that the terminal phenyl ring is involved in a  $\pi$ -edge stacking interaction with Phe43. Hence it is plausible that the configuration at the piperidic acid would have a more substantial influence on BpMip inhibition than at the side chain. However, this highlights the importance of performing a cell-based infection model, as not all trends gained by anti-PPIase and FP data may necessarily be reflected. The question of whether this is due to properties such as cell permeability of the compounds or additional targets being addressed requires further investigation.

Replacement of the pyridine moiety with a pyridine-*N*-oxide is well tolerated (cf. *S,S*-**22d** vs. *S,S*-**21d**), sometimes even superior (cf. *S,S*-**22g** vs. *S,S*-**21g**). In the side chain, the benzyl group seems superior to an ethylbenzene group (cf. *S,S*-**21a** vs. *S,S*-**21e**). Interestingly, the replacement of the benzene ring by a (second) pyridine in the side chain considerably increases the effectiveness (*S,R/S*-**10f** vs. *S,R/S*-**10e**).

In addition to the recommendation of an additional side chain, other screening's observations were also confirmed, such as the good tolerance of replacement of the piperidic ester with an amide (cf. *S,S*-**21a** vs. *S,S*-**10a**) and the superiority of a *para*-fluoro substitution at the aromatic of the sulfonamide moiety (cf. *S,S*-**21i** vs. *S,S*-**28i**).

When incubated with non-infected RAW264.7 cells as a control, all compounds were found to induce only low cytotoxicity by themselves (see SI).

**Table 2.** Percent reduction in *B. pseudomallei* (*B.ps.*)-induced cytotoxicity in RAW264.7 murine macrophages when treated with Mip inhibitors. Percentage of survival of *N. meningitidis* and *N. gonorrhoeae* in RAW264.7 murine macrophages treated with Mip inhibitors at 50  $\mu$ M compared to untreated control. Mean of a minimum of three biological replicates, each with technical duplicates. SD are given in the SI.

Inhibitor	% <i>B.ps.</i> -induced cytotoxicity RAW264.7	<i>Nm</i> survival, % of control in RAW264.7 cells	<i>Ng</i> survival, % of control in RAW264.7 cells
9	68.9	41.1	27.1
11	71.0	19.6	21.5
<i>R,S,S</i> -10a	68.5	38.4	65.1
<i>S,R</i> -10a	65.9	26.0	73.2
<i>S,S</i> -10a	72.5	41.5	64.6
<i>R,R</i> -10a	74.3	21.0	58.6
<i>R,S</i> -10a	82.7	35.2	68.4
<i>S,S</i> -21a	63.4	25.0	40.9
<i>S,R</i> -21a	30.4	60.8	70.6
<i>R,S,S</i> -22a	46.2	76.0	45.4
<i>R,S,S</i> -10b	96.8	52.5	65.1
<i>R,S,S</i> -10c	94.3	58.0	35.4
<i>R,S,S</i> -10d	93.2	36.9	ND
<i>S,S</i> -10d	87.8	13.0	19.1
<i>S,S</i> -21d	46.8	56.2	61.7
<i>S,S</i> -22d	61.5	71.3	56.4
<i>S,R/S</i> -10e	93.4	16.4	63.5
<i>R,R/S</i> -10e	95.7	21.2	ND
<i>S,S</i> -10e	70.6	16.0	19.8
<i>S,R</i> -10e	97.6	67.7	53.6
<i>S,S</i> -21e	75.4	34.1	71.5
<i>S,R</i> -21e	88.7	69.9	41.9
<i>S,R/S</i> -10f	35.6	84.4	52.0
<i>S,S</i> -21g	68.0	47.9	50.8
<i>S,S</i> -22g	51.7	52.8	44.2
<i>S,S</i> -21h	55.4	45.7	35.2
<i>S,S</i> -28i	78.5	22.6	28.0
<i>S,S</i> -21i	46.7	51.4	31.4

### Screening Enzymatic Anti-PPIase Activity Against Mips from *Neisseria* Species

The high conservation of the PPIase domain of Mip proteins results in Mip inhibitors exhibiting activity in a wide range of pathogens.<sup>8, 53</sup> Consequently, the compound library optimized against BpMip was subsequently tested against the two Mip proteins of *N. meningitidis* – NmMip and NEIS0004 (see **Table 1**). The use of NmMip was also expected to provide information on the

effect of compounds against *N. gonorrhoeae* since the analogs NgMip and NmMip possess more than 97% similarity in the gene sequence of the PPIase region. As in the case of BpMip, for both Mip proteins of *N. meningitidis*, the introduction of a side chain has a drastic effect on the activity of the inhibitors in the protease-coupled enzyme assay (cf. **9**: 38% reduction (NEIS0004), resp. 48% (NmMip) vs. *S,S*-**10a**: 93% (NEIS0004), resp. 90% (NmMip) reduction).

The anti-PPIase data of NEIS0004 (12 kDa) appear to be more similar to those of BpMip than the data of the larger NmMip (cf. *S,S*-**10e**, *S,S*-**10d**, and *R/S,S*-**10c**). This difference is most likely due to the fact that NEIS0004 is similar to the Mip-like (ML1) proteins, which BpMip is a part of, while NmMip is structured like a traditional Mip protein with a dimerization domain and is localized to the outer membrane of the bacteria. ML1 proteins are predicted to exist in other cellular compartments. Since this library was designed against BpMip, an ML1 protein, the inhibition was more similar to that of NEIS0004.<sup>12, 25, 32</sup>

Against NEIS0004, substances with an (*S,S*)-configuration (cf. *S,S*-**10a**) and partially containing the (*S,S*)-diastereomer (cf. *R/S,S*-**10d** and *R/S,S*-**10a**) show a high inhibition of the enzymatic activity, while compounds with unfavorable stereochemistry show poorer inhibition (cf. *S,R*-**10a**, *R,R*-**10a**). The larger NmMip protein shows the same preference for an (*S,S*)-configuration (cf. the **10a** stereoisomers). However, some other stereoisomers exhibit an anti-enzymatic activity against NmMip, while they don't show any in the case of BpMip and NEIS0004 (cf. *R,S*-**10a**, *S,R*-**10a**, *R,R*-**10a**).

The introduction of *para*-fluoro substituents at the sulfonamide benzene ring as well as at the aromatic side chain seems to be beneficial for PPIase inhibition of NmMip (cf. *S,S*-**21a** vs. *S,S*-**21g** and *S,S*-**21i** vs. *S,S*-**28i**) and tolerated for NEIS0004 (cf. *S,S*-**21i** vs. *S,S*-**28i**). Particularly in the case of NmMip, there is a preference for a benzyl moiety as a side chain (cf. *S,S*-**10a** and *S,S*-**21g**). Tolerance towards a pipercolic amide (cf. *S,S*-**21e** vs. *S,S*-**10e**) and a reduction in anti-PPIase activity upon introduction of a *N*-pyridine oxide (cf. *S,S*-**21d** vs. *S,S*-**22d**) were found to be similar for NEIS0004 and NmMip as for BpMip.

### **Mip Inhibitors Reduce *N. meningitidis* Survival in RAW264.7 Murine Macrophages**

Meningococcal invasion of the epithelial layer occurs via a transcellular pathway dependent on major adhesins such as type IV pili (Tfp).<sup>27</sup> Once it has moved through the epithelial layer, *N. meningitidis* circulates in the body, where it is phagocytosed by macrophages. Macrophages are



able to kill bacteria through a series of intracellular killing mechanisms to which the bacteria have developed resistance.<sup>57</sup> Previously, it was shown that both Mip inhibitors **9** and **11** significantly reduced the ability of *N. meningitidis* to invade epithelial cells to approximately 30%.<sup>8</sup> In the present study, we focused on the survival of the pathogen in macrophages in the presence of Mip inhibitors. To determine whether treatment with compounds sensitizes bacteria to intracellular killing, the survival of meningococci over 6 h in RAW264.7 murine macrophages was examined. Standardized *N. meningitidis* serogroup B cells were pre-treated with 50  $\mu$ M compounds for 1 h and subsequently allowed to invade and be phagocytosed by the macrophages at a multiplicity of infection of 100. Following 6 h of incubation, macrophage cells were lysed, and the meningococci survival was enumerated (cf. **Table 2**).

The cell-based assay shows the effectiveness of the studied Mip inhibitors in sensitizing macrophages to killing *N. meningitidis* almost entirely as bacterial survival drops to as low as 13% (cf. *S,S*-**10d**, **11**, and *S,S*-**10e**, see **Table 2**). Interestingly, **11**, which lacks a side chain, also strongly sensitizes macrophages to *N. meningitidis* killing. However, since this does not hold true for **9**, and **11** possesses long ether chains attached to the aromatic that could mimic a side chain, conclusions about the importance of the side chain cannot be unambiguously drawn from this.

The results of the survival assay are largely in agreement with those of the PPIase screening, but there are some deviations, such as the stereochemical preference (cf. *S,S*-**10a** and its stereoisomers). The most potent inhibitors feature a *S*-configuration at the pipercolic acid, respectively an (*S,S*)-configuration. However, *R,R*-**10a** inhibits the PPIase activity of NmMip (51.3% remaining PPIase activity) and NEIS0004 (total remaining PPIase activity) rather weakly, yet in the cell-based assay shows a 79% reduction in bacteria load in macrophages. Possible reasons for differences in the assays are discussed in the following subsection of the *N. gonorrhoeae* cell-based assay.

Contrary to the *B. pseudomallei* studies and, therefore, a conceivable starting point for future selectivity tuning, the best activity can be seen with ester compounds, and *para*-fluorination at the aromatics tends to negatively impact the potency (cf. *S,S*-**21i** vs. *S,S*-**28i** and *S,S*-**21g** vs. *S,S*-**21a**). Furthermore, in the case of *N. meningitidis*, *N*-oxide formation of the pyridine moiety reduces efficacy (cf. *S,S*-**21d** vs. *S,S*-**22d**).

## Mip Inhibitors Reduce *N. gonorrhoeae* Survival in RAW264.7 Murine Macrophages

In a follow-up to Reimer *et al.*, who found reduced intracellular survival of *N. gonorrhoeae* in PMNs in the presence of Mip inhibitors, the library of side chain-bearing Mip inhibitors was examined for whether they sensitize infected RAW264.7 mouse macrophages to eliminate the bacteria (see **Table 2**).<sup>53</sup> As a result, it was shown that substances such as **11**, *S,S*-**10d**, and *S,S*-**10e** (at a concentration of 50  $\mu$ M) lead to a reduction in pathogen load by up to 80%. Interestingly, the positive effect of an additional sidechain is only weakly pronounced here (cf. **9** and **11**). Furthermore, the preference for one particular stereoisomer is not the same for all compounds investigated (cf. *S,S*-**10e** vs. *S,R*-**10e** and *S,S*-**21e** vs. *S,R*-**21e**). However, the compounds showing the best activity feature a *S*-configuration on the piperidine moiety and a *S*-configuration on the side chain, if present. Similar to *N. meningitidis* and in contrast to *B. pseudomallei*, there seems to be a preference for pipercolic esters over amides (cf. *S,S*-**10e** vs. *S,S*-**21e**, *S,S*-**21d** vs. *S,S*-**10d**) with only few exceptions. This might be because esters adopt a different spatial arrangement and flexibility than the  $sp^2$  hybridized amides. Moreover, the amide proton might exhibit unfavorable interactions with the binding pocket.

Fluorine substitution of the benzene rings has a slightly negative to no effect (cf. *S,S*-**21a** vs. *S,S*-**21g**, *S,S*-**21i** vs. *S,S*-**28i**), while *N*-oxide formation of the pyridine moiety seems to be well-tolerated (cf. *S,S*-**21g** vs. *S,S*-**22g**).

In some cases, PPIase-trends for NmMip differ significantly from those obtained in the survival assay (cf. **11**, *R/S,S*-**10a**, and *S,S*-**10a**). This suggests that the effect of the compound does not depend solely on its inhibitory potential on the PPIase activity of the Mip protein, an observation reported by Reimer *et al.* for related inhibitors of NgMip and CtrMip.<sup>53</sup> This may also indicate the possibility that some compounds inhibit the function of NgMip not only by inhibiting PPIase activity. The fact that NgMip gene knockout lowers survival in macrophages, but strong inhibition of PPIase by some compounds does not lead to a strong effect in the survival assay might suggest that NgMip has other important functions besides PPIase activity that affect survival in macrophages, such as chaperone activity.<sup>12</sup> Another possibility could be a decreased cell-permeability of some compounds or that the inhibitors affect another bacterial or cellular protein involved in infection.

## Solubility and Cytotoxicity Studies

Solubility studies of a selection of substances demonstrate that the insertion of an aromatic side chain typically leads to decreased solubility, presumably supported by intramolecular  $\pi$ - $\pi$  stacking (cf. *S,S*-**10a** ( $26.6 \pm 0.3$   $\mu\text{g/mL}$ ) vs. **11** ( $239$   $\mu\text{g/mL}$ )). *Para*-fluorination of the aromatics also decreases solubility as the electronegative fluorine atom withdraws electron density (cf. *S,S*-**21a** ( $125.0 \pm 8.8$   $\mu\text{g/mL}$ ) vs. *S,S*-**21g** ( $13.5 \pm 2.2$   $\mu\text{g/mL}$ )). Replacement of the pipercolic ester with an amide results in a slight increase in solubility (cf. *S,S*-**10a** ( $26.6 \pm 0.3$   $\mu\text{g/mL}$ ) vs. *S,S*-**21a** ( $125.0 \pm 8.8$   $\mu\text{g/mL}$ )). Aliphatic side chains have higher solubility than aromatic side chains (cf. *S,S*-**21g** ( $13.5 \pm 2.2$   $\mu\text{g/mL}$ ) vs. *S,S*-**21d** ( $390 \pm 21$   $\mu\text{g/mL}$ )), falling within the range of substances without side chain. The addition of a pyridine residue to the side chain (cf. *S,R/S*-**10f**) or, more pronounced, the oxidation of the pyridine residue to the *N*-oxide significantly increases solubility (cf. *S,S*-**21g** ( $13.5 \pm 2.2$   $\mu\text{g/mL}$ ) vs. *S,S*-**22g** ( $1494 \pm 16$   $\mu\text{g/mL}$ )). The solubility of different stereoisomers is comparable and differs by a maximum of  $65$   $\mu\text{g/mL}$  (cf. *S,S*-**21a** vs. *S,R*-**21a**, *S,R*-**10e** vs. *S,S*-**10e**).

A selection of the most active substances was tested for cytotoxicity against murine fibroblasts (NIH 3T3) and human embryonal kidney (HEK 293T) cells in a colorimetric WST-1 assay. All Mip inhibitors except for the fluorinated compounds *S,S*-**21g** and *S,S*-**21d** showed excellent cytotoxicity profiles with  $\text{IC}_{50}$  values above  $100$   $\mu\text{M}$  (see SI). Interestingly, other substances containing *para*-fluoro-substituted benzenes did not exhibit cytotoxicity (cf. *S,S*-**21i** and *S,S*-**28i**). However, replacing the pyridine with a pyridine-*N*-oxide eliminated the cytotoxic effects of *S,S*-**21g** (to *S,S*-**22g**) and *S,S*-**21d** (to *S,S*-**22d**).

## 4.3 Conclusion

Our study demonstrates that introducing a side chain into the rapamycin-derived Mip inhibitor backbone significantly improves the affinity and enzymatic inhibition of the Mip proteins of *B. pseudomallei* and *N. meningitidis*. Thus, this supports our hypothesis of the combination of two binding modes derived from crystal structure analysis. Several Mip inhibitors showed promising activity in cell-based assays, reducing *B. pseudomallei*-induced cytotoxicity in infected macrophages by up to 70% and sensitizing infected macrophages to kill *N. meningitidis* by up to 87% and *N. gonorrhoeae* by up to 80%. While there does not appear to be a discrete inhibitor with excellent

activity against all pathogens, certain compromises in activity allow the identification of structurally similar broad-spectrum Mip inhibitors such as *S,S*-**21a**, *S,S*-**21i**, and *S,S*-**21h**, which share a *S,S*-configuration, an aromatic side chain, and a pipercolic amide. *B. pseudomallei*-selectivity can be improved by introducing a second pyridine or using an *R*-configuration at the side chain. A *para*-fluoro substitution, especially at the aromatic of the sulfonamide moiety, also provides this selectivity-increasing effect. Selectivity for *Neisseria* species over *B. pseudomallei* can be enhanced by adding an aliphatic side chain (cf. *S,S*-**10d**) or an ethylbenzene moiety (*S,S*-**10e**) to a pipercolic ester inhibitor or by omitting the side chain (cf. **11**). As found by Seufert *et al.*, an *R*-configuration at the pipercolic moiety has a strong negative effect on activity.<sup>52</sup> Our results are in agreement with Iwasaki *et al.*, who, on the one hand, demonstrated the high similarity of the formed active sites of BpMip and NmMip by homology modeling.<sup>8</sup> On the other hand, minor changes, such as the mutation of phenylalanine (Phe53) in BpMip to valine in NmMip, resulted in the existence of different docking poses with comparable binding energies<sup>8</sup> and possibly led to the observed species-dependent SAR. All in all, *S,S*-**22g** may be a promising lead compound for BpMip and *B. pseudomallei*, and *S,S*-**10d** may be suitable for *N. meningitidis* and *N. gonorrhoeae* and the respective Mip proteins. The Mip inhibitors shown are novel, non-cytotoxic compounds with promising potential for developing Mip-targeted drugs to combat a broad spectrum of infectious diseases.

#### 4.4 Experimental Section

##### Organic Synthesis

**General.** Reagents used for the synthesis were obtained from *Alfa Aesar* (Ward Hill, USA), *Merck* (Darmstadt, Germany), *Avantor* (Darmstadt, Germany), *TCI Deutschland GmbH* (Eschborn, Germany), *Fisher Scientific* (Schwerte, Germany), and *ABCR* (Karlsruhe, Germany). The purchased chemicals were used without further purification. Dry solvents for organic synthesis were produced and stored according to general procedures.<sup>58</sup> All syntheses were performed under an argon or nitrogen protective atmosphere using Schlenk technique.

**Gravity-driven column chromatography.** For gravity-driven column chromatography, silica gel 60 (0.063–0.200 nm) purchased from *Merck* (Darmstadt, Germany) or basic aloxide 90 (0.050–0.200 nm) purchased from *Macherey-Nagel* (Düren, Germany) were used. One of the following isocratic methods was typically used: SiO<sub>2</sub>, PE/EtOAc = 3:1; SiO<sub>2</sub>, DCM/MeOH = 20:1; aloxide basic III, DCM/MeOH = 20:1.

**Flash chromatography.** For purification by medium pressure liquid chromatography (MPLC, flash chromatography), a *puriFlash*<sup>®</sup>430 system from Interchim (Montluçon, France) with an integrated UV diode array detector (DAD) covering a scanning range of 200 – 600 nm was used. Non-UV-active compounds were detected using a *Flash-ELSD* (evaporative light scattering detector) version 2011 from *Interchim* (Montluçon, France). The following pre-packed columns were used: *Chromabond Flash*, type: RS15 C18 ec, 16 g from *Macherey-Nagel* (Düren, Germany); *puriFlash*, type: SI-Std (IR-50SI), 12 g and 25 g from *Interchim* (Montluçon, France); and *FlashPure EcoFlex*, type: alumina neutral, 24 g from *Büchi Labortechnik AG* (Flawil, Switzerland). One of the following methods was typically used: SiO<sub>2</sub>, A: PE, B: EtOAc, gradient: 0→100% B; SiO<sub>2</sub>, A: DCM, B: MeOH, gradient: 0→30% B; RP 18, A: H<sub>2</sub>O + 1% FA, B: MeOH + 1% FA, gradient: 5→100% B.

**HPLC.** Purity analysis was carried out using an HPLC system from *Shimadzu Scientific instruments* (Kyoto, Japan). Mobile phase A was Milli-Q<sup>®</sup>-water with 0.1% formic acid (FA) added, while mobile phase B was MeOH with 0.1% FA. The gradient started with 5% of mobile phase B and the ratio of mobile phase B was increased to 100% over 8 min and held for 4 min. For re-equilibration, the mobile phase B ratio was reduced from 100% to 5% in another 4 min. Subsequently, the column was flushed with 5% B for 2 min. The flow rate was set to 1.0 mL/min. The injection volume was 20 µL. The UV signal at 254 nm was chosen for detection, the oven temperature was rt.

**TLC.** Thin layer chromatography (TLC) was performed on pre-coated silica gel glass plates SIL G-25 or aluminum sheets coated with aluminum oxide ALUGRAM Alox N/UV254 from *Macherey-Nagel* (Düren, Germany). Spots were evidenced by quenching at 254 nm or intrinsic fluorescence at 365 nm.

**Purity.** All purities of the compounds were verified by HPLC. All final compounds synthesized had purities above 95%. Purity data are given in the SI.

**Mass spectrometry.** Electrospray ionization (ESI) mass spectra were measured with a *Shimadzu LCMS-2020* (*Shimadzu Scientific instruments*, Kyoto, Japan). Data are reported as mass-to-charge ratio (m/z) of the respective positively charged molecular ions.

**Determination of Diastereomeric Ratio.** Diastereomers were distinguished analytically by <sup>1</sup>H NMR spectroscopy based on the signal integrals of the protons at the two stereocenters. More

specifically, by the signals at the C2, C3 or C6 position of the piperidine ring and at the hinge position of the side chain. The diastereomeric ratio was calculated by the ratio of the integrals of equivalent peaks of the two diastereomers.

**High-Resolution Mass Spectrometry.** High-resolution mass spectrometry (HRMS) was performed using an *Agilent* Infinity II LC-system (Waldbronn, Germany) consisting of a quaternary pump, a thermostatted autosampler, and a thermostatted column compartment, coupled to a *Sciex* X500R QTOF mass spectrometer (Concord, Ontario, Canada) equipped with a Turbo V™ Ion Source (ESI). Automatic calibration of the mass spectrometer was performed using the provided tuning solution for ESI (*Sciex*, Concord, Ontario, Canada). Mobile phase A was a mixture of water and 0.1% formic acid (FA), while mobile phase B was acetonitrile containing 0.1% FA. An isocratic elution of 50% B with a stop time of 1.5 min was used. The flow rate was set to 1 mL/min, and the injection volume was 10 µL. The parameters for the HRMS experiment were optimized by flow-injection using positive polarity (Gas1: 50 psi, Gas2: 50 psi, Curtain gas: 25 psi, Ionspray voltage: 5500 V, Temperature: 500 °C, Declustering potential: 70 +/- 10 V, Collision energy: 10 V). The mass accuracy is given as an error in ppm and was calculated adapted from Lermyte<sup>59</sup>: mass error (ppm) =  $(|(m/z)_{found} - (m/z)_{calculated}| \times 1\,000\,000) / (m/z)_{calculated}$ .

**Infrared Spectroscopy (IR).** IR spectra were recorded on a *Jasco*-FT-IR-6100 system (*Jasco Deutschland GmbH*, Groß-Umstadt, Germany) in combination with a diamond ATR accessory. The wave numbers of characteristic absorption bands are given in [cm<sup>-1</sup>].

**Nuclear Magnetic Resonance Spectroscopy.** <sup>1</sup>H (400.132 MHz) and <sup>13</sup>C (100.613 MHz) NMR spectra were recorded on a *Bruker* AV 400 instrument (*Bruker Biospin*, Ettlingen, Germany) at a temperature of 300 K. The residual <sup>1</sup>H-solvent signal (containing one less deuterium atom than the perdeuterated solvent) was used as an internal standard for <sup>1</sup>H spectra. For <sup>13</sup>C spectra, the solvent signals resulting from the <sup>13</sup>C atoms in natural abundance in the perdeuterated solvent were used for calibration. ACN-d<sub>3</sub>: <sup>1</sup>H: 1.94 ppm, <sup>13</sup>C: 1.32 ppm, 118.26 ppm; CDCl<sub>3</sub>: <sup>1</sup>H: 7.26 ppm, <sup>13</sup>C: 77.16 ppm; CD<sub>3</sub>OD: <sup>1</sup>H: 3.31 ppm, <sup>13</sup>C: 49.00 ppm; DMSO-d<sub>6</sub>: <sup>1</sup>H: 2.50 ppm, <sup>13</sup>C: 39.52 ppm.<sup>60</sup> Abbreviations for multiplicity are: s, singlet; d, doublet; t, triplet; m, multiplet; br, broad; dd, doublet of doublets; ddd, doublet of doublets of doublets. MestReNova® (version 6.0.2-5475) software (*Mestrelab Research S.L.*, Santiago de Compostela, Spain) or Topspin® (version 3.2-pl7) software (*Bruker Biospin*, Ettlingen, Germany) was applied for processing of NMR spectra.

**Melting points.** To determine melting points, an MP70 melting point system (*Mettler-Toledo GmbH*, Gießen, Germany) was used.

**Solubility.** To determine thermodynamic solubility, the continuous shake flask protocol of Hiltensperger *et al.* was applied, using an extended stirring time of up to 48 h to ensure thermodynamic equilibrium.<sup>61</sup> The protocol and data are given in the SI.

**Substances known from literature.** Synthesis of (*R/S*)-1-(benzylsulfonyl)piperidine-2-carboxylic acid (**14**) was performed according to Juli *et al.*<sup>6</sup> Synthesis of lead structures **9** and **11** has been described by Seufert *et al.*<sup>52</sup> 2-Hydroxy-4-phenylbutanoic acid<sup>62</sup>, (*S*)-2-hydroxy-4-phenylbutanoic acid<sup>63</sup>, (*R*)-2-hydroxy-4-phenylbutanoic acid<sup>64</sup>, (*S*)-2-hydroxy-3-methylbutanoic acid<sup>65</sup>, (*S*)-2-hydroxy-4-methylpentanoic acid<sup>65</sup>, (*2S,3S*)-2-hydroxy-3-methylpentanoic acid<sup>65</sup>, and (*R*)-2-hydroxy-4-methylpentanoic acid<sup>66</sup> were prepared according to general procedure F. Allyl (*S*)-2-hydroxy-3-methylbutanoate<sup>67</sup>, allyl (*S*)-2-hydroxy-4-methylpentanoate<sup>68</sup>, and allyl (*2S,3S*)-2-hydroxy-3-methylpentanoate<sup>69</sup> were prepared according to general procedure H. Analytical data was in agreement with the cited literature.

### General Procedures.

**General procedure A.** Esterification and amidation was carried out according to Seufert *et al.*<sup>52</sup> First, the corresponding carboxylic acid (1 equiv) was dissolved in dry DCM (30–40 mL per 1 mmol limiting reactant). In the case of esterifications, EDC·HCl (1.2 equiv) and DMAP (0.2–1 equiv) was added under ice cooling. In the case of amidations was added under ice cooling an auxiliary base (DIPEA, NMM or NEt<sub>3</sub>; 1–4 equiv) and either a combination of EDC·HCl (1.2 equiv) and HOBT (0.2–1 equiv) or HBTU alone (1.2–2 equiv). After stirring for 15 min, the corresponding amine or alcohol (1–1.2 equiv) was added to the solution under ice cooling. The reaction was allowed to warm up to rt and stirred until completion, monitored by TLC. The mixture was then washed several times with saturated ammonium chloride solution, brine, and water (2 × 50 mL per step). After separation of the phases, the combined organic phases were dried over Na<sub>2</sub>SO<sub>4</sub> and filtered. The organic solvent was removed *in vacuo*, and the crude product was purified by column chromatography or flash chromatography.

**General procedure B.** According to Seufert *et al.*,<sup>52</sup> the Boc-protection group was cleaved at rt using an excess of TFA (2–10 mL) in dry DCM (10–20 mL). After completion, monitored by TLC (usually around 24 h), the reaction was neutralized with a sat. NaHCO<sub>3</sub> solution and extracted

with DCM (3 × 50 mL). After separation of the phases, the combined organic layers were dried over Na<sub>2</sub>SO<sub>4</sub>, filtered, and the solvent was removed *in vacuo* to give the crude product, which was used in the next step without further purification.

**General procedure C.** According to Seufert *et al.*,<sup>52</sup> to a solution of the piperidine-derivative (1 equiv) in dry DCM (20 mL per 1 mmol limiting reactant), *N*-methylmorpholine (NMM) (1.5–3 equiv) or DIPEA (1.5–3 equiv) and the corresponding sulfonyl chloride (phenylmethanesulfonyl chloride or (4-fluorophenyl)methanesulfonyl chloride) (1 equiv) were added and stirred at rt. After the reaction was completed according to TLC monitoring, the organic layer was washed consecutively with 2M HCl (50 mL), water (50 mL), and sat. NaHCO<sub>3</sub> solution (50 mL). The phases were separated, and the organic phase was dried over Na<sub>2</sub>SO<sub>4</sub>. The desiccant was filtered off, the solvent was removed *in vacuo*, and the product was purified using column chromatography or flash chromatography.

**General procedure D.** According to a modified protocol by Franz *et al.*,<sup>70</sup> the allylester (1 equiv) was dissolved in dry THF (10 mL per 1 mmol limiting reactant) and cooled to 0 °C. Pd(PPh<sub>3</sub>)<sub>4</sub> (0.1 equiv) and morpholine (1.05 equiv) were added, and the mixture was stirred at 0°C for 2 h. The solvent was removed *in vacuo*, and the residue was dissolved in DCM and washed with 1M HCl (3 × 50 mL). The organic phase was filtered using Celite® to remove excess palladium. The solvent was removed *in vacuo*, and the crude oily product was purified using column chromatography or flash chromatography.

**General procedure E.** According to a modified procedure by Patil *et al.*,<sup>71</sup> the pyridine-bearing compound (1 equiv) was diluted in EtOAc (5 mL per 100 μmol), and *m*-CPBA (2 equiv) was added slowly under ice cooling. The reaction mixture was immediately allowed to warm to rt and stirred for 2–18 h until completion, indicated by TLC. Subsequently, the reaction solution was directly loaded onto silica gel and purified by flash chromatography.

**General procedure F.** For the synthesis of α-hydroxy acids, according to a modified protocol by Casalme *et al.*,<sup>72</sup> the amino acid (1 equiv) dissolved in 1M H<sub>2</sub>SO<sub>4</sub> (2 equiv) was cooled to 0 °C. A saturated aqueous solution of NaNO<sub>2</sub> (6 equiv) was added dropwise over 5 h at 0 °C. The mixture was then allowed to warm to rt and stirred overnight. Subsequently, the reaction solution was diluted with water (50 mL) and extracted with Et<sub>2</sub>O (4 × 50 mL). The combined organic phases were washed with brine (50 mL), and the solvent was removed *in vacuo*. The crude product was



used for the next step without further purification.

**General Procedure G.** According to Schwenk *et al.*,<sup>73</sup> the corresponding amino acid (1 equiv) was suspended in an excess of allyl alcohol (2 mL per 1 mmol amino acid) and cooled to 0 °C. Thionyl chloride (2–3 equiv) was added dropwise, and the mixture was slowly warmed to 60 °C. After 8 h of stirring at 60 °C, the reaction mixture was cooled to rt and stirred for another 12 h. After the addition of cooled Et<sub>2</sub>O (150 mL), the resulting precipitate was filtered through a glass filter frit, washed further with diethyl ether (2 × 150 mL), and the solvent was removed *in vacuo*. If necessary, the product was purified by flash chromatography.

**General Procedure H.** For allyl protection of the α-hydroxy acids, according to Yao *et al.*,<sup>74</sup> the corresponding α-hydroxy acid was dissolved in dry DMF (15 mL), and Na<sub>2</sub>CO<sub>3</sub> (1.2 equiv) was added. Subsequently, allyl bromide (4 equiv) was carefully added at rt, and the reaction mixture was stirred until completion, monitored by TLC. Subsequently, the reaction mixture was diluted with water (50 mL) and extracted with Et<sub>2</sub>O (4 × 50 mL). The combined organic phases were washed with 3M HCl (70 mL) and saturated NaHCO<sub>3</sub> solution (70 mL) and dried over Na<sub>2</sub>SO<sub>4</sub>. After filtration, the solvent was removed *in vacuo*. If necessary, the product was purified by flash chromatography.

### Synthesis of the *R/S*-Pipelic Ester Derivatives.

#### (*S*)-1-(Allyloxy)-3-methyl-1-oxobutan-2-yl (*R/S*)-1-(benzylsulfonyl)piperidine-2-carboxylate (*R/S,S*-15b)

*R/S,S*-15b was synthesized according to general procedure A using 160 mg (1.01 mmol) of allyl (*S*)-2-hydroxy-3-methylbutanoate, **14** (286 mg, 1.01 mmol), EDC·HCl (230 mg, 1.21 mmol), and DMAP (70 mg, 0.51 mmol) in dry DCM (40 mL). The crude oily product was purified by column chromatography (SiO<sub>2</sub>, PE/EtOAc = 10:1). Compound *R/S,S*-15b was obtained as a yellow oil (1.94 g, 4.58 mmol, 81%). R<sub>f</sub>: 0.4 (DC<sub>SIL</sub>; PE/EtOAc = 10:1; KMnO<sub>4</sub>), IR (ATR),  $\tilde{\nu}$  [cm<sup>-1</sup>]: 2952, 2871, 1737, 1455, 1337, 1188, 1125, 1072, 1058, 966, 697. Diastereomeric ratio: 45:55. <sup>1</sup>H NMR (CDCl<sub>3</sub>,  $\delta$  [ppm], J [Hz]): 7.46–7.43 (m, 2H), 7.38–7.33 (m, 3H), 5.96–5.85 (m, 1H), 5.38–5.30 (m, 1H), 5.28–5.23 (m, 1H), 4.97 (d, *J* = 4.1, 1H), 4.71–4.61 (m, 3H), 4.27 (s, 2H), 3.48–3.45 (m, 1H), 3.30–3.15 (m, 1H), 2.34–2.25 (m, 2H), 1.72–1.30 (m, 5H), 1.06–0.98 (m, 6H). <sup>1</sup>H NMR (CDCl<sub>3</sub>,  $\delta$  [ppm], J [Hz]): 7.46–7.43 (m, 2H), 7.38–7.33 (m, 3H), 5.96–5.85 (m, 1H), 5.38–5.30 (m, 1H), 5.28–5.23 (m, 1H), 4.97 (d, *J* = 4.1, 1H), 4.71–4.61 (m, 2H), 4.57–

4.55 (m, 1H), 4.24–4.22 (m, 2H), 3.48–3.45 (m, 1H), 3.30–3.15 (m, 1H), 2.34–2.25 (m, 1H), 2.18–2.14 (m, 1H), 1.72–1.30 (m, 5H), 1.06–0.98 (m, 6H).  $^{13}\text{C}$  NMR ( $\text{CDCl}_3$ ,  $\delta$  [ppm]): 171.6, 169.0, 131.5, 131.1 (2C), 129.5, 128.7 (2C), 128.6, 119.2, 77.8, 65.9, 59.1, 56.1, 43.6, 30.3, 28.1, 25.2, 20.2, 18.9, 17.2.  $^{13}\text{C}$  NMR ( $\text{CDCl}_3$ ,  $\delta$  [ppm]): 171.4, 169.0, 131.5, 131.1 (2C), 129.4, 128.7 (2C), 128.5, 119.2, 77.5, 65.9, 58.8, 55.8, 43.5, 30.3, 27.8, 25.0, 20.2, 18.9, 17.0.

**(S)-3-Methyl-1-oxo-1-((pyridin-3-ylmethyl)amino)butan-2-yl (*R/S*)-1-(benzylsulfonyl)piperidine-2-carboxylate (*R/S,S*-10b)**

In a first step, *R/S,S*-15b (300 mg, 0.71 mmol) was deprotected according to general procedure D using 60 mg of  $\text{Pd}(\text{PPh}_3)_4$  (0.05 mmol) and 70  $\mu\text{L}$  of morpholine (0.75 mmol) in dry THF (10 mL). The intermediate product was further reacted with 3-picolylamine (80  $\mu\text{L}$ , 0.85 mmol), EDC·HCl (164 mg, 0.85 mmol), and HOBt (48 mg, 0.37 mmol) in dry DCM (30 mL) according to general procedure A. Purification using column chromatography ( $\text{SiO}_2$ , PE/EtOAc = 3:1) afforded compound *R/S,S*-10b as a colorless oil (256 mg, 0.54 mmol, 76%),  $R_f$ : 0.5 ( $\text{DC}_{\text{SiO}_2}$ ; EtOAc/PE = 3:2). IR (ATR),  $\tilde{\nu}$  [ $\text{cm}^{-1}$ ]: 3360, 2965, 1739, 1672, 1536, 1455, 1334, 1199, 1125, 1058, 951, 697. Diastereomeric ratio: 47:53.  $^1\text{H}$  NMR ( $\text{CDCl}_3$ ,  $\delta$  [ppm],  $J$  [Hz]): 8.59–8.57 (m, 1H), 8.52–8.50 (m, 1H), 7.76–7.69 (m, 2H), 7.41–7.35 (m, 5H), 7.30–7.26 (m, 1H), 5.29 (d,  $J$  = 3.0, 1H), 4.47–4.43 (m, 2H), 4.28–4.26 (m, 1H), 4.22 (s, 2H), 3.40–3.35 (m, 1H), 3.13–3.06 (m, 1H), 2.43–2.31 (m, 1H), 2.19–2.17 (m, 1H), 1.64–1.25 (m, 5H), 0.97–0.92 (m, 6H).

$^1\text{H}$  NMR ( $\text{CDCl}_3$ ,  $\delta$  [ppm],  $J$  [Hz]): 8.59–8.57 (m, 1H), 8.52–8.50 (m, 1H), 7.76–7.69 (m, 2H), 7.41–7.35 (m, 5H), 7.30–7.26 (m, 1H), 5.16 (d,  $J$  = 3.0, 1H), 4.47–4.43 (m, 2H), 4.22 (s, 2H), 4.11–4.09 (m, 1H), 3.23–3.20 (m, 1H), 3.02–2.95 (m, 1H), 2.43–2.31 (m, 1H), 2.03 (m, 1H), 1.64–1.25 (m, 5H), 0.97–0.92 (m, 6H).  $^{13}\text{C}$  NMR ( $\text{CDCl}_3$ ,  $\delta$  [ppm]): 170.4, 169.4, 148.9, 148.1, 136.8, 134.5, 130.9 (2C), 129.2, 129.0 (2C), 128.9, 123.9, 79.4, 59.6, 57.2, 44.2, 40.6, 31.0, 27.0, 24.6, 20.3, 19.4, 16.9.  $^{13}\text{C}$  NMR ( $\text{CDCl}_3$ ,  $\delta$  [ppm]): 170.2, 169.2, 148.8, 147.8, 136.7, 134.5, 130.9 (2C), 129.2, 129.0 (2C), 128.8, 123.8, 79.1, 59.0, 56.1, 44.1, 40.6, 30.7, 27.0, 24.6, 19.7, 18.7, 16.6. LC/MS ( $m/z$ ) 474.35 [ $\text{M}+\text{H}$ ] $^+$ . Purity (HPLC, *both diastereomers in total*): 99.1%,  $t_R$  = 7.84 min, 8.12 min. HRMS ( $m/z$ )  $\text{C}_{24}\text{H}_{31}\text{N}_3\text{O}_5\text{S}$ , [ $\text{M}+\text{H}$ ] $^+$ , calculated 474.20572, found 474.20675, error 2.2 ppm.

**Synthesis of the Specific Pipecolic Ester Stereo Isomers.****(S)-2-Hydroxy-4-methyl-N-(pyridin-3-ylmethyl)pentanamide (S-17d)**

Compound **S-17d** was prepared according to general procedure A using 1.37 g of (*S*)-2-hydroxy-4-methoxypentanoic acid (10.4 mmol), HOBt (1.40 g, 10.4 mmol), EDC·HCl (1.98 g, 10.4 mmol), and 3-(aminomethyl)pyridine (1.16 mL, 11.4 mmol) in dry DCM (45 mL). After stirring at rt for 21 h and workup according to the general procedure, the crude oily product was purified by column chromatography (SiO<sub>2</sub>, DCM/MeOH 9:1 + 0.5% FA). Compound **S-17d** was obtained as a colorless oil (1.64 g, 7.38 mmol, 71%).  $R_f = 0.79$  (DC<sub>SIL</sub>; DCM/MeOH = 5:1), **IR** (ATR),  $\tilde{\nu}$  [cm<sup>-1</sup>]: 3319, 2049, 2955, 2870, 1645, 1522, 1427, 1277, 790, 734, 711. **<sup>1</sup>H NMR** (CDCl<sub>3</sub>,  $\delta$  [ppm],  $J$  [Hz]): 8.41–8.37 (m, 2H), 7.60 (d,  $J = 7.8$ , 1H), 7.46 (t,  $J = 6.2$ , 1H), 7.22 (dd,  $J = 7.8$ , 4.9, 1H), 4.99 (br s, 1H), 4.47 (dd,  $J = 15.2$ , 6.2, 1H), 4.36 (dd,  $J = 15.2$ , 6.2, 1H), 4.18–4.14 (m, 1H), 1.90–1.78 (m, 1H), 1.65–1.62 (m, 1H), 1.54–1.50 (m, 1H), 0.93–0.88 (m, 6H).

**<sup>13</sup>C NMR** (CDCl<sub>3</sub>,  $\delta$  [ppm]): 175.6, 148.5, 148.4, 136.1, 134.5, 123.9, 70.7, 43.8, 40.5, 24.6, 23.6, 21.4.

**2-Oxo-4-(pyridin-3-yl)-N-(pyridin-3-ylmethyl)butanamide (18)**

Potassium (*E*)-2-oxo-4-(pyridin-3-yl)but-3-enoate was synthesized following a modified procedure by Stecher *et al.*<sup>75</sup> After obtaining the free acid by reaction with hydrochloric acid, (*E*)-2-oxo-4-(pyridin-3-yl)but-3-enoic acid (3.00 g, 16.9 mmol) was hydrogenated in the microwave (450 W, 15 bar H<sub>2</sub>) in isopropanol (50 mL) under Pd/C catalysis according to Slavinska *et al.*<sup>76</sup> The obtained 2-oxo-4-(pyridin-3-yl)butanoic acid (2.00 g, 11.1 mmol) was further reacted according to general procedure A using EDC·HCl (2.55 g, 13.3 mmol), HOBt (75 mg, 0.56 mmol), and DIPEA (3.00 mL, 17.2 mmol) in dry DCM (200 mL). Purification by column chromatography (SiO<sub>2</sub>, DCM/MeOH 9:1) afforded compound **18** as a yellow oil (2.70 g, 10.0 mmol, 90%).  $R_f = 0.4$  (DC<sub>SIL</sub>; EtOAc/MeOH = 4:1), **IR** (ATR),  $\tilde{\nu}$  [cm<sup>-1</sup>]: 3183, 2362, 1676, 1425, 1095, 1028, 706. **<sup>1</sup>H NMR** (CDCl<sub>3</sub>,  $\delta$  [ppm],  $J$  [Hz]): 8.54–8.50 (m, 2H), 8.47–8.43 (m, 2H), 7.61–7.52 (m, 2H), 7.47–7.45 (m, 1H), 7.28–7.19 (m, 2H), 4.48 (m, 2H), 3.30 (t,  $J = 7.3$ , 2H), 2.94 (t,  $J = 7.3$ , 2H), **<sup>13</sup>C NMR** (CDCl<sub>3</sub>,  $\delta$  [ppm]): 197.4, 160.0, 149.9, 149.4 (2C), 147.8, 136.2, 135.8 (2C), 132.8, 123.8, 123.6, 41.0, 38.1, 26.4.

**(*R/S*)-2-Hydroxy-4-(pyridin-3-yl)-*N*-(pyridin-3-ylmethyl)butanamide (19)**

Following a protocol by Ideguchi *et al.*,<sup>77</sup> **18** (2.70 g, 10.04 mmol) was dissolved in 50 mL MeOH and NaBH<sub>4</sub> (0.75 g, 20.0 mmol) was added in portions under ice cooling. After stirring the reaction mixture at 0°C for 30 min, excess NaBH<sub>4</sub> was deactivated with 2M HCl and the solution was neutralized. The solvent was removed *in vacuo*, the residue was taken up in DCM (50 mL) and washed with water (2 × 50 mL). After separation of the phases, the solvent was removed *in vacuo* and the crude oily product was purified by column chromatography (SiO<sub>2</sub>, EtOAc/MeOH = 2:1) to give **19** as a white oily solid (660 mg, 2.43 mmol, 25%). R<sub>f</sub>: 0.4 (DC<sub>SIL</sub>; EtOAc/MeOH = 2:1), IR (ATR),  $\tilde{\nu}$  [cm<sup>-1</sup>]: 3253, 2356, 1645, 1523, 1424, 1098, 709. <sup>1</sup>H NMR (CDCl<sub>3</sub>,  $\delta$  [ppm], J [Hz]): 8.46–8.41 (m, 2H), 8.31–8.30 (m, 2H), 7.63–7.55 (m, 3H), 7.24–7.18 (m, 2H), 4.53 (dd, *J* = 15.1, 6.5, 1H), 4.39 (dd, *J* = 15.1, 5.8, 1H), 4.11 (dd, *J* = 15.1, 6.5, 1H), 2.79–2.77 (m, 2H), 2.20–2.12 (m, 1H), 2.00–1.92 (m, 1H). <sup>13</sup>C NMR (CDCl<sub>3</sub>,  $\delta$  [ppm]): 174.8, 149.5, 148.7, 148.5, 147.0, 137.3, 136.9, 136.1, 134.5, 123.9 (2C), 41.0, 38.1, 26.4.

**1-(*tert*-Butyl) 2-((*S*)-4-methyl-1-oxo-1-((pyridin-3-ylmethyl)amino)pentan-2-yl) (*S*)-piperidine-1,2-dicarboxylate (*S,S*-20d)**

*S,S*-**20d** was prepared following general procedure A using 1.36 g of *S*-**17d** (6.10 mmol), (*S*)-1-Boc-piperidine-2-carboxylic acid (1.54 g, 6.71 mmol), EDC·HCl (1.75 g, 9.15 mmol), and DMAP (0.15 g, 1.22 mmol) in dry DCM (200 mL). After stirring at rt for 4 h and workup according to general procedure A, the crude oily product was purified by column chromatography (SiO<sub>2</sub>, DCM/MeOH 15:1). Compound *S,S*-**20d** was obtained as a colorless oil (1.29 g, 2.97 mmol, 49%). IR (ATR),  $\tilde{\nu}$  [cm<sup>-1</sup>]: 3310, 2935, 2865, 1739, 1686, 1364, 1156, 1042, 930, 870, 777, 735. <sup>1</sup>H NMR (CDCl<sub>3</sub>,  $\delta$  [ppm], J [Hz]): 8.55–8.51 (m, 2H), 7.74 (br s, 1H), 7.68–7.66 (m, 1H), 7.29–7.26 (m, 1H), 5.37–5.35 (m, 1H), 4.75–4.74 (m, 1H), 4.48–4.46 (m, 1H), 4.40–4.38 (m, 1H), 3.93 (br d, *J* = 12.8, 1H), 2.75 (ddd, *J* = 12.8, 12.8, 2.5, 1H), 2.35 (br d, *J* = 13.0, 1H), 1.80–1.60 (m, 6H), 1.48–1.42 (m, 1H), 1.34 (s, 9H), 1.20–1.10 (m, 1H), 0.95–0.93 (m, 6H). <sup>13</sup>C NMR (CDCl<sub>3</sub>,  $\delta$  [ppm]): 171.2, 170.8, 157.9, 149.6, 148.9, 135.8, 134.0, 123.6, 80.9, 73.5, 54.7, 43.1, 40.9, 40.8, 28.4 (3C), 26.0, 25.0, 24.6, 23.5, 21.4, 21.0.

**1-(*tert*-Butyl) 2-((*R/S*)-1-oxo-4-(pyridin-3-yl)-1-((pyridin-3-ylmethyl)amino)butan-2-yl) (*S*)-piperidine-1,2-dicarboxylate (*S,R/S*-20f)**

*S,R/S*-20f was synthesized according to general procedure A using 660 mg of **19** (2.43 mmol), EDC·HCl (560 mg, 2.91 mmol), and DMAP (148 mg, 1.22 mmol) in dry DCM (50 mL).

After purification by column chromatography (SiO<sub>2</sub>, EtOAc/MeOH = 4:1), compound *S,R/S*-20f was obtained as a yellowish oil (700 mg, 1.45 mmol, 60%). R<sub>f</sub>: 0.5 (DC<sub>SIL</sub>; EtOAc/MeOH = 4:1).

**IR** (ATR),  $\tilde{\nu}$  [cm<sup>-1</sup>]: 3323, 2933, 2360, 1743, 1671, 1155, 719. Diastereomeric ratio: 53:47.

**<sup>1</sup>H NMR** (CDCl<sub>3</sub>,  $\delta$  [ppm], J [Hz]): 8.55–8.43 (m, 4H), 7.67–7.54 (m, 2H), 7.28–7.25 (m, 2H), 5.36–5.35 (m, 1H), 4.81–4.79 (m, 1H), 4.58–4.36 (m, 2H), 4.01–3.97 (m, 1H), 3.34–3.29 (m, 1H), 2.74–2.58 (m, 3H), 2.35–1.47 (m, 7H), 1.37–1.35 (m, 9H). **<sup>1</sup>H NMR** (CDCl<sub>3</sub>,  $\delta$  [ppm], J [Hz]): 8.55–8.43 (m, 4H), 7.67–7.54 (m, 2H), 7.28–7.25 (m, 2H), 5.27–5.25 (m, 1H), 4.58–4.36 (m, 3H), 3.68–3.64 (m, 1H), 2.84–2.82 (m, 1H), 2.74–2.58 (m, 2H), 2.35–1.47 (m, 8H), 1.37–1.35 (m, 9H). **<sup>13</sup>C NMR** (CDCl<sub>3</sub>,  $\delta$  [ppm]): 172.1, 169.7, 157.2, 149.4, 148.7, 148.4, 147.6, 136.8, 136.5, 136.2, 134.0, 123.8 (2C), 81.0, 73.7, 54.8, 43.2, 40.8, 33.6, 28.7, 28.4, 26.7, 24.5, 20.9. **<sup>13</sup>C NMR** (CDCl<sub>3</sub>,  $\delta$  [ppm]): 170.9, 169.7, 157.2, 149.2, 148.7, 148.4, 147.1, 136.8, 136.5, 136.2, 134.0, 123.8 (2C), 81.0, 73.2, 54.8, 43.2, 40.8, 32.8, 28.7, 28.4, 26.0, 24.5, 20.2.

**(*S*)-4-Methyl-1-oxo-1-((pyridin-3-ylmethyl)amino)pentan-2-yl (*S*)-1-(benzylsulfonyl)piperidine-2-carboxylate (*S,S*-10d)**

Following general procedure B, *S,S*-20d (500 mg, 1.15 mmol) was first deprotected using TFA (1.0 mL, 13.0 mmol) in dry DCM (4.0 mL) stirring at rt for 1 d. After workup according to general procedure B, 208 mg of the amine intermediate (623  $\mu$ mol) was reacted according to general procedure C using NMM (0.21 mL, 1.87 mmol) and phenylmethanesulfonyl chloride (220 mg, 1.15 mmol) in dry DCM (3 mL). After stirring at rt for 3 d, the reaction was worked up according to the general procedure and purified by flash chromatography (run 1: SiO<sub>2</sub>, 2  $\times$  12 g, A: CHCl<sub>3</sub>, B: MeOH, gradient: 0  $\rightarrow$  20% B; run 2: RP 18, A: H<sub>2</sub>O, B: MeOH, gradient: 5  $\rightarrow$  70% B). *S,S*-10d was obtained as a colorless oily solid (135 mg, 277  $\mu$ mol, 44%). R<sub>f</sub> = 0.55 (DC<sub>SIL</sub>; DCM/MeOH = 15:1). **IR** (ATR),  $\tilde{\nu}$  [cm<sup>-1</sup>]: 3354, 3061, 3036, 2952, 1739, 1671, 1536, 1335, 1175, 825, 792, 741, 697. **<sup>1</sup>H NMR** (CDCl<sub>3</sub>,  $\delta$  [ppm], J [Hz]): 8.54 (br s, 2H), 7.70–7.58 (m, 2H), 7.46–7.30 (m, 5H), 7.25 (br s, 1H), 5.41–5.31 (m, 1H), 4.49–4.35 (m, 2H), 4.20 (m, 2H),

4.08 (d,  $J = 4.3$ , 1H), 3.36 (br d,  $J = 13.0$ , 1H), 3.02 (ddd,  $J = 13.0$ , 13.0, 2.7, 1H), 2.20–2.00 (m, 2H), 1.83–1.73 (m, 2H), 1.70–1.60 (m, 2H), 1.41–1.22 (m, 2H), 1.19–0.97 (m, 1H), 0.95–0.88 (m, 6H).  $^{13}\text{C}$  NMR ( $\text{CDCl}_3$ ,  $\delta$  [ppm]): 170.4, 170.3, 149.5, 148.6, 135.8, 134.1, 130.9 (2C), 129.2, 128.9 (2C), 128.8, 123.6, 74.1, 59.5, 57.0, 44.3, 41.2, 40.7, 27.1, 25.0, 24.6, 23.3, 21.5, 20.3. LC/MS ( $m/z$ ) 488.45  $[\text{M}+\text{H}]^+$ . Purity (HPLC): 98.9%,  $t_{\text{R}} = 8.46$  min. HRMS ( $m/z$ )  $\text{C}_{25}\text{H}_{33}\text{N}_3\text{O}_5\text{S}$ ,  $[\text{M}+\text{H}]^+$ , calculated 488.22137, found 488.22235, error 2.0 ppm.

**(*R/S*)-1-Oxo-4-(pyridin-3-yl)-1-((pyridin-3-ylmethyl)amino)butan-2-yl (*S*)-1-(benzylsulfonyl)piperidine-2-carboxylate (*S,R/S*-10f)**

*S,R/S*-20f was Boc-protected following general procedure B using 2.00 mL TFA in dry DCM (20 mL). After workup according to the general procedure, the free amine intermediate (555 mg, 1.45 mmol) was further reacted according to general procedure C using phenylmethanesulfonyl chloride (276 mg, 1.45 mmol) and NMM (175  $\mu\text{L}$ , 1.60 mmol) in dry DCM (30 mL). After purification by flash chromatography ( $\text{SiO}_2$ , A: DCM, B: MeOH, gradient: 0  $\rightarrow$  30% B), *S,R/S*-10f was obtained as a colorless oil (380 mg, 0.71 mmol, 48%).  $R_f$ : 0.3 ( $\text{DC}_{\text{Sil}}$ ; EtOAc = 100%). IR (ATR),  $\tilde{\nu}$  [ $\text{cm}^{-1}$ ]: 3345, 3033, 2933, 1739, 1672, 1322, 1125, 696. Diastereomeric ratio: 53:47.  $^1\text{H}$  NMR ( $\text{CDCl}_3$ ,  $\delta$  [ppm],  $J$  [Hz]): 8.59–8.57 (m, 1H), 8.52–8.50 (m, 1H), 8.43–8.39 (m, 2H), 7.82–7.64 (m, 2H), 7.52–7.50 (m, 1H), 7.41–7.36 (m, 5H), 7.26–7.23 (m, 2H), 5.38–5.37 (m, 1H), 4.46–4.37 (m, 2H), 4.24–4.22 (m, 3H), 3.42–3.40 (m, 1H), 3.06–2.93 (m, 1H), 2.79–2.56 (m, 3H), 2.27–2.15 (m, 3H), 1.69–1.57 (m, 2H), 1.40–1.27 (m, 2H).  $^1\text{H}$  NMR ( $\text{CDCl}_3$ ,  $\delta$  [ppm],  $J$  [Hz]): 8.59–8.57 (m, 1H), 8.52–8.50 (m, 1H), 8.43–8.39 (m, 2H), 7.82–7.64 (m, 2H), 7.52–7.50 (m, 1H), 7.41–7.36 (m, 5H), 7.26–7.23 (m, 2H), 5.27–5.25 (m, 1H), 4.46–4.37 (m, 2H), 4.24–4.22 (m, 2H), 4.13–4.11 (m, 1H), 3.25–3.21 (m, 1H), 3.06–2.93 (m, 1H), 2.79–2.56 (m, 3H), 2.27–2.15 (m, 2H), 2.05–2.02 (m, 1H), 1.69–1.57 (m, 2H), 1.40–1.27 (m, 2H).  $^{13}\text{C}$  NMR ( $\text{CDCl}_3$ ,  $\delta$  [ppm]): 170.0, 169.1, 149.6, 149.4, 148.6, 147.6, 136.6, 136.3, 136.1, 134.1, 130.9 (2C), 129.3, 128.94 (2C), 128.90, 123.7 (2C), 74.5, 59.6, 57.0, 44.6, 40.8, 33.6, 28.3, 27.0, 24.6, 20.4.  $^{13}\text{C}$  NMR ( $\text{CDCl}_3$ ,  $\delta$  [ppm]): 169.8, 169.1, 149.5, 149.3, 148.5, 147.3, 136.4, 136.2, 136.1, 134.0, 130.9 (2C), 129.1, 128.86 (2C), 128.8, 123.7 (2C), 74.3, 59.0, 56.3, 44.3, 40.8, 33.1, 27.7, 26.8, 24.6, 19.8. LC/MS ( $m/z$ ) 537.10  $[\text{M}+\text{H}]^+$ , 269.20  $[\text{M}+2\text{H}]^{2+}$ . Purity (HPLC, *both diastereomers in total*):

98.8%,  $t_R = 6.52$  min, 6.59 min. HRMS (m/z)  $C_{28}H_{32}N_4O_5S$ ,  $[M+H]^+$ , calculated 537.21662, found 537.21764, error 1.9 ppm.

### Synthesis of the Pipecolic Amide Derivatives.

#### (*S*)-1-(Allyloxy)-3-(4-fluorophenyl)-1-oxopropan-2-aminium chloride (*S*-23g)

*S*-23g was synthesized following general procedure G using 2450 mg of (*S*)-2-amino-3-(4-fluorophenyl)propanoic acid (13.4 mmol), allyl alcohol (29.1 mL, 428 mmol), thionyl chloride (6.05 mL, 82.9 mmol) and additional DMF (1.0 mL, 12.9 mmol). After purification according to the general procedure, compound *S*-23g was obtained as a white oily solid (2300 mg, 8.86 mmol, 66%),  $R_f$ : 0.6 ( $DC_{SIL}$ ; DCM/MeOH = 20:1;  $KMnO_4$ ). IR (ATR),  $\tilde{\nu}$  [ $cm^{-1}$ ]: 3151, 2996, 2791, 1738, 1602, 1509, 1489, 1219, 1192, 991, 938, 822.  $^1H$  NMR ( $CD_3OD$ ,  $\delta$  [ppm], J [Hz]): 7.31–7.26 (m, 2H), 7.13–7.07 (m, 2H), 5.97–5.85 (m, 1H), 5.37–5.26 (m, 2H), 4.71–4.69 (m, 2H), 4.34–4.32 (m, 1H), 3.29–3.13 (m, 2H).  $^{13}C$  NMR ( $CD_3OD$ ,  $\delta$  [ppm], J [Hz]): 169.7, 164.9 (d,  $J_{CF} = 245.0$ , 1C), 132.4 (d,  $J_{CF} = 8.2$ , 2C), 132.4, 131.3 (d,  $J_{CF} = 3.3$ , 1C), 120.0, 116.8 (d,  $J_{CF} = 21.8$ , 2C), 68.0, 55.2, 36.6.

#### *tert*-Butyl (*S*)-2-(((*S*)-1-(allyloxy)-3-(4-fluorophenyl)-1-oxopropan-2-yl)carbamoyl)piperidine-1-carboxylate (*S,S*-24g)

*S*-23g (1950 mg, 7.51 mmol) was reacted according to general procedure A using (*S*)-1-Boc-piperidine-2-carboxylic acid (1.81 g, 7.88 mmol), HBTU (3.28 g, 8.64 mmol), and  $NEt_3$  (1.10 mL, 15.0 mmol) in dry DCM (200 mL). After stirring at rt for 4 d and workup according to general procedure A, the crude oily product was purified by column chromatography (aloxide basic III, PE/EtOAc/MeOH 90:30:4). *S,S*-24g was obtained as a colorless oil (3100 mg, 7.13 mmol, 95%).  $R_f$ : 0.66 ( $DC_{ALOX}$ ; PE/EtOAc/MeOH = 9:3:0.4;  $KMnO_4$ ). IR (ATR),  $\tilde{\nu}$  [ $cm^{-1}$ ]: 3330, 2974, 2937, 1740, 1671, 1508, 1158, 988, 928, 822.  $^1H$  NMR ( $CDCl_3$ ,  $\delta$  [ppm], J [Hz]): 7.13–7.05 (m, 2H), 7.01–6.92 (m, 2H), 6.61–6.32 (m, 1H), 5.92–5.82 (m, 1H), 5.31 (d,  $J = 17.2$ , 1H), 5.26 (d,  $J = 10.5$ , 1H), 4.87 (br s, 1H), 4.70 (br s, 1H), 4.61 (d,  $J = 5.9$ , 2H), 4.10–3.78 (m, 1H), 3.24–2.98 (m, 2H), 2.44 (br s, 1H), 2.26–2.18 (m, 1H), 1.80–1.20 (m, 5H), 1.44 (s, 9H).  $^{13}C$  NMR ( $CDCl_3$ ,  $\delta$  [ppm]): 171.1, 162.2 (d,  $^1J_{CF} = 245.5$ , 1C), 131.8, 131.5, 131.0 (d,  $^3J_{CF} = 7.8$ , 2C), 119.4, 115.6 (d,  $^2J_{CF} = 21.7$ , 2C), 80.9, 66.3, 55.5 & 54.1 (br s, 1C, *rotamers*), 53.2, 42.4 & 41.1 (br s, 1C, *rotamers*), 28.4 (3C), 25.6, 24.9, 20.5.

**Allyl-(*S*)-2-((*S*)-1-((4-fluorobenzyl)sulfonyl)piperidine-2-carboxamido)-3-(4-fluorophenyl)-propanoate (*S,S*-25g)**

*S,S*-24g (3060 mg, 7.04 mmol) was Boc-protected following general procedure B using TFA (10 mL) in dry DCM (10 mL). After stirring at rt for 3 d and workup according to the general procedure, the amine intermediate (1.80 g, 5.38 mmol) was reacted according to general procedure C, using (4-fluorophenyl)methanesulfonyl chloride (1.36 g, 6.51 mmol) and DIPEA (3.00 mL, 17.2 mmol) in dry DCM (60 mL). After stirring at rt for 3 d and workup according to the general procedure, the crude oily product was purified by flash chromatography (run 1: SiO<sub>2</sub>, A: DCM, B: MeOH, gradient: 0→30% B; run 2: RP 18, A: H<sub>2</sub>O + 0.1% FA, B: MeOH + 0.1% FA, gradient: 5→100% B). Compound *S,S*-25g was obtained as a colorless solid (448 mg, 0.95 mmol, 16%). R<sub>f</sub>: 0.44 (DC<sub>ALOX</sub>; PE/EtOAc/MeOH = 15:5:0.5; KMnO<sub>4</sub>). IR (ATR),  $\tilde{\nu}$  [cm<sup>-1</sup>]: 3356, 2939, 1739, 1667, 1603, 1508, 1327, 1215, 1180, 1147, 1061, 835, 715. Mp: 104–106 °C. <sup>1</sup>H NMR (CDCl<sub>3</sub>,  $\delta$  [ppm], J [Hz]): 7.44–7.38 (m, 2H), 7.16–7.10 (m, 2H), 7.09–7.03 (m, 2H), 7.00–6.93 (m, 2H), 6.65 (d, *J* = 7.9, 1H), 5.89 (ddt, *J* = 17.0, 10.3, 5.9, 1H), 5.32 (d, *J* = 17.0, 1H), 5.27 (d, *J* = 10.3, 1H), 4.86–4.79 (m, 1H), 4.63 (d, *J* = 5.9, 2H), 4.30 (br d, *J* = 4.2, 1H), 4.20 (br s, 2H), 3.43 (br d, *J* = 13.4, 1H), 3.23 (dd, *J* = 14.1, 5.4, 1H), 3.01 (dd, *J* = 14.1, 7.6, 1H), 2.69 (ddd, *J* = 13.4, 13.4, 2.7, 1H), 2.12 (d, *J* = 13.3, 1H), 1.63–1.54 (m, 1H), 1.48–1.18 (m, 4H). <sup>13</sup>C NMR (CDCl<sub>3</sub>,  $\delta$  [ppm]): 170.9, 170.0, 163.2 (d, <sup>1</sup>*J*<sub>CF</sub> = 248.7, 1C), 162.2 (d, <sup>1</sup>*J*<sub>CF</sub> = 245.6, 1C), 132.7 (d, <sup>3</sup>*J*<sub>CF</sub> = 8.4, 2C), 131.7 (d, <sup>4</sup>*J*<sub>CF</sub> = 3.3, 1C), 131.5, 131.0 (d, <sup>3</sup>*J*<sub>CF</sub> = 8.0, 2C), 124.9 (d, <sup>4</sup>*J*<sub>CF</sub> = 3.3, 1C), 119.4, 115.9 (d, <sup>2</sup>*J*<sub>CF</sub> = 21.7, 2C), 115.7 (d, <sup>2</sup>*J*<sub>CF</sub> = 21.4, 2C), 66.4, 58.2, 56.3, 53.6, 43.7, 37.2, 26.4, 24.8, 19.9. LC/MS (*m/z*) 507.25 [M+H]<sup>+</sup>. Purity (HPLC): 95.0%, t<sub>R</sub> = 9.58 min. HRMS (*m/z*) C<sub>25</sub>H<sub>28</sub>F<sub>2</sub>N<sub>2</sub>O<sub>5</sub>S, [M+H]<sup>+</sup>, calculated 507.17598, found 507.17627, error 0.6 ppm.

**(*S*)-1-((4-Fluorobenzyl)sulfonyl)-*N*-((*S*)-3-(4-fluorophenyl)-1-oxo-1-((pyridin-3-ylmethyl)amino)propan-2-yl)piperidine-2-carboxamide (*S,S*-21g)**

*S,S*-25g (375 mg, 740  $\mu$ mol) was allyl-protected according to general procedure D using Pd(PPh<sub>3</sub>)<sub>4</sub> (86 mg, 74  $\mu$ mol) and morpholine (70  $\mu$ L, 0.80 mmol) in dry THF (30 mL). After stirring at rt for 21 h, the reaction mixture was worked up according to the general procedure. The crude oily intermediate product was purified by flash chromatography (SiO<sub>2</sub>, A: PE, B: EtOAc/MeOH 9:1 + 0.1% FA, gradient: 0→100% B) to obtain the carboxylic acid intermediate



as a colorless solid (290 mg, 622  $\mu\text{mol}$ , 84%). Subsequently, the intermediate product (277 mg, 590  $\mu\text{mol}$ ) was reacted according to general procedure A using HBTU (262 mg, 690  $\mu\text{mol}$ ), 3-picolylamine (90  $\mu\text{L}$ , 0.88 mmol), and DIPEA (0.21 mL, 1.21 mmol) in dry DCM (30 mL). After stirring at rt for 4 d and workup according to the general procedure, the crude oily product was purified by flash chromatography (RP 18, A:  $\text{H}_2\text{O}$  + 0.2% FA, B: MeOH + 0.2% FA, gradient: 5  $\rightarrow$  100% B). Compound *S,S*-**21g** was obtained as a colorless solid (205 mg, 0.37 mmol, 62%).  $R_f$ : 0.56 ( $\text{DC}_{\text{SIL}}$ ; DCM/MeOH = 10:1). **IR** (ATR),  $\tilde{\nu}$  [ $\text{cm}^{-1}$ ]: 3290, 3068, 2941, 1650, 1603, 1508, 1326, 1220, 1183, 1126, 839, 773, 711. **Mp**: 78  $^\circ\text{C}$ .  **$^1\text{H}$  NMR** ( $\text{CDCl}_3$ ,  $\delta$  [ppm],  $J$  [Hz]): 8.55–8.44 (m, 2H), 7.56–7.52 (m, 1H), 7.38–7.32 (m, 2H), 7.26–7.21 (m, 1H), 7.16–7.02 (m, 5H), 6.94–6.80 (m, 3H), 4.75–4.66 (m, 1H), 4.45–4.30 (m, 2H), 4.22–4.11 (m, 3H), 3.34 (br d,  $J$  = 13.5, 1H), 3.20 (dd,  $J$  = 14.2, 5.9, 1H), 2.97 (dd,  $J$  = 14.2, 8.6, 1H), 2.58 (ddd,  $J$  = 13.5, 13.5, 2.9, 1H), 2.07 (br d,  $J$  = 13.9, 1H), 1.54–1.44 (m, 1H), 1.43–1.35 (m, 1H), 1.33–1.22 (m, 1H), 1.20–1.09 (m, 1H), 1.09–0.96 (m, 1H).  **$^{13}\text{C}$  NMR** ( $\text{CDCl}_3$ ,  $\delta$  [ppm]): 170.6, 170.4, 163.3 (d,  $^1J_{\text{CF}}$  = 249.3, 1C), 162.1 (d,  $^1J_{\text{CF}}$  = 245.8, 1C), 149.4, 149.0, 135.7, 133.6, 132.6 (d,  $^3J_{\text{CF}}$  = 8.3, 2C), 132.3 (d,  $^4J_{\text{CF}}$  = 3.2, 1C), 130.8 (d,  $^3J_{\text{CF}}$  = 7.9, 2C), 124.4 (d,  $^4J_{\text{CF}}$  = 3.4, 1C), 123.7, 116.1 (d,  $^2J_{\text{CF}}$  = 21.8, 2C), 115.8 (d,  $^2J_{\text{CF}}$  = 21.3, 2C), 57.9, 57.0, 54.6, 43.8, 41.2, 36.9, 25.9, 24.5, 19.6. **LC/MS** ( $m/z$ ) 557.45 [ $\text{M}+\text{H}$ ] $^+$ . **Purity** (HPLC): 97.0%,  $t_R$  = 8.10 min, **HRMS**  $\text{C}_{28}\text{H}_{30}\text{F}_2\text{N}_4\text{O}_4\text{S}$ , [ $\text{M}+\text{H}$ ] $^+$ , calculated 557.20286, found 557.20306, error: 0.4 ppm.

**3-(((*S*)-2-(((*S*)-1-((4-Fluorobenzyl)sulfonyl)piperidine-2-carboxamido)-3-(4-fluorophenyl)-propanamido)methyl)pyridine 1-oxide (*S,S*-**22g**)**

*S,S*-**21g** (10 mg, 18  $\mu\text{mol}$ ) was reacted according to general procedure E using 6.00 mg of *m*-CPBA (34.8  $\mu\text{mol}$ ) in 4 mL of EtOAc. After stirring overnight, the reaction mixture was loaded directly onto silica gel and purified by flash chromatography ( $\text{SiO}_2$ , 2  $\cdot$  4 g, A: DCM, B: MeOH, gradient: 0  $\rightarrow$  30% B). Compound *S,S*-**22g** was obtained as a colorless solid (6.0 mg, 11  $\mu\text{mol}$ , 58%).  $R_f$ : 0.48 ( $\text{DC}_{\text{SIL}}$ ; DCM/MeOH = 9:1). **IR** (ATR),  $\tilde{\nu}$  [ $\text{cm}^{-1}$ ]: 3292, 3073, 2968, 1656, 1508, 1335, 1222, 1183, 1157, 841, 817, 774. **Mp**: 98  $^\circ\text{C}$ .  **$^1\text{H}$  NMR** ( $\text{CD}_3\text{OD}$ ,  $\delta$  [ppm],  $J$  [Hz]): 8.26 (br s, 1H), 8.21 (d,  $J$  = 6.0, 1H), 7.48–7.39 (m, 4H), 7.27–7.21 (m, 2H), 7.13–7.06 (m, 2H), 7.02–6.95 (m, 2H), 4.62–4.56 (m, 1H), 4.36–4.18 (m, 5H), 3.47–3.42 (m, 1H), 3.20 (ddd,  $J$  = 12.7, 12.7, 2.5, 1H), 3.15–2.92 (m, 2H), 2.03 (br d,  $J$  = 13.7, 1H), 1.65–1.47 (m, 3H), 1.40–1.19 (m, 2H).  **$^{13}\text{C}$  NMR** ( $\text{CD}_3\text{OD}$ ,  $\delta$  [ppm],  $J$  [Hz]): 173.6, 173.3, 164.35 (d,  $^1J_{\text{CF}}$  = 246.2, 1C), 163.29

(d,  $^1J_{CF} = 243.8$ , 1C), 140.6, 139.5, 139.0, 134.14 (d,  $^3J_{CF} = 8.3$ , 2C), 134.14 (d,  $^4J_{CF} = 3.4$ , 1C), 132.1 (d,  $^3J_{CF} = 8.0$ , 2C), 130.1, 127.7, 127.0 (d,  $^4J_{CF} = 3.3$ , 1C), 116.26 (d,  $^2J_{CF} = 21.9$ , 2C), 116.22 (d,  $^2J_{CF} = 21.5$ , 2C), 58.0, 57.1, 56.3, 44.7, 40.9, 37.8, 28.6, 25.8, 20.6. LC/MS (m/z) 573.10 [M+H]<sup>+</sup>. Purity (HPLC): 97.4%,  $t_R = 9.00$  min, HRMS (m/z) C<sub>28</sub>H<sub>30</sub>F<sub>2</sub>N<sub>4</sub>O<sub>5</sub>S, [M+H]<sup>+</sup>, calculated 573.19777, found 573.19779, error: 0.0 ppm.

***tert*-Butyl (*S*)-(1-oxo-3-(4-(prop-2-yn-1-yloxy)phenyl)-1-((pyridin-3-ylmethyl)amino)-propan-2-yl)carbamate (*S*-26h)**

(*S*)-2-((*tert*-Butoxycarbonyl)amino)-3-(4-(prop-2-yn-1-yloxy)phenyl)propanoic acid (639 mg, 2.00 mmol) was amide-coupled to 3-picolylamine (244  $\mu$ L, 2.40 mmol) according to general procedure A using DIPEA (696  $\mu$ L, 4.00 mmol) and HBTU (833 g, 2.20 mmol) in dry DCM (80 mL). After stirring at rt for 5 d, the reaction was worked up according to the general procedure and purified by column chromatography (aloxide basic III, Cy/EtOAc/MeOH = 10:10:1) and flash chromatography (RP 18, A: H<sub>2</sub>O, B: MeOH, gradient: 5  $\rightarrow$  100% B). Compound *S*-26h was obtained as a white solid (640 mg, 1.56 mmol, 78%). R<sub>f</sub>: 0.56 (DC<sub>SIL</sub>; DCM/MeOH = 10:1). Mp: 164 °C. IR (ATR),  $\tilde{\nu}$  [cm<sup>-1</sup>]: 3303, 3030, 2989, 1680, 1666, 1507, 1288, 827, 811, 751, 715. <sup>1</sup>H NMR (CD<sub>3</sub>OD,  $\delta$  [ppm], J [Hz]): 8.50–8.36 (m, 2H), 7.58 (d,  $J = 7.5$ , 1H), 7.40–7.31 (m, 1H), 7.12 (d,  $J = 8.5$ , 2H), 6.87 (d,  $J = 8.5$ , 2H), 4.70–4.68 (m, 2H), 4.40 (d,  $J = 15.3$ , 1H), 4.31 (d,  $J = 15.2$ , 1H), 4.24 (t,  $J = 7.2$ , 1H), 2.98 (dd,  $J = 13.7, 7.0$ , 1H), 2.92 (t,  $J = 2.4$ , 1H), 2.82 (dd,  $J = 13.6, 8.0$ , 1H), 1.39 (br s, 9H). <sup>13</sup>C NMR (CD<sub>3</sub>OD,  $\delta$  [ppm]): 174.5, 158.1, 158.0, 149.4, 148.7, 137.6, 136.4, 131.4 (2C), 131.2, 125.2, 116.0 (2C), 80.7, 79.9, 76.7, 57.8, 56.6, 41.4, 38.4, 28.7.

***tert*-Butyl (*S*)-2-(((*S*)-1-oxo-3-(4-(prop-2-yn-1-yloxy)phenyl)-1-((pyridin-3-ylmethyl)amino)propan-2-yl)carbamoyl)piperidine-1-carboxylate (*S,S*-27h)**

*S*-26h (310 mg, 757  $\mu$ mol) was Boc-deprotected according to general procedure B using TFA (9.00 mL) and dry DCM (10 mL). After stirring at rt for 1 d, the reaction was worked up according to the general procedure. The intermediate product (318 mg, 757  $\mu$ mol) was amide-coupled to (*S*)-1-Boc-piperidine-2-carboxylic acid (196 mg, 856  $\mu$ mol) following general procedure A using HBTU (282 mg, 744  $\mu$ mol) and DIPEA (1.04 mL, 5.95 mmol) in dry DCM (40 mL). After stirring at rt for 2 d and workup according to the general procedure, the crude oily product was

purified by flash chromatography (aloxide (neutral), A: DCM, B: MeOH, gradient: 0→30% B). Compound *S,S*-**27h** was obtained as a slightly yellowish solid (380 mg, 730  $\mu\text{mol}$ , 98%).  $R_f$ : 0.50 ( $\text{DC}_{\text{SIL}}$ ; DCM/MeOH = 10:1). Mp: 77 °C. **IR** (ATR),  $\tilde{\nu}$  [ $\text{cm}^{-1}$ ]: 3286, 3061, 2968, 2940, 1648, 1509, 869, 785, 773, 707.  **$^1\text{H}$  NMR** ( $\text{CDCl}_3$ ,  $\delta$  [ppm],  $J$  [Hz]): 8.48 (dd,  $J = 4.8, 1.8, 1\text{H}$ ), 8.43 (d,  $J = 1.8, 1\text{H}$ ), 7.46 (d,  $J = 7.8, 1\text{H}$ ), 7.21 (dd,  $J = 7.8, 4.8, 1\text{H}$ ), 7.11–7.05 (m, 2H), 6.89–6.84 (m, 2H), 6.67 (br s, 1H), 6.47–6.43 (m, 1H), 4.71–4.65 (m, 1H), 4.67–4.63 (m, 2H), 4.63–4.59 (m, 1H), 4.44–4.30 (m, 2H), 3.82 (br s, 1H), 3.06 (d,  $J = 7.1, 2\text{H}$ ), 2.50 (t,  $J = 2.4, 1\text{H}$ ), 2.43 (br s, 1H), 2.18–2.10 (m, 1H), 1.59–1.43 (m, 3H), 1.40 (s, 9H), 1.37–1.22 (m, 2H).  **$^{13}\text{C}$  NMR** ( $\text{CDCl}_3$ ,  $\delta$  [ppm]): 171.8, 170.9, 156.8, 155.7, 149.4, 149.0, 135.6, 133.7, 130.4 (2C), 129.4, 123.7, 115.4 (2C), 81.0, 78.6, 75.7, 56.0, 55.2, 54.4, 41.1 (2C), 37.1, 28.4 (3C), 25.5, 24.7, 20.4.

**(*S*)-1-(Benzylsulfonyl)-*N*-((*S*)-1-oxo-3-(4-(prop-2-yn-1-yloxy)phenyl)-1-(pyridin-3-ylmethyl)amino)propan-2-yl)piperidine-2-carboxamide (*S,S*-**21h**)**

*S,S*-**27h** (450 mg, 864  $\mu\text{mol}$ ) was Boc-protected according to General Procedure B using TFA (5 mL) and dry DCM (5 mL). After stirring at rt for 1 d, workup was conducted according to the general procedure. The intermediate product (363 mg, 863  $\mu\text{mol}$ ) was subsequently treated with phenylmethanesulfonyl chloride (330 mg, 1.73 mmol) and NMM (960  $\mu\text{L}$ , 8.63 mmol) in dry DCM (45 mL) according to general procedure C. After stirring at rt for 5 d, the reaction was worked up according to the general procedure. Purification by flash chromatography (RP 18, A:  $\text{H}_2\text{O}$ , B: MeOH, gradient: 40→80% B) afforded *S,S*-**21h** as a white solid (240 mg, 418  $\mu\text{mol}$ , 48%),  $R_f$ : 0.51 ( $\text{DC}_{\text{SIL}}$ ; DCM/MeOH = 9:1). Mp: 123 °C. **IR** (ATR),  $\tilde{\nu}$  [ $\text{cm}^{-1}$ ]: 3289, 2938, 2120, 1650, 1508, 1350, 1322, 1180, 823, 780, 739.  **$^1\text{H}$  NMR** ( $\text{CDCl}_3$ ,  $\delta$  [ppm],  $J$  [Hz]): 8.51 (dd,  $J = 4.8, 1.7, 1\text{H}$ ), 8.48 (d,  $J = 1.7, 1\text{H}$ ), 7.53–7.49 (m, 1H), 7.40–7.35 (m, 5H), 7.25–7.21 (m, 1H), 7.10–7.06 (m, 2H), 6.89–6.83 (m, 2H), 6.71 (t,  $J = 5.8, 1\text{H}$ ), 6.57 (d,  $J = 8.3, 1\text{H}$ ), 4.73–4.65 (m, 1H), 4.65–4.60 (m, 2H), 4.45–4.33 (m, 2H), 4.22 (s, 2H), 4.07 (br d,  $J = 4.3, 1\text{H}$ ), 3.32 (br d,  $J = 13.6, 1\text{H}$ ), 3.22 (dd,  $J = 14.4, 5.9, 1\text{H}$ ), 2.96 (dd,  $J = 14.4, 8.9, 1\text{H}$ ), 2.48–2.38 (m, 2H), 2.10 (br d,  $J = 13.8, 1\text{H}$ ), 1.50–0.87 (m, 5H).  **$^{13}\text{C}$  NMR** ( $\text{CDCl}_3$ ,  $\delta$  [ppm]): 170.8, 170.5, 156.8, 149.4, 149.0, 135.6, 133.7, 130.8 (2C), 130.3 (2C), 129.5, 129.3, 129.0 (2C), 128.6, 123.7, 115.4 (2C), 78.6, 75.6, 58.8, 57.1, 56.0, 54.6, 43.8, 41.1, 36.7, 25.6, 24.3, 19.6. LC/MS ( $m/z$ ) 575.20 [ $\text{M}+\text{H}$ ] $^+$ . Purity (HPLC): 99.2%,  $t_R = 8.18$  min. HRMS ( $m/z$ )  $\text{C}_{31}\text{H}_{34}\text{N}_4\text{O}_5\text{S}$ , [ $\text{M}+\text{H}$ ] $^+$ , calculated 575.23227, found 575.23197, error: 0.5 ppm.

### Fluorescence Polarization Competition Assay for Inhibitor Screening against BpMip

$K_i$  values for the Mip inhibitors with BpMip were determined using fluorescence polarization, according to similar procedures by Kozany *et al.*<sup>78</sup> and Scheuplein *et al.*<sup>55</sup> Briefly, binding is measured by displacement of the fluorescent tracer from the tracer-protein complex by the respective inhibitor under investigation. Tracer **29** (see SI) was diluted in DMSO to obtain a stock solution of 40  $\mu\text{M}$ . All further dilution steps were performed with the assay buffer (20 mM HEPES, 0.002% TritonX-100, 13.4 mM KCl) to a final concentration of 10 nM, which is four times higher than the final concentration in the well. All compounds were also prepared as a stock DMSO solution, followed by three different dilution series on three different days. Subsequently, 15  $\mu\text{L}$  each of the compound and tracer were mixed with 30  $\mu\text{L}$  of BpMip (stock solution 0.5  $\mu\text{M}$ ) into black 384-well plates (Greiner Bio-One, Kremsmünster, Austria, #781900) to obtain final concentrations of 2.5 nM of the fluorescent ligand and 250 nM of BpMip in the well. To ensure a state of equilibrium, incubation was performed for 30 minutes in the dark at room temperature. Finally, fluorescence polarization was measured (Mithras LB 940, Berthold Technologies, Bad Wildbad, Germany), and the competition curves were analyzed using GraphPad Prism 8.0.1.<sup>79</sup>

### Cell Cytotoxicity Assay

Possible cytotoxicity of the Mip inhibitors was investigated by a formazan (WST-1) assay. The resulting data is given in the SI. NIH 3T3 fibroblast (CRL-1658; ATCC, Manassas, VA) and HEK 293T cells (CRL-1573, ATCC, Manassas, VA) were harvested from exponentially growing subconfluent monolayer. The cells were maintained in 75  $\text{cm}^2$  culture flasks in growth medium (DMEM high-glucose containing heat-inactivated 10% FCS and 1% P/S) at 37 °C under 5%  $\text{CO}_2$ . NIH 3T3 and HEK 293T cells were seeded in triplets using 96-well plates (NIH 3T3:  $40 \times 10^3$  cells/mL, HEK 293T:  $50 \times 10^3$  cells/mL, 100  $\mu\text{L}$  per well) and were grown for 48 h (method A), respectively 24 h (method B) at 37 °C and 5%  $\text{CO}_2$ . Dilution series of each Mip inhibitor from 2  $\mu\text{M}$  to 200  $\mu\text{M}$  (method A) or from 0.391  $\mu\text{M}$  to 200  $\mu\text{M}$  (method B) were prepared in growth medium and added (1:1 [V/V]) to the cells, leading to inhibitor concentrations of (method A) 1  $\mu\text{M}$  to 100  $\mu\text{M}$  or (method B) 0.195  $\mu\text{M}$  to 100  $\mu\text{M}$ . The final concentration of DMSO was 1% at the highest inhibitor concentration and lower at the dilutions, respectively. The cells were then incubated for 24 h at 37 °C and 5%  $\text{CO}_2$ . Untreated cells were used as control. Cell viability was

assessed using the WST-1 colorimetric assay following the manufacturer's instructions. 10  $\mu$ L WST-1 reagent was added to each well, and cells were incubated at 37 °C and 5% CO<sub>2</sub>, according to manufacturer instructions. After 1 h, 2 h, and 3 h, the absorbance of the soluble formazan product at 450 nm as well as background noise at 630 nm was determined using a SPECTRAmax 250 microplate reader (Molecular Devices, Sunnyvale, USA).

#### **Materials and Methods: Protein Purification and Protease-Coupled PPIase Enzymatic Assay**

Recombinant BpMip, NmMip, and NEIS0004 were expressed and purified as described in the Supplementary Information and by Iwasaki *et al.*<sup>8</sup> with some modifications. The PPIase assay was performed as described in the Supplementary Information and by Vivoli *et al.*<sup>80</sup> and Fischer *et al.*<sup>81</sup>

#### **Materials and Methods: Measurement of *B. pseudomallei*-Inducted Macrophage Cytotoxicity**

The cytotoxicity assays were performed as described by Begley *et al.* and Iwasaki *et al.*<sup>7, 8</sup> Briefly, RAW264.7 murine macrophages (ATCC-TIBX71) were seeded into 24-well tissue culture plates and used at a density of 1x10<sup>6</sup> cells/mL in Dulbecco's modified Eagle medium (DMEM; Gibco) supplemented with 10% v/v fetal bovine serum (FBS; Gibco), 1X GlutaMAX (Gibco) and penicillin-streptomycin (10,000 U/mL; Gibco). *B. pseudomallei* K96243 overnight cultures were standardized into Leibovitz L-15 medium (L15; Gibco) supplemented with 10% v/v FBS and 1X GlutaMAX) to an absorbance at 580 nm of 0.4. A 1:10 dilution of the *B. pseudomallei* culture was treated with 50  $\mu$ M of each inhibitor or DMSO alone (vehicle control) for 1 h at 37 °C. Pre-treated *B. pseudomallei* were allowed to infect RAW264.7 murine macrophages at a multiplicity of infection (MOI) of approximately 10:1 for 30 min at 37 °C. Post-infection, the extracellular bacteria were removed, cells washed three times with phosphate buffer saline (PBS) and treated with 1 mL L15 supplemented with 1 mg/mL kanamycin for 30 min at 37 °C to kill any remaining extracellular bacteria. Infected RAW264.7 murine macrophage cells were incubated for 24 h at 37 °C in 1 mL L15 supplemented with 250  $\mu$ g/mL kanamycin with appropriate inhibitor at 50  $\mu$ M before the supernatant was tested for lactate dehydrogenase (LDH) release using the Cytotoxicity Detection Kit (Roche), following the manufacturer's instructions. All results are presented as the means of three independent experiments containing two technical repeats. Infected cells treated with DMSO (Sigma) and uninfected cells were included as controls. To express the results as the percentage of wild-type cytotoxicity, the LDH activity in test compound wells was compared to

that in wells infected with *B. pseudomallei* K96243 treated with DMSO. Spontaneous release (LDH release following incubation of uninfected cells with the corresponding inhibitor or DMSO) was subtracted from the final values to account for the presence of any off-target effects of these compounds. All statistical analyses were carried out using a Student's t-test and analyzed using GraphPad Prism v.9.0.1 from Dotmatics (Boston, Massachusetts, USA).

### **Materials and Methods: *N. meningitidis* and *N. gonorrhoeae* intracellular survival assays**

RAW264.7 murine macrophages (ATCC-TIBX71) were seeded into 96-well tissue culture plates and used at a density of  $1 \times 10^6$  cells/mL in Dulbecco's modified Eagle medium (DMEM; Gibco) supplemented with 10% v/v fetal bovine serum (FBS; Gibco) and 1X GlutaMAX (Gibco)). *N. meningitidis* serogroup B or *N. gonorrhoeae* FA19 were harvested from a 14 h agar plate culture, resuspended in DMEM and normalized to an optical density of 0.4 (550 nm). For each experiment, the actual number of bacteria was confirmed by viable count of the inoculum. Bacteria were pre-incubated with 50  $\mu$ M of either DMSO or relevant inhibitors for 1 h prior to infection of RAW274.7 murine macrophages at a multiplicity of infection of 100 whereby they were incubated for 6 h and incubated in 5% CO<sub>2</sub> at 37 °C. Following 6 h of incubation, extracellular bacteria were then removed by washing the monolayers once with PBS and then the addition of DMEM with 100  $\mu$ g/mL gentamicin (Agri-Bio) for 1 h. The monolayers were washed once again with PBS to remove gentamycin, and macrophage cells were lysed with 1% (w/v) saponin (Sigma) in DMEM to release the intracellular bacteria. The number of intracellular bacteria was enumerated by viable count. Three biological replicates containing two technical repeats were performed for each strain. All statistical analyses were carried out using the Student's t-test using Graphpad Prism v.9.0.1.

### **Author Information**

#### **Corresponding Authors**

M.S-T.: email, [mitali.sarkar-tyson@uwa.edu.au](mailto:mitali.sarkar-tyson@uwa.edu.au)

U.H.: email, [ulrike.holzgrabe@uni-wuerzburg.de](mailto:ulrike.holzgrabe@uni-wuerzburg.de)

## ORCID

Nicolas J. Scheuplein: 0000-0003-3261-7964

Nicole M. Bzdyl: 0000-0003-2204-1172

Theresa Lohr: 0000-0001-6473-0983

Ulrike Holzgrabe: 0000-0002-0364-7278

Mitali Sarkar-Tyson: 0000-0002-6764-8499

## Notes

The authors declare no competing financial interest.

## Acknowledgments

Lukas Kirchner is thanked for performing the HRMS measurements. Marcus Gutmann and Simon Reiländer helped to perform the cytotoxicity measurements against HEK and NIH cells. Markus Zehe is thanked for the preparation of **Figure 2**. This work was supported by the North Atlantic Treaty Organization (NATO, Brussels, Belgium; grant SPS 984835), the German Research Foundation (DFG, Bonn, Germany; grant SFB 630), and The Federal Ministry of Education and Research (BMBF, Germany, Berlin; project number 16GW0212 “iMIP”) given to UH. This paper includes research that was supported by DMTC Limited (Australia). The authors have prepared this paper in accordance with the intellectual property rights granted to partners from the original DMTC project.

## Author Contribution

‡ N.J.S. is the first author, and \* U.H. and \* M.S.T. are equal corresponding authors. N.J.S. carried out the organic synthesis, solubility studies, and cytotoxicity assay and wrote most of the manuscript. N.M.B. performed the protease-coupled PPIase assay, the cell-based assays, and protein purification and wrote the corresponding methods. T.L. performed the FPA with BpMip and wrote the corresponding method, also did the cytotoxicity assay, and helped with proofreading the manuscript. E.A.K. supported the *in vitro* testing. A.H. supported the organic synthesis. U.H. corrected the manuscript. M.S.T. also corrected the manuscript.

## Abbreviations Used

AMR, antimicrobial resistance; ATR, attenuated total reflectance; AV, anti-virulence; Boc,

*tert*-butyloxycarbonyl; B.ps., *Burkholderia pseudomallei*; BpMip, *Burkholderia pseudomallei* Mip; C18, octyldecylsilane; config. pip., stereochemical configuration of the pipercolic acid; DAD, diode array detection; DIPEA, *N,N*-diisopropylethylamine; EDC·HCl, 1-Ethyl-3-(3-dimethylaminopropyl)carbodiimide hydrochloride; ELSD, evaporative light scattering detector; ESCs, extended-spectrum cephalosporins; EtOAc, ethyl acetate; FKBP, FK506 binding protein; FPA, fluorescence polarization assay; HBTU, hexafluorophosphate benzotriazole tetramethyl uronium; HOBt, 1-hydroxybenzotriazole; IMD, invasive meningococcal disease; inh., inhibitor;  $K_D$ , dissociation constant; kDa, kilodaltons; LDH, lactose dehydrogenase; Lp, *Legionella pneumophila*; MIP, macrophage infectivity potentiator; mTOR, mammalian target of rapamycin; NB, no binding; ND, not determined; NEt<sub>3</sub>, triethylamine; Ng, *N. gonorrhoeae*; Nm, *Neisseria meningitidis*; NMM, *N*-methylmorpholine; Pd, palladium; PMNs, polymorphonuclear neutrophils; PPIase, peptidylprolyl *cis-trans* isomerase; SD, standard deviation; STI, sexually transmitted infection; Tfp, type IV pili.

### Supplementary Material

The supplementary material includes the organic synthesis and analytical data of all synthesized compounds, a protocol of protein purification and the enzymatic protease-coupled PPIase assay, as well as detailed solubility data, including the protocol and cytotoxicity data of a selection of compounds. Data including SD of *in vitro* tests performed, HPLC purity data, and <sup>1</sup>H NMR spectra of the tested compounds are also given.



#### 4.5 References

- (1) Reardon, S. WHO warns against 'post-antibiotic' era. *Nature* **2014**. DOI: 10.1038/nature.2014.15135.
- (2) Kwon, J. H.; Powderly, W. G. The post-antibiotic era is here. *Science* **2021**, *373* (6554), 471. DOI: 10.1126/science.abl5997.
- (3) Lakemeyer, M.; Zhao, W.; Mandl, F. A.; Hammann, P.; Sieber, S. A. Thinking Outside the Box- Novel Antibacterials To Tackle the Resistance Crisis. *Angew. Chem. Int. Ed. Engl.* **2018**, *57* (44), 14440-14475. DOI: 10.1002/anie.201804971.
- (4) Richter, M. F.; Drown, B. S.; Riley, A. P.; Garcia, A.; Shirai, T.; Svec, R. L.; Hergenrother, P. J. Predictive compound accumulation rules yield a broad-spectrum antibiotic. *Nature* **2017**, *545* (7654), 299-304. DOI: 10.1038/nature22308.
- (5) Lim, K. Y. L.; Mullally, C. A.; Haese, E. C.; Kibble, E. A.; McCluskey, N. R.; Mikucki, E. C.; Thai, V. C.; Stubbs, K. A.; Sarkar-Tyson, M.; Kahler, C. M. Anti-Virulence Therapeutic Approaches for *Neisseria gonorrhoeae*. *Antibiotics* **2021**, *10* (2). DOI: 10.3390/antibiotics10020103.
- (6) Juli, C.; Sippel, M.; Jäger, J.; Thiele, A.; Weiwad, M.; Schweimer, K.; Rösch, P.; Steinert, M.; Sottriffer, C. A.; Holzgrabe, U. Pipecolic acid derivatives as small-molecule inhibitors of the *Legionella* MIP protein. *J. Med. Chem.* **2011**, *54* (1), 277-283. DOI: 10.1021/jm101156y.
- (7) Begley, D. W.; Fox, D., 3rd; Jenner, D.; Juli, C.; Pierce, P. G.; Abendroth, J.; Muruthi, M.; Safford, K.; Anderson, V.; Atkins, K.; Barnes, S. R.; Moen, S. O.; Raymond, A. C.; Stacy, R.; Myler, P. J.; Staker, B. L.; Harmer, N. J.; Norville, I. H.; Holzgrabe, U.; Sarkar-Tyson, M.; Edwards, T. E.; Lorimer, D. D. A structural biology approach enables the development of antimicrobials targeting bacterial immunophilins. *Antimicrob. Agents Chemother.* **2014**, *58* (3), 1458-1467. DOI: 10.1128/AAC.01875-13.
- (8) Iwasaki, J.; Lorimer, D. D.; Vivoli-Vega, M.; Kibble, E. A.; Peacock, C. S.; Abendroth, J.; Mayclin, S. J.; Dranow, D. M.; Pierce, P. G.; Fox, D.; Lewis, M.; Bzdyl, N. M.; Kristensen, S. S.; Inglis, T. J. J.; Kahler, C. M.; Bond, C. S.; Hasenkopf, A.; Seufert, F.; Schmitz, J.; Marshall, L. E.; Scott, A. E.; Norville, I. H.; Myler, P. J.; Holzgrabe, U.; Harmer, N. J.; Sarkar-Tyson, M. Broad-spectrum in vitro activity of macrophage infectivity potentiator inhibitors against Gram-negative bacteria and *Leishmania major*. *J. Antimicrob. Chemother.* **2022**, *77* (6), 1625-1634.

DOI: 10.1093/jac/dkac065.

(9) Schiene-Fischer, C.; Yu, C. Receptor accessory folding helper enzymes: the functional role of peptidyl prolylcis/transisomerases. *FEBS Lett.* **2001**, *495* (1-2), 1-6. DOI: 10.1016/s0014-5793(01)02326-2.

(10) Scheuplein, N. J.; Bzdyl, N. M.; Kibble, E. A.; Lohr, T.; Holzgrabe, U.; Sarkar-Tyson, M. Targeting Protein Folding: A Novel Approach for the Treatment of Pathogenic Bacteria. *J. Med. Chem.* **2020**, *63* (22), 13355-13388. DOI: 10.1021/acs.jmedchem.0c00911.

(11) Helbig, J.; Lück, P.; Steinert, M.; Jacobs, E.; Witt, M. Immunolocalization of the Mip protein of intracellularly and extracellularly grown *Legionella pneumophila*. *Let. Appl. Microbiol.* **2001**, *32* (2), 83-88. DOI: 10.1046/j.1472-765x.2001.00861.x.

(12) Leuzzi, R.; Serino, L.; Scarselli, M.; Savino, S.; Fontana, M. R.; Monaci, E.; Taddei, A.; Fischer, G.; Rappuoli, R.; Pizza, M. Ng-MIP, a surface-exposed lipoprotein of *Neisseria gonorrhoeae*, has a peptidyl-prolyl cis/trans isomerase (PPIase) activity and is involved in persistence in macrophages. *Mol. Microbiol.* **2005**, *58* (3), 669-681. DOI: 10.1111/j.1365-2958.2005.04859.x.

(13) Norville, I. H.; Harmer, N. J.; Harding, S. V.; Fischer, G.; Keith, K. E.; Brown, K. A.; Sarkar-Tyson, M.; Titball, R. W. A *Burkholderia pseudomallei* macrophage infectivity potentiator-like protein has rapamycin-inhibitable peptidylprolyl isomerase activity and pleiotropic effects on virulence. *Infect. Immun.* **2011**, *79* (11), 4299-4307. DOI: 10.1128/IAI.00134-11.

(14) Rasch, J.; Unal, C. M.; Klages, A.; Karsli, U.; Heinsohn, N.; Brouwer, R.; Richter, M.; Dellmann, A.; Steinert, M. Peptidyl-Prolyl-cis/trans-Isomerases Mip and PpiB of *Legionella pneumophila* Contribute to Surface Translocation, Growth at Suboptimal Temperature, and Infection. *Infect. Immun.* **2019**, *87* (1). DOI: 10.1128/IAI.00939-17.

(15) Cianciotto, N. P.; Eisenstein, B. I.; Mody, C. H.; Toews, G. B.; Engleberg, N. C. A *Legionella pneumophila* gene encoding a species-specific surface protein potentiates initiation of intracellular infection. *Infect. Immun.* **1989**, *57* (4), 1255-1262. DOI: 10.1128/iai.57.4.1255-1262.1989.

(16) Kohler, R.; Fanghanel, J.; Konig, B.; Luneberg, E.; Frosch, M.; Rahfeld, J. U.; Hilgenfeld, R.; Fischer, G.; Hacker, J.; Steinert, M. Biochemical and functional analyses of the Mip protein: influence of the N-terminal half and of peptidylprolyl isomerase activity on the virulence of *Legionella pneumophila*. *Infect. Immun.* **2003**, *71* (8), 4389-4397.

DOI: 10.1128/IAI.71.8.4389-4397.2003.

(17) Wagner, C.; Khan, A. S.; Kamphausen, T.; Schmausser, B.; Ünal, C.; Lorenz, U.; Fischer, G.; Hacker, J.; Steinert, M. Collagen binding protein Mip enables *Legionella pneumophila* to transmigrate through a barrier of NCI-H292 lung epithelial cells and extracellular matrix. *Cell. Microbiol.* **2007**, *9* (2), 450-462. DOI: 10.1111/j.1462-5822.2006.00802.x.

(18) Limmathurotsakul, D.; Golding, N.; Dance, D. A. B.; Messina, J. P.; Pigott, D. M.; Moyes, C. L.; Rolim, D. B.; Bertherat, E.; Day, N. P. J.; Peacock, S. J.; Hay, S. I. Predicted global distribution of *Burkholderia pseudomallei* and burden of melioidosis. *Nat. Microbiol.* **2016**, *1* (1). DOI: 10.1038/nmicrobiol.2015.8.

(19) Rhodes, K. A.; Schweizer, H. P. Antibiotic resistance in *Burkholderia* species. *Drug Resist. Updat.* **2016**, *28*, 82-90. DOI: 10.1016/j.drug.2016.07.003.

(20) Cheng, A. C.; Currie, B. J. Melioidosis: epidemiology, pathophysiology, and management. *Clin. Microbiol. Rev.* **2005**, *18* (2), 383-416. DOI: 10.1128/CMR.18.2.383-416.2005.

(21) Currie, B. J. Melioidosis: evolving concepts in epidemiology, pathogenesis, and treatment. *Semin. Respir. Crit. Care Med.* **2015**, *36* (1), 111-125. DOI: 10.1055/s-0034-1398389.

(22) Norville, I. H.; Breitbach, K.; Eske-Pogodda, K.; Harmer, N. J.; Sarkar-Tyson, M.; Titball, R. W.; Steinmetz, I. A novel FK-506-binding-like protein that lacks peptidyl-prolyl isomerase activity is involved in intracellular infection and in vivo virulence of *Burkholderia pseudomallei*. *Microbiology (Reading)* **2011**, *157* (Pt 9), 2629-2638. DOI: 10.1099/mic.0.049163-0.

(23) Norville, I. H.; O'Shea, K.; Sarkar-Tyson, M.; Zheng, S.; Titball, R. W.; Varani, G.; Harmer, N. J. The structure of a *Burkholderia pseudomallei* immunophilin-inhibitor complex reveals new approaches to antimicrobial development. *Biochem. J.* **2011**, *437* (3), 413-422.

(24) Ceymann, A.; Horstmann, M.; Ehses, P.; Schweimer, K.; Paschke, A. K.; Steinert, M.; Faber, C. Solution structure of the *Legionella pneumophila* Mip-rapamycin complex. *BMC Struct. Biol.* **2008**, *8*, 17. DOI: 10.1186/1472-6807-8-17.

(25) Hung, M. C.; Salim, O.; Williams, J. N.; Heckels, J. E.; Christodoulides, M. The *Neisseria meningitidis* macrophage infectivity potentiator protein induces cross-strain serum bactericidal activity and is a potential serogroup B vaccine candidate. *Infect. Immun.* **2011**, *79* (9), 3784-3791. DOI: 10.1128/IAI.05019-11.

(26) Caugant, D. A.; Maiden, M. C. Meningococcal carriage and disease--population biology and

evolution. *Vaccine* **2009**, *27 Suppl 2*, B64-70. DOI: 10.1016/j.vaccine.2009.04.061.

(27) Hollingshead, S.; Tang, C. M. An Overview of *Neisseria meningitidis*. *Methods Mol. Biol.* **2019**, *1969*, 1-16. DOI: 10.1007/978-1-4939-9202-7\_1.

(28) Liu, G.; Tang, C. M.; Exley, R. M. Non-pathogenic *Neisseria*: members of an abundant, multi-habitat, diverse genus. *Microbiology (Reading)* **2015**, *161* (7), 1297-1312. DOI: 10.1099/mic.0.000086.

(29) Sharip, A.; Sorvillo, F.; Redelings, M. D.; Mascola, L.; Wise, M.; Nguyen, D. M. Population-based analysis of meningococcal disease mortality in the United States: 1990-2002. *Pediatr. Infect. Dis. J.* **2006**, *25* (3), 191-194. DOI: 10.1097/01.inf.0000202065.03366.0c.

(30) Wu, H. M.; Harcourt, B. H.; Hatcher, C. P.; Wei, S. C.; Novak, R. T.; Wang, X.; Juni, B. A.; Glennen, A.; Boxrud, D. J.; Rainbow, J.; Schmink, S.; Mair, R. D.; Theodore, M. J.; Sander, M. A.; Miller, T. K.; Kruger, K.; Cohn, A. C.; Clark, T. A.; Messonnier, N. E.; Mayer, L. W.; Lynfield, R. Emergence of ciprofloxacin-resistant *Neisseria meningitidis* in North America. *N. Engl. J. Med.* **2009**, *360* (9), 886-892. DOI: 10.1056/NEJMoa0806414.

(31) McNamara, L. A.; Potts, C.; Blain, A. E.; Retchless, A. C.; Reese, N.; Swint, S.; Lonsway, D.; Karlsson, M.; Lunquest, K.; Sweitzer, J. J.; Wang, X.; Hariri, S.; Fox, L. M.; Antimicrobial-Resistant *Neisseria meningitidis*, T. Detection of Ciprofloxacin-Resistant, beta-Lactamase-Producing *Neisseria meningitidis* Serogroup Y Isolates - United States, 2019-2020. *Morb. Mortal. Wkly. Rep.* **2020**, *69* (24), 735-739. DOI: 10.15585/mmwr.mm6924a2.

(32) Sampson, B. A.; Gotschlich, E. C. *Neisseria meningitidis* encodes an FK506-inhibitable rotamase. *Proc. Natl. Acad. Sci. USA* **1992**, *89* (4), 1164-1168. DOI: 10.1073/pnas.89.4.1164.

(33) Echenique-Rivera, H.; Muzzi, A.; Del Tordello, E.; Seib, K. L.; Francois, P.; Rappuoli, R.; Pizza, M.; Serruto, D. Transcriptome analysis of *Neisseria meningitidis* in human whole blood and mutagenesis studies identify virulence factors involved in blood survival. *PLoS Pathog.* **2011**, *7* (5), e1002027. DOI: 10.1371/journal.ppat.1002027.

(34) Bielecka, M. K.; Devos, N.; Gilbert, M.; Hung, M. C.; Weynants, V.; Heckels, J. E.; Christodoulides, M. Recombinant protein truncation strategy for inducing bactericidal antibodies to the macrophage infectivity potentiator protein of *Neisseria meningitidis* and circumventing potential cross-reactivity with human FK506-binding proteins. *Infect. Immun.* **2015**, *83* (2), 730-742. DOI: 10.1128/IAI.01815-14.

- (35) Christodoulides, M. Update on the Neisseria Macrophage Infectivity Potentiator-Like PPIase Protein. *Front. cell. infect. microbiol.* **2022**, *12*. DOI: 10.3389/fcimb.2022.861489.
- (36) Rowley, J.; Vander Hoorn, S.; Korenromp, E.; Low, N.; Unemo, M.; Abu-Raddad, L. J.; Chico, R. M.; Smolak, A.; Newman, L.; Gottlieb, S.; Thwin, S. S.; Broutet, N.; Taylor, M. M. Chlamydia, gonorrhoea, trichomoniasis and syphilis: global prevalence and incidence estimates, 2016. *Bull. World Health Organ.* **2019**, *97* (8), 548-562P. DOI: 10.2471/BLT.18.228486.
- (37) Whelan, J.; Abbing-Karahagopian, V.; Serino, L.; Unemo, M. Gonorrhoea: a systematic review of prevalence reporting globally. *BMC Infect. Dis.* **2021**, *21* (1), 1152. DOI: 10.1186/s12879-021-06381-4.
- (38) Unemo, M.; Seifert, H. S.; Hook, E. W., 3rd; Hawkes, S.; Ndowa, F.; Dillon, J. R. Gonorrhoea. *Nat. Rev. Dis. Primers* **2019**, *5* (1), 79. DOI: 10.1038/s41572-019-0128-6.
- (39) Unemo, M.; Shafer, W. M. Antimicrobial Resistance in Neisseria gonorrhoeae in the 21st Century: Past, Evolution, and Future. *Clin. Microbiol. Rev.* **2014**, *27* (3), 587-613. DOI: 10.1128/cmr.00010-14.
- (40) Eyre, D. W.; Sanderson, N. D.; Lord, E.; Regisford-Reimmer, N.; Chau, K.; Barker, L.; Morgan, M.; Newnham, R.; Golparian, D.; Unemo, M.; Crook, D. W.; Peto, T. E.; Hughes, G.; Cole, M. J.; Fifer, H.; Edwards, A.; Andersson, M. I. Gonorrhoea treatment failure caused by a Neisseria gonorrhoeae strain with combined ceftriaxone and high-level azithromycin resistance, England, February 2018. *Eurosurveillance* **2018**, *23* (27). DOI: 10.2807/1560-7917.ES.2018.23.27.1800323.
- (41) Starnino, S.; Leuzzi, R.; Ghisetti, V.; De Francesco, M. A.; Cusini, M.; Impara, G.; Galluppi, E.; Pizza, M.; Stefanelli, P. Molecular analysis of two novel Neisseria gonorrhoeae virulent components: the macrophage infectivity potentiator and the outer membrane protein A. *New Microbiol.* **2010**, *33* (2), 167-170.
- (42) Escobar, A.; Rodas, P. I.; Acuna-Castillo, C. Macrophage-Neisseria gonorrhoeae Interactions: A Better Understanding of Pathogen Mechanisms of Immunomodulation. *Front. Immunol.* **2018**, *9*, 3044. DOI: 10.3389/fimmu.2018.03044.
- (43) Yang, D.; Rosen, M. K.; Schreiber, S. L. A composite FKBP12-FK506 surface that contacts calcineurin. *J. Am. Chem. Soc.* **1993**, *115* (2), 819-820. DOI: 10.1021/ja00055a081.
- (44) Van Duyne, G. D.; Standaert, R. F.; Karplus, P. A.; Schreiber, S. L.; Clardy, J. Atomic

structure of FKBP-FK506, an immunophilin-immunosuppressant complex. *Science* **1991**, *252* (5007), 839-842. DOI: 10.1126/science.1709302.

(45) Heitman, J.; Movva, N. R.; Hall, M. N. Targets for cell cycle arrest by the immunosuppressant rapamycin in yeast. *Science* **1991**, *253* (5022), 905-909. DOI: 10.1126/science.1715094.

(46) Sabers, C. J.; Martin, M. M.; Brunn, G. J.; Williams, J. M.; Dumont, F. J.; Wiederrecht, G.; Abraham, R. T. Isolation of a protein target of the FKBP12-rapamycin complex in mammalian cells. *J. Biol. Chem.* **1995**, *270* (2), 815-822. DOI: 10.1074/jbc.270.2.815.

(47) Fischer, G.; Bang, H.; Ludwig, B.; Mann, K.; Hacker, J. Mip protein of *Legionella pneumophila* exhibits peptidyl-prolyl-cis/trans isomerase (PPlase) activity. *Mol. Microbiol.* **1992**, *6* (10), 1375-1383. DOI: 10.1111/j.1365-2958.1992.tb00858.x.

(48) Griffith, J. P.; Kim, J. L.; Kim, E. E.; Sintchak, M. D.; Thomson, J. A.; Fitzgibbon, M. J.; Fleming, M. A.; Caron, P. R.; Hsiao, K.; Navia, M. A. X-ray structure of calcineurin inhibited by the immunophilin-immunosuppressant FKBP12-FK506 complex. *Cell* **1995**, *82* (3), 507-522. DOI: 10.1016/0092-8674(95)90439-5.

(49) Liang, J.; Choi, J.; Clardy, J. Refined structure of the FKBP12-rapamycin-FRB ternary complex at 2.2 Å resolution. *Acta Crystallogr. D Biol. Crystallogr.* **1999**, *55* (Pt 4), 736-744. DOI: 10.1107/s09074444998014747.

(50) Banaszynski, L. A.; Liu, C. W.; Wandless, T. J. Characterization of the FKBP.rapamycin.FRB ternary complex. *J. Am. Chem. Soc.* **2005**, *127* (13), 4715-4721. DOI: 10.1021/ja043277y.

(51) Pomplun, S.; Sippel, C.; Hahle, A.; Tay, D.; Shima, K.; Klages, A.; Unal, C. M.; Riess, B.; Toh, H. T.; Hansen, G.; Yoon, H. S.; Bracher, A.; Preiser, P.; Rupp, J.; Steinert, M.; Hausch, F. Chemogenomic Profiling of Human and Microbial FK506-Binding Proteins. *J. Med. Chem.* **2018**, *61* (8), 3660-3673. DOI: 10.1021/acs.jmedchem.8b00137.

(52) Seufert, F.; Kuhn, M.; Hein, M.; Weiwad, M.; Vivoli, M.; Norville, I. H.; Sarkar-Tyson, M.; Marshall, L. E.; Schweimer, K.; Bruhn, H.; Rosch, P.; Harmer, N. J.; Sotriffer, C. A.; Holzgrabe, U. Development, synthesis and structure-activity-relationships of inhibitors of the macrophage infectivity potentiator (Mip) proteins of *Legionella pneumophila* and *Burkholderia pseudomallei*. *Bioorg. Med. Chem.* **2016**, *24* (21), 5134-5147. DOI: 10.1016/j.bmc.2016.08.025.

(53) Reimer, A.; Seufert, F.; Weiwad, M.; Ebert, J.; Bzdyl, N. M.; Kahler, C. M.; Sarkar-Tyson, M.; Holzgrabe, U.; Rudel, T.; Kozjak-Pavlovic, V. Inhibitors of macrophage infectivity

potentiator-like PPIases affect neisserial and chlamydial pathogenicity. *Int. J. Antimicrob. Agents* **2016**, *48* (4), 401-408. DOI: 10.1016/j.ijantimicag.2016.06.020.

(54) Rossi, A. M.; Taylor, C. W. Analysis of protein-ligand interactions by fluorescence polarization. *Nat. Protoc.* **2011**, *6* (3), 365-387. DOI: 10.1038/nprot.2011.305.

(55) Scheuplein, N. J.; Lohr, T.; Vivoli Vega, M.; Ankrett, D.; Seufert, F.; Kirchner, L.; Harmer, N. J.; Holzgrabe, U. Fluorescent probe for the identification of potent inhibitors of the macrophage infectivity potentiator (Mip) protein of *Burkholderia pseudomallei*. Unpublished results. Work submitted for publication. **2023**.

(56) Wiersinga, W. J.; van der Poll, T.; White, N. J.; Day, N. P.; Peacock, S. J. Melioidosis: insights into the pathogenicity of *Burkholderia pseudomallei*. *Nat. Rev. Microbiol.* **2006**, *4* (4), 272-282. DOI: 10.1038/nrmicro1385.

(57) Wang, X.; Sjolinder, M.; Gao, Y.; Wan, Y.; Sjolinder, H. Immune Homeostatic Macrophages Programmed by the Bacterial Surface Protein NhhA Potentiate Nasopharyngeal Carriage of *Neisseria meningitidis*. *mBio* **2016**, *7* (1), e01670-01615. DOI: 10.1128/mBio.01670-15.

(58) S. Hünig, P. K., G. Märkl, J. Sauer. *Arbeitsmethoden in der organischen Chemie*. Lehmanns Verlag: Berlin, 2006.

(59) Lermyte, F. Chapter 1 Modern Mass Spectrometry and Advanced Fragmentation Methods. In *Advanced Fragmentation Methods in Biomolecular Mass Spectrometry: Probing Primary and Higher Order Structure with Electrons, Photons and Surfaces*, The Royal Society of Chemistry, 2021; pp 1-14.

(60) Fulmer, G. R.; Miller, A. J. M.; Sherden, N. H.; Gottlieb, H. E.; Nudelman, A.; Stoltz, B. M.; Bercaw, J. E.; Goldberg, K. I. NMR Chemical Shifts of Trace Impurities: Common Laboratory Solvents, Organics, and Gases in Deuterated Solvents Relevant to the Organometallic Chemist. *Organometallics* **2010**, *29* (9), 2176-2179. DOI: 10.1021/om100106e.

(61) Hiltensperger, G.; Hecht, N.; Kaiser, M.; Rybak, J. C.; Hoerst, A.; Dannenbauer, N.; Muller-Buschbaum, K.; Bruhn, H.; Esch, H.; Lehmann, L.; Meinel, L.; Holzgrabe, U. Quinolone Amides as Antitrypanosomal Lead Compounds with In Vivo Activity. *Antimicrob. Agents Chemother.* **2016**, *60* (8), 4442-4452. DOI: 10.1128/AAC.01757-15.

(62) Tang, G.; Cheng, C.-H. Synthesis of  $\alpha$ -Hydroxy Carboxylic Acids via a Nickel(II)-Catalyzed Hydrogen Transfer Process. *Adv. Synth. Catal.* **2011**, *353* (11-12), 1918-1922. DOI:

10.1002/adsc.201100241.

(63) Meng, Q.; Zhu, L.; Zhang, Z. Highly Enantioselective Sequential Hydrogenation of Ethyl 2-Oxo-4-arylbut-3-enoate to Ethyl 2-Hydroxy-4-arylbutyrate. *J. Org. Chem.* **2008**, *73* (18), 7209-7212. DOI: 10.1021/jo801140j.

(64) Sugai, T.; Ohta, H. A Simple Preparation of (R)-2-Hydroxy-4-phenyl-butanoic Acid. *Chem. Biol. Technol. Agric.* **1991**, *55* (1), 293-294. DOI: 10.1080/00021369.1991.10870526.

(65) Guyon, H.; Boussonniere, A.; Castanet, A. S. Readily Accessible 1,2-Amino Ether Ligands for Enantioselective Intramolecular Carbolithiation. *J. Org. Chem.* **2017**, *82* (9), 4949-4957. DOI: 10.1021/acs.joc.7b00423.

(66) Pettit, G. R.; Hu, S.; Knight, J. C.; Chapuis, J.-C. Antineoplastic Agents. 571. Total Synthesis of Bacillistatin 2. *J. Nat. Prod.* **2009**, *72* (3), 372-379. DOI: 10.1021/np800607x.

(67) Liang, B.; Portonovo, P.; Vera, M. D.; Xiao, D.; Joullie, M. M. The first total synthesis of (-)-tamandarin A. *Org. Lett.* **1999**, *1* (8), 1319-1322. DOI: 10.1021/ol9910058.

(68) Lai, Q.; Wu, M.; Wang, R.; Lai, W.; Tao, Y.; Lu, Y.; Wang, Y.; Yu, L.; Zhang, R.; Peng, Y.; Jiang, X.; Fu, Y.; Wang, X.; Zhang, Z.; Guo, C.; Liao, W.; Zhang, Y.; Kang, T.; Chen, H.; Yao, Y.; Gou, L.; Yang, J. Cryptophycin-55/52 based antibody-drug conjugates: Synthesis, efficacy, and mode of action studies. *Eur. J. Med. Chem.* **2020**, *199*, 112364. DOI: 10.1016/j.ejmech.2020.112364.

(69) Manaviazar, S.; Nockemann, P.; Hale, K. J. Total Synthesis of the GRP78-Downregulatory Macrolide (+)-Prunustatin A, the Immunosuppressant (+)-SW-163A, and a JBIR-04 Diastereoisomer That Confirms JBIR-04 Has Nonidentical Stereochemistry to (+)-Prunustatin A. *Org. Lett.* **2016**, *18* (12), 2902-2905. DOI: 10.1021/acs.orglett.6b01235.

(70) Franz, N.; Menin, L.; Klok, H.-A. A Post-Modification Strategy for the Synthesis of Uniform, Hydrophilic/Hydrophobic Patterned  $\alpha$ -Hydroxy Acid Oligomers. *Eur. J. Org. Chem.* **2009**, *2009* (31), 5390-5405. DOI: 10.1002/ejoc.200900663.

(71) Patil, V. V.; Gayakwad, E. M.; Shankarling, G. S. m-CPBA Mediated Metal Free, Rapid Oxidation of Aliphatic Amines to Oximes. *J. Org. Chem.* **2016**, *81* (3), 781-786. DOI: 10.1021/acs.joc.5b01740.

(72) Casalme, L. O.; Yamauchi, A.; Sato, A.; Petitbois, J. G.; Nogata, Y.; Yoshimura, E.; Okino, T.; Umezawa, T.; Matsuda, F. Total synthesis and biological activity of dolastatin 16. *Org. Biomol.*



- Chem.* **2017**, *15* (5), 1140-1150, 10.1039/C6OB02657E. DOI: 10.1039/C6OB02657E.
- (73) Schwenk, S.; Ronco, C.; Oberheide, A.; Arndt, H.-D. Biomimetic Synthesis of Urukthapelstatin A by Aza-Wittig Ring Contraction. *Eur. J. Org. Chem.* **2016**, *2016* (28), 4795-4799. DOI: 10.1002/ejoc.201600994.
- (74) Yao, G.; Pan, Z.; Wu, C.; Wang, W.; Fang, L.; Su, W. Efficient Synthesis and Stereochemical Revision of Coibamide A. *J. Am. Chem. Soc.* **2015**, *137* (42), 13488-13491. DOI: 10.1021/jacs.5b09286.
- (75) Stecher, E. D.; Ryder, H. F. Ionization Constants and Rates of Ester Hydrolysis in the Benzylidenepyruvic Acid Series. *J. Am. Chem. Soc.* **1952**, *74* (17), 4392-4395. DOI: 10.1021/ja01137a045.
- (76) Slavinska, V.; Sile, D.; Rozentals, G.; Balodis, Y.; Popelis, J.; Lukevics, E. Hydrogenation of the Sodium Salt of 2-Oxo-4-(3-pyridyl)butenoic Acid on Palladium Black. *Chem. Heterocycl. Compd.* **2002**, *38* (7), 801-804. DOI: 10.1023/A:1020677503143.
- (77) Ideguchi, T.; Yamada, T.; Shirahata, T.; Hirose, T.; Sugawara, A.; Kobayashi, Y.; Omura, S.; Sunazuka, T. Asymmetric total synthesis of neoxaline. *J. Am. Chem. Soc.* **2013**, *135* (34), 12568-12571. DOI: 10.1021/ja406657v.
- (78) Kozany, C.; Marz, A.; Kress, C.; Hausch, F. Fluorescent probes to characterise FK506-binding proteins. *ChemBioChem* **2009**, *10* (8), 1402-1410. DOI: 10.1002/cbic.200800806.
- (79) Wang, Z.-X. An exact mathematical expression for describing competitive binding of two different ligands to a protein molecule. *FEBS Lett.* **1995**, *360* (2), 111-114. DOI: 10.1016/0014-5793(95)00062-e.
- (80) Vivoli, M.; Renou, J.; Chevalier, A.; Norville, I. H.; Diaz, S.; Juli, C.; Atkins, H.; Holzgrabe, U.; Renard, P. Y.; Sarkar-Tyson, M.; Harmer, N. J. A miniaturized peptidyl-prolyl isomerase enzyme assay. *Anal. Biochem.* **2017**, *536*, 59-68. DOI: 10.1016/j.ab.2017.08.004.
- (81) Fischer, G.; Bang, H.; Mech, C. Detection of enzyme catalysis for cis-trans-isomerization of peptide bonds using proline-containing peptides. *Biomed. Biochim. Acta* **1984**, *43* (10), 1101-1111.

#### 4.6 SUPPORTING INFORMATION - Analysis of Structure–Activity-Relationships of Novel Inhibitors of the Macrophage Infectivity Potentiator (Mip) Proteins of *Neisseria meningitidis*, *Neisseria gonorrhoeae*, and *Burkholderia pseudomallei*

Nicolas J. Scheuplein<sup>1‡</sup>, Nicole M. Bzdyl<sup>2</sup>, Theresa Lohr<sup>1</sup>, Emily A. Kibble<sup>2,3</sup>, Anja Hasenkopf<sup>1</sup>, Mitali Sarkar-Tyson<sup>2\*</sup>, Ulrike Holzgrabe<sup>1\*</sup>

<sup>1</sup> Institute of Pharmacy and Food Chemistry, University of Würzburg, Am Hubland, 97074 Würzburg, Germany

<sup>2</sup> Marshall Centre for Infectious Diseases Research and Training, School of Biomedical Sciences, University of Western Australia, 6009, Perth, Australia

<sup>3</sup> DMTC Limited, Level 1, 620 High Street, Kew VIC 3101, Australia.

‡first author; \*equal corresponding authors

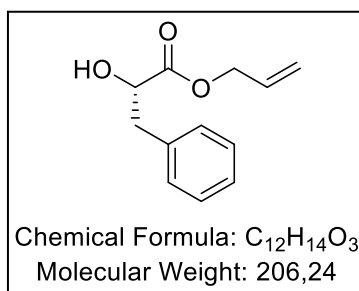
##### 4.6.1 Organic Synthesis

*General procedures and equipment can be found in the main part of the paper.*

*Additional general information which may facilitate the interpretation of the experimental data is given here.*

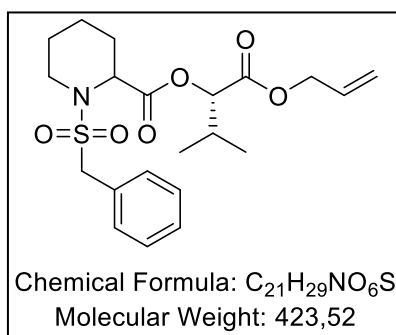
**To <sup>1</sup>H NMR.** In the <sup>1</sup>H NMR spectra, several signals corresponding to the protons of the pipercolic acid exhibit signal broadening. This phenomenon can be attributed to the quadrupolar relaxation arising from the neighboring nitrogen atom ( $I(^{14}N) = 1$ ). Consequently, as an example, the anticipated ddd coupling pattern for the equatorial H6 proton of the piperidine ring is often obscured, resulting in the appearance of a broadened doublet. To facilitate improved comparability during re-synthesis, the term "broad doublet" (br d) will be employed in the subsequent experimental part.

**To Flash chromatography.** For each specific compound and its corresponding flash chromatography method, only the initial and final percentages of the gradient are provided, in addition to the stationary and mobile phases. The detailed procedure for each compound can be described as follows: 0 – 5 min: Isocratic elution with the initial composition of mobile phase A and B; 5 – 45 min: Gradient elution transitioning from the initial to the final ratio of mobile phase A and B; 45 – 50 min: Isocratic elution with the final composition of mobile phase A and B.

4.6.1.1 Synthesis of the *R/S*-Pipecolic Ester DerivativesAllyl (*S*)-2-hydroxy-3-phenylpropanoate (*S*-13a; Lab-ID: AN232)

The allyl protection of (*S*)-2-hydroxy-3-phenylpropanoic acid (800 mg, 4.81 mmol) was carried out following general procedure H using allyl bromide (1.24 mL, 14.44 mmol) and sodium carbonate (560 mg, 5.29 mmol) in dry DMF (15 mL). After workup according to the general procedure, the crude oily product was purified by column chromatography (SiO<sub>2</sub>, PE/EtOAc = 5:1). Compound **S-13a** was obtained as a colorless oil (752 mg, 73%). R<sub>f</sub>: 0.61 (DC<sub>SIL</sub>; PE/EtOAc = 5:1; KMnO<sub>4</sub>). IR (ATR),  $\tilde{\nu}$  [cm<sup>-1</sup>]: 3451, 2935, 1725, 1454, 1176, 1090, 990, 697. <sup>1</sup>H NMR (CDCl<sub>3</sub>,  $\delta$  [ppm], J [Hz]): 7.24–7.14 (m, 5H), 5.88–5.78 (m, 1H), 5.29–5.20 (ddq, *J* = 17.2, 10.0, 1.2, 2H), 4.59 (dt, *J* = 5.9, 1.2, 2H), 4.43–4.39 (m, 1H), 3.07 (dd, *J* = 13.9, 4.5, 1H), 2.91 (dd, *J* = 13.9, 6.8, 1H), 2.65 (d, *J* = 6.2, 1H). <sup>13</sup>C NMR (CDCl<sub>3</sub>,  $\delta$  [ppm]): 173.8, 135.9, 130.9, 129.5 (2C), 128.8 (2C), 127.4, 119.2, 71.2, 66.4, 40.3.

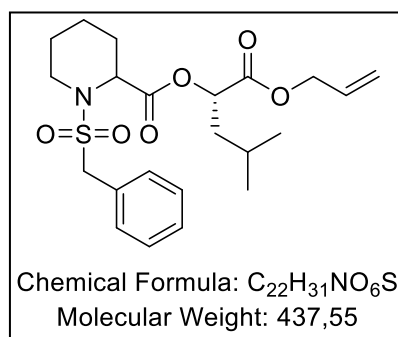
(*S*)-1-(Allyloxy)-3-methyl-1-oxobutan-2-yl (*R/S*)-1-(benzylsulfonyl)piperidine-2-carboxylate (*R/S,S*-15b; Lab-ID: AN125)



**R/S,S-15b** was synthesized according to general procedure A using 160 mg (1.01 mmol) of allyl (*S*)-2-hydroxy-3-methylbutanoate, (*R/S*)-1-(benzylsulfonyl)piperidine-2-carboxylic acid (**14**, 286 mg, 1.01 mmol), EDC·HCl (230 mg, 1.21 mmol), and DMAP (70 mg, 0.51 mmol) in dry DCM (40 mL). The crude oily product was purified by column chromatography (SiO<sub>2</sub>, PE/EtOAc

= 10:1). Compound *R/S,S-15b* was obtained as a yellow oil (1.94 g, 4.58 mmol, 81%).  $R_f$ : 0.4 (DC<sub>SIL</sub>; PE/EtOAc = 10:1; KMnO<sub>4</sub>), IR (ATR),  $\tilde{\nu}$  [cm<sup>-1</sup>]: 2952, 2871, 1737, 1455, 1337, 1188, 1125, 1072, 1058, 966, 697. Diastereomeric ratio: 45:55. <sup>1</sup>H NMR (CDCl<sub>3</sub>,  $\delta$  [ppm], J [Hz]): 7.46–7.43 (m, 2H), 7.38–7.33 (m, 3H), 5.96–5.85 (m, 1H), 5.38–5.30 (m, 1H), 5.28–5.23 (m, 1H), 4.97 (d,  $J$  = 4.1, 1H), 4.71–4.61 (m, 3H), 4.27 (s, 2H), 3.48–3.45 (m, 1H), 3.30–3.15 (m, 1H), 2.34–2.25 (m, 2H), 1.72–1.30 (m, 5H), 1.06–0.98 (m, 6H). <sup>1</sup>H NMR (CDCl<sub>3</sub>,  $\delta$  [ppm], J [Hz]): 7.46–7.43 (m, 2H), 7.38–7.33 (m, 3H), 5.96–5.85 (m, 1H), 5.38–5.30 (m, 1H), 5.28–5.23 (m, 1H), 4.97 (d,  $J$  = 4.1, 1H), 4.71–4.61 (m, 2H), 4.57–4.55 (m, 1H), 4.24–4.22 (m, 2H), 3.48–3.45 (m, 1H), 3.30–3.15 (m, 1H), 2.34–2.25 (m, 1H), 2.18–2.14 (m, 1H), 1.72–1.30 (m, 5H), 1.06–0.98 (m, 6H). <sup>13</sup>C NMR (CDCl<sub>3</sub>,  $\delta$  [ppm]): 171.6, 169.0, 131.5, 131.1 (2C), 129.5, 128.7 (2C), 128.6, 119.2, 77.8, 65.9, 59.1, 56.1, 43.6, 30.3, 28.1, 25.2, 20.2, 18.9, 17.2. <sup>13</sup>C NMR (CDCl<sub>3</sub>,  $\delta$  [ppm]): 171.4, 169.0, 131.5, 131.1 (2C), 129.4, 128.7 (2C), 128.5, 119.2, 77.5, 65.9, 58.8, 55.8, 43.5, 30.3, 27.8, 25.0, 20.2, 18.9, 17.0.

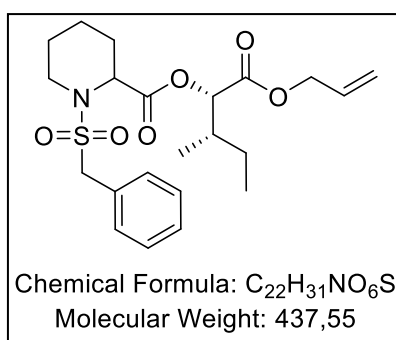
(*S*)-1-(Allyloxy)-4-methyl-1-oxopentan-2-yl (*R/S*)-1-(benzylsulfonyl)piperidine-2-carboxylate (*R/S,S-15d*; Lab-ID: AN123)



*R/S,S-15d* was synthesized according to general procedure A using allyl (*S*)-2-hydroxy-4-methylpentanoate (940 mg, 5.46 mmol), (*R/S*)-1-(benzylsulfonyl)piperidine-2-carboxylic acid (1.50 g, 5.46 mmol), EDC·HCl (1.26 g, 6.55 mmol), and DMAP (340 mg, 2.73 mmol) in dry DCM (200 mL). *R/S,S-15d* was obtained as a yellow oil (1.94 g, 4.42 mmol, 81%),  $R_f$ : 0.35 (DC<sub>SIL</sub>; PE/EtOAc = 10:1; KMnO<sub>4</sub>), IR (ATR),  $\tilde{\nu}$  [cm<sup>-1</sup>]: 2953, 2869, 1738, 1455, 1337, 1187, 1125, 1072, 1057, 966, 697. Diastereomeric ratio: 47:53. <sup>1</sup>H NMR (CDCl<sub>3</sub>,  $\delta$  [ppm], J [Hz]): 7.46–7.44 (m, 2H), 7.37–7.34 (m, 3H), 5.95–5.85 (m, 1H), 5.37–5.30 (m, 1H), 5.28–5.23 (m, 1H), 5.14–5.10 (m, 1H), 4.69–4.66 (m, 3H), 4.27 (s, 2H), 3.48–3.45 (m, 1H), 3.28–3.15 (m, 1H), 2.30–2.26 (m, 1H), 1.91–1.30 (m, 8H), 0.98–0.93 (m, 6H). <sup>1</sup>H NMR (CDCl<sub>3</sub>,  $\delta$  [ppm], J

[Hz]): 7.46–7.44 (m, 2H), 7.37–7.34 (m, 3H), 5.95–5.85 (m, 1H), 5.37–5.30 (m, 1H), 5.28–5.23 (m, 1H), 5.14–5.10 (m, 1H), 4.69–4.66 (m, 3H), 4.24–4.22 (m, 2H), 3.48–3.45 (m, 1H), 3.28–3.15 (m, 1H), 2.19–2.13 (m, 1H), 1.91–1.30 (m, 8H), 0.98–0.93 (m, 6H).  $^{13}\text{C}$  NMR ( $\text{CDCl}_3$ ,  $\delta$  [ppm]): 171.4, 170.0, 131.5, 131.1 (2C), 129.5, 128.7 (2C), 128.6, 119.2, 72.0, 66.1, 58.9, 55.9, 43.6, 39.8, 28.1, 25.2, 24.8, 23.2, 21.8, 20.3.  $^{13}\text{C}$  NMR ( $\text{CDCl}_3$ ,  $\delta$  [ppm]): 171.4, 170.0, 131.5, 131.1 (2C), 129.4, 128.6 (2C), 128.5, 119.2, 71.8, 66.1, 58.8, 55.8, 43.4, 39.8, 27.8, 25.2, 24.6, 23.2, 21.4, 20.2.

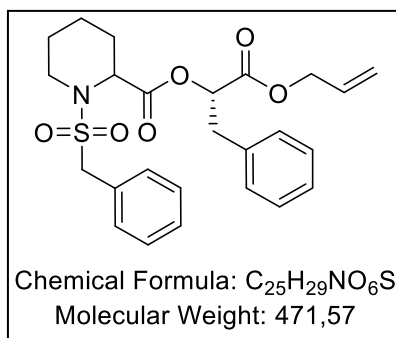
(2*S*,3*S*)-1-(Allyloxy)-3-methyl-1-oxopentan-2-yl (*R/S*)-1-(benzylsulfonyl)piperidine-2-carboxylate (*R/S,S*-15c; Lab-ID: AN124)



*R/S,S*-15c was synthesized following general procedure A using 600 mg (3.52 mmol) of allyl (2*S*,3*S*)-2-hydroxy-3-methylpentanoate, (*R/S*)-1-(benzylsulfonyl)piperidine-2-carboxylic acid (1.00 g, 3.52 mmol), EDC·HCl (810 mg, 4.22 mmol), and DMAP (215 mg, 1.76 mmol) in dry DCM (140 mL). Compound *R/S,S*-15c was obtained as yellow oil (1.49 g, 3.41 mmol, 97%).  $R_f$ : 0.45 ( $\text{DC}_{\text{SIL}}$ ; PE/EtOAc = 10:1;  $\text{KMnO}_4$ ), IR (ATR),  $\tilde{\nu}$  [ $\text{cm}^{-1}$ ]: 2953, 2871, 1737, 1455, 1337, 1188, 1171, 1073, 1057, 966, 697. Diastereomeric ratio: 50:50.  $^1\text{H}$  NMR ( $\text{CDCl}_3$ ,  $\delta$  [ppm], J [Hz]): 7.46–7.43 (m, 2H), 7.37–7.34 (m, 3H), 5.94–5.86 (m, 1H), 5.37–5.31 (m, 1H), 5.28–5.23 (m, 1H), 5.02 (d,  $J = 4.2$ , 1H), 4.66–4.62 (m, 3H), 4.27 (s, 2H), 3.48–3.45 (m, 1H), 3.30–3.15 (m, 1H), 2.29–2.26 (m, 1H), 2.08–2.01 (m, 1H), 1.72–1.25 (m, 7H), 1.03–0.99 (dd,  $J = 10.8, 6.9$ , 3H), 0.95–0.90 (td,  $J = 7.4, 3.9$ , 3H).  $^1\text{H}$  NMR ( $\text{CDCl}_3$ ,  $\delta$  [ppm], J [Hz]): 7.46–7.43 (m, 2H), 7.37–7.34 (m, 3H), 5.94–5.86 (m, 1H), 5.37–5.31 (m, 1H), 5.28–5.23 (m, 1H), 4.98 (d,  $J = 4.2$ , 1H), 4.66–4.62 (m, 2H), 4.57–4.56 (m, 1H), 4.24–4.22 (m, 2H), 3.48–3.45 (m, 1H), 3.30–3.15 (m, 1H), 2.19–2.17 (m, 1H), 2.08–2.01 (m, 1H), 1.72–1.25 (m, 7H), 1.03–0.99 (dd,  $J = 10.8, 6.9$ , 3H), 0.95–0.90 (td,  $J = 7.4, 3.9$ , 3H).  $^{13}\text{C}$  NMR ( $\text{CDCl}_3$ ,  $\delta$  [ppm]): 171.5, 169.1, 131.5, 131.1 (2C), 129.5, 128.7 (2C), 128.6, 119.2, 77.3, 66.0, 59.1, 56.1, 43.6, 36.8, 28.1, 25.2,

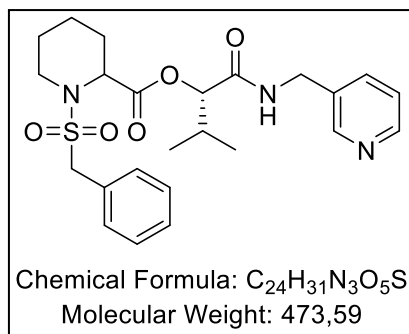
24.7, 20.2, 15.6, 11.7.  $^{13}\text{C}$  NMR ( $\text{CDCl}_3$ ,  $\delta$  [ppm]): 171.4, 169.0, 131.5, 131.0 (2C), 129.4, 128.6 (2C), 128.6, 119.2, 77.0, 66.0, 58.9, 55.8, 43.5, 36.8, 27.9, 25.1, 24.5, 20.2, 15.6, 11.7.

(*S*)-1-(Allyloxy)-1-oxo-3-phenylpropan-2-yl (*R/S*)-1-(benzylsulfonyl)piperidine-2-carboxylate  
(*R/S,S*-15a; Lab-ID: AN232II)



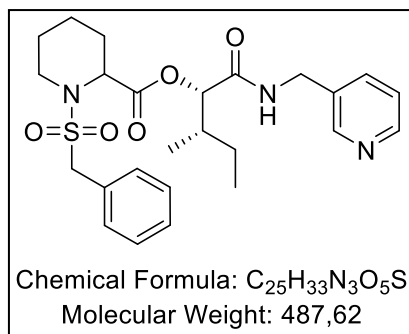
*R/S,S*-15a was synthesized following general procedure A using 220 mg (1.07 mmol) of *S*-13a, (*R/S*)-1-(benzylsulfonyl)piperidine-2-carboxylic acid (302 mg, 1.07 mmol), EDC·HCl (245 mg, 1.28 mmol), and DMAP (66 mg, 0.54 mmol) in dry DCM (40 mL). The crude oily product was purified by column chromatography ( $\text{SiO}_2$ , PE/EtOAc = 10:1). Compound *R/S,S*-15a was obtained as yellow oil (430 mg, 0.91 mmol, 85%).  $R_f$ : 0.5 ( $\text{DC}_{\text{SIL}}$ ; PE/EtOAc = 10:1;  $\text{KMnO}_4$ ). IR (ATR),  $\tilde{\nu}$  [ $\text{cm}^{-1}$ ]: 2963, 2869, 1742, 1455, 1336, 1186, 1175, 1073, 1056, 966, 697. Diastereomeric ratio: 55:45.  $^1\text{H}$  NMR ( $\text{CDCl}_3$ ,  $\delta$  [ppm], J [Hz]): 7.43–7.20 (m, 10H), 5.93–5.80 (m, 1H), 5.37–5.24 (m, 3H), 4.66–4.62 (m, 3H), 4.66–4.62 (m, 3H), 4.17–4.16 (m, 2H), 3.44–3.41 (m, 1H), 3.32–3.11 (m, 2H), 3.08–3.01 (m, 1H), 2.25–1.97 (m, 1H), 1.74–1.30 (m, 3H), 0.90–0.86 (m, 2H).  $^{13}\text{C}$  NMR ( $\text{CDCl}_3$ ,  $\delta$  [ppm]): 170.9, 168.8, 135.5, 131.4, 131.2 (2C), 129.4 (2C), 129.3, 128.7 (2C), 128.6 (2C), 128.5, 127.4, 119.2, 73.6, 66.4, 58.7, 55.7, 43.4, 37.4, 28.1, 25.2, 20.2.  $^1\text{H}$  NMR ( $\text{CDCl}_3$ ,  $\delta$  [ppm], J [Hz]): 7.43–7.20 (m, 10H), 5.93–5.80 (m, 1H), 5.37–5.24 (m, 3H), 4.66–4.62 (m, 3H), 4.66–4.62 (m, 3H), 4.17–4.16 (m, 2H), 3.44–3.41 (m, 1H), 3.32–3.11 (m, 2H), 3.08–3.01 (m, 1H), 2.25–1.97 (m, 1H), 1.74–1.30 (m, 3H), 0.90–0.86 (m, 2H).  $^{13}\text{C}$  NMR ( $\text{CDCl}_3$ ,  $\delta$  [ppm]): 170.9, 168.8, 135.5, 131.4, 131.2 (2C), 129.4 (2C), 129.3, 128.7 (2C), 128.6 (2C), 128.5, 127.4, 119.2, 73.6, 66.4, 58.7, 55.7, 43.4, 37.4, 28.1, 25.2, 20.2.

**(S)-3-Methyl-1-oxo-1-((pyridin-3-ylmethyl)amino)butan-2-yl (R/S)-1-(benzylsulfonyl)piperidine-2-carboxylate (R/S,S-10b; Lab-ID: AN131)**



In a first step, **R/S,S-15b** (300 mg, 0.71 mmol) was deprotected according to general procedure D using 60 mg of Pd(PPh<sub>3</sub>)<sub>4</sub> (0.05 mmol) and 70  $\mu$ L of morpholine (0.75 mmol) in dry THF (10 mL). The intermediate product was further reacted with 3-picolylamine (80  $\mu$ L, 0.85 mmol), EDC·HCl (164 mg, 0.85 mmol), and HOBT (48 mg, 0.37 mmol) in dry DCM (30 mL) according to general procedure A. Purification using column chromatography (SiO<sub>2</sub>, PE/EtOAc = 3:1) afforded compound **R/S,S-10b** as a colorless oil (256 mg, 0.54 mmol, 76%), R<sub>f</sub>: 0.5 (DC<sub>SIL</sub>; EtOAc/PE = 3:2). IR (ATR),  $\tilde{\nu}$  [cm<sup>-1</sup>]: 3360, 2965, 1739, 1672, 1536, 1455, 1334, 1199, 1125, 1058, 951, 697. Diastereomeric ratio: 47:53. <sup>1</sup>H NMR (CDCl<sub>3</sub>,  $\delta$  [ppm], J [Hz]): 8.59–8.57 (m, 1H), 8.52–8.50 (m, 1H), 7.76–7.69 (m, 2H), 7.41–7.35 (m, 5H), 7.30–7.26 (m, 1H), 5.29 (d, J = 3.0, 1H), 4.47–4.43 (m, 2H), 4.28–4.26 (m, 1H), 4.22 (s, 2H), 3.40–3.35 (m, 1H), 3.13–3.06 (m, 1H), 2.43–2.31 (m, 1H), 2.19–2.17 (m, 1H), 1.64–1.25 (m, 5H), 0.97–0.92 (m, 6H). <sup>1</sup>H NMR (CDCl<sub>3</sub>,  $\delta$  [ppm], J [Hz]): 8.59–8.57 (m, 1H), 8.52–8.50 (m, 1H), 7.76–7.69 (m, 2H), 7.41–7.35 (m, 5H), 7.30–7.26 (m, 1H), 5.16 (d, J = 3.0, 1H), 4.47–4.43 (m, 2H), 4.22 (s, 2H), 4.11–4.09 (m, 1H), 3.23–3.20 (m, 1H), 3.02–2.95 (m, 1H), 2.43–2.31 (m, 1H), 2.03 (m, 1H), 1.64–1.25 (m, 5H), 0.97–0.92 (m, 6H). <sup>13</sup>C NMR (CDCl<sub>3</sub>,  $\delta$  [ppm]): 170.4, 169.4, 148.9, 148.1, 136.8, 134.5, 130.9 (2C), 129.2, 129.0 (2C), 128.9, 123.9, 79.4, 59.6, 57.2, 44.2, 40.6, 31.0, 27.0, 24.6, 20.3, 19.4, 16.9. <sup>13</sup>C NMR (CDCl<sub>3</sub>,  $\delta$  [ppm]): 170.2, 169.2, 148.8, 147.8, 136.7, 134.5, 130.9 (2C), 129.2, 129.0 (2C), 128.8, 123.8, 79.1, 59.0, 56.1, 44.1, 40.6, 30.7, 27.0, 24.6, 19.7, 18.7, 16.6. LC/MS (m/z) 474.35 [M+H]<sup>+</sup>. Purity (HPLC, *both diastereomers in total*): 99.1%, t<sub>R</sub> = 7.84 min, 8.12 min. HRMS (m/z) C<sub>24</sub>H<sub>31</sub>N<sub>3</sub>O<sub>5</sub>S, [M+H]<sup>+</sup>, calculated 474.20572, found 474.20675, error 2.2 ppm.

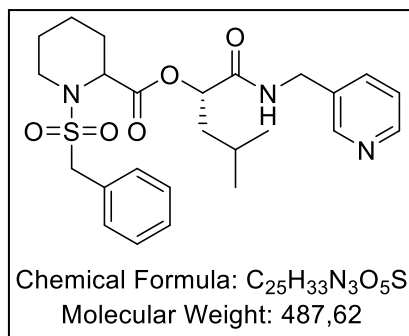
(2*S*,3*S*)-3-Methyl-1-oxo-1-((pyridin-3-ylmethyl)amino)pentan-2-yl (*R/S*)-1-(benzylsulfonyl)piperidine-2-carboxylate (*R/S,S*-10c; Lab-ID: AN132)



In a first step, *R/S,S*-15c (720 mg, 1.65 mmol) was deprotected using 150 mg of Pd(Ph<sub>3</sub>)<sub>4</sub> (150 mg, 0.08 mmol) and morpholine (150 μL, 1.73 mmol) in dry THF (20 mL) following general procedure D. The intermediate product (656 mg, 1.65 mmol) was further reacted with 3-picolylamine (208 μL, 1.98 mmol), EDC·HCl (382 mg, 1.98 mmol), and HOBT (116 mg, 0.42 mmol) in dry DCM (70 mL) according to general procedure A. Compound *R/S,S*-10c was obtained as a colorless oil (450 mg, 0.92 mmol, 56%), R<sub>f</sub>: 0.5 (DC<sub>SIL</sub>; EtOAc/PE = 3:2), IR (ATR),  $\tilde{\nu}$  [cm<sup>-1</sup>]: 3359, 2964, 2937, 2877, 1738, 1671, 1536, 1455, 1334, 1175, 1125, 1059, 917, 795, 698. Diastereomeric ratio: 51:49. <sup>1</sup>H NMR (CDCl<sub>3</sub>, δ [ppm], J [Hz]): 8.57–8.55 (m, 1H), 8.51–8.49 (m, 1H), 7.73–7.65 (m, 2H), 7.40–7.33 (m, 5H), 7.26–7.23 (m, 1H), 5.32 (d, *J* = 3.1, 1H), 4.44 (dd, *J* = 9.9, 6.0, 2H), 4.26–4.24 (m, 1H), 4.20 (s, 2H), 3.38–3.35 (m, 1H), 3.09–2.93 (m, 1H), 2.17–1.99 (m, 2H), 1.63–1.24 (m, 7H), 0.94–0.87 (m, 6H). <sup>1</sup>H NMR (CDCl<sub>3</sub>, δ [ppm], J [Hz]): 8.57–8.55 (m, 1H), 8.51–8.49 (m, 1H), 7.73–7.65 (m, 2H), 7.40–7.33 (m, 5H), 7.26–7.23 (m, 1H), 5.21 (d, *J* = 3.1, 1H), 4.44 (dd, *J* = 9.9, 6.0, 2H), 4.20 (s, 2H), 4.10–4.08 (m, 1H), 3.22–3.19 (m, 1H), 3.09–2.93 (m, 1H), 2.17–1.99 (m, 2H), 1.63–1.24 (m, 7H), 0.94–0.87 (m, 6H). <sup>13</sup>C NMR (CDCl<sub>3</sub>, δ [ppm]): 170.3, 169.2, 149.2, 148.4, 136.4, 134.3, 130.9 (2C), 129.2, 128.8 (2C), 128.7, 123.7, 79.2, 59.6, 57.1, 44.4, 40.7, 37.5, 27.1, 24.6, 24.4, 20.3, 15.8, 12.0. <sup>13</sup>C NMR (CDCl<sub>3</sub>, δ [ppm]): 170.1, 169.0, 149.2, 148.2, 136.3, 134.3, 130.9 (2C), 129.0, 128.8 (2C), 128.7, 123.6, 78.8, 59.0, 56.2, 44.1, 40.6, 37.5, 27.0, 24.6, 24.4, 19.7, 15.1, 11.7. LC/MS (m/z) 488.40 [M+H]<sup>+</sup>. Purity (HPLC, both diastereomers in total): 97.3%, t<sub>R</sub> = 8.17 min, 8.47 min. HRMS (m/z) C<sub>25</sub>H<sub>33</sub>N<sub>3</sub>O<sub>5</sub>S, [M+H]<sup>+</sup>, calculated 488.22137, found 488.22225, error 1.8 ppm.

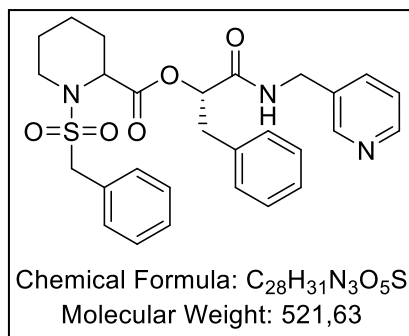


**(S)-4-methyl-1-oxo-1-((pyridin-3-ylmethyl)amino)pentan-2-yl (R/S)-1-(benzylsulfonyl)piperidine-2-carboxylate (R/S,S-10d; Lab-ID: AN133)**



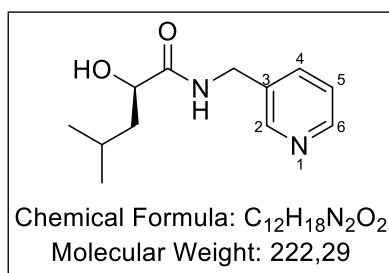
In a first step, *R/S,S-15d* (900 mg, 2.05 mmol) was deprotected using 160 mg of Pd(PPh<sub>3</sub>)<sub>4</sub> (0.14 mmol) and morpholine (200 μL, 2.15 mmol) in dry THF (20 mL) following general procedure D. The intermediate product (819 mg, 2.05 mmol) was then reacted with 3-picolylamine (273 μL, 2.48 mmol), EDC·HCl (473 mg, 2.48 mmol), and HOBT (138 mg, 1.03 mmol) in dry DCM (80 mL) according to general procedure A. Compound *R/S,S-10d* was obtained as a colorless oil (721 mg, 1.48 mmol, 72%), R<sub>f</sub>: 0.5 (DC<sub>SIL</sub>; EtOAc/PE = 3:2), IR (ATR),  $\tilde{\nu}$  [cm<sup>-1</sup>]: 3357, 2952, 2870, 1738, 1672, 1536, 1455, 1334, 1174, 1125, 1057, 921, 697. Diastereomeric ratio: 60:40. <sup>1</sup>H NMR (CDCl<sub>3</sub>, δ [ppm], J [Hz]): 8.57–8.55 (m, 1H), 8.51–8.49 (m, 1H), 7.69–7.65 (m, 2H), 7.40–7.33 (m, 5H), 7.28–7.24 (m, 1H), 5.38–5.34 (m, 1H), 4.45–4.41 (m, 2H), 4.21–4.20 (m, 3H), 3.37–3.34 (m, 1H), 3.06–2.99 (m, 1H), 2.16 (m, 1H), 1.80–1.74 (m, 2H), 1.67–1.24 (m, 5H), 1.06–1.02 (m, 1H), 0.92–0.90 (m, 6H). <sup>1</sup>H NMR (CDCl<sub>3</sub>, δ [ppm], J [Hz]): 8.57–8.55 (m, 1H), 8.51–8.49 (m, 1H), 7.69–7.65 (m, 2H), 7.40–7.33 (m, 5H), 7.28–7.24 (m, 1H), 5.27–5.24 (m, 1H), 4.45–4.41 (m, 2H), 4.21–4.20 (m, 2H), 4.11–4.09 (m, 1H), 3.21–3.19 (m, 1H), 3.06–2.99 (m, 1H), 1.99–1.97 (m, 1H), 1.80–1.74 (m, 2H), 1.67–1.24 (m, 5H), 1.06–1.02 (m, 1H), 0.92–0.90 (m, 6H). <sup>13</sup>C NMR (CDCl<sub>3</sub>, δ [ppm]): 170.5, 170.3, 149.0, 148.2, 136.5, 134.3, 130.9 (2C), 129.2, 129.0 (2C), 128.9, 123.8, 74.0, 59.5, 56.8, 44.1, 41.1, 40.7, 27.1, 24.9, 24.7, 23.1, 21.7, 20.2. <sup>13</sup>C NMR (CDCl<sub>3</sub>, δ [ppm]): 170.3, 170.2, 149.0, 148.0, 136.4, 134.3, 130.9 (2C), 129.0, 128.9 (2C), 128.8, 123.7, 73.9, 59.0, 56.1, 44.1, 40.9, 40.5, 27.1, 24.7, 24.6, 23.1, 21.5, 19.7. LC/MS (m/z) 488.45 [M+H]<sup>+</sup>. Purity (HPLC, *both diastereomers in total*): 98.4%, t<sub>R</sub> = 8.26 min, 8.47 min. HRMS (m/z) C<sub>25</sub>H<sub>33</sub>N<sub>3</sub>O<sub>5</sub>S, [M+H]<sup>+</sup>, calculated 488.22137, found 488.22150, error 0.3 ppm.

(*S*)-1-Oxo-3-phenyl-1-((pyridin-3-ylmethyl)amino)propan-2-yl-(*R/S*)-1-(benzylsulfonyl)piperidine-2-carboxylate (*R/S,S*-10a; Lab-ID: ANCH37)

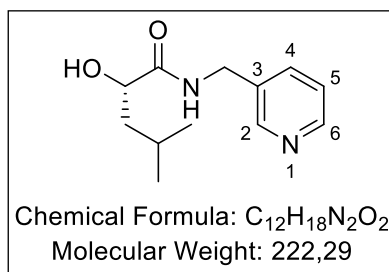


The cleavage of the allyl ester of *R/S,S*-15a (400 mg, 0.85 mmol) was carried out following general procedure D using 50 mg of Pd(PPh<sub>3</sub>)<sub>4</sub> (0.04 mmol) and morpholine (100 μL, 0.89 mmol) in dry THF (10 mL). For the subsequent amidation of the intermediate product (337 mg, 0.85 mmol) general procedure A was applied using 100 μL of 3-picolylamine (1.02 mmol), EDC·HCl (230 mg, 1.02 mmol), and HOBT (58 mg, 0.43 mmol) in dry DCM (40 mL). Purification using column chromatography (SiO<sub>2</sub>, PE/EtOAc = 3:1) afforded compound *R/S,S*-10a as a colorless oil (542 mg, 1.11 mmol, 56%), R<sub>f</sub>: 0.5 (DC<sub>SIL</sub>; EtOAc/PE = 3:2). IR (ATR),  $\tilde{\nu}$  [cm<sup>-1</sup>]: 3361, 2941, 1737, 1697, 1539, 1455, 1315, 1188, 1122, 1056, 932, 695, 610. Diastereomeric ratio: 58:42. <sup>1</sup>H NMR (CDCl<sub>3</sub>,  $\delta$  [ppm], J [Hz]): 8.57–8.52 (m, 2H), 7.77–7.58 (m, 2H), 7.38–7.17 (m, 11H), 5.67 (dd, *J* = 9.2, 3.9, 1H), 4.50–4.33 (m, 2H), 4.18–4.16 (m, 3H), 3.48–3.43 (dd, *J* = 14.7, 3.9, 1H), 3.20–3.00 (m, 3H), 1.97–1.93 (m, 1H), 1.51–1.06 (m, 5H). <sup>1</sup>H NMR (CDCl<sub>3</sub>,  $\delta$  [ppm], J [Hz]): 8.57–8.52 (m, 2H), 7.77–7.58 (m, 2H), 7.38–7.17 (m, 10H), 7.26–7.23 (m, 1H), 5.50–5.47 (dd, *J* = 9.2, 3.9, 1H), 4.50–4.33 (m, 2H), 4.18–4.16 (m, 2H), 3.99–3.96 (m, 1H), 3.36–3.32 (dd, *J* = 13.0, 3.0, 1H), 3.20–3.00 (m, 2H), 2.60 (td, *J* = 14.7, 3.9, 1H), 1.70–1.66 (m, 1H), 1.51–1.06 (m, 5H). <sup>13</sup>C NMR (CDCl<sub>3</sub>,  $\delta$  [ppm]): 170.3, 169.2, 148.5, 147.5, 137.2, 136.0, 134.5, 130.9 (2C), 129.6 (2C), 129.0, 128.9 (2C), 128.8, 128.5 (2C), 127.1, 124.0, 75.4, 59.3, 56.8, 44.0, 40.7, 38.0, 27.1, 24.4, 19.5. <sup>13</sup>C NMR (CDCl<sub>3</sub>,  $\delta$  [ppm]): 170.1, 169.0, 148.3, 147.5, 137.0, 135.8, 134.5, 130.7 (2C), 129.4 (2C), 129.0, 128.9 (2C), 128.7, 128.5 (2C), 127.1, 123.8, 75.1, 59.0, 56.0, 43.7, 40.7, 38.0, 27.0, 24.6, 19.4. LC/MS (*m/z*) 522.10 [M+H]<sup>+</sup>. Purity (HPLC, both diastereomers in total): 99.0%, *t<sub>R</sub>* = 8.38 min, 8.55 min. HRMS (*m/z*) C<sub>28</sub>H<sub>31</sub>N<sub>3</sub>O<sub>5</sub>S, [M+H]<sup>+</sup>, calculated 522.20572, found 522.20598, error 0.5 ppm.

## 4.6.1.2 Synthesis of the Specific Pipecolic Ester Stereo Isomers

**(*R*)-2-Hydroxy-4-methyl-*N*-(pyridin-3-ylmethyl)pentanamide (*R*-17d; Lab-ID: NJS182)**

Compound *R*-17d was prepared according to general procedure A using 1.89 g (*R*)-2-hydroxy-4-methoxypentanoic acid (14.3 mmol), HOBT (1.93 g, 14.3 mmol), EDC·HCl (2.74 g, 15.2 mmol), and 3-picolylamine (2.20 mL, 21.5 mmol) in dry DCM (200 mL). The crude oily product was purified by column chromatography (SiO<sub>2</sub>, DCM/MeOH 9:1 + 0.5% FA) to obtain *R*-17d as a colorless solid (1.08 g, 4.86 mmol, 34%), R<sub>f</sub>: 0.79 (DC<sub>SIL</sub>; EtOAc/MeOH = 5:1), mp: 47 – 48 °C, IR (ATR),  $\tilde{\nu}$  [cm<sup>-1</sup>]: 3326, 2955, 1639, 1521, 1421, 1281, 1171, 1044, 789, 711. <sup>1</sup>H NMR (CDCl<sub>3</sub>,  $\delta$  [ppm], J [Hz]): 8.53 (br s, 1H, *CH*-2), 8.51 (d, <sup>3</sup>J = 4.5, 1H, *CH*-6), 7.72–7.68 (m, 1H, *CH*-4), 7.32 (dd, <sup>3</sup>J = 7.8, 4.5, 1H, *CH*-5), 7.12 (br s, 1H, *NH*), 4.50 (dd, <sup>2</sup>J = 11.0, <sup>3</sup>J = 6.2, 2H, *CH*<sub>2</sub>C-3), 4.25–4.18 (m, 1H, HO*CH*CO), 1.93–1.77 (m, 1H, *CH*(CH<sub>3</sub>)<sub>2</sub>), 1.74–1.68 (m, 1H, *CH*CH<sub>2</sub>CH), 1.60–1.51 (m, 1H, *CH*CH<sub>2</sub>CH), 1.00–0.92 (m, 6H, *CH*<sub>3</sub>). <sup>13</sup>C NMR (CDCl<sub>3</sub>,  $\delta$  [ppm]): 174.8 (1C, CONH), 149.1 (1C, *CH*-2), 148.9 (1C, *CH*-6), 135.9 (1C, *CH*-4), 134.2 (1C, *C*-3), 123.8 (1C, *CH*-5), 71.0 (1C, HO*CH*CO), 43.9 (1C, *CH*CH<sub>2</sub>CH), 40.6 (1C, CONHCH<sub>2</sub>), 24.7 (1C, *CH*(CH<sub>3</sub>)<sub>2</sub>), 21.5 (2C, *CH*<sub>3</sub>) ppm.

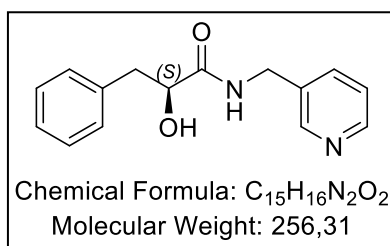
**(*S*)-2-Hydroxy-4-methyl-*N*-(pyridin-3-ylmethyl)pentanamide (*S*-17d; Lab-ID: NJS170)**

Compound *S*-17d was prepared according to general procedure A using 1.37 g of (*S*)-2-hydroxy-4-methoxypentanoic acid (10.4 mmol), HOBT (1.40 g, 10.4 mmol), EDC·HCl (1.98 g, 10.4 mmol), and 3-(aminomethyl)pyridine (1.16 mL, 11.4 mmol) in dry DCM (45 mL). After stirring at rt for 21 h and workup according to the general procedure, the crude oily product was

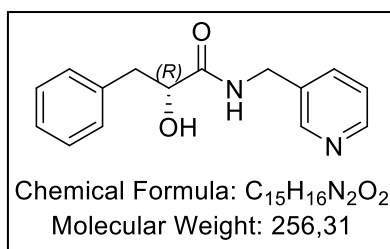
purified by column chromatography (SiO<sub>2</sub>, DCM/MeOH 9:1 + 0.5% FA). Compound *S*-17d was obtained as a colorless oil (1.64 g, 7.38 mmol, 71%).  $R_f = 0.79$  (DC<sub>SIL</sub>; DCM/MeOH = 5:1), IR (ATR),  $\tilde{\nu}$  [cm<sup>-1</sup>]: 3319, 2049, 2955, 2870, 1645, 1522, 1427, 1277, 790, 734, 711. <sup>1</sup>H NMR (CDCl<sub>3</sub>,  $\delta$  [ppm], J [Hz]):

<sup>1</sup>H NMR (CDCl<sub>3</sub>): 8.41–8.37 (m, 2H, *CH*-2, 6), 7.60 (d, <sup>3</sup>J = 7.8, 1H, *CH*-4), 7.46 (t, <sup>3</sup>J = 6.2, 1H, *NH*), 7.22 (dd, <sup>3</sup>J = 7.8, 4.9, 1H, *CH*-5), 4.99 (br s, 1H, *OH*), 4.47 (dd, <sup>2</sup>J = 15.2, <sup>3</sup>J = 6.2, 1H, *NHCH*<sub>2</sub>), 4.36 (dd, <sup>2</sup>J = 15.2, <sup>3</sup>J = 6.2, 1H, *NHCH*<sub>2</sub>), 4.18–4.14 (m, 1H, *CHOH*), 1.90–1.78 (m, 1H, *CH*(CH<sub>3</sub>)<sub>2</sub>), 1.65–1.62 (m, 1H, *CHCH*<sub>2</sub>), 1.54–1.50 (m, 1H, *CHCH*<sub>2</sub>), 0.93–0.88 (m, 6H, *CH*<sub>3</sub>). <sup>13</sup>C NMR (CDCl<sub>3</sub>,  $\delta$  [ppm]): 175.6 (1C, *CONH*), 148.5 (1C, *CH*-2), 148.4 (1C, *CH*-6), 136.1 (1C, *CH*-4), 134.5 (1C, *C*-3), 123.9 (1C, *CH*-5), 70.7 (1C, *CHOH*), 43.8 (1C, *CHCH*<sub>2</sub>CH), 40.5 (1C, *CONHCH*<sub>2</sub>), 24.6 (1C, *CH*(CH<sub>3</sub>)<sub>2</sub>), 23.6 (1C, *CH*<sub>3</sub>), 21.4 (1C, *CH*<sub>3</sub>).

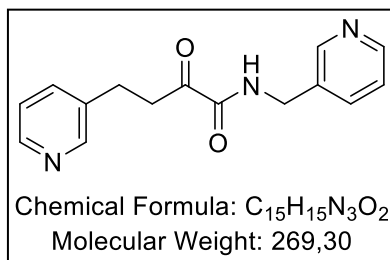
**(*S*)-2-Hydroxy-3-phenyl-*N*-(pyridin-3-ylmethyl)propanamide (*S*-17a; Lab-ID: AN281)**



Amidation of L-phenyl lactic acid (1.00 g, 6.02 mmol) and 3-picolylamine (410  $\mu$ L, 6.02 mmol) was carried out following general procedure A using 1.34 g of EDC·HCl (7.22 mmol) and HOBT (406 mg, 3.01 mmol) in dry DCM (240 mL). The product was obtained as a colorless oil (1.18 g, 4.60 mmol, 76%),  $R_f = 0.69$  (DC<sub>SIL</sub>; EtOAc/MeOH = 10:1). IR (ATR),  $\tilde{\nu}$  [cm<sup>-1</sup>]: 3329, 3154, 2925, 2851, 1737, 1651, 1515, 1071, 705. <sup>1</sup>H NMR (CDCl<sub>3</sub>,  $\delta$  [ppm], J [Hz]): 8.95–8.93 (m, 1H), 8.51–8.49 (m, 1H), 8.17–8.13 (m, 2H), 7.67–7.64 (m, 1H), 7.22–7.20 (m, 5H), 4.57–4.42 (m, 3H), 3.19–3.15 (m, 1H), 2.94–2.89 (m, 1H). <sup>13</sup>C NMR (CDCl<sub>3</sub>,  $\delta$  [ppm]): 171.9, 148.7, 148.2, 136.5, 135.7, 135.1, 129.8 (2C), 128.4 (2C), 126.1, 124.2, 74.1, 42.8, 40.9.

**(R)-2-Hydroxy-3-phenyl-N-(pyridin-3-ylmethyl)propanamide (R-17a; Lab-ID: AN283)**

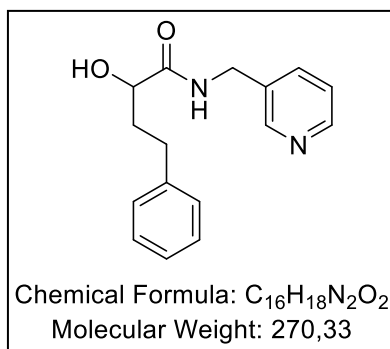
Amidation of D-phenyl lactic acid (1.00 g, 6.02 mmol) with 3-picolylamine (0.41 mL, 6.02 mmol) was carried out following general procedure A using 1.34 g of EDC·HCl (7.22 mmol) and HOBT (406 mg, 3.01 mmol) in dry DCM (240 mL). Compound **R-17a** was obtained as a colorless oil (671 mg, 2.61 mmol, 45%), *R<sub>f</sub>*: 0.73 (DC<sub>SIL</sub>; EtOAc/MeOH = 10:1). **IR** (ATR),  $\tilde{\nu}$  [cm<sup>-1</sup>]: 3329, 3154, 2925, 2851, 1737, 1651, 1515, 1071, 705. **<sup>1</sup>H NMR** (CDCl<sub>3</sub>,  $\delta$  [ppm], J [Hz]): 8.70–8.68 (m, 1H), 8.46–8.44 (m, 1H), 7.88–7.86 (m, 2H), 7.64–7.62 (m, 1H), 7.46–7.44 (m, 1H), 7.23–7.21 (m, 5H), 4.50–4.40 (m, 3H), 3.22–3.18 (m, 1H), 2.95–2.90 (m, 1H). **<sup>13</sup>C NMR** (CDCl<sub>3</sub>,  $\delta$  [ppm]): 171.9, 148.7, 148.2, 136.3, 134.7, 135.1, 129.8 (2C), 127.9 (2C), 126.1, 124.2, 74.5, 42.8, 40.9.

**2-Oxo-4-(pyridin-3-yl)-N-(pyridin-3-ylmethyl)butanamide (18; Lab-ID: AN346)**

Potassium (*E*)-2-oxo-4-(pyridin-3-yl)but-3-enoate was synthesized following a modified procedure by Stecher *et al.*<sup>1</sup> After obtaining the free acid by reaction with hydrochloric acid, (*E*)-2-oxo-4-(pyridin-3-yl)but-3-enoic acid (3.00 g, 16.9 mmol) was hydrogenated in the microwave (450 W, 15 bar H<sub>2</sub>) in isopropanol (50 mL) under Pd/C catalysis according to Slavinska *et al.*<sup>2</sup> The obtained 2-oxo-4-(pyridin-3-yl)butanoic acid (2.00 g, 11.1 mmol) was further reacted according to general procedure A using EDC·HCl (2.55 g, 13.3 mmol), HOBT (75 mg, 0.56 mmol), and DIPEA (3.00 mL, 17.2 mmol) in dry DCM (200 mL). Purification by column chromatography (SiO<sub>2</sub>, DCM/MeOH 9:1) afforded compound **18** as a yellow oil (2.70 g, 10.0 mmol, 90%). *R<sub>f</sub>*: 0.4 (DC<sub>SIL</sub>; EtOAc/MeOH = 4:1), **IR** (ATR),  $\tilde{\nu}$  [cm<sup>-1</sup>]: 3183, 2362, 1676, 1425, 1095, 1028, 706. **<sup>1</sup>H NMR** (CDCl<sub>3</sub>,  $\delta$  [ppm], J [Hz]): 8.54–8.50 (m, 2H), 8.47–8.43 (m, 2H), 7.61–7.52 (m, 2H),

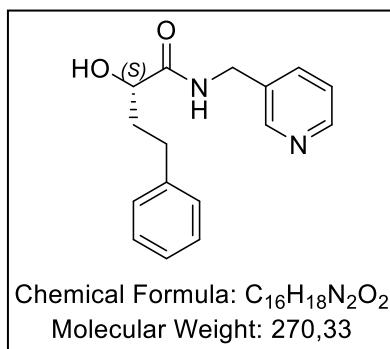
7.47–7.45 (m, 1H), 7.28–7.19 (m, 2H), 4.48 (m, 2H), 3.30 (t,  $J = 7.3$ , 2H), 2.94 (t,  $J = 7.3$ , 2H),  $^{13}\text{C}$  NMR ( $\text{CDCl}_3$ ,  $\delta$  [ppm]): 197.4, 160.0, 149.9, 149.4 (2C), 147.8, 136.2, 135.8 (2C), 132.8, 123.8, 123.6, 41.0, 38.1, 26.4.

**(*R/S*)-2-Hydroxy-4-phenyl-*N*-(pyridin-3-ylmethyl)butanamide (*R/S*-17e; Lab-ID: AN314)**



Amidation of (*R/S*)-2-hydroxy-4-phenylbutanoic acid (5.40 g, 30.0 mmol) with 3-picolylamine (3.25 mL, 30.0 mmol) was carried out following general procedure A using 6.90 g of EDC·HCl (36.0 mmol), DIPEA (6.00 mL, 34.4 mmol), and HOBT (2.00 g, 15.0 mmol) in dry DCM (400 mL). Compound *R/S*-17e was obtained as a white solid (3.71 g, 21.8 mmol, 45%),  $R_f$ : 0.29 ( $\text{DC}_{\text{SIL}}$ ; EtOAc/MeOH = 10:1). IR (ATR),  $\tilde{\nu}$  [ $\text{cm}^{-1}$ ]: 3449, 3026, 2924, 1716, 1645, 1495, 1236, 857, 694.  $^1\text{H}$  NMR ( $\text{CDCl}_3$ ,  $\delta$  [ppm],  $J$  [Hz]): 8.50–8.49 (m, 2H), 7.71–7.69 (m, 1H), 7.32–7.24 (m, 7H), 4.59–4.54 (dd,  $J = 15.2, 6.4$ , 1H), 4.46 (dd,  $J = 15.2, 9.9$ , 1H), 4.26–4.23 (dd,  $J = 8.4, 3.6$ , 1H), 2.86–2.82 (m, 2H), 2.28–2.24 (m, 1H), 2.07–1.98 (m, 1H).  $^{13}\text{C}$  NMR ( $\text{CDCl}_3$ ,  $\delta$  [ppm]): 174.6, 148.5, 148.3, 141.3, 136.4, 134.5, 128.7 (2C), 128.6 (2C), 126.2, 124.0, 71.6, 40.6, 36.4, 31.5.

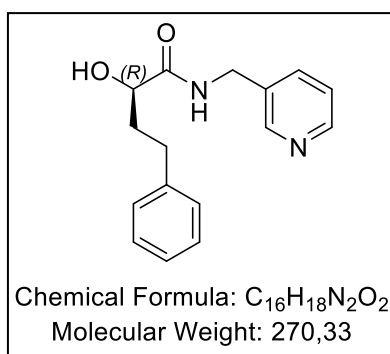
**(*S*)-2-Hydroxy-4-phenyl-*N*-(pyridin-3-ylmethyl)butanamide (*S*-17e; Lab-ID: AN263II)**



Amidation of (*S*)-2-hydroxy-4-phenylbutanoic acid (1.87 g, 10.4 mmol) with 3-picolylamine (1.16 mL, 11.4 mmol) was carried out following general procedure A using EDC·HCl (1.98 g,

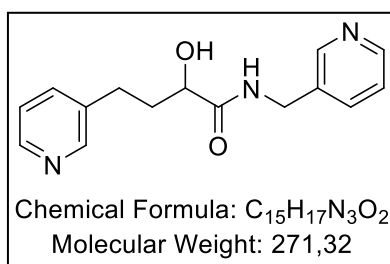
10.4 mmol) and HOBT (1.40 g, 10.4 mmol) in dry DCM (300 mL). The product was obtained as a white solid (1.30 g, 4.81 mmol, 46%),  $R_f$ : 0.29 (DC<sub>SIL</sub>; EtOAc/MeOH = 10:1). IR (ATR),  $\tilde{\nu}$  [cm<sup>-1</sup>]: 3449, 3026, 2924, 1716, 1645, 1495, 1236, 857, 694. <sup>1</sup>H NMR (CDCl<sub>3</sub>,  $\delta$  [ppm], J [Hz]): 8.50–8.49 (m, 2H), 7.71–7.69 (m, 1H), 7.32–7.24 (m, 7H), 4.59–4.54 (dd,  $J$  = 15.2, 6.4, 1H), 4.48–4.43 (dd,  $J$  = 15.2, 9.9, 1H), 4.26–4.23 (dd,  $J$  = 8.4, 3.6, 1H), 2.86–2.82 (m, 2H), 2.28–2.24 (m, 1H), 2.07–1.98 (m, 1H). <sup>13</sup>C NMR (CDCl<sub>3</sub>,  $\delta$  [ppm]): 174.6, 148.5, 148.3, 141.3, 136.4, 134.5, 128.7 (2C), 128.6 (2C), 126.2, 124.0, 71.6, 40.6, 36.4, 31.5.

**(*R*)-2-Hydroxy-4-phenyl-*N*-(pyridin-3-ylmethyl)butanamide (*R*-17e; Lab-ID: AN351II)**



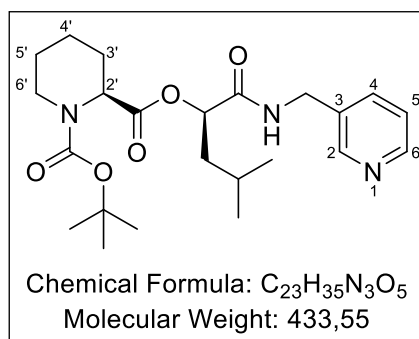
Amidation of (*R*)-2-hydroxy-4-phenylbutanoic acid (1.57 g, 8.75 mmol) and 3-picolylamine (0.92 mL, 9.00 mmol) was carried out following general procedure A using EDC·HCl (1.67 g, 8.75 mmol) and HOBT (1.07 g, 8.00 mmol) in dry DCM (300 mL). *R*-17e was obtained as a white solid (1.42 g, 5.25 mmol, 60%),  $R_f$ : 0.29 (DC<sub>SIL</sub>; EtOAc/MeOH = 10:1). IR (ATR),  $\tilde{\nu}$  [cm<sup>-1</sup>]: 3449, 3026, 2924, 1716, 1645, 1495, 1236, 857, 694. <sup>1</sup>H NMR (CDCl<sub>3</sub>,  $\delta$  [ppm], J [Hz]): 8.50–8.49 (m, 2H), 7.71–7.69 (m, 1H), 7.32–7.24 (m, 7H), 4.59–4.54 (dd,  $J$  = 15.2, 6.4, 1H), 4.48–4.43 (dd,  $J$  = 15.2, 9.9, 1H), 4.26–4.23 (dd,  $J$  = 8.4, 3.6, 1H), 2.86–2.82 (m, 2H), 2.28–2.24 (m, 1H), 2.07–1.98 (m, 1H). <sup>13</sup>C NMR (CDCl<sub>3</sub>,  $\delta$  [ppm]): 174.6, 148.5, 148.3, 141.3, 136.4, 134.5, 128.7 (2C), 128.6 (2C), 126.2, 124.0, 71.6, 40.6, 36.4, 31.5.

**(*R/S*)-2-Hydroxy-4-(pyridin-3-yl)-*N*-(pyridin-3-ylmethyl)butanamide (19; Lab-ID: AN347)**



Following a protocol by Ideguchi *et al.*,<sup>3</sup> 2-oxo-4-(pyridin-3-yl)-*N*-(pyridin-3-ylmethyl)-butanamide (**18**, 2.70 g, 10.04 mmol) was dissolved in 50 mL MeOH and NaBH<sub>4</sub> (0.75 g, 20.0 mmol) was added in portions under ice cooling. After stirring the reaction mixture at 0°C for 30 min, excess NaBH<sub>4</sub> was deactivated with 2M HCl and the solution was neutralized. The solvent was removed in vacuo, the residue was taken up in DCM (50 mL) and washed with water (2 × 50 mL). After separation of the phases, the solvent was removed in vacuo and the crude oily product was purified by column chromatography (SiO<sub>2</sub>, EtOAc/MeOH = 2:1) to give **19** as a white oily solid (660 mg, 2.43 mmol, 25%). R<sub>f</sub>: 0.4 (DC<sub>SIL</sub>; EtOAc/MeOH = 2:1), **IR** (ATR),  $\tilde{\nu}$  [cm<sup>-1</sup>]: 3253, 2356, 1645, 1523, 1424, 1098, 709. <sup>1</sup>H NMR (CDCl<sub>3</sub>,  $\delta$  [ppm], J [Hz]): 8.46–8.41 (m, 2H), 8.31–8.30 (m, 2H), 7.63–7.55 (m, 3H), 7.24–7.18 (m, 2H), 4.53 (dd, *J* = 15.1, 6.5, 1H), 4.39 (dd, *J* = 15.1, 5.8, 1H), 4.11 (dd, *J* = 15.1, 6.5, 1H), 2.79–2.77 (m, 2H), 2.20–2.12 (m, 1H), 2.00–1.92 (m, 1H). <sup>13</sup>C NMR (CDCl<sub>3</sub>,  $\delta$  [ppm]): 174.8, 149.5, 148.7, 148.5, 147.0, 137.3, 136.9, 136.1, 134.5, 123.9 (2C), 41.0, 38.1, 26.4.

**1-(*tert*-Butyl) 2-((*R*)-4-methyl-1-oxo-1-((pyridin-3-ylmethyl)amino)pentan-2-yl) (*S*)-piperidine-1,2-dicarboxylate (*S,R*-20d; Lab-ID: NJS190)**

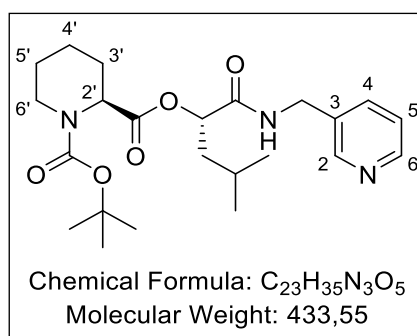


Esterification of *R*-**17d** (200 mg, 0.90 mmol) and (*S*)-1-Boc-piperidine-2-carboxylic acid (206 mg, 0.90 mmol) was carried out following general procedure A using EDC·HCl (207 mg, 1.08 mmol) and DMAP (121 mg, 0.99 mmol) in dry DCM (15 mL). After stirring at rt for 24 h and workup according to general procedure A, the crude oily product was purified by flash chromatography (RP 18, A: H<sub>2</sub>O + 1%FA, B: MeOH + 1% FA, gradient: 5 → 100% B). *S,R*-20d was obtained as a colorless oil (55 mg, 0.13 mmol, 14%). R<sub>f</sub>: 0.41 (DC<sub>SIL</sub>; DCM/MeOH = 14:1). **IR** (ATR),  $\tilde{\nu}$  [cm<sup>-1</sup>]: 3312, 2956, 2935, 1743, 1686, 1392, 1365, 1154, 773, 711. <sup>1</sup>H NMR (CDCl<sub>3</sub>,  $\delta$  [ppm], J [Hz]): 8.55–8.50 (m, 2H, *CH*-2,6), 7.32 (s, 1H, *NH*), 7.62 (d, <sup>3</sup>*J* = 7.8, 1H, *CH*-4), 7.25–7.20 (m, 1H, *CH*-5), 5.27 (dd, <sup>3</sup>*J* = 9.4, 3.9, 1H, COO*CH*CONH), 4.55–4.30 (m, 3H, *CH*<sub>2</sub>C-3,



$CH-2'$ ), 3.67–3.60 (m, 1H,  $CH_2-6'$ ), 3.33–3.28 (m, 1H,  $CH_2-6'$ ), 2.02–1.94 (m, 1H,  $CH(CH_3)_2$ ), 1.89–1.57 (m, 6H,  $CHCH_2CH$ ,  $CH_2-3',5'$ ), 1.46–1.42 (m, 2H,  $CH-4'$ ), 1.35 (s, 9H,  $C(CH_3)_3$ ), 0.96–0.88 (m, 6H,  $CH(CH_3)_2$ ).  $^{13}C$  NMR ( $CDCl_3$ ,  $\delta$  [ppm]): 172.4 (1C,  $CONH$ ), 170.7 (1C,  $COO$ ), 157.2 (1C,  $Boc-NCOO$ ), 149.1 (1C,  $CH-2$ ), 148.7 (1C,  $CH-6$ ), 135.5 (1C,  $CH-4$ ), 134.5 (1C,  $C-3$ ), 123.7 (1C,  $CH-5$ ), 80.8 (1C,  $C(CH_3)_3$ ), 72.9 (1C,  $COOCHCONH$ ), 54.7 (1C,  $CH-2'$ ), 43.0 (1C,  $CH_2-6'$ ), 40.8 (1C,  $CH_2C-3$ ), 40.4 (1C,  $CHCH_2CH$ ), 28.4 (3C,  $C(CH_3)_3$ ), 26.6 (1C,  $CH_2-3'$ ), 24.8 (1C,  $CH(CH_3)_2$ ), 24.4 (1C,  $CH_2-5'$ ), 23.4 (1C,  $CH(CH_3)_2$ ), 21.2 (1C,  $CH(CH_3)_2$ ), 20.1 (1C,  $CH_2-4'$ ).

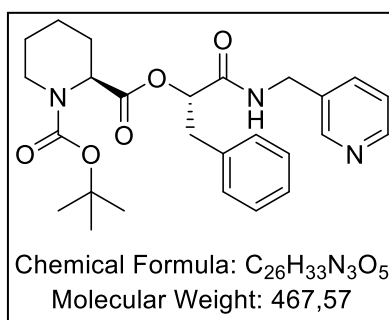
**1-(*tert*-Butyl) 2-((*S*)-4-methyl-1-oxo-1-((pyridin-3-ylmethyl)amino)pentan-2-yl) (*S*)-piperidine-1,2-dicarboxylate (*S,S*-20d; Lab-ID: NJS174)**



*S,S*-20d was prepared following general procedure A using 1.36 g of *S*-17d (6.10 mmol), (*S*)-1-Boc-piperidine-2-carboxylic acid (1.54 g, 6.71 mmol), EDC·HCl (1.75 g, 9.15 mmol), and DMAP (0.15 g, 1.22 mmol) in dry DCM (200 mL). After stirring at rt for 4 h and workup according to general procedure A, the crude oily product was purified by column chromatography ( $SiO_2$ , DCM/MeOH 15:1). Compound *S,S*-20d was obtained as a colorless oil (1.29 g, 2.97 mmol, 49%). IR (ATR),  $\tilde{\nu}$  [ $cm^{-1}$ ]: 3310, 2935, 2865, 1739, 1686, 1364, 1156, 1042, 930, 870, 777, 735.  $^1H$  NMR ( $CDCl_3$ ,  $\delta$  [ppm], J [Hz]): 8.55–8.51 (m, 2H,  $CH-2,6$ ), 7.74 (br s, 1H,  $NH$ ), 7.68–7.66 (m, 1H,  $CH-4$ ), 7.29–7.26 (m, 1H,  $CH-5$ ), 5.37–5.35 (m, 1H,  $CHOCO$ ), 4.75–4.74 (m, 1H,  $CH-2'$ ), 4.48–4.46 (m, 1H,  $NHCH_2$ ), 4.40–4.38 (m, 1H,  $NHCH_2$ ), 3.93 (d,  $^2J = 12.8$ , 1H,  $CH_2-6'$ ), 2.75 (ddd,  $^2J = 12.8$ ,  $^3J = 12.8$ , 2.5, 1H,  $CH_2-6'$ ), 2.35 (br d,  $^2J = 13.0$ , 1H,  $CH_2-3'$ ), 1.80–1.60 (m, 6H,  $CH(CH_3)_2$ ,  $CH_2$ ,  $CH_2-3',4',5'$ ), 1.48–1.42 (m, 1H,  $CH_2-5'$ ), 1.34 (s, 9H,  $C(CH_3)_3$ ), 1.20–1.10 (m, 1H,  $CH_2-4'$ ), 0.95–0.93 (m, 6H,  $CH(CH_3)_2$ ).  $^{13}C$  NMR ( $CDCl_3$ ,  $\delta$  [ppm]): 171.2 (1C,  $CONH$ ), 170.8 (1C,  $COO$ ), 157.9 (1C,  $Boc-NCOO$ ), 149.6 (1C,  $CH-2$ ), 148.9 (1C,  $CH-6$ ), 135.8 (1C,  $CH-4$ ), 134.0 (1C,  $C-3$ ), 123.6 (1C,  $CH-5$ ), 80.9 (1C,  $C(CH_3)_3$ ),

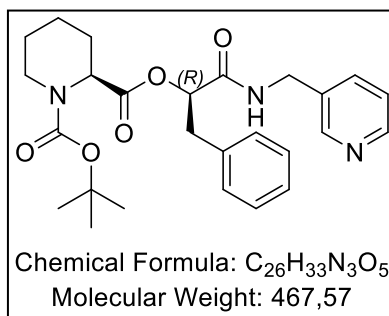
73.5 (1C, COOCHCONH), 54.7 (1C, CH-2'), 43.1 (1C, CH<sub>2</sub>-6'), 40.9 (1C, CHCH<sub>2</sub>CH), 40.8 (1C, CH<sub>2</sub>C-3), 28.4 (3C, C(CH<sub>3</sub>)<sub>3</sub>), 26.0 (1C, CH<sub>2</sub>-3'), 25.0 (1C, CH(CH<sub>3</sub>)<sub>2</sub>), 24.6 (1C, CH<sub>2</sub>-5'), 23.5 (1C, CH(CH<sub>3</sub>)<sub>2</sub>), 21.4 (1C, CH(CH<sub>3</sub>)<sub>2</sub>), 21.0 (1C, CH<sub>2</sub>-4').

**1-(*tert*-Butyl) 2-((*S*)-1-oxo-3-phenyl-1-((pyridin-3-ylmethyl)amino)propan-2-yl) (*S*)-piperidine-1,2-dicarboxylate (*S,S*-20a; Lab-ID: AN290)**



Esterification of *S*-17a (1.38 g, 5.38 mmol) and (*S*)-1-Boc-piperidine-2-carboxylic acid (1.23 g, 5.38 mmol) was carried out following general procedure A using 1.24 g of EDC·HCl (6.46 mmol) and DMAP (328 mg, 2.69 mmol) in dry DCM (200 mL). Compound *S,S*-20a was obtained as a colorless oil (1.18 g, 2.52 mmol, 47%), R<sub>f</sub>: 0.55 (DC<sub>SII</sub>; EtOAc/PE = 95:5). IR (ATR),  $\tilde{\nu}$  [cm<sup>-1</sup>]: 3318, 2974, 2932, 2862, 1745, 1666, 1364, 1155, 699. <sup>1</sup>H NMR (CDCl<sub>3</sub>,  $\delta$  [ppm], J [Hz]): 8.52–8.50 (m, 2H), 7.67–7.60 (m, 2H), 7.28–7.19 (m, 6H), 5.67–5.65 (m, 1H), 4.71–4.69 (m, 1H), 4.51–4.37 (m, 2H), 3.81–3.78 (m, 1H), 3.42–3.36 (m, 1H), 3.07–3.01 (m, 1H), 2.52 (td, *J* = 13.0, 2.9, 1H), 2.24–2.22 (m, 1H), 1.56–1.46 (m, 4H), 1.31 (s, 9H), 0.87–0.81 (m, 1H). <sup>13</sup>C NMR (CDCl<sub>3</sub>,  $\delta$  [ppm]): 170.9, 169.7, 157.8, 148.9, 148.2, 136.3, 136.1, 134.1, 129.5 (2C), 128.5 (2C), 127.1, 123.7, 80.7, 74.8, 54.4, 42.7, 40.8, 38.1, 28.4 (3C), 25.9, 24.4, 20.5.

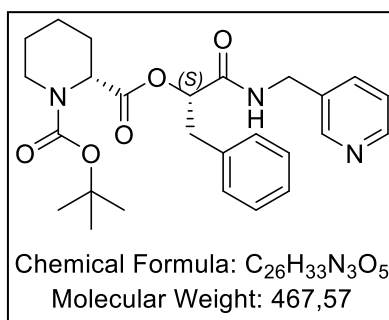
**1-(*tert*-Butyl) 2-((*R*)-1-oxo-3-phenyl-1-((pyridin-3-ylmethyl)amino)propan-2-yl) (*S*)-piperidine-1,2-dicarboxylate (*S,R*-20a; Lab-ID: AN293)**



Esterification of *R*-17a (670 mg, 2.61 mmol) and (*S*)-1-Boc-piperidine-2-carboxylic acid (600 mg,

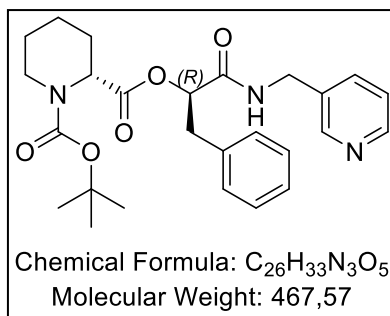
2.61 mmol) was carried out following general procedure A using 601 mg of EDC·HCl (3.12 mmol) and DMAP (1.31 mmol, 160 mg) in dry DCM (100 mL). Compound *S,R*-20a was obtained as a colorless oil (860 mg, 1.83 mmol, 70%),  $R_f$ : 0.50 (DC<sub>SIL</sub>; EtOAc/PE = 95:5). IR (ATR),  $\tilde{\nu}$  [cm<sup>-1</sup>]: 3318, 2974, 2932, 2862, 1745, 1666, 1364, 1155, 699. <sup>1</sup>H NMR (CDCl<sub>3</sub>,  $\delta$  [ppm], J [Hz]): 8.50–8.48 (m, 2H), 7.49–7.47 (m, 1H), 7.25–7.20 (m, 7H), 5.51–5.48 (m, 1H), 4.58–4.28 (m, 3H), 3.63–3.61 (m, 1H), 3.40–3.07 (m, 3H), 1.67–1.57 (m, 5H), 1.33 (s, 9H), 1.19–1.17 (m, 1H). <sup>13</sup>C NMR (CDCl<sub>3</sub>,  $\delta$  [ppm]): 171.9, 169.4, 157.2, 149.1, 148.8, 136.4, 135.1, 133.9, 129.5 (2C), 128.5 (2C), 127.0, 123.6, 80.8, 74.3, 54.4, 42.8, 40.8, 37.7, 28.4 (3C), 26.3, 24.4, 19.9.

1-(*tert*-Butyl) 2-((*S*)-1-oxo-3-phenyl-1-((pyridin-3-ylmethyl)amino)propan-2-yl) (*R*)-piperidine-1,2-dicarboxylate (*R,S*-20a; Lab-ID: AN306)



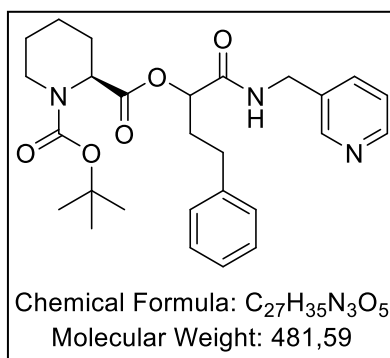
Esterification of *S*-17a (279 mg, 1.09 mmol) and (*R*)-1-Boc-piperidine-2-carboxylic acid (250 mg, 1.09 mmol) was carried out following general procedure A using EDC·HCl (250 mg, 1.31 mmol) and DMAP (66 mg, 0.55 mmol) in dry DCM (40 mL). Compound *R,S*-20a was obtained as a colorless oil (276 mg, 0.59 mmol, 52%),  $R_f$ : 0.51 (DC<sub>SIL</sub>; EtOAc/PE = 95:5). IR (ATR),  $\tilde{\nu}$  [cm<sup>-1</sup>]: 3337, 3024, 2955, 1745, 1671, 1264, 1154, 711. <sup>1</sup>H NMR (CDCl<sub>3</sub>,  $\delta$  [ppm], J [Hz]): 8.49–8.46 (m, 2H), 7.50–7.48 (m, 1H), 7.26–7.19 (m, 6H), 5.51–5.48 (m, 1H), 4.58–4.26 (m, 3H), 3.63–3.61 (m, 1H), 3.41–3.39 (m, 1H), 3.23–3.21 (m, 1H), 3.11–3.09 (m, 1H), 1.67–1.42 (m, 5H), 1.33 (s, 9H), 1.20–1.17 (m, 1H). <sup>13</sup>C NMR (CDCl<sub>3</sub>,  $\delta$  [ppm]): 177.6, 175.7, 152.8, 149.3, 148.8, 135.3, 136.1, 134.1, 129.6 (2C), 128.5 (2C), 127.0, 123.6, 81.7, 74.2, 54.5, 42.7, 40.8, 37.8, 28.4 (3C), 25.9, 24.3, 20.5.

1-(*tert*-Butyl) 2-((*R*)-1-oxo-3-phenyl-1-((pyridin-3-ylmethyl)amino)propan-2-yl) (*R*)-piperidine-1,2-dicarboxylate (*R,R*-20a; Lab-ID: AN305)



Esterification of *R*-17a (279 mg, 1.09 mmol) and (*R*)-1-Boc-piperidine-2-carboxylic acid (250 mg, 1.09 mmol) was carried out following general procedure A using EDC·HCl (250 mg, 1.31 mmol) and DMAP (66 mg, 0.55 mmol) in dry DCM (40 mL). Compound *R,R*-20a was obtained as a colorless oil (350 mg, 0.75 mmol, 62%), *R*<sub>f</sub>: 0.51 (DC<sub>SIL</sub>; EtOAc/PE = 95:5). IR (ATR),  $\tilde{\nu}$  [cm<sup>-1</sup>]: 3345, 3030, 2955, 1745, 1671, 1413, 1264, 1154, 707. <sup>1</sup>H NMR (CDCl<sub>3</sub>,  $\delta$  [ppm], J [Hz]): 8.50–8.48 (m, 2H), 7.64–7.56 (m, 2H), 7.26–7.16 (m, 6H), 5.66–5.64 (m, 1H), 4.69–4.67 (m, 1H), 4.48–4.34 (m, 2H), 3.79–3.76 (m, 1H), 3.39–3.35 (m, 1H), 3.04–2.99 (m, 1H), 2.53–2.46 (m, 1H), 2.20–2.17 (m, 1H), 1.53–1.44 (m, 4H), 1.29 (s, 9H), 0.89–0.78 (m, 1H). <sup>13</sup>C NMR (CDCl<sub>3</sub>,  $\delta$  [ppm]): 170.9, 169.7, 157.8, 149.0, 148.4, 136.2, 136.1, 134.1, 129.5 (2C), 128.5 (2C), 127.1, 123.7, 80.6, 74.7, 54.5, 42.7, 40.7, 38.1, 28.4 (3C), 25.9, 24.4, 20.5.

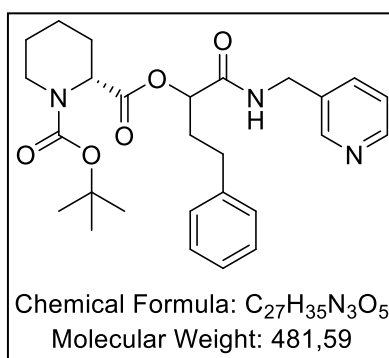
1-(*tert*-Butyl) 2-((*R/S*)-1-oxo-4-phenyl-1-((pyridin-3-ylmethyl)amino)butan-2-yl) (*S,S*)-piperidine-1,2-dicarboxylate (*S,S*-20e; Lab-ID: AN315)



Esterification of *R/S*-17e (1.27 g, 5.55 mmol) with (*S*)-1-Boc-piperidine-2-carboxylic acid (1.50 g, 5.55 mmol) was carried out following general procedure A using 1.28 g of EDC·HCl (6.66 mmol) and DMAP (340 mg, 2.78 mmol) in dry DCM (200 mL). Compound *S,S*-20e was obtained as a colorless oil (1.45 g, 3.01 mmol, 54%). *R*<sub>f</sub>: 0.48 (DC<sub>SIL</sub>; EtOAc = 100%). IR (ATR),  $\tilde{\nu}$  [cm<sup>-1</sup>]:

3320, 2931, 2857, 1742, 1671, 1532, 1392, 1154, 700. Diastereomeric ratio: 55:45.  $^1\text{H NMR}$  ( $\text{CDCl}_3$ ,  $\delta$  [ppm], J [Hz]): 8.54–8.48 (m, 2H), 7.63–7.61 (m, 1H), 7.35–7.15 (m, 7H), 5.37–5.35 (m, 1H), 4.58–4.33 (m, 3H), 3.68–3.65 (m, 1H), 3.34–3.32 (m, 1H), 2.67–2.65 (m, 2H), 2.38–1.94 (m, 3H), 1.82–1.56 (m, 6H), 1.37–1.35 (m, 9H).  $^{13}\text{C NMR}$  ( $\text{CDCl}_3$ ,  $\delta$  [ppm]): 170.8, 169.8, 157.7, 149.0, 148.8, 140.5, 135.6, 133.8, 128.6 (2C), 128.4 (2C), 126.3, 123.5, 80.9, 74.09, 54.7, 43.0, 40.8, 33.5, 31.5, 28.4 (3C), 24.5, 20.9, 20.2.  $^1\text{H NMR}$  ( $\text{CDCl}_3$ ,  $\delta$  [ppm], J [Hz]): 8.54–8.48 (m, 2H), 7.62 (m, 1H), 7.35–7.15 (m, 7H), 5.26–5.24 (m, 1H), 4.80–4.78 (m, 1H), 4.58–4.33 (m, 2H), 4.00–3.96 (m, 1H), 2.80 (td,  $J = 19.4, 3.0$ , 1H), 2.67–2.65 (m, 2H), 2.38–1.94 (m, 3H), 1.82–1.56 (m, 6H), 1.37–1.35 (m, 9H).  $^{13}\text{C NMR}$  ( $\text{CDCl}_3$ ,  $\delta$  [ppm]): 170.8, 169.8, 157.7, 149.0, 148.8, 140.5, 135.6, 133.8, 128.6 (2C), 128.4 (2C), 126.3, 123.5, 80.9, 73.67, 54.7, 43.0, 40.8, 33.5, 31.5, 28.4 (3C), 24.5, 20.9, 20.2.

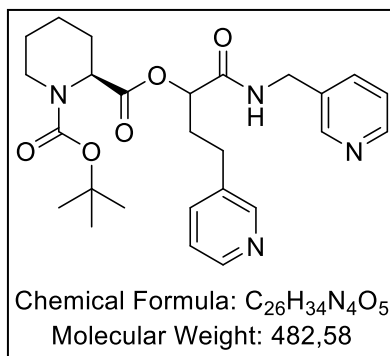
**1-(*tert*-Butyl) 2-((*R/S*)-1-oxo-4-phenyl-1-((pyridin-3-ylmethyl)amino)butan-2-yl) (*2R*)-piperidine-1,2-dicarboxylate (*R,R/S*-20e; AN316)**



Esterification of *R/S*-17e (1.27 g, 5.55 mmol) with (*R*)-1-Boc-piperidine-2-carboxylic acid (1.50 g, 5.55 mmol) was carried out following general procedure A using 1.28 g of EDC·HCl (6.66 mmol) and DMAP (340 mg, 2.78 mmol) in dry DCM (200 mL). Compound *R,R/S*-20e was obtained as a white oily solid (1.46 g, 21.8 mmol, 55%).  $R_f$ : 0.50 ( $\text{DC}_{\text{SiH}}$ ; EtOAc = 100%). IR (ATR),  $\tilde{\nu}$  [ $\text{cm}^{-1}$ ]: 3319, 2932, 2857, 1742, 1676, 1532, 1393, 1154, 1041, 700. Diastereomeric ratio: 57:43.  $^1\text{H NMR}$  ( $\text{CDCl}_3$ ,  $\delta$  [ppm], J [Hz]): 8.55–8.48 (m, 2H), 7.64–7.62 (m, 1H), 7.29–7.14 (m, 7H), 5.37–5.35 (m, 1H), 4.81–4.79 (m, 1H), 4.53–4.37 (m, 2H), 4.01–3.99 (m, 1H), 3.34–3.32 (m, 1H), 2.69–2.65 (m, 2H), 2.38–1.96 (m, 3H), 1.81–1.46 (m, 6H), 1.37–1.35 (m, 9H).  $^{13}\text{C NMR}$  ( $\text{CDCl}_3$ ,  $\delta$  [ppm]): 170.1, 157.2, 149.2, 148.9, 140.6, 135.8, 135.3, 128.8 (2C), 128.5 (2C), 126.4, 123.7, 80.9, 74.1, 54.7, 43.0, 40.8, 34.0, 31.6, 28.4 (3C), 24.5, 21.2, 20.2.  $^1\text{H NMR}$  ( $\text{CDCl}_3$ ,  $\delta$  [ppm], J [Hz]): 8.55–8.48 (m, 2H), 7.64–7.62 (m, 1H), 7.29–7.14 (m, 7H), 5.28–

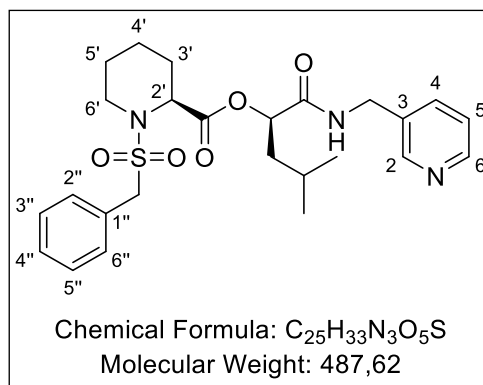
5.26 (m, 1H), 4.53–4.37 (m, 3H), 3.70–3.68 (m, 1H), 2.84–2.77 (m, 1H), 2.69–2.65 (m, 2H), 2.38–1.96 (m, 3H), 1.81–1.46 (m, 6H), 1.37–1.35 (m, 9H).  $^{13}\text{C}$  NMR ( $\text{CDCl}_3$ ,  $\delta$  [ppm]): 170.1, 157.2, 149.2, 148.9, 140.6, 135.8, 135.3, 128.6 (2C), 128.4 (2C), 126.4, 123.7, 80.9, 73.7, 54.7, 43.0, 40.8, 33.3, 31.4, 28.4 (3C), 24.5, 20.9, 20.2.

1-(*tert*-Butyl) 2-((*R/S*)-1-oxo-4-(pyridin-3-yl)-1-((pyridin-3-ylmethyl)amino)butan-2-yl) (*S*)-piperidine-1,2-dicarboxylate (*S,R/S*-20f; AN348)



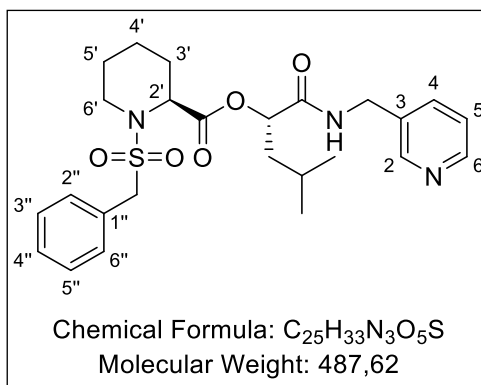
*S,R/S*-20f was synthesized according to general procedure A using 660 mg of **19** (2.43 mmol), EDC·HCl (560 mg, 2.91 mmol), and DMAP (148 mg, 1.22 mmol) in dry DCM (50 mL). After purification by column chromatography ( $\text{SiO}_2$ , EtOAc/MeOH = 4:1), compound *S,R/S*-20f was obtained as a yellowish oil (700 mg, 1.45 mmol, 60%).  $R_f$ : 0.5 ( $\text{DC}_{\text{SIL}}$ ; EtOAc/MeOH = 4:1). IR (ATR),  $\tilde{\nu}$  [ $\text{cm}^{-1}$ ]: 3323, 2933, 2360, 1743, 1671, 1155, 719. Diastereomeric ratio: 53:47.  $^1\text{H}$  NMR ( $\text{CDCl}_3$ ,  $\delta$  [ppm], J [Hz]): 8.55–8.43 (m, 4H), 7.67–7.54 (m, 2H), 7.28–7.25 (m, 2H), 5.36–5.35 (m, 1H), 4.81–4.79 (m, 1H), 4.58–4.36 (m, 2H), 4.01–3.97 (m, 1H), 3.34–3.29 (m, 1H), 2.74–2.58 (m, 3H), 2.35–1.47 (m, 7H), 1.37–1.35 (m, 9H).  $^1\text{H}$  NMR ( $\text{CDCl}_3$ ,  $\delta$  [ppm], J [Hz]): 8.55–8.43 (m, 4H), 7.67–7.54 (m, 2H), 7.28–7.25 (m, 2H), 5.27–5.25 (m, 1H), 4.58–4.36 (m, 3H), 3.68–3.64 (m, 1H), 2.84–2.82 (m, 1H), 2.74–2.58 (m, 2H), 2.35–1.47 (m, 8H), 1.37–1.35 (m, 9H).  $^{13}\text{C}$  NMR ( $\text{CDCl}_3$ ,  $\delta$  [ppm]): 172.1, 169.7, 157.2, 149.4, 148.7, 148.4, 147.6, 136.8, 136.5, 136.2, 134.0, 123.8 (2C), 81.0, 73.7, 54.8, 43.2, 40.8, 33.6, 28.7, 28.4, 26.7, 24.5, 20.9.  $^{13}\text{C}$  NMR ( $\text{CDCl}_3$ ,  $\delta$  [ppm]): 170.9, 169.7, 157.2, 149.2, 148.7, 148.4, 147.1, 136.8, 136.5, 136.2, 134.0, 123.8 (2C), 81.0, 73.2, 54.8, 43.2, 40.8, 32.8, 28.7, 28.4, 26.0, 24.5, 20.2.

**(*R*)-4-Methyl-1-oxo-1-((pyridin-3-ylmethyl)amino)pentan-2-yl (*S*)-1-(benzylsulfonyl)piperidine-2-carboxylate (*S,R*-10d; Lab-ID: NJS195)**



*S,R*-20d (50 mg, 0.12 mmol) was Boc-protected according to general procedure B using 2 mL of TFA in dry DCM (5 mL). After stirring at rt for 18 h, the reaction was worked up according to the general procedure. Subsequently, the intermediate product (29.7 mg, 89  $\mu$ mol) was further reacted according to general procedure C using NMM (69  $\mu$ L, 0.62 mmol) and phenylmethanesulfonyl chloride (41 mg, 0.21 mmol) in dry DCM (20 mL). After stirring at rt for 4 d and workup according to the general procedure, the crude oily product was purified by flash chromatography (SiO<sub>2</sub>, A: DCM, B: MeOH, gradient: 0  $\rightarrow$  30% B) giving the product as a colorless oily solid (26 mg, 53  $\mu$ mol, 60%).  $R_f$  = 0.53 (DC<sub>SIL</sub>; DCM/MeOH = 15:1). IR (ATR),  $\tilde{\nu}$  [cm<sup>-1</sup>]: 3356, 3063, 3032, 2956, 1740, 1670, 1540, 1335, 1172, 826, 790, 731, 697. <sup>1</sup>H NMR (CDCl<sub>3</sub>,  $\delta$  [ppm], J [Hz]): 8.56 (s, 1H, CH-2), 8.50 (d, <sup>3</sup>J = 3.9, 1H, CH-6), 7.65 (br d, <sup>3</sup>J = 7.8, 1H, CH-4), 7.42–7.34 (m, 5H, CH-2''–6''), 7.27 (br s, 1H, NH), 7.25–7.22 (m, 1H, CH-5), 5.30–5.23 (m, 1H, COOCH), 4.49–4.38 (m, 2H, CHCH<sub>2</sub>CH), 4.21–4.19 (m, 3H, SO<sub>2</sub>CH<sub>2</sub>, CH-2'), 3.21 (br d, <sup>2</sup>J = 12.3, 1H, CH<sub>2</sub>-6'), 3.06 (ddd, <sup>2</sup>J = 12.3, <sup>3</sup>J = 12.3, 2.6, 1H, CH<sub>2</sub>-6'), 2.01–1.93 (m, 1H, CH<sub>2</sub>-3'), 1.90–1.73 (m, 3H, CH<sub>2</sub>C-3, CH<sub>2</sub>-5'), 1.71–1.30 (m, 5H, CH<sub>2</sub>-3', 4', 5'), 0.96–0.88 (m, 6H, CH(CH<sub>3</sub>)<sub>2</sub>). <sup>13</sup>C NMR (CDCl<sub>3</sub>,  $\delta$  [ppm]): 170.5 (1C, CONH), 170.2 (1C, COO), 149.5 (1C, CH-2), 148.8 (1C, CH-6), 136.0 (1C, CH-4), 134.1 (br 1C, C-3), 131.0 (2C, CH-2'', 6''), 129.03 (1C, CH-4''), 129.01 (1C, C-1''), 128.8 (2C, CH-3'', 5''), 123.6 (1C, CH-5), 73.9 (1C, COOCHCONH), 59.1 (1C, SO<sub>2</sub>CH<sub>2</sub>), 56.2 (1C, CH-2'), 44.2 (1C, CH<sub>2</sub>-6'), 41.0 (1C, CH<sub>2</sub>C-3), 40.8 (1C, CHCH<sub>2</sub>CH), 27.1 (1C, CH<sub>2</sub>-3'), 24.7 (br 2C, CH(CH<sub>3</sub>)<sub>2</sub>, CH<sub>2</sub>-5''), 23.2 (1C, CH(CH<sub>3</sub>)<sub>2</sub>), 21.9 (1C, CH(CH<sub>3</sub>)<sub>2</sub>), 19.7 (1C, CH<sub>2</sub>-4''). LC/MS (m/z) 488.50 [M+H]<sup>+</sup>. Purity (HPLC): 95.1%,  $t_R$  = 8.47 min. HRMS (m/z) C<sub>25</sub>H<sub>33</sub>N<sub>3</sub>O<sub>5</sub>S, [M+H]<sup>+</sup>, calculated 488.22137, found 488.22146, error 0.2 ppm.

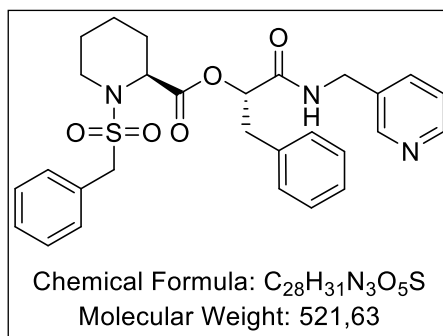
**(S)-4-Methyl-1-oxo-1-((pyridin-3-ylmethyl)amino)pentan-2-yl (S)-1-(benzylsulfonyl)piperidine-2-carboxylate (S,S-10d; NJS178)**



Following general procedure B, *S,S*-**20d** (500 mg, 1.15 mmol) was first deprotected using TFA (1.0 mL, 13.0 mmol) in dry DCM (4.0 mL) stirring at rt for 1 d. After workup according to general procedure B, 208 mg of the amine intermediate (623  $\mu$ mol) was reacted according to general procedure C using NMM (0.21 mL, 1.87 mmol) and phenylmethanesulfonyl chloride (220 mg, 1.15 mmol) in dry DCM (3 mL). After stirring at rt for 3 d, the reaction was worked up according to the general procedure and purified by flash chromatography (run 1: SiO<sub>2</sub>, 2  $\times$  12 g, A: CHCl<sub>3</sub>, B: MeOH, gradient: 0  $\rightarrow$  20% B; run 2: RP 18, A: H<sub>2</sub>O, B: MeOH, gradient: 5  $\rightarrow$  70% B). *S,S*-**10d** was obtained as a colorless oily solid (135 mg, 277  $\mu$ mol, 44%).  $R_f$  = 0.55 (DC<sub>SIL</sub>; DCM/MeOH = 15:1). IR (ATR),  $\tilde{\nu}$  [cm<sup>-1</sup>]: 3354, 3061, 3036, 2952, 1739, 1671, 1536, 1335, 1175, 825, 792, 741, 697. <sup>1</sup>H NMR (CDCl<sub>3</sub>,  $\delta$  [ppm], J [Hz]): 8.54 (br s, 2H, CH-2,6), 7.70–7.58 (m, 2H, CH-4, NH), 7.46–7.30 (m, 5H, CH-2''–6''), 7.25 (br s, 1H, CH-5), 5.41–5.31 (m, 1H, COOCH), 4.49–4.35 (m, 2H, CHCH<sub>2</sub>CH), 4.20 (m, 2H, SO<sub>2</sub>CH<sub>2</sub>), 4.08 (d, <sup>3</sup>J = 4.3, 1H, CH-2'), 3.36 (br d, <sup>2</sup>J = 13.0, 1H, CH<sub>2</sub>-6'), 3.02 (ddd, <sup>2</sup>J = 13.0, <sup>3</sup>J = 13.0, 2.7, 1H, CH<sub>2</sub>-6'), 2.20–2.00 (m, 2H, CH<sub>2</sub>-3', NH), 1.83–1.73 (m, 2H, CH<sub>2</sub>C-3), 1.70–1.60 (m, 2H, CH<sub>2</sub>-4',5'), 1.41–1.22 (m, 2H, CH<sub>2</sub>-3',5'), 1.19–0.97 (m, 1H, CH<sub>2</sub>-4'), 0.95–0.88 (m, 6H, CH(CH<sub>3</sub>)<sub>2</sub>). <sup>13</sup>C NMR (CDCl<sub>3</sub>,  $\delta$  [ppm]): 170.4 (1C, *pip*-CO), 170.3 (1C, CONH), 149.5 (1C, CH-2), 148.6 (1C, CH-6), 135.8 (1C, CH-4), 134.1 (br 1C, C-3), 130.9 (2C, CH-2'',6''), 129.2 (1C, CH-4''), 128.9 (2C, CH-3'',5''), 128.8 (1C, C-1''), 123.6 (1C, CH-5), 74.1 (1C, COOCHCONH), 59.5 (1C, SO<sub>2</sub>CH<sub>2</sub>), 57.0 (1C, CH-2'), 44.3 (1C, CH<sub>2</sub>-6'), 41.2 (1C, CH<sub>2</sub>C-3), 40.7 (1C, CHCH<sub>2</sub>CH), 27.1 (1C, CH<sub>2</sub>-3'), 25.0 (1C, CH(CH<sub>3</sub>)<sub>2</sub>), 24.6 (1C, CH<sub>2</sub>-5''), 23.3 (1C, CH(CH<sub>3</sub>)<sub>2</sub>), 21.5 (1C, CH(CH<sub>3</sub>)<sub>2</sub>), 20.3 (1C, CH<sub>2</sub>-4''). LC/MS (m/z) 488.45 [M+H]<sup>+</sup>. Purity (HPLC): 98.9%,  $t_R$  = 8.46 min. HRMS (m/z) C<sub>25</sub>H<sub>33</sub>N<sub>3</sub>O<sub>5</sub>S, [M+H]<sup>+</sup>, calculated 488.22137, found 488.22235, error 2.0 ppm.

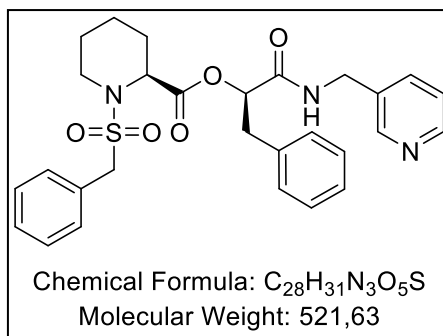


**(S)-1-Oxo-3-phenyl-1-((pyridin-3-ylmethyl)amino)propan-2-yl (S)-1-(benzylsulfonyl)piperidine-2-carboxylate (S,S-10a; Lab-ID: AN296)**



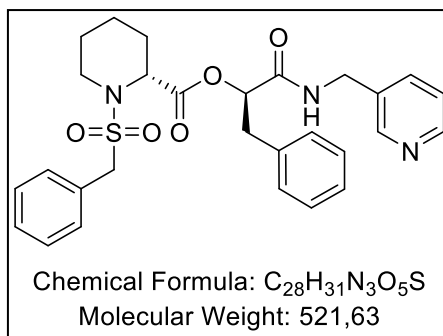
**S,S-20a** (860 mg, 1.84 mmol) was Boc-protected following general procedure B using 2.00 mL TFA in dry DCM (20 mL). After workup according to the general procedure, the free amine intermediate (650 mg, 1.77 mmol) was further reacted according to general procedure C using phenylmethanesulfonyl chloride (337 mg, 1.77 mmol) and NMM (210  $\mu$ L, 1.95 mmol) in dry DCM (35 mL). Compound **S,S-10a** was obtained as a colorless oil (300 mg, 0.57 mmol, 32%),  $R_f$ : 0.41 (DC<sub>SIL</sub>; EtOAc/PE = 95:5). IR (ATR),  $\tilde{\nu}$  [ $cm^{-1}$ ]: 3349, 3050, 2943, 1740, 1671, 1536, 1321, 1124, 697.  $^1H$  NMR (CDCl<sub>3</sub>,  $\delta$  [ppm], J [Hz]): 8.54 (d,  $J$  = 1.8, 1H), 8.51 (dd,  $J$  = 4.8, 1.7, 1H), 7.70 (t,  $J$  = 5.7, 1H), 7.58 (dt,  $J$  = 7.8, 1.9, 1H), 7.37–7.17 (m, 11H), 5.66 (dd,  $J$  = 9.2, 3.9, 1H), 4.48–4.37 (m, 2H), 4.14 (s, 2H), 3.96–3.94 (m, 1H), 3.45 (dd,  $J$  = 14.7, 4.0, 1H), 3.11 (dd,  $J$  = 14.7, 9.2, 1H), 3.13–3.11 (m, 1H), 2.59 (td,  $J$  = 13.0, 2.9, 1H), 1.96–1.92 (m, 1H), 1.34–1.08 (m, 4H), 0.45–0.35 (m, 1H).  $^{13}C$  NMR (CDCl<sub>3</sub>,  $\delta$  [ppm]): 170.1, 169.2, 149.7, 148.8, 136.1, 135.8, 133.8, 130.8 (2C), 129.5 (2C), 129.2 (2C), 128.9 (2C), 128.6, 127.1 (2C), 123.5, 75.4, 59.4, 56.8, 43.7, 40.8, 38.0, 27.1, 24.3, 19.4. LC/MS ( $m/z$ ) 522.10 [M+H]<sup>+</sup>. Purity (HPLC): 96.5%,  $t_R$  = 8.55 min. HRMS ( $m/z$ )  $C_{28}H_{31}N_3O_5S$ , [M+H]<sup>+</sup>, calculated 522.20572, found 522.20657, error 1.6 ppm.

**(*R*)-1-Oxo-3-phenyl-1-((pyridin-3-ylmethyl)amino)propan-2-yl (*S*)-1-(benzylsulfonyl)piperidine-2-carboxylate (*S,R*-10a; Lab-ID: AN297)**



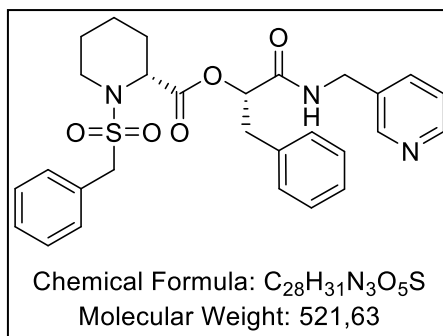
*S,R*-20a (860 mg, 1.84 mmol) was Boc-protected following general procedure B using 2.00 mL TFA in dry DCM (20 mL). After workup according to the general procedure, the free amine intermediate (650 mg, 1.77 mmol) was further reacted according to general procedure C using phenylmethanesulfonyl chloride (337 mg, 1.77 mmol) and NMM (210  $\mu$ L, 1.95 mmol) in dry DCM (30 mL). Compound *S,R*-10a was obtained as a colorless oil (320 mg, 0.61 mmol, 35%),  $R_f$ : 0.42 (DC<sub>SIL</sub>; EtOAc/PE = 95:5). IR (ATR),  $\tilde{\nu}$  [cm<sup>-1</sup>]: 3349, 3039, 2943, 1744, 1684, 1536, 1323, 1124, 697. <sup>1</sup>H NMR (CDCl<sub>3</sub>,  $\delta$  [ppm], J [Hz]): 8.50–8.48 (m, 2H), 7.50–7.48 (m, 1H), 7.38–7.33 (m, 5H), 7.24–7.15 (m, 6H), 7.09 (t,  $J$  = 5.8, 1H), 5.50–5.47 (dd,  $J$  = 8.4, 4.0, 1H), 4.49–4.43 (dd,  $J$  = 14.9, 6.4, 1H), 4.36–4.31 (dd,  $J$  = 14.9, 5.8, 1H), 4.16 (m, 2H), 4.12 (m, 1H), 3.36–3.31 (dd,  $J$  = 14.4, 4.0, 1H), 3.17–3.13 (m, 1H), 3.09–3.03 (dd,  $J$  = 14.4, 8.4, 1H), 3.03–2.98 (m, 1H), 1.69–1.65 (m, 1H), 1.50–1.25 (m, 4H), 1.09–1.06 (m, 1H). <sup>13</sup>C NMR (CDCl<sub>3</sub>,  $\delta$  [ppm]): 170.2, 168.9, 149.5, 148.8, 135.9, 135.8, 133.7, 130.9 (2C), 129.6 (2C), 129.0 (2C), 128.7 (2C), 128.5, 127.1 (2C), 123.6, 75.1, 59.1, 56.0, 44.1, 40.8, 38.0, 26.9, 24.6, 19.5. LC/MS (m/z) 522.10 [M+H]<sup>+</sup>. Purity (HPLC): 99.5%,  $t_R$  = 8.41 min. HRMS (m/z) C<sub>28</sub>H<sub>31</sub>N<sub>3</sub>O<sub>5</sub>S, [M+H]<sup>+</sup>, calculated 522.20572, found 522.20601, error 0.6 ppm.

**(*R*)-1-Oxo-3-phenyl-1-((pyridin-3-ylmethyl)amino)propan-2-yl (*R*)-1-(benzylsulfonyl)piperidine-2-carboxylate (*R,R*-10a; Lab-ID: AN309)**



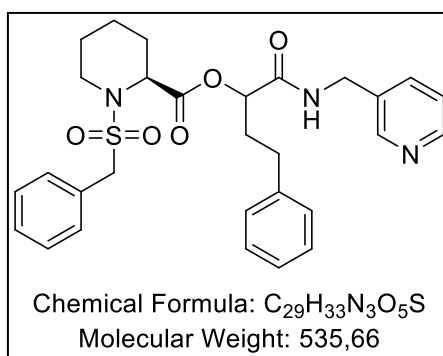
*R,R*-20a (350 mg, 0.75 mmol) was Boc-protected following general procedure B using 3.00 mL TFA in dry DCM (20 mL). After workup according to the general procedure, the free amine intermediate (284 mg, 0.78 mmol) was further reacted according to general procedure C using phenylmethanesulfonyl chloride (150 mg, 0.78 mmol) and NMM (100  $\mu$ L, 0.94 mmol) in dry DCM (20 mL). *R,R*-10a was obtained as a colorless oil (120 mg, 0.23 mmol, 31%),  $R_f$ : 0.40 (DC<sub>SIL</sub>; EtOAc/PE = 95:5). IR (ATR),  $\tilde{\nu}$  [cm<sup>-1</sup>]: 3345, 3062, 2933, 1739, 1671, 1537, 1322, 1192, 1124, 697. <sup>1</sup>H NMR (CDCl<sub>3</sub>,  $\delta$  [ppm], J [Hz]): 8.55–8.51 (m, 2H), 7.73 (t, 1H,  $J$  = 5.6), 7.65–7.63 (m, 1H), 7.37–7.25 (m, 5H), 7.23–7.15 (m, 6H), 5.68–5.64 (dd, 1H,  $J$  = 9.2, 3.9), 4.50–4.38 (m, 2H), 4.16 (m, 2H), 3.96 (m, 1H), 3.47–3.43 (dd, 1H,  $J$  = 14.7, 3.9), 3.15–3.10 (m, 1H), 3.13–3.07 (dd, 1H,  $J$  = 14.7, 9.2), 2.63–2.56 (td,  $J$  = 13.0, 2.9, 1H), 1.96–1.93 (m, 1H), 1.34–1.07 (m, 4H), 0.45–0.35 (m, 1H). <sup>13</sup>C NMR (CDCl<sub>3</sub>,  $\delta$  [ppm]): 170.1, 169.2, 148.9, 147.9, 136.6, 136.0, 134.3, 130.8 (2C), 129.5 (2C), 129.2 (2C), 128.9 (2C), 128.6, 127.1 (2C), 123.8, 75.4, 59.4, 56.8, 43.7, 40.7, 38.0, 27.1, 24.3, 19.4. LC/MS ( $m/z$ ) 522.50 [M+H]<sup>+</sup>,  $t_R$  = 8.52 min. Purity (HPLC): 95.6%. HRMS ( $m/z$ ) C<sub>28</sub>H<sub>31</sub>N<sub>3</sub>O<sub>5</sub>S, [M+H]<sup>+</sup>, calculated 522.20572, found 522.20569, error 0.1 ppm.

**(*S*)-1-Oxo-3-phenyl-1-((pyridin-3-ylmethyl)amino)propan-2-yl (*R*)-1-(benzylsulfonyl)piperidine-2-carboxylate (*R,S*-10a; Lab-ID: AN310)**



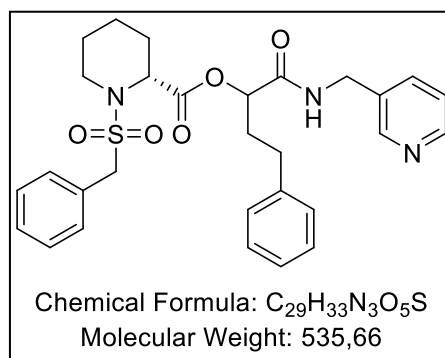
*R,S*-20a (276 mg, 0.60 mmol) was Boc-protected following general procedure B using 3.00 mL TFA in dry DCM (20 mL). After workup according to the general procedure, the free amine intermediate (200 mg, 0.55 mmol) was further reacted according to general procedure C using phenylmethanesulfonyl chloride (104 mg, 0.55 mmol) and NMM (70  $\mu$ L, 0.66 mmol) in dry DCM (10 mL). *R,S*-10a was obtained as a colorless oil (80 mg; 0.15 mmol, 28%),  $R_f$ : 0.41 (DC<sub>SIL</sub>; EtOAc/PE = 95:5). IR (ATR),  $\tilde{\nu}$  [cm<sup>-1</sup>]: 3362, 3034, 1736, 1696, 1540, 1299, 1179, 778, 693. <sup>1</sup>H NMR (CDCl<sub>3</sub>,  $\delta$  [ppm], J [Hz]): 8.53–8.50 (m, 2H), 7.67–7.65 (m, 1H), 7.38–7.16 (m, 12H), 5.48 (dd,  $J$  = 8.4, 3.9, 1H), 4.54 (dd,  $J$  = 15.0, 6.3, 1H), 4.38 (dd,  $J$  = 15.0, 5.8, 1H), 4.20–4.16 (m, 3H), 3.34 (dd,  $J$  = 14.4, 4.0, 1H), 3.21–3.18 (m, 1H), 3.07 (dd,  $J$  = 14.4, 8.4, 1H), 3.05–2.99 (m, 1H), 1.72–1.68 (m, 1H), 1.52–1.23 (m, 4H), 1.12–1.06 (m, 1H). <sup>13</sup>C NMR (CDCl<sub>3</sub>,  $\delta$  [ppm]): 170.3, 169.0, 147.3, 146.5, 135.8, 135.2, 130.9, 129.7 (2C), 129.6 (2C), 129.0 (2C), 128.9 (2C), 128.5, 127.2 (2C), 124.4, 75.1, 59.1, 56.0, 44.0, 40.6, 37.9, 26.9, 24.6, 19.5. LC/MS (m/z) 522.45 [M+H]<sup>+</sup>. Purity (HPLC): 98.5%,  $t_R$  = 8.38 min. HRMS (m/z) C<sub>28</sub>H<sub>31</sub>N<sub>3</sub>O<sub>5</sub>S, [M+H]<sup>+</sup>, calculated 522.20572, found 522.20608, error 0.7 ppm.

**(*R/S*)-1-Oxo-4-phenyl-1-((pyridin-3-ylmethyl)amino)butan-2-yl (*S*)-1-(benzylsulfonyl)piperidine-2-carboxylate (*S,R/S*-10e; Lab-ID: AN319)**



*S,R/S-20e* (1.45 g, 3.00 mmol) was Boc-protected following general procedure B using 2.00 mL TFA in dry DCM (20 mL). After workup according to the general procedure, the free amine intermediate (440 mg, 1.15 mmol) was further reacted according to general procedure C using phenylmethanesulfonyl chloride (260 mg, 1.38 mmol) and NMM (150  $\mu$ L, 1.38 mmol) in dry DCM (20 mL). *S,R/S-10e* was obtained as a colorless oil (90 mg; 0.16 mmol, 15%),  $R_f$ : 0.60 (DC<sub>SIL</sub>; EtOAc/PE = 95:5). IR (ATR),  $\tilde{\nu}$  [ $\text{cm}^{-1}$ ]: 3308, 3046, 2921, 2852, 1741, 1671, 1536, 1322, 1125, 695. Diastereomeric ratio: 55:45.  $^1\text{H NMR}$  ( $\text{CDCl}_3$ ,  $\delta$  [ppm],  $J$  [Hz]): 8.63–8.61 (m, 1H), 8.54–8.52 (m, 1H), 7.83–7.79 (m, 2H), 7.41–7.36 (m, 6H), 7.26–7.12 (m, 5H), 5.38 (t,  $J$  = 5.6, 1H), 4.50–4.44 (m, 2H), 4.27–4.25 (m, 3H), 3.42–3.39 (m, 1H), 3.11–3.04 (m, 1H), 2.70–2.62 (m, 2H), 2.24–2.21 (m, 3H), 1.65–1.59 (m, 2H), 1.39–1.09 (m, 3H).  $^{13}\text{C NMR}$  ( $\text{CDCl}_3$ ,  $\delta$  [ppm]): 170.2, 169.6, 147.6, 146.7, 140.6, 138.1, 135.2, 130.9 (2C), 129.2, 128.8 (2C), 128.7 (2C), 128.5 (2C), 126.4 (2C), 124.3, 74.8, 59.5, 57.0, 44.5, 40.6, 34.0, 31.4, 27.1, 24.6, 20.4.  $^1\text{H NMR}$  ( $\text{CDCl}_3$ ,  $\delta$  [ppm],  $J$  [Hz]): 8.63–8.61 (m, 1H), 8.54–8.52 (m, 1H), 7.83–7.79 (m, 2H), 7.41–7.36 (m, 6H), 7.26–7.12 (m, 5H), 5.25 (t,  $J$  = 5.6, 1H), 4.50–4.44 (m, 2H), 4.27–4.25 (m, 2H), 4.16–4.14 (m, 1H), 3.29–3.25 (m, 1H), 3.11–3.04 (m, 1H), 2.70–2.62 (m, 2H), 2.24–2.21 (m, 2H), 2.01–1.99 (m, 1H), 1.65–1.59 (m, 2H), 1.39–1.09 (m, 3H).  $^{13}\text{C NMR}$  ( $\text{CDCl}_3$ ,  $\delta$  [ppm]): 170.2, 169.6, 147.6, 146.7, 140.6, 138.1, 135.2, 130.9 (2C), 129.0, 128.8 (2C), 128.7 (2C), 128.5 (2C), 126.2 (2C), 124.3, 74.8, 59.0, 56.1, 44.2, 40.6, 33.5, 30.7, 27.1, 24.6, 19.7. LC/MS ( $m/z$ ) 536.45 [ $\text{M} + \text{H}$ ] $^+$ . Purity (HPLC, *both diastereomers in total*): 99.3%,  $t_R$  = 8.69 min, 8.89 min. HRMS ( $m/z$ )  $\text{C}_{29}\text{H}_{33}\text{N}_3\text{O}_5\text{S}$ , [ $\text{M} + \text{H}$ ] $^+$ , calculated 536.22137, found 536.22152, error 0.3 ppm.

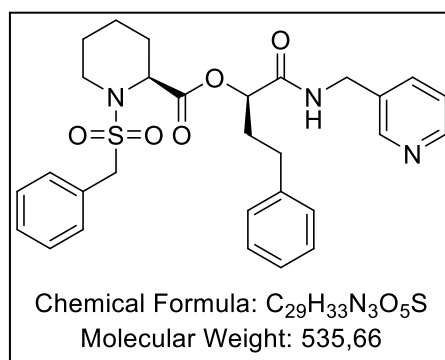
**(*R/S*)-1-Oxo-4-phenyl-1-((pyridin-3-ylmethyl)amino)butan-2-yl (*R*)-1-(benzylsulfonyl)piperidine-2-carboxylate (*R,R/S-10e*; Lab-ID: AN320)**



*R,R/S-20e* (1.45 g, 3.00 mmol) was Boc-protected following general procedure B using 2.00 mL

TFA in dry DCM (20 mL). After workup according to the general procedure, the free amine intermediate (230 mg, 0.60 mmol) was further reacted according to general procedure C using phenylmethanesulfonyl chloride (137 mg, 0.72 mmol) and NMM (80  $\mu$ L, 0.72 mmol) in dry DCM (12 mL). *R,R/S-10e* was obtained as a colorless oil (102 mg, 0.19 mmol, 31%),  $R_f$ : 0.60 (DC<sub>SIL</sub>; EtOAc/PE = 95:5). IR (ATR),  $\tilde{\nu}$  [ $\text{cm}^{-1}$ ]: 3349, 3044, 2921, 2852, 1741, 1671, 1536, 1322, 1125, 695. Diastereomeric ratio: 54:46.  $^1\text{H NMR}$  ( $\text{CDCl}_3$ ,  $\delta$  [ppm],  $J$  [Hz]): 8.59–8.58 (m, 1H), 8.51–8.49 (m, 1H), 7.78–1.76 (m, 1H), 7.70–7.66 (m, 1H), 7.41–7.34 (m, 6H), 7.27–7.11 (m, 5H), 5.38 (t,  $J$  = 5.6, 1H), 4.45–4.43 (m, 2H), 4.26–4.23 (m, 3H), 3.42–3.39 (m, 1H), 3.10–2.99 (m, 1H), 2.72–2.60 (m, 2H), 2.24–2.22 (m, 3H), 1.64–1.56 (m, 2H), 1.39–1.09 (m, 3H).  $^{13}\text{C NMR}$  ( $\text{CDCl}_3$ ,  $\delta$  [ppm]): 170.2, 169.6, 147.6, 146.7, 140.6, 138.1, 135.2, 130.9 (2C), 129.2, 128.8 (2C), 128.7 (2C), 128.5 (2C), 126.4 (2C), 124.3, 74.8, 59.5, 57.0, 44.5, 40.6, 34.0, 31.4, 27.1, 24.6, 20.4.  $^1\text{H NMR}$  ( $\text{CDCl}_3$ ,  $\delta$  [ppm],  $J$  [Hz]): 8.59–8.58 (m, 1H), 8.51–8.49 (m, 1H), 7.56–7.54 (m, 1H), 7.70–7.66 (m, 1H), 7.41–7.34 (m, 6H), 7.27–7.11 (m, 5H), 5.25 (t,  $J$  = 5.6, 1H), 4.45–4.43 (m, 2H), 4.26–4.23 (m, 2H), 4.14–4.12 (m, 1H), 3.26–3.23 (m, 1H), 3.10–2.99 (m, 1H), 2.72–2.60 (m, 2H), 2.24–2.22 (m, 2H), 2.01–1.99 (m, 1H), 1.64–1.56 (m, 2H), 1.39–1.09 (m, 3H).  $^{13}\text{C NMR}$  ( $\text{CDCl}_3$ ,  $\delta$  [ppm]): 170.2, 169.6, 147.6, 146.7, 140.6, 138.1, 135.2, 130.9 (2C), 129.0, 128.8 (2C), 128.7 (2C), 128.5 (2C), 126.2 (2C), 124.3, 74.8, 59.0, 56.1, 44.2, 40.6, 33.5, 30.7, 27.1, 24.6, 19.7. LC/MS ( $m/z$ ) 536.50 [ $\text{M}+\text{H}$ ] $^+$ . Purity (HPLC, *both diastereomers in total*): 95.2%,  $t_R$  = 8.68 min, 8.87 min. HRMS ( $m/z$ )  $\text{C}_{29}\text{H}_{33}\text{N}_3\text{O}_5\text{S}$ , [ $\text{M}+\text{H}$ ] $^+$ , calculated 536.22137, found 536.22097, error 0.7 ppm.

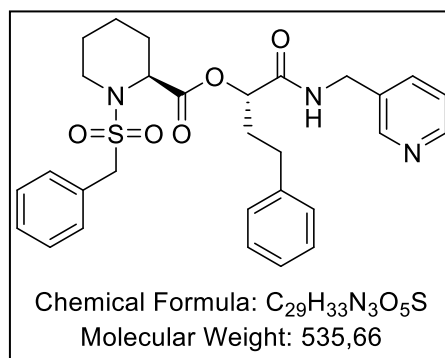
**(*R*)-1-Oxo-4-phenyl-1-((pyridin-3-ylmethyl)amino)butan-2-yl (*S*)-1-(benzylsulfonyl)piperidine-2-carboxylate (*S,R-10e*; Lab-ID: AN351)**



Esterification of *R-17e* (1.27 g, 5.55 mmol) and (*S*)-1-Boc-piperidine-2-carboxylic acid (1.50 g, 5.55 mmol) was conducted following general procedure A using 1.28 g of EDC·HCl (6.66 mmol)

and DMAP (340 mg, 2.78 mmol) in dry DCM (200 mL). The intermediate product was Boc-deprotected following general procedure B using 2.00 mL TFA in dry DCM (20 mL). After workup according to the general procedure, the free amine intermediate (233 mg, 0.61 mmol) was further reacted according to general procedure C using phenylmethanesulfonyl chloride (133 mg, 0.70 mmol) and NMM (80  $\mu$ L, 0.72 mmol) in dry DCM (12 mL). *S,R*-**10e** was obtained as a colorless oil (102 mg, 0.19 mmol, 31%),  $R_f$ : 0.58 (DC<sub>SIL</sub>; EtOAc/PE = 95:5), **IR** (ATR),  $\tilde{\nu}$  [ $\text{cm}^{-1}$ ]: 2921, 2852, 1741, 1671, 1536, 1322, 1125, 695. **<sup>1</sup>H NMR** (CDCl<sub>3</sub>,  $\delta$  [ppm], J [Hz]): 8.63–8.53 (m, 2H), 7.77–7.75 (m, 1H), 7.55–7.52 (m, 1H), 7.39–7.37 (m, 5H), 7.34–7.32 (m, 1H), 7.26–7.12 (m, 5H), 5.26 (t,  $J$  = 5.6, 1H), 4.52–4.40 (m, 2H), 4.27–4.23 (m, 3H), 3.27–3.24 (m, 1H), 3.06–3.03 (m, 1H), 2.73–2.59 (m, 2H), 2.24–2.20 (m, 2H), 2.01–1.99 (m, 1H), 1.61–1.58 (m, 2H), 1.42–1.31 (m, 3H). **<sup>13</sup>C NMR** (CDCl<sub>3</sub>,  $\delta$  [ppm]): 170.1, 169.6, 148.1, 147.6, 140.7, 137.3, 134.8, 130.9 (2C), 129.1, 129.0, 128.8 (2C), 128.6 (2C), 128.5 (2C), 126.3, 124.1, 74.8, 59.0, 56.2, 44.2, 40.7, 33.5, 30.8, 26.9, 24.6, 19.9. LC/MS ( $m/z$ ) 536.50 [M+H]<sup>+</sup>. Purity (HPLC): 95.1%,  $t_R$  = 8.68 min. HRMS ( $m/z$ ) C<sub>29</sub>H<sub>33</sub>N<sub>3</sub>O<sub>5</sub>S, [M+H]<sup>+</sup>, calculated 536.22137, found 536.22245, error 2.0 ppm.

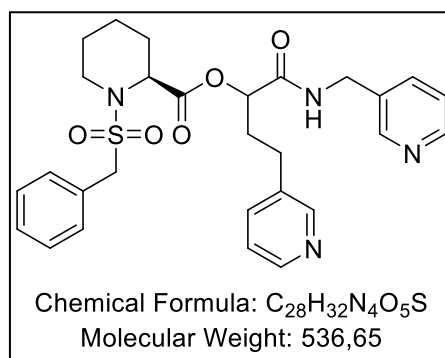
**(*S*)-1-Oxo-4-phenyl-1-((pyridin-3-ylmethyl)amino)butan-2-yl (*S*)-1-(benzylsulfonyl)piperidine-2-carboxylate (*S,S*-**10e**; Lab-ID: AN263)**



Esterification of *S*-**17e** (0.92 g, 4.00 mmol) and (*S*)-1-Boc-piperidine-2-carboxylic acid (1.08 g, 5.55 mmol) was conducted following general procedure A using 0.92 g of EDC·HCl (4.80 mmol) and DMAP (245 mg, 2.00 mmol) in dry DCM (160 mL). The intermediate product was Boc-deprotected following general procedure B using 2.00 mL TFA in dry DCM (20 mL). After workup according to the general procedure, the free amine intermediate (233 mg, 0.61 mmol) was further reacted according to general procedure C using phenylmethanesulfonyl chloride (140 mg, 0.74 mmol) and NMM (80  $\mu$ L, 0.81 mmol) in dry DCM (15 mL). *S,S*-**10e** was obtained as a

colorless oil (102 mg, 31%),  $R_f$ : 0.58 (DC<sub>SIL</sub>; EtOAc/PE = 95:5), **IR** (ATR),  $\tilde{\nu}$  [cm<sup>-1</sup>]: 2921, 2852, 1741, 1671, 1536, 1322, 1125, 695. **<sup>1</sup>H NMR** (CDCl<sub>3</sub>,  $\delta$  [ppm],  $J$  [Hz]): 8.58 (s, 1H), 8.52 (d,  $J$  = 4.5, 1H), 7.75 (t,  $J$  = 5.8, 1H), 7.67 (d,  $J$  = 7.8, 1H), 7.42–7.37 (m, 5H), 7.27–7.12 (m, 6H), 5.38 (t,  $J$  = 5.6, 1H), 4.45–4.43 (m, 2H), 4.23 (s, 2H), 4.13–4.11 (m, 1H), 3.42–3.39 (m, 1H), 3.05 (td,  $J$  = 13.0, 2.7, 1H), 2.75–2.60 (m, 2H), 2.26–2.15 (m, 3H), 1.68–1.62 (m, 2H), 1.36–1.29 (m, 2H), 1.15–1.09 (m, 1H). **<sup>13</sup>C NMR** (CDCl<sub>3</sub>,  $\delta$  [ppm]): 170.1, 169.4, 149.1, 148.2, 140.6, 136.3, 134.2, 130.9 (2C), 129.2, 128.9 (2C), 128.8, 128.6 (2C), 128.5 (2C), 126.3, 123.7, 74.8, 59.5, 57.0, 44.7, 40.7, 34.0, 31.3, 27.1, 24.6, 20.4. LC/MS (m/z) 536.50 [M+H]<sup>+</sup>. Purity (HPLC, *both diastereomers in total*): 95.4%,  $t_R$  = 8.89 min. HRMS (m/z) C<sub>29</sub>H<sub>33</sub>N<sub>3</sub>O<sub>5</sub>S, [M+H]<sup>+</sup>, calculated 536.22137, found 536.22170, error 0.6 ppm.

**(*R/S*)-1-Oxo-4-(pyridin-3-yl)-1-((pyridin-3-ylmethyl)amino)butan-2-yl (*S*)-1-(benzylsulfonyl)piperidine-2-carboxylate (*S,R/S*-10f; Lab-ID: AN350)**



*S,R/S*-**20f** was Boc-protected following general procedure B using 2.00 mL TFA in dry DCM (20 mL). After workup according to the general procedure, the free amine intermediate (555 mg, 1.45 mmol) was further reacted according to general procedure C using phenylmethanesulfonyl chloride (276 mg, 1.45 mmol) and NMM (175  $\mu$ L, 1.60 mmol) in dry DCM (30 mL). After purification by flash chromatography (SiO<sub>2</sub>, A: DCM, B: MeOH, gradient: 0  $\rightarrow$  30% B), *S,R/S*-**10f** was obtained as a colorless oil (380 mg, 0.71 mmol, 48%).  $R_f$ : 0.3 (DC<sub>SIL</sub>; EtOAc = 100%). **IR** (ATR),  $\tilde{\nu}$  [cm<sup>-1</sup>]: 3345, 3033, 2933, 1739, 1672, 1322, 1125, 696. Diastereomeric ratio: 53:47. **<sup>1</sup>H NMR** (CDCl<sub>3</sub>,  $\delta$  [ppm],  $J$  [Hz]): 8.59–8.57 (m, 1H), 8.52–8.50 (m, 1H), 8.43–8.39 (m, 2H), 7.82–7.64 (m, 2H), 7.52–7.50 (m, 1H), 7.41–7.36 (m, 5H), 7.26–7.23 (m, 2H), 5.38–5.37 (m, 1H), 4.46–4.37 (m, 2H), 4.24–4.22 (m, 3H), 3.42–3.40 (m, 1H), 3.06–2.93 (m, 1H), 2.79–2.56 (m, 3H), 2.27–2.15 (m, 3H), 1.69–1.57 (m, 2H), 1.40–1.27 (m, 2H). **<sup>1</sup>H NMR** (CDCl<sub>3</sub>,  $\delta$  [ppm],  $J$  [Hz]): 8.59–8.57 (m, 1H), 8.52–8.50 (m, 1H), 8.43–8.39 (m, 2H), 7.82–7.64 (m, 2H),

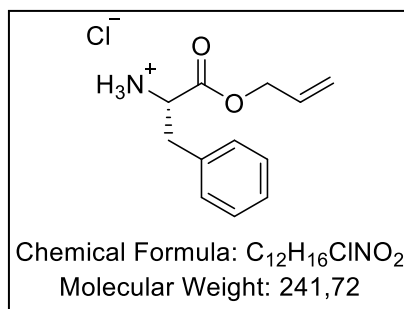


7.52–7.50 (m, 1H), 7.41–7.36 (m, 5H), 7.26–7.23 (m, 2H), 5.27–5.25 (m, 1H), 4.46–4.37 (m, 2H), 4.24–4.22 (m, 2H), 4.13–4.11 (m, 1H), 3.25–3.21 (m, 1H), 3.06–2.93 (m, 1H), 2.79–2.56 (m, 3H), 2.27–2.15 (m, 2H),

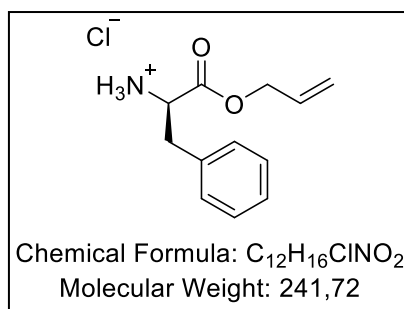
2.05–2.02 (m, 1H), 1.69–1.57 (m, 2H), 1.40–1.27 (m, 2H).  $^{13}\text{C}$  NMR ( $\text{CDCl}_3$ ,  $\delta$  [ppm]): 170.0, 169.1, 149.6, 149.4, 148.6, 147.6, 136.6, 136.3, 136.1, 134.1, 130.9 (2C), 129.3, 128.94 (2C), 128.90, 123.7 (2C), 74.5, 59.6, 57.0, 44.6, 40.8, 33.6, 28.3, 27.0, 24.6, 20.4.  $^{13}\text{C}$  NMR ( $\text{CDCl}_3$ ,  $\delta$  [ppm]): 169.8, 169.1, 149.5, 149.3, 148.5, 147.3, 136.4, 136.2, 136.1, 134.0, 130.9 (2C), 129.1, 128.86 (2C), 128.8, 123.7 (2C), 74.3, 59.0, 56.3, 44.3, 40.8, 33.1, 27.7, 26.8, 24.6, 19.8. LC/MS ( $m/z$ ) 537.10  $[\text{M}+\text{H}]^+$ , 269.20  $[\text{M}+2\text{H}]^{2+}$ . Purity (HPLC, *both diastereomers in total*): 98.8%,  $t_{\text{R}} = 6.52$  min, 6.59 min. HRMS ( $m/z$ )  $\text{C}_{28}\text{H}_{32}\text{N}_4\text{O}_5\text{S}$ ,  $[\text{M}+\text{H}]^+$ , calculated 537.21662, found 537.21764, error 1.9 ppm.

#### 4.6.1.3 Synthesis of the Pipecolic Amide Derivatives

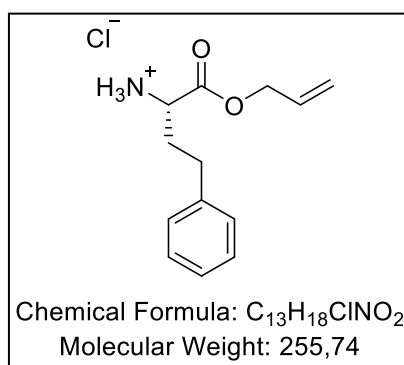
##### Allyl-L-phenylalaninate hydrochloride (*S*-23a; Lab-ID: AN230)



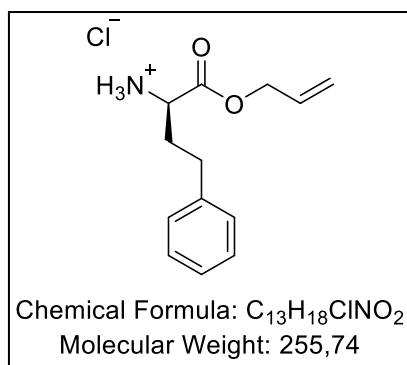
*S*-23a was synthesized according to general procedure G using 1.00 g of L-phenylalanine (6.05 mmol) and thionyl chloride (1.00 mL, 13.3 mmol) in allyl alcohol (12 mL, 181.6 mmol). The product was obtained as a white oily solid (957 mg, 3.96 mmol, 66%).  $R_f$ : 0.1 ( $\text{DC}_{\text{SIL}}$ ; PE/EtOAc = 4:1;  $\text{KMnO}_4$ ). IR (ATR),  $\tilde{\nu}$  [ $\text{cm}^{-1}$ ]: 3032, 2875, 1731, 1482, 1224, 823, 730.  $^1\text{H}$  NMR ( $\text{DMSO}-d_6$ ,  $\delta$  [ppm],  $J$  [Hz]): 8.60 (s, 3H), 7.34–7.27 (m, 5H), 5.95–5.90 (m, 1H), 5.39–5.27 (m, 2H), 4.64–4.62 (m, 2H), 4.08 (t,  $J = 6.3$ , 1H), 3.14 (d,  $J = 6.3$ , 2H).  $^{13}\text{C}$  NMR ( $\text{DMSO}-d_6$ ,  $\delta$  [ppm]): 170.1, 135.2, 131.7, 129.5 (2C), 128.5 (2C), 127.2, 118.2, 66.1, 52.5, 33.8.

**Allyl-D-phenylalaninate hydrochloride (*R*-23a, Lab-ID: AN353)**

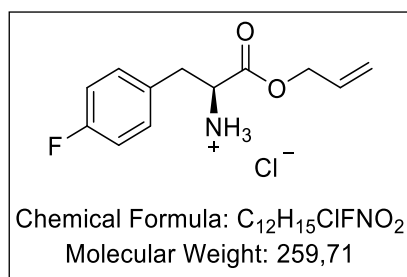
*R*-23a was synthesized according to general procedure G using 1.00 g of D-phenylalanine (6.05 mmol) and thionyl chloride (1.00 mL, 13.3 mmol) in allyl alcohol (12 mL, 181.6 mmol). Compound *R*-23a was obtained as a white oily solid (930 mg; 64%), *R*<sub>f</sub>: 0.1 (DC<sub>SIL</sub>; PE/EtOAc = 4:1; KMnO<sub>4</sub>). IR (ATR),  $\tilde{\nu}$  [cm<sup>-1</sup>]: 3032, 2875, 1731, 1482, 1224, 823, 730. <sup>1</sup>H NMR (DMSO-d<sub>6</sub>,  $\delta$  [ppm], *J* [Hz]): 8.60 (s, 3H), 7.33–7.26 (m, 5H), 5.95–5.89 (m, 1H), 5.37–5.28 (m, 2H), 4.67–4.65 (m, 2H), 4.11 (t, *J* = 6.3, 1H), 3.10 (d, *J* = 6.3, 2H). <sup>13</sup>C NMR (DMSO-d<sub>6</sub>,  $\delta$  [ppm]): 170.3, 135.1, 131.5, 129.5 (2C), 128.5 (2C), 127.1, 118.5, 65.8, 53.3, 35.8.

**Allyl-L-homophenylalaninate hydrochloride (*S*-23e; Lab-ID: AN229)**

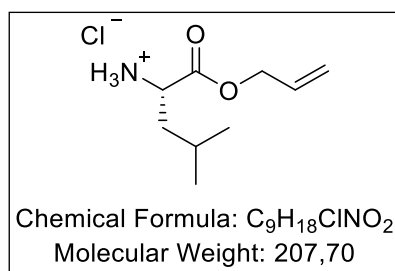
*S*-23e was synthesized according to general procedure G using 500 mg of L-homophenylalanine (2.79 mmol) and thionyl chloride (0.50 mL, 6.14 mmol) in allyl alcohol (5.70 mL, 83.7 mmol). Compound *S*-23e was obtained as a white oily solid (420 mg; 60%), *R*<sub>f</sub>: 0.1 (DC<sub>SIL</sub>; PE/EtOAc = 4:1; KMnO<sub>4</sub>). IR (ATR),  $\tilde{\nu}$  [cm<sup>-1</sup>]: 3052, 2857, 1741, 1582, 1519, 1263, 1192, 956, 700. <sup>1</sup>H NMR (DMSO-d<sub>6</sub>,  $\delta$  [ppm], *J* [Hz]): 8.76 (s, 3H), 7.32–7.21 (m, 5H), 5.98–5.91 (m, 1H), 5.39 (dd, *J* = 17.2, 1.4, 1H), 5.29 (dd, *J* = 10.5, 1.4, 1H), 4.70–4.66 (m, 2H), 4.05–4.03 (m, 1H), 2.80–2.62 (m, 2H), 2.13–2.08 (m, 2H). <sup>13</sup>C NMR (DMSO-d<sub>6</sub>,  $\delta$  [ppm]): 169.0, 140.2, 131.7, 128.5 (2C), 128.3 (2C), 126.2, 118.8, 65.9, 51.5, 31.8, 30.2.

**Allyl-D-homophenylalaninate hydrochloride (*R*-23e; Lab-ID: AN352I)**

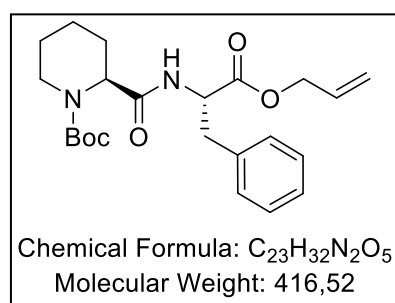
D-Homophenylalanine (500 mg, 2.79 mmol) was treated with allyl alcohol (5.70 mL, 83.7 mmol) and thionyl chloride (0.50 mL, 6.14 mmol) following general procedure G to obtain compound *R*-23e as a white oily solid (462 mg, 1.81 mmol, 65%),  $R_f$ : 0.1 (DC<sub>SIL</sub>; PE/EtOAc = 4:1; KMnO<sub>4</sub>). IR (ATR),  $\tilde{\nu}$  [cm<sup>-1</sup>]: 3045, 2853, 1741, 1581, 1518, 1263, 1096, 956, 700. <sup>1</sup>H NMR (DMSO-d<sub>6</sub>,  $\delta$  [ppm], J [Hz]): 8.85 (s, 3H), 7.32–7.18 (m, 5H), 6.00–5.90 (m, 1H), 5.43–5.37 (m, 1H), 5.30–5.27 (m, 1H), 4.69–4.67 (m, 2H), 4.04–4.02 (m, 1H), 2.83–2.76 (m, 1H), 2.69–2.61 (m, 1H), 2.18–2.08 (m, 2H). <sup>13</sup>C NMR (DMSO-d<sub>6</sub>,  $\delta$  [ppm]): 169.0, 140.3, 131.8, 128.5 (2C), 128.3 (2C), 126.2, 118.7, 65.9, 51.5, 31.8, 30.3.

**(*S*)-1-(Allyloxy)-3-(4-fluorophenyl)-1-oxopropan-2-aminium chloride (*S*-23g; Lab-ID: NJS216)**

*S*-23g was synthesized following general procedure G using 2450 mg of (*S*)-2-amino-3-(4-fluorophenyl)propanoic acid (13.4 mmol), allyl alcohol (29.1 mL, 428 mmol), thionyl chloride (6.05 mL, 82.9 mmol) and additional DMF (1.0 mL, 12.9 mmol). After purification according to the general procedure, compound *S*-23g was obtained as a white oily solid (2300 mg, 8.86 mmol, 66%),  $R_f$ : 0.6 (DC<sub>SIL</sub>; DCM/MeOH = 20:1; KMnO<sub>4</sub>). IR (ATR),  $\tilde{\nu}$  [cm<sup>-1</sup>]: 3151, 2996, 2791, 1738, 1602, 1509, 1489, 1219, 1192, 991, 938, 822. No IR data, melting point or  $R_f$  value were found in the literature. The NMR data are in agreement with Shang et al.<sup>3</sup>

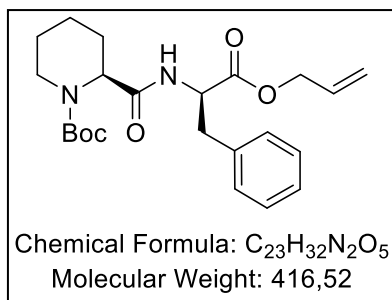
**Allyl-L-isoleucinate hydrochloride (*S*-23d; Lab-ID: NJS214)**

L-Leucine (2.00 g, 15.3 mmol) was treated with allyl alcohol (37.0 mL, 544 mmol) and thionyl chloride (4.00 mL, 54.8 mmol) in additional dry DCM (2 mL) following general procedure G to give *S*-23d as a colorless oil (2200 mg, 13.0 mmol, 84%), *R*<sub>f</sub>: 0.66 (DC<sub>ALOX</sub>; DCM/MeOH = 10:1; KMnO<sub>4</sub>). Data was consistent with the literature.<sup>4</sup>

***tert*-Butyl (*S*)-2-(((*S*)-1-(allyloxy)-1-oxo-3-phenylpropan-2-yl)carbamoyl)piperidine-1-carboxylate (*S,S*-24a; Lab-ID: AN234)**

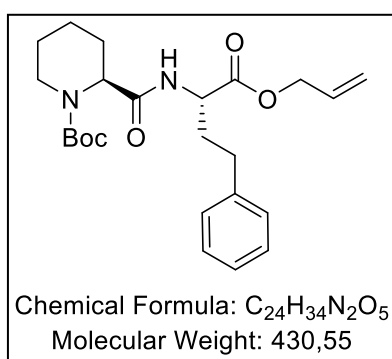
For the amidation of *S*-23a with (*S*)-1-Boc-piperidine-2-carboxylic acid (837 mg, 3.64 mmol), general procedure A was followed using 762 mg of EDC·HCl (3.97 mmol) and HOBT (223 mg, 1.66 mmol) in dry DCM (130 mL). *S,S*-24a was obtained as a yellow oil (915 mg, 2.20 mmol, 65%), *R*<sub>f</sub>: 0.36 (DC<sub>SIL</sub>; PE/EtOAc = 4:1; KMnO<sub>4</sub>). **IR** (ATR),  $\tilde{\nu}$  [cm<sup>-1</sup>]: 3340, 3004, 2935, 2859, 1741, 1677, 1509, 1455, 1158, 1031, 699. **<sup>1</sup>H NMR** (CDCl<sub>3</sub>,  $\delta$  [ppm], *J* [Hz]): 7.29–7.22 (m, 3H), 7.14–7.12 (m, 2H), 6.93–6.91 (m, 1H), 5.92–5.82 (m, 1H), 5.33–5.28 (dd, *J* = 17.2, 1.3, 1H), 5.25 (dd, *J* = 10.5, 1.1, 1H), 4.92–4.90 (m, 1H), 4.70–4.61 (m, 1H), 4.62 (d, *J* = 5.8, 2H), 4.01–3.84 (m, 1H), 3.24 (dd, *J* = 14.0, 5.7, 1H), 3.05 (dd, *J* = 14.0, 7.2, 1H), 2.37–2.21 (m, 2H), 1.43 (s, 9H), 1.59–1.31 (m, 5H). **<sup>13</sup>C NMR** (CDCl<sub>3</sub>,  $\delta$  [ppm]): 171.2, 170.9, 154.5, 136.0, 131.6, 129.4 (2C), 128.7 (2C), 127.3, 119.2, 80.7, 66.2, 53.1, 48.9, 42.3, 38.2, 28.4, 25.6, 24.9, 20.5.

***tert*-Butyl (*S*)-2-(((*R*)-1-(allyloxy)-1-oxo-3-phenylpropan-2-yl)carbamoyl)piperidine-1-carboxylate (*S,R*-24a; Lab-ID: AN354)**



For the amidation of *R*-23a (800 mg, 3.31 mmol) with (*S*)-1-Boc-piperidine-2-carboxylic acid (837 mg, 3.64 mmol) general procedure A was followed using 762 mg of EDC·HCl (3.97 mmol) and 223 mg of HOBT (1.66 mmol) in dry DCM (130 mL). *S,R*-24a was obtained as a yellow oil (688 mg, 1.65 mmol, 51%),  $R_f$ : 0.36 (DC<sub>SIL</sub>; PE/EtOAc = 4:1; KMnO<sub>4</sub>). IR (ATR),  $\tilde{\nu}$  [cm<sup>-1</sup>]: 3340, 3008, 2935, 2859, 1741, 1677, 1509, 1455, 1158, 1031, 699. <sup>1</sup>H NMR (CDCl<sub>3</sub>,  $\delta$  [ppm], J [Hz]): 7.28–7.24 (m, 3H), 7.12–7.10 (m, 2H), 6.57–6.55 (m, 1H), 5.91–5.82 (m, 1H), 5.33–5.24 (m, 2H), 4.93–4.88 (m, 1H), 4.79–4.65 (m, 1H), 4.61 (d,  $J$  = 5.8, 2H), 4.04–3.94 (m, 1H), 3.12–3.10 (m, 2H), 2.77–2.75 (m, 1H), 2.29–2.27 (m, 1H), 1.44 (s, 9H), 1.62–1.26 (m, 5H). <sup>13</sup>C NMR (CDCl<sub>3</sub>,  $\delta$  [ppm]): 171.3, 171.0, 154.6, 135.8, 131.6, 129.3 (2C), 128.8 (2C), 127.3, 119.3, 80.7, 66.2, 53.1, 48.9, 42.6, 38.0, 28.5, 25.0, 24.9, 20.7.

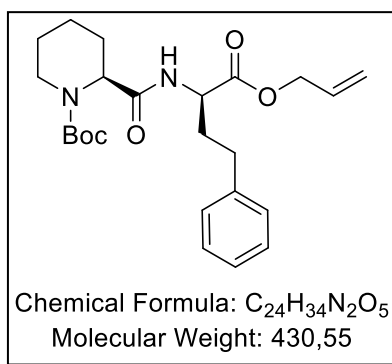
***tert*-Butyl (*S*)-2-(((*S*)-1-(allylamino)-1-oxo-4-phenylbutan-2-yl)carbamoyl)piperidine-1-carboxylate (*S,S*-24e; Lab-ID: AN235)**



For the amidation of *S*-23e (370 mg, 1.45 mmol) with (*S*)-1-Boc-piperidine-2-carboxylic acid (366 mg, 1.60 mmol), general procedure A was followed using 334 mg of EDC·HCl (1.74 mmol), HOBT (100 mg, 0.73 mmol) and NMM (200  $\mu$ L, 1.74 mmol) in dry DCM (60 mL). *S,S*-24e was obtained as a yellow oil (520 mg, 1.21 mmol, 83%),  $R_f$ : 0.5 (DC<sub>SIL</sub>; PE/EtOAc = 4:1; KMnO<sub>4</sub>).

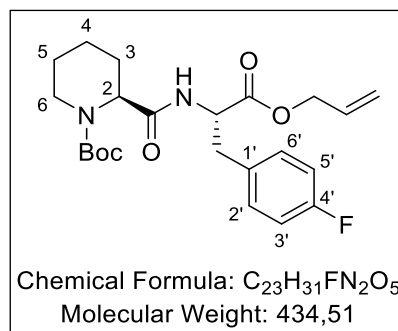
IR (ATR),  $\tilde{\nu}$  [ $\text{cm}^{-1}$ ]: 3341, 3012, 2935, 2862, 1737, 1684, 1365, 1249, 1158, 927, 699.  $^1\text{H NMR}$  ( $\text{CDCl}_3$ ,  $\delta$  [ppm],  $J$  [Hz]): 7.30–7.14 (m, 5H), 6.93–6.91 (m, 1H), 5.94–5.85 (m, 1H), 5.32 (dq,  $J = 17.3, 1.5, 1\text{H}$ ), 5.26 (dq,  $J = 10.5, 1.2, 1\text{H}$ ), 4.77–4.63 (m, 2H), 4.60 (dt,  $J = 5.9, 1.5, 2\text{H}$ ), 4.15–4.02 (m, 1H), 3.80–3.78 (m, 1H), 2.67–2.61 (m, 2H), 2.31–2.17 (m, 2H), 2.06–1.96 (m, 1H), 1.50 (s, 9H), 1.65–1.41 (m, 5H).  $^{13}\text{C NMR}$  ( $\text{CDCl}_3$ ,  $\delta$  [ppm]): 171.7, 171.3, 165.3, 140.7, 131.6, 128.7 (2C), 128.5 (2C), 126.3, 119.2, 80.9, 66.1, 53.2, 42.6, 34.4, 31.9, 28.5, 25.6, 25.0, 20.5.

*tert*-Butyl (*S*)-2-(((*R*)-1-(allylamino)-1-oxo-4-phenylbutan-2-yl)carbamoyl)piperidine-1-carboxylate (*S,R*-**24e**; Lab-ID: AN352II)



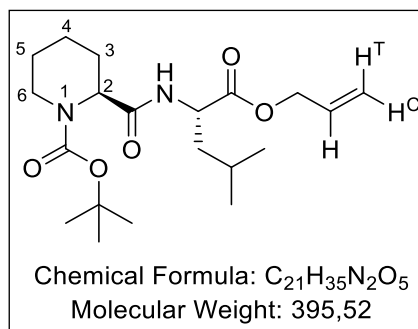
For the amidation of *R*-**23e** (400 mg, 1.56 mmol) with (*S*)-1-Boc-piperidine-2-carboxylic acid (428 mg, 1.87 mmol), general procedure A was followed using 300 mg of EDC·HCl (1.56 mmol), HOBT (42 mg, 0.31 mmol), and NMM (210  $\mu\text{L}$ , 1.87 mmol) in dry DCM (60 mL). *S,R*-**24e** was obtained as a colorless oil (468 mg, 1.09 mmol, 70%),  $R_f$ : 0.5 ( $\text{DC}_{\text{SIL}}$ ; PE/EtOAc = 4:1;  $\text{KMnO}_4$ ). IR (ATR),  $\tilde{\nu}$  [ $\text{cm}^{-1}$ ]: 3341, 3009, 2935, 2862, 1737, 1684, 1365, 1249, 1158, 927, 699.  $^1\text{H NMR}$  ( $\text{CDCl}_3$ ,  $\delta$  [ppm],  $J$  [Hz]): 7.30–7.14 (m, 5H), 6.66–6.64 (m, 1H), 5.94–5.84 (m, 1H), 5.33 (dq,  $J = 17.3, 1.5, 1\text{H}$ ), 5.26 (dq,  $J = 10.5, 1.2, 1\text{H}$ ), 4.82–4.80 (m, 1H), 4.70–4.64 (m, 1H), 4.61–4.58 (m, 2H), 4.12–4.02 (m, 1H), 2.93–2.86 (m, 1H), 2.67–2.62 (m, 2H), 2.32–2.17 (m, 2H), 2.04–1.96 (m, 1H), 1.50 (s, 9H), 1.65–1.41 (m, 5H).  $^{13}\text{C NMR}$  ( $\text{CDCl}_3$ ,  $\delta$  [ppm]): 171.9, 171.4, 162.5, 140.6, 131.6, 128.7 (2C), 128.5 (2C), 126.4, 119.2, 80.9, 66.1, 53.2, 42.3, 34.0, 31.8, 28.5, 25.5, 25.0, 20.6.

*tert*-Butyl (*S*)-2-(((*S*)-1-(allyloxy)-3-(4-fluorophenyl)-1-oxopropan-2-yl)carbamoyl)piperidine-1-carboxylate (*S,S*-24g; Lab-ID: NJS218)



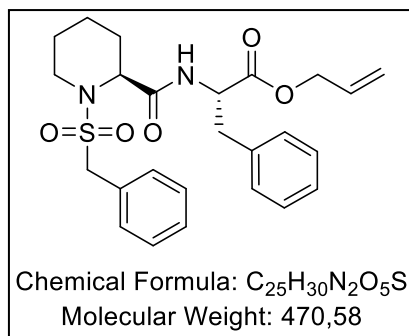
*S*-23g (1950 mg, 7.51 mmol) was reacted according to general procedure A using (*S*)-1-Boc-piperidine-2-carboxylic acid (1.81 g, 7.88 mmol), HBTU (3.28 g, 8.64 mmol), and NEt<sub>3</sub> (1.10 mL, 15.0 mmol) in dry DCM (200 mL). After stirring at rt for 4 d and workup according to general procedure A, the crude oily product was purified by column chromatography (aloxide basic III, PE/EtOAc/MeOH 90:30:4). *S,S*-24g was obtained as a colorless oil (3100 mg, 7.13 mmol, 95%). R<sub>f</sub>: 0.66 (DC<sub>ALOX</sub>; PE/EtOAc/MeOH = 9:3:0.4; KMnO<sub>4</sub>). IR (ATR),  $\tilde{\nu}$  [cm<sup>-1</sup>]: 3330, 2974, 2937, 1740, 1671, 1508, 1158, 988, 928, 822. <sup>1</sup>H NMR (CDCl<sub>3</sub>,  $\delta$  [ppm], J [Hz]): 7.13–7.05 (m, 2H, CH-2',6'), 7.01–6.92 (m, 2H, CH-3',5'), 6.61–6.32 (m, 1H, NH, rotamers), 5.92–5.82 (m, 1H, CH<sub>2</sub>CHCH<sub>2</sub>), 5.31 (d, 1H, OCH<sub>2</sub>CHCH<sup>trans</sup><sub>2</sub>, <sup>3</sup>J = 17.2), 5.26 (d, 1H, OCH<sub>2</sub>CHCH<sup>cis</sup><sub>2</sub>, <sup>3</sup>J = 10.5), 4.87 (br s, 1H, NHCHCOO), 4.70 (br s, 1H, CH-2), 4.61 (d, 2H, OCH<sub>2</sub>CH, <sup>3</sup>J = 5.9), 4.10–3.78 (m, 1H, CH<sub>2</sub>-6), 3.24–2.98 (m, 2H, CHCH<sub>2</sub>C<sub>q</sub>), 2.44 (br s, 1H, CH<sub>2</sub>-6, rotamers), 2.26–2.18 (m, 1H, CH<sub>2</sub>-3), 1.80–1.20 (m, 5H, CH<sub>2</sub>-3,4,5), 1.44 (s, 9H, C(CH<sub>3</sub>)<sub>3</sub>). <sup>13</sup>C NMR (CDCl<sub>3</sub>,  $\delta$  [ppm]): 171.1 (1C, COOCH<sub>2</sub>), 162.2 (d, <sup>1</sup>J<sub>CF</sub> = 245.5, 1C, C-4'), 131.8 (br 1C, C-1'), 131.5 (1C, OCH<sub>2</sub>CHCH<sub>2</sub>), 131.0 (d, <sup>3</sup>J<sub>CF</sub> = 7.8, 2C, CH-2',6'), 119.4 (1C, OCH<sub>2</sub>CHCH<sub>2</sub>), 115.6 (d, <sup>2</sup>J<sub>CF</sub> = 21.7, 2C, CH-3',5'), 80.9 (1C, OC(CH<sub>3</sub>)<sub>3</sub>), 66.3 (1C, OCH<sub>2</sub>CH), 55.5 & 54.1 (br 1C, CH-2, rotamers), 53.2 (1C, NHCHCO), 42.4 & 41.1 (br 1C, CH<sub>2</sub>-6, rotamers), 28.4 (3C, C(CH<sub>3</sub>)<sub>3</sub>), 25.6 (s, br, 1C, CH<sub>2</sub>-3), 24.9 (1C, CH<sub>2</sub>-5), 20.5 (1C, CH<sub>2</sub>-4).

*tert*-Butyl (*S*)-2-(((*S*)-1-(allyloxy)-4-methyl-1-oxopentan-2-yl)carbamoyl)piperidine-1-carboxylate (*S,S*-24d; Lab-ID: NJS226)

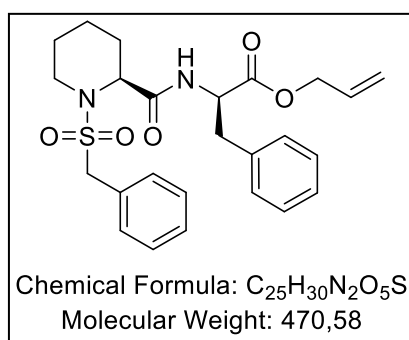


For the amidation of *S*-23d (2.20 g, 12.9 mmol) with (*S*)-1-Boc-piperidine-2-carboxylic acid (3.77 g, 16.4 mmol), general procedure A was followed using HBTU (5.73 g, 15.1 mmol) and NEt<sub>3</sub> (3.00 mL, 21.5 mmol) in DMF (due to solubility, 50 mL). After stirring at rt for 3 d and workup following general procedure A, the crude oily product was purified by column chromatography (aloxide basic III, Cy/EtOAc/MeOH = 15:4:1) and flash chromatography (SiO<sub>2</sub>, ELSD, A: CyH, B: EtOAc/MeOH 95:5, gradient: 10 → 100% B). Compound *S,S*-24d was obtained as a colorless solid (1.90 g, 4.97 mmol, 39%). R<sub>f</sub>: 0.51 (DC<sub>SIL</sub>; CyH/EtOAc/MeOH = 15:4:1; KMnO<sub>4</sub>). IR (ATR),  $\tilde{\nu}$  [cm<sup>-1</sup>]: 3315, 2956, 2936, 2869, 2160, 1737, 1687, 1666, 1544, 1383, 1277, 930, 780. <sup>1</sup>H NMR (CDCl<sub>3</sub>,  $\delta$  [ppm], J [Hz]): 6.65–6.20 (m, 1H, NH), 5.95–5.83 (m, 1H, CH<sub>2</sub>CHCH<sub>2</sub>), 5.32 (dd, 1H, OCH<sub>2</sub>CHCH<sup>trans</sup>, <sup>3</sup>J = 17.2, <sup>2</sup>J = 1.2), 5.24 (dd, <sup>3</sup>J = 10.5, <sup>2</sup>J = 1.2, 1H, OCH<sub>2</sub>CHCH<sup>cis</sup>), 4.74 (s, 1H, NHCHCO), 4.62–4.60 (m, 2H, OCH<sub>2</sub>CH), 4.59 (s, 1H, CH-2), 4.20–3.90 (m, 1H, CH<sub>2</sub>-6), 2.75 (br s, 1H, CH<sub>2</sub>-6), 2.26 (br s, 1H, CH<sub>2</sub>-3), 1.70–1.35 (m, 8H, CH<sub>2</sub>-3,4,5, NHCHCH<sub>2</sub>, CH<sub>2</sub>CH(CH<sub>3</sub>)<sub>2</sub>), 1.48 (s, 9H, C(CH<sub>3</sub>)<sub>3</sub>), 0.94 (d, <sup>3</sup>J = 5.9, 6H, C(CH<sub>3</sub>)<sub>2</sub>) ppm. <sup>13</sup>C NMR (CDCl<sub>3</sub>,  $\delta$  [ppm], J [Hz]): 172.5 (1C, COOCH<sub>2</sub>), 171.2 (1C, CONH) 155.6 (br 1C, NCOOC(CH<sub>3</sub>)<sub>3</sub>), 131.8 (1C, OCH<sub>2</sub>CHCH<sub>2</sub>), 118.8 (1C, OCH<sub>2</sub>CHCH<sub>2</sub>), 80.9 (1C, OC(CH<sub>3</sub>)<sub>3</sub>), 65.9 (1C, OCH<sub>2</sub>CH), 55.7 & 53.8 (br 1C, CH<sub>2</sub>-2, (rotamers)), 50.9 (1C, NHCHCO), 42.6 (br 1C, CH<sub>2</sub>-6), 41.7 (1C, NHCHCH<sub>2</sub>), 28.5 (3C, C(CH<sub>3</sub>)<sub>3</sub>), 25.5 (br 1C, CH<sub>2</sub>-3), 25.1 (2C, CH(CH<sub>3</sub>)<sub>2</sub>), 23.0 (1C, CH<sub>2</sub>-5), 21.9 (1C, CH(CH<sub>3</sub>)<sub>2</sub>), 20.6 (1C, CH<sub>2</sub>-4).



Allyl ((*S*)-1-(benzylsulfonyl)piperidine-2-carbonyl)-L-phenylalaninate*(S,S*-25a; Lab-ID: AN244)

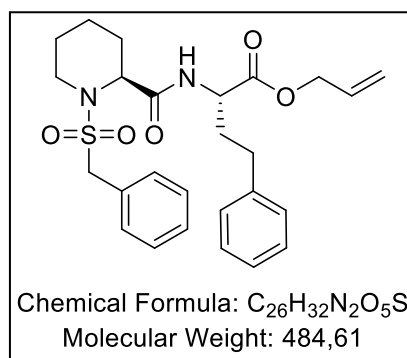
*S,S*-24a was Boc-protected following general procedure B using 5.00 mL of TFA in dry DCM (20 mL). After workup according to the general procedure, the free amine intermediate (736 mg, 2.33 mmol) was further reacted according to general procedure C using phenylmethanesulfonyl chloride (530 mg, 2.79 mmol) and NMM (300  $\mu$ L, 2.56 mmol) in dry DCM (50 mL). *S,S*-25a was obtained as a yellow oil (720 mg, 1.53 mmol, 66%). *R*<sub>f</sub>: 0.45 (DC<sub>SIL</sub>; PE/EtOAc = 2:1; KMnO<sub>4</sub>). IR (ATR),  $\tilde{\nu}$  [cm<sup>-1</sup>]: 3344, 3033, 2953, 2938, 1732, 1666, 1534, 1455, 1259, 694. <sup>1</sup>H NMR (CDCl<sub>3</sub>,  $\delta$  [ppm], J [Hz]): 7.43–7.36 (m, 5H), 7.28–7.14 (m, 5H), 6.66 (d, *J* = 8.0, 1H), 5.94–5.84 (m, 1H), 5.35–5.25 (m, 2H), 4.88–4.83 (m, 1H), 4.66–4.64 (m, 2H), 4.30–4.28 (m, 1H), 4.23 (s, 2H), 3.40–3.37 (m, 1H), 3.27 (dd, *J* = 14.0, 5.4, 1H), 3.28 (dd, *J* = 14.0, 8.0, 1H), 2.59–2.52 (m, 1H), 2.13–2.09 (m, 1H), 1.58–1.19 (m, 5H). <sup>13</sup>C NMR (CDCl<sub>3</sub>,  $\delta$  [ppm]): 171.1, 169.9, 136.0, 131.6, 130.9 (2C), 129.4 (2C), 129.1, 129.0, 128.9 (2C), 128.8 (2C), 127.3, 119.2, 66.2, 59.0, 56.4, 53.5, 42.3, 37.9, 26.0, 24.6, 19.8.

Allyl ((*S*)-1-(benzylsulfonyl)piperidine-2-carbonyl)-D-phenylalaninate (*S,R*-25a; Lab-ID: AN356)

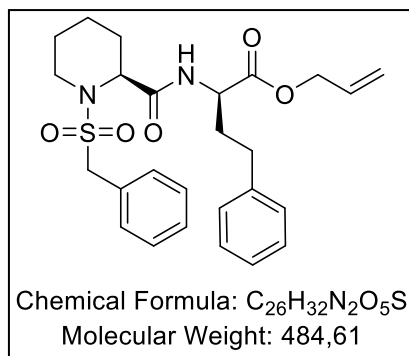
*S,R*-24a (600 mg, 1.28 mmol) was Boc-protected following general procedure B using 3.00 mL of TFA in dry DCM (20 mL). After workup according to the general procedure, the free amine

intermediate (500 mg, 1.58 mmol) was further reacted according to general procedure C using phenylmethanesulfonyl chloride (360 mg, 1.90 mmol) and NMM (170  $\mu$ L, 1.58 mmol) in dry DCM (30 mL). *S,R*-**25a** was obtained as a yellow oil (505 mg, 1.07 mmol, 68%),  $R_f$ : 0.45 (DC<sub>SII</sub>; PE/EtOAc = 2:1; KMnO<sub>4</sub>). IR (ATR),  $\tilde{\nu}$  [cm<sup>-1</sup>]: 3344, 3033, 2953, 2938, 1732, 1666, 1534, 1455, 1259, 916, 694. <sup>1</sup>H NMR (CDCl<sub>3</sub>,  $\delta$  [ppm], J [Hz]): 7.41–7.36 (m, 5H), 7.29–7.13 (m, 5H), 6.68 (d,  $J$  = 8.0, 1H), 5.91–5.82 (m, 1H), 5.33–5.24 (m, 2H), 4.85–4.83 (m, 1H), 4.63–4.60 (m, 2H), 4.31–4.29 (m, 1H), 4.24–4.22 (m, 2H), 3.54–3.50 (m, 1H), 3.18–3.00 (m, 3H), 2.17–2.14 (m, 1H), 1.60–1.23 (m, 5H). <sup>13</sup>C NMR (CDCl<sub>3</sub>,  $\delta$  [ppm]): 171.1, 169.9, 135.7, 131.6, 130.9 (2C), 129.4 (2C), 129.1, 129.0, 128.9 (2C), 128.8 (2C), 127.3, 119.2, 66.2, 59.0, 56.4, 53.4, 43.8, 37.9, 26.0, 24.5, 19.8.

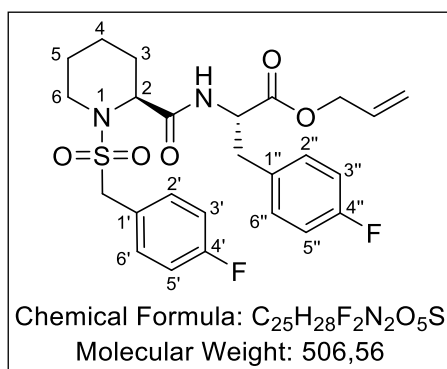
**(*S*)-*N*-((*S*)-1-(Allylamino)-1-oxo-4-phenylbutan-2-yl)-1-(benzylsulfonyl)piperidine-2-carboxamide (*S,S*-**25e**; Lab-ID: AN245)**



*S,S*-**24e** (520 mg, 1.20 mmol) was Boc-protected following general procedure B using 3.00 mL of TFA in dry DCM (20 mL). After workup according to the general procedure, the free amine intermediate (328 mg, 0.99 mmol) was further reacted according to general procedure C using phenylmethanesulfonyl chloride (227 mg, 1.20 mmol) and NMM (120  $\mu$ L, 1.09 mmol) in dry DCM (20 mL). *S,S*-**25e** was obtained as a yellow oil (345 mg, 0.71 mmol, 72%),  $R_f$ : 0.55 (DC<sub>SII</sub>; PE/EtOAc = 2:1; KMnO<sub>4</sub>). IR (ATR),  $\tilde{\nu}$  [cm<sup>-1</sup>]: 3345, 3030, 2955, 2938, 1731, 1670, 1530, 1455, 1254, 917, 695. <sup>1</sup>H NMR (CDCl<sub>3</sub>,  $\delta$  [ppm], J [Hz]): 7.48–7.36 (m, 5H), 7.28–7.16 (m, 5H), 6.80 (d,  $J$  = 7.7, 1H), 5.94–5.87 (m, 1H), 5.35–5.24 (m, 2H), 4.62–4.56 (m, 3H), 4.33–4.31 (m, 3H), 3.60–3.62 (m, 1H), 3.07–2.99 (m, 1H), 2.67 (t,  $J$  = 8.0, 2H), 2.25–2.01 (m, 3H), 1.63–1.21 (m, 5H). <sup>13</sup>C NMR (CDCl<sub>3</sub>,  $\delta$  [ppm]): 171.6, 170.2, 140.6, 131.6, 130.9 (2C), 129.1, 129.0, 128.8 (2C), 128.7 (2C), 128.6 (2C), 126.4, 119.2, 66.2, 59.1, 56.4, 52.5, 44.3, 33.9, 31.9, 26.2, 24.6, 19.9.

**(*R*)-*N*-((*S*)-1-(Allylamino)-1-oxo-4-phenylbutan-2-yl)-1-(benzylsulfonyl)piperidine-2-carboxamide (*S*,*R*-25e; Lab-ID: AN352III)**

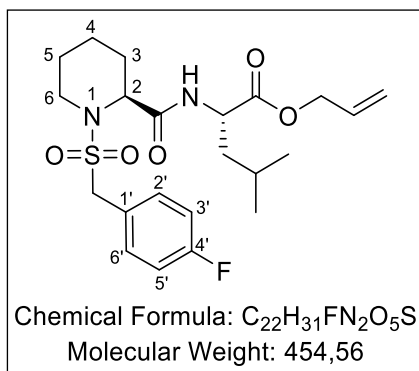
*S*,*R*-24e (400 mg, 0.93 mmol) was Boc-protected following general procedure B using 3.00 mL of TFA in dry DCM (20 mL). After workup according to the general procedure, the free amine intermediate (297 mg, 0.90 mmol) was further reacted according to general procedure C using phenylmethanesulfonyl chloride (205 mg, 1.08 mmol) and NMM (110  $\mu$ L, 0.99 mmol) in dry DCM (20 mL). *S*,*R*-25e was obtained as a colorless oil (266 mg, 0.55 mmol, 61%), R<sub>f</sub>: 0.55 (DC<sub>SIL</sub>; PE/EtOAc = 2:1; KMnO<sub>4</sub>). IR (ATR),  $\tilde{\nu}$  [cm<sup>-1</sup>]: 3345, 3030, 2955, 2938, 1731, 1670, 1533, 1454, 1264, 1147, 917, 695. <sup>1</sup>H NMR (CDCl<sub>3</sub>,  $\delta$  [ppm], J [Hz]): 7.48–7.37 (m, 5H), 7.29–7.16 (m, 5H), 6.79 (d, *J* = 8.02, 1H), 5.93–5.86 (m, 1H), 5.35–5.24 (m, 2H), 4.64–4.57 (m, 3H), 4.33–4.31 (m, 3H), 3.66–3.64 (m, 1H), 3.24–3.14 (m, 1H), 2.65 (t, *J* = 8.0, 2H), 2.25–2.17 (m, 2H), 2.00–1.95 (m, 1H), 1.63–1.28 (m, 5H). <sup>13</sup>C NMR (CDCl<sub>3</sub>,  $\delta$  [ppm]): 171.7, 170.0, 140.6, 131.7, 130.9 (2C), 129.1, 129.0, 128.9 (2C), 128.6 (2C), 128.4 (2C), 126.3, 119.2, 66.2, 58.7, 56.5, 52.2, 44.0, 33.8, 31.7, 25.8, 24.5, 19.9.

**Allyl-(*S*)-2-((*S*)-1-((4-fluorobenzyl)sulfonyl)piperidine-2-carboxamido)-3-(4-fluorophenyl)-propanoate (*S*,*S*-25g; Lab-ID: NJS230)**

*S*,*S*-24g (3060 mg, 7.04 mmol) was Boc-protected following general procedure B using TFA

(10 mL) in dry DCM (10 mL). After stirring at rt for 3 d and workup according to the general procedure, the amine intermediate (1.80 g, 5.38 mmol) was reacted according to general procedure C, using (4-fluorophenyl)methanesulfonyl chloride (1.36 g, 6.51 mmol) and DIPEA (3.00 mL, 17.2 mmol) in dry DCM (60 mL). After stirring at rt for 3 d and workup according to the general procedure, the crude oily product was purified by flash chromatography (run 1: SiO<sub>2</sub>, A: DCM, B: MeOH, gradient: 0→30% B; run 2: RP 18, A: H<sub>2</sub>O + 0.1% FA, B: MeOH + 0.1% FA, gradient: 5→100% B). Compound **S,S-25g** was obtained as a colorless solid (448 mg, 0.95 mmol, 16%). R<sub>f</sub>: 0.44 (DC<sub>ALOX</sub>; PE/EtOAc/MeOH = 15:5:0.5; KMnO<sub>4</sub>). IR (ATR),  $\tilde{\nu}$  [cm<sup>-1</sup>]: 3356, 2939, 1739, 1667, 1603, 1508, 1327, 1215, 1180, 1147, 1061, 835, 715. Mp: 104–106 °C. <sup>1</sup>H NMR (CDCl<sub>3</sub>,  $\delta$  [ppm], J [Hz]): 7.44–7.38 (m, 2H, CH-2',6'), 7.16–7.10 (m, 2H, CH-2'',6''), 7.09–7.03 (m, 2H, CH-3',5'), 7.00–6.93 (m, 2H, CH-3'',5''), 6.65 (d, <sup>3</sup>J = 7.9, 1H, CONH), 5.89 (ddt, <sup>3</sup>J<sub>trans</sub> = 17.0, <sup>3</sup>J<sub>cis</sub> = 10.3, <sup>3</sup>J = 5.9, 1H, CH<sub>2</sub>CHCH<sub>2</sub>), 5.32 (d, <sup>3</sup>J = 17.0, 1H, H<sup>trans</sup>), 5.27 (d, <sup>3</sup>J = 10.3, 1H, H<sup>cis</sup>), 4.86–4.79 (m, 1H, NHCHCOO), 4.63 (d, <sup>3</sup>J = 5.9, 2H, OCH<sub>2</sub>CHCH<sub>2</sub>), 4.30 (br d, <sup>3</sup>J = 4.2, 1H, CH-2), 4.20 (br s, 2H, SO<sub>2</sub>CH<sub>2</sub>), 3.43 (br d, <sup>2</sup>J = 13.4, 1H, CH<sub>2</sub>-6), 3.23 (dd, <sup>2</sup>J = 14.1, <sup>3</sup>J = 5.4, 1H, NHCHCH<sub>2</sub>), 3.01 (dd, <sup>2</sup>J = 14.1, <sup>3</sup>J = 7.6, 1H, NHCHCH<sub>2</sub>), 2.69 (ddd, <sup>2</sup>J = 13.4, <sup>3</sup>J = 13.4, 2.7, 1H, CH<sub>2</sub>-6), 2.12 (d, <sup>2</sup>J = 13.3, 1H, CH<sub>2</sub>-3), 1.63–1.54 (m, 1H, CH<sub>2</sub>-4), 1.48–1.18 (m, 4H, CH<sub>2</sub>-3,4,5). <sup>13</sup>C NMR (CDCl<sub>3</sub>,  $\delta$  [ppm]): 170.9 (1C, NHCHCOO), 170.0 (1C, CH-2CONH), 163.2 (d, <sup>1</sup>J<sub>CF</sub> = 248.7, 1C, C-4'), 162.2 (d, <sup>1</sup>J<sub>CF</sub> = 245.6, 1C, C-4''), 132.7 (d, <sup>3</sup>J<sub>CF</sub> = 8.4, 2C, CH-2',6'), 131.7 (d, <sup>4</sup>J<sub>CF</sub> = 3.3, 1C, C-1''), 131.5 (1C, OCH<sub>2</sub>CHCH<sub>2</sub>), 131.0 (d, <sup>3</sup>J<sub>CF</sub> = 8.0, 2C, CH-2'',6''), 124.9 (d, <sup>4</sup>J<sub>CF</sub> = 3.3, 1C, C-1'), 119.4 (1C, CH<sub>2</sub>CHCH<sub>2</sub>), 115.9 (d, <sup>2</sup>J<sub>CF</sub> = 21.7, 2C, CH-3',5'), 115.7 (d, <sup>2</sup>J<sub>CF</sub> = 21.4, 2C, CH-3'',5''), 66.4 (1C, OCH<sub>2</sub>CH), 58.2 (1C, SO<sub>2</sub>CH<sub>2</sub>), 56.3 (1C, CH-2), 53.6 (1C, NHCHCOO), 43.7 (1C, CH<sub>2</sub>-6), 37.2 (1C, NHCHCH<sub>2</sub>), 26.4 (1C, CH<sub>2</sub>-3), 24.8 (1C, CH<sub>2</sub>-5), 19.9 (1C, CH<sub>2</sub>-4). LC/MS (m/z) 507.25 [M+H]<sup>+</sup>. Purity (HPLC): 95.0%, t<sub>R</sub> = 9.58 min. HRMS (m/z) C<sub>25</sub>H<sub>28</sub>F<sub>2</sub>N<sub>2</sub>O<sub>5</sub>S, [M+H]<sup>+</sup>, calculated 507.17598, found 507.17627, error 0.6 ppm.

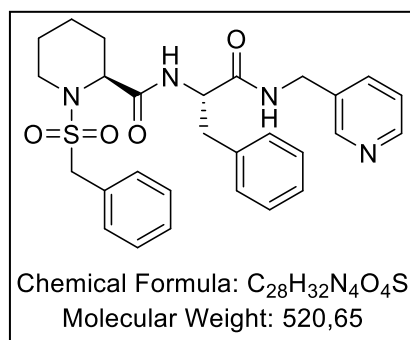
Allyl-(*S*)-1-((4-fluorobenzyl)sulfonyl)piperidine-2-carbonyl)-*L*-leucinate (*S,S*-25d; Lab-ID: NJS234)



*S,S*-24d (200 mg, 462 μmol) was Boc-protected according to general procedure B using TFA (3.00 mL) in dry DCM (10 mL). After stirring at rt for 1 d and workup according to the general procedure, the amine intermediate (1.40 g, 4.96 mmol) was reacted according to general procedure C using (4-fluorophenyl)methanesulfonyl chloride (1.35 g, 6.45 mmol) and NMM (2.50 mL, 22.7 mmol) in dry DCM (100 mL). After stirring for 3 d and workup according to the general procedure, the crude oily product was purified consecutively by column chromatography (SiO<sub>2</sub>, EtOAc/PE/MeOH 1:3:0.05) and flash chromatography (run 1: SiO<sub>2</sub>, A: CyH, B: EtOAc/MeOH/FA (95:5:0.05); gradient: 0 → 100% B; run 2: RP 18, A: H<sub>2</sub>O + 0.1% FA, B: MeOH + 0.1% FA, gradient: 5 → 100% B). Compound *S,S*-25d was obtained as a colorless oil (1.39 g, 3.06 mmol, 62%). R<sub>f</sub>: 0.71 (DC<sub>ALOX3</sub>; PE/EtOAc/MeOH = 3:1:0.05; KMnO<sub>4</sub>). IR (ATR),  $\tilde{\nu}$  [cm<sup>-1</sup>]: 3532, 3359, 3078, 2953, 2870, 1739, 1674, 1604, 1508, 1365, 1327, 1292, 1175, 1126, 1058, 840, 711. Mp: 89 °C. <sup>1</sup>H NMR (CDCl<sub>3</sub>, δ [ppm], J [Hz]): 7.47–7.41 (m, 2H, CH-2',6'), 7.10–7.03 (m, 2H, CH-3',5'), 6.51 (d, <sup>3</sup>J = 8.3, 1H, NH), 5.96–5.85 (m, 1H, CH<sub>2</sub>CHCH<sub>2</sub>), 5.33 (d, <sup>3</sup>J = 17.1, 1H, CH<sub>2</sub>CHCH<sub>2</sub>), 5.25 (d, <sup>3</sup>J = 10.5, 1H, CH<sub>2</sub>CHCH<sub>2</sub>), 4.68–4.56 (m, 3H, CH<sub>2</sub>CHCH<sub>2</sub>, NHCHCO), 4.38 (br s, 1H, CH-2), 4.30–4.21 (m, 2H, SO<sub>2</sub>CH<sub>2</sub>), 3.57 (d, <sup>2</sup>J = 13.1, 1H, CH<sub>2</sub>-6), 3.07 (ddd, <sup>2</sup>J = 13.1, <sup>3</sup>J = 13.1, 2.5, 1H, CH<sub>2</sub>-6), 2.21–2.16 (m, 1H, CH<sub>2</sub>-3), 1.73–1.46 (m, 7H, CH<sub>2</sub>-3,4,5, CH<sub>2</sub>CH(CH<sub>3</sub>)<sub>2</sub>, CH(CH<sub>3</sub>)<sub>2</sub>), 1.39–1.24 (m, 1H, CH<sub>2</sub>-4), 0.97–0.94 (m, 6H, CH(CH<sub>3</sub>)<sub>2</sub>). <sup>13</sup>C NMR (CDCl<sub>3</sub>, δ [ppm]): 172.3 (1C, COOCH<sub>2</sub>), 170.3 (1C, CONH), 163.2 (d, <sup>1</sup>J<sub>CF</sub> = 248, 1C, C-4'), 132.7 (d, <sup>3</sup>J<sub>CF</sub> = 8.3, 2C, CH-2',6'), 131.7 (1C, CH<sub>2</sub>CHCH<sub>2</sub>), 125.0 (d, <sup>4</sup>J<sub>CF</sub> = 3.5, 1C, C-1'), 118.9 (1C, CH<sub>2</sub>CHCH<sub>2</sub>), 115.9 (d, <sup>2</sup>J<sub>CF</sub> = 21.6, 2C, CH-3',5'), 66.1 (1C, COOCH<sub>2</sub>), 58.1 (1C, SO<sub>2</sub>CH<sub>2</sub>), 56.3 (br 1C, CH-2), 51.2 (br 1C,

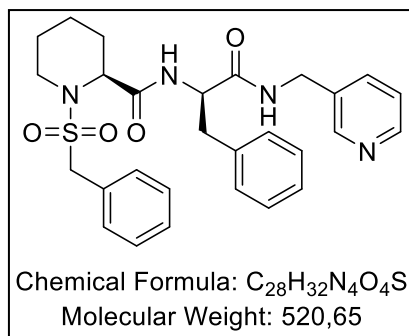
NHCHCO), 44.0 (1C, CH<sub>2</sub>-6), 41.3 (1C, CH<sub>2</sub>CH(CH<sub>3</sub>)<sub>2</sub>), 26.7 (1C, CH<sub>2</sub>-3), 25.1 (1C, CH(CH<sub>3</sub>)<sub>2</sub>), 25.0 (1C, CH<sub>2</sub>-5), 23.0 (2C, CH(CH<sub>3</sub>)<sub>2</sub>), 21.9 (1C, CH(CH<sub>3</sub>)<sub>2</sub>), 20.0 (1C, CH<sub>2</sub>-4).

**(S)-1-(Benzylsulfonyl)-N-((S)-1-oxo-3-phenyl-1-((pyridin-3-ylmethyl)amino)propan-2-yl)piperidine-2-carboxamide (S,S-21a; Lab-ID: AN258)**

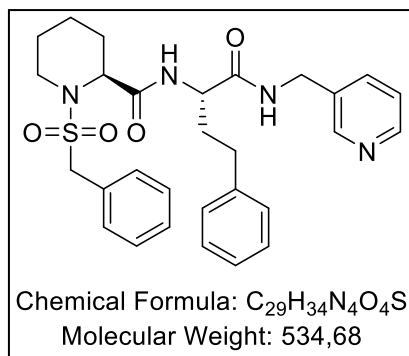


*S,S*-**25a** was allyl-deprotected according to general procedure D using Pd(PPh<sub>3</sub>)<sub>4</sub> (25 mg, 0.02 mmol) and morpholine (20 μL, 0.22 mmol) in dry THF (10 mL). After workup according to the general procedure, the carboxylic acid intermediate (90 mg, 0.21 mmol) was further reacted according to general procedure A using 3-picolylamine (30 μL, 0.25 mmol), EDC·HCl (48 mg, 0.25 mmol), and HOBT (15 mg, 0.11 mmol) in dry DCM (10 mL). *S,S*-**21a** was obtained as a white oily solid (89 mg, 0.17 mmol, 82%), R<sub>f</sub>: 0.2 (DC<sub>SIL</sub>; EtOAc = 100%). IR (ATR),  $\tilde{\nu}$  [cm<sup>-1</sup>]: 3268, 3030, 2936, 1731, 1650, 1540, 1495, 1322, 1146, 1056, 1029, 697. <sup>1</sup>H NMR (CDCl<sub>3</sub>,  $\delta$  [ppm], J [Hz]): 8.60–8.58 (m, 2H), 7.60–7.58 (m, 1H), 7.37 (s, 5H), 7.29–7.14 (m, 6H), 6.92 (t, J = 5.6, 1H), 6.65 (d, J = 8.3, 1H), 4.79–4.73 (m, 1H), 4.41–4.39 (m, 2H), 4.23 (s, 2H), 4.10–4.08 (m, 1H), 3.31–3.29 (m, 2H), 3.03–2.97 (m, 1H), 2.68–2.66 (m, 1H), 2.44–2.36 (m, 1H), 2.11–2.09 (m, 1H), 1.45–0.87 (m, 4H). <sup>13</sup>C NMR (CDCl<sub>3</sub>,  $\delta$  [ppm]): 170.9, 170.6, 148.5, 147.9, 136.6 (2C), 134.8, 130.7 (2C), 129.2 (2C), 129.0 (2C), 128.9 (2C), 128.5, 127.2 (2C), 123.9, 58.7, 57.0, 54.5, 43.7, 41.0, 37.5, 25.6, 24.3, 19.5. LC/MS (m/z) 521.45 [M+H]<sup>+</sup>. Purity (HPLC): 97.9%, t<sub>R</sub> = 7.89 min. HRMS (m/z) C<sub>28</sub>H<sub>32</sub>N<sub>4</sub>O<sub>4</sub>S, [M+H]<sup>+</sup>, calculated 521.22170, found 521.22088, error 1.6 ppm.

(*S*)-1-(Benzylsulfonyl)-*N*-((*R*)-1-oxo-3-phenyl-1-((pyridin-3-ylmethyl)amino)propan-2-yl)piperidine-2-carboxamide (*S,R*-21a; Lab-ID: AN358)



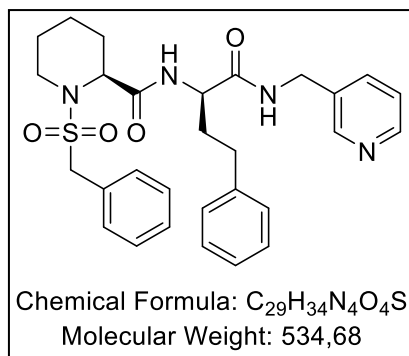
*S,R*-25a was allyl-deprotected according to general procedure D using Pd(PPh<sub>3</sub>)<sub>4</sub> (50 mg, 0.04 mmol) and morpholine (40 μL, 0.44 mmol) in dry THF (10 mL). After workup according to the general procedure, the carboxylic acid intermediate (150 mg, 0.40 mmol) was further reacted according to general procedure A using 3-picolyamine (50 μL, 0.44 mmol), EDC·HCl (85 mg, 0.44 mmol), and HOBT (27 mg, 0.20 mmol) in dry DCM (20 mL). *S,R*-21a was obtained as a white oily solid (100 mg, 0.20 mmol, 49%), R<sub>f</sub>: 0.2 (DC<sub>SIL</sub>; EtOAc = 100%). IR (ATR),  $\tilde{\nu}$  [cm<sup>-1</sup>]: 3296, 3032, 2939, 1649, 1534, 1322, 1125, 697. <sup>1</sup>H NMR (CDCl<sub>3</sub>, δ [ppm], J [Hz]): 8.46–8.44 (m, 2H), 7.55–7.53 (m, 1H), 7.41–7.35 (m, 5H), 7.25–7.20 (m, 6H), 6.94 (t, *J* = 5.9, 1H), 6.82 (d, *J* = 7.8, 1H), 4.67–4.65 (m, 1H), 4.36 (d, *J* = 6.0, 2H), 4.27–4.18 (m, 2H), 4.13–4.11 (m, 1H), 3.35–3.33 (m, 1H), 3.14 (dd, *J* = 13.9, 7.9, 1H), 3.05–2.96 (m, 2H), 2.67 (m, 1H), 1.89–1.86 (m, 1H), 1.45–1.19 (m, 4H). <sup>13</sup>C NMR (CDCl<sub>3</sub>, δ [ppm]): 171.0, 170.9, 148.6, 148.0, 136.6, 136.5, 134.3, 130.9 (2C), 129.3 (2C), 129.0 (2C), 128.9 (2C), 128.8, 127.1 (2C), 123.9, 58.8, 56.7, 54.8, 44.2, 41.0, 37.8, 26.9, 24.5, 19.8. LC/MS (*m/z*) 521.45 [M+H]<sup>+</sup>. Purity (HPLC): 99.3%, t<sub>R</sub> = 7.90 min. HRMS (*m/z*) C<sub>28</sub>H<sub>32</sub>N<sub>4</sub>O<sub>4</sub>S, [M+H]<sup>+</sup>, calculated 521.22170, found 521.22135, error: 0.7 ppm.

**(S)-1-(Benzylsulfonyl)-N-((S)-1-oxo-4-phenyl-1-((pyridin-3-ylmethyl)amino)butan-2-yl)piperidine-2-carboxamide (S,S-21e; Lab-ID: AN259)**

*S,S*-**25e** (345 mg, 0.71 mmol) was allyl-deprotected according to general procedure D using Pd(PPh<sub>3</sub>)<sub>4</sub> (82 mg, 0.07 mmol) and morpholine (60 μL, 0.75 mmol) in dry THF (10 mL). After workup according to the general procedure, the carboxylic acid intermediate (315 mg, 0.71 mmol) was further reacted according to general procedure A using 3-picolylamine (90 μL, 0.85 mmol), EDC·HCl (163 mg, 0.85 mmol), and HOBT (50 mg, 0.36 mmol) in dry DCM (30 mL). *S,S*-**21e** was obtained as a colorless oil (102 mg, 0.19 mmol, 31%), R<sub>f</sub>: 0.35 (DC<sub>SIL</sub>; EtOAc = 100%). IR (ATR),  $\tilde{\nu}$  [cm<sup>-1</sup>]: 3287, 3029, 2921, 2852, 1741, 1671, 1536, 1322, 1125, 695. <sup>1</sup>H NMR (CDCl<sub>3</sub>,  $\delta$  [ppm], J [Hz]): 8.52–8.47 (m, 2H), 7.65–7.63 (m, 1H), 7.43–7.36 (m, 5H), 7.25–7.11 (m, 7H), 6.85 (d, *J* = 8.1, 1H), 4.49–4.40 (m, 3H), 4.29 (s, 2H), 4.19–4.17 (m, 1H), 3.49–3.46 (m, 1H), 2.99–2.93 (m, 1H), 2.64 (t, *J* = 7.9, 2H), 2.27–2.22 (m, 1H), 2.10–2.07 (m, 1H), 2.01–1.95 (m, 1H), 1.57–1.49 (m, 2H), 1.32–1.25 (m, 3H). <sup>13</sup>C NMR (CDCl<sub>3</sub>,  $\delta$  [ppm]): 171.4, 170.9, 148.6, 148.1, 140.7, 136.4, 134.4, 130.9 (2C), 129.1 (2C), 129.0, 128.7 (3C), 128.5, 126.3 (2C), 123.9, 58.8, 56.9, 53.4, 44.1, 41.0, 33.5, 32.1, 26.1, 24.6, 19.8. LC/MS (*m/z*) 535.50 [M+H]<sup>+</sup>. Purity (HPLC): 99.2%, t<sub>R</sub> = 8.19 min. HRMS (*m/z*) C<sub>29</sub>H<sub>34</sub>N<sub>4</sub>O<sub>4</sub>S, [M+H]<sup>+</sup>, calculated 535.23735, found 535.23729, error: 0.1 ppm.

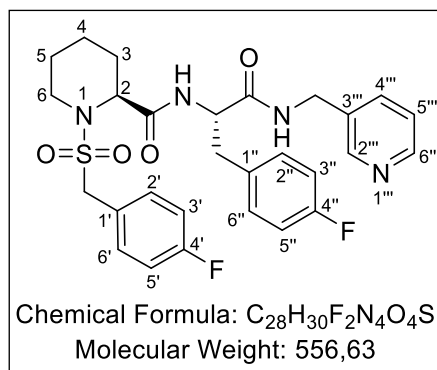


**(S)-1-(Benzylsulfonyl)-N-((R)-1-oxo-4-phenyl-1-((pyridin-3-ylmethyl)amino)butan-2-yl)piperidine-2-carboxamide (S,R-21e; Lab-ID: AN352)**



*S,R-25e* (150 mg, 0.31 mmol) was allyl-deprotected according to general procedure D using Pd(PPh<sub>3</sub>)<sub>4</sub> (35 mg, 0.03 mmol) and morpholine (30 μL, 0.33 mmol) in dry THF (10 mL). After workup according to the general procedure, the carboxylic acid intermediate (137 mg, 0.31 mmol) was further reacted according to general procedure A using 3-picolylamine (45 μL, 0.37 mmol), EDC·HCl (70 mg, 0.37 mmol), and HOBT (22 mg, 0.16 mmol) in dry DCM (10 mL). *S,R-21e* was obtained as a colorless oil (58 mg, 0.11 mmol, 33%), R<sub>f</sub>: 0.35 (DC<sub>SII</sub>; EtOAc = 100%). IR (ATR),  $\tilde{\nu}$  [cm<sup>-1</sup>]: 3035, 2921, 2852, 1741, 1671, 1536, 1322, 1125, 695. <sup>1</sup>H NMR (CDCl<sub>3</sub>,  $\delta$  [ppm], J [Hz]): 8.63–8.53 (m, 2H), 7.76–7.74 (m, 1H), 7.55–7.52 (m, 1H), 7.38 (s, 5H), 7.33–7.30 (m, 1H), 7.27–7.12 (m, 6H), 5.25 (t, *J* = 5.6, 1H), 4.49 (dd, *J* = 14.9, 6.2, 1H), 4.42 (dd, *J* = 14.9, 5.9, 1H), 4.27–4.25 (m, 1H), 4.23 (s, 2H), 3.27–3.24 (m, 1H), 3.06–3.03 (m, 1H), 2.73–2.59 (m, 2H), 2.24–2.20 (m, 2H), 2.03–2.00 (m, 1H), 1.61–1.58 (m, 2H), 1.42–1.31 (m, 3H). <sup>13</sup>C NMR (CDCl<sub>3</sub>,  $\delta$  [ppm]): 170.1, 169.5, 148.5, 147.6, 140.7, 137.2, 134.8, 130.9 (2C), 129.1, 129.0, 128.8 (2C), 128.6, 128.5 (2C), 126.3 (2C), 124.1, 74.8, 59.0, 56.2, 44.1, 40.7, 33.5, 30.8, 27.0, 24.6, 19.8. LC/MS (*m/z*) 535.45 [M+H]<sup>+</sup>. Purity (HPLC): 97.9%, t<sub>R</sub> = 8.20 min, HRMS (*m/z*) C<sub>29</sub>H<sub>34</sub>N<sub>4</sub>O<sub>4</sub>S, [M+H]<sup>+</sup>, calculated 535.23735, found 535.23660, error: 1.4 ppm.

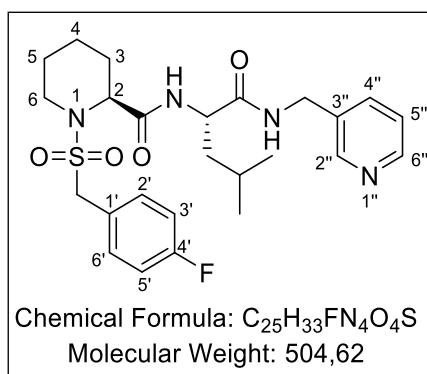
(*S*)-1-((4-Fluorobenzyl)sulfonyl)-*N*-((*S*)-3-(4-fluorophenyl)-1-oxo-1-(pyridin-3-ylmethyl)amino)propan-2-yl)piperidine-2-carboxamide (*S,S*-21g; Lab-ID: NJS227)



*S,S*-25g (375 mg, 740  $\mu$ mol) was allyl-deprotected according to general procedure D using Pd(PPh<sub>3</sub>)<sub>4</sub> (86 mg, 74  $\mu$ mol) and morpholine (70  $\mu$ L, 0.80 mmol) in dry THF (30 mL). After stirring at rt for 21 h, the reaction mixture was worked up according to the general procedure. The crude oily intermediate product was purified by flash chromatography (SiO<sub>2</sub>, A: PE, B: EtOAc/MeOH 9:1 + 0.1% FA, gradient: 0  $\rightarrow$  100% B) to obtain the carboxylic acid intermediate as a colorless solid (290 mg, 622  $\mu$ mol, 84%). Subsequently, the intermediate product (277 mg, 590  $\mu$ mol) was reacted according to general procedure A using HBTU (262 mg, 690  $\mu$ mol), 3-picolyamine (90  $\mu$ L, 0.88 mmol), and DIPEA (0.21 mL, 1.21 mmol) in dry DCM (30 mL). After stirring at rt for 4 d and workup according to the general procedure, the crude oily product was purified by flash chromatography (RP 18, A: H<sub>2</sub>O + 0.2% FA, B: MeOH + 0.2% FA, gradient: 5  $\rightarrow$  100% B). Compound *S,S*-21g was obtained as a colorless solid (205 mg, 0.37 mmol, 62%). R<sub>f</sub>: 0.56 (DC<sub>SIL</sub>; DCM/MeOH = 10:1). IR (ATR),  $\tilde{\nu}$  [cm<sup>-1</sup>]: 3290, 3068, 2941, 1650, 1603, 1508, 1326, 1220, 1183, 1126, 839, 773, 711. Mp: 78 °C. <sup>1</sup>H NMR (CDCl<sub>3</sub>,  $\delta$  [ppm], J [Hz]): 8.55–8.44 (m, 2H, CH-6''', 2'''), 7.56–7.52 (m, 1H, CH-4'''), 7.38–7.32 (m, 2H, CH-2', 6'), 7.26–7.21 (m, 1H, CH-5'''), 7.16–7.02 (m, 5H, CH-2'', 6'', 3', 5', NH), 6.94–6.80 (m, 3H, CH-3'', 5'', NH), 4.75–4.66 (m, 1H, NHCHCO), 4.45–4.30 (m, 2H, NHCH<sub>2</sub>), 4.22–4.11 (m, 3H, SO<sub>2</sub>CH<sub>2</sub>, CH-2), 3.34 (br d, <sup>2</sup>J = 13.5, 1H, CH<sub>2</sub>-6), 3.20 (dd, <sup>2</sup>J = 14.2, <sup>3</sup>J = 5.9, 1H, NHCHCH<sub>2</sub>), 2.97 (dd, <sup>2</sup>J = 14.2, <sup>3</sup>J = 8.6, 1H, NHCHCH<sub>2</sub>), 2.58 (ddd, <sup>2</sup>J = 13.5, <sup>3</sup>J = 13.5, 2.9, 1H, CH<sub>2</sub>-6), 2.07 (br d, <sup>2</sup>J = 13.9, 1H, CH<sub>2</sub>-3), 1.54–1.44 (m, 1H, CH<sub>2</sub>-4), 1.43–1.35 (m, 1H, CH<sub>2</sub>-5), 1.33–1.22 (m, 1H, CH<sub>2</sub>-3), 1.20–1.09 (m, 1H, CH<sub>2</sub>-5), 1.09–0.96 (m, 1H, CH<sub>2</sub>-4). <sup>13</sup>C NMR (CDCl<sub>3</sub>,  $\delta$  [ppm]): 170.6 (1C, CONHCH<sub>2</sub>), 170.4 (1C, CHCO), 163.3 (d, <sup>1</sup>J<sub>CF</sub> = 249.3, 1C, CF'), 162.1 (d, <sup>1</sup>J<sub>CF</sub> = 245.8, 1C, CF''), 149.4 (1C, CH-2'''), 149.0 (1C, CH-6'''), 135.7 (1C, CH-4'''), 133.6 (1C,

$C-3''$ ), 132.6 (d,  $^3J_{CF} = 8.3$ , 2C,  $CH-2',6'$ ), 132.3 (d,  $^4J_{CF} = 3.2$ , 1C,  $C-1''$ ), 130.8 (d,  $^3J_{CF} = 7.9$ , 2C,  $CH-2'',6''$ ), 124.4 (d,  $^4J_{CF} = 3.4$ , 1C,  $C-1'$ ), 123.7 (1C,  $CH-5''$ ), 116.1 (d,  $^2J_{CF} = 21.8$ , 2C,  $CH-3',5'$ ), 115.8 (d,  $^2J_{CF} = 21.3$ , 2C,  $CH-3'',5''$ ), 57.9 (1C,  $SO_2CH_2$ ), 57.0 (1C,  $CH-2$ ), 54.6 (1C,  $NHCH$ ), 43.8 (1C,  $CH_2-6$ ), 41.2 (1C,  $NHCH_2$ ), 36.9 (1C,  $NHCHCH_2$ ), 25.9 (1C,  $CH_2-3$ ), 24.5 (1C,  $CH_2-5$ ), 19.6 (1C,  $CH_2-4$ ). LC/MS (m/z) 557.45  $[M+H]^+$ . Purity (HPLC): 97.0%,  $t_R = 8.10$  min, HRMS  $C_{28}H_{30}F_2N_4O_4S$ ,  $[M+H]^+$ , calculated 557.20286, found 557.20306, error: 0.4 ppm.

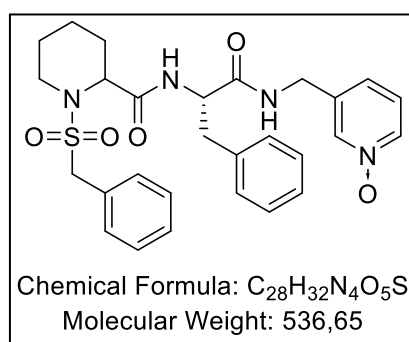
**(S)-1-((4-Fluorobenzyl)sulfonyl)-N-((S)-4-methyl-1-oxo-1-((pyridin-3-ylmethyl)-amino)-pentan-2-yl)piperidine-2-carboxamide (S,S-21d; Lab-ID: NJS224)**



**S,S-25d** (1.30 g, 2.87 mmol) was allyl-protected according to general procedure D using  $Pd(PPh_3)_4$  (332 mg, 287  $\mu$ mol) and morpholine (260  $\mu$ L, 3.01 mmol) in dry THF (30 mL). After stirring at rt for 4 d, the reaction mixture was worked up according to the general procedure. The crude oily product was purified by flash chromatography (run 1:  $SiO_2$ , A: PE, B: EtOAc/MeOH 9:1 + 0.1% FA, gradient: 0  $\rightarrow$  100% B; run 2: RP 18, A:  $H_2O$  + 0.1% FA, B: MeOH + 0.1% FA, gradient: 30  $\rightarrow$  100% B) to obtain the carboxylic acid intermediate as a colorless oily solid (740 mg, 1.79 mmol, 62%). 681 mg of the intermediate product (1.64 mmol) were further treated according to general procedure A using DIPEA (180  $\mu$ L, 1.80 mmol), 3-picolylamine (260  $\mu$ L, 2.55 mmol), and HBTU (917 mg, 2.42 mmol) in dry DCM (45 mL). After stirring at rt for 5 d and workup according to the general procedure, the crude oily product was purified by column chromatography (aloxide basic III, Cy/EtOAc/MeOH/FA = 50:48:1.9:0.1) and flash chromatography (run 1: RP 18, A:  $H_2O$  + 0.1% FA, B: MeOH + 0.1% FA, gradient: 5  $\rightarrow$  100% B; run 2: RP 18, A:  $H_2O$  + 0.1% FA, B: ACN + 0.1% FA, gradient: 5  $\rightarrow$  100% B). Compound **S,S-21d** was obtained as a colorless solid (479 mg, 0.95 mmol, 58%).  $R_f$ : 0.35 ( $DC_{ALOX}$ ; CyH/EtOAc/MeOH/FA =

10:10:1:0.1). IR (ATR),  $\tilde{\nu}$  [cm<sup>-1</sup>]: 3286, 3053, 2953, 2869, 1648, 1604, 1541, 1508, 1355, 1327, 1222, 1184, 1126, 975, 840, 772, mp: 70 °C. <sup>1</sup>H NMR (CDCl<sub>3</sub>,  $\delta$  [ppm], J [Hz]): 8.52–8.49 (m, 2H, CH-2<sup>''</sup>,6<sup>''</sup>), 7.61–7.57 (m, 1H, CH-4<sup>''</sup>), 7.42–7.37 (m, 2H, CH-2<sup>'</sup>,6<sup>'</sup>), 7.25–7.21 (m, 1H, CH-5<sup>''</sup>), 7.12–7.05 (m, 2H, CH-3<sup>'</sup>,5<sup>'</sup>), 6.79 (t, <sup>3</sup>J = 5.6, 1H, CONHCH), 6.57–6.54 (m, 1H, NHCH<sub>2</sub>), 4.50–4.44 (m, 1H, NHCHCO), 4.42 (d, <sup>3</sup>J = 6.0, 2H, NHCH<sub>2</sub>), 4.24 (br s, 2H, SO<sub>2</sub>CH<sub>2</sub>), 4.22–4.18 (m, 1H, CH-2), 3.52 (d, <sup>2</sup>J = 13.5, 1H, CH<sub>2</sub>-6), 3.03–2.93 (br s, 1H, CH<sub>2</sub>-6), 2.22–2.15 (m, 1H, CH<sub>2</sub>-3), 1.83–1.73 (m, 1H, CH<sub>2</sub>CH(CH<sub>3</sub>)<sub>2</sub>), 1.69–1.53 (m, 4H, CH(CH<sub>3</sub>)<sub>2</sub>, CH<sub>2</sub>CH(CH<sub>3</sub>)<sub>2</sub>, CH<sub>2</sub>-4,5), 1.46–1.24 (m, 3H, CH<sub>2</sub>-3,4,5), 0.94 (d, <sup>3</sup>J = 6.3, 3H, CH(CH<sub>3</sub>)<sub>2</sub>), 0.91 (d, <sup>3</sup>J = 6.3, 3H, CH(CH<sub>3</sub>)<sub>2</sub>). <sup>13</sup>C NMR (CDCl<sub>3</sub>,  $\delta$  [ppm]): 171.8 (1C, CONHCH<sub>2</sub>), 170.6 (1C, CH-2CONH), 163.3 (d, <sup>1</sup>J<sub>CF</sub> = 249, 1C, C-4<sup>'</sup>), 149.3 (1C, CH-2<sup>''</sup>), 149.0 (1C, CH-6<sup>''</sup>), 135.6 (1C, CH-4<sup>''</sup>), 133.9 (1C, CH-3<sup>''</sup>), 132.7 (d, <sup>3</sup>J<sub>CF</sub> = 8.4, 2C, CH-2<sup>'</sup>,6<sup>'</sup>), 124.5 (d, <sup>4</sup>J<sub>CF</sub> = 3.4, 1C, C-1<sup>'</sup>), 123.7 (1C, CH-5<sup>''</sup>), 116.1 (d, <sup>2</sup>J<sub>CF</sub> = 21.7, 2C, CH-3<sup>'</sup>,5<sup>'</sup>), 57.9 (1C, SO<sub>2</sub>CH<sub>2</sub>), 57.0 (1C, CH-2), 52.3 (1C, NHCHCO), 44.2 (1C, CH<sub>2</sub>-6), 41.1 (1C, NHCH<sub>2</sub>), 40.5 (1C, CH<sub>2</sub>CH(CH<sub>3</sub>)<sub>2</sub>), 26.3 (1C, CH<sub>2</sub>-3), 25.2 (1C, CH<sub>2</sub>CH(CH<sub>3</sub>)<sub>2</sub>), 24.8 (1C, CH<sub>2</sub>-5), 23.2 (1C, CH(CH<sub>3</sub>)<sub>2</sub>), 21.7 (1C, CH(CH<sub>3</sub>)<sub>2</sub>), 19.9 (1C, CH<sub>2</sub>-4). LC/MS (m/z) 505.10 [M+H]<sup>+</sup>. Purity (HPLC): 99.0%, t<sub>R</sub> = 7.74 min, HRMS (m/z) C<sub>25</sub>H<sub>33</sub>FN<sub>4</sub>O<sub>4</sub>S, [M+H]<sup>+</sup>, calculated 505.22793, found 505.22772, error: 0.4 ppm.

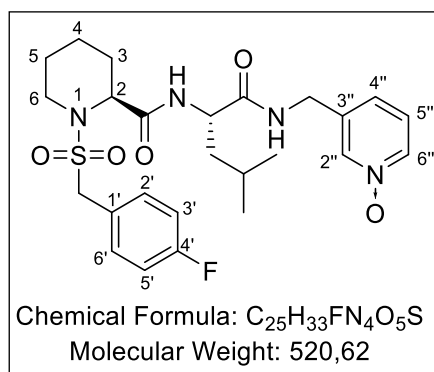
**3-(((S)-2-((R/S)-1-(Benzylsulfonyl)piperidine-2-carboxamido)-3-phenylpropanamido)-methyl)pyridine 1-oxide (R/S,S-22a; Lab-ID: TL75)**



*S,S*-**21a** (75 mg, 0.14 mmol) was reacted with *m*-CPBA (50 mg, 0.28 mmol) in EtOAc (5 mL) following general procedure E. After stirring at rt for 2 h, additional EtOAc (20 mL) was added and the solution was washed with sat. NaHCO<sub>3</sub> solution (3 × 20 mL) and water (3 × 20 mL). After separation of the phases, the crude oily product was purified by column chromatography (SiO<sub>2</sub>, EtOAc/PE/MeOH = 4:2:1). *R/S,S*-**22a** was obtained as a white oily solid (60 mg,

0.11 mmol, 78%),  $R_f$ : 0.38 ( $DC_{SIL}$ ; DCM/MeOH = 10:1). IR (ATR),  $\tilde{\nu}$  [ $cm^{-1}$ ]: 3262, 3038, 2933, 1656, 1519, 1325, 1135, 786, 691. During basic purification, isomerization of the pipercolic acid stereocenter occurred. Diastereomeric ratio: 58:42.  $^1H$  NMR (ACN- $d_3$ ,  $\delta$  [ppm], J [Hz]): 8.03 (s, 1H), 7.96 (d,  $J$  = 6.4, 1H), 7.51 (t,  $J$  = 5.9, 1H), 7.42–7.33 (m, 5H), 7.29–7.01 (m, 8H), 4.72–4.58 (m, 1H), 4.35–4.16 (m, 5H), 3.46–3.44 (m, 1H), 3.22–3.12 (m, 1H), 2.95–2.85 (m, 2H), 2.03–2.01 (m, 1H), 1.58–1.26 (m, 4H), 1.16–1.00 (m, 1H).  $^1H$  NMR (ACN- $d_3$ ,  $\delta$  [ppm], J [Hz]): 8.04 (s, 1H), 7.92 (d,  $J$  = 6.2, 1H), 7.58 (t,  $J$  = 5.9, 1H), 7.42–7.33 (m, 5H), 7.29–7.01 (m, 8H), 4.72–4.58 (m, 1H), 4.35–4.16 (m, 5H), 3.45 (d,  $J$  = 12.5, 1H), 3.26 (td,  $J$  = 12.7, 3.1, 1H), 2.95–2.85 (m, 2H), 1.83–1.81 (m, 1H), 1.58–1.26 (m, 4H), 1.16–1.00 (m, 1H).  $^{13}C$  NMR (ACN- $d_3$ ,  $\delta$  [ppm]): 171.8, 171.2, 140.6, 139.3, 138.6, 137.8, 131.5 (2C), 129.9 (2C), 129.0–128.8 (5C), 127.3, 126.6, 125.6, 58.3, 56.4, 55.1, 43.8, 40.2, 37.9, 27.0, 24.8, 19.9.  $^{13}C$  NMR (ACN- $d_3$ ,  $\delta$  [ppm]): 171.8, 171.2, 140.6, 139.4, 138.4, 138.0, 131.5 (2C), 129.9 (2C), 129.0–128.8 (5C), 127.2, 126.6, 125.5, 58.1, 56.3, 55.1, 43.9, 40.2, 37.9, 28.0, 25.0, 19.9. LC/MS (m/z) 537.10  $[M+H]^+$ . Purity (HPLC, both diastereomers in total): 99.5%,  $t_R$  = 9.08 min; HRMS (m/z)  $C_{28}H_{32}N_4O_5S$ ,  $[M+H]^+$ , calculated 537.21662, found 537.21776, error: 2.1 ppm.

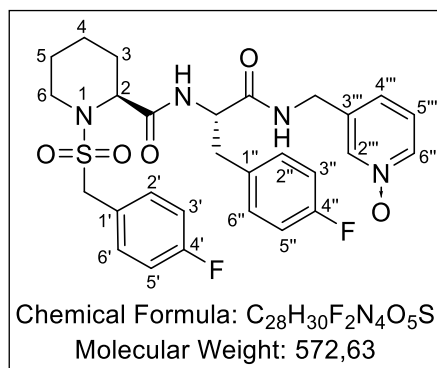
**3-(((S)-2-(((S)-1-((4-Fluorobenzyl)sulfonyl)piperidine-2-carboxamido)-4-methylpentanamido)methyl)pyridine 1-oxide (S,S-22d; Lab-ID: NJS256)**



*S,S*-**21d** (25 mg, 50  $\mu$ mol) was reacted according to general procedure E using 21 mg of *m*-CPBA (99  $\mu$ mol) in EtOAc (4 mL). After stirring at rt for 2 h, the crude oily product was purified by flash chromatography (run 1:  $SiO_2$ , A: DCM, B: MeOH, gradient: 0  $\rightarrow$  30% B; run 2: RP 18, A:  $H_2O$ , B: ACN, gradient: 5  $\rightarrow$  60% B). Compound *S,S*-**22d** was obtained as a white solid (20 mg, 38  $\mu$ mol, 77%).  $R_f$ : 0.39 ( $DC_{SIL}$ ; DCM/MeOH = 9:1). IR (ATR),  $\tilde{\nu}$  [ $cm^{-1}$ ]: 3400–3200, 3070, 2952, 2871, 1654, 1541, 1508, 1336, 1223, 1180, 772, 761, 754, 716. Mp: 87  $^{\circ}C$ .  $^1H$  NMR ( $CD_3OD$ ,  $\delta$

[ppm], J [Hz]): 8.31 (br s, 1H, *CH*-2<sup>''</sup>), 8.23–8.20 (m, 1H, *CH*-6<sup>''</sup>), 7.57–7.53 (m, 1H, *CH*-4<sup>''</sup>), 7.51–7.44 (m, 3H, *CH*-2',6',5<sup>''</sup>), 7.14–7.06 (m, 2H, *CH*-3',5<sup>''</sup>), 4.48–4.26 (m, 6H, NH*CHCO*, NH*CH*<sub>2</sub>, *CH*-2, SO<sub>2</sub>*CH*<sub>2</sub>), 3.51–3.41 (m, 2H, *CH*<sub>2</sub>-6), 2.11–2.03 (m, 1H, *CH*<sub>2</sub>-3), 1.72–1.54 (m, 6H, *CH*<sub>2</sub>CH(CH<sub>3</sub>)<sub>2</sub>, *CH*(CH<sub>3</sub>)<sub>2</sub>, *CH*<sub>2</sub>-3,4,5), 1.47–1.32 (m, 2H, *CH*<sub>2</sub>-4,5), 0.98 (d, <sup>3</sup>J = 6.4, 3H, CH(CH<sub>3</sub>)<sub>2</sub>), 0.95 (d, <sup>3</sup>J = 6.4, 3H, CH(CH<sub>3</sub>)<sub>2</sub>). <sup>13</sup>C NMR (CD<sub>3</sub>OD, δ [ppm], J [Hz]): 175.3 (1C, CONHCH<sub>2</sub>C-3<sup>''</sup>), 173.8 (1C, C-2CONH), 164.3 (d, <sup>1</sup>J<sub>CF</sub> = 246.3, 1C, C-4<sup>''</sup>), 140.9 (1C, C-3<sup>''</sup>), 139.4 (1C, *CH*-2<sup>''</sup>), 139.0 (s, 1C, *CH*-6<sup>''</sup>), 134.1 (d, <sup>3</sup>J<sub>CF</sub> = 8.4, 2C, *CH*-2',6'), 130.0 (1C, *CH*-4<sup>''</sup>), 127.7 (1C, *CH*-5<sup>''</sup>), 127.2 (d, <sup>4</sup>J<sub>CF</sub> = 3.3, 1C, C-1<sup>''</sup>), 116.3 (d, <sup>2</sup>J<sub>CF</sub> = 21.8, 2C, *CH*-3',-5'), 57.9 (1C, SO<sub>2</sub>CH<sub>2</sub>), 57.0 (1C, *CH*-2), 53.4 (1C, NH*CHCO*), 44.8 (1C, *CH*<sub>2</sub>-6), 41.6 (1C, NHCH<sub>2</sub>), 40.9 (1C, *CH*<sub>2</sub>CH(CH<sub>3</sub>)<sub>2</sub>), 29.0 (1C, *CH*<sub>2</sub>-3), 26.00 (1C, *CH*<sub>2</sub>-5), 25.95 (1C, CH(CH<sub>3</sub>)<sub>2</sub>), 23.3 (1C, CH(CH<sub>3</sub>)<sub>2</sub>), 22.0 (1C, CH(CH<sub>3</sub>)<sub>2</sub>), 20.7 (1C, *CH*<sub>2</sub>-4). LC/MS (m/z) 521.15 [M+H]<sup>+</sup>. Purity (HPLC): 99.4%, t<sub>R</sub> = 8.74 min, HRMS (m/z) C<sub>25</sub>H<sub>33</sub>FN<sub>4</sub>O<sub>5</sub>S, [M+H]<sup>+</sup>, calculated 521.22285, found 521.22230, error: 1.1 ppm.

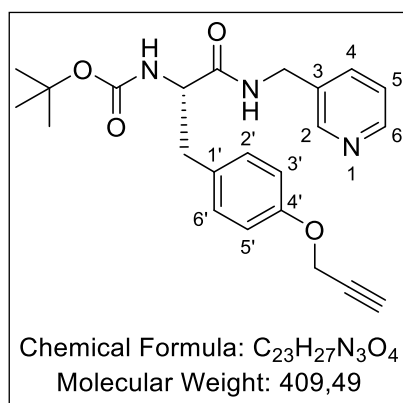
**3-(((*S*)-2-(((*S*)-1-((4-Fluorobenzyl)sulfonyl)piperidine-2-carboxamido)-3-(4-fluorophenyl)-propanamido)methyl)pyridine 1-oxide (*S,S*-22g; Lab-ID: NJS250)**



*S,S*-21g (10 mg, 18 μmol) was reacted according to general procedure E using 6.00 mg of m-CPBA (34.8 μmol) in 4 mL of EtOAc. After stirring overnight, the reaction mixture was loaded directly onto silica gel and purified by flash chromatography (SiO<sub>2</sub>, 2 · 4 g, A: DCM, B: MeOH, gradient: 0 → 30% B). Compound *S,S*-22g was obtained as a colorless solid (6.0 mg, 11 μmol, 58%). R<sub>f</sub>: 0.48 (DC<sub>SIL</sub>; DCM/MeOH = 9:1). IR (ATR),  $\tilde{\nu}$  [cm<sup>-1</sup>]: 3292, 3073, 2968, 1656, 1508, 1335, 1222, 1183, 1157, 841, 817, 774. Mp: 98 °C. <sup>1</sup>H NMR (CD<sub>3</sub>OD, δ [ppm], J [Hz]): 8.26 (br s, 1H, *CH*-2<sup>''</sup>), 8.21 (d, <sup>3</sup>J = 6.0, 1H, *CH*-6<sup>''</sup>), 7.48–7.39 (m, 4H, *CH*-4<sup>''</sup>,5<sup>''</sup>,2',6'), 7.27–7.21 (m, 2H, *CH*-2<sup>''</sup>,6<sup>''</sup>), 7.13–7.06 (m, 2H, *CH*-3',5<sup>''</sup>), 7.02–6.95 (m, 2H, *CH*-3<sup>''</sup>,5<sup>''</sup>), 4.62–4.56 (m,

<sup>1</sup>H, NHCHCO), 4.36–4.18 (m, 5H, NHCH<sub>2</sub>, CH-2, SO<sub>2</sub>CH<sub>2</sub>), 3.47–3.42 (m, CH<sub>2</sub>-6, 1H), 3.20 (ddd, <sup>2</sup>J = 12.7, <sup>3</sup>J = 12.7, 2.5, 1H, CH<sub>2</sub>-6), 3.15–2.92 (m, 2H, NHCHCH<sub>2</sub>), 2.03 (br d, <sup>2</sup>J = 13.7, 1H, CH-3), 1.65–1.47 (m, 3H, CH<sub>2</sub>-3,4,5), 1.40–1.19 (m, 2H, CH<sub>2</sub>-4,5). <sup>13</sup>C NMR (CD<sub>3</sub>OD, δ [ppm], J [Hz]): 173.6 (1C, CONHCH<sub>2</sub>C-3''), 173.3 (1C, C-2CONH), 164.35 (d, <sup>1</sup>J<sub>CF</sub> = 246.2, C-4'), 163.29 (d, <sup>1</sup>J<sub>CF</sub> = 243.8, C-4''), 140.6 (1C, C-3''), 139.5 (1C, CH-2''), 139.0 (s, 1C, CH-6''), 134.14 (d, <sup>3</sup>J<sub>CF</sub> = 8.3, 2C, ), 134.14 (d, <sup>4</sup>J<sub>CF</sub> = 3.4), 132.1 (d, <sup>3</sup>J<sub>CF</sub> = 8.0, 2C), 130.1, 127.7, 127.0 (d, <sup>4</sup>J<sub>CF</sub> = 3.3), 116.26 (d, <sup>2</sup>J<sub>CF</sub> = 21.9, 2C), 116.22 (d, <sup>2</sup>J<sub>CF</sub> = 21.5, 2C), 58.0, 57.1, 56.3, 44.7, 40.9, 37.8, 28.6 (1C, CH<sub>2</sub>-3), 25.8 (1C, CH<sub>2</sub>-5), 20.6 (1C, CH<sub>2</sub>-4). LC/MS (m/z) 573.10 [M+H]<sup>+</sup>. Purity (HPLC): 97.4%, t<sub>R</sub> = 9.00 min, HRMS (m/z) C<sub>28</sub>H<sub>30</sub>F<sub>2</sub>N<sub>4</sub>O<sub>5</sub>S, [M+H]<sup>+</sup>, calculated 573.19777, found 573.19779, error: 0.0 ppm.

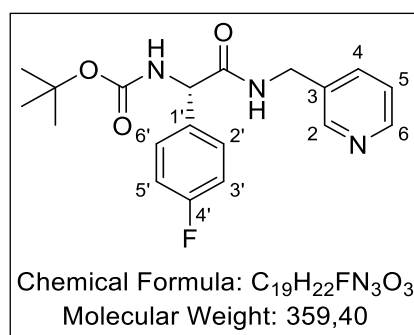
***tert*-Butyl (S)-(1-oxo-3-(4-(prop-2-yn-1-yloxy)phenyl)-1-((pyridin-3-ylmethyl)amino)-propan-2-yl)carbamate (S-26h; Lab-ID: NJS240)**



(S)-2-((*tert*-Butoxycarbonyl)amino)-3-(4-(prop-2-yn-1-yloxy)phenyl)propanoic acid (639 mg, 2.00 mmol) was amide-coupled to 3-picolylamine (244 μL, 2.40 mmol) according to general procedure A using DIPEA (696 μL, 4.00 mmol) and HBTU (833 g, 2.20 mmol) in dry DCM (80 mL). After stirring at rt for 5 d, the reaction was worked up according to the general procedure and purified by column chromatography (aloxide basic III, Cy/EtOAc/MeOH = 10:10:1) and flash chromatography (RP 18, A: H<sub>2</sub>O, B: MeOH, gradient: 5 → 100% B). Compound S-26h was obtained as a white solid (640 mg, 1.56 mmol, 78%). R<sub>f</sub>: 0.56 (DC<sub>SIL</sub>; DCM/MeOH = 10:1). Mp: 164 °C. IR (ATR),  $\tilde{\nu}$  [cm<sup>-1</sup>]: 3303, 3030, 2989, 1680, 1666, 1507, 1288, 827, 811, 751, 715. <sup>1</sup>H NMR (CD<sub>3</sub>OD, δ [ppm], J [Hz]): 8.50–8.36 (m, 2H, CH-2,6), 7.58 (d, <sup>3</sup>J = 7.5, 1H, CH-4), 7.40–7.31 (m, 1H, CH-5), 7.12 (d, <sup>3</sup>J = 8.5, 2H, CH-2',6'), 6.87 (d, <sup>3</sup>J = 8.5, 2H, CH-3',5'), 4.69 (d, <sup>4</sup>J = 2.3, 2H, OCH<sub>2</sub>CCH), 4.43–4.27 (m, 2H, NHCH<sub>2</sub>C-3), 4.24 (t, <sup>3</sup>J = 7.5, 1H,

NHCHCO), 2.98 (dd,  $^2J = 13.6$ ,  $^3J = 7.5$ , 1H,  $\text{CH}_2\text{C}-1'$ ), 2.92 (t,  $^4J = 2.3$ , 1H, *alkine-CH*), 2.82 (dd,  $^2J = 13.6$ ,  $^3J = 7.5$ , 1H,  $\text{CH}_2\text{C}-1'$ ), 1.39 (br s, 9H, *Boc-CH*<sub>3</sub>).  $^{13}\text{C}$  NMR (CD<sub>3</sub>OD,  $\delta$  [ppm]): 174.5 (1C, CONH), 158.1 (1C, COO), 158.0 (1C, *C-4'*), 149.4 (1C, *CH-2*), 148.7 (1C, *CH-6*), 137.6 (1C, *CH-4*), 136.4 (1C, *C-3*), 131.4 (2C, *CH-2',6'*), 131.2 (1C, *C-1'*), 125.2 (1C, *CH-5*), 116.0 (2C, *CH-3',5'*), 80.7 (1C, *Boc-C*<sub>q</sub>), 79.9 (1C, *alkine-C*<sub>q</sub>), 76.7 (1C, *alkine-CH*), 57.8 (1C, OCH<sub>2</sub>CCH), 56.6 (1C, NHCHCO), 41.4 (1C,  $\text{CH}_2\text{C}-3$ ), 38.4 (1C,  $\text{CH}_2\text{C}-1'$ ), 28.7 (3C, *Boc-CH*<sub>3</sub>).

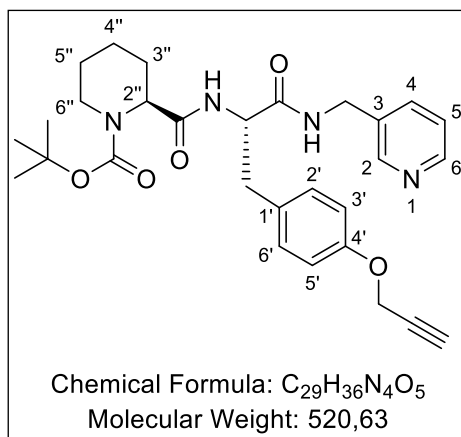
*tert*-Butyl (*S*)-(1-(4-fluorophenyl)-2-oxo-2-((pyridin-3-ylmethyl)amino)ethyl)carbamate (*S*-26i; Lab-ID: NJS255)



(*S*)-*N*-Boc-4-Fluorophenylglycine (275 mg, 1.02 mmol) was amide-coupled to 3-picolylamine (146  $\mu\text{L}$ , 1.43 mmol) according to general procedure A using DIPEA (0.4 mL, 2.3 mmol) and HBTU (426 mg, 1.12 mmol) in dry DCM (40 mL). After stirring at rt for 3 d and workup according to the general procedure, the crude oily product was purified by flash chromatography (aloxide (neutral), A: DCM, B: MeOH, gradient: 0  $\rightarrow$  25% B). *S*-26i was obtained as a colorless oil (340 mg, 946  $\mu\text{mol}$ , 93%).  $R_f$ : 0.61 (DC<sub>SIL</sub>, DCM/MeOH = 9:1). IR (ATR),  $\tilde{\nu}$  [cm<sup>-1</sup>]: 3300, 3062, 2975, 2929, 1701, 1662, 1604, 1507, 795, 745, 711.  $^1\text{H}$  NMR (CDCl<sub>3</sub>,  $\delta$  [ppm], J [Hz]): 8.42 (dd,  $^3J = 4.8$ ,  $^4J = 1.7$ , 1H, *CH-6*), 8.35 (d,  $^4J = 1.7$ , 1H, *CH-2*), 7.44 (d,  $^3J = 7.8$ , 1H, *CH-4*), 7.34–7.29 (m, 2H, *CH-2',6'*), 7.16 (dd,  $^3J = 7.8$ , 4.8, 1H, *CH-5*), 7.04 (br s, 1H, *NH*), 7.01–6.94 (m, 2H, *CH-3',5'*), 5.87 (br s, 1H, *NH*), 5.23 (br s, 1H, HNC $\text{HCO}$ ), 4.45–4.32 (m, 2H, HNC $\text{H}_2\text{C}-3$ ), 1.36 (s, 9H, *CH*<sub>3</sub>).  $^{13}\text{C}$  NMR (CDCl<sub>3</sub>,  $\delta$  [ppm]): 170.6 (1C, CONH), 162.7 (d,  $^1J_{\text{CF}} = 247.4$ , 1C, *C-4'*), 155.3 (1C, COO), 149.0 (1C, *CH-2*), 148.9 (1C, *CH-6*), 135.4 (1C, *CH-4*), 134.1 (d,  $^4J_{\text{CF}} = 2.9$ , 1C, *C-1'*), 133.7 (1C, *C-3*), 129.0 (d,  $^3J_{\text{CF}} = 8.3$ , 2C, *CH-2',6'*), 123.7 (1C, *CH-5*), 116.0 (d,  $^2J_{\text{CF}} = 21.7$ , 2C, *CH-3',5'*), 80.5 (1C, *C(CH*<sub>3</sub>)<sub>3</sub>), 57.9 (1C, NHCHCO), 41.2 (1C, NHCH<sub>2</sub>C-3), 28.4 (3C, *CH*<sub>3</sub>).



*tert*-Butyl (*S*)-2-(((*S*)-1-oxo-3-(4-(prop-2-yn-1-yloxy)phenyl)-1-((pyridin-3-ylmethyl)-amino)propan-2-yl)carbamoyl)piperidine-1-carboxylate (*S,S*-27h; Lab-ID: NJS242)

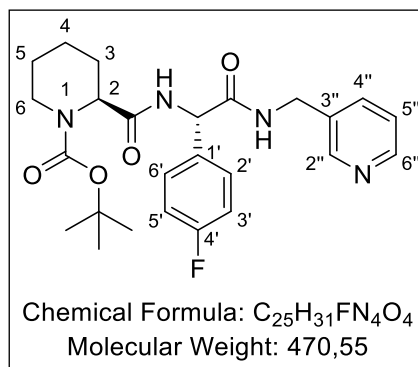


*S*-26h (310 mg, 757  $\mu$ mol) was Boc-protected according to general procedure B using TFA (9.00 mL) and dry DCM (10 mL). After stirring at rt for 1 d, the reaction was worked up according to the general procedure. The intermediate product (318 mg, 757  $\mu$ mol) was amide-coupled to (*S*)-1-Boc-piperidine-2-carboxylic acid (196 mg, 856  $\mu$ mol) following general procedure A using HBTU (282 mg, 744  $\mu$ mol) and DIPEA (1.04 mL, 5.95 mmol) in dry DCM (40 mL). After stirring at rt for 2 d and workup according to the general procedure, the crude oily product was purified by flash chromatography (aloxide (neutral), A: DCM, B: MeOH, gradient: 0 $\rightarrow$ 30% B). Compound *S,S*-27h was obtained as a slightly yellowish solid (380 mg, 730  $\mu$ mol, 98%). *R*<sub>f</sub>: 0.50 (DC<sub>SIL</sub>; DCM/MeOH = 10:1). Mp: 77 °C. IR (ATR),  $\tilde{\nu}$  [cm<sup>-1</sup>]: 3286, 3061, 2968, 2940, 1648, 1509, 869, 785, 773, 707. <sup>1</sup>H NMR (CDCl<sub>3</sub>,  $\delta$  [ppm], J [Hz]):

8.48 (dd, <sup>3</sup>J = 4.8, <sup>4</sup>J = 1.8, 1H, CH-6), 8.43 (d, <sup>4</sup>J = 1.8, 1H, CH-2), 7.46 (d, <sup>3</sup>J = 7.8, 1H, CH-4), 7.21 (dd, <sup>3</sup>J = 7.8, 4.8, 1H, CH-5), 7.11–7.05 (m, 2H, CH-2',6'), 6.89–6.84 (m, 2H, CH-3',5'), 6.67 (br s, 1H, NHCH<sub>2</sub>C-3), 6.47–6.43 (m, 1H, CH-2''CONH), 4.71–4.65 (m, 1H, NHCHCONH), 4.67–4.63 (m, 2H, OCH<sub>2</sub>CCH), 4.63–4.59 (m, 1H, pip-CH-2''), 4.44–4.30 (m, 2H, NHCH<sub>2</sub>C-3), 3.82 (br s, 1H, pip-CH<sub>2</sub>-6''), 3.06 (d, <sup>3</sup>J = 7.1, 2H, CH<sub>2</sub>C-1'), 2.50 (t, J = 2.4, 1H, alkine-CH), 2.43 (br s, 1H, pip-CH<sub>2</sub>-6''), 2.18–2.10 (m, 1H, pip-CH<sub>2</sub>-3''), 1.59–1.43 (m, 3H, pip-CH<sub>2</sub>-3'',4'',5''), 1.40 (s, 9H, Boc-CH<sub>3</sub>), 1.37–1.22 (m, 2H, pip-CH<sub>2</sub>-4'',5''). <sup>13</sup>C NMR (CDCl<sub>3</sub>,  $\delta$  [ppm]): 171.8 (1C, pip-CH-2''CONH), 170.9 (1C, NHCHCONH), 156.8 (1C, CH-4'), 155.7 (1C, Boc-NCOO), 149.4 (1C, CH-2), 149.0 (1C, CH-6), 135.6 (1C, CH-4), 133.7 (1C, C-3), 130.4 (2C, CH-2',6'), 129.4 (1C, C-1'), 123.7 (1C, CH-5), 115.4 (2C, CH-5'), 81.0 (1C, Boc-C<sub>q</sub>), 78.6 (1C, alkine-C<sub>q</sub>), 75.7 (1C, alkine-CH), 56.0 (1C, OCH<sub>2</sub>CCH), 55.2 (1C,

*pip-CH-2''*), 54.4 (1C, NHCHCO), 41.1 (2C, CH<sub>2</sub>-6, CH<sub>2</sub>C-3), 37.1 (1C, CH<sub>2</sub>C-1'), 28.4 (3C, Boc-CH<sub>3</sub>), 25.5 (1C, CH<sub>2</sub>-3''), 24.7 (1C, CH<sub>2</sub>-5''), 20.4 (1C, CH<sub>2</sub>-4'').

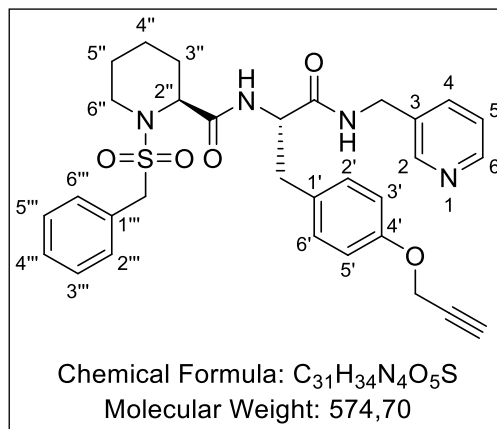
***tert*-Butyl (*S*)-2-(((*S*)-1-(4-fluorophenyl)-2-oxo-2-((pyridin-3-ylmethyl)amino)ethyl)-carbamoyl)piperidine-1-carboxylate (*S,S*-27i; Lab-ID: NJS258)**



*S*-26i (450 mg, 1.25 mmol) was Boc-protected according to general procedure B using TFA (5.0 mL, 66.0 mmol) in dry DCM (20 mL). After stirring at rt for 1 d, the reaction was worked up according to the general procedure. The intermediate product (245 mg, 946 μmol) was further reacted with (*S*)-1-Boc-piperidine-2-carboxylic acid (317 mg, 1.38 mmol) according to general procedure A using HBTU (395 mg, 1.04 mmol) and DIPEA (1.00 mL) in dry DCM (15 mL). After stirring at rt for 1 d, the reaction was worked up according to the general procedure and the crude oily product was purified by flash chromatography (aloxide (neutral), A: CHCl<sub>3</sub>, B: MeOH, 0 → 30% B). *S,S*-27i was obtained as a white solid (440 mg, 935 μmol, 99%). R<sub>f</sub>: 0.78 (DC<sub>ALOX</sub>; DCM/MeOH = 10:1). Mp: 147 °C. IR (ATR),  $\tilde{\nu}$  [cm<sup>-1</sup>]: 3318, 3042, 2941, 1646, 1507, 1364, 1158, 837, 712. <sup>1</sup>H NMR (CDCl<sub>3</sub>, δ [ppm], J [Hz]): 8.50–8.46 (m, 2H, CH-2'',6''), 7.62–7.56 (m, 1H, CH-4''), 7.39–7.27 (m, 3H, CH-5'',2',6'), 7.01 (t, <sup>3</sup>J = 8.6, 2H, CH-3',5'), 6.83 (br s, 1H, CH-2CONH), 5.49 (d, <sup>3</sup>J = 6.7, 1H, NHCHCOO), 4.72 (br s, 1H, CH-2), 4.51–4.39 (m, 2H, HNCH<sub>2</sub>C-3''), 3.96 (br s, 1H, CH<sub>2</sub>-6), 3.01 (br s, 1H, NHCH<sub>2</sub>C-3''), 2.68 (br s, 1H, CH<sub>2</sub>-6), 2.16–2.09 (m, 1H, CH<sub>2</sub>-3), 1.62–1.30 (m, 5H, CH<sub>2</sub>-3,4,5), 1.45 (s, 9H, CH<sub>3</sub>). <sup>13</sup>C NMR (CDCl<sub>3</sub>, δ [ppm]): 171.5 (1C, HNCHCONH), 169.9 (1C, C-2CONH), 162.8 (d, <sup>1</sup>J<sub>CF</sub> = 247.6, 1C, C-4'), 156.0 (br 1C, COO), 149.0 (1C, CH-2), 148.9 (1C, CH-6), 135.5 (1C, CH-4''), 134.0 (d, <sup>4</sup>J<sub>CF</sub> = 3.3, 1C, C-1'), 133.7 (1C, C-3''), 129.0 (d, <sup>3</sup>J<sub>CF</sub> = 8.3, 2C, CH-2',6'), 123.7 (1C, C-5''), 116.1 (d, <sup>2</sup>J<sub>CF</sub> = 21.7, 2C, CH-3',5'), 81.1 (1C, C(CH<sub>3</sub>)<sub>3</sub>), 56.6 (1C, NHCHCO), 54.8 (1C, CH-2), 42.9 (br 1C, CH<sub>2</sub>-6), 41.3 (1C, HNCH<sub>2</sub>C-3''), 28.4 (3C, CH<sub>3</sub>), 25.7 (1C, CH<sub>2</sub>-3), 24.8 (1C,

CH<sub>2</sub>-5), 20.5 (1C, CH<sub>2</sub>-4).

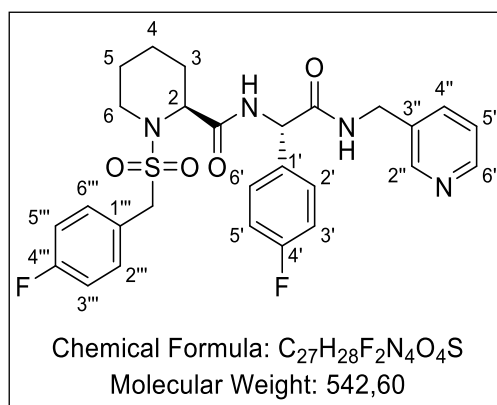
(*S*)-1-(Benzylsulfonyl)-*N*-((*S*)-1-oxo-3-(4-(prop-2-yn-1-yloxy)phenyl)-1-((pyridin-3-ylmethyl)amino)propan-2-yl)piperidine-2-carboxamide (*S,S*-21h; Lab-ID: NJS244)



*S,S*-27h (450 mg, 864 μmol) was Boc-protected according to General Procedure B using TFA (5 mL) and dry DCM (5 mL). After stirring at rt for 1 d, workup was conducted according to the general procedure. The intermediate product (363 mg, 863 μmol) was subsequently treated with phenylmethanesulfonyl chloride (330 mg, 1.73 mmol) and NMM (960 μL, 8.63 mmol) in dry DCM (45 mL) according to general procedure C. After stirring at rt for 5 d, the reaction was worked up according to the general procedure. Purification by flash chromatography (RP 18, A: H<sub>2</sub>O, B: MeOH, gradient: 40→80% B) afforded *S,S*-21h as a white solid (240 mg, 418 μmol, 48%), R<sub>f</sub>: 0.51 (DC<sub>SIL</sub>; DCM/MeOH = 9:1). Mp: 123 °C. IR (ATR),  $\tilde{\nu}$  [cm<sup>-1</sup>]: 3289, 2938, 2120, 1650, 1508, 1350, 1322, 1180, 823, 780, 739. <sup>1</sup>H NMR (CDCl<sub>3</sub>, δ [ppm], J [Hz]): 8.51 (dd, <sup>3</sup>J = 4.8, <sup>4</sup>J = 1.7, 1H, CH-6), 8.48 (d, <sup>4</sup>J = 1.7, 1H, CH-2), 7.53–7.49 (m, 1H, CH-4), 7.40–7.35 (m, 5H, CH-2'''–6'''), 7.25–7.21 (m, 1H, CH-5), 7.10–7.06 (m, 2H, CH-2',6'), 6.89–6.83 (m, 2H, CH-3',5'), 6.71 (t, <sup>3</sup>J = 5.8, 1H, NHCH<sub>2</sub>C-3), 6.57 (d, <sup>3</sup>J = 8.3, 1H, CH-2''CONH), 4.73–4.65 (m, 1H, HNCHCO), 4.65–4.60 (m, 2H, OCH<sub>2</sub>C), 4.45–4.33 (m, 2H, CH<sub>2</sub>C-3), 4.22 (s, 2H, CH<sub>2</sub>SO<sub>2</sub>), 4.07 (br d, <sup>3</sup>J = 4.3, 1H, CH-2''), 3.32 (br d, <sup>2</sup>J = 13.6, 1H, CH<sub>2</sub>-6''), 3.22 (dd, <sup>2</sup>J = 14.4, <sup>3</sup>J = 5.9, 1H, CH<sub>2</sub>C-1'), 2.96 (dd, <sup>2</sup>J = 14.4, <sup>3</sup>J = 8.9, 1H, CH<sub>2</sub>C-1'), 2.48–2.38 (m, 2H, alkene-CH, CH<sub>2</sub>-6''), 2.10 (br d, <sup>2</sup>J = 13.8, 1H, CH<sub>2</sub>-3''), 1.50–0.87 (m, 5H, CH<sub>2</sub>-3'',4'',5''). <sup>13</sup>C NMR (CDCl<sub>3</sub>, δ [ppm]): 170.8 (1C, CONHCH<sub>2</sub>C-3), 170.5 (1C, pip-C-2''CONH), 156.8 (1C, C-4'), 149.4 (1C, CH-2), 149.0 (1C, CH-6), 135.6 (1C, CH-4), 133.7 (1C, C-3), 130.8 (2C, CH-2''',6'''), 130.3 (2C, CH-2',6'), 129.5 (1C, C-1'), 129.3 (1C, CH-4'''), 129.0 (2C,

CH-3''',5'''), 128.6 (1C, CH-1'''), 123.7 (1C, CH-5), 115.4 (2C, CH-3',5'), 78.6 (1C, *alkine-C*), 75.6 (1C, *alkine-CH*), 58.8 (1C, CH<sub>2</sub>SO<sub>2</sub>), 57.1 (1C, CH-2''), 56.0 (1C, HNCHCO), 54.6 (1C, OCH<sub>2</sub>C), 43.8 (1C, CH<sub>2</sub>-6''), 41.1 (1C, CH<sub>2</sub>C-3), 36.7 (1C, CHCH<sub>2</sub>C-1), 25.6 (1C, CH<sub>2</sub>-3''), 24.3 (1C, CH<sub>2</sub>-5''), 19.6 (1C, CH<sub>2</sub>-4''). LC/MS (m/z) 575.20 [M+H]<sup>+</sup>. Purity (HPLC): 99.2%, t<sub>R</sub> = 8.18 min. HRMS (m/z) C<sub>31</sub>H<sub>34</sub>N<sub>4</sub>O<sub>5</sub>S, [M+H]<sup>+</sup>, calculated 575.23227, found 575.23197, error: 0.5 ppm.

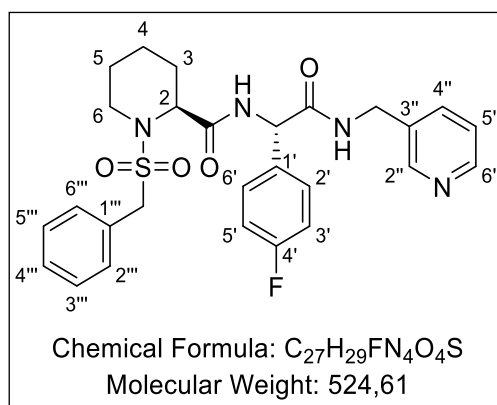
**(S)-1-((4-Fluorobenzyl)sulfonyl)-N-((S)-1-(4-fluorophenyl)-2-oxo-2-((pyridin-3-ylmethyl)-amino)ethyl)piperidine-2-carboxamide (S,S-21i; Lab-ID: NJS260)**



*S,S*-**27i** (200 mg, 425 μmol) was first Boc-protected according to general procedure B using 4 mL of TFA in dry DCM (20 mL). After stirring at rt for 1 d, the reaction was worked up according to the general procedure. Subsequently, the intermediate product (TFA salt, 254 mg, 425 μmol) was reacted according to general procedure C using (4-fluorophenyl)methanesulfonyl chloride (160 mg, 765 μmol) and DIPEA (740 μL, 4.25 mmol) in dry DCM (20 mL). After stirring at rt for 4 d and workup according to the general procedure, the crude oily product was purified by flash chromatography (run 1: RP 18, A: H<sub>2</sub>O, B: MeOH, gradient: 5 → 70% B; run 2: RP 18, A: H<sub>2</sub>O + 0.1% FA, B: MeOH + 0.1% FA, gradient: 5 → 60% B). Compound *S,S*-**21i** was obtained as a white solid (40 mg, 74 μmol, 17%). R<sub>f</sub>: 0.47 (DC<sub>SIL</sub>; DCM/MeOH = 10:1), Mp: 105 °C. IR (ATR),  $\tilde{\nu}$  [cm<sup>-1</sup>]: 3289, 3061, 2939, 1652, 1604, 1507, 1326, 1223, 1183, 837, 773. <sup>1</sup>H NMR (CDCl<sub>3</sub>, δ [ppm], J [Hz]): 8.58–8.38 (m, 2H, CH-2'',6''), 7.54 (d, <sup>3</sup>J = 7.7, 1H, CH-4''), 7.46 (d, <sup>3</sup>J = 6.7, 1H, CH-2CONH), 7.38–7.31 (m, 4H, CH-2',6',2''',6'''), 7.25–7.22 (br s, 1H, CH-5''), 7.07–6.97 (m, 4H, CH-3',5',3''',5'''), 6.77 (br s, 1H, C-3''CH<sub>2</sub>NH), 5.48 (d, <sup>3</sup>J = 6.7, 1H, HNCHCO), 4.49–4.39 (m, 2H, HNCH<sub>2</sub>C-3''), 4.34–4.29 (m, 1H, CH-2) 4.23–4.11 (m, 2H, SO<sub>2</sub>CH<sub>2</sub>), 3.45 (br d, <sup>2</sup>J = 12.5, 1H, CH<sub>2</sub>-6), 2.98 (ddd, <sup>2</sup>J = 12.5, <sup>3</sup>J = 12.5, 2.5,

<sup>1</sup>H, CH<sub>2</sub>-6), 2.12 (br d, <sup>2</sup>J = 13.3, 1H, CH<sub>2</sub>-3), 1.62–1.42 (m, 3H, CH<sub>2</sub>-3,4,5), 1.36–1.26 (m, 2H, CH<sub>2</sub>-4,5). <sup>13</sup>C NMR (CDCl<sub>3</sub>, δ [ppm], J [Hz]): 170.3 (1C, CH-2CONH), 169.8 (1C, CONHCH<sub>2</sub>C-3''), 163.2 (d, <sup>1</sup>J<sub>CF</sub> = 248.6, 1C, C-4'), 162.9 (d, <sup>1</sup>J<sub>CF</sub> = 248.2, 1C, C-4'''), 148.6 (1C, CH-2''), 148.4 (1C, CH-6''), 136.2 (1C, CH-4''), 133.4 (d, <sup>1</sup>J<sub>CF</sub> = 3.3, 1C, C-1'), 132.7 (d, <sup>3</sup>J<sub>CF</sub> = 8.4, 2C, CH-2''',6'''), 131.5 (1C, C-3''), 129.3 (d, <sup>3</sup>J<sub>CF</sub> = 8.3, 2C, CH-2',6'), 124.7 (d, <sup>4</sup>J<sub>CF</sub> = 3.3, 1C, C-1'''), 123.9 (br 1C, CH-5''), 116.3 (d, <sup>2</sup>J<sub>CF</sub> = 21.7, 2C, CH-3',5'), 115.9 (d, <sup>2</sup>J<sub>CF</sub> = 21.7, 2C, CH-3''',5'''), 58.0 (1C, SO<sub>2</sub>CH<sub>2</sub>), 57.0 (1C, HNCHCO), 56.6 (1C, CH-2), 44.1 (1C, CH<sub>2</sub>-6), 41.4 (1C, HNCH<sub>2</sub>C-3''), 26.8 (1C, CH<sub>2</sub>-3), 24.8 (1C, CH<sub>2</sub>-5), 19.8 (1C, CH<sub>2</sub>-4). LC/MS (m/z) 543.10 [M+H]<sup>+</sup>. Purity (HPLC): 99.0%, t<sub>R</sub> = 7.74 min. HRMS (m/z) C<sub>27</sub>H<sub>28</sub>F<sub>2</sub>N<sub>4</sub>O<sub>4</sub>S, [M+H]<sup>+</sup>, calculated 543.18721, found 543.18764, error: 0.8 ppm.

**(S)-1-(Benzylsulfonyl)-N-((S)-1-(4-fluorophenyl)-2-oxo-2-((pyridin-3-ylmethyl)amino)ethyl)piperidine-2-carboxamide (S,S-28i; Lab-ID: NJS261)**

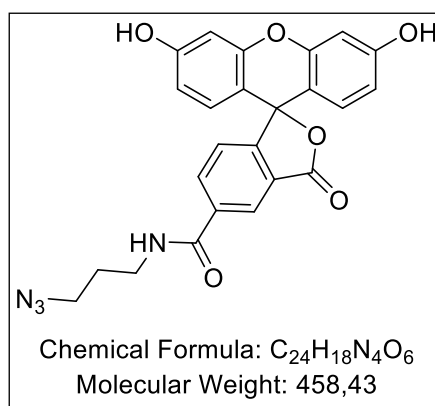


*S,S*-**27i** (200 mg, 425 μmol) was Boc-protected according to general procedure B using 4 mL of TFA in dry DCM (20 mL). After stirring at rt for 1 d, the reaction was worked up according to the general procedure. Subsequently, the intermediate product (85 mg, 229 μmol) was reacted according to general procedure C using phenylmethanesulfonyl chloride (101 mg, 482 μmol) and DIPEA (120 μL, 688 μmol) in dry DCM (15 mL). After stirring at rt for 2 d and workup according to the general procedure, the crude oily product was purified by flash chromatography (RP 18, A: H<sub>2</sub>O + 0.1% FA, B: MeOH + 0.1% FA, gradient: 5 → 100% B). Compound *S,S*-**28i** was obtained as a white, slightly yellowish oily solid (40 mg, 76 μmol, 33%). R<sub>f</sub>: 0.50 (DC<sub>SIL</sub>; DCM/MeOH = 10:1). Mp: 143 °C. IR (ATR),  $\tilde{\nu}$  [cm<sup>-1</sup>]: 3300, 3063, 3037, 2935, 1650, 1507, 1323, 1183, 837, 784, 737, 698. <sup>1</sup>H NMR (CDCl<sub>3</sub>, δ [ppm], J [Hz]): 8.47–8.33 (m, 2H, CH-2'',6''), 7.59 (d, <sup>3</sup>J = 7.0, 1H, CH-2CONH), 7.50 (d, <sup>3</sup>J = 7.7, 1H, CH-4''), 7.38–7.29 (m, 8H, CH-2',6',2''',6''',3''',

5''',4''',NHCH<sub>2</sub>C-3''), 7.21–7.15 (br s, 1H, CH-5''), 6.94 (t, <sup>3</sup>J = 8.5, 2H, CH-3',5'), 5.54 (d, <sup>3</sup>J = 7.0, 1H, HNCHCO), 4.44–4.31 (m, 2H, HNCH<sub>2</sub>C-3''), 4.29–4.25 (m, 1H, CH-2) 4.22–4.18 (m, 2H, SO<sub>2</sub>CH<sub>2</sub>), 3.42 (br d, <sup>2</sup>J = 12.7, 1H, CH<sub>2</sub>-6), 2.96 (ddd, <sup>2</sup>J = 12.7, <sup>3</sup>J = 12.7, 2.3, 1H, CH<sub>2</sub>-6), 2.02 (br d, <sup>2</sup>J = 13.0, 1H, CH<sub>2</sub>-3), 1.55–1.20 (m, 5H, CH<sub>2</sub>-3,4,5). <sup>13</sup>C NMR (CDCl<sub>3</sub>, δ [ppm], J [Hz]): 170.4 (1C, CH-2CONH), 169.9 (1C, NHCHCONH), 162.7 (d, <sup>1</sup>J<sub>CF</sub> = 247.7, 1C, C-4'), 148.4 (1C, CH-2''), 148.1 (1C, CH-6''), 136.2 (1C, CH-4''), 134.2 (1C, C-3''), 133.5 (d, <sup>1</sup>J<sub>CF</sub> = 3.2, 1C, C-1'), 129.1 (d, <sup>3</sup>J<sub>CF</sub> = 8.3, 2C, CH-2',6'), 129.08 (1C, C-1'''), 128.9 (2C, CH-2'',6'''), 128.80 (2C, CH-3''',5'''), 128.78 (1C, CH-4'''), 123.9 (br 1C, CH-5''), 116.0 (d, <sup>2</sup>J<sub>CF</sub> = 21.7, 2C, CH-3',5'), 58.8 (1C, SO<sub>2</sub>CH<sub>2</sub>), 56.7 (1C, HNCHCO), 56.5 (1C, CH-2), 44.0 (1C, CH<sub>2</sub>-6), 41.1 (1C, HNCH<sub>2</sub>C-3''), 26.5 (1C, CH<sub>2</sub>-3), 24.6 (1C, CH<sub>2</sub>-5), 19.7 (1C, CH<sub>2</sub>-4). LC/MS (m/z) 525.35 [M+H]<sup>+</sup>. Purity (HPLC): 96.9%, t<sub>R</sub> = 7.65 min. HRMS (m/z) C<sub>27</sub>H<sub>29</sub>FN<sub>4</sub>O<sub>4</sub>S, [M+H]<sup>+</sup>, calculated 525.19663, found 525.19591, error: 1.4 ppm.

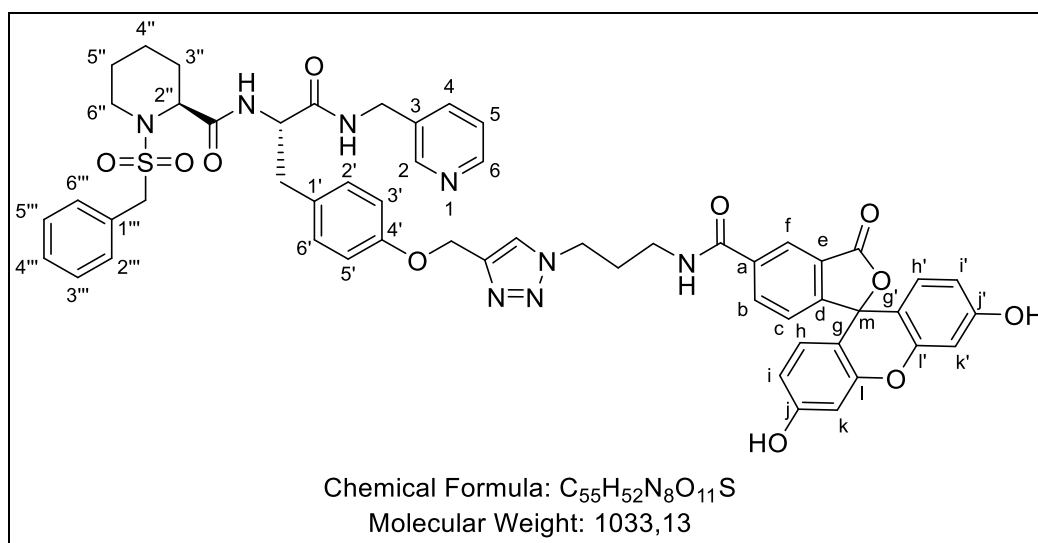
#### 4.6.1.4 Synthesis of the FP Probe

*N*-(3-Azidopropyl)-3',6'-dihydroxy-3-oxo-3H-spiro[isobenzofuran-1,9'-xanthene]-5-carboxamide (30; Lab-ID: NJS253)



**30** was synthesized according to Rossi *et al.*<sup>5</sup> and Farzan *et al.*<sup>6</sup> to give the product quantitatively (36 mg, 78 μmol, >99%, Lit.<sup>6</sup>: 89%) as a yellow powder. R<sub>f</sub>: 0.57 (DC<sub>SIL</sub>; DCM/MeOH/FA = 10:1:0.1). Mp: 193 – 195°C (Lit.<sup>6</sup>: decomposition > 210 °C. IR (ATR),  $\tilde{\nu}$  [cm<sup>-1</sup>]: 3400–2600, 2957, 2922, 2090, 1735, 1604, 1588, 1541, 1108, 845. Analytical data are in agreement with the literature from Farzan *et al.*<sup>6</sup>, but no IR spectrum was described before.

(*S*)-1-(Benzylsulfonyl)-*N*-((*S*)-3-(4-((1-(3-(3',6'-dihydroxy-3-oxo-3*H*-spiro[isobenzofuran-1,9'-xanthene]-5-carboxamido)propyl)-1*H*-1,2,3-triazol-4-yl)methoxy)phenyl)-1-oxo-1-((pyridin-3-ylmethyl)amino)propan-2-yl)piperidine-2-carboxamide (**29**; Lab-ID: NJS254)



According to a modified protocol by Donnelly *et al.*,<sup>7</sup> to a solution of *S,S*-**21h** (37.6 mg, 65.4 μmol) in a mixture of acetonitrile, DCM, and EtOH (10:4:1, 15 mL), was given sodium ascorbate (23.0 mg, 116 μmol), copper(II) sulfate pentahydrate (20.0 mg, 80.1 μmol), tris((1-benzyl-4-triazolyl)methyl)amine (TBTA, 11.0 mg, 20.7 μmol) and *N*-(3-Azidopropyl)-3',6'-dihydroxy-3-oxo-3*H*-spiro[isobenzofuran-1,9'-xanthene]-5-carboxamide<sup>6</sup> (**30**, 30.0 mg, 65.4 μmol) at rt. After stirring for 9 d at rt, the mixture was loaded directly onto silica gel and purified by flash chromatography (run 1: SiO<sub>2</sub>, A: CHCl<sub>3</sub> + 1% FA, B: MeOH + 1% FA, gradient: 0→30% B; run 2: RP 18, A: H<sub>2</sub>O, B: MeOH, gradient: 5→100% B). **29** was obtained as an orange solid (52.0 mg, 50.3 μmol, 77%). R<sub>f</sub>: 0.40 (DC<sub>SIL</sub>; DCM/MeOH = 20:3), mp: 160 °C. IR (ATR),  $\tilde{\nu}$  [cm<sup>-1</sup>]: 3600 – 3000, 3058, 2930, 1749, 1648, 1604, 846, 818, 791, 698. <sup>1</sup>H NMR (DMSO-*d*<sub>6</sub>,  $\delta$  [ppm], J [Hz]): 8.94 (s, 1H, *inhibitor-CH*-6), 8.61 (s, 1H, *inhibitor-CH*-2), 8.49 (s, 1H, *fluorescein-CH*-f), 8.32–8.18 (m, 2H, *fluorescein-CH*-b, *triazole-CH*), 8.10–8.06 (m, 1H, *NHCOC*-a), 7.78–7.27 (m, 10H, *fluorescein-CH*-c,h,h'; *inhibitor-CH*-4,5,2'',3'',5'',6'', *inhibitor-CONHCH*<sub>2</sub>C-3), 7.15 (d, <sup>3</sup>J = 7.6, 2H, *CH*-2',6'), 6.89 (d, <sup>3</sup>J = 7.6, 2H, *CH*-3',5'), 6.80–6.43 (m, 6H, *fluorescein-CH*-i,i',k,k', *inhibitor-CH*-4'', *fluorescein-NHCO*), 5.03 (s, 2H, *triazole-CCH*<sub>2</sub>O), 4.63–4.52 (m, 1H, *inhibitor-NHCHCO*), 4.52–4.43 (m, 2H, *triazole-NCH*<sub>2</sub>), 4.40–4.29 (m, 3H, *inhibitor-NHCH*<sub>2</sub>C-3, *inhibitor-CH*-2''), 4.26 (d, <sup>2</sup>J = 13.6, 1H, SO<sub>2</sub>CH<sub>2</sub>), 4.13 (d, <sup>2</sup>J = 13.6, 1H, SO<sub>2</sub>CH<sub>2</sub>), 3.44–3.38 (m, 1H, *pip-CH*<sub>2</sub>-6'', *behind residual water*), 3.37–

3.33 (m, 2H,  $\text{CH}_2\text{NHCOC-a}$ ), 3.24–3.20 (m, 1H,  $\text{pip-CH}_2\text{-6''}$ ), 3.02–2.96 (m, 1H,  $\text{inhibitor-CH}_2\text{C-1'}$ ), 2.87–2.76 (m, 1H,  $\text{inhibitor-CH}_2\text{C-1'}$ ), 2.21–2.07 (m, 2H,  $\text{linker-CH}_2\text{CH}_2\text{CH}_2$ ), 1.99 (d,  $^2J = 12.4$ , 1H,  $\text{pip-CH}_2\text{-3}$ ), 1.54–1.40 (m, 3H,  $\text{pip-CH}_2\text{-3''}, 4'', 5''$ ), 1.17–1.01 (m, 2H,  $\text{pip-CH}_2\text{-4''}, 5''$ ). The signals of the fluorescein-hydroxy-OH (2H) are masked by the signal of residual water (3.62–3.27).  $^{13}\text{C}$  NMR (DMSO- $d_6$ ,  $\delta$  [ppm], J [Hz]): 171.1 (1C,  $\text{inhibitor-CONHCH}_2\text{C-3}$ ), 170.5 (1C,  $\text{pip-CONH}$ ), 168.3 (1C,  $\text{fluorescein-COO}$ ), 165.0 (1C,  $\text{fluorescein-NHCOC-a}$ ), 160.8 (2C,  $\text{fluorescein-C-j}, \text{j'}$ ), 157.1 (1C,  $\text{inhibitor-C-4'}$ ), 156.7 (1C,  $\text{fluorescein-C-d}$ ), 152.3 (2C,  $\text{fluorescein-C-l}, \text{l'}$ ), 148.8 (1C,  $\text{inhibitor-CH-2}$ ), 147.9 (1C,  $\text{inhibitor-CH-6}$ ), 142.7 (1C,  $\text{triazole-C}_q$ ), 137.7 (1C,  $\text{fluorescein-C-a}$ ), 136.1 (2C,  $\text{inhibitor-CH-3, 4}$ ), 134.8 (1C,  $\text{fluorescein-C-e}$ ), 134.3 (1C,  $\text{fluorescein-CH-b}$ ), 130.9 (2C,  $\text{fluorescein-CH-h}, \text{h'}$ ), 130.2 (2C,  $\text{inhibitor-CH-2'}, 6'$ ), 129.83 (1C,  $\text{C-1''}$ ), 129.77 (1C,  $\text{inhibitor-C-1'}$ ), 129.2 (1C,  $\text{inhibitor-CH-4''}$ ), 128.2 (2C,  $\text{inhibitor-CH-3''}, 5''$ ), 128.0 (2C,  $\text{inhibitor-CH-2''}, 6''$ ), 124.61 (1C,  $\text{inhibitor-CH-5}$ ), 124.58 (1C,  $\text{triazole-CH}$ ), 124.54 (1C,  $\text{fluorescein-CH-c}$ ), 123.8 (1C,  $\text{fluorescein-CH-f}$ ), 114.3 (2C,  $\text{inhibitor-CH-3'}, 5'$ ), 113.4 (2C,  $\text{fluorescein-CH-i}, \text{i'}$ ), 109.3 (2C,  $\text{fluorescein-C-g}, \text{g'}$ ), 102.4 (2C,  $\text{fluorescein-CH-k}, \text{k'}$ ), 78.6 (1C,  $\text{fluorescein-C-m}$ ), 61.1 (1C,  $\text{triazole-CCH}_2\text{O}$ ), 57.0 (1C,  $\text{CH}_2\text{SO}_2$ ), 54.7 (1C,  $\text{inhibitor-CH-2''}$ ), 54.2 (1C,  $\text{inhibitor-NHCHCO}$ ), 47.4 (1C,  $\text{triazole-NCH}_2$ ), 42.7 (1C,  $\text{pip-CH}_2\text{-6''}$ ), 40.0 (under DMSO peak, 1C,  $\text{inhibitor-HNCH}_2\text{C-3}$ ), 36.7 (1C,  $\text{CH}_2\text{NHCOC-a}$ ), 36.6 (1C,  $\text{CH}_2\text{C-1'}$ ), 29.7 (1C,  $\text{linker-CH}_2\text{CH}_2\text{CH}_2$ ), 27.6 (1C,  $\text{pip-CH}_2\text{-3''}$ ), 24.4 (1C,  $\text{pip-CH}_2\text{-5''}$ ), 19.1 (1C,  $\text{CH}_2\text{-4''}$ ). LC/MS (m/z) 517.30  $[\text{M}+2\text{H}]^{2+}$ , 345.15  $[\text{M}+3\text{H}]^{3+}$ . Purity (HPLC): 98.5%,  $t_R = 8.57$  min. HRMS (m/z)  $\text{C}_{55}\text{H}_{52}\text{N}_8\text{O}_{11}\text{S}$ ,  $[\text{M}+\text{H}]^+$ , calculated 1033.35490, found 1033.35225, error: 2.6 ppm.

#### 4.6.2 Materials and Methods: Protein Purification and Protease-Coupled PPIase Enzymatic Assay

Recombinant protein production and purification was conducted as previously described by Iwasaki *et al.*<sup>8</sup> with some modifications. The open reading frame (ORF) encoding BpMip (BPSS1823) was amplified and cloned into pET15b (Novagen) for recombinant protein purification with an N-terminal Hisx6 tag. The ORF encoding NmMip (NEIS1487), minus the signal peptide (first 17 amino acids), was amplified and cloned into pET28a(+) with a C-terminal Hisx6 tag. The ORF of NEIS0004 was amplified and cloned into pET-M11 with an N-terminal fusion with a Maltose Binding Protein (MBP) to allow for soluble expression as well as a C-terminal



Hisx6 tag. Expression constructs were sequenced prior to protein purification studies. Large scale protein expression was conducted as follows. An overnight culture of *E. coli* BL21 pLysS (DE3) containing the expression construct was diluted 1:50 in LB containing appropriate antibiotics. Flasks containing 800mL of culture were incubated at 37 °C with agitation until reaching an optical density (590nm) of 0.4-0.6. Cultures were induced by adding 1 mM isopropyl  $\beta$ -D-1-thiogalactopyranoside (IPTG) and incubated at 37 °C with agitation for a further 2 hours. Bacterial cells were harvested by centrifugation (4000 x g, 10 min, 4 °C), supernatant discarded and pellets stored at -20 °C.

Immediately prior to purification, cell pellets were thawed on ice and resuspended in Binding Buffer (BB) (50 mM NaCl, 50 mM HEPES, 10 % v/v Glycerol, 25 mM Imidazole, pH 7.5) with the addition of 2 $\mu$ l Benzonase nuclease (Sigma Aldrich), Lysozyme (0.2 mg/ml; Sigma Aldrich) and dissolved protease inhibitor pellet (ThermoFisher Scientific). Cell pellets were disrupted via sonication using the Ultrasonic Processor XL-2020 (Misonix) (five cycles of one minute sonication, one minute on ice). Samples were centrifuged (14100 x g, 15 min) to separate the soluble protein from insoluble protein. A HisTrap Nickel Affinity Column (5mL HisTrap HP, GE Healthcare Life Sciences) was equilibrated with 5X column volumes (CV) BB. Protein sample was filtered (Filtropur S 0.2, Sarstedt) and loaded manually onto the equilibrated HisTrap column. The column was washed with 5X CV BB before being subjected to a 10 % step-wise gradient of BB to elution buffer (EB) (150 mM NaCl, 50 mM HEPES, 10% v/v glycerol, 500 mM Imidazole. pH 7.5), followed by a 2X CV EB wash. Each elution fraction was collected and evaluated by SDS-PAGE and Coomassie Blue staining for the presence of purified recombinant protein. Fractions with purified protein were pooled and the protein concentration determined by optical density using a Nanodrop 2000 UV-Vis Spectrophotometer (ThermoFisher Scientific). Protein was aliquoted into one time use volumes for subsequent enzymatic assays.

The PPIase assay was performed as described by Vivoli *et al.*<sup>9</sup> and Fischer *et al.*<sup>10</sup>

A protease-coupled enzymatic assay was used to detect inhibition of PPIase activity. The enzymatic assay was conducted as follows; recombinant Mip protein (BpMip = 83  $\mu$ M; NmMip = 100  $\mu$ M; NEIS0004 = 89  $\mu$ M) was co-incubated for 6 min with 10  $\mu$ L succinyl-ala-phe-pro-phe-*p*-nitroanilide (SAPPP) (10 mg/mL in DMSO, Bachem), 400 nm inhibitor and 35 mM HEPES buffer (pH 7.8, Sigma-Aldrich) to a total volume of 1.25 mL at 4 °C. Following the 6 min

equilibration step, 250  $\mu\text{L}$  of  $\alpha$ -Chymotrypsin (5 mg/mL in 35 mM HEPES buffer; Sigma-Aldrich) was added to the cuvette. Cleavage of the chromophore, *p*-nitroanilide, was measured at 390 nm at 2 second intervals for 900 seconds using a Shimadzu 1800 UV/Vis spectrophotometer. Inhibition studies were conducted three times on independent days. All data fitting and statistical analyses were performed using GraphPad Prism 9.0.1. The pseudo-first-order rate constant was calculated by using one-phase association of non-linear regression. The calculated  $K_{\text{obs}}$  (minus the  $K_{\text{uncatalysed}}$ ) values were then used in the analysis of inhibitor efficacy. The percentage of remaining  $K_{\text{obs}}$  relative to the DMSO-treated recombinant protein was calculated.

#### 4.6.3 Solubility and Cytotoxicity

To determine the thermodynamic solubility, the continuous shake flask protocol, according to Hiltensperger *et al.*, was applied.<sup>11</sup> Three samples each were prepared by weighing out 1 – 2 mg of the substance to be tested and adding 1.00 mL of PBS buffer (pH = 7.4) to produce a saturated solution. The samples were incubated in a thermomixer (37 °C, 800 rpm), and after 15 min, 24 h and 48 h, 100  $\mu\text{L}$  were taken and centrifuged (10 min, 13000  $\text{min}^{-1}$ , 17 g, 20 °C). From the supernatant, 40  $\mu\text{L}$  were taken and measured on an *Agilent 1100 series* HPLC system from *Agilent Technologies* (Santa Clara, California, USA) using the method described below. The HPLC system was equipped with a degasser (G1322A), a binary pump (G1312A), a sample changer (G1313A), a DAD detector (G1315B) and a column oven (G1316A). The *Agilent Chemstation* software by *Agilent Technologies* (Santa Clara, California, USA) was used to analyze the data. To determine the thermodynamic solubility, the data after 48 hours was used. To prepare the calibration curves, stock solutions of the respective compounds (10 mM) were first prepared in methanol and diluted to the concentrations 1 mM, 500  $\mu\text{M}$ , 250  $\mu\text{M}$ , 200  $\mu\text{M}$ , 100  $\mu\text{M}$ , 50  $\mu\text{M}$ , 25  $\mu\text{M}$  and 10  $\mu\text{M}$ . Samples were measured using the HPLC method shown below and the peak area obtained was plotted against concentration to obtain the calibration curve. The data is representative of three independent experiments and the values are given as mean (SD).

Column: Eurosphere II, 5  $\mu\text{m}$ , 150 x 4.6 mm, *Knauer* (Berlin, Germany)  
Eluent: Milli-Q® water (A), acetonitrile (B)  
Gradient elution: 0–3 min: 5% (B)  
3–8 min: 5  $\rightarrow$  100% (B)  
8–10 min: 100% (B)

	10–11 min: 100 → 5% (B)
	11–13 min: 5% (B)
Injection volume:	5 $\mu$ L
Flow rate:	1.00 mL/min
Temperature:	30 °C
Detection:	262 nm

#### **Preparation of the PBS buffer**

2.0 g sodium chloride (NaCl)

50 mg potassium chloride (KCl)

355 mg disodium hydrogen phosphate ( $\text{Na}_2\text{HPO}_4$ )

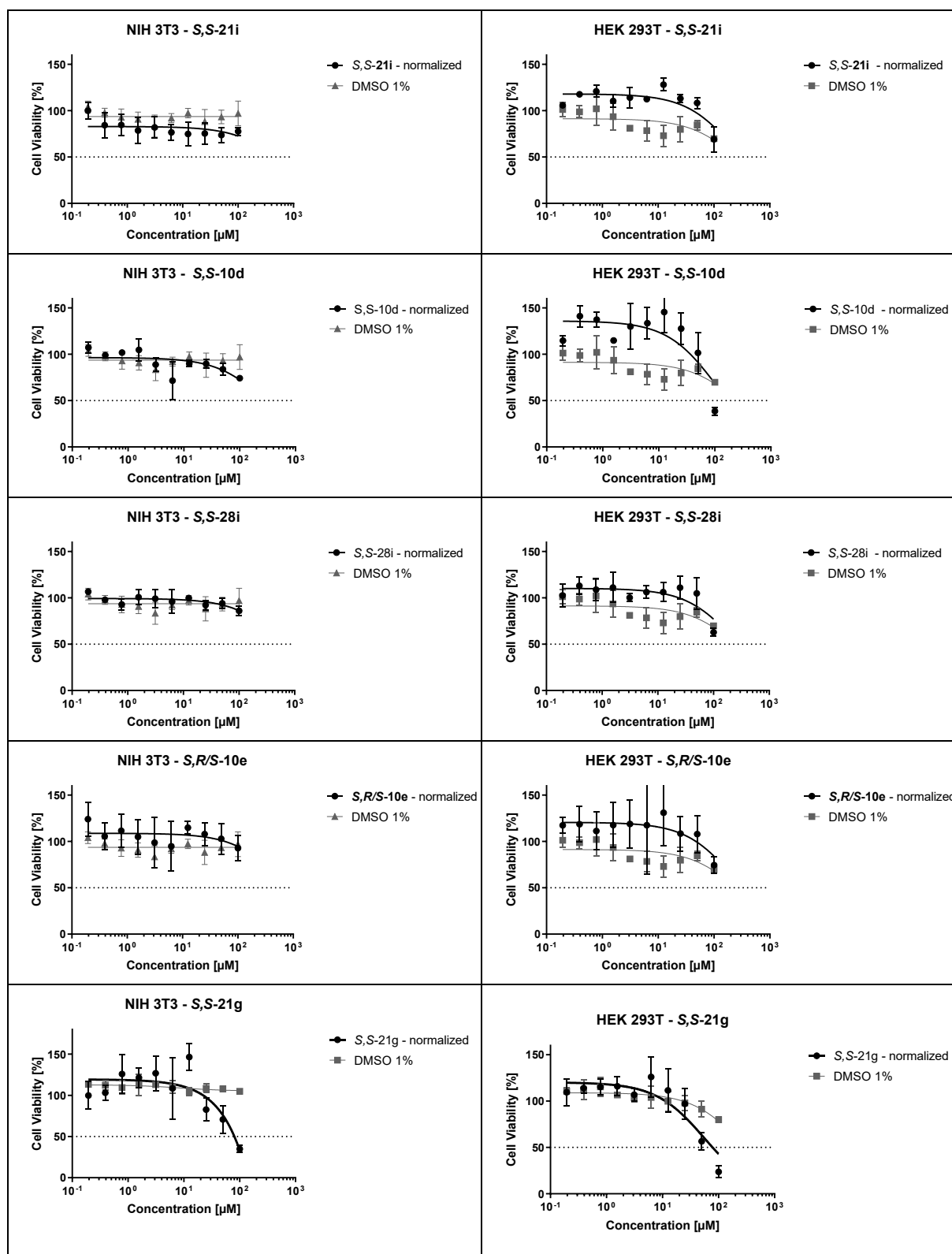
68 mg potassium dihydrogen phosphate ( $\text{KH}_2\text{PO}_4$ )

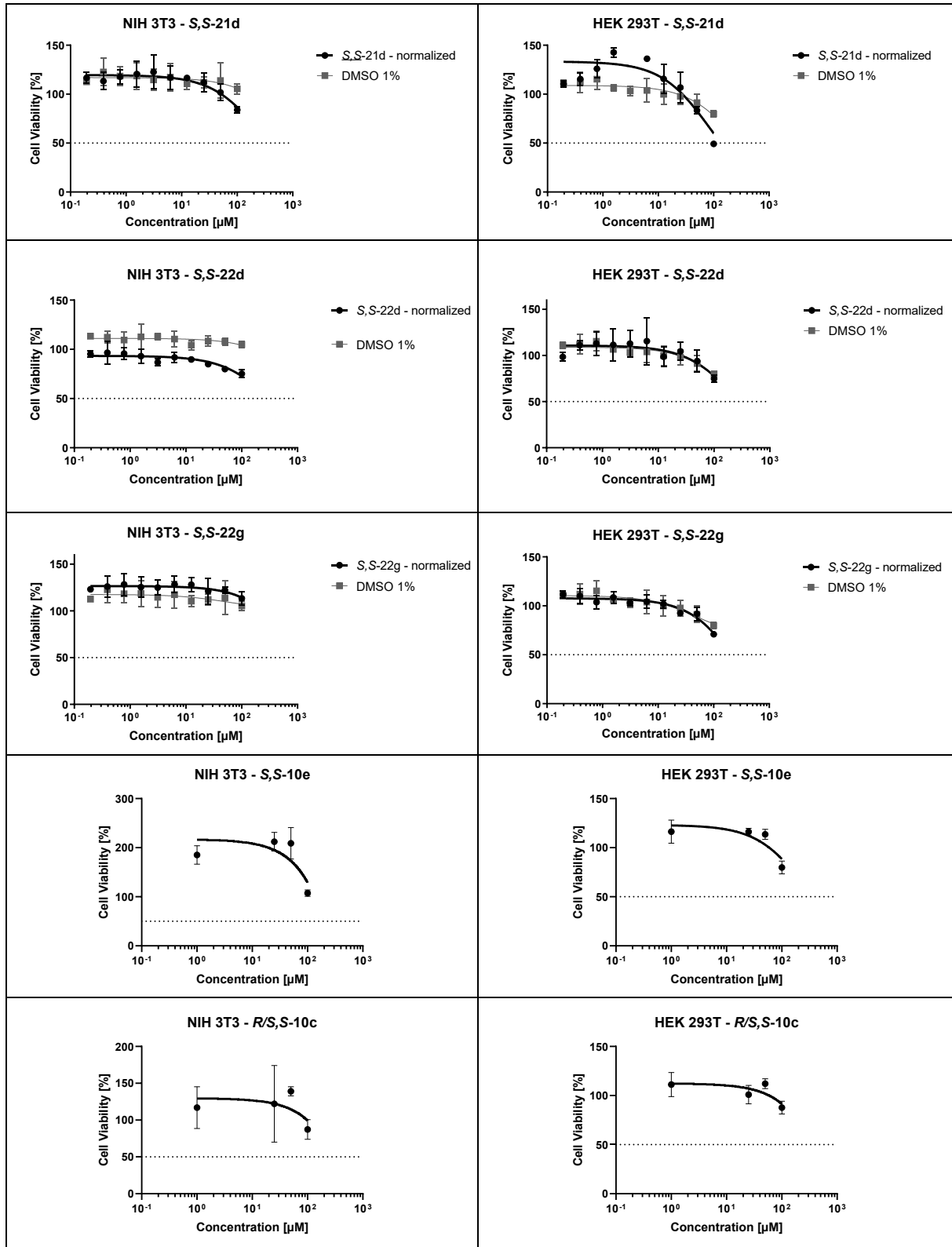
All substances were dissolved in 200 mL Millipore water, the pH was adjusted to 7.40 with 1 M NaOH and then made up to 250 mL with Millipore water.

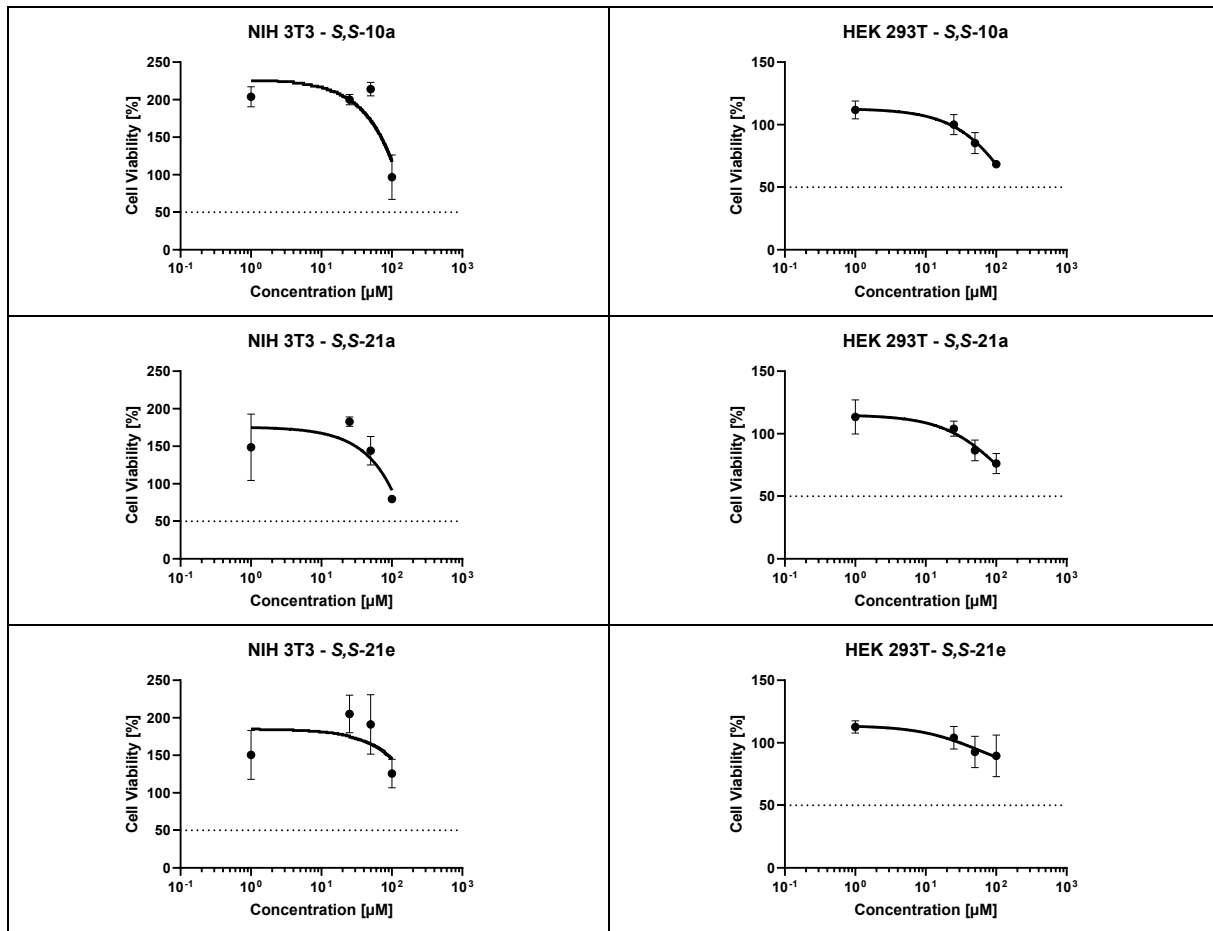
**Table 1.** Cytotoxicity and solubility data of a selection of Mip inhibitors. The determination of cell cytotoxicity against NIH 3T3 and HEK 293T cells, using a WST-1 formazan assay, is described in the experimental part of the main paper. *Mean ± SD, n = 3.*

Inhibitor	Cytotoxicity NIH 3T3 & HEK 293T (IC <sub>50</sub> , μM) <i>*Method A, Method B (described in Exp. Part)</i>	Solubility [μg/mL]
<b>9</b>	> 100 (HEK 293T) <sup>B</sup>	ND
<b>11</b>	> 100 (HEK 293T) <sup>B</sup>	239.0 ± 0.0
<i>R,S,S-10a</i>	ND	26.3 ± 1.2
<i>S,R-10a</i>	ND	Insoluble
<i>S,S-10a</i>	> 100 (NIH3T3) <sup>A</sup> > 100 (HEK293T) <sup>A</sup>	26.6 ± 0.3
<i>R,R-10a</i>	ND	Degradation
<i>R,S-10a</i>	ND	Degradation
<i>S,S-21a</i>	> 100 (NIH3T3) <sup>A</sup> > 100 (HEK293T) <sup>A</sup>	125.0 ± 8.8
<i>S,R-21a</i>	ND	61.1 ± 12.7
<i>R/S,S-22a</i>	ND	ND
<i>R/S,S-10b</i>	ND	290.6 ± 47.9
<i>R/S,S-10c</i>	> 100 (NIH3T3) <sup>A</sup> > 100 (HEK293T) <sup>A</sup>	172.0 ± 13.0
<i>R/S,S-10d</i>	ND	97.0 ± 4.6
<i>S,R-10d</i>	ND	ND
<i>S,S-10d</i>	> 100 (NIH3T3) <sup>B</sup> > 100 (HEK293T) <sup>B</sup>	ND
<i>S,S-21d</i>	> 100 (NIH3T3) <sup>B</sup> > 50 (HEK293T) <sup>B</sup>	390.0 ± 21.0
<i>S,S-22d</i>	> 100 (NIH3T3) <sup>B</sup> > 100 (HEK293T) <sup>B</sup>	1820.0 ± 137.0
<i>S,R/S-10e</i>	> 100 (NIH3T3) <sup>B</sup> > 100 (HEK293T) <sup>B</sup>	Insoluble
<i>R,R/S-10e</i>	ND	Insoluble
<i>S,S-10e</i>	> 100 (NIH3T3) <sup>A</sup> > 100 (HEK293T) <sup>A</sup>	14.9 ± 1.0
<i>S,R-10e</i>	ND	30.3 ± 10.0
<i>S,S-21e</i>	> 100 (NIH3T3) <sup>A</sup> > 100 (HEK293T) <sup>A</sup>	48.7 ± 6.5
<i>S,R-21e</i>	ND	56.6 ± 2.2
<i>S,R/S-10f</i>	ND	328.0 ± 26.0
<i>S,S-21g</i>	> 50 (NIH3T3) <sup>B</sup> > 50 (HEK293T) <sup>B</sup>	13.5 ± 2.2
<i>S,S-22g</i>	> 100 (NIH3T3) <sup>B</sup> > 100 (HEK293T) <sup>B</sup>	1494.0 ± 16.0
<i>S,S-25g</i>	ND	ND
<i>S,S-21h</i>	ND	ND
<i>S,S-28i</i>	> 100 (NIH3T3) <sup>B</sup> > 100 (HEK293T) <sup>B</sup>	ND
<i>S,S-21i</i>	> 100 (NIH3T3) <sup>B</sup> > 100 (HEK293T) <sup>B</sup>	ND

**Table 2.** Dose Response Curves of the Measured Cytotoxicity of the Substances, n = 3.

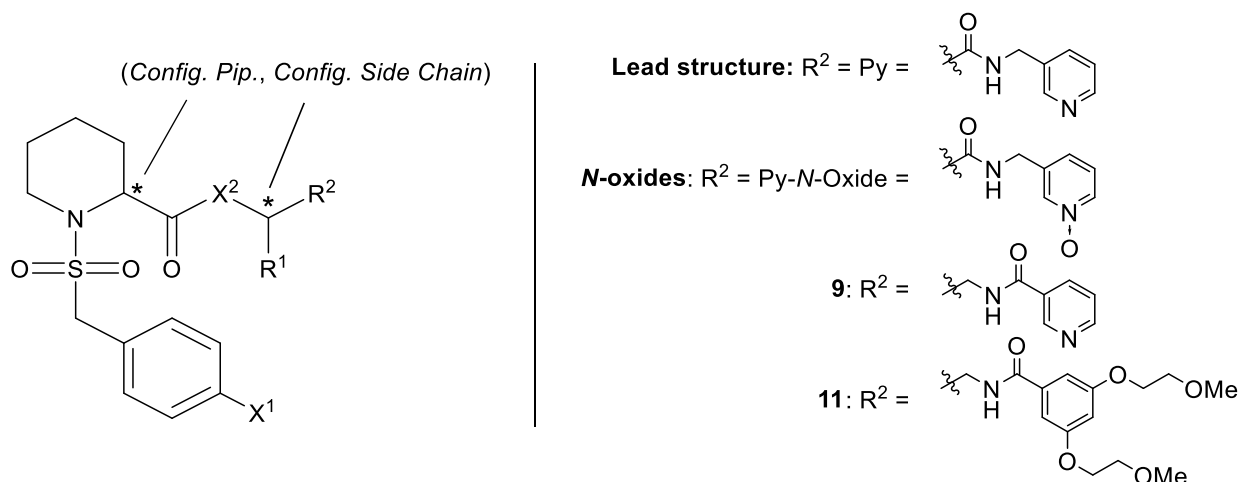






#### 4.6.4 Data and Standard Deviation of the FPA, the Protease-coupled PPIase Assays, and the *in vitro* RAW264.7 Murine Macrophage Infection Assays

**Table 3.** General structure and overview of the synthesized Mip inhibitors and their results in the FPA and protease-coupled enzymatic assay, including SD. *ND* = not determined. *NB* = no binding.



Inhibitor	Config. Pip. *	X <sup>1</sup>	X <sup>2</sup>	Side Chain Code	Side Chain R <sup>1</sup>	Config Side Chain *	R <sup>2</sup>	FPA K <sub>i</sub> [nM], BpMip, n = 3	BpMip %remaining activity at 400 nM inh., n = 3	NmMip %remaining activity at 400 nM inh., n = 3	NEIS0004 %remaining activity at 400 nM inh., n = 3	
<b>9</b>	S	H	O	Xxx	Xxx	Xxx	See above	3959.7±789.9	50.3±3.6	52.2±12.6	61.9±21.1	
<b>11</b>	S	H	O	Xxx	Xxx	Xxx	See above	1055.2±276.1	52.3±4.6	85.0±13.8	88.9±15.5	
<i>R/S,S-10a</i>	<i>R/S</i>	H	O	A		S	Py	48.8±0.0	15.9±0.9	14.0±2.4	6.9±1.2	
<i>S,R-10a</i>	S	H	O	A		R	Py	41115.5±6186.5	151.1±10.9	51.1±4.6	106.0±15.6	
<i>S,S-10a</i>	S	H	O	A		S	Py	122.1±40.3	7.0±0.6	10.0±3.9	6.7±0.6	
<i>R,R-10a</i>	R	H	O	A		R	Py	NB	154.6±22.0	51.3±6.4	107.5±25.0	
<i>R,S-10a</i>	R	H	O	A		S	Py	42421.0±4110.2	146.8±28.6	27.2±5.1	122.4±17.0	
<i>S,S-21a</i>	S	H	NH	A		S	Py	34.7±34.3	23.7±9.3	27.3±3.7	8.5±3.8	
<i>S,R-21a</i>	S	H	NH	A		R	Py	625.6±126.2	21.5±2.0	87.9±5.9	45.4±15.8	
<i>R/S,S-22a</i>	<i>R/S</i>	H	NH	A		S	Py-N-Oxide	4450.7±595.7	51.9±3.8	66.7±7.9	45.5±19.0	
<i>R/S,S-10b</i>	<i>R/S</i>	H	O	B			S	Py	1084.1±210.6	13.9±3.0	25.2±9.6	10.9±2.0
<i>R/S,S-10c</i>	<i>R/S</i>	H	O	C			<i>R/S</i>	Py	3131.4±2477.7	16.8±2.8	73.3±10.0	9.4±1.5
<i>R/S,S-10d</i>	<i>R/S</i>	H	O	D		S	Py	15.8±8.5	17.4±1.9	22.1±8.5	3.4±0.7	
<i>S,R-10d</i>	S	H	O	D		R	Py	2520.5±156.3	ND	ND	ND	
<i>S,S-10d</i>	S	H	O	D		S	Py	60.5±22.4	4.8±0.5	35.6±3.9	3.8±0.4	
<i>S,S-21d</i>	S	F	NH	D		S	Py	45.6±7.3	5.8±1.4	23.6±2.9	4.2±0.9	
<i>S,S-22d</i>	S	F	NH	D		S	Py-N-Oxide	148.0±15.6	21.0±1.9	44.4±3.8	23.8±5.0	



Inhibitor	Config. Pip. *	X <sup>1</sup>	X <sup>2</sup>	Side Chain Code	Side Chain R <sup>1</sup>	Config Side Chain *	R <sup>2</sup>	FPA K <sub>i</sub> [nM], BpMip, n = 3	BpMip %remaining activity at 400 nM inh., n = 3	NmMip %remaining activity at 400 nM inh., n = 3	NEIS0004 %remaining activity at 400 nM inh., n = 3
<i>S,R/S-10e</i>	<i>S</i>	H	O	E		<i>R/S</i>	Py	207.0±70.6	28.7±1.8	47.0±4.9	8.4±5.2
<i>R,R/S-10e</i>	<i>R</i>	H	O	E		<i>R/S</i>	Py	NB	139.6±16.9	93.7±8.4	119.2±26.6
<i>S,S-10e</i>	<i>S</i>	H	O	E		<i>S</i>	Py	15.3±12.0	14.8±1.4	54.0±6.3	11.1±2.9
<i>S,R-10e</i>	<i>S</i>	H	O	E		<i>R</i>	Py	3381.3±1437.6	100.6±15.7	83.5±7.3	70.0±28.0
<i>S,S-21e</i>	<i>S</i>	H	NH	E		<i>S</i>	Py	10.5±7.5	17.6±1.5	44.8±4.0	12.9±7.5
<i>S,R-21e</i>	<i>S</i>	H	NH	E		<i>R</i>	Py	320.0±69.7	23.4±2.0	83.7±5.3	39.9±14.9
<i>S,R/S-10f</i>	<i>S</i>	H	O	F		<i>R/S</i>	Py	4155.0±695.7	32.6±2.7	82.0±6.9	32.8±4.1
<i>S,S-21g</i>	<i>S</i>	F	NH	G		<i>S</i>	Py	18.8±18.6	12.5±1.6	11.5±2.7	37.2±13.1
<i>S,S-22g</i>	<i>S</i>	F	NH	G		<i>S</i>	Py- <i>N</i> -Oxide	1312.9±342.8	40.9±2.5	49.4±3.7	24.0±13.0
<i>S,S-25g</i>	<i>S</i>	F	NH	G		<i>S</i>		NB	ND	ND	ND
<i>S,S-21h</i>	<i>S</i>	H	NH	H		<i>S</i>	Py	34.3±0.0	4.4±0.8	12.3±2.4	4.9±1.1
<i>S,S-28i</i>	<i>S</i>	H	NH	I		<i>S</i>	Py	73.2±69.4	11.3±1.0	63.5±1.1	27.2±4.6
<i>S,S-21i</i>	<i>S</i>	F	NH	I		<i>S</i>	Py	17.0±0.0	13.5±1.4	43.3±3.9	30.6±3.4

**Table 4.** Percent reduction in *B. pseudomallei* (*B.ps.*)-induced cytotoxicity in RAW264.7 murine macrophages when treated with Mip inhibitors. Percentage of survival of *N. meningitidis* (Nm) and *N. gonorrhoeae* (Ng) in RAW264.7 murine macrophages treated with Mip inhibitors at 50 µM compared to untreated control. Mean of a minimum of three biological replicates, each with technical duplicates, ± SD.

Inhibitor	% <i>B.ps.</i> -induced cytotoxicity in RAW264.7 cells	<i>Nm</i> survival, % of control in RAW264.7 cells	<i>Ng</i> survival, % of control in RAW264.7 cells
<b>9</b>	68.9±14.3	41.1±25.5	27.1±7.6
<b>11</b>	71.0±20.5	19.6±14.6	21.5±4.7
<i>R/S,S-10a</i>	68.5±23.3	38.4±9.9	65.1±15.3
<i>S,R-10a</i>	65.9±18.2	26.0±13.4	73.2±16.3
<i>S,S-10a</i>	72.5±23.9	41.5±5.3	64.6±17.1
<i>R,R-10a</i>	74.3±12.3	21.0±10.9	58.6±25.8
<i>R,S-10a</i>	82.7±16.4	35.2±22.6	68.4±13.6
<i>S,S-21a</i>	63.4±16.3	25.0±7.9	40.9±17.7
<i>S,R-21a</i>	30.4±18.5	60.8±8.6	70.6±23.5
<i>R/S,S-22a</i>	46.2±20.4	76.0±15.8	45.4±21.2
<i>R/S,S-10b</i>	96.8±23.1	52.5±17.4	65.1±13.3
<i>R/S,S-10c</i>	94.3±19.7	58.0±15.2	35.4±11.3
<i>R/S,S-10d</i>	93.2±15.4	36.9±18.9	ND
<i>S,S-10d</i>	87.8±24.6	13.0±13.0	19.1±8.5
<i>S,S-21d</i>	46.8±24.0	56.2±13.9	61.7±20.7
<i>S,S-22d</i>	61.5±15.8	71.3±9.4	56.4±18.6

Inhibitor	% <i>B.ps.</i> -induced cytotoxicity in RAW264.7 cells	<i>Nm</i> survival, % of control in RAW264.7 cells	<i>Ng</i> survival, % of control in RAW264.7 cells
<i>S,R/S-10e</i>	93.4±28.4	16.4±6.2	63.5±13.7
<i>R,R/S-10e</i>	95.7±26.5	21.2±11.3	ND
<i>S,S-10e</i>	70.6±17.4	16.0±6.9	19.8±11.8
<i>S,R-10e</i>	97.6±29.1	67.7±18.7	53.6±24.3
<i>S,S-21e</i>	75.4±32.6	34.1±3.3	71.5±21.7
<i>S,R-21e</i>	88.7±35.3	69.9±7.9	41.9±17.7
<i>S,R/S-10f</i>	35.6±14.3	84.4±20.5	52.0±15.4
<i>S,S-21g</i>	68.0±25.1	47.9±14.4	50.8±23.9
<i>S,S-22g</i>	51.7±16.4	52.8±21.5	44.2±13.1
<i>S,S-21h</i>	55.4±26.9	45.7±15.0	35.2±21.3
<i>S,S-28i</i>	78.5±19.7	22.6±22.6	28.0±9.1
<i>S,S-21i</i>	46.7±19.7	51.4±29.8	31.4±15.2

**Table 5.** Mip inhibitor cytotoxicity against RAW264.7 murine macrophages. Murine macrophages were co-incubated with 50  $\mu$ M of Mip inhibitor or DMSO (solvent control) for 24 hours before the lactose dehydrogenase (LDH) release was measured as per manufacturer's protocol (Roche). Mean of a minimum of three biological repeats, each with technical duplicates,  $\pm$  SD.

Inhibitor	% Inhibitor-induced cytotoxicity RAW264.7 cells
<b>9</b>	7.07 $\pm$ 6.97
<b>11</b>	10.36 $\pm$ 10.96
<i>R/S,S-10a</i>	13.77 $\pm$ 10.00
<i>S,R-10a</i>	8.10 $\pm$ 5.85
<i>S,S-10a</i>	9.84 $\pm$ 4.13
<i>R,R-10a</i>	5.37 $\pm$ 7.08
<i>R,S-10a</i>	3.99 $\pm$ 7.14
<i>S,S-21a</i>	7.62 $\pm$ 6.66
<i>S,R-21a</i>	12.04 $\pm$ 2.98
<i>R/S,S-22a</i>	10.69 $\pm$ 4.90
<i>R/S,S-10b</i>	9.88 $\pm$ 6.26
<i>R/S,S-10c</i>	5.28 $\pm$ 2.92
<i>R/S,S-10d</i>	4.90 $\pm$ 4.01
<i>S,S-10d</i>	2.55 $\pm$ 6.74
<i>S,S-21d</i>	8.26 $\pm$ 8.19
<i>S,S-22d</i>	5.36 $\pm$ 3.06
<i>S,R/S-10e</i>	6.35 $\pm$ 7.81
<i>R,R/S-10e</i>	9.97 $\pm$ 9.86
<i>S,S-10e</i>	7.33 $\pm$ 8.81
<i>S,R-10e</i>	5.08 $\pm$ 5.37
<i>S,S-21e</i>	7.30 $\pm$ 7.02
<i>S,R-21e</i>	2.96 $\pm$ 1.11
<i>S,R/S-10f</i>	17.75 $\pm$ 7.77
<i>S,S-21g</i>	6.99 $\pm$ 10.03
<i>S,S-22g</i>	14.76 $\pm$ 4.22
<i>S,S-21h</i>	9.26 $\pm$ 9.75
<i>S,S-28i</i>	2.71 $\pm$ 1.84
<i>S,S-21i</i>	10.46 $\pm$ 4.39

4.6.5 Table with All Analytical or Biological Data as a Summary of SI Tables 01 to 05

**Table 6.** Table with all analytical or biological data as a summary of SI tables 01 to 05. The description can be found in the mentioned SI tables.

Inhibitor	SMILES	PPA RI (n), $\mu\text{g}/\text{ml}$ , $n=3$	Biophysical Scrambling activity at 400 nm (h), $n=3$	Biophysical Scrambling activity at 400 nm (h), $n=3$	NEISS004 Scrambling activity at 400 nm (h), $n=3$	% B <sub>1</sub> induced cytotoxicity BAW264.7 $n=3$ (minimum of 3)	Nm survival, % of control in BAW264.7 cells $n=3$ (minimum of 3)	Nt survival, % of control in BAW264.7 cells $n=3$ (minimum of 3)	Cytotoxicity Measured by HEK 293T (IC50, $\mu\text{M}$ ) Method (A/B)	Solubility ( $\mu\text{g}/\text{ml}$ )	% inhibitor-induced cytotoxicity BAW264.7 cells, $n=3$ (minimum of 3)
9	O=C1C=CC(=O)C=C(C)C=C1	3959.73789.9	50.313.6	52.212.6	61.921.1	68.914.3	41.125.5	27.127.6	> 100 [HEK 293T]B	ND	7.0746.97
11	O=C1C=CC(=O)C=C(C)C=C1	1055.21276.1	52.334.6	85.0113.8	88.915.5	71.0120.5	19.614.6	21.54.7	> 100 [HEK 293T]B	239.010.0	10.36110.96
R/S-10a	O=C1C=CC(=O)C=C(C)C=C1	48.810.0	15.910.9	14.012.4	6.911.2	68.5123.3	38.419.9	65.115.3	ND	26.311.2	13.77110.00
S/R-10a	O=C1C=CC(=O)C=C(C)C=C1	4115.5186.5	151.114.6	51.114.6	106.015.6	65.918.2	26.013.4	71.216.3	ND	insoluble	8.1015.85
S/S-10a	O=C1C=CC(=O)C=C(C)C=C1	122.1140.3	7.016.6	10.013.9	6.716.6	72.5123.9	41.516.3	64.617.1	> 100 [NH43T]A > 100 [HEK293T]A	26.610.3	9.844.13
R/R-10a	O=C1C=CC(=O)C=C(C)C=C1	NS	154.6122.0	53.316.4	107.5125.0	74.3112.3	21.0110.9	58.6125.8	ND	degradation	5.3717.08
R/S-10a	O=C1C=CC(=O)C=C(C)C=C1	42421.04110.2	146.8128.6	27.245.1	122.4417.0	82.7116.4	35.2122.6	68.4413.6	ND	degradation	3.9917.14
S/S-21a	O=C1C=CC(=O)C=C(C)C=C1	34.713.3	23.719.3	27.313.7	8.513.8	63.4116.3	25.017.9	40.917.7	> 100 [NH43T]A > 100 [HEK293T]A	125.018.8	7.6246.66
S/R-21a	O=C1C=CC(=O)C=C(C)C=C1	625.6126.2	21.512.0	87.915.9	45.415.8	30.418.5	60.818.6	70.6123.5	ND	61.1112.7	12.0421.98
R/S-22a	O=C1C=CC(=O)C=C(C)C=C1	4450.71395.7	51.913.8	66.717.9	45.319.0	46.2120.4	76.015.8	45.4121.2	ND	ND	10.6914.90
R/S-10b	O=C1C=CC(=O)C=C(C)C=C1	1084.11210.6	13.913.0	25.219.6	10.912.0	96.8123.1	52.5117.4	65.1113.3	ND	290.6147.9	9.8816.36
R/S-10c	O=C1C=CC(=O)C=C(C)C=C1	3131.412477.7	16.812.8	73.3110.0	9.415.1	94.3119.7	58.015.2	35.4111.3	> 100 [NH43T]A > 100 [HEK293T]A	172.0113.0	5.2812.92
R/S-10d	O=C1C=CC(=O)C=C(C)C=C1	15.818.5	17.411.9	22.114.5	3.410.7	93.2115.4	36.9118.9	ND	ND	97.014.6	4.9014.01
S/R-10d	O=C1C=CC(=O)C=C(C)C=C1	2520.51156.3	ND	ND	ND	ND	ND	ND	ND	ND	ND
S/S-10d	O=C1C=CC(=O)C=C(C)C=C1	60.5122.4	4.810.5	35.613.9	3.810.4	87.8124.6	13.0113.0	19.118.5	> 100 [NH43T]B > 100 [HEK293T]B	ND	2.5516.74
S/S-21d	O=C1C=CC(=O)C=C(C)C=C1	45.617.3	5.811.4	23.612.9	4.216.9	46.8124.0	56.2113.9	61.7120.7	> 100 [NH43T]B > 50 [HEK293T]B	390.0121.0	8.2618.19
S/S-22d	O=C1C=CC(=O)C=C(C)C=C1	148.0115.6	21.011.9	44.413.8	23.815.0	61.5115.8	71.319.4	56.4118.6	> 100 [NH43T]B > 100 [HEK293T]B	182.01137.0	5.3613.06
S/R/S-10e	O=C1C=CC(=O)C=C(C)C=C1	207.0170.6	28.711.8	47.014.9	8.415.2	93.4128.4	16.416.2	63.5113.7	> 100 [NH43T]B > 100 [HEK293T]B	insoluble	6.3517.81
R/R/S-10e	O=C1C=CC(=O)C=C(C)C=C1	NS	139.6116.9	93.718.4	119.2126.6	95.7136.5	21.2111.3	ND	ND	insoluble	9.9719.86
S/S-10e	O=C1C=CC(=O)C=C(C)C=C1	15.3112.0	14.811.4	54.016.3	11.112.9	70.6117.4	16.016.9	19.8111.8	> 100 [NH43T]A > 100 [HEK293T]A	14.911.0	7.3318.81
S/R-10e	O=C1C=CC(=O)C=C(C)C=C1	3381.31437.6	100.6115.7	83.517.3	70.0128.0	97.6129.1	67.718.7	53.6134.3	ND	30.3110.0	5.0815.37
S/S-21e	O=C1C=CC(=O)C=C(C)C=C1	10.517.5	17.611.5	44.814.0	12.917.5	75.4121.6	34.113.3	71.5121.7	> 100 [NH43T]A > 100 [HEK293T]A	48.716.5	7.3017.02
S/R-21e	O=C1C=CC(=O)C=C(C)C=C1	320.0169.7	23.412.0	83.715.3	39.914.9	88.7135.3	69.917.9	41.917.7	ND	56.612.2	2.9611.11
S/R/S-10f	O=C1C=CC(=O)C=C(C)C=C1	4155.01495.7	32.612.7	82.016.9	32.814.1	35.6114.3	84.4120.5	52.0115.4	ND	328.0126.0	17.7517.77
S/S-21f	O=C1C=CC(=O)C=C(C)C=C1	18.8118.6	12.313.6	11.514.7	37.2113.1	68.0125.1	47.9144.4	50.8123.9	> 50 [NH43T]B > 100 [HEK293T]B	13.512.2	6.99110.03
S/S-22f	O=C1C=CC(=O)C=C(C)C=C1	1312.91342.8	40.912.5	49.413.7	24.0113.0	51.7116.4	52.8121.5	44.2113.1	> 100 [NH43T]B > 100 [HEK293T]B	1494.0116.0	14.7614.22
S/S-25f	O=C1C=CC(=O)C=C(C)C=C1	NS	ND	ND	ND	ND	ND	ND	ND	ND	ND
S/S-21h	O=C1C=CC(=O)C=C(C)C=C1	94.310.0	4.410.8	12.312.4	4.911.1	55.4126.9	45.7115.0	35.2121.3	ND	ND	9.2619.75
S/S-28f	O=C1C=CC(=O)C=C(C)C=C1	73.2169.4	11.311.0	63.511.1	27.214.6	78.5119.7	22.6122.6	28.019.1	> 100 [NH43T]B > 100 [HEK293T]B	ND	2.7111.84
S/S-23f	O=C1C=CC(=O)C=C(C)C=C1	17.010.0	13.511.4	43.313.9	30.613.4	46.7119.7	51.4129.8	31.4115.2	> 100 [HEK293T]B	ND	10.4614.39

#### 4.6.6 References (*Supporting Information*)

- (1) Stecher, E. D.; Ryder, H. F. Ionization Constants and Rates of Ester Hydrolysis in the Benzylidenepyruvic Acid Series. *J. Am. Chem. Soc.* **1952**, *74* (17), 4392-4395. DOI: 10.1021/ja01137a045.
- (2) Slavinska, V.; Sile, D.; Rozentals, G.; Balodis, Y.; Popelis, J.; Lukevics, E. Hydrogenation of the Sodium Salt of 2-Oxo-4-(3-pyridyl)butenoic Acid on Palladium Black. *Chem. Heterocycl. Compd.* **2002**, *38* (7), 801-804. DOI: 10.1023/A:1020677503143.
- (3) Shang, L.; Ma, Y.; He, S.; Shang, C. Preparing method and application of Michael receptor enterovirus 71 inhibitor. CN110105348, 2019.
- (4) Hanna, C. C.; Kulkarni, S. S.; Watson, E. E.; Premdjee, B.; Payne, R. J. Solid-phase synthesis of peptide selenoesters via a side-chain anchoring strategy. *Chem. Commun.* **2017**, *53* (39), 5424-5427. DOI: 10.1039/c7cc00823f.
- (5) Rossi, F. M.; Kao, J. P. Practical method for the multigram separation of the 5- and 6-isomers of carboxyfluorescein. *Bioconjug. Chem.* **1997**, *8* (4), 495-497. DOI: 10.1021/bc970078d.
- (6) Farzan, V. M.; Ulashchik, E. A.; Martynenko-Makaev, Y. V.; Kvach, M. V.; Aparin, I. O.; Brylev, V. A.; Prikazchikova, T. A.; Maklakova, S. Y.; Majouga, A. G.; Ustinov, A. V.; Shipulin, G. A.; Shmanai, V. V.; Korshun, V. A.; Zatsepin, T. S. Automated Solid-Phase Click Synthesis of Oligonucleotide Conjugates: From Small Molecules to Diverse N-Acetylgalactosamine Clusters. *Bioconjug. Chem.* **2017**, *28* (10), 2599-2607. DOI: 10.1021/acs.bioconjchem.7b00462.
- (7) Donnelly, P. S.; Zanatta, S. D.; Zammit, S. C.; White, J. M.; Williams, S. J. 'Click' cycloaddition catalysts: copper(I) and copper(II) tris(triazolylmethyl)amine complexes. *Chem. Commun.* **2008**, (21), 2459-2461. DOI: 10.1039/b719724a.
- (8) Iwasaki, J.; Lorimer, D. D.; Vivoli-Vega, M.; Kibble, E. A.; Peacock, C. S.; Abendroth, J.; Mayclin, S. J.; Dranow, D. M.; Pierce, P. G.; Fox, D.; Lewis, M.; Bzdyl, N. M.; Kristensen, S. S.; Inglis, T. J. J.; Kahler, C. M.; Bond, C. S.; Hasenkopf, A.; Seufert, F.; Schmitz, J.; Marshall, L. E.; Scott, A. E.; Norville, I. H.; Myler, P. J.; Holzgrabe, U.; Harmer, N. J.; Sarkar-Tyson, M. Broad-spectrum in vitro activity of macrophage infectivity potentiator inhibitors against Gram-negative bacteria and *Leishmania major*. *J. Antimicrob. Chemother.* **2022**, *77* (6), 1625-1634. DOI: 10.1093/jac/dkac065.

(9) Vivoli, M.; Renou, J.; Chevalier, A.; Norville, I. H.; Diaz, S.; Juli, C.; Atkins, H.; Holzgrabe, U.; Renard, P. Y.; Sarkar-Tyson, M.; Harmer, N. J. A miniaturized peptidyl-prolyl isomerase enzyme assay. *Anal. Biochem.* **2017**, *536*, 59-68. DOI: 10.1016/j.ab.2017.08.004.

(10) Fischer, G.; Bang, H.; Mech, C. Detection of enzyme catalysis for cis-trans-isomerization of peptide bonds using proline-containing peptides. *Biomed. Biochim. Acta* **1984**, *43* (10), 1101-1111.

(11) Hiltensperger, G.; Hecht, N.; Kaiser, M.; Rybak, J. C.; Hoerst, A.; Dannenbauer, N.; Muller-Buschbaum, K.; Bruhn, H.; Esch, H.; Lehmann, L.; Meinel, L.; Holzgrabe, U. Quinolone Amides as Antitrypanosomal Lead Compounds with In Vivo Activity. *Antimicrob. Agents Chemother.* **2016**, *60* (8), 4442-4452. DOI: 10.1128/AAC.01757-15.

## IV General Discussion

Here, overarching findings and future perspectives of research on inhibitors of the Macrophage Infectivity Potentiator (Mip) protein will be highlighted. In order to avoid replicating subchapter III\_4, particular observations will be singled out and discussed in-depth here.

### Evolution of Mip Inhibitors Derived from Rapamycin

In the past, natural products have been the most important source of antibiotic lead compounds. Considering the last 40 years, about 60% of all new chemical entities in the field of antibacterial agents were based on or derived from natural products.<sup>14</sup> The Mip inhibitors developed here can also be assigned to this category. They are derived from rapamycin and FK506, structurally similar, immunosuppressive natural products produced by the bacteria *Streptomyces hygroscopicus* and *Streptomyces tsukubensis*, respectively.<sup>109, 119</sup> By rational design, i.e., omission of the so-called *effector domain* (cf. Figure 21), responsible for the immunosuppressive effect, it was possible to produce small molecule inhibitors that address the Mip protein of *Legionella pneumophila* (LpMip), the causative agent of Legionnaires' disease.<sup>119</sup>

The virulence factor Mip has emerged as a promising antimicrobial target. Mip proteins belong to the FK506 binding proteins (FKBPs) and the immunophilin family of peptidyl-prolyl *cis-trans* isomerase (PPIase) enzymes. The C-terminal PPIase domain is highly conserved over a broad spectrum of pathogens' Mip proteins.<sup>146</sup> The *cis-trans* isomerization of peptide bonds preceding a proline residue is known to be a rate-limiting reaction in the process of protein folding.<sup>147, 148</sup> PPIases catalyze this inherently slow reaction, increasing the protein-folding rate.<sup>149</sup>

The predominantly surface-exposed Mip proteins have been demonstrated to play a crucial role in the virulence of various pathogenic bacteria and parasites. Upon deletion of the corresponding genes, a reduction in the survival of several pathogens, such as *L. pneumophila* and *Burkholderia pseudomallei*, was observed in animal infection models.<sup>150, 151</sup>

Over the past decade, the previously mentioned small molecule inhibitors featuring a pipercolic acid backbone (cf. Figure 21) have been developed. These Mip targeting inhibitors have shown promising potential to combat a broad spectrum of microbial infections *in vitro*.<sup>114, 119, 152</sup>

---

*The bibliography for this chapter can be found at the end of this thesis (chapter VII).*

Figure 21 displays the evolution of Mip inhibitor lead structures of the Holzgrabe research group and the corresponding crystal structures. Key modifications from **39** (*CJ168*) to **41** (*SF235*) were the replacement of the trimethoxy-benzene moiety with nicotinamide, which resulted in an improved cytotoxicity profile, higher solubility, and enhanced affinity towards BpMip.<sup>152, 153</sup> Introduction of an amide linker in **41** likewise resulted in enhanced solubility and higher chemical stability compared to the nicotinic acid ester derivatives studied.<sup>152, 153</sup>

In this study, a library of piperolic acid ester and amide derivatives was synthesized, featuring a diverse range of side chains and distinct stereochemical arrangements. Analysis of BpMip/inhibitor co-crystal structures had revealed that the inhibitors could assume two distinct binding poses. By incorporating an additional side chain into the linker connecting the piperolic moiety and the pyridine ring, it was anticipated that a single molecule might accommodate both binding conformations.

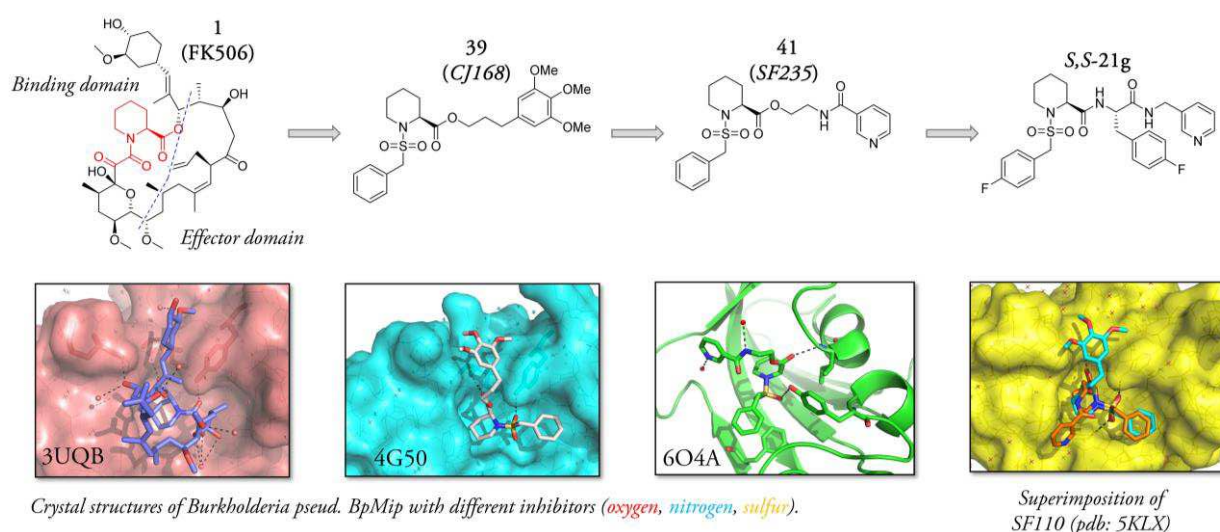


Figure 21. Evolution of Mip inhibitors developed in the Holzgrabe research group.

In the design of novel inhibitors, such as **S,S-21g** (cf. Figure 1), the pyridine moiety was maintained constant due to its aforementioned advantages.<sup>119, 152</sup> The piperidine-sulfonamide moiety was also preserved, as it had demonstrated to be indispensable for Mip inhibition.<sup>119, 152</sup> Exchange of the piperidine-2-carboxylate by an amide group aimed to enhance both chemical and metabolic stability of the compounds. Employing a benzyl and a *para*-fluorobenzyl group at the sulfonamide moiety had been found to be favorable for PPIase inhibition against BpMip.<sup>152</sup> Furthermore, the *para*-fluorine substitution at the benzene rings on both the sulfonamide moiety and the side chain



was intended to impede metabolism, such as CYP-mediated hydroxylation. The amide position on the pyridine residue was altered compared to lead compound **41** to facilitate synthetic accessibility. This modification enabled the introduction of side chains using cost-effective amino acids and simplified the preparation of the inhibitors through mild amidation and esterification reactions, preserving the stereochemical integrity of the compounds.

A number of substances examined in the side chain paper (subchapter III\_4) were synthesized by Anja Hasenkopf (*see appendix for details*).<sup>142</sup> Binding affinity towards BpMip was measured by means of FPA by Theresa Lohr.<sup>20</sup>

### **Side Chain Introduction Increases BpMip Binding Affinity and Enzymatic Inhibition**

The introduction of a side chain significantly enhances the inhibition of BpMip PPIase activity and binding affinity. Thus, the  $K_i$  can be lowered from a micromolar to a double-digit nanomolar range, supporting the hypothesis of combining two binding modes in one molecule (e.g.,  $K_i$  (**S,S-21i**) = 17 nM). The proper configuration at both stereo centers is crucial for effective binding affinity and enzymatic inhibition of BpMip. A comparison among all four stereo isomers of various Mip inhibitors (e.g., **10a**) showed that the *S* configuration at both stereocenters is preferred. Moreover, BpMip's enzymatic activity can be almost completely inhibited (by up to 96%) using compounds such as **S,S-21d** and **S,S-21h**.

Interestingly, the differences between aromatic and aliphatic side chains are not substantial. However, this does not necessarily represent a disadvantage. Rather, it means that a wide variety of residues are conceivable on this side. Consequently, in the future, this will allow the tuning of distinct properties, such as solubility, by the introduction of a hydrophilic residue.

By attaching the side chain in an overall *S,S* configuration, an improvement by a factor of 100 in binding affinity to BpMip was achieved. So far, variations of the side chain-bearing inhibitors suggest that it is unlikely to achieve a similarly significant improvement by further modification.

In fact, a point has now been reached where it can be debated whether a higher binding affinity is still desirable. As binding affinity to microbial Mip proteins increases, the binding affinity to off-targets such as the human FKBP12 protein is likely to increase as well.

### Binding of Mip Inhibitors to Human FKBP

Pomplun and colleagues examined the binding affinity of structurally related C5-substituted [4.3.1]-aza-bicyclic sulfonamides to a series of human FK506-binding proteins (FKBPs), including FKBP12, FKBP51, and FKBP52, as well as to microbial Mip proteins such as *Plasmodium falciparum* Mip and LpMip.<sup>140</sup> Their findings revealed that the investigated inhibitors consistently demonstrate stronger binding to human FKBP12 than to microbial Mip proteins. This could potentially cause reduced active drug concentrations *in vivo* to target microbial Mips and may even result in unwanted side effects.

The pipercolic amide derivatives **S,S-21d** and **S,S-21g** were also investigated for their binding to human FKBP by the Hausch group. Fortunately, a different order was found here.  $K_i$  values decreased in the following sequence: FKBP51 > FKBP52 > FKBP12.6 > FKBP12 ~ TcMip > BpMip (see Table 8).

Table 8. Results of the FPA for **S,S-21g** and **S,S-21d** using different human and microbial FKBP. Testing against human FKBP was performed by the Hausch research group. n=3.

Mip Inhibitor	$K_i$ FKBP51 [nM]	$K_i$ FKBP52 [nM]	$K_i$ FKBP12.6 [nM]	$K_i$ FKBP12 [nM]	$K_i$ TcMip [nM]	$K_i$ BpMip [nM]
<b>S,S-21g</b>	5261 ± 2021	3731 ± 1179	281 ± 36.4	380	388	19 ± 18
<b>S,S-21d</b>	3133 ± 375	1601 ± 282	112 ± 15	82 ± 11	669	46 ± 7

For the pipercolic amide derivatives, especially for **S,S-21g**, binding to BpMip is more potent than to the human FKBP. This altered order may indicate that the open form of **S,S-21d** and **S,S-21g** ( $K_{i,FKBP12} / K_{i,BpMip} = 20$ ) has a selectivity advantage for microbial over human FKBP, in contrast to the bridged variant of Pomplun *et al.*

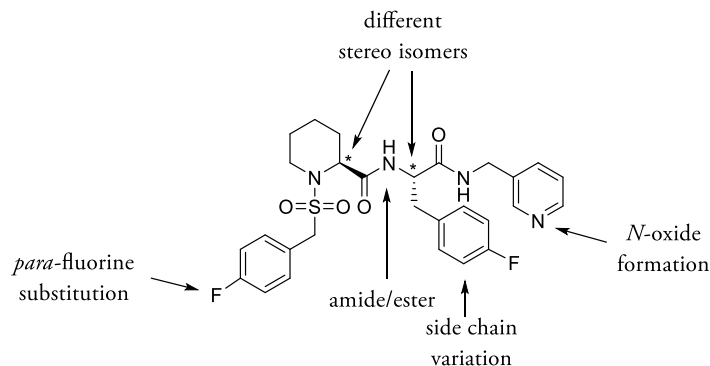
However, since the  $K_i$  values of the pipercolic amide derivatives against human FKBP12 are in the two- to three-digit nanomolar range, it can be assumed that microbial inhibition in the absence of FKBP12 inhibition may also be difficult for this kind of Mip inhibitors.

It should therefore be investigated whether binding of the pipercolic amide derivatives to FKBP12 could lead to immunosuppression or other side effects. Looking at the structure, an immunosuppressive effect is not to be expected due to the absence of an *effector domain* like in rapamycin. Nevertheless, a final clarification prior to a human application would probably be advisable.

### Overview of SAR Findings from the Side Chain Paper

The novel Mip inhibitors, equipped with side chains, have shown significant improvements in cell-based assays. Thus, they led to a reduction in *B. pseudomallei*-induced cytotoxicity within infected macrophages by up to 70%. Moreover, they sensitized infected macrophages to eliminate *N. meningitidis* and *N. gonorrhoeae* infections by up to 87% and 80%, respectively. The detailed discussion given in III\_4.2 will not be repeated here. Rather, Table 9 provides a general overview of the structural modifications and SARs found.

Table 9. General overview of the structural modifications and SAR results from the side chain paper. The Mip inhibitors help to reduce the cytotoxicity induced by *B. pseudomallei* on macrophages. They also help to (re)sensitize infected macrophages to kill *Neisseria species*. For more details, see chapter III\_4.



Molecule Feature	BpMip inhibition (FPA & PPIase)	NEIS0004 inhibition (PPIase)	NmMip inhibition (PPIase)	Reduction of <i>Bps</i> -induced cytotoxicity on macrophages	Resensitizing infected macrophages to eliminate <i>N. meningitidis</i>	Resensitizing infected macrophages to eliminate <i>N. gonorrhoeae</i>
Side Chain Addition	↑↑	↑↑	↑↑	↑↑	↑/→ ***	→
<i>S,S</i> Configuration vs. <i>R,S</i> ; <i>S,R</i> ; and <i>R,R</i>	↑↑	↑↑	↑/→	↑*	↑/→ ***	↑/→ ***

Molecule Feature	BpMip inhibition (FPA & PPIase)	NEIS0004 inhibition (PPIase)	NmMip inhibition (PPIase)	Reduction of <i>Bps</i> -induced cytotoxicity on macrophages	Resensitizing infected macrophages to eliminate <i>N. meningitidis</i>	Resensitizing infected macrophages to eliminate <i>N. gonorrhoeae</i>
Pip.- amide instead of an ester	↑	→	→	↑	↓	↓
<i>p</i> -Fluorine substitution @ benzene	↑	→	↑	↑**	↓	↓
<i>N</i> -pyridine-oxide	↓	↓	↓	↑/→	↓	→

↑↑: strong enhancing effect, ↑: enhancing effect, ↑/→ enhancing to no effect, ↓ worsening effect. Bps: *Burkholderia pseudomallei*, pip: piperidic. \* Clear preference for an *S*-configuration at the piperidine ring, but not at the side chain; \*\*especially at the sulfonamide; \*\*\* not unambiguously.

Table 9 demonstrates that the rationally performed modifications to the Mip inhibitor scaffold have the most significant beneficial impact on BpMip and *B. pseudomallei*. This is not surprising since the first screening that inspired the structural changes was performed with BpMip. Also, the idea of an additional side chain originated from the co-crystal structures of BpMip. This observation strongly suggests that species-selective development may be worthwhile.

In addition, Table 9 reveals an apparent difference between the SAR results from the PPIase assays with NEIS0004 and NmMip and the cell-based assays against the two *Neisseria* species. Whether this is due to parameters such as membrane permeation, off-targets such as human FKBP, or protein binding will be an exciting research point in the future. The goal should be to ensure even better screening for *Neisseria*-selective Mip inhibitors so that the trends found are more reflected in the cell-based data.

### Confirmation of the FPA as Superior Screening Method for BpMip Inhibitors

For screening the side chain-bearing BpMip inhibitors, a fluorescence polarization assay (FPA) established together with Theresa Lohr was employed. The modified FP probe **29**, which also possesses a side chain, was used for this purpose. With a  $K_D$  of  $63 \pm 10$  nM, **29** can effectively compete with newly developed Mip inhibitors. The observed trends for BpMip in the FPA align well with those from the previously utilized protease-coupled PPIase assay, indicating a high degree of congruence.

This observation should not be underestimated, as it confirms the application of the FPA using a broader library than previously employed. The consistency of the test results favors the use of the newly developed FPA, as it is faster, more robust, and closer to physiological conditions (see subchapter III\_2). Temperature-dependent FP measurements revealed that the binding of the former FP probe to BpMip is enthalpy-driven, underscoring the importance of conducting measurements as close to physiological conditions as possible.

The formerly used protease-coupled PPIase assay had to be conducted at 4–8 °C to slow down the spontaneous, uncatalyzed *cis–trans* isomerization of the substrate, *N*-succinylated tetrapeptide-4-nitroanilides (pNA). Even under cooled conditions, typical halftime of the uncatalyzed *cis–trans* isomerization is only about 100 s.<sup>73, 154</sup> The newly developed FPA measures binding affinity to BpMip protein instead of enzymatic activity and therefore can be performed closer to physiological conditions at a temperature of 20–25 °C. The results of the developed FP probes are shown in Table 10. Additionally, suitability as an FP tracer is assessed, with a brief rationale for unsuitable cases.

Table 10. Results of the developed FP probes. The color indicates whether the FP probe is suitable for screening with the respective Mip protein. The FPA was conducted by T. Lohr; *yellow: not suitable; light green: suitable; green: highly suitable.*

FP Probe	Structural Features	$K_D$ (TcMip)	$K_D$ (LpMip)	$K_D$ (BpMip)	Conclusion
<b>30</b> (NJS106)	- no side chain inhibitor moiety - linker length: 10 atoms - fluorescein	8.1 ± 0.0 μM* (n=1)	7.37 ± 1.15 μM* (n=1)	1.20 ± 0.12 μM*** (n=3)	Works (only) for BpMip
<b>31</b> (NJS166)	- no side chain inhibitor moiety - linker length: 4 atoms - fluorescein	26.8 ± 6.7 μM* (n=3)	ND	3.8 ± 0.5 μM (n=2)	Linker too short; works only for BpMip, but worse than <b>30</b>
<b>32</b> (NJS205)	- side chain inhibitor moiety - linker length: 12 atoms - rhodamine derivative (TAMRA)	271 ± 148 nM** (n=3)	12.9 ± 5.8 μM** (n=1)	67 ± 52 nM** (n=2)	TAMRA fluorophore leads to unstable FP signal due to solubility problem
<b>29</b> (NJS254)	- side chain inhibitor moiety - linker length: 10 atoms - fluorescein	815 ± 8 nM (n=3)	1461 ± 5 nM (n=5)	63 ± 10 nM (n=3)	Works for TcMip, LpMip, and BpMip

\* upper plateau not reached due to weak binding \*\* DMSO/solubility problem

\*\*\* 2.0 ± 0.0 μM (0.5% DMSO-adjusted)

Thus, **29** is not only a suitable FP probe for BpMip, TcMip, and LpMip. In addition, due to its high binding affinity, it is also expected to be a valuable tracer for structurally related Mip proteins of other pathogens.

Further insights were gained from the methodology and results of the FP probe and FPA development process: First, our findings demonstrate that FP probes can be designed rationally. Here, analysis of crystal structures is indispensable to determine features such as suitable linker attachment points or linker length.

Second, it has been shown that binding affinity is not everything in FP probes. Non-obvious properties such as aggregation behavior or binding affinity in the presence of DMSO are also critical to consider.

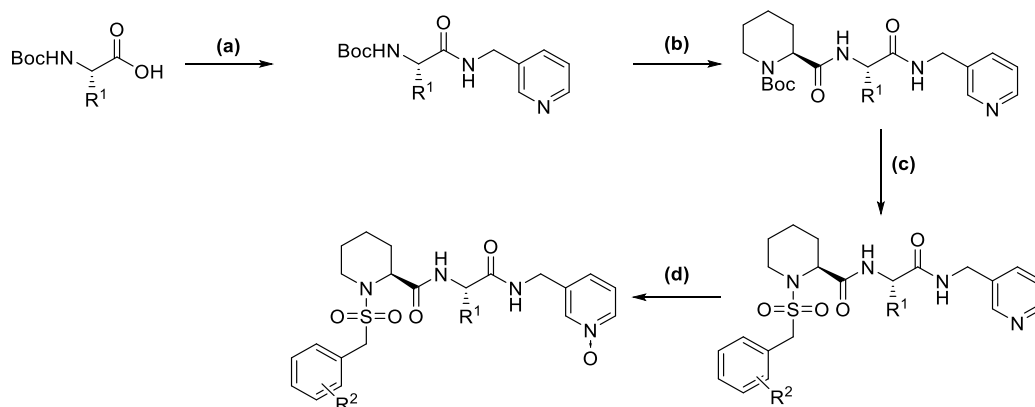
### **A Comparative Analysis of Synthetic Routes for Stereochemically Pure Pipecolic Amide Mip Inhibitors**

In this study, two distinct synthesis routes for stereochemically pure pipecolic amide Mip inhibitors were developed, featuring a series of amidation, protection/deprotection (either Boc or allyl), and sulfonamide preparation steps. The first approach utilized allyl protection groups (see subchapter III\_4.2), allowing for late-stage variation of the pyridine moiety. The second method made use of Boc-protected reagents, which allowed late variation of the sulfonamide moiety. A comprehensive and detailed analysis of the synthetic routes for Mip inhibitors is presented in subchapter III\_4.2. However, the primary focus of this discussion is to identify the most efficient, straightforward, and consequently, the recommended route. The Boc-protection group strategy, henceforth referred to as *Boc-approach*, clearly stands out in this regard. It is not only the shortest synthetic route but also obviates the need for allyl groups and Pd-catalyzed cleavages, rendering it more appealing from a toxicological standpoint, which is crucial for potential scale-up.

Moreover, this synthesis route allows for late-stage variation of the sulfonamide moiety. This is advantageous, as previous FPA results for BpMip indicate that the pyridine moiety has already reached an optimum. In contrast, the sulfonamide moiety still offers room for variation, potentially leading to increased affinity. However, it is important to note that this observation might not necessarily apply to other Mip proteins.

Briefly, the synthesis route starts with coupling a Boc-protected amino acid, which defines the

molecule's side chain, to 3-picolylamine using HBTU and DIPEA to form the amide. The Boc-protection group is then cleaved with TFA, followed by amide coupling to the Boc-protected *S*-pipercolic acid using HBTU and DIPEA. Subsequent TFA cleavage of the Boc-protection group enables *N*-sulfonamide formation with the corresponding sulfonyl chloride derivative, yielding the final Mip inhibitor. If an *N*-oxide is desired, the Mip inhibitor can be treated with *m*-CPBA in EtOAc.



**Scheme 11.** Synthesis scheme of the recommended pathway – the *Boc-approach* – for stereochemically pure *S*-pipercolic amide derivatives that allows a late variation of the sulfonamide moiety. R<sup>1</sup>: aliphatic or aromatic side chains, R<sup>2</sup>: substituents, such as F, Cl, NO<sub>2</sub>, etc., are conceivable. **Reagents and conditions:** (a) 3-picolylamine, HBTU, DIPEA, DCM, 0°C → rt; (b) i) TFA, rt; ii) *N*-Boc-(*S*)-pipercolic acid, HBTU, DIPEA, DCM, 0°C → rt; (c) i) TFA, rt; ii) phenylmethanesulfonyl chloride or an analog, NEt<sub>3</sub>, DCM, rt; (d) *m*-CPBA, EtOAc, rt.

Notably, the synthesis steps employed in the *Boc-approach* are straightforward, generally taking no more than a day to perform and featuring simple workup procedures. Purifying intermediates by column or flash chromatography is recommended after amide/ester/sulfonamide coupling reactions. In contrast, primary or secondary amine intermediates obtained from the deprotection steps are more challenging to purify using column chromatography. However, as Boc deprotection usually proceeds without by-products, purification by extraction is sufficient at this point.

It has been observed that only the Boc-protected intermediates and final stages exhibit long-term storage capabilities. On the other hand, primary/secondary amine intermediates tend to react at room temperature, likely due to the nucleophilicity of the amino groups. Consequently, it is advised to either store these intermediates in the dark at -18°C or to proceed with further reactions within a few days.

### Stereochemistry and Chiral HPLC Analysis

The basic hydrolysis used in the preparation of racemic (*R/S*)-1 (benzylsulfonyl)piperidine-2-carboxylate, previously used to prepare diastereomeric mixtures of Mip inhibitors, was omitted, as it was known to cause racemization.

Additionally, care was taken during synthesis and workup to avoid too basic conditions ( $\text{pH} > 9$ ) once the pipercolic acid moiety was introduced. The use of auxiliary bases such as DIPEA,  $\text{NEt}_3$ , NMM, and  $\text{NaHCO}_3$  proved to be well tolerated. To ensure the correct stereochemistry, pure isomers were used as starting materials, and synthetic procedures known for retaining stereochemistry were employed. From the introduction of the second stereo center, differentiation of diastereomers via  $^1\text{H}$  NMR became possible and was conducted. The absence of diastereomers in the prepared pure stereoisomers in NMR, as evidenced by a single data set, also implies the absence of enantiomers due to potential racemization. Moreover, a chiral, isocratic HPLC method was developed to resolve all four stereo isomers, utilizing a chiral *Amylose I* column (see III\_3.5). Using this chiral HPLC method, products from each developed synthetic route were tested. In each case, a stereochemical purity greater than 95% was obtained. For future synthesis, it is recommended to check the stereochemistry by chiral HPLC if an unusual doubling of signals in the NMR or an unexpected double-peak in the LC-MS chromatogram is observed.

### Preparing for *in-vivo* Testing

The fluorine substitution on the benzene rings of the molecules appears to have a good effect on the binding to BpMip, judging from the results in the FPA. However, fluorination can also have a negative impact. Thus, fluorination seems to increase cytotoxicity (cf. **S,S-21g** and **S,S-21d**). Interestingly, this effect can be overcome by oxidation to the *N*-oxide.

However, the lipophilicity of the compounds also increases slightly upon fluorination (estimate:  $\text{ClogP} = 3.57$  for **S,S-21g** (*two fluorine substituents*) and  $3.28$  for **S,S-21** (*no fluorine substituent*)). Furthermore, the addition of an aromatic side chain by itself increases lipophilicity.

Firstly, this heightened lipophilicity results in reduced water solubility, exemplified by **S,S-21g**'s low solubility of only  $13.5 \pm 2.2 \mu\text{g/mL}$ . However, this effect could be somewhat improved by incorporating an aliphatic side chain (e.g., **S,S-21d**) or via *N*-oxidation.



### Plasma Protein Binding (PPB)

A higher ClogP value also suggests an increased likelihood of elevated plasma protein binding (PPB) to proteins such as albumin, alpha1-acid glycoprotein, and lipoproteins. Miriam Volpp used a continuous ultrafiltration method to measure binding of **41** (*SF235*) to human serum albumin (HSA). As a result, protein binding was relatively high at  $79.2 \pm 3.2\%$ , with two binding sites at albumin.<sup>155, 156</sup> Considering the generally higher ClogP value, there is a risk that compounds with side chains may exhibit even higher protein binding.

Plasma protein binding (PPB) data is frequently used in drug discovery to prioritize compounds for *in vivo* studies. The extent of protein binding is important to know because it is only the unbound fraction of a drug that is able to bind to an enzyme and induce a pharmacological effect.<sup>157</sup> Knowledge about PPB aids in predicting drug-drug interactions, estimating therapeutic indices, and developing pharmacokinetic/pharmacodynamic relationships<sup>158</sup>

However, the debate on the impact of PPB on *in vivo* efficacy and its relevance in drug development is still ongoing.<sup>158-160</sup> On one hand, risks exist, such as if binding to plasma proteins is too high or irreversible, unbound drug concentrations may not reach therapeutic levels.<sup>160</sup> On the other hand, there can also be advantages of moderate PPB. For example, PPB may also improve antimicrobial efficacy when plasma proteins act as drug reservoirs.<sup>160</sup> This might result in drug concentrations remaining above the bacterial minimum inhibitory concentration for longer.<sup>160</sup>

According to Di *et al.*, PPB alone has limited relevance to *in vivo* efficacy, and structural modifications to alter PPB are generally not recommended<sup>158</sup>. Smith *et al.* argue that the critical factor is the unbound drug concentration at the site of action.<sup>161</sup> Enhancing factors such as solubility, membrane permeation, metabolic stability, and mitigating efflux (e.g., by P-glycoprotein 1) can contribute to increasing this concentration.<sup>161</sup> Consequently, in addition to PPB determination, which can be achieved, e.g., by ultrafiltration<sup>156, 157</sup>, or equilibrium dialysis, the other parameters mentioned by Smith *et al.* should also be optimized.<sup>160, 161</sup>

Taken together, while PPB determination will be an important step toward *in vivo* experiments, it should not be the primary directive for structural modifications.

### Membrane Permeability

Of the parameters mentioned by Smith *et al.*,<sup>161</sup> solubility and metabolism of the Mip inhibitors have been investigated and are the focus of further research. Investigations of metabolism using liver microsomes and mass spectrometric analysis were performed in collaboration with Theresa Lohr. These studies are currently being continued, and will consequently be reported in the respective PhD thesis.<sup>162</sup>

The study of membrane permeation and efflux, such as through P-glycoprotein 1, remains unexplored to date. During the drug design process, membrane permeability is a crucial characteristic to evaluate, especially for small molecules targeting intracellular components. Their effectiveness largely relies on their capacity to traverse the membrane.

It would be of interest to study the cell permeability of charged molecules that normally require active transporters, such as the *N*-oxide derivatives.<sup>163</sup> In this regard, it might initially be sufficient to apply molecular dynamics (MD) computational modeling as reported by Bennion *et al.* or Hoffmann *et al.*<sup>164, 165</sup> Investigating these mechanisms may provide valuable insights and could potentially facilitate the progression to *in vivo* testing.

### Broad Spectrum Screening

A further step will be the investigation of the side chain-bearing Mip inhibitors against the related TcMip and LpMip protein. These investigations are still ongoing and part of a more comprehensive screening by Theresa Lohr and Nicholas Harmer.<sup>162</sup> Preliminary results show that the order of binding affinity decreases in the following order: BpMip > TcMip > LpMip. Interestingly, this order is also that of the protein masses, with LpMip as the heaviest of the three, with an increasing *N*-terminal dimerization domain from BpMip (no dimerization domain) toward LpMip. With the help of side chain-bearing Mip inhibitors, Ute Hellmich and colleagues are investigating whether this difference in structure leads to different protein dynamics, which in turn affects binding affinity.

### Testing the Anti-Virulence Hypothesis

Lastly, it is of great interest to test the hypothesis that targeting the virulence factor Mip reduces the risk of resistance development.<sup>166</sup> As anti-virulence drugs interact with non-essential targets, it is generally assumed that they do not induce resistance; however, this has been questioned.<sup>167, 168</sup> Experimental data have indicated the emergence of resistance, demonstrating the complex evolution and selection of resistance by some anti-virulence drugs.<sup>169</sup>

Additionally, given that anti-virulence therapeutics focus on nonessential targets, it is probable that they will be employed in combination with antibiotics to effectively eliminate the targeted pathogen.<sup>168, 170</sup> Although such investigations have not yet been conducted with Mip inhibitors, undertaking this step is imperative. It can be anticipated that only a combination therapy approach will yield the necessary antimicrobial efficacy to ensure success in clinical trials.<sup>168</sup>

### Concluding Remarks

In light of the increasing prevalence of antibiotic resistance, the World Health Organization and a number of researchers have recently underscored the imminent threat of an upcoming *post-antibiotic era*.<sup>2, 171</sup> It is my hope that the findings presented in this dissertation contribute to our collective efforts in preventing this dystopian scenario and furthering our understanding of how to effectively address this pressing global challenge.

## V Summary

In the face of increasing antibiotic resistance, the search for innovative anti-infectives is becoming increasingly urgent and requires discovering new modes of action. One promising approach is that of anti-virulence, which aims to target bacterial proteins that play a critical role in disease causation and progression without interfering with bacterial growth, thus probably reducing the selection pressure for resistance.<sup>172, 173</sup>

This dissertation focuses on the antivirulence factor “macrophage infectivity potentiator” protein (Mip) that belongs to the FK506 binding proteins (FKBPs) and the immunophilin family of peptidyl-prolyl *cis-trans* isomerase (PPIase) enzymes. These microbial enzymes have been shown to be essential for virulence in a variety of pathogenic bacteria and parasites. Deletion of the respective genes resulted in decreased bacterial survival of multiple pathogens, including *Legionella pneumophila* and *Burkholderia pseudomallei* in animal infection models.<sup>150, 151</sup> In the past decade, small molecule inhibitors with a pipercolic acid backbone derived from rapamycin, lacking the moiety responsible for the immunosuppressive effect, have been developed, inhibiting Mip and showing promising activity in fighting microbial infections *in vitro*.<sup>119, 152</sup>

Within a wider project, three central topics in the target-based drug discovery (TDD) process for Mip inhibitors are addressed. (1) Development of a fluorescent probe allowing the screening of potential Mip inhibitors in a fluorescence polarization assay (FPA), (2) designing novel Mip inhibitors bearing a side chain targeting a broad spectrum of pathogens, and (3) gaining insight into the metabolism of Mip inhibitors and identifying active metabolites to improve understanding of the pharmacokinetics.

A side project focused on biotinylation of antileishmanial compounds derived from pulverized rhizomes of *Valeriana wallichii* known to have *in vitro* antileishmanial activity against *Leishmania major* promastigotes.<sup>74, 78</sup> Hereby, target identification of this previous phenotypic drug discovery (PDD) process, was to be enabled. Thus, a more targeted, structure-based development of the active compounds was to be enabled. To this end, three tracer molecules were successfully synthesized, paving the way for future target pull-down experiments.

In pursuit of a deeper understanding of Mip proteins and the immunophilin superfamily, a comprehensive review of existing research in this field was written.<sup>21</sup> This effort aimed to

consolidate knowledge about Mip proteins and lay a solid foundation for future investigations into this promising broad-spectrum target family.

The first major research focus was to develop a suitable fluorescent probe for the Mip protein of *Burkholderia pseudomallei* (BpMip), the causative agent of melioidosis. Thereby, a robust screening of new Mip inhibitors in a fluorescence polarization assay (FPA) was to be achieved. This was necessary since the previously used protease-coupled PPIase assay suffered from some drawbacks, such as the need for low, non-physiological temperatures (4–8°C) and a lack of robustness.<sup>73</sup> Thus, a fluorescein-labeled probe **30** (*NJS106*) was designed and synthesized, derived from previous Mip inhibitors (cf. Figure 22). As a result, **30** enabled performing an FPA with BpMip. Temperature dependence analysis revealed BpMip ligand binding to be mainly controlled by enthalpic effects, supporting the choice of an assay performed closer to physiological conditions.<sup>48</sup>

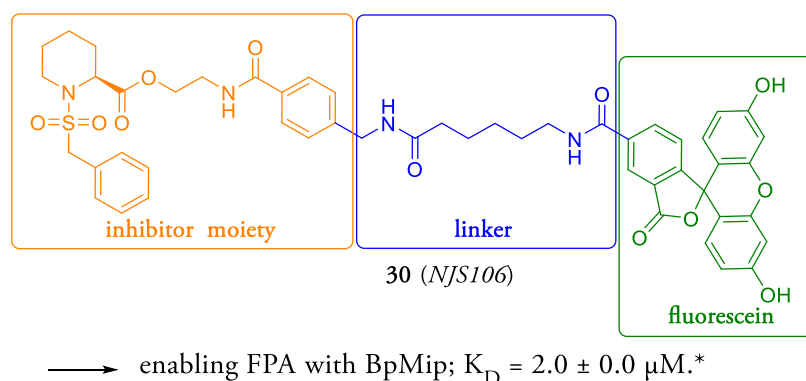
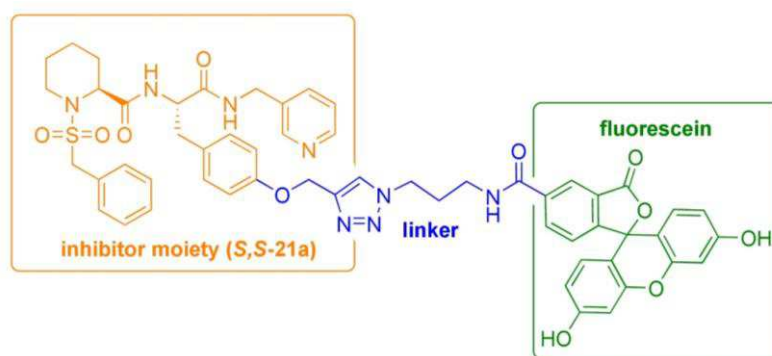


Figure 22. Chemical structure of the developed FP probe **30** (*NJS106*), suitable for screening BpMip inhibitors.  
\*0.5% DMSO-adjusted value

Development continued to find adapted FP probes for the related Mip proteins of the parasite *Trypanosoma cruzi* (TcMip) and the Gram-negative bacterium *Legionella pneumophila* (LpMip). Reducing the linker length between the inhibitor moiety and the fluorophore adversely affected binding. In contrast, the addition of a side chain to the inhibitor moiety ultimately led to the synthesis of **29**, an effective FP probe for the screening of small molecule inhibitors of BpMip, TcMip, and LpMip (cf. Figure 24).

Thus, not only is **29** a suitable FP probe for the aforementioned Mip proteins, but it is also anticipated to be a useful tracer for related Mip proteins of other pathogens as well, such as those of *N. meningitidis*, *N. gonorrhoeae*, and others, representing an exciting task for further research.

29 (*NJS254*)

→ enabling FPA with: BpMip,  $K_D = 63 \pm 10$  nM  
 LpMip,  $K_D = 1461 \pm 5$  nM  
 TcMip,  $K_D = 815 \pm 8$  nM

Figure 23. Chemical structure of the developed FP probe **29**, suitable for a wide range of pathogens' Mip proteins: BpMip, LpMip, and TcMip.

In the second research focus, the Mip inhibitor backbone was modified to enhance its affinity and enzymatic inhibition of the related Mip proteins of *B. pseudomallei* and *N. meningitidis*, the latter being the causative agent of meningitis. Prior analysis of BpMip-inhibitor complex crystal structures indicated that the inhibitors can adopt two different binding poses. By introducing a side chain to the linker connecting the piperolic moiety and the pyridine, it was expected that a single molecule could accommodate both binding modes. This included testing aliphatic and aromatic side chains, piperolic ester and amide derivatives, as well as several variants of stereo isomers.

The newly developed, side chain-bearing Mip inhibitors demonstrated substantially improved outcomes not only in the FPA and protease-coupled enzyme assay but also in the cell-based assays. Hence, they helped to reduce *B. pseudomallei*-induced cytotoxicity in infected macrophages by up to 70% and sensitized infected macrophages to eliminate *N. meningitidis* and *N. gonorrhoeae* by up to 87% and 80%, respectively.

While no individual inhibitor exhibited exceptional activity against all pathogens, certain trade-offs in activity enabled the identification of structurally analogous broad-spectrum Mip inhibitors, such as **S,S-21a**, **S,S-21i**, and **S,S-21h** (cf. Figure 24).

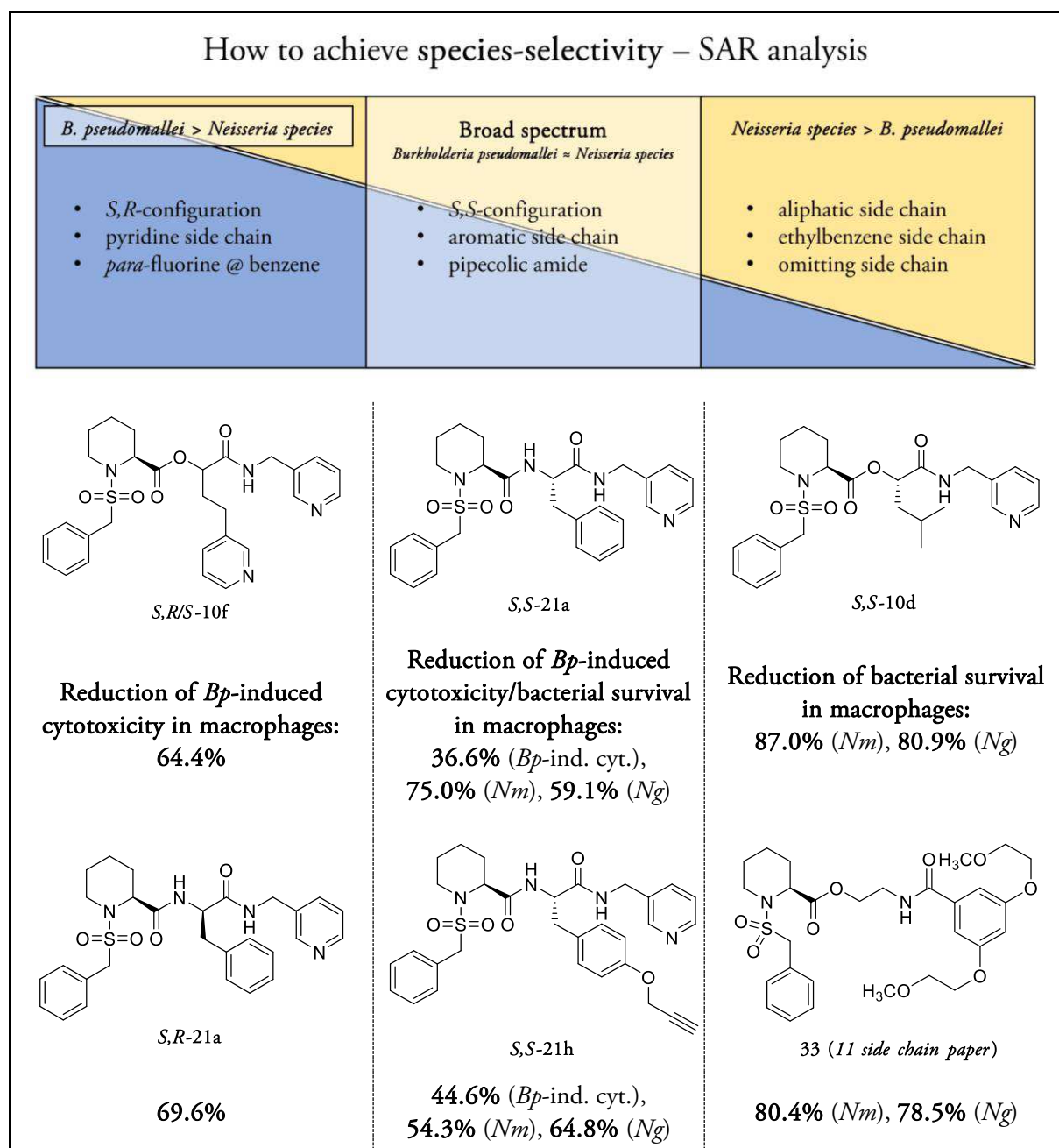


Figure 24. SAR analysis of how to achieve species-selectivity for the tested Mip inhibitors regarding *B. pseudomallei* (*Bp*), *N. meningitidis* (*Nm*), and *N. gonorrhoeae* (*Ng*) with exemplary representatives.

These inhibitors share an *S,S*-configuration, an aromatic side chain, and a pipercolic amide. Selectivity for *B. pseudomallei* could be enhanced by employing an *R*-configuration at the side chain (*S,R*-21a), incorporating a second pyridine (*S,R/S*-10f), or introducing a *para*-fluorine to the benzene ring of the sulfonamide moiety. To improve selectivity for *Neisseria* species over *B. pseudomallei*, an aliphatic side chain (e.g., *S,S*-10d) or an ethylbenzene moiety (*S,S*-10e) could be added to a pipercolic ester inhibitor, or alternatively, the side chain could be omitted (e.g., 33 (11, SF354, cf. Figure 24).

As found by Seufert *et al.*, an *R*-configuration at the pipercolic moiety showed a strong negative effect on activity.<sup>152</sup> While the preference for an *S,S*-configuration of inhibitors for the pure Mip protein was clear, this was not always the case in the cell-based assays, potentially indicating the presence of off-target effects.

The results obtained here were in agreement with Iwasaki *et al.*, who demonstrated the high similarity of the formed active sites of BpMip and NmMip by homology modeling.<sup>114</sup> However, minor changes, such as the mutation of phenylalanine (Phe53) in BpMip to valine in NmMip, resulted in the existence of different docking poses with comparable binding energies in the Iwasaki-study<sup>114</sup> and possibly led to the observed species-dependent SAR. Finally, new lead compounds were identified, considering the results in the cell-based assay, as well as properties such as solubility and cytotoxicity: **S,S-22g** for BpMip and *B. pseudomallei*, and **S,S-10d** for *N. meningitidis* and *N. gonorrhoeae* (see Figure 25).

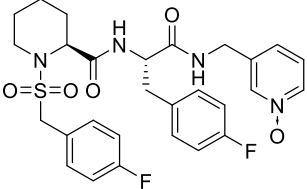
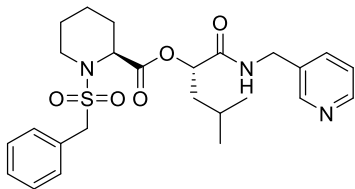
<p align="center"><b>BpMip</b> <i>B. pseudomallei</i></p>	<p align="center"><b>NmMip, NEIS0004</b> <i>N. meningitidis</i> and <i>N. gonorrhoeae</i></p>
 <p align="center"><b>S,S-22g</b></p> <p><i>Reduction of Bp-induced cytotoxicity in macrophages:</i> <b>48.3%</b></p> <p><i>Remaining PPIase act. @400 nM:</i> <b>40.9 ± 2.5%</b></p> <p><i>Solubility:</i> <b>1494.0 ± 16.0 µg/mL</b></p> <p><i>Cytotoxicity:</i> <b>IC<sub>50</sub> &gt; 100 µM (NIH3T3; HEK293T)</b></p>	 <p align="center"><b>S,S-10d</b></p> <p><i>Reduction of bacterial load in macrophages:</i> <b>87.0% (Nm), 80.9% (Ng)</b></p> <p><i>Remaining PPIase act. @400 nM:</i> <b>35.6 ± 3.9% (NmMip); 3.8 ± 0.4% (NEIS0004)</b></p> <p><i>Solubility:</i> <b>97.0 ± 4.6 µg/mL*</b></p> <p><i>Cytotoxicity:</i> <b>IC<sub>50</sub> &gt; 100 µM (NIH3T3; HEK293T)</b></p>

Figure 25. Chemical structures of the new lead compounds **S,S-22g** and **S,S-10d**. Results in the cell-based assay, as well as properties such as solubility and cytotoxicity, were considered. \**S,R/S*-10d.

The third research focus addressed the metabolic transformation of Mip inhibitors in human liver microsomes, aiming to identify active metabolites and enhance the metabolic stability of the compounds. By means of mass spectrometry methods, ester cleavages, hydroxylations, *N*-oxide formation, and to a lesser extent, amide cleavages were found to be of significant importance. These findings prompted the modification of the inhibitor structures through the exchange of ester groups



with amide groups, the introduction of *para*-fluorine substituents at the benzene rings (cf. **S,S-21g**), and *N*-oxidation of the pyridine moiety.

With regard to the *N*-oxides, FPA and enzymatic testing revealed only a slightly reduced affinity for the Mip proteins of *B. pseudomallei* and *Neisseria* species. *In vitro* cell-based testing of the *N*-oxides showed improved efficacy against *B. pseudomallei* (cf. Figure 25), indicating that active metabolites likely play a crucial role *in vivo*.

In summary, this dissertation has made meaningful contributions to the development of Mip inhibitors as potential anti-infective agents. It provides insights into the design, synthesis, and optimization of these compounds while addressing challenges in screening, metabolism, and drug-likeness. Future research should focus on exploring cell permeability, off-target effects, *in vivo* efficacy, and resistance development to ensure the successful translation of these promising Mip inhibitors into effective therapeutic strategies against a broad spectrum of infectious diseases.

## VI Zusammenfassung

Angesichts zunehmender Antibiotikaresistenzen gewinnt die Suche nach innovativen Antiinfektiva immer mehr an Bedeutung und erfordert die Erforschung neuer Wirkmechanismen. Ein vielversprechender Ansatz ist der der Anti-Virulenz. Dieser zielt darauf ab, bakterielle Proteine zu adressieren, die eine entscheidende Rolle bei Krankheitsverursachung und Krankheitsverlauf spielen, ohne dabei das Bakterienwachstum zu beeinträchtigen. Somit wird höchstwahrscheinlich der Selektionsdruck für Resistenzen verringert.<sup>172, 173</sup>

Diese Dissertation konzentriert sich auf das "Macrophage infectivity potentiator"-Protein (Mip), einen Antivirulenzfaktor der zu den FK506-bindenden Proteinen (FKBPs) und der Immunophilin-Familie der Peptidyl-Prolyl-*cis-trans*-Isomerase (PPIase) Enzyme gehört. Diese mikrobiellen Enzyme sind erwiesenermaßen für die Virulenz einer Vielzahl von pathogenen Bakterien und Parasiten wichtig. Die Deletion der entsprechenden Gene führte in Tierinfektionsmodellen zu einem verringerten bakteriellen Überleben mehrerer Krankheitserreger, darunter *Legionella pneumophila* und *Burkholderia pseudomallei*.<sup>150, 151</sup> In den letzten zehn Jahren wurden niedermolekulare Inhibitoren mit einem von Rapamycin abgeleiteten Pipecolinsäure-Grundgerüst entwickelt, bei denen der, für die immunsuppressive Wirkung verantwortliche, Teil fehlt. Diese hemmen Mip und zeigen eine vielversprechende Aktivität bei der Bekämpfung mikrobieller Infektionen *in vitro*.<sup>119, 152</sup>

Insgesamt wurden in dieser Arbeit drei zentrale Themen im Target-basierten Wirkstofffindungsprozess (TDD) für Mip-Inhibitoren behandelt. (1) Die Entwicklung einer fluoreszierenden Sonde, die das Screening potenzieller Mip-Inhibitoren in einem Fluoreszenzpolarisationsassay (FPA) ermöglicht, (2) die Entwicklung neuartiger Mip-Inhibitoren mit einer Seitenkette, die auf ein breites Spektrum von Krankheitserregern abzielt, und (3) die Untersuchung der Metabolisierung der Mip-Inhibitoren und die Identifizierung aktiver Metabolite, um die Pharmakokinetik dieser Substanzklasse besser zu verstehen.

Ein Nebenprojekt konzentrierte sich auf die Biotinylierung von antileishmanialen Wirkstoffen, die aus pulverisierten Rhizomen von *Valeriana wallichii* gewonnen wurden und von denen bekannt ist, dass sie *in vitro* eine antileishmaniale Wirkung gegen *Leishmania major* Promastigoten besitzen.

<sup>74, 78</sup> Hierdurch sollte die Target-Identifizierung dieses früheren Phänotyp-basierten Wirkstofffindungsprozesses (PDD) ermöglicht werden. So sollte eine gezieltere, strukturbasierte

Entwicklung der Wirkstoffe ermöglicht werden. Zu diesem Zweck wurden drei Tracer-Moleküle erfolgreich synthetisiert, die den Weg für künftige Target-Pull-Down-Experimente ebnen.

Um ein tieferes Verständnis der Mip-Proteine und der Immunophilin-Superfamilie zu erlangen, wurde ein umfassender Überblick über die bisherige Forschung auf diesem Gebiet verfasst.<sup>21</sup> Ziel dieser Bemühungen war es, das Wissen über Mip-Proteine zu bündeln und eine solide Grundlage für künftige Untersuchungen dieser vielversprechenden Target-Familie mit breitem Wirkungsspektrum zu schaffen.

Den ersten Forschungsschwerpunkt stellte die Entwicklung einer geeigneten Fluoreszenzsonde für das Mip-Protein von *Burkholderia pseudomallei* (BpMip) dar, dem Erreger der Melioidose. Hierdurch sollte ein robustes Screening neuer Mip-Inhibitoren in einem Fluoreszenzpolarisationsassay (FPA) erreicht werden. Dies war notwendig, da der bisher verwendete proteasegekoppelte PPIase-Assay einige Nachteile aufwies, wie z. B. die Notwendigkeit niedriger, unphysiologischer Temperaturen (4-8°C) und einen Mangel an Robustheit.<sup>73</sup> Es wurde eine Fluorescein-markierte Sonde **30** (NJS106) entwickelt und synthetisiert, die von früheren Mip-Inhibitoren abgeleitet wurde (vgl. Figure 26). Sonde **30** ermöglichte das Screening von BpMip Inhibitoren mittels FPA. Die Analyse der Temperaturabhängigkeit ergab, dass die Bindung des BpMip-Liganden hauptsächlich durch enthalpische Effekte bestimmt wird, was für die Wahl eines Tests spricht, der näher an physiologischen Bedingungen durchgeführt wird.<sup>48</sup>

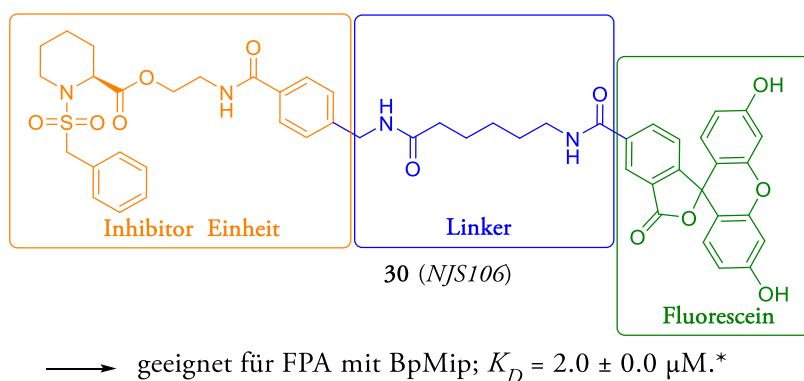
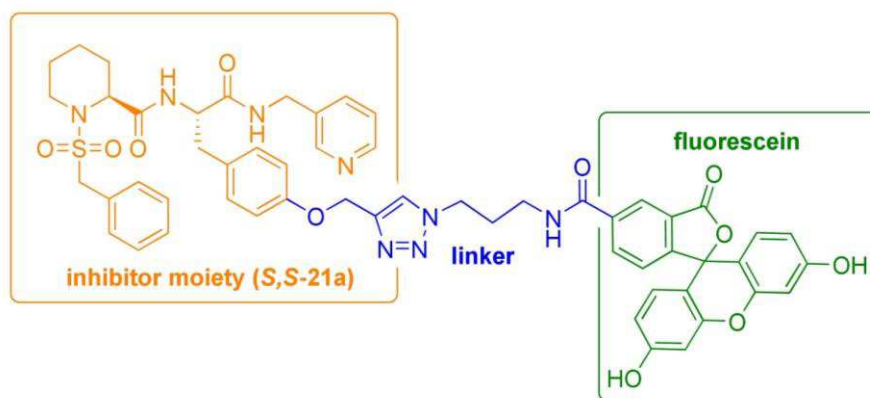


Figure 26. Chemische Struktur der entwickelten FP-Sonde **30** (NJS106), die für das Screening von BpMip-Inhibitoren geeignet ist. \*0.5% DMSO-angepasster Wert.

Die Entwicklung wurde fortgesetzt, um angepasste FP-Sonden für die verwandten Mip-Proteine des Parasiten *Trypanosoma cruzi* (TcMip) und des gramnegativen Bakteriums *Legionella pneumophila* (LpMip) zu finden. Eine Verkürzung der Linkerlänge zwischen dem Inhibitorteil und

dem Fluorophor beeinträchtigte die Bindung zum Target. Im Gegensatz dazu führte das Anbringen einer Seitenkette an den Inhibitorteil schließlich zur Synthese von **29**, einer leistungsfähigen FP-Sonde für das Screening von niedermolekularen Inhibitoren von BpMip, TcMip und LpMip.

Darüber hinaus ist **29** nicht nur eine geeignete FP-Sonde für die oben genannten Mip-Proteine, sondern dürfte auch ein nützlicher Tracer für verwandte Mip-Proteine anderer Krankheitserreger sein, wie z. B. die von *N. meningitidis*, *N. gonorrhoeae* und anderen.



**29** (NJS254)

→ geeignet für FPA mit: BpMip,  $K_D = 63 \pm 10$  nM

LpMip,  $K_D = 1461 \pm 5$  nM

TcMip,  $K_D = 815 \pm 8$  nM

Figure 27. Strukturformel der entwickelten FP-Sonde **29**, die für eine Vielzahl von Mip-Proteinen von Krankheitserregern geeignet ist: BpMip, LpMip und TcMip.

Im zweiten Forschungsschwerpunkt wurde das Mip-Inhibitor-Grundgerüst modifiziert, um die Affinität und die enzymatische Hemmung der verwandten Mip-Proteine von *B. pseudomallei* und *N. meningitidis*, dem Erreger der Meningitis, zu verbessern. Vorherige Analysen der Kristallstrukturen von BpMip-Inhibitorkomplexen zeigten, dass die Inhibitoren zwei verschiedene Bindungspositionen einnehmen können. Es wurde erwartet, dass durch die Einführung einer Seitenkette am Linker, welcher die Pipecolin-Einheit und das Pyridin verbindet, ein einziges Molekül beide Bindungspositionen annehmen könnte. Zu diesem Zweck wurden aliphatische und aromatische Seitenketten, Pipecolinsäureester- und -amid-Derivate sowie mehrere Varianten von Stereo-Isomeren getestet.

Die neu entwickelten Mip-Inhibitoren mit Seitenkette zeigten nicht nur im FPA- und im Proteasegekoppelten Enzym-Assay, sondern auch in den zellbasierten Assays deutlich verbesserte

Ergebnisse. So trugen diese Moleküle dazu bei, die von *B. pseudomallei* ausgelöste Zytotoxizität in infizierten Makrophagen um bis zu 70% zu verringern. Darüber hinaus half die Behandlung mit Mip Inhibitoren, infizierte Makrophagen dafür zu sensibilisieren, *N. meningitidis* und *N. gonorrhoeae* bis zu 87 % bzw. 80 % zu eliminieren.

Auch wenn kein einzelner Inhibitor eine herausragende Aktivität gegen sämtliche Krankheitserreger aufwies, ermöglichten bestimmte Kompromisse hinsichtlich der Aktivität die Identifizierung strukturell ähnlicher Mip-Inhibitoren mit breitem Wirkungsspektrum, wie *S,S*-21a, *S,S*-21i und *S,S*-21h (vgl. Figure 27).

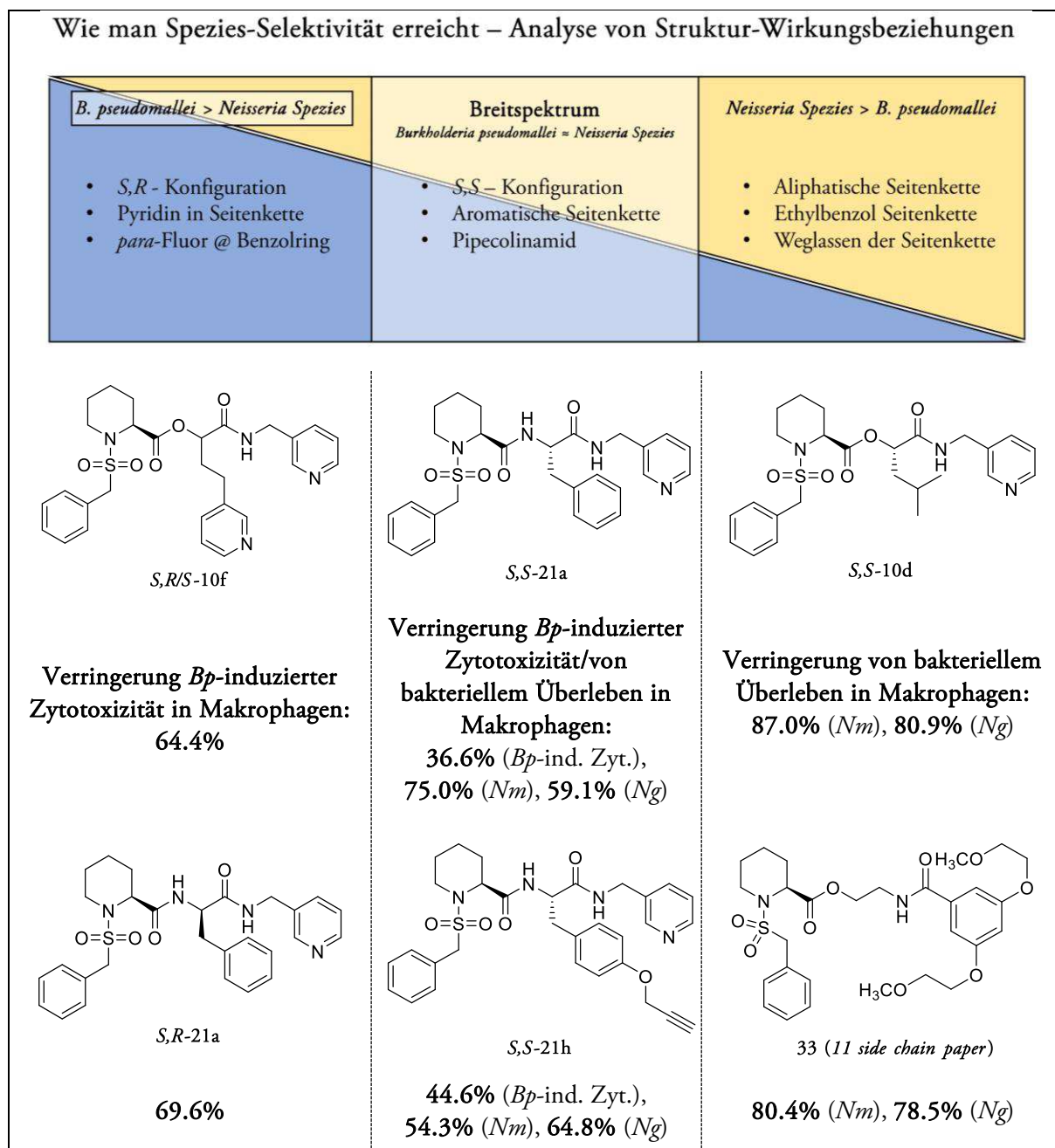


Figure 28. SAR-Analyse zum Erreichen von Spezies-Selektivität für die getesteten Mip-Inhibitoren hinsichtlich *B. pseudomallei* (*Bp*), *N. meningitidis* (*Nm*) und *N. gonorrhoeae* (*Ng*) mit exemplarischen Inhibitoren.

Diese Inhibitoren zeichnen sich durch eine *S,S*-Konfiguration, eine aromatische Seitenkette und ein Pipecolinsäureamid aus. Die Selektivität für *B. pseudomallei* konnte durch eine *R*-Konfiguration an der Seitenkette (*S,R*-21a), den Einbau eines zweiten Pyridins (*S,R/S*-10f) oder eine *para*-Fluor-Substitution am Benzolring der Sulfonamideinheit erhöht werden. Um die Selektivität für *Neisseria*-Spezies gegenüber *B. pseudomallei* zu verbessern, kann einem Pipecolinsäureester-Inhibitor eine aliphatische Seitenkette (z. B. *S,S*-10d) oder eine Ethylbenzolgruppe (*S,S*-10e) hinzugefügt oder aber auch die Seitenkette komplett weggelassen werden (z. B. **33** (11, SF354, vgl. Figure 28)).

Wie von Seufert *et al.* festgestellt, wirkte sich eine *R*-Konfiguration an der Pipecolin-Einheit stark negativ auf die Aktivität aus.<sup>152</sup> Während die Präferenz für eine *S,S*-Konfiguration der Inhibitoren für das reine Mip-Protein eindeutig war, war dies bei den zellbasierten Assays nicht immer der Fall, was möglicherweise auf Off-Target-Effekte hinweist.

Die hier erzielten Ergebnisse stimmten mit denen von Iwasaki *et al.* überein, welche die große Ähnlichkeit der gebildeten Bindetaschen von BpMip und NmMip durch Homologiemodellierung nachwiesen.<sup>114</sup> Geringfügige Unterschiede, wie die Änderung von Phenylalanin (Phe53) in BpMip zu Valin in NmMip, führten in der Iwasaki-Studie zu unterschiedlichen Docking-Posen mit ähnlichen Bindungsenergien<sup>114</sup> und hierdurch möglicherweise zu der beobachteten speziesabhängigen SAR hier. Schließlich wurden unter Berücksichtigung der Ergebnisse im zellbasierten Assay sowie der Eigenschaften wie Löslichkeit und Zytotoxizität neue Leitverbindungen identifiziert: *S,S*-22g für BpMip und *B. pseudomallei* und *S,S*-10d für *N. meningitidis* und *N. gonorrhoeae* (siehe Figure 29).

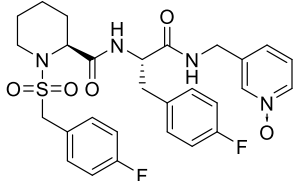
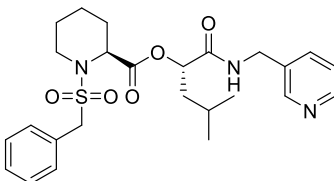
BpMip <i>B. pseudomallei</i>	NmMip, NEIS0004 <i>N. meningitidis</i> und <i>N. gonorrhoeae</i>
 <p style="text-align: center;">S,S-22g</p>	 <p style="text-align: center;">S,S-10d</p>
<p style="text-align: center;"><i>Reduktion der Bp-induzierten Zytotoxizität in Makrophagen: 48.3%</i></p> <p style="text-align: center;"><i>Verbleibende PPIase Aktivität @ 400 nM:</i> <b>40.9 ± 2.5%</b></p> <p style="text-align: center;"><i>Löslichkeit: 1494.0 ± 16.0 µg/mL</i></p> <p><i>Zytotoxizität: IC<sub>50</sub> &gt; 100 µM (NIH3T3; HEK293T)</i></p>	<p style="text-align: center;"><i>Reduktion der Bakterienlast in Makrophagen:</i> <b>87.0% (Nm), 80.9% (Ng)</b></p> <p style="text-align: center;"><i>Verbleibende PPIase Aktivität @ 400 nM:</i> <b>35.6 ± 3.9% (NmMip); 3.8 ± 0.4% (NEIS0004)</b></p> <p style="text-align: center;"><i>Löslichkeit: 97.0 ± 4.6 µg/mL*</i></p> <p><i>Zytotoxizität: IC<sub>50</sub> &gt; 100 µM (NIH3T3; HEK293T)</i></p>

Figure 29. Chemische Strukturen der neuen Leitverbindungen *S,S*-22g und *S,S*-10d. Ergebnisse im zellbasierten Assay sowie Eigenschaften wie Löslichkeit und Zytotoxizität wurden berücksichtigt. \*S,R/S-10d.

Der dritte Forschungsschwerpunkt befasste sich mit der metabolischen Transformation von Mip-Inhibitoren in menschlichen Lebermikrosomen mit dem Ziel, aktive Metabolite zu identifizieren und die metabolische Stabilität der Verbindungen zu erhöhen. Mithilfe von massenspektrometrischen Methoden wurde festgestellt, dass Esterspaltungen, Hydroxylierungen, *N*-Oxidbildung und in geringerem Maße auch Amidspaltungen von entscheidender Bedeutung sind. Diese Erkenntnisse führten dazu, dass die Inhibitorstrukturen durch den Austausch von Ester- gegen Amidgruppen, die Einführung von *para*-Fluoro-Substituenten an den Benzolringen (vgl. **S,S-21g**) und *N*-Oxidation des Pyridinrestes verändert wurden.

Hinsichtlich der *N*-Oxide ergaben FPA- und Enzymtestungen nur eine leicht verringerte Affinität zu den Mip-Proteinen von *B. pseudomallei* und den *Neisseria*-Spezies. *In-vitro*-Zelltests der *N*-Oxide zeigten zudem eine verbesserte Wirksamkeit gegen *B. pseudomallei* (siehe Figure 29), was nahelegt, dass die aktiven Metabolite möglicherweise eine entscheidende Rolle *in vivo* spielen.

Zusammenfassend lässt sich sagen, dass diese Dissertation einen wichtigen Beitrag zur Entwicklung von Mip-Inhibitoren als potenzielle Antiinfektiva geleistet hat. Sie bietet Einblicke in das Design, die Synthese und die Optimierung dieser Verbindungen und geht dabei auf die Herausforderungen des Screenings, des Metabolismus und der Medikamenteneignung ein.

Zukünftige Forschungsvorhaben sollten sich auf die Untersuchung von Zellpermeabilität, Off-Target-Effekten, der *in-vivo*-Wirksamkeit und der Resistenzentwicklung konzentrieren. So kann die erfolgreiche Weiterentwicklung dieser vielversprechenden Mip-Inhibitoren hin zu wirksamen therapeutischen Strategien gegen ein breites Spektrum von Infektionskrankheiten sichergestellt werden.

**VII Bibliography**

(1) Hughes, J. P.; Rees, S.; Kalindjian, S. B.; Philpott, K. L. Principles of early drug discovery. *Br. J. Pharmacol.* **2011**, *162* (6), 1239-1249.

DOI: 10.1111/j.1476-5381.2010.01127.x

(2) Kwon, J. H.; Powderly, W. G. The post-antibiotic era is here. *Science* **2021**, *373* (6554), 471.

DOI: 10.1126/science.abl5997

(3) Murray, C. J. L.; Ikuta, K. S.; Sharara, F.; Swetschinski, L.; Robles Aguilar, G.; Gray, A.; et al. Global burden of bacterial antimicrobial resistance in 2019: a systematic analysis. *Lancet* **2022**, *399* (10325), 629-655.

DOI: 10.1016/s0140-6736(21)02724-0

(4) Samsdodd, F. Target-based drug discovery: is something wrong? *Drug Discov. Today* **2005**, *10* (2), 139-147.

DOI: 10.1016/s1359-6446(04)03316-1

(5) Emmerich, C. H.; Gamboa, L. M.; Hofmann, M. C. J.; Bonin-Andresen, M.; Arbach, O.; Schendel, P.; et al. Improving target assessment in biomedical research: the GOT-IT recommendations. *Nat. Rev. Drug. Discov.* **2021**, *20* (1), 64-81.

DOI: 10.1038/s41573-020-0087-3

(6) Swinney, D. C. Phenotypic vs. target-based drug discovery for first-in-class medicines. *Clin. Pharmacol. Ther.* **2013**, *93* (4), 299-301.

DOI: 10.1038/clpt.2012.236

(7) Wang, S.; Tian, Y.; Wang, M.; Wang, M.; Sun, G. B.; Sun, X. B. Advanced Activity-Based Protein Profiling Application Strategies for Drug Development. *Front. Pharmacol.* **2018**, *9*, 353.

DOI: 10.3389/fphar.2018.00353

(8) Kiriiri, G. K.; Njogu, P. M.; Mwangi, A. N. Exploring different approaches to improve the success of drug discovery and development projects: a review. *Future J. Pharm. Sci.* **2020**, *6* (1).

DOI: 10.1186/s43094-020-00047-9



(9) Wildey, M. J.; Haunso, A.; Tudor, M.; Webb, M.; Connick, J. H. Chapter Five - High-Throughput Screening. In *Annu. Rep. Med. Chem.*, Goodnow, R. A. Ed.; Vol. 50; Academic Press, 2017; pp 149-195.

DOI: 10.1016/bs.armc.2017.08.004.

(10) Terstappen, G. C.; Schlupen, C.; Raggiaschi, R.; Gaviraghi, G. Target deconvolution strategies in drug discovery. *Nat. Rev. Drug Discov.* **2007**, *6* (11), 891-903.

DOI: 10.1038/nrd2410

(11) Kotz, J. Phenotypic screening, take two. *SciBX* **2012**, *5* (15), 380-380.

DOI: 10.1038/scibx.2012.380

(12) Batool, M.; Ahmad, B.; Choi, S. A Structure-Based Drug Discovery Paradigm. *Int. J. Mol. Sci.* **2019**, *20* (11).

DOI: 10.3390/ijms20112783

(13) Miethke, M.; Pieroni, M.; Weber, T.; Bronstrup, M.; Hammann, P.; Halby, L.; et al. Towards the sustainable discovery and development of new antibiotics. *Nat. Rev. Chem.* **2021**, *5* (10), 726-749.

DOI: 10.1038/s41570-021-00313-1

(14) Newman, D. J.; Cragg, G. M. Natural Products as Sources of New Drugs over the Nearly Four Decades from 01/1981 to 09/2019. *J. Nat. Prod.* **2020**, *83* (3), 770-803.

DOI: 10.1021/acs.jnatprod.9b01285

(15) Richter, M. F.; Drown, B. S.; Riley, A. P.; Garcia, A.; Shirai, T.; Svec, R. L.; et al. Predictive compound accumulation rules yield a broad-spectrum antibiotic. *Nature* **2017**, *545* (7654), 299-304.

DOI: 10.1038/nature22308

(16) Lewis, K. The Science of Antibiotic Discovery. *Cell* **2020**, *181* (1), 29-45.

DOI: 10.1016/j.cell.2020.02.056

(17) Ege, N.; Bouguenina, H.; Tatari, M.; Chopra, R. Phenotypic screening with target identification and validation in the discovery and development of E3 ligase modulators. *Cell Chem. Biol.* **2021**, *28* (3), 283-299.

DOI: 10.1016/j.chembiol.2021.02.011

(18) Katsuno, K.; Burrows, J. N.; Duncan, K.; Hooft van Huijsduijnen, R.; Kaneko, T.; Kita, K.; et al. Hit and lead criteria in drug discovery for infectious diseases of the developing world. *Nat. Rev. Drug Discov.* **2015**, *14* (11), 751-758.

DOI: 10.1038/nrd4683

(19) Chen, X.; Wang, Y.; Ma, N.; Tian, J.; Shao, Y.; Zhu, B.; et al. Target identification of natural medicine with chemical proteomics approach: probe synthesis, target fishing and protein identification. *Signal Transduct. Target. Ther.* **2020**, *5* (1), 72.

DOI: 10.1038/s41392-020-0186-y

(20) Rossi, A. M.; Taylor, C. W. Analysis of protein-ligand interactions by fluorescence polarization. *Nat. Protoc.* **2011**, *6* (3), 365-387.

DOI: 10.1038/nprot.2011.305

(21) Scheuplein, N. J.; Bzdyl, N. M.; Kibble, E. A.; Lohr, T.; Holzgrabe, U.; Sarkar-Tyson, M. Targeting Protein Folding: A Novel Approach for the Treatment of Pathogenic Bacteria. *J. Med. Chem.* **2020**, *63* (22), 13355-13388.

DOI: 10.1021/acs.jmedchem.0c00911

(22) Lakemeyer, M.; Zhao, W.; Mandl, F. A.; Hammann, P.; Sieber, S. A. Thinking Outside the Box—Novel Antibacterials To Tackle the Resistance Crisis. *Angew. Chem. Int. Ed.* **2018**, *57* (44), 14440-14475.

DOI: 10.1002/anie.201804971

(23) Bar-Peled, L.; Kemper, E. K.; Suci, R. M.; Vinogradova, E. V.; Backus, K. M.; Horning, B. D.; et al. Chemical Proteomics Identifies Druggable Vulnerabilities in a Genetically Defined Cancer. *Cell* **2017**, *171* (3), 696-709 e623.

DOI: 10.1016/j.cell.2017.08.051

(24) Rix, U.; Superti-Furga, G. Target profiling of small molecules by chemical proteomics. *Nat. Chem. Biol.* **2009**, *5* (9), 616-624.

DOI: 10.1038/nchembio.216

(25) Cravatt, B. F.; Wright, A. T.; Kozarich, J. W. Activity-based protein profiling: from enzyme chemistry to proteomic chemistry. *Annu. Rev. Biochem.* **2008**, *77*, 383-414.

DOI: 10.1146/annurev.biochem.75.101304.124125

(26) Harding, M. W.; Galat, A.; Uehling, D. E.; Schreiber, S. L. A receptor for the immunosuppressant FK506 is a cis-trans peptidyl-prolyl isomerase. *Nature* **1989**, *341* (6244), 758-760.

DOI: 10.1038/341758a0

(27) Chen, X.; Li, W.; Xu, C.; Wang, J.; Zhu, B.; Huang, Q.; et al. Comparative profiling of analog targets: a case study on resveratrol for mouse melanoma metastasis suppression. *Theranostics* **2018**, *8* (13), 3504-3516.

DOI: 10.7150/thno.24336

(28) Blake, R. A. Target validation in drug discovery. *Methods Mol. Biol.* **2007**, *356*, 367-377.

DOI: 10.1385/1-59745-217-3:367

(29) Bunnage, M. E. Getting pharmaceutical R&D back on target. *Nat. Chem. Biol.* **2011**, *7* (6), 335-339.

DOI: 10.1038/nchembio.581

(30) Dowden, H.; Munro, J. Trends in clinical success rates and therapeutic focus. *Nat. Rev. Drug Discov.* **2019**, *18* (7), 495-496.

DOI: 10.1038/d41573-019-00074-z

(31) Strovel, J.; Sittampalam, S.; Coussens, N. P.; Hughes, M.; Inglese, J.; Kurtz, A.; et al. Early Drug Discovery and Development Guidelines: For Academic Researchers, Collaborators, and Start-up Companies. In *Assay Guidance Manual*, Markossian, S., Grossman, A., Brimacombe, K., et al., e. Eds.; Eli Lilly & Company and NCATS, 2016.

(32) Egner, U.; Hillig, R. C. A Structural View on Druggability. In *Structural Biology in Drug Discovery*, John Wiley & Sons (Hoboken), 2020; pp 23-52.

DOI: 10.1002/9781118681121.ch2.

(33) Egner, U.; Hillig, R. C. A structural biology view of target drugability. *Expert Opin. Drug Discov.* **2008**, *3* (4), 391-401.

DOI: 10.1517/17460441.3.4.391

(34) Vogel, G. Nobel Prizes. A knockout award in medicine. *Science* **2007**, *318* (5848), 178-179.

DOI: 10.1126/science.318.5848.178

(35) Yu, L.; Coelho, J. E.; Zhang, X.; Fu, Y.; Tillman, A.; Karaoz, U.; et al. Uncovering multiple molecular targets for caffeine using a drug target validation strategy combining A 2A receptor knockout mice with microarray profiling. *Physiol. Genomics* **2009**, *37* (3), 199-210.

DOI: 10.1152/physiolgenomics.90353.2008

(36) Glasson, S. S. In vivo osteoarthritis target validation utilizing genetically-modified mice. *Curr. Drug Targets* **2007**, *8* (2), 367-376.

DOI: 10.2174/138945007779940061

(37) Cohen, J. CRISPR, the revolutionary genetic ‘scissors,’ honored by Chemistry Nobel. *Science* **2020**.

DOI: 10.1126/science.abf0540

(38) Smurnyy, Y.; Cai, M.; Wu, H.; McWhinnie, E.; Tallarico, J. A.; Yang, Y.; et al. DNA sequencing and CRISPR-Cas9 gene editing for target validation in mammalian cells. *Nat. Chem. Biol.* **2014**, *10* (8), 623-625.

DOI: 10.1038/nchembio.1550

(39) Floris, M.; Olla, S.; Schlessinger, D.; Cucca, F. Genetic-Driven Druggable Target Identification and Validation. *Trends Genet.* **2018**, *34* (7), 558-570.

DOI: 10.1016/j.tig.2018.04.004

(40) Silver, L. L. Appropriate Targets for Antibacterial Drugs. *Cold Spring Harb. Perspect. Med.* **2016**, *6* (12).

DOI: 10.1101/cshperspect.a030239

(41) Maia, E. H. B.; Assis, L. C.; de Oliveira, T. A.; da Silva, A. M.; Taranto, A. G. Structure-Based Virtual Screening: From Classical to Artificial Intelligence. *Front. Chem.* **2020**, *8*, 343.

DOI: 10.3389/fchem.2020.00343

(42) Service, R. 'The game has changed.' AI triumphs at solving protein structures. *Science* **2020**.

DOI: 10.1126/science.abf9367

(43) Jumper, J.; Evans, R.; Pritzel, A.; Green, T.; Figurnov, M.; Ronneberger, O.; et al. Highly accurate protein structure prediction with AlphaFold. *Nature* **2021**, *596* (7873), 583-589.

DOI: 10.1038/s41586-021-03819-2

(44) Zhang, J. H.; Chung, T. D.; Oldenburg, K. R. A Simple Statistical Parameter for Use in Evaluation and Validation of High Throughput Screening Assays. *J. Biomol. Screen.* **1999**, *4* (2), 67-73.

DOI: 10.1177/108705719900400206

(45) Albrecht, C. Joseph R. Lakowicz: Principles of fluorescence spectroscopy, 3rd Edition. *Anal. Bioanal. Chem.* **2008**, *390* (5), 1223-1224.

DOI: 10.1007/s00216-007-1822-x

(46) Owicki, J. C. Fluorescence polarization and anisotropy in high throughput screening: perspectives and primer. *J. Biomol. Screen.* **2000**, *5* (5), 297-306.

DOI: 10.1177/108705710000500501

(47) Moerke, N. J. Fluorescence Polarization (FP) Assays for Monitoring Peptide-Protein or Nucleic Acid-Protein Binding. *Curr. Protoc. Chem. Biol.* **2009**, *1* (1), 1-15.

DOI: 10.1002/9780470559277.ch090102

(48) Scheuplein, N. J.; Lohr, T.; Vivoli Vega, M.; Ankrett, D.; Seufert, F.; Kirchner, L.; et al. Fluorescent probe for the identification of potent inhibitors of the macrophage infectivity potentiator (Mip) protein of *Burkholderia pseudomallei*. *SLAS Discov.* **2023**.

DOI: 10.1016/j.slasd.2023.03.004

(49) Yu, J.; Lan, L.; Lewin, S. J.; Rogers, S. A.; Roy, A.; Wu, X.; et al. Identification of novel small molecule Beclin 1 mimetics activating autophagy. *Oncotarget* **2017**, 8 (31), 51355-51369.

DOI: 10.18632/oncotarget.17977

(50) Daina, A.; Michielin, O.; Zoete, V. SwissADME: a free web tool to evaluate pharmacokinetics, drug-likeness and medicinal chemistry friendliness of small molecules. *Sci. Rep.* **2017**, 7, 42717.

DOI: 10.1038/srep42717

(51) Lipinski, C. A.; Lombardo, F.; Dominy, B. W.; Feeney, P. J. Experimental and computational approaches to estimate solubility and permeability in drug discovery and development settings IPII of original article: S0169-409X(96)00423-1. The article was originally published in *Advanced Drug Delivery Reviews* 23 (1997) 3–25. 1. *Adv. Drug Deliv. Rev.* **2001**, 46 (1-3), 3-26.

DOI: 10.1016/s0169-409x(00)00129-0

(52) Veber, D. F.; Johnson, S. R.; Cheng, H. Y.; Smith, B. R.; Ward, K. W.; Kopple, K. D. Molecular properties that influence the oral bioavailability of drug candidates. *J. Med. Chem.* **2002**, 45 (12), 2615-2623.

DOI: 10.1021/jm020017n

(53) Chagas, C. M.; Moss, S.; Alisaraie, L. Drug metabolites and their effects on the development of adverse reactions: Revisiting Lipinski's Rule of Five. *Int. J. Pharm.* **2018**, 549 (1-2), 133-149.

DOI: 10.1016/j.ijpharm.2018.07.046

(54) O'Hagan, S.; Swainston, N.; Handl, J.; Kell, D. B. A 'rule of 0.5' for the metabolite-likeness of approved pharmaceutical drugs. *Metabolomics* **2015**, 11 (2), 323-339.

DOI: 10.1007/s11306-014-0733-z

(55) Doak, B. C.; Over, B.; Giordanetto, F.; Kihlberg, J. Oral druggable space beyond the rule of 5: insights from drugs and clinical candidates. *Chem. Biol.* **2014**, 21 (9), 1115-1142.

DOI: 10.1016/j.chembiol.2014.08.013

(56) Wunberg, T.; Hendrix, M.; Hillisch, A.; Lobell, M.; Meier, H.; Schmeck, C.; et al. Improving the hit-to-lead process: data-driven assessment of drug-like and lead-like screening hits. *Drug Discov. Today* **2006**, *11* (3-4), 175-180.

DOI: 10.1016/s1359-6446(05)03700-1

(57) Burrows, J. N.; Leroy, D.; Lotharius, J.; Waterson, D. Challenges in antimalarial drug discovery. *Future Med. Chem.* **2011**, *3* (11), 1401-1412.

DOI: 10.4155/fmc.11.91

(58) Ridgway, D.; Tuszynski, J. A.; Tam, Y. K. Reassessing models of hepatic extraction. *J. Biol. Phys.* **2003**, *29* (1), 1-21.

DOI: 10.1023/A:1022531403741

(59) Sahi, J.; Grepper, S.; Smith, C. Hepatocytes as a tool in drug metabolism, transport and safety evaluations in drug discovery. *Curr. Drug Discov. Technol.* **2010**, *7* (3), 188-198.

DOI: 10.2174/157016310793180576

(60) Masimirembwa, C. M.; Bredberg, U.; Andersson, T. B. Metabolic stability for drug discovery and development: pharmacokinetic and biochemical challenges. *Clin. Pharmacokinet.* **2003**, *42* (6), 515-528.

DOI: 10.2165/00003088-200342060-00002

(61) Lecluyse, E. L.; Alexandre, E. Isolation and culture of primary hepatocytes from resected human liver tissue. *Methods Mol. Biol.* **2010**, *640*, 57-82.

DOI: 10.1007/978-1-60761-688-7\_3

(62) Fry, J. R. The metabolism of drugs by isolated hepatocytes. *Q. Rev. Drug. Metab. Drug Interact.* **1982**, *4* (2-3), 99-122.

DOI: 10.1515/dmdi.1982.4.2-3.99

(63) Oprea, T. I.; Davis, A. M.; Teague, S. J.; Leeson, P. D. Is there a difference between leads and drugs? A historical perspective. *J. Chem. Inf. Comput. Sci.* **2001**, *41* (5), 1308-1315.

DOI: 10.1021/ci010366a

(64) van Breemen, R. B.; Li, Y. Caco-2 cell permeability assays to measure drug absorption. *Expert. Opin. Drug Metab. Toxicol.* **2005**, *1* (2), 175-185.

DOI: 10.1517/17425255.1.2.175

(65) Sanguinetti, M. C.; Tristani-Firouzi, M. hERG potassium channels and cardiac arrhythmia. *Nature* **2006**, *440* (7083), 463-469.

DOI: 10.1038/nature04710

(66) Ames, B. N.; McCann, J.; Yamasaki, E. Methods for detecting carcinogens and mutagens with the salmonella/mammalian-microsome mutagenicity test. *Mutat. Res. - Environ. Mutagen. Rel. Sub.* **1975**, *31* (6), 347-363.

DOI: 10.1016/0165-1161(75)90046-1

(67) Adan, A.; Kiraz, Y.; Baran, Y. Cell Proliferation and Cytotoxicity Assays. *Curr. Pharm. Biotechnol.* **2016**, *17* (14), 1213-1221.

DOI: 10.2174/1389201017666160808160513

(68) Roux, S.; Sable, E.; Porsolt, R. D. Primary observation (Irwin) test in rodents for assessing acute toxicity of a test agent and its effects on behavior and physiological function. *Curr. Protoc. Pharmacol.* **2005**, *Chapter 10*, Unit 10 10.

DOI: 10.1002/0471141755.ph1010s27

(69) Eisenblatter, T.; Teichert, L. Dose Linearity and Proportionality. In *Drug Discovery and Evaluation: Methods in Clinical Pharmacology*, Vogel, H. G., Maas, J., Gebauer, A. Eds.; Springer Berlin, 2011; pp 23-40.

DOI: 10.1007/978-3-540-89891-7\_5.

(70) Beckonert, O.; Keun, H. C.; Ebbels, T. M.; Bundy, J.; Holmes, E.; Lindon, J. C.; et al. Metabolic profiling, metabolomic and metabonomic procedures for NMR spectroscopy of urine, plasma, serum and tissue extracts. *Nat. Protoc.* **2007**, *2* (11), 2692-2703.

DOI: 10.1038/nprot.2007.376



(71) Harrison, R. K. Phase II and phase III failures: 2013-2015. *Nat. Rev. Drug Discov.* **2016**, *15* (12), 817-818.

DOI: 10.1038/nrd.2016.184

(72) Ünal, C. M.; Steinert, M. Microbial peptidyl-prolyl cis/trans isomerases (PPIases): virulence factors and potential alternative drug targets. *Microbiol. Mol. Biol. Rev.* **2014**, *78* (3), 544-571.

DOI: 10.1128/MMBR.00015-14

(73) Vivoli, M.; Renou, J.; Chevalier, A.; Norville, I. H.; Diaz, S.; Juli, C.; et al. A miniaturized peptidyl-prolyl isomerase enzyme assay. *Anal. Biochem.* **2017**, *536*, 59-68.

DOI: 10.1016/j.ab.2017.08.004

(74) Glaser, J.; Schultheis, M.; Hazra, S.; Hazra, B.; Moll, H.; Schurigt, U.; et al. Antileishmanial lead structures from nature: analysis of structure-activity relationships of a compound library derived from caffeic Acid bornyl ester. *Molecules* **2014**, *19* (2), 1394-1410.

DOI: 10.3390/molecules19021394

(75) Mann, S.; Frasca, K.; Scherrer, S.; Henao-Martinez, A. F.; Newman, S.; Ramanan, P.; et al. A Review of Leishmaniasis: Current Knowledge and Future Directions. *Curr. Trop. Med. Rep.* **2021**, *8* (2), 121-132.

DOI: 10.1007/s40475-021-00232-7

(76) Sasidharan, S.; Saudagar, P. Leishmaniasis: where are we and where are we heading? *Parasitol. Res.* **2021**, *120* (5), 1541-1554.

DOI: 10.1007/s00436-021-07139-2

(77) Mohan, S.; Revill, P.; Malvolti, S.; Malhame, M.; Sculpher, M.; Kaye, P. M. Estimating the global demand curve for a leishmaniasis vaccine: A generalisable approach based on global burden of disease estimates. *PLOS Negl. Trop. Dis.* **2022**, *16* (6), e0010471.

DOI: 10.1371/journal.pntd.0010471

(78) Glaser, J. PhD Thesis: Antileishmanial compounds from Nature - Elucidation of the active principles of an extract from *Valeriana wallichii* rhizomes. University of Würzburg, 2015.

(79) Glaser, J.; Schultheis, M.; Moll, H.; Hazra, B.; Holzgrabe, U. Antileishmanial and cytotoxic compounds from *Valeriana wallichii* and identification of a novel nepetolactone derivative. *Molecules* **2015**, *20* (4), 5740-5753.

DOI: 10.3390/molecules20045740

(80) Masic, A.; Valencia Hernandez, A. M.; Hazra, S.; Glaser, J.; Holzgrabe, U.; Hazra, B.; et al. Cinnamic Acid Bornyl Ester Derivatives from *Valeriana wallichii* Exhibit Antileishmanial In Vivo Activity in *Leishmania major*-Infected BALB/c Mice. *PLoS One* **2015**, *10* (11), e0142386.

DOI: 10.1371/journal.pone.0142386

(81) Glaser, J.; Schurigt, U.; Suzuki, B. M.; Caffrey, C. R.; Holzgrabe, U. Anti-Schistosomal Activity of Cinnamic Acid Esters: Eugenyl and Thymyl Cinnamate Induce Cytoplasmic Vacuoles and Death in Schistosomula of *Schistosoma mansoni*. *Molecules* **2015**, *20* (6), 10873-10883.

DOI: 10.3390/molecules200610873

(82) Cuatrecasas, P. Affinity chromatography. *Annu. Rev. Biochem.* **1971**, *40*, 259-278.

DOI: 10.1146/annurev.bi.40.070171.001355

(83) Cuatrecasas, P.; Wilchek, M.; Anfinsen, C. B. Selective enzyme purification by affinity chromatography. *Proc. Natl. Acad. Sci. U.S.A.* **1968**, *61* (2), 636-643.

DOI: 10.1073/pnas.61.2.636

(84) Christopoulos, T. K.; Diamandis, E. P. The biotin-(strept)avidin system: principles and applications in biotechnology. *Clin. Chem.* **1991**, *37* (5), 625-636.

DOI: 10.1093/clinchem/37.5.625

(85) L. Mpye, K.; Gildenhuis, S.; Mosebi, S. The effects of temperature on streptavidin-biotin binding using affinity isothermal titration calorimetry. *AIMS Biophys.* **2020**, *7* (4), 236-247.

DOI: 10.3934/biophys.2020018

(86) Green, N. M. Avidin. In *Advances in Protein Chemistry*, Anfinsen, C. B., Edsall, J. T., Richards, F. M. Eds.; Vol. 29; Academic Press, 1975; pp 85-133.

DOI: 10.1016/S0065-3233(08)60411-8.

(87) Bayer, E. A.; Wilchek, M. Application of avidin—biotin technology to affinity-based separations. *J. Chromatogr. A* **1990**, *510*, 3-11.

DOI: 10.1016/s0021-9673(01)93733-1

(88) Greenberg, A.; Breneman, C. M.; Liebman, J. F. *The amide linkage: Structural significance in chemistry, biochemistry, and materials science*; John Wiley & Sons: 2000.

(89) Yi, C. M.; Yu, J.; Kim, H.; Lee, N. R.; Kim, S. W.; Lee, N. J.; et al. Identification of actin as a direct proteomic target of berberine using an affinity-based chemical probe and elucidation of its modulatory role in actin assembly. *Chem. Commun. (Camb)* **2017**, *53* (52), 7045-7047.

DOI: 10.1039/c7cc02789c

(90) Lehmann, A. PhD Thesis: Development of potential inhibitors of the heat shock components HSF1 and HSP70 on the model of the multiple myeloma. University of Würzburg, 2017.

(91) Castelvechi, D.; Ledford, H. Chemists who invented revolutionary 'click' reactions win Nobel. *Nature* **2022**, *610* (7931), 242-243.

DOI: 10.1038/d41586-022-03087-8

(92) Nagl, P. A. PhD Thesis: Chemistry meets Cancer Immunotherapy: Synthesis and Characterization of Hapten-like Compounds for Selective Immunotherapy. University of Würzburg, 2022.

(93) Donnelly, P. S.; Zanatta, S. D.; Zammit, S. C.; White, J. M.; Williams, S. J. 'Click' cycloaddition catalysts: copper(I) and copper(II) tris(triazolylmethyl)amine complexes. *Chem. Commun.* **2008**, (21), 2459-2461.

DOI: 10.1039/b719724a

(94) S. Hünig, P. K., G. Märkl, J. Sauer. *Arbeitsmethoden in der organischen Chemie*. Lehmanns Verlag: Berlin, 2006.

(95) Fulmer, G. R.; Miller, A. J. M.; Sherden, N. H.; Gottlieb, H. E.; Nudelman, A.; Stoltz, B. M.; et al. NMR Chemical Shifts of Trace Impurities: Common Laboratory Solvents, Organics, and

Gases in Deuterated Solvents Relevant to the Organometallic Chemist. *Organometallics* **2010**, *29* (9), 2176-2179.

DOI: 10.1021/om100106e

(96) Becker, H. *Organikum: organisch-chemisches Grundpraktikum, 20. Auflage*; Johann Ambrosius Barth Verlag, Leipzig: 1996.

(97) Gavrilyuk, J. I.; Wuellner, U.; Barbas, C. F., 3rd. Beta-lactam-based approach for the chemical programming of aldolase antibody 38C2. *Bioorg Med Chem Lett* **2009**, *19* (5), 1421-1424.

DOI: 10.1016/j.bmcl.2009.01.028

(98) Salvagnini, C.; Gharbi, S.; Boxus, T.; Marchand-Brynaert, J. Synthesis and evaluation of a small library of graftable thrombin inhibitors derived from (L)-arginine. *Eur. J. Med. Chem.* **2007**, *42* (1), 37-53.

DOI: 10.1016/j.ejmech.2006.07.010

(99) Nagl, P. Master Thesis: Synthesis and Characterization of Hapten Compounds for Selective Immunotherapy. University of Würzburg, 2015.

(100) Patent. Inventor(s): Hawkins, L. D.; Ishizaka, S. T. Immunomodulatory compounds and methods of use thereof. Patent Number: US7915238B2, 2011.

(101) Fernandez-Megia, E.; Correa, J.; Rodríguez-Meizoso, I.; Riguera, R. A Click Approach to Unprotected Glycodendrimers. *Macromolecules* **2006**, *39* (6), 2113-2120.

DOI: 10.1021/ma052448w

(102) Risseuw, M. D.; De Clercq, D. J.; Lievens, S.; Hillaert, U.; Sinnaeve, D.; Van den Broeck, F.; et al. A "clickable" MTX reagent as a practical tool for profiling small-molecule-intracellular target interactions via MASPIT. *ChemMedChem* **2013**, *8* (3), 521-526.

DOI: 10.1002/cmdc.201200493

(103) Goncalves, M.; Estieu-Gionnet, K.; Berthelot, T.; Lain, G.; Bayle, M.; Cannon, X.; et al. Design, synthesis, and evaluation of original carriers for targeting vascular endothelial growth factor receptor interactions. *Pharm. Res.* **2005**, *22* (8), 1411-1421.

DOI: 10.1007/s11095-005-5265-9

(104) Sun, Q.; Yao, C. J.; Konig, B. A triphenylphosphine mediated photo-rearrangement and methanol addition of aryl chalcones to 1-propanones. *Photochem. Photobiol. Sci.* **2015**, *14* (5), 948-952.

DOI: 10.1039/c5pp00009b

(105) Bunce, R. A.; Nammalwar, B. ( $\pm$ )-2-Aryl-2,3-dihydro-4(1H)-quinolinones by a tandem reduction-Michael addition reaction. *J. Heterocycl. Chem.* **2011**, *48* (3), 613-619.

DOI: 10.1002/jhet.624

(106) Kirubavathy, S. J.; Velmurugan, R.; Parameswari, K.; Chitra, S. Synthesis, characterization and biological evaluation of Cu(II), Co(III) and Fe(III) complexes of 2-benzoyl-3-(nitrophenyl)quinoxaline. *Int. J. Pharm. Sci.* **2014**, *5* (6), 2498-2507, 2410.

DOI: 10.13040/ijpsr.0975-8232.5(6).2498-07

(107) Patent. Inventor(s): Bradshaw, C.; Sakamuri, S.; Fu, Y.; Oates, B.; Desharnais, J.; Tumelty, D. Glucagon-like protein-1 receptor (glp-1r) agonist compounds. Patent Number: CA2674112A1, 2008.

(108) Kobayashi, T.; Kikumoto, R. Synthesis of quino(4,3-c)quinoline derivatives and polycarbocyclic quino(4,3-c)quinolines. *Tetrahedron* **1965**, *21* (8), 1903-1905.

DOI: 10.1016/s0040-4020(01)98329-2

(109) Begley, D. W.; Fox, D., 3rd; Jenner, D.; Juli, C.; Pierce, P. G.; Abendroth, J.; et al. A structural biology approach enables the development of antimicrobials targeting bacterial immunophilins. *Antimicrob. Agents Chemother.* **2014**, *58* (3), 1458-1467.

DOI: 10.1128/AAC.01875-13

(110) Banaszynski, L. A.; Liu, C. W.; Wandless, T. J. Characterization of the FKBP center dot rapamycin, FRB ternary complex (vol 127, pg 4715, 2005). *J. Am. Chem. Soc.* **2006**, *128* (49), 15928.

DOI: 10.1021/ja0699788

(111) Kozany, C.; Marz, A.; Kress, C.; Hausch, F. Fluorescent probes to characterise FK506-binding proteins. *ChemBioChem* **2009**, *10* (8), 1402-1410.

DOI: 10.1002/cbic.200800806

(112) Hall, M. D.; Yasgar, A.; Peryea, T.; Braisted, J. C.; Jadhav, A.; Simeonov, A.; et al. Fluorescence polarization assays in high-throughput screening and drug discovery: a review. *Methods Appl. Fluoresc.* **2016**, *4* (2), 022001.

DOI: 10.1088/2050-6120/4/2/022001

(113) Moro, A.; Ruiz-Cabello, F.; Fernandez-Cano, A.; Stock, R. P.; Gonzalez, A. Secretion by *Trypanosoma cruzi* of a peptidyl-prolyl cis-trans isomerase involved in cell infection. *EMBO J.* **1995**, *14* (11), 2483-2490.

DOI: 10.1002/j.1460-2075.1995.tb07245.x

(114) Iwasaki, J.; Lorimer, D. D.; Vivoli-Vega, M.; Kibble, E. A.; Peacock, C. S.; Abendroth, J.; et al. Broad-spectrum in vitro activity of macrophage infectivity potentiator inhibitors against Gram-negative bacteria and *Leishmania major*. *J. Antimicrob. Chemother.* **2022**, *77* (6), 1625-1634.

DOI: 10.1093/jac/dkac065

(115) Aneja, A.; Mathur, N.; Bhatnagar, P. K.; Mathur, P. C. Triple-FRET Technique for Energy Transfer Between Conjugated Polymer and TAMRA Dye with Possible Applications in Medical Diagnostics. *J. Biol. Phys.* **2008**, *34* (5), 487-493.

DOI: 10.1007/s10867-008-9107-y

(116) Shiba, A.; Kinoshita-Kikuta, E.; Kinoshita, E.; Koike, T. TAMRA/TAMRA Fluorescence Quenching Systems for the Activity Assay of Alkaline Phosphatase. *Sensors (Basel)* **2017**, *17* (8).

DOI: 10.3390/s17081877

(117) Sapsford, K. E.; Berti, L.; Medintz, I. L. Materials for fluorescence resonance energy transfer analysis: beyond traditional donor-acceptor combinations. *Angew. Chem. Int. Ed. Engl.* **2006**, *45* (28), 4562-4589.

DOI: 10.1002/anie.200503873

(118) Wiederschain, G. Y. The Molecular Probes handbook. A guide to fluorescent probes and labeling technologies. *Biochemistry (Moscow)* **2011**, *76* (11), 1276-1276.

DOI: 10.1134/s0006297911110101

(119) Juli, C.; Sippel, M.; Jäger, J.; Thiele, A.; Weiwad, M.; Schweimer, K.; et al. Pipecolic acid derivatives as small-molecule inhibitors of the Legionella MIP protein. *J. Med. Chem.* **2011**, *54* (1), 277-283.

DOI: 10.1021/jm101156y

(120) Jorgensen, F. P.; Bols, M. An Inexpensive and Scalable Synthesis of Shld. *J. Org. Chem.* **2018**, *83* (11), 6050-6055.

DOI: 10.1021/acs.joc.8b00698

(121) Keenan, T.; Yaeger, D. R.; Courage, N. L.; Rollins, C. T.; Pavone, M. E.; Rivera, V. M.; et al. Synthesis and activity of bivalent FKBP12 ligands for the regulated dimerization of proteins. *Bioorg. Med. Chem.* **1998**, *6* (8), 1309-1335.

DOI: 10.1016/s0968-0896(98)00125-4

(122) Mori, A.; Miyakawa, Y.; Ohashi, E.; Haga, T.; Maegawa, T.; Sajiki, H. Pd/C-catalyzed chemoselective hydrogenation in the presence of diphenylsulfide. *Org. Lett.* **2006**, *8* (15), 3279-3281.

DOI: 10.1021/ol061147j

(123) Hanson, K. R. Applications of the Sequence Rule. I. Naming the Paired Ligands g,g at a Tetrahedral Atom Xggij. II. Naming the Two Faces of a Trigonal Atom Yghi. *J. Am. Chem. Soc.* **1966**, *88* (12), 2731-2742.

DOI: 10.1021/ja00964a022

(124) Eschmann, C.; Song, L.; Schreiner, P. R. London Dispersion Interactions Rather than Steric Hindrance Determine the Enantioselectivity of the Corey-Bakshi-Shibata Reduction. *Angew. Chem. Int. Ed. Engl.* **2021**, *60* (9), 4823-4832.

DOI: 10.1002/anie.202012760

- (125) Corey, E. J.; Bakshi, R. K.; Shibata, S. Highly enantioselective borane reduction of ketones catalyzed by chiral oxazaborolidines. Mechanism and synthetic implications. *J. Am. Chem. Soc.* **1987**, *109* (18), 5551-5553.  
DOI: 10.1021/ja00252a056
- (126) Hirao, A.; Itsuno, S.; Nakahama, S.; Yamazaki, N. Asymmetric reduction of aromatic ketones with chiral alkoxy-amineborane complexes. *J. Chem. Soc., Chem. Commun.* **1981**, (7).  
DOI: 10.1039/c39810000315
- (127) Clayden, J.; Greeves, N.; Warren, S. G. *Organic chemistry*; Oxford Univ. Press: Oxford [u.a.], 2012.
- (128) Mathre, D. J.; Shinkai, I.; Zaidlewicz, M.; Krzemiński, M.; Łączkowski, K.; Patti, A.; et al. Tetrahydro-1-methyl-3,3-diphenyl-1H, 3H-pyrrolo[1,2-c][1,3,2]oxazaborole. In *Encyclopedia of Reagents for Organic Synthesis*, John Wiley & Sons (Hoboken), 2013.  
DOI: 10.1002/047084289X.rt035s.pub3.
- (129) Mandal, D. K. Chapter 7 - Ionic reactions 2: Diastereoselectivity and asymmetric synthesis. In *Stereochemistry and Organic Reactions*, Mandal, D. K. Ed.; Academic Press, 2021; pp 303-374.  
DOI: 10.1016/B978-0-12-824092-2.00007-1.
- (130) Vedejs, E.; Denmark, S. E. *Lewis Base Catalysis in Organic Synthesis*; Wiley-VCH Verlag Weinheim: 2016.  
DOI: 10.1002/9783527675142.
- (131) London, F. The general theory of molecular forces. *Transactions of the Faraday Society* **1937**, *33*.  
DOI: 10.1039/tf937330008b
- (132) Kumar, S.; Reddy, L. C.; Kumar, Y.; Kumar, A.; Singh, B. K.; Kumar, V.; et al. Arylalkyl ketones, benzophenones, desoxybenzoin and chalcones inhibit TNF-alpha induced expression of ICAM-1: structure-activity analysis. *Arch. Pharm. (Weinheim)* **2012**, *345* (5), 368-377.  
DOI: 10.1002/ardp.201100279



(133) Hu, D. X.; Grice, P.; Ley, S. V. Rotamers or diastereomers? An overlooked NMR solution. *J. Org. Chem.* **2012**, *77* (11), 5198-5202.

DOI: 10.1021/jo300734r

(134) Huggins, M. T.; Kesharwani, T.; Buttrick, J.; Nicholson, C. Variable Temperature NMR Experiment Studying Restricted Bond Rotation. *J. Chem. Educ.* **2020**, *97* (5), 1425-1429.

DOI: 10.1021/acs.jchemed.0c00057

(135) Talk, R. A.; El-Tunsi, A.; Robertson, C. C.; Coldham, I. Regioselective Lithiation and Electrophilic Quenching of N-Boc-3-phenyltetrahydroisoquinoline. *Eur. J. Org. Chem.* **2019**, *2019* (31-32), 5294-5301.

DOI: 10.1002/ejoc.201900238

(136) Günther, H. *NMR spectroscopy*; Wiley: Chichester [u.a.], 1998.

(137) Cox, C.; Lectka, T. Solvent Effects on the Barrier to Rotation in Carbamates. *J. Org. Chem.* **1998**, *63* (8), 2426-2427.

DOI: 10.1021/jo9800863

(138) Oberg, C. T.; Carlsson, S.; Fillion, E.; Leffler, H.; Nilsson, U. J. Efficient and expedient two-step pyranose-retaining fluorescein conjugation of complex reducing oligosaccharides: galectin oligosaccharide specificity studies in a fluorescence polarization assay. *Bioconjug. Chem.* **2003**, *14* (6), 1289-1297.

DOI: 10.1021/bc034130j

(139) Farzan, V. M.; Ulashchik, E. A.; Martynenko-Makaev, Y. V.; Kvach, M. V.; Aparin, I. O.; Brylev, V. A.; et al. Automated Solid-Phase Click Synthesis of Oligonucleotide Conjugates: From Small Molecules to Diverse N-Acetylgalactosamine Clusters. *Bioconjug. Chem.* **2017**, *28* (10), 2599-2607.

DOI: 10.1021/acs.bioconjchem.7b00462

(140) Pomplun, S.; Sippel, C.; Hahle, A.; Tay, D.; Shima, K.; Klages, A.; et al. Chemogenomic Profiling of Human and Microbial FK506-Binding Proteins. *J. Med. Chem.* **2018**, *61* (8), 3660-3673.

DOI: 10.1021/acs.jmedchem.8b00137

(141) Lermyte, F. Chapter 1 Modern Mass Spectrometry and Advanced Fragmentation Methods. In *Advanced Fragmentation Methods in Biomolecular Mass Spectrometry: Probing Primary and Higher Order Structure with Electrons, Photons and Surfaces*, The Royal Society of Chemistry, 2021; pp 1-14.

DOI: 10.1039/9781839161056-00001.

(142) Scheuplein, N. J.; Bzdyl, N. M.; Lohr, T.; Kibble, E. A.; Hasenkopf, A.; Sarkar-Tyson, M.; et al. Analysis of Structure–Activity-Relationships of Novel Inhibitors of the Macrophage Infectivity Potentiator (Mip) Proteins of *Neisseria meningitidis*, *Neisseria gonorrhoeae*, and *Burkholderia pseudomallei*. *unpublished results* **2023**.

(143) Lameijer, L. N.; Ernst, D.; Hopkins, S. L.; Meijer, M. S.; Askes, S. H. C.; Le Devedec, S. E.; et al. A Red-Light-Activated Ruthenium-Caged NAMPT Inhibitor Remains Phototoxic in Hypoxic Cancer Cells. *Angew. Chem. Int. Ed. Engl.* **2017**, *56* (38), 11549-11553.

DOI: 10.1002/anie.201703890

(144) Mori, M.; Washioka, Y.; Urayama, T.; Yoshiura, K.; Chiba, K.; Ban, Y. Palladium-catalyzed carbonylation. A new synthesis of .alpha.-methylene .gamma.-, .delta.-, .epsilon.-lactams and lactones including bicyclic lactams of pyrrolizidine and indolizidine skeletons. *J. Org. Chem.* **1983**, *48* (22), 4058-4067.

DOI: 10.1021/jo00170a037

(145) Carta, F.; Vullo, D.; Maresca, A.; Scozzafava, A.; Supuran, C. T. Mono-/dihydroxybenzoic acid esters and phenol pyridinium derivatives as inhibitors of the mammalian carbonic anhydrase isoforms I, II, VII, IX, XII and XIV. *Bioorg. Med. Chem.* **2013**, *21* (6), 1564-1569.

DOI: 10.1016/j.bmc.2012.05.019

(146) Unal, C. M.; Steinert, M. FKBP's in bacterial infections. *Biochim. Biophys. Acta* **2015**, *1850* (10), 2096-2102.

DOI: 10.1016/j.bbagen.2014.12.018

(147) Brandts, J. F.; Halvorson, H. R.; Brennan, M. Consideration of the Possibility that the slow step in protein denaturation reactions is due to cis-trans isomerism of proline residues. *Biochemistry* **1975**, *14* (22), 4953-4963.

DOI: 10.1021/bi00693a026

(148) Lang, K.; Schmid, F. X.; Fischer, G. Catalysis of protein folding by prolyl isomerase. *Nature* **1987**, *329* (6136), 268-270.

DOI: 10.1038/329268a0

(149) Schiene-Fischer, C.; Yu, C. Receptor accessory folding helper enzymes: the functional role of peptidyl prolylcis/transisomerases. *FEBS Lett.* **2001**, *495* (1-2), 1-6.

DOI: 10.1016/s0014-5793(01)02326-2

(150) Kohler, R.; Fanghanel, J.; Konig, B.; Luneberg, E.; Frosch, M.; Rahfeld, J. U.; et al. Biochemical and functional analyses of the Mip protein: influence of the N-terminal half and of peptidylprolyl isomerase activity on the virulence of *Legionella pneumophila*. *Infect. Immun.* **2003**, *71* (8), 4389-4397.

DOI: 10.1128/IAI.71.8.4389-4397.2003

(151) Norville, I. H.; Harmer, N. J.; Harding, S. V.; Fischer, G.; Keith, K. E.; Brown, K. A.; et al. A *Burkholderia pseudomallei* macrophage infectivity potentiator-like protein has rapamycin-inhibitable peptidylprolyl isomerase activity and pleiotropic effects on virulence. *Infect. Immun.* **2011**, *79* (11), 4299-4307.

DOI: 10.1128/IAI.00134-11

(152) Seufert, F.; Kuhn, M.; Hein, M.; Weiwad, M.; Vivoli, M.; Norville, I. H.; et al. Development, synthesis and structure-activity-relationships of inhibitors of the macrophage infectivity potentiator (Mip) proteins of *Legionella pneumophila* and *Burkholderia pseudomallei*. *Bioorg. Med. Chem.* **2016**, *24* (21), 5134-5147.

DOI: 10.1016/j.bmc.2016.08.025

(153) Seufert, F. PhD Thesis: Mip-Inhibitoren. University of Würzburg, 2016.

- (154) Caporale, A.; Mascanzoni, F.; Farina, B.; Sturlese, M.; Di Sorbo, G.; Fattorusso, R.; et al. FRET-Protease-Coupled Peptidyl-Prolyl cis-trans Isomerase Assay: New Internally Quenched Fluorogenic Substrates for High-Throughput Screening. *J. Biomol. Screen.* **2016**, *21* (7), 701-712. DOI: 10.1177/1087057116650402
- (155) Volpp, M. PhD Thesis: Determination of plasma protein binding of low-affinity ligands using Ephedra alkaloids as an example. University of Würzburg, 2021.
- (156) Volpp, M.; Holzgrabe, U. Determination of plasma protein binding for sympathomimetic drugs by means of ultrafiltration. *Eur. J. Pharm. Sci.* **2019**, *127*, 175-184. DOI: 10.1016/j.ejps.2018.10.027
- (157) Heinze, A.; Holzgrabe, U. Determination of the extent of protein binding of antibiotics by means of an automated continuous ultrafiltration method. *Int. J. Pharm.* **2006**, *311* (1-2), 108-112. DOI: 10.1016/j.ijpharm.2005.12.022
- (158) Di, L. An update on the importance of plasma protein binding in drug discovery and development. *Expert Opin. Drug Discov.* **2021**, *16* (12), 1453-1465. DOI: 10.1080/17460441.2021.1961741
- (159) Hann, E.; Malagu, K.; Stott, A.; Vater, H. The importance of plasma protein and tissue binding in a drug discovery program to successfully deliver a preclinical candidate. *Prog. Med. Chem.* **2022**, *61*, 163-214. DOI: 10.1016/bs.pmch.2022.04.002
- (160) Ahmed, H.; Bergmann, F.; Zeitlinger, M. Protein Binding in Translational Antimicrobial Development-Focus on Interspecies Differences. *Antibiotics (Basel)* **2022**, *11* (7). DOI: 10.3390/antibiotics11070923
- (161) Smith, D. A.; Di, L.; Kerns, E. H. The effect of plasma protein binding on in vivo efficacy: misconceptions in drug discovery. *Nat. Rev. Drug Discov.* **2010**, *9* (12), 929-939. DOI: 10.1038/nrd3287

(162) Lohr, T. PhD Thesis: TcMip Inhibitors (working title). To be published in 2023/24. University of Würzburg, 2023.

(163) Cooper, G.; Hausman, R. E. *The cell: a molecular approach*. Sinauer Associates; URL: <https://www.ncbi.nlm.nih.gov/books/NBK9839/> ; acc. 19.04.2023: 2000.

(164) Bennion, B. J.; Be, N. A.; McNerney, M. W.; Lao, V.; Carlson, E. M.; Valdez, C. A.; et al. Predicting a Drug's Membrane Permeability: A Computational Model Validated With in Vitro Permeability Assay Data. *J. Phys. Chem. B* **2017**, *121* (20), 5228-5237.

DOI: 10.1021/acs.jpbc.7b02914

(165) Hoffmann, C.; Centi, A.; Menichetti, R.; Bereau, T. Molecular dynamics trajectories for 630 coarse-grained drug-membrane permeations. *Sci. Data* **2020**, *7* (1), 51.

DOI: 10.1038/s41597-020-0391-0

(166) West, K. H. J.; Gahan, C. G.; Kierski, P. R.; Calderon, D. F.; Zhao, K.; Czuprynski, C. J.; et al. Sustained Release of a Synthetic Autoinducing Peptide Mimetic Blocks Bacterial Communication and Virulence In Vivo. *Angew. Chem.* **2022**, *134* (24).

DOI: 10.1002/ange.202201798

(167) Allen, R. C.; Popat, R.; Diggle, S. P.; Brown, S. P. Targeting virulence: can we make evolution-proof drugs? *Nat. Rev. Microbiol.* **2014**, *12* (4), 300-308.

DOI: 10.1038/nrmicro3232

(168) Theuretzbacher, U.; Piddock, L. J. V. Non-traditional Antibacterial Therapeutic Options and Challenges. *Cell Host Microbe* **2019**, *26* (1), 61-72.

DOI: 10.1016/j.chom.2019.06.004

(169) Totsika, M. Benefits and Challenges of Antivirulence Antimicrobials at the Dawn of the Post-Antibiotic Era. *Drug Deliv. Lett.* **2016**, *6* (1), 30-37.

DOI: 10.2174/2210303106666160506120057

(170) Rezzoagli, C.; Archetti, M.; Mignot, I.; Baumgartner, M.; Kummerli, R. Combining antibiotics with antivirulence compounds can have synergistic effects and reverse selection for antibiotic resistance in *Pseudomonas aeruginosa*. *PLoS Biol.* **2020**, *18* (8), e3000805.

DOI: 10.1371/journal.pbio.3000805

(171) Reardon, S. WHO warns against 'post-antibiotic' era. *Nature* **2014**.

DOI: 10.1038/nature.2014.15135

(172) Rasko, D. A.; Sperandio, V. Anti-virulence strategies to combat bacteria-mediated disease. *Nat. Rev. Drug Discov.* **2010**, *9* (2), 117-128.

DOI: 10.1038/nrd3013

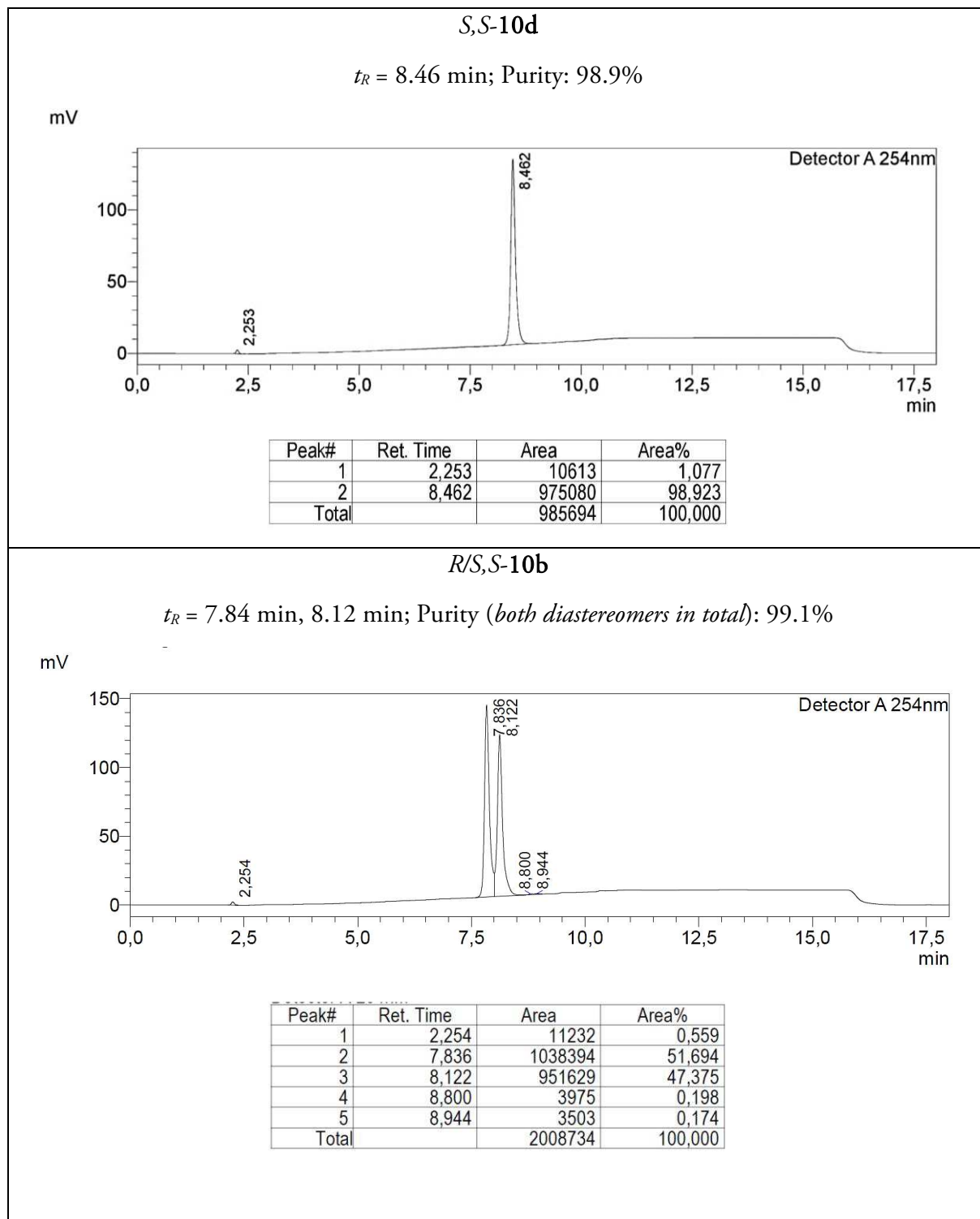
(173) Cegelski, L.; Marshall, G. R.; Eldridge, G. R.; Hultgren, S. J. The biology and future prospects of antivirulence therapies. *Nat. Rev. Microbiol.* **2008**, *6* (1), 17-27.

DOI: 10.1038/nrmicro1818

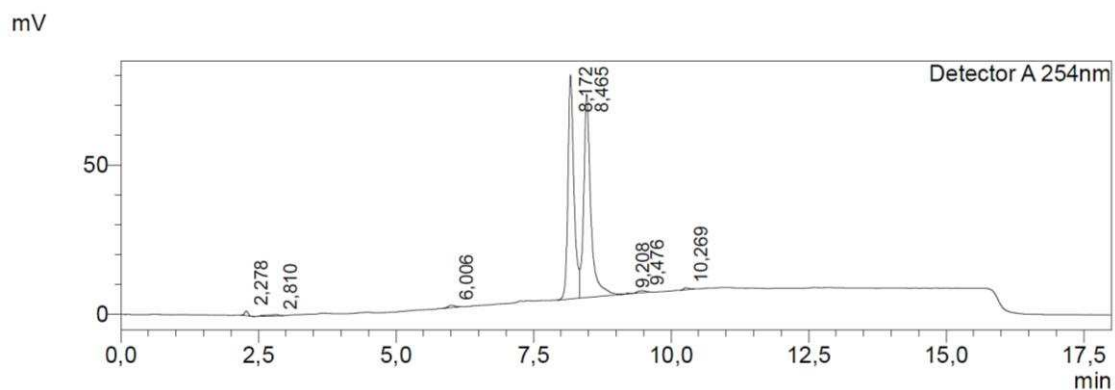
## VIII Appendix

## 1 HPLC Purity Data

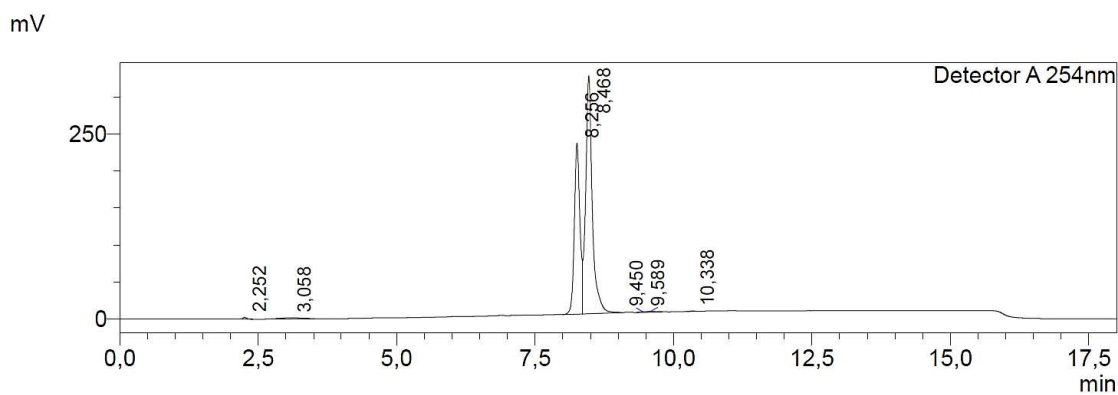
The HPLC method used is described in chapter III\_4.4. HPLC chromatograms of the FP paper (SLAS Discovery), including the chromatogram of probe **30** (NJS106), can be found in chapter III\_2.8.1.



## VIII Appendix

*R/S,S-10c* $t_R = 8.17 \text{ min}, 8.47 \text{ min}; \text{Purity (both diastereomers in total): } 97.3\%$ 

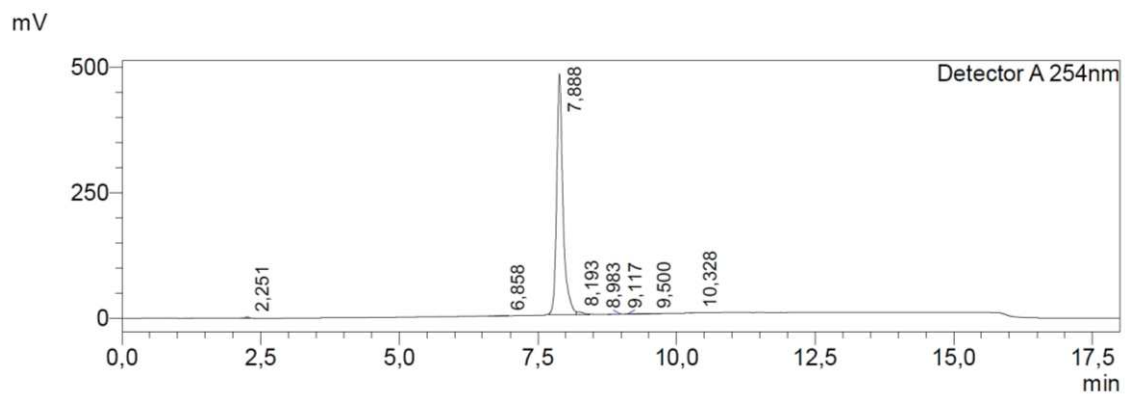
Peak#	Ret. Time	Area	Area%
1	2,278	6827	0,560
2	2,810	7355	0,603
3	6,006	6299	0,516
4	8,172	572401	46,932
5	8,465	613723	50,320
6	9,208	1727	0,142
7	9,476	6928	0,568
8	10,269	4377	0,359
Total		1219637	100,000

*R/S,S-10d* $t_R = 8.26 \text{ min}, 8.47 \text{ min}; \text{Purity (both diastereomers in total): } 98.4\%$ 

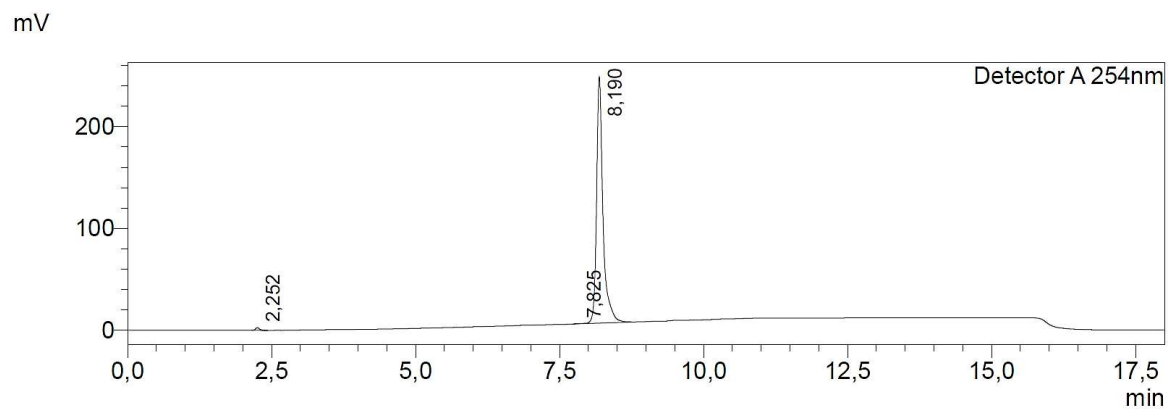
Peak#	Ret. Time	Area	Area%
1	2,252	11052	0,254
2	3,058	37256	0,858
3	8,256	1616137	37,211
4	8,468	2658299	61,206
5	9,450	6801	0,157
6	9,589	9741	0,224
7	10,338	3930	0,090
Total		4343216	100,000



## VIII Appendix

**S,S-21a** $t_R = 7.89$  min; Purity: 97.9%

Peak#	Ret. Time	Area	Area%
1	2,251	11156	0,289
2	6,858	1568	0,041
3	7,888	3773873	97,879
4	8,193	56117	1,455
5	8,983	2895	0,075
6	9,117	2009	0,052
7	9,500	4800	0,124
8	10,328	3214	0,083
Total		3855633	100,000

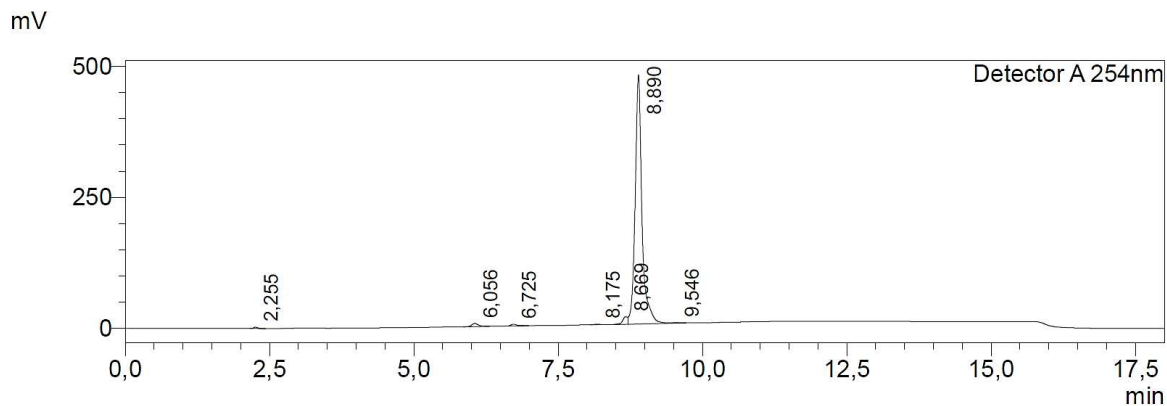
**S,S-21e** $t_R = 8.19$  min; Purity: 99.2%

Peak#	Ret. Time	Area	Area%
1	2,252	11867	0,627
2	7,825	3297	0,174
3	8,190	1877844	99,199
Total		1893008	100,000

VIII Appendix

**S,S-10e**

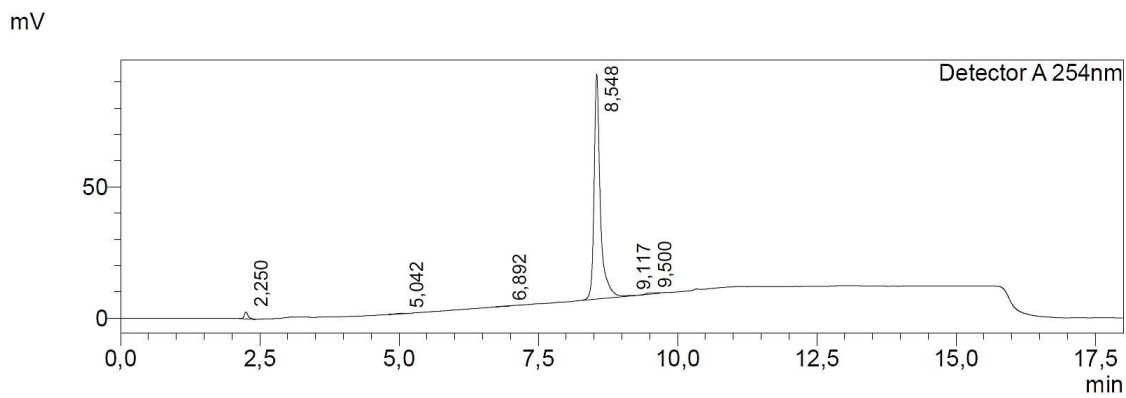
$t_R = 8.89$  min; Purity: 95.4%



Peak#	Ret. Time	Area	Area%
1	2,255	11727	0,288
2	6,056	48913	1,200
3	6,725	27117	0,665
4	8,175	5862	0,144
5	8,669	83331	2,045
6	8,890	3886310	95,354
7	9,546	12390	0,304
Total		4075651	100,000

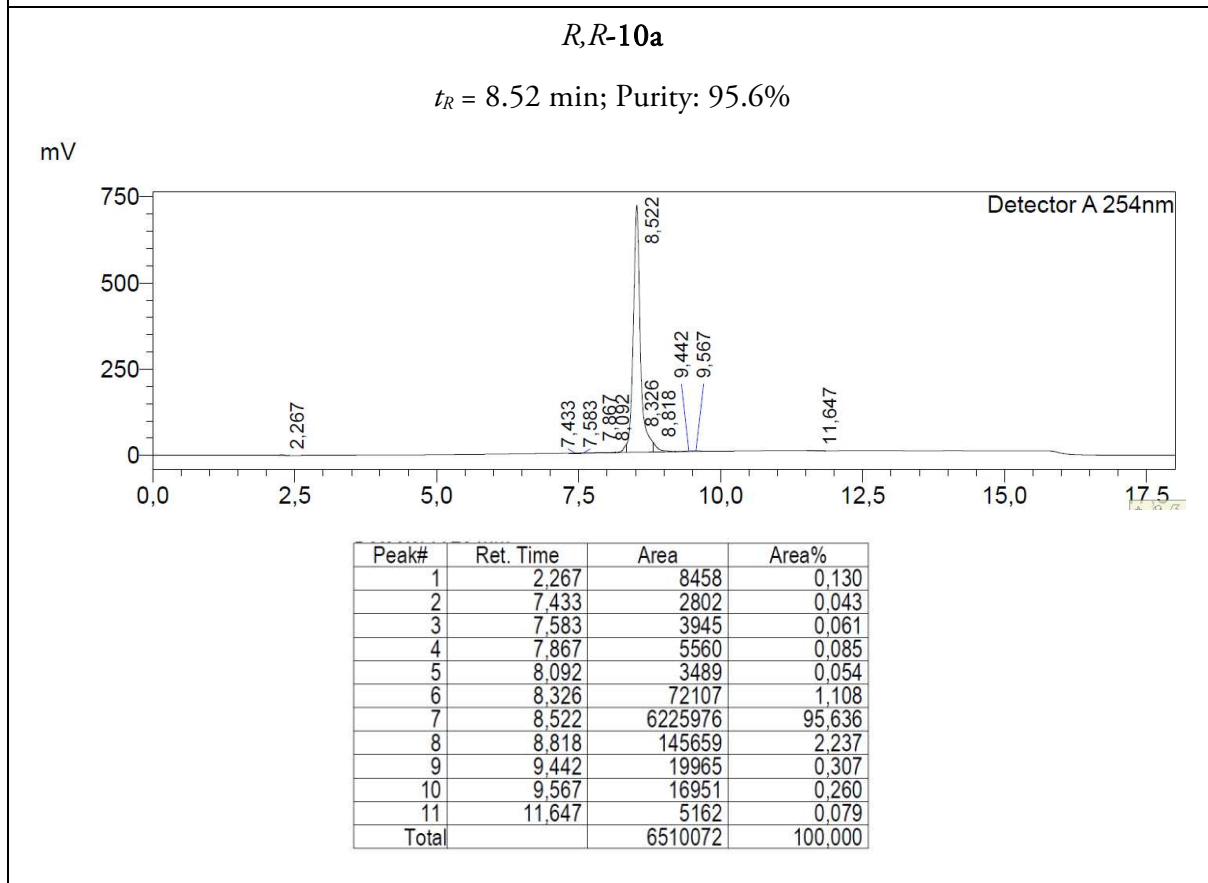
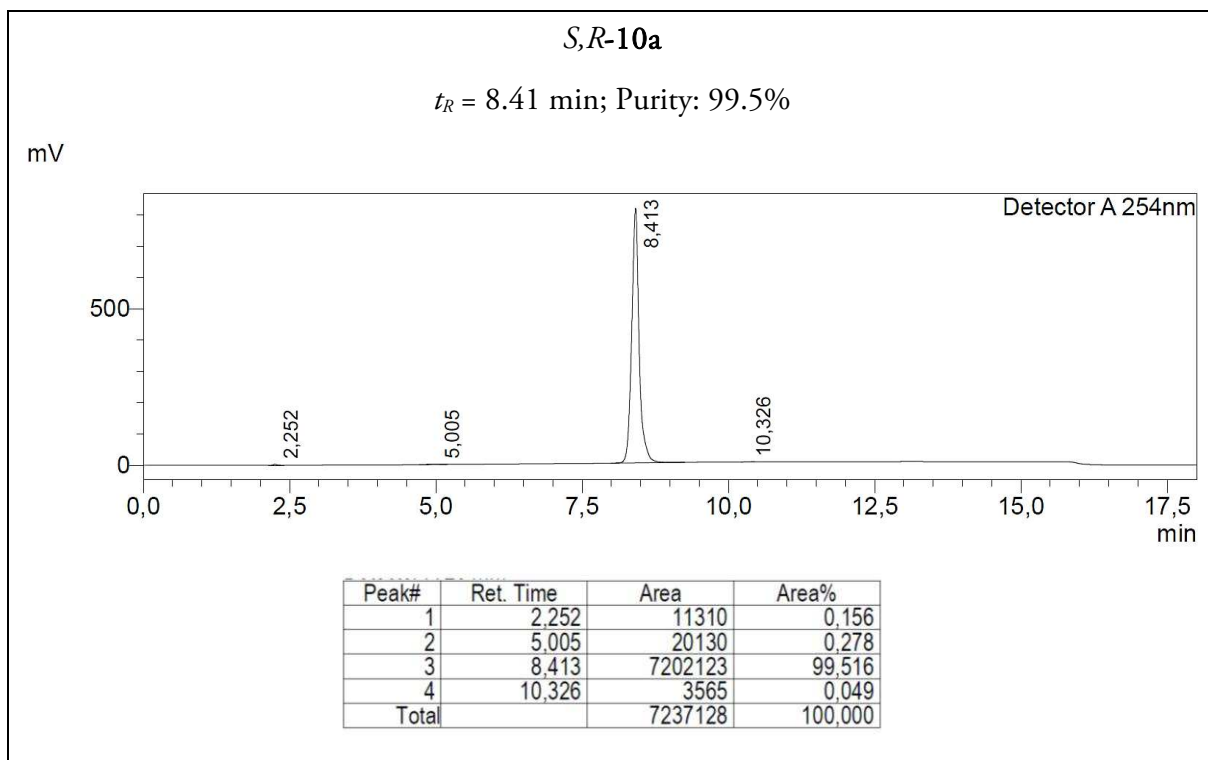
**S,S-10a**

$t_R = 8.55$  min; Purity: 96.5%

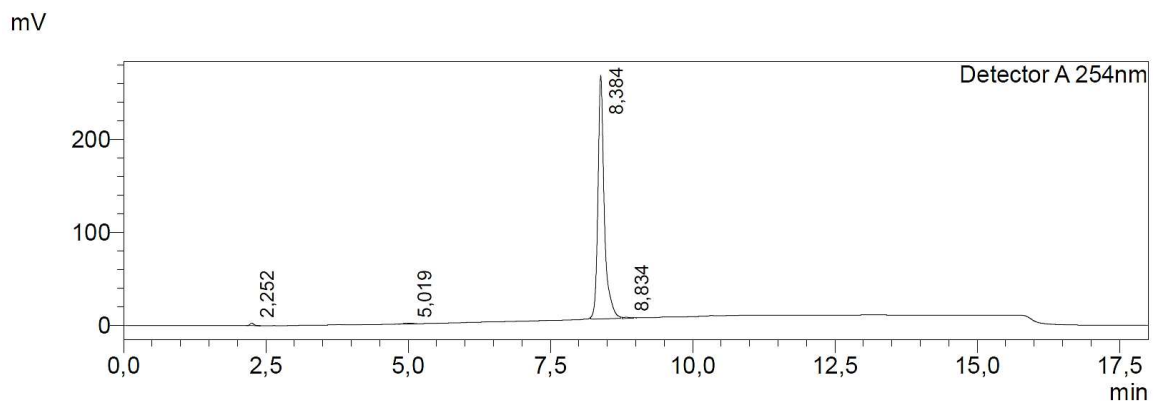


Peak#	Ret. Time	Area	Area%
1	2,250	12307	1,771
2	5,042	2192	0,315
3	6,892	1019	0,147
4	8,548	670450	96,483
5	9,117	2449	0,352
6	9,500	6472	0,931
Total		694889	100,000

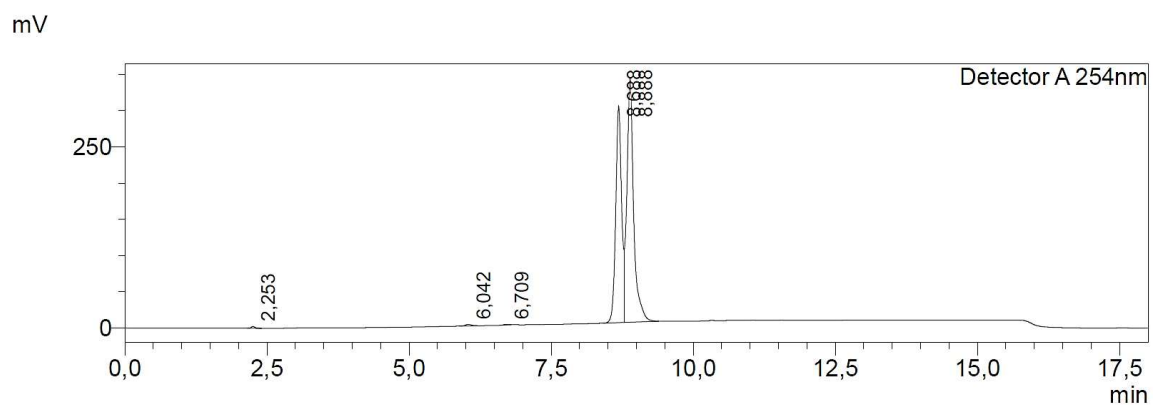
VIII Appendix



## VIII Appendix

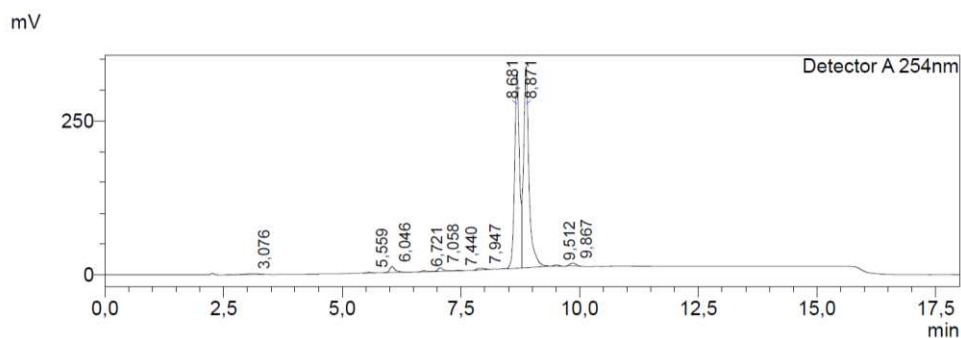
***R,S-10a*** $t_R = 8.38 \text{ min}$ ; Purity: 98.5%

Peak#	Ret. Time	Area	Area%
1	2,252	11672	0,567
2	5,019	6540	0,318
3	8,384	2027461	98,499
4	8,834	12691	0,617
Total		2058364	100,000

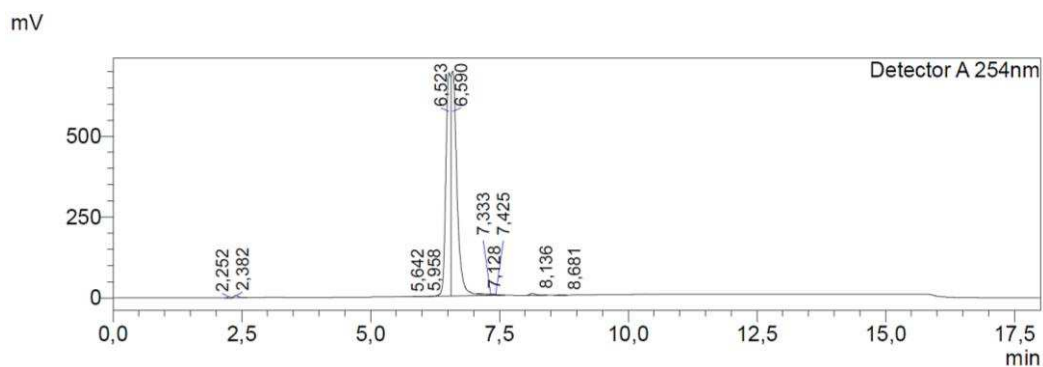
***S,R/S-10e*** $t_R = 8.69 \text{ min}, 8.89 \text{ min}$ ; Purity (*both diastereomers in total*): 99.3%

Peak#	Ret. Time	Area	Area%
1	2,253	11446	0,230
2	6,042	16579	0,333
3	6,709	5911	0,119
4	8,688	2135924	42,847
5	8,888	2815190	56,473
Total		4985051	100,000

## VIII Appendix

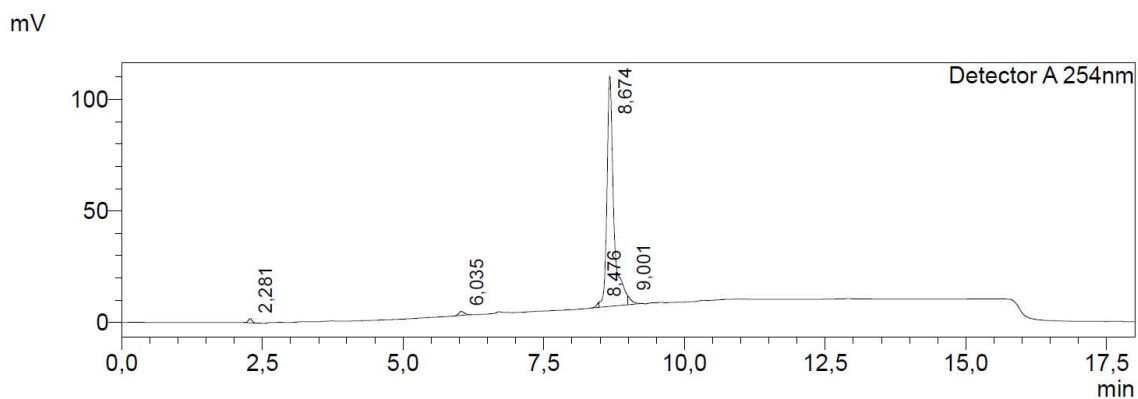
*R,R/S-10e* $t_R = 8.68 \text{ min}, 8.87 \text{ min}$ ; Purity (both diastereomers in total): 95.2%

Peak#	Ret. Time	Area	Area%
1	3,076	19199	0,378
2	5,559	7251	0,143
3	6,046	73637	1,449
4	6,721	11503	0,226
5	7,058	47196	0,929
6	7,440	6684	0,132
7	7,947	27313	0,538
8	8,681	2215348	43,600
9	8,871	2620782	51,580
10	9,512	12487	0,246
11	9,867	39646	0,780
Total		5081045	100,000

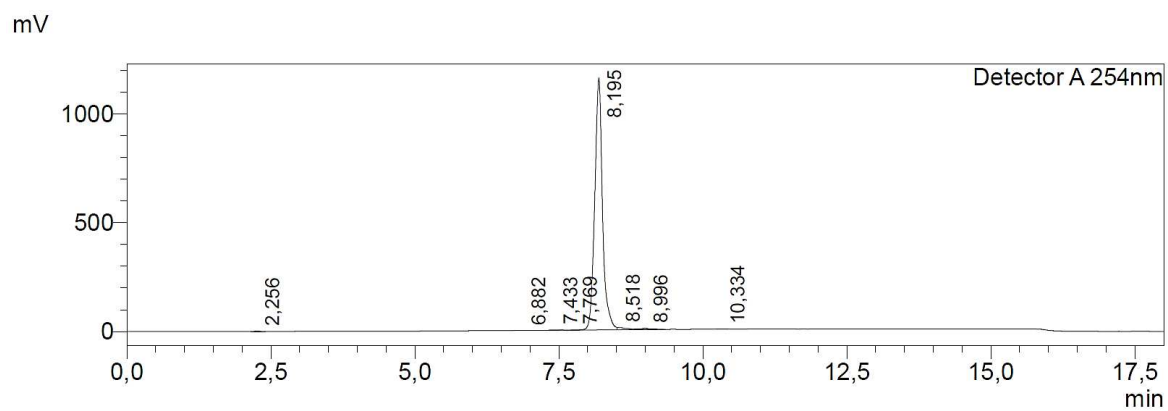
*S,R/S-10f* $t_R = 6.52 \text{ min}, 6.59 \text{ min}$ ; Purity (both diastereomers in total): 98.8%

Peak#	Ret. Time	Area	Area%
1	2,252	9955	0,098
2	2,382	34679	0,343
3	5,642	1333	0,013
4	5,958	1674	0,017
5	6,523	4439748	43,900
6	6,590	5555570	54,934
7	7,128	10700	0,106
8	7,333	3046	0,030
9	7,425	6515	0,064
10	8,136	44719	0,442
11	8,681	5285	0,052
Total		10113225	100,000

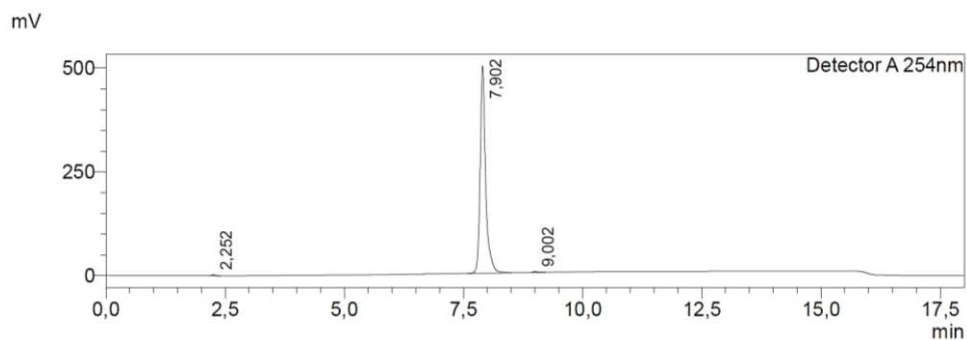
## VIII Appendix

*S,R-10e* $t_R = 8.67$  min; Purity: 95.1%

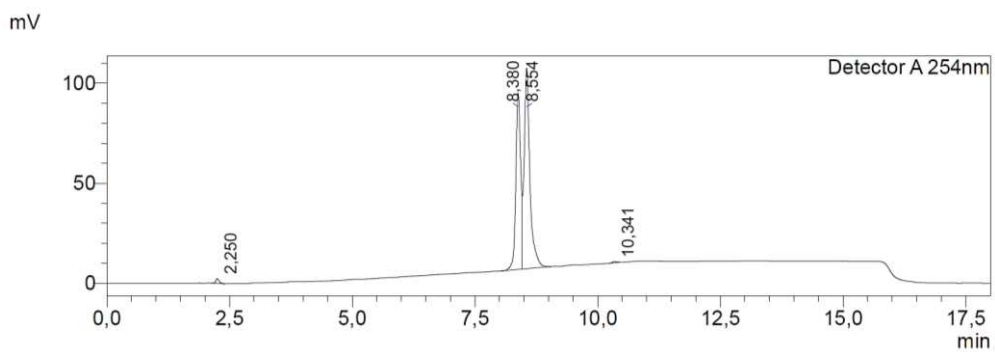
Peak#	Ret. Time	Area	Area%
1	2,281	8168	0,898
2	6,035	12849	1,413
3	8,476	6656	0,732
4	8,674	864919	95,136
5	9,001	16544	1,820
Total		909137	100,000

*S,R-21e* $t_R = 8.20$  min; Purity: 97.9%

Peak#	Ret. Time	Area	Area%
1	2,256	11048	0,099
2	6,882	4635	0,042
3	7,433	4543	0,041
4	7,769	16815	0,151
5	8,195	10896837	97,893
6	8,518	148831	1,337
7	8,996	45063	0,405
8	10,334	3566	0,032
Total		11131336	100,000

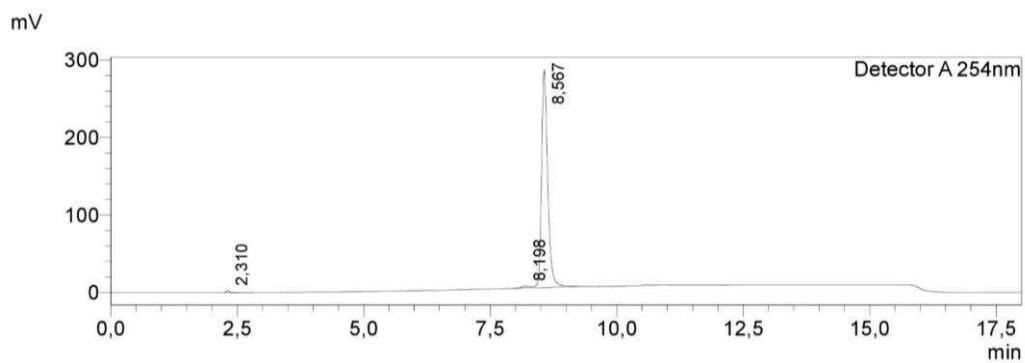
***S,R-21a*** $t_R = 7.90$  min; Purity: 99.3%

Peak#	Ret. Time	Area	Area%
1	2,252	11564	0,291
2	7,902	3951810	99,284
3	9,002	16944	0,426
Total		3980318	100,000

***R/S,S-10a*** $t_R = 8.38$  min,  $8.55$  min; Purity (both diastereomers in total): 99.0%

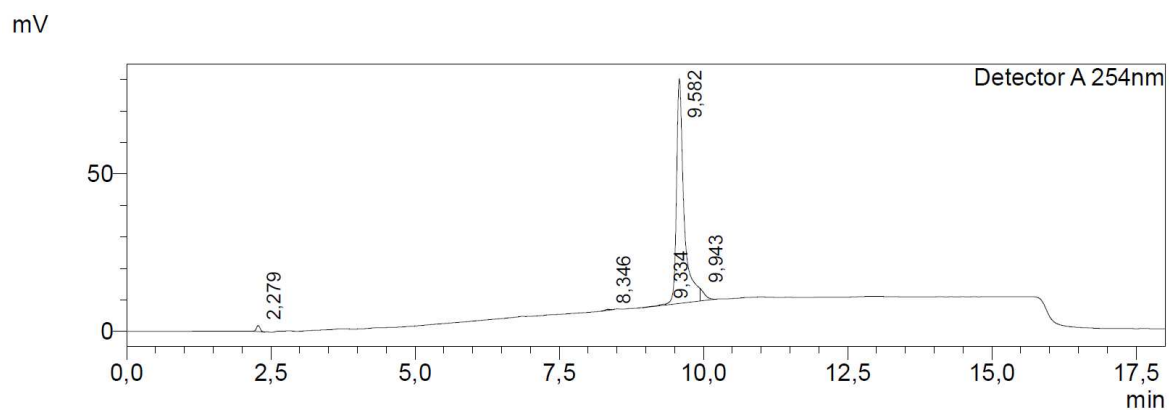
Peak#	Ret. Time	Area	Area%
1	2,250	11415	0,792
2	8,380	606765	42,081
3	8,554	820412	56,897
4	10,341	3321	0,230
Total		1441914	100,000

## 29 (NJS254)

 $t_R = 8.57$  min; Purity: 98.5%

Peak#	Ret. Time	Area	Area%
1	2,310	10021	0,411
2	8,198	25938	1,065
3	8,567	2400366	98,524
Total		2436325	100,000

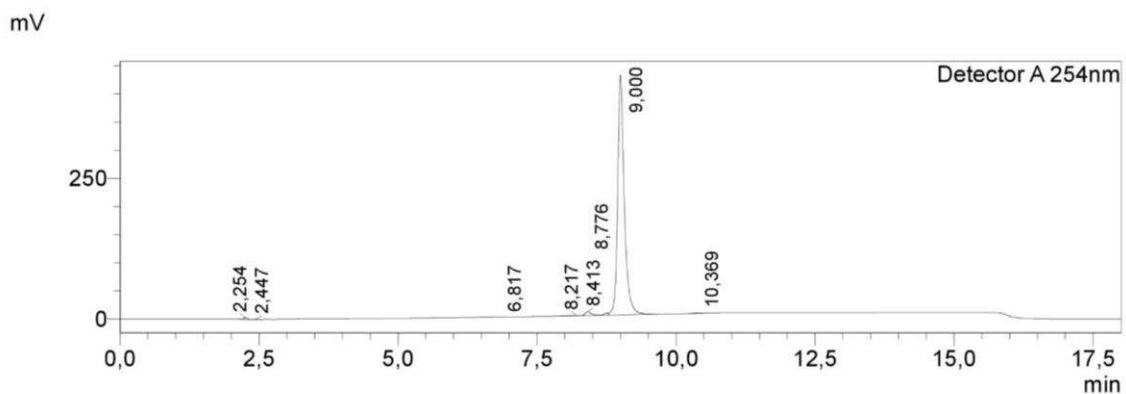
## S,S-25g

 $t_R = 9.58$  min; Purity: 95.0%

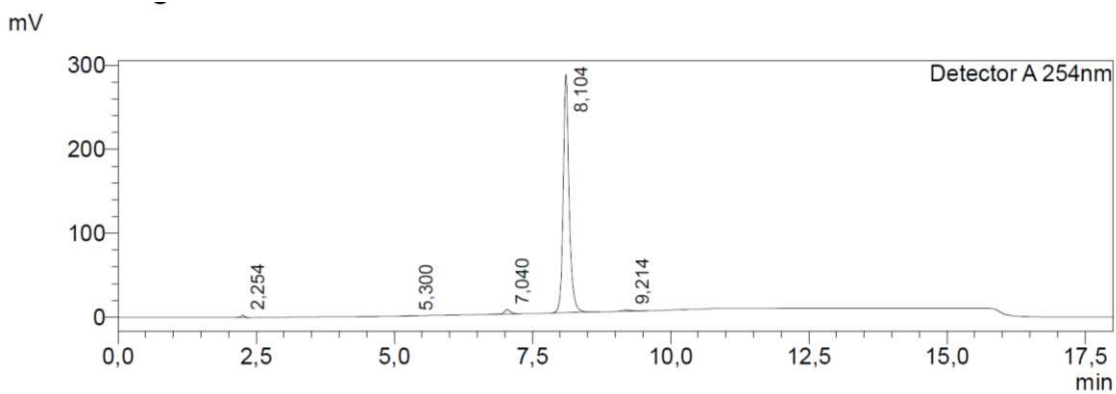
Peak#	Ret. Time	Area	Area%
1	2,279	8407	1,238
2	8,346	1735	0,255
3	9,334	2675	0,394
4	9,582	645500	95,025
5	9,943	20978	3,088
Total		679295	100,000



## VIII Appendix

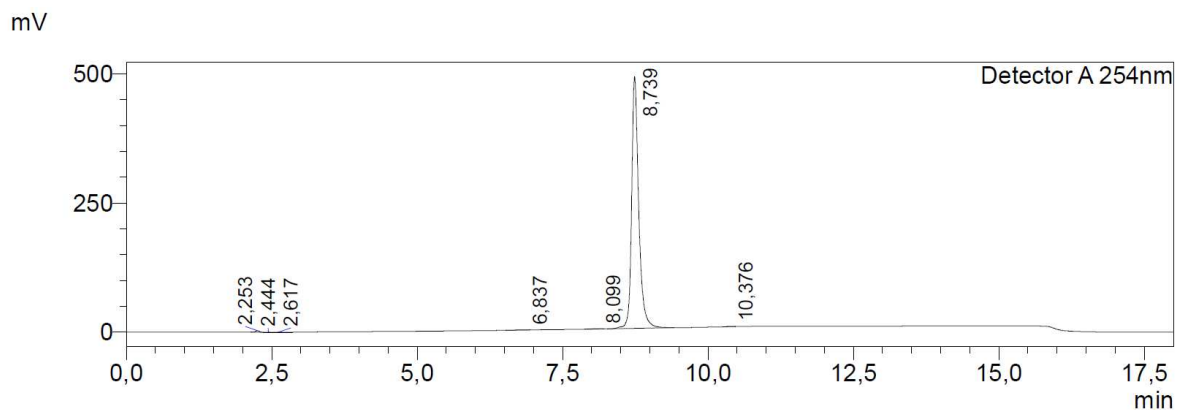
*S,S*-22g $t_R = 9.00$  min; Purity: 97.4%

Peak#	Ret. Time	Area	Area%
1	2,254	12191	0,336
2	2,447	1410	0,039
3	6,817	1616	0,045
4	8,217	4199	0,116
5	8,413	52654	1,450
6	8,776	20271	0,558
7	9,000	3536512	97,356
8	10,369	3706	0,102
Total		3632561	100,000

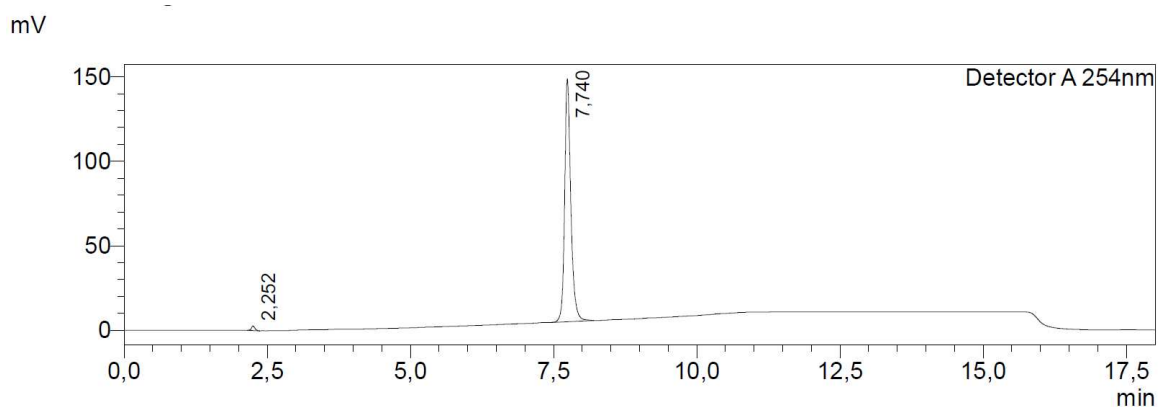
*S,S*-21g $t_R = 8.10$  min; Purity: 97.0%

Peak#	Ret. Time	Area	Area%
1	2,254	11063	0,505
2	5,300	2584	0,118
3	7,040	39509	1,804
4	8,104	2124285	97,002
5	9,214	12506	0,571
Total		2189946	100,000

## VIII Appendix

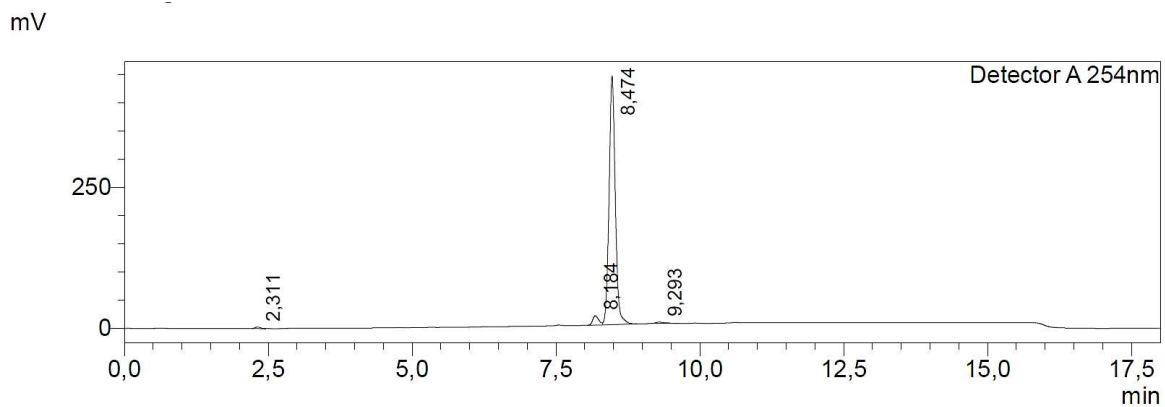
**S,S-22d** $t_R = 8.74$  min; Purity: 99.4%

Peak#	Ret. Time	Area	Area%
1	2,253	12195	0,294
2	2,444	1443	0,035
3	2,617	1098	0,026
4	6,837	2762	0,067
5	8,099	4291	0,104
6	8,739	4118792	99,402
7	10,376	2969	0,072
Total		4143551	100,000

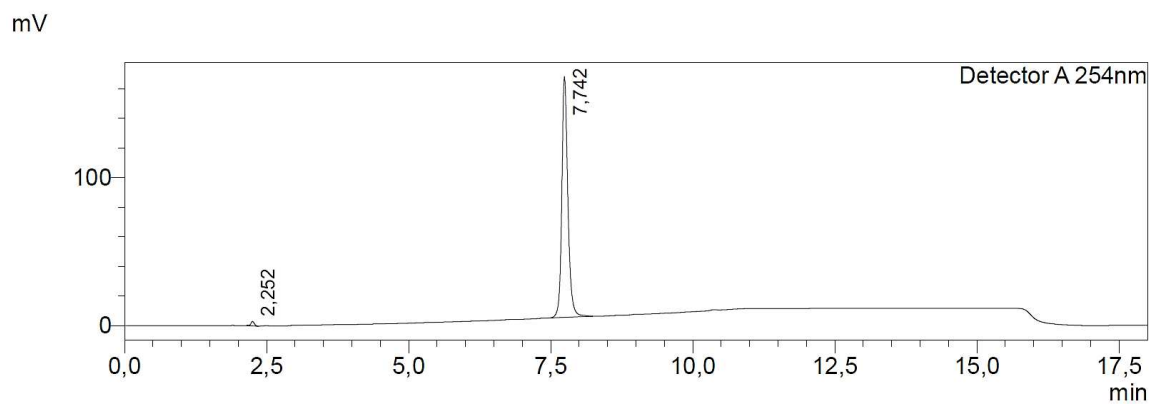
**S,S-21d** $t_R = 7.74$  min; Purity: 99.0%

Peak#	Ret. Time	Area	Area%
1	2,252	10693	0,979
2	7,740	1081655	99,021
Total		1092348	100,000

## VIII Appendix

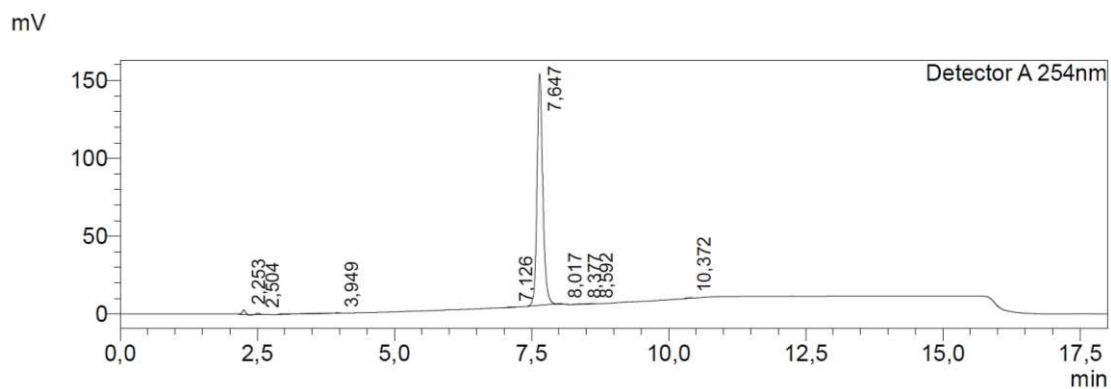
**S,R-10d** $t_R = 8.47$  min; Purity: 95.1%

Peak#	Ret. Time	Area	Area%
1	2,311	14929	0,429
2	8,184	120449	3,465
3	8,474	3304796	95,067
4	9,293	36118	1,039
Total		3476293	100,000

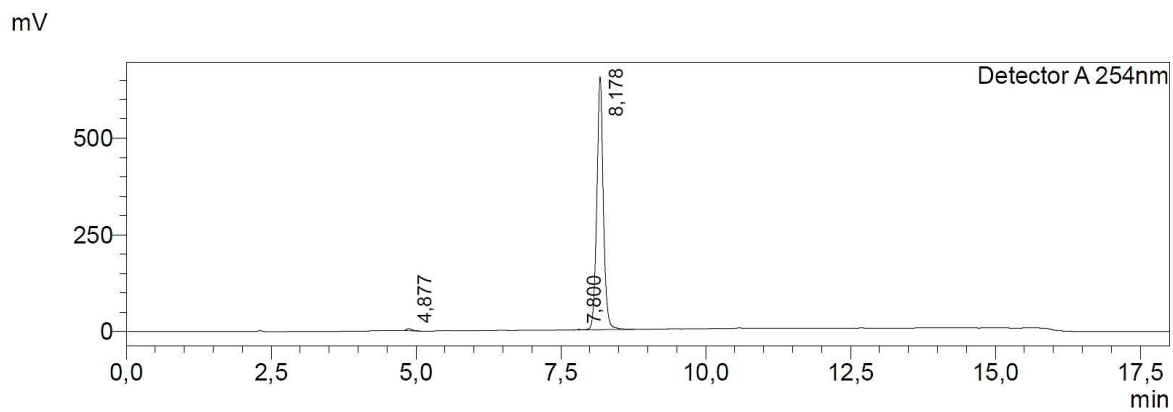
**S,S-21i** $t_R = 7.74$  min; Purity: 99.0%

Peak#	Ret. Time	Area	Area%
1	2,252	11828	0,966
2	7,742	1212328	99,034
Total		1224157	100,000

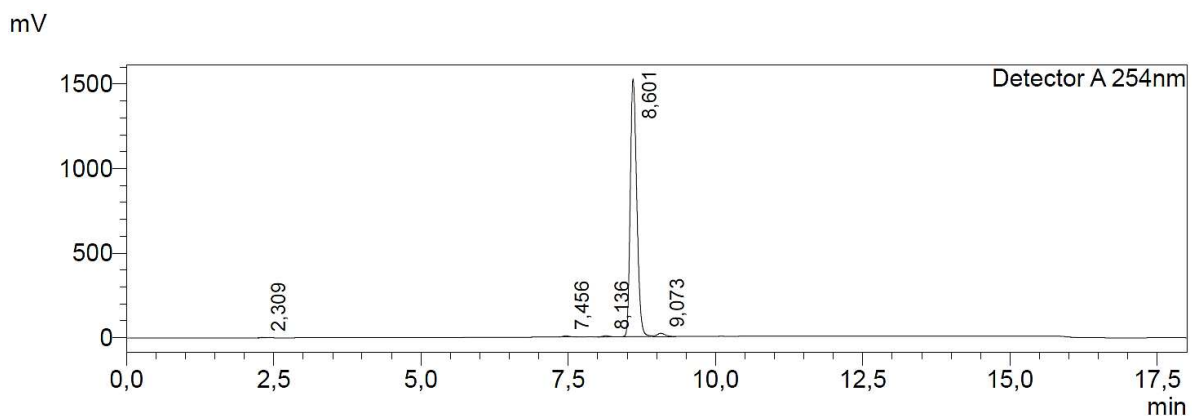
## VIII Appendix

**S,S-28i** $t_R = 7.65$  min; Purity: 96.9%

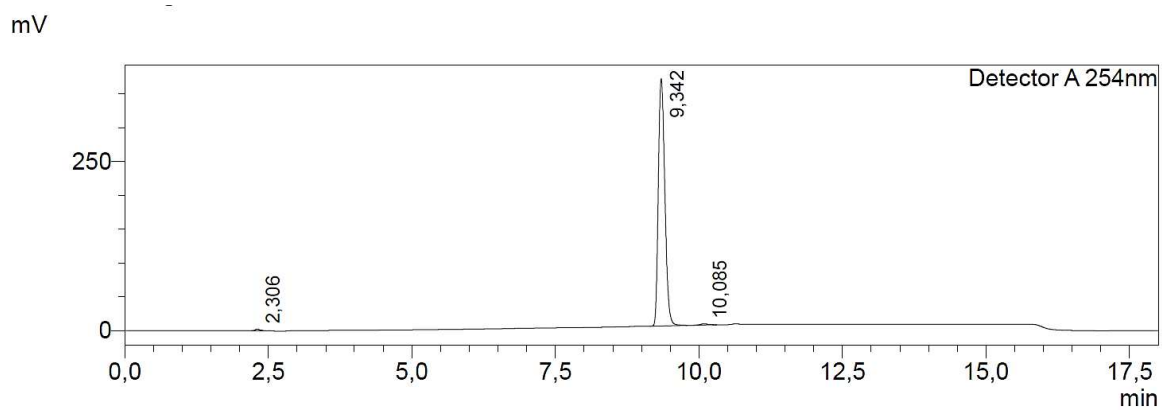
Peak#	Ret. Time	Area	Area%
1	2,253	12219	1,093
2	2,504	4597	0,411
3	3,949	7855	0,702
4	7,126	1814	0,162
5	7,647	1083438	96,879
6	8,017	2113	0,189
7	8,377	2126	0,190
8	8,592	1491	0,133
9	10,372	2685	0,240
Total		1118340	100,000

**S,S-21h** $t_R = 8.18$  min; Purity: 99.2%

Peak#	Ret. Time	Area	Area%
1	4,877	35022	0,677
2	7,800	8947	0,173
3	8,178	5132518	99,151
Total		5176487	100,000

**9\* (SF235)** $t_R = 8.60$  min, Purity: 97.7%

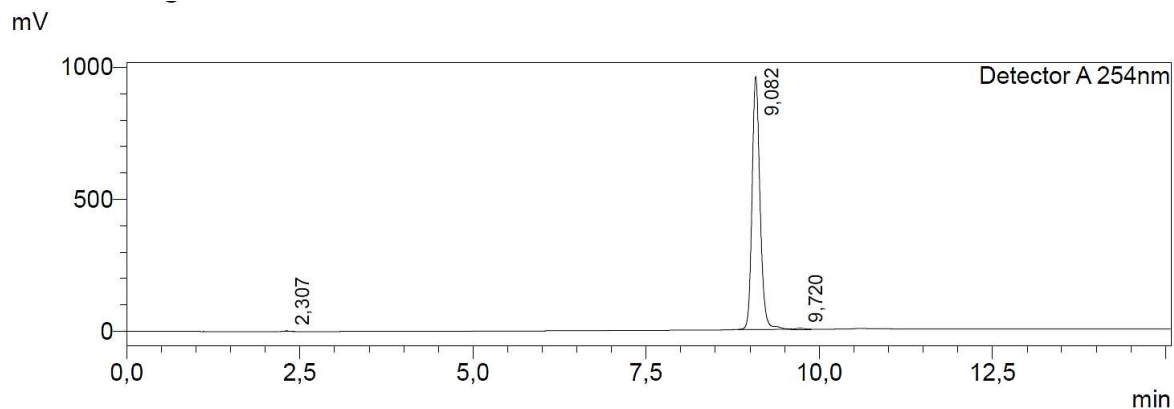
Peak#	Ret. Time	Area	Area%
1	2,309	9329	0,077
2	7,456	47420	0,392
3	8,136	47084	0,389
4	8,601	11822969	97,668
5	9,073	178457	1,474
Total		12105258	100,000

*\*side chain paper numbering***11\* (SF354)** $t_R = 9.34$  min, Purity: 99.0%

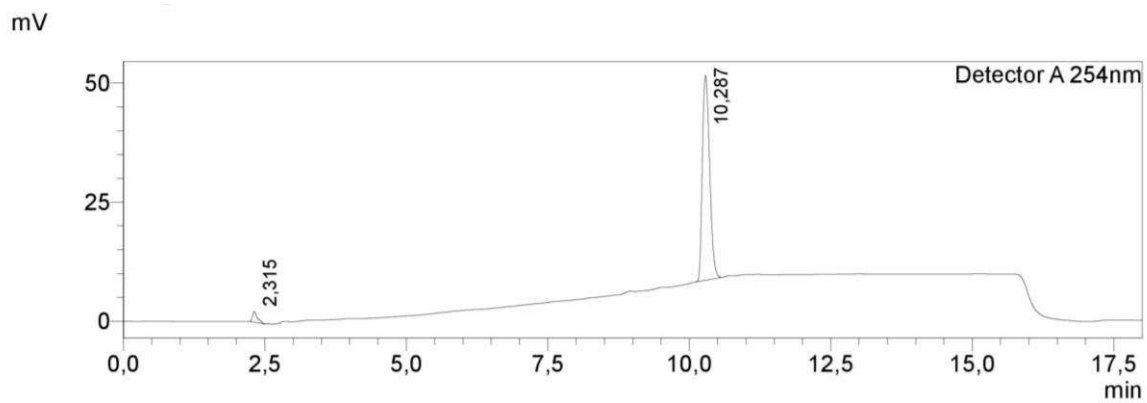
Peak#	Ret. Time	Area	Area%
1	2,306	12787	0,437
2	9,342	2892442	98,957
3	10,085	17686	0,605
Total		2922915	100,000

*\*side chain paper numbering*

## VIII Appendix

*R/S,S-22a* $t_R = 9.08$  min, Purity: 99.5%

Peak#	Ret. Time	Area	Area%
1	2,307	10118	0,131
2	9,082	7678910	99,455
3	9,720	31948	0,414
Total		7720976	100,000

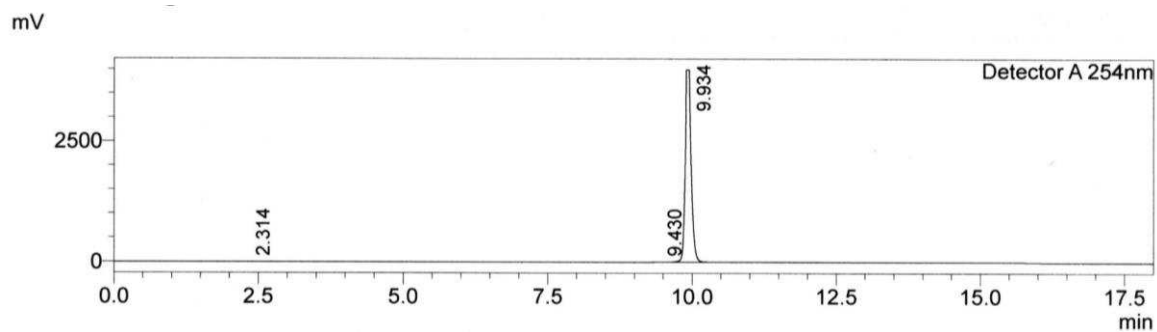
*47 (NJS175)* $t_R = 10.29$  min; Purity: 96.6%

Peak#	Ret. Time	Area	Area%
1	2,315	13677	3,396
2	10,287	389101	96,604
Total		402778	100,000

VIII Appendix

22 (NJS36)

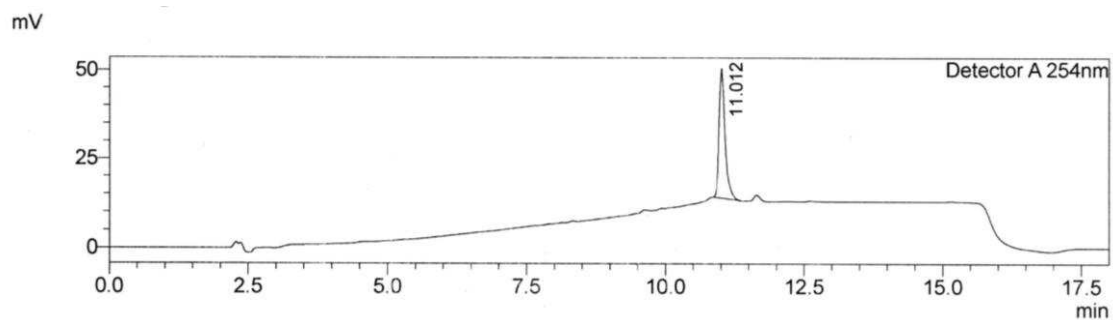
$t_R = 9.93$  min; Purity: 99.7%



Peak#	Ret. Time	Area	Height	Area%
1	2.314	45493	4437	0.160
2	9.430	32961	4776	0.116
3	9.934	28265815	3993519	99.723
Total		28344269	4002732	100.000

11 (NJS25)

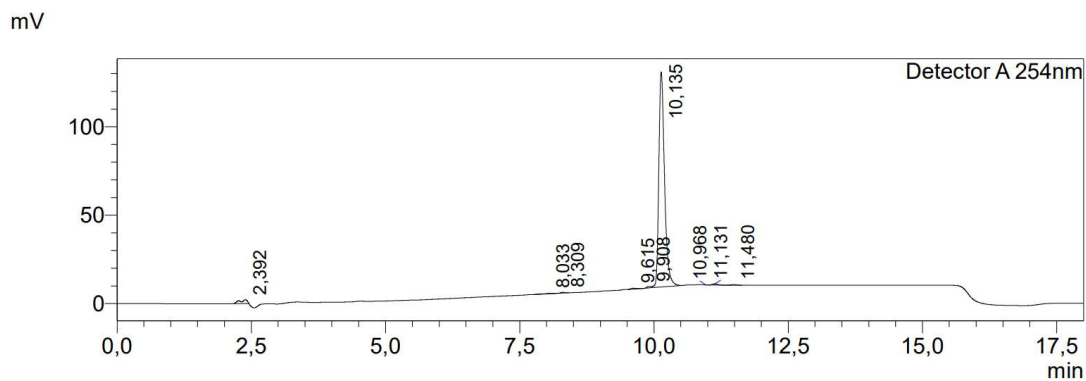
$t_R = 11.01$  min; Purity: >99%



Peak#	Ret. Time	Area	Height	Area%
1	11.012	274493	36605	100.000
Total		274493	36605	100.000

12 (NJS28)

$t_R = 10.14$  min; Purity: 95.7 %

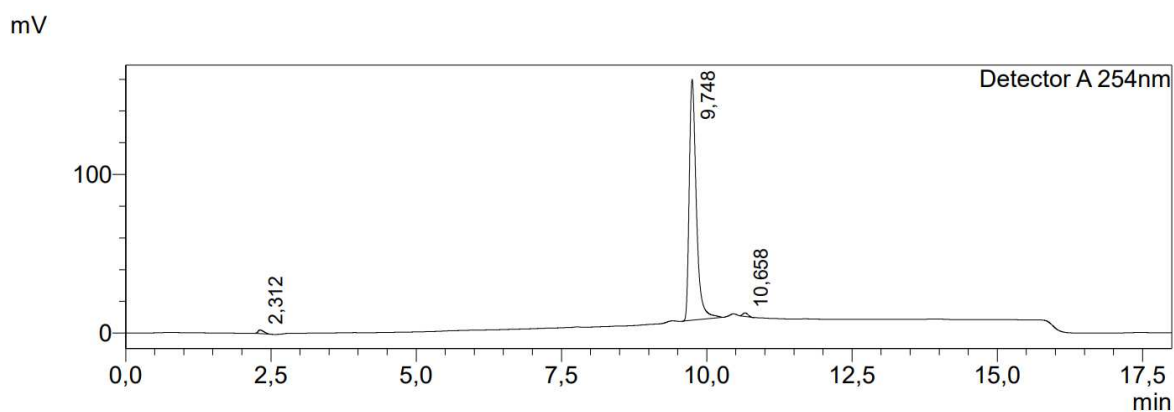


VIII Appendix

Peak#	Ret. Time	Area	Area%
1	2,392	20567	2,196
2	8,033	2962	0,316
3	8,309	2510	0,268
4	9,615	3596	0,384
5	9,908	4512	0,482
6	10,135	896062	95,688
7	10,968	-11	-0,001
8	11,131	4186	0,447
9	11,480	2060	0,220
Total		936443	100,000

32 (NJS205)

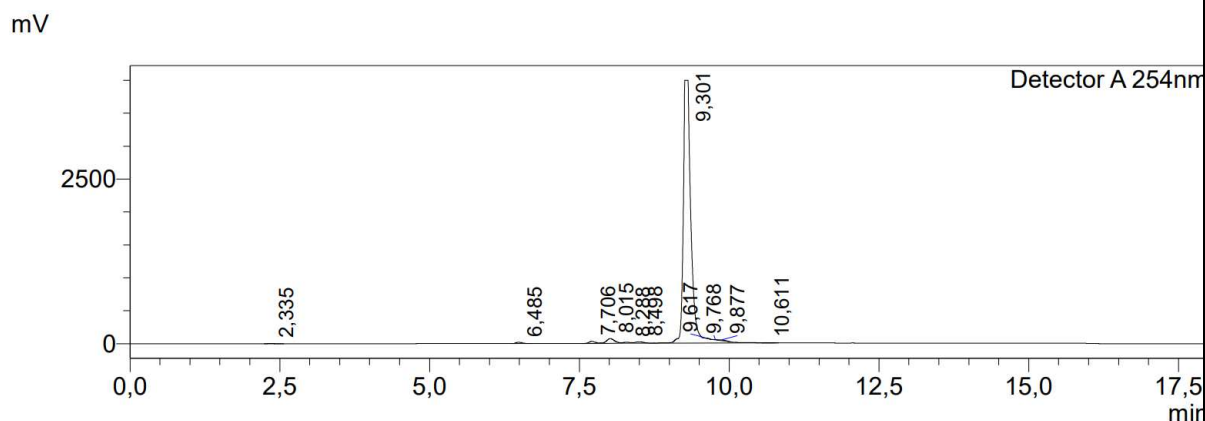
$t_R = 9.75$  min; Purity: 95.7 %



Peak#	Ret. Time	Area	Area%
1	2,312	15358	1,168
2	9,748	1285520	97,774
3	10,658	13905	1,058
Total		1314782	100,000

31 (NJS166)

$t_R = 9.30$  min; Purity: 95.9 %



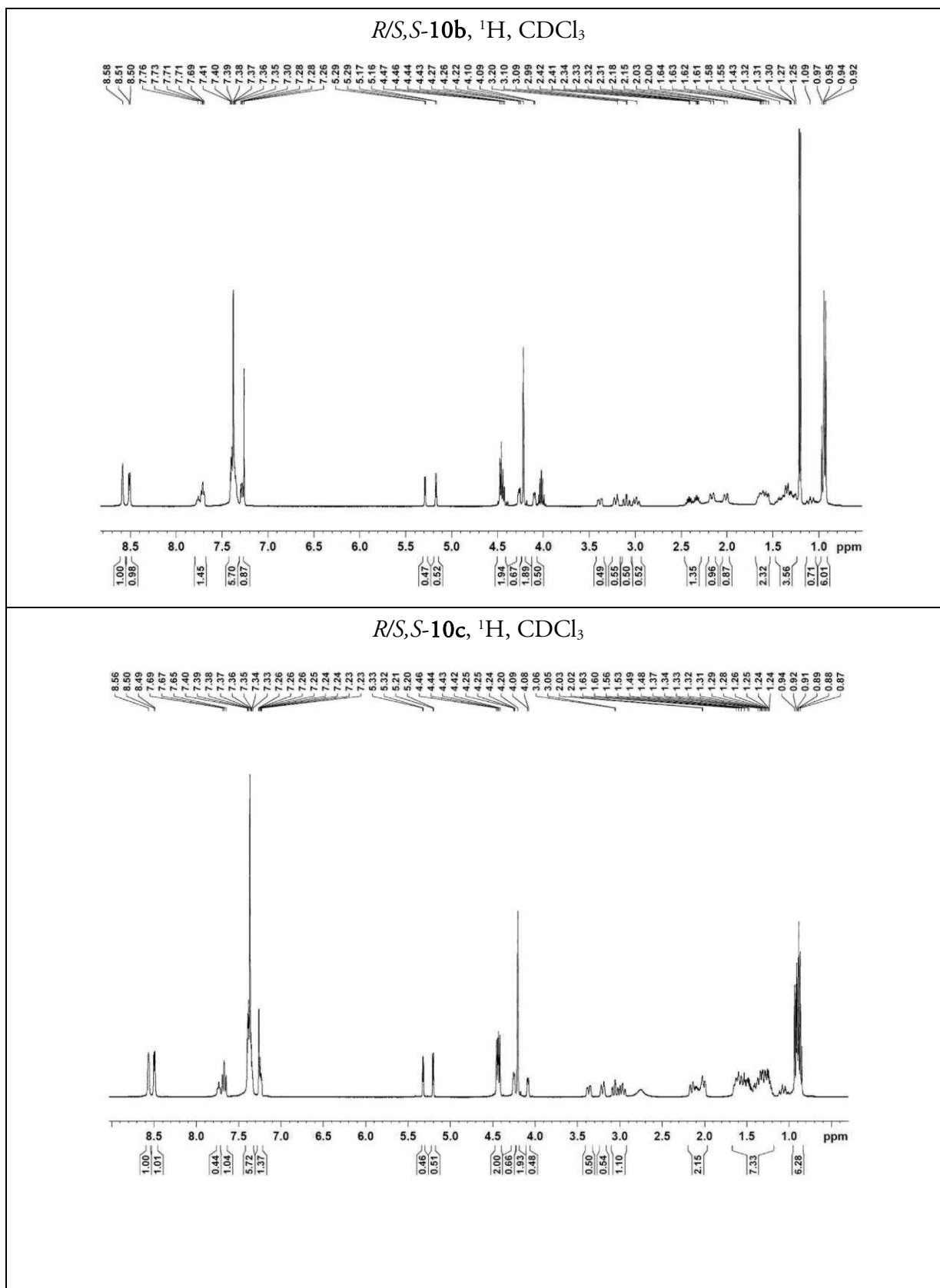


## VIII Appendix

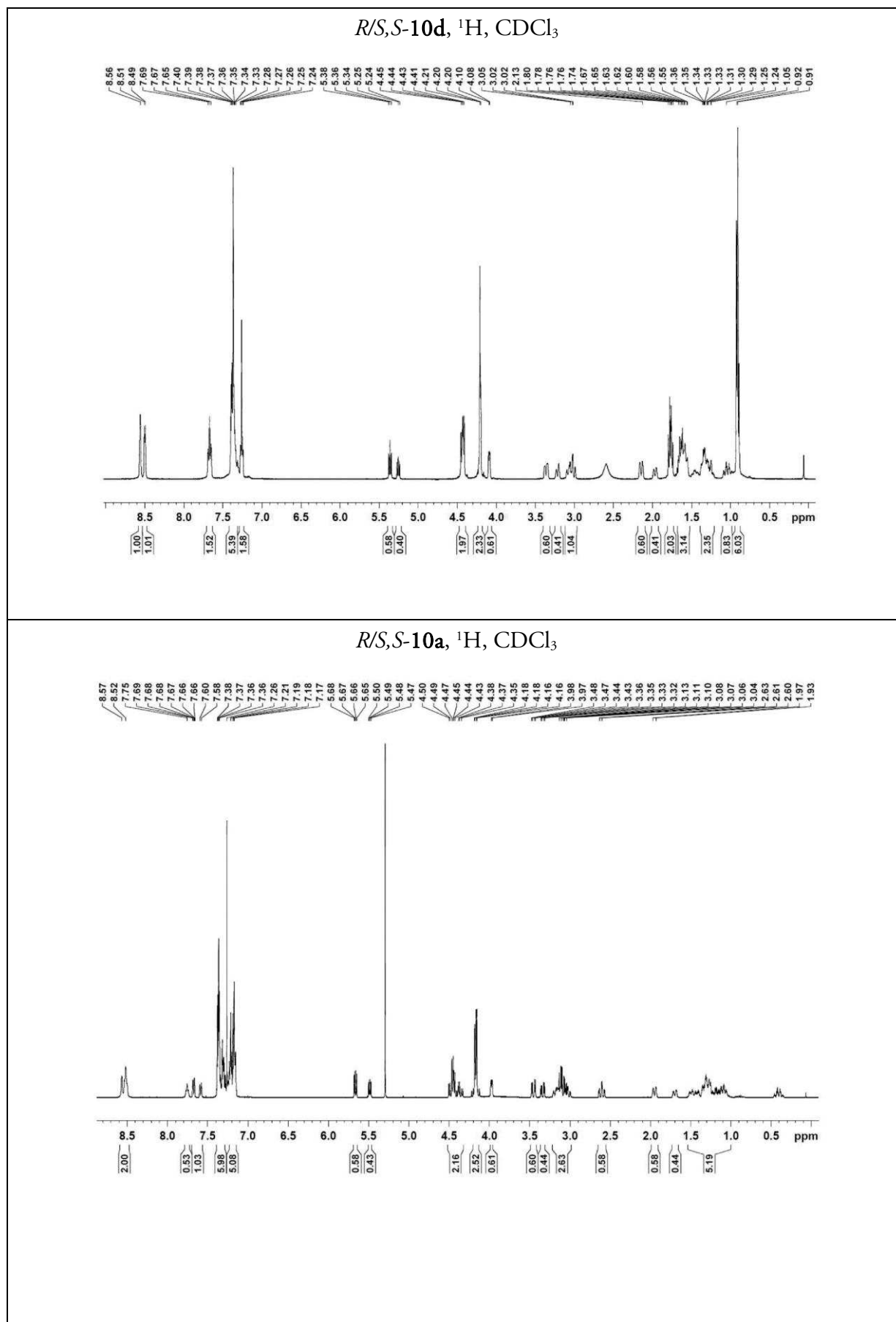
Peak#	Ret. Time	Area	Area%
1	2,335	18586	0,050
2	6,485	130132	0,349
3	7,706	216917	0,582
4	8,015	668408	1,792
5	8,288	134340	0,360
6	8,498	215477	0,578
7	9,301	35756020	95,858
8	9,617	27811	0,075
9	9,768	42961	0,115
10	9,877	84798	0,227
11	10,611	5653	0,015
Total		37301103	100,000

2  $^1\text{H}$  NMR Spectra

NMR spectra of the FP paper (*SLAS Discovery*), including the spectrum of probe **30** (*NJS106*), can be found in chapter III\_2.8.2.

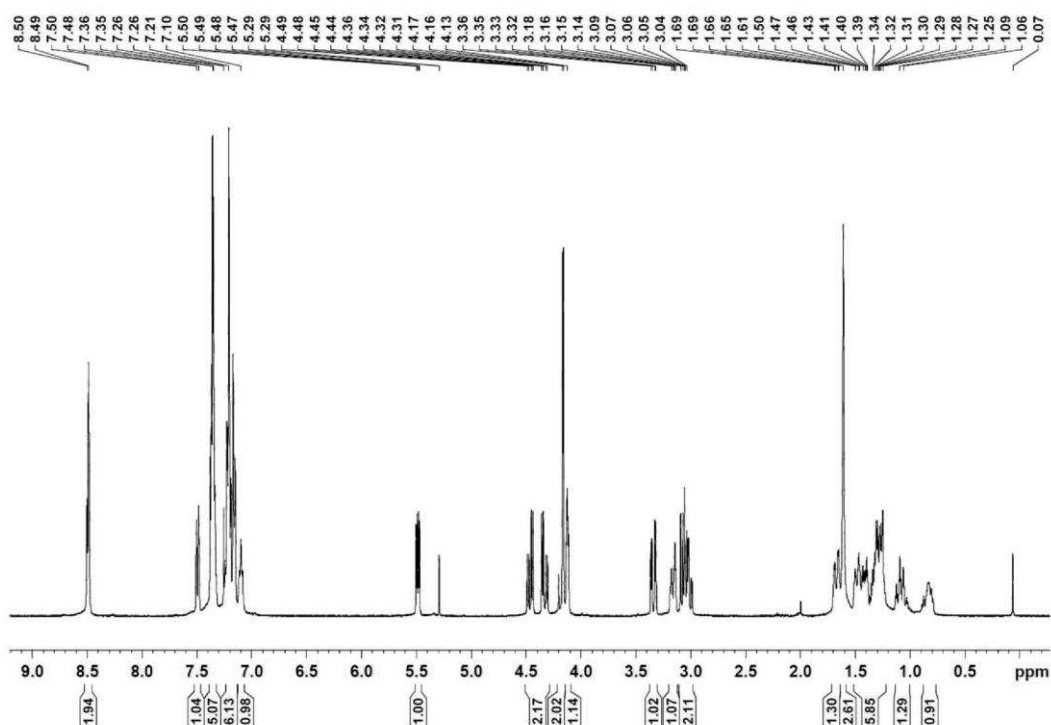


## VIII Appendix

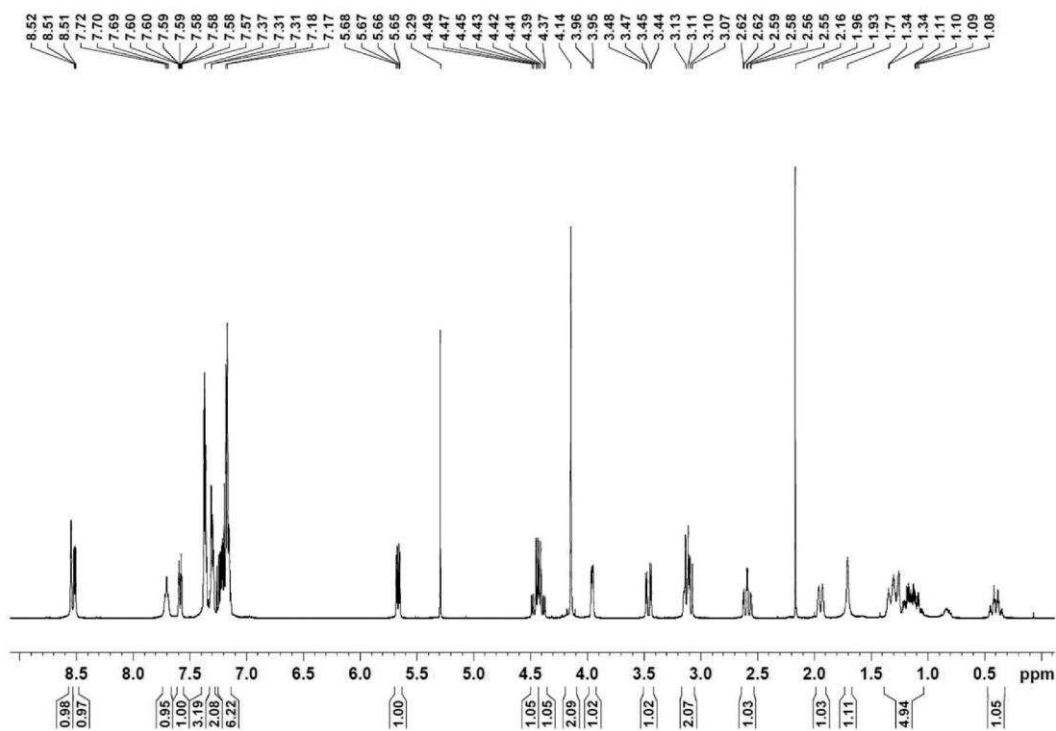


VIII Appendix

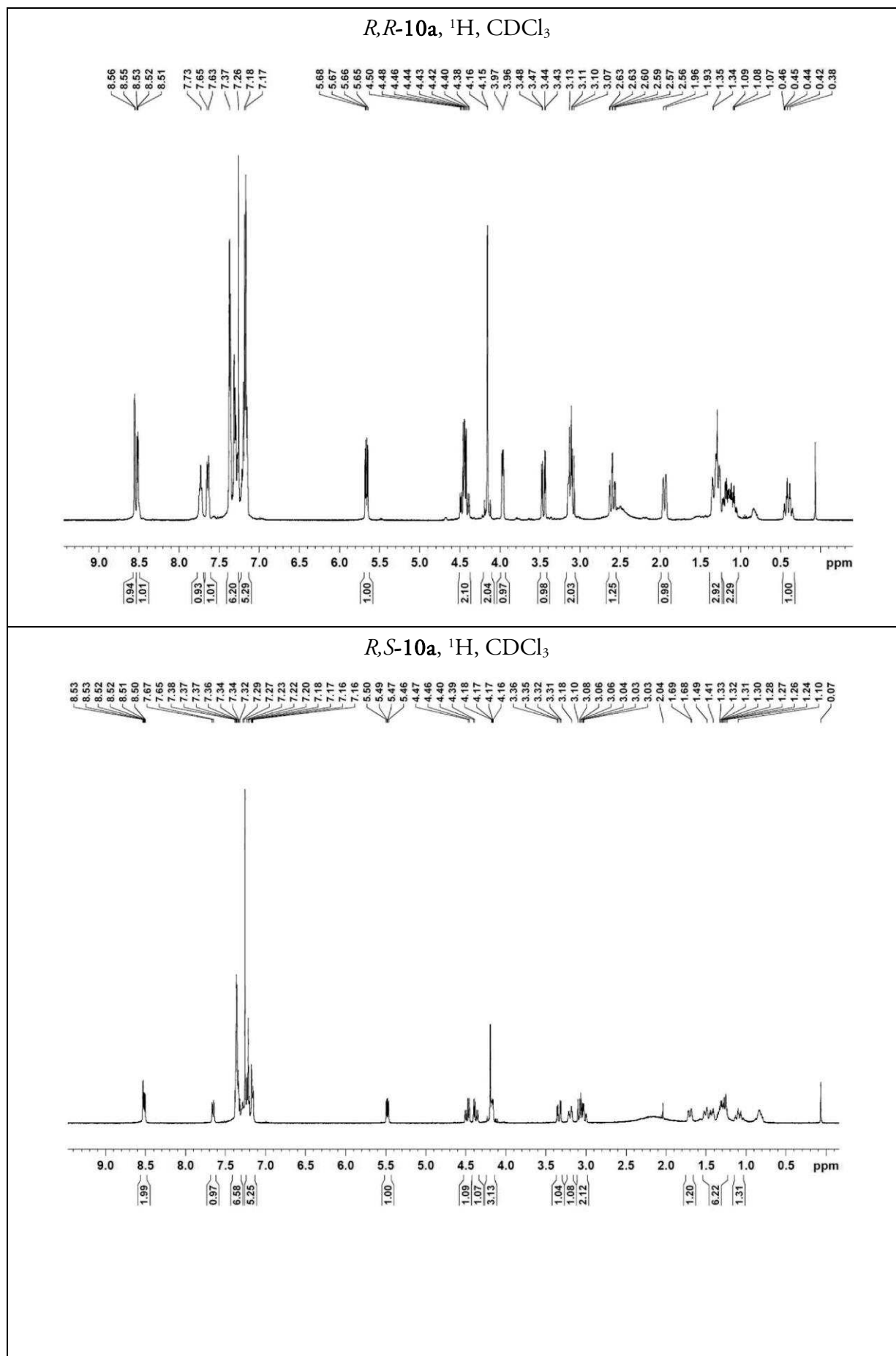
*S,R*-10a, <sup>1</sup>H, CDCl<sub>3</sub>



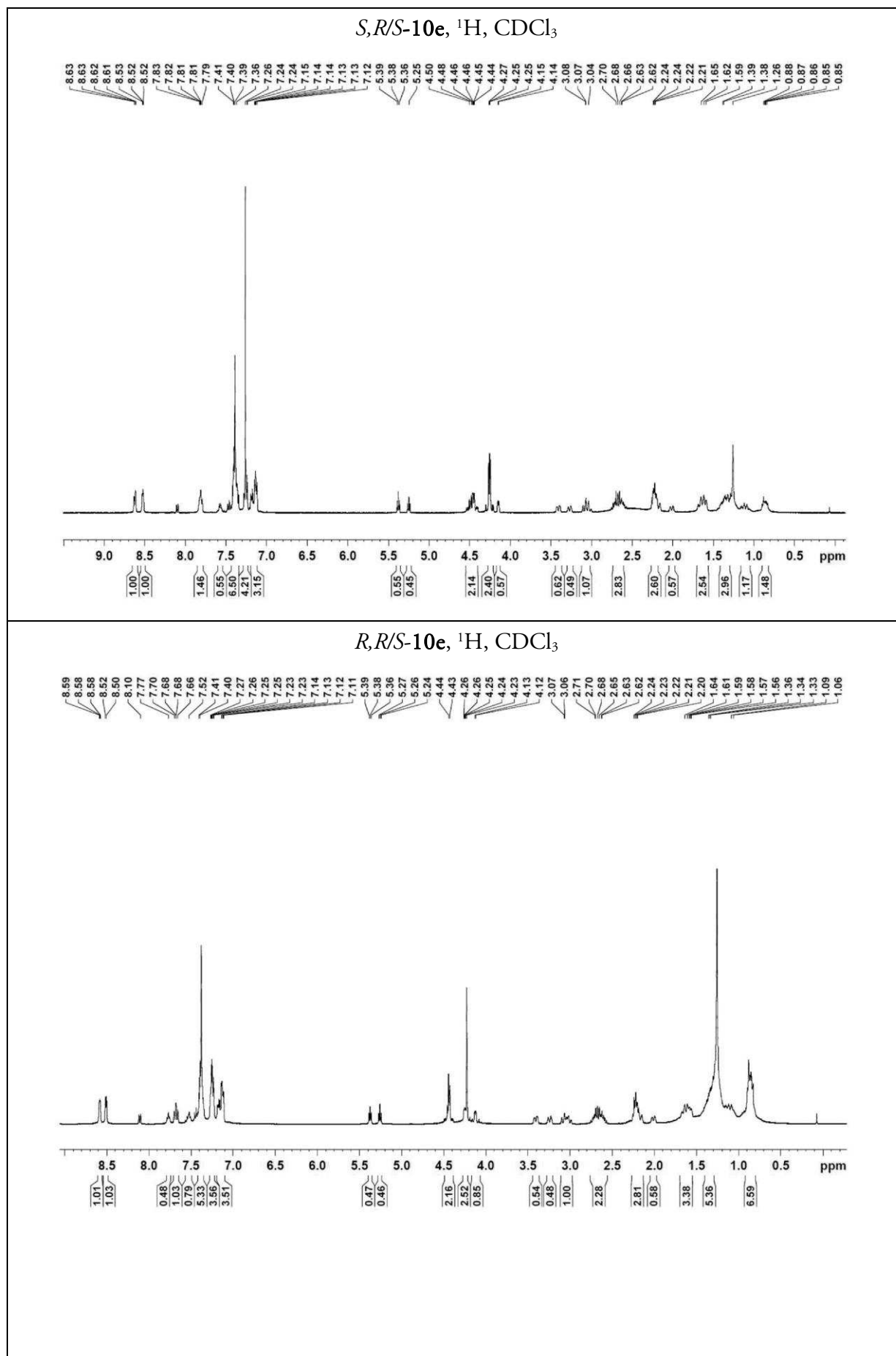
*S,S*-10a, <sup>1</sup>H, CDCl<sub>3</sub>



## VIII Appendix

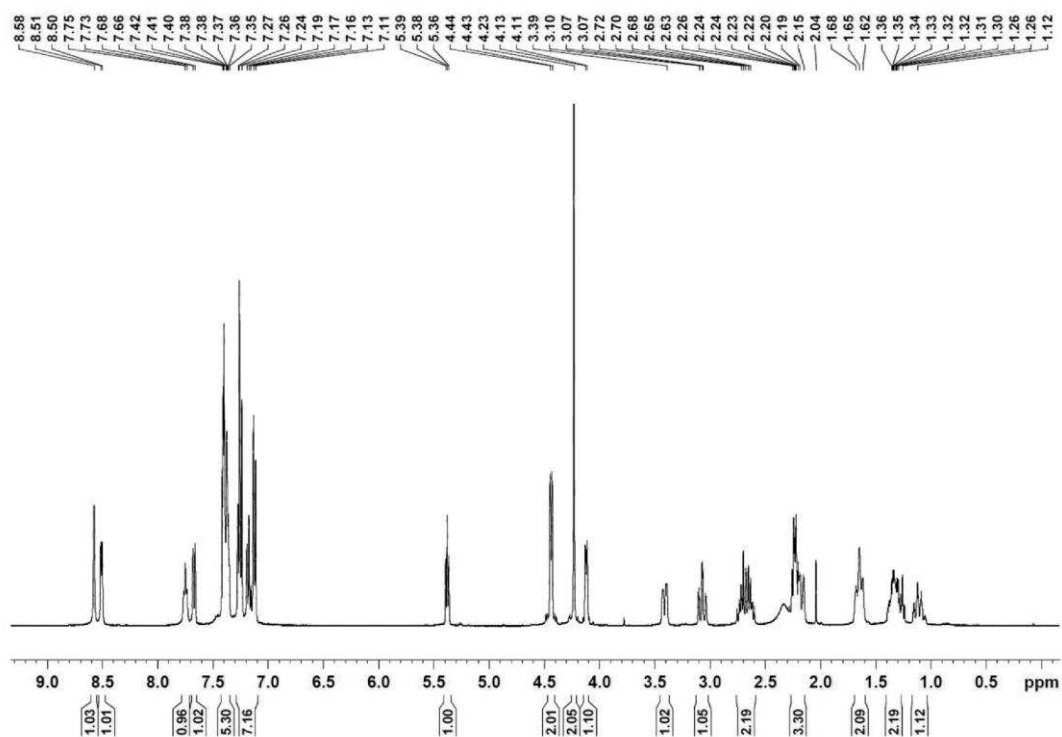


## VIII Appendix

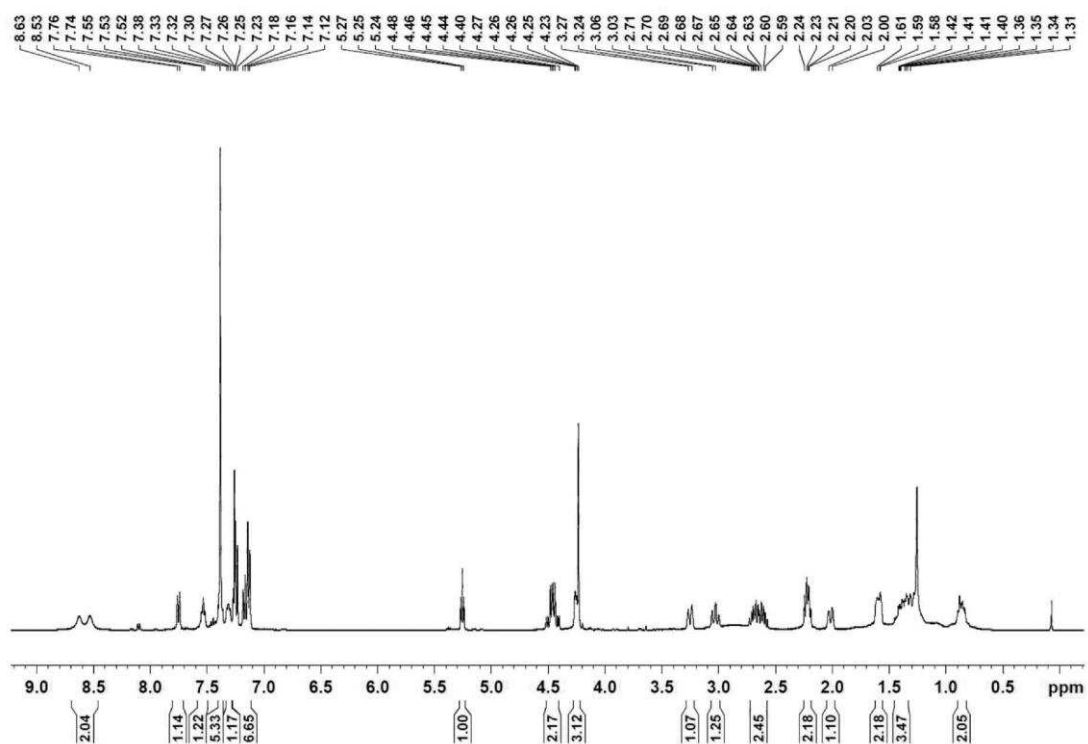


VIII Appendix

*S,S*-10e, <sup>1</sup>H, CDCl<sub>3</sub>

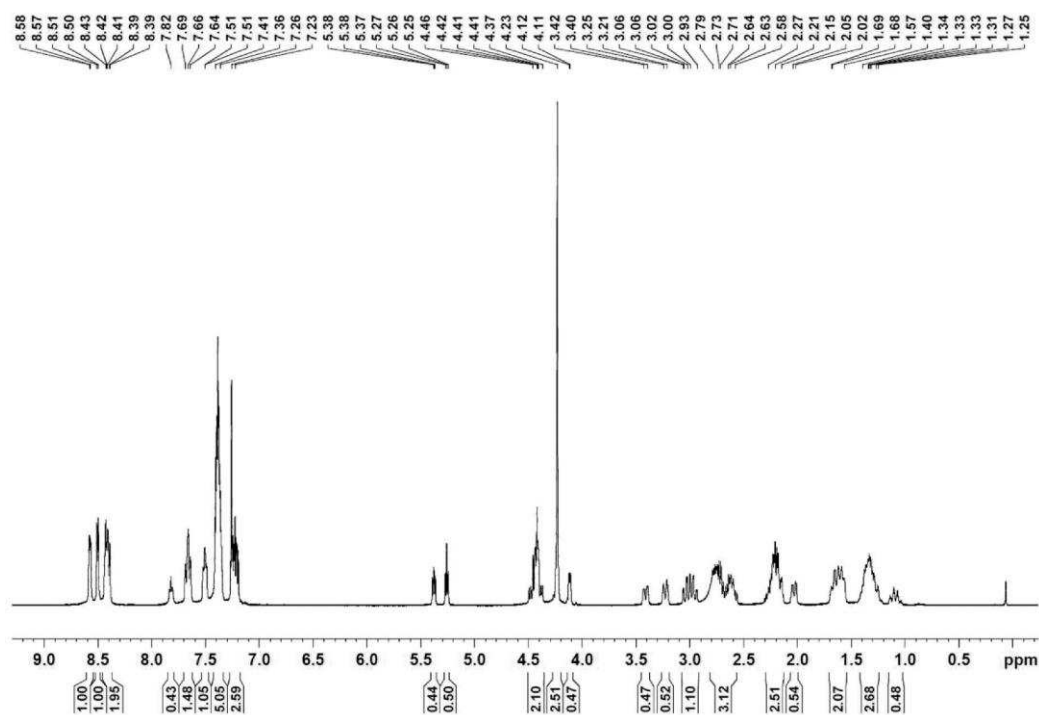


*S,R*-10e, <sup>1</sup>H, CDCl<sub>3</sub>

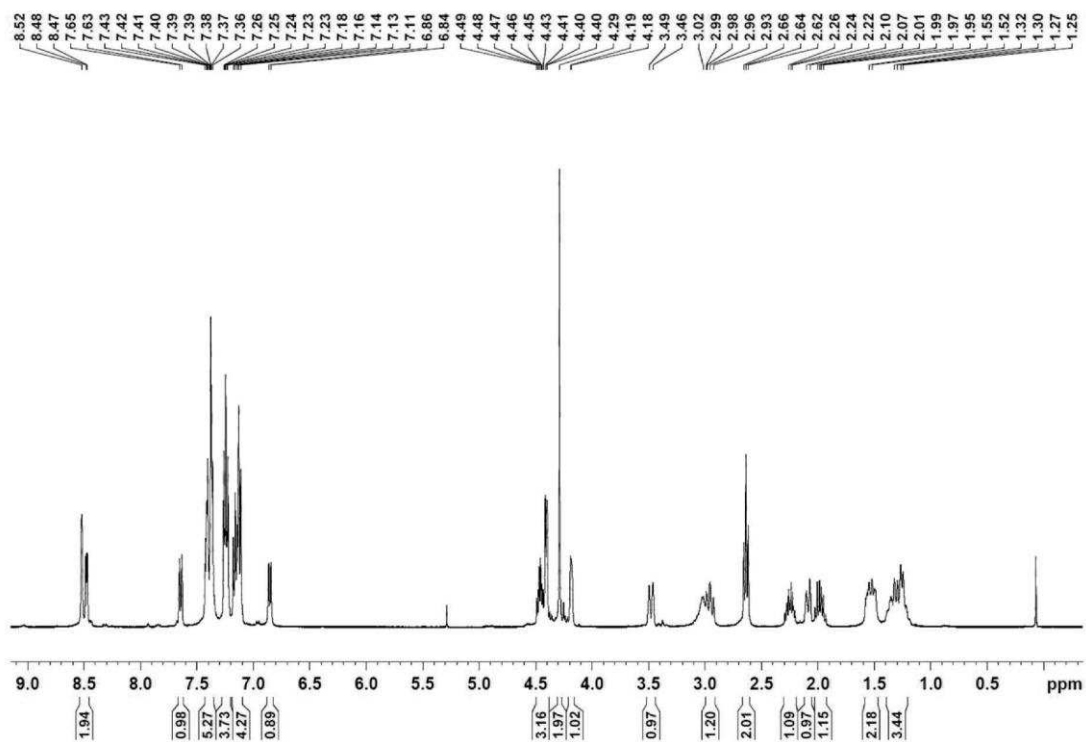


VIII Appendix

*S,S*-10f, <sup>1</sup>H, CDCl<sub>3</sub>



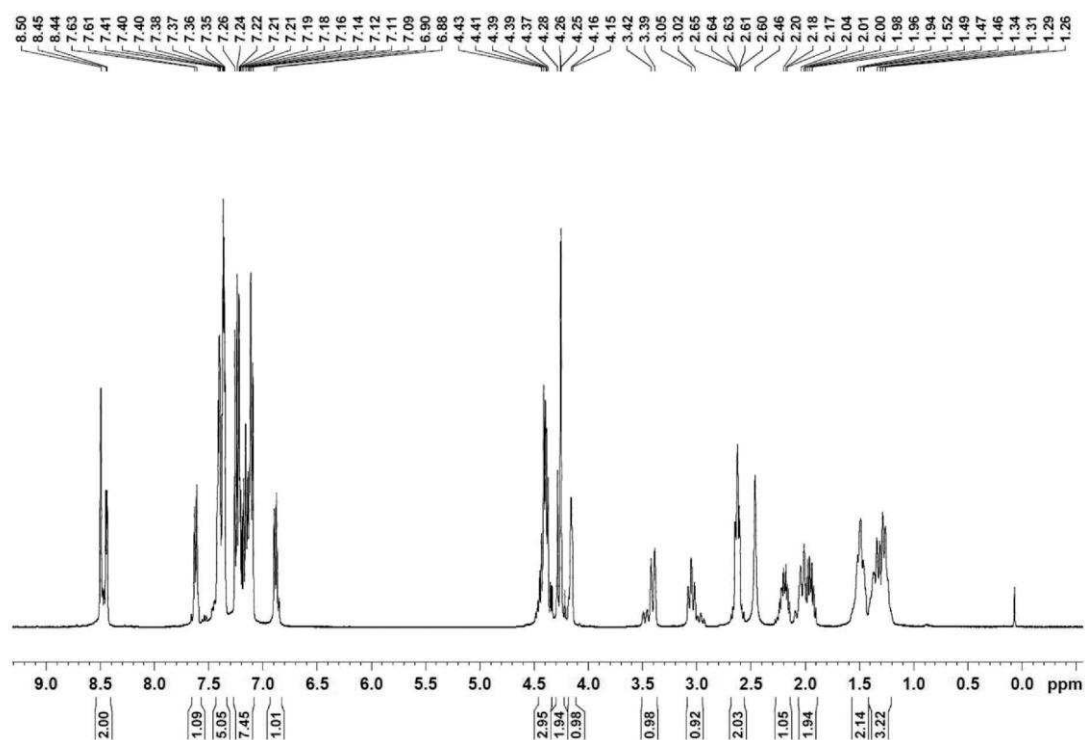
*S,S*-21e, <sup>1</sup>H, CDCl<sub>3</sub>



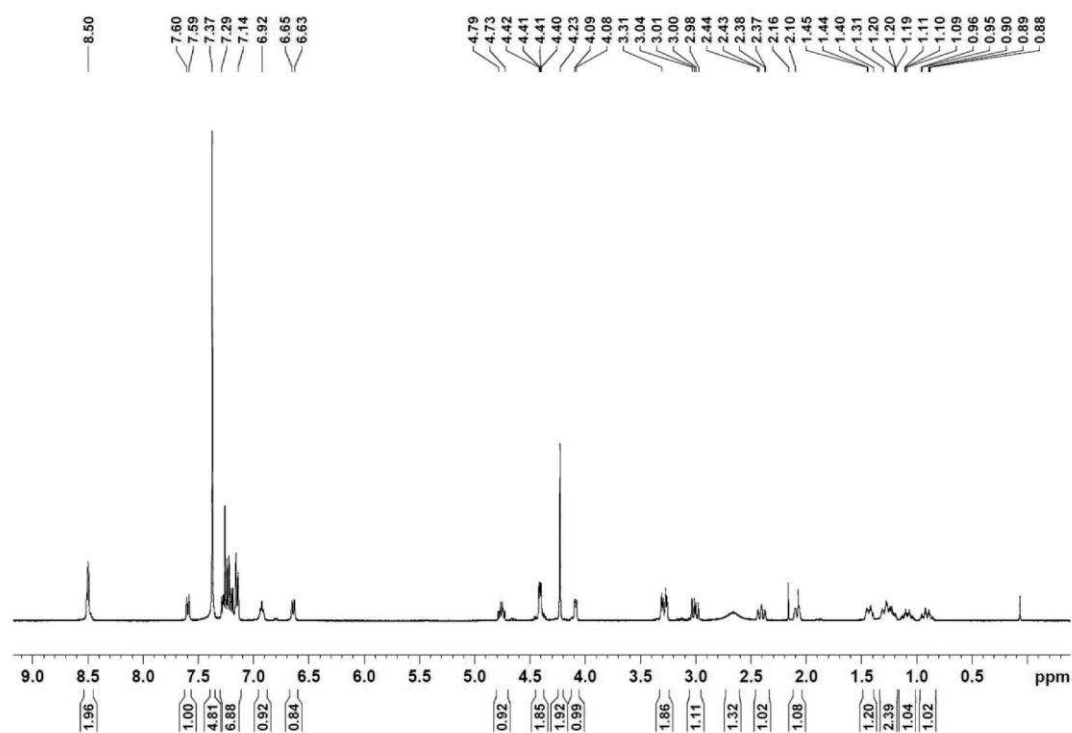


VIII Appendix

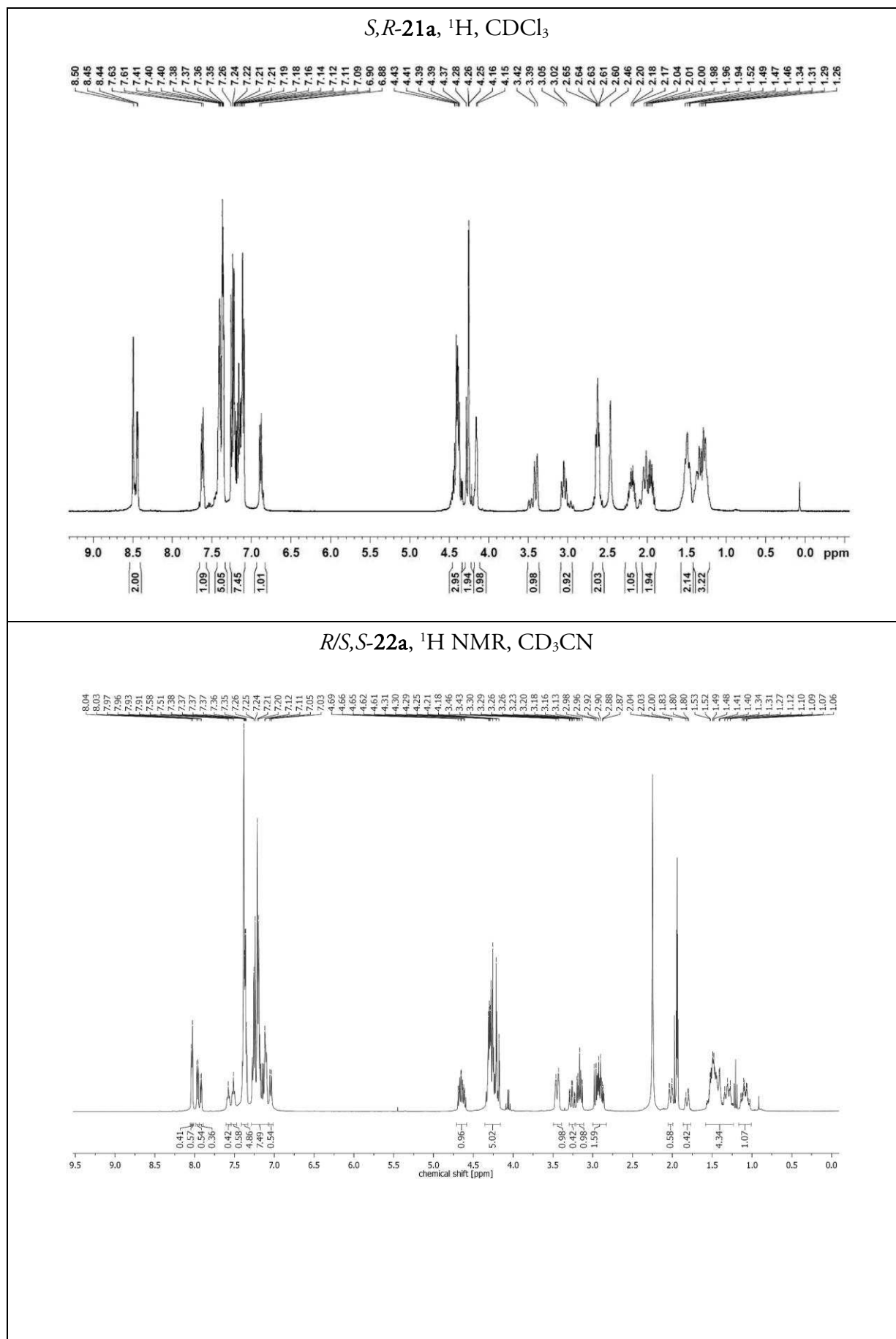
*S,R*-21e,  $^1\text{H}$ ,  $\text{CDCl}_3$



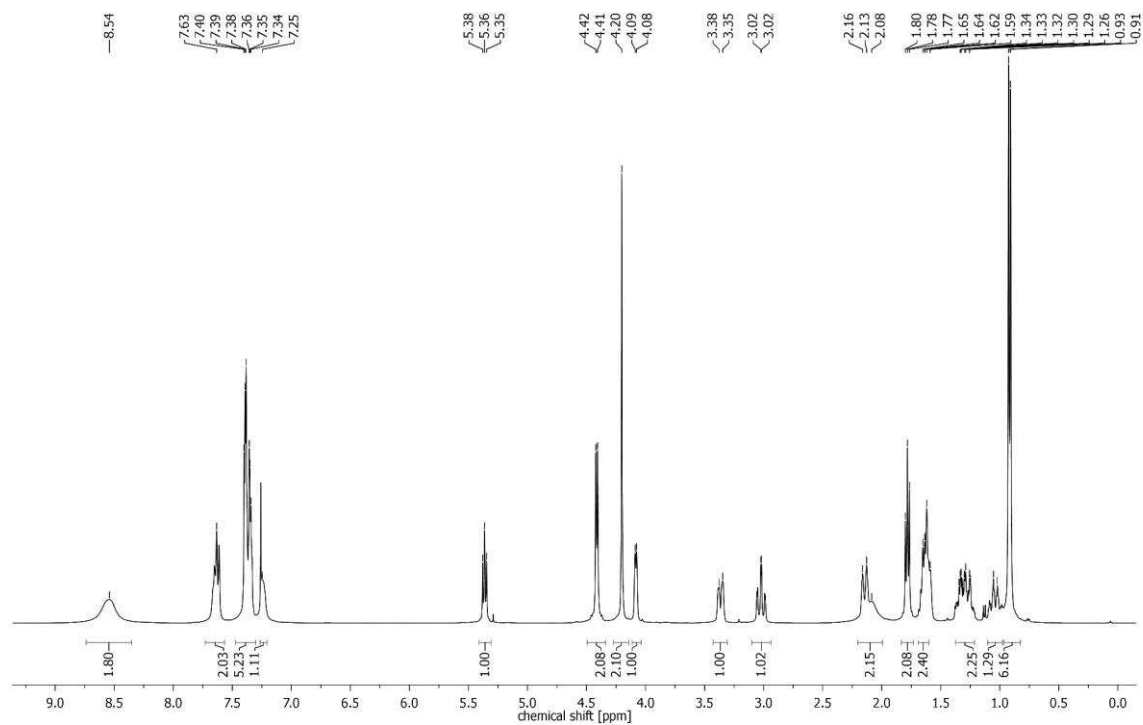
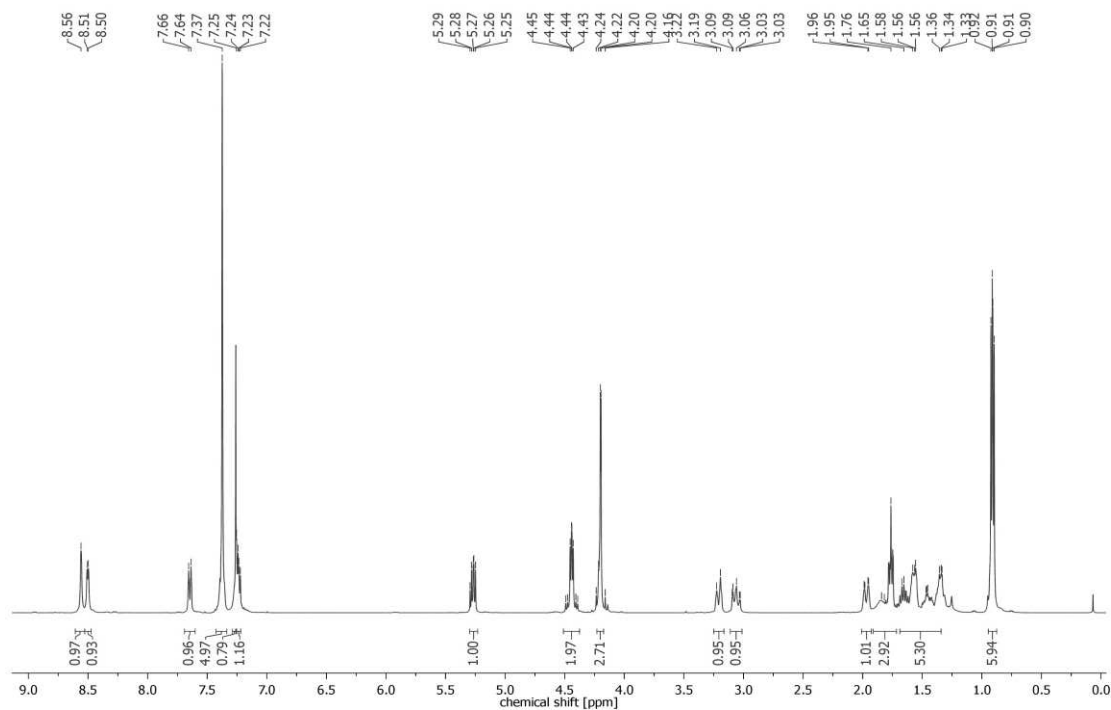
*S,S*-21a,  $^1\text{H}$ ,  $\text{CDCl}_3$



## VIII Appendix

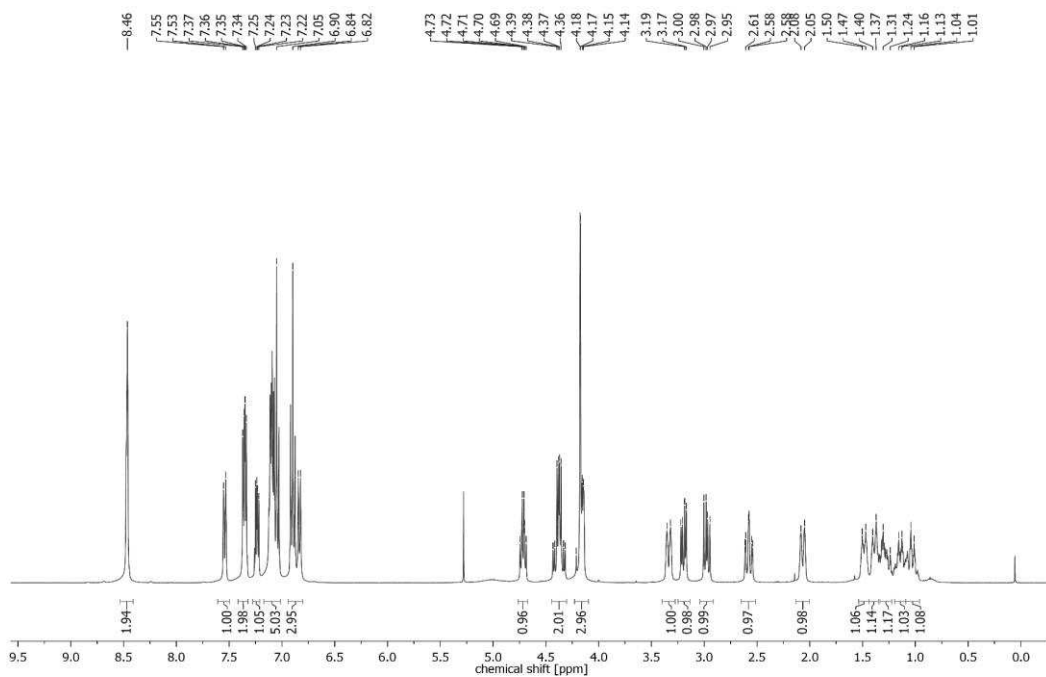


## VIII Appendix

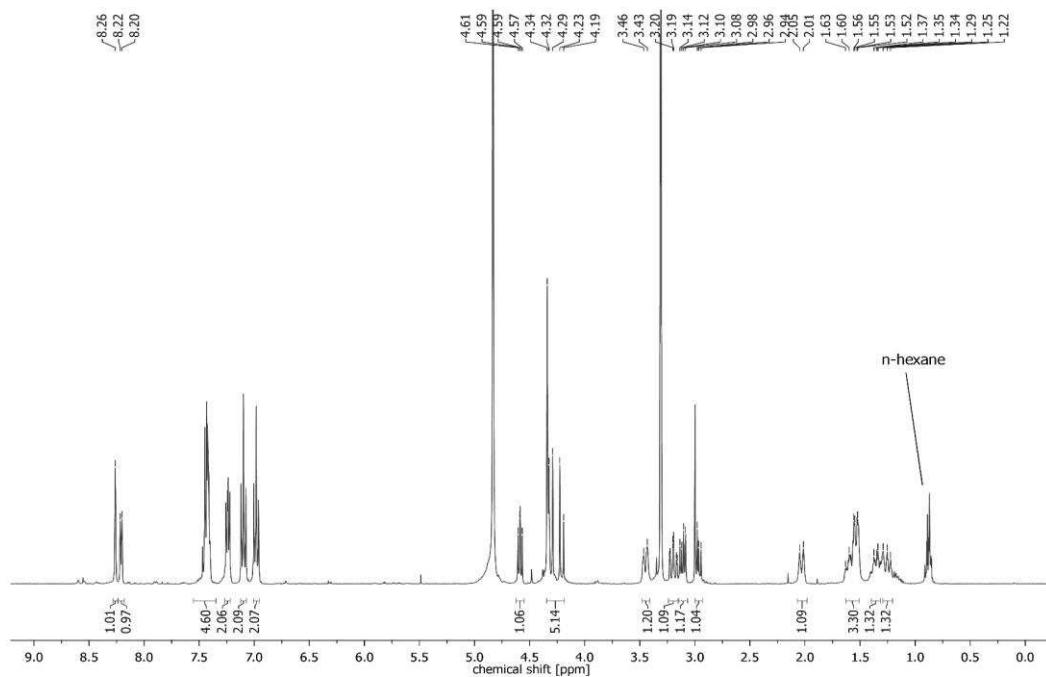
*S,S*-10d,  $^1\text{H}$ ,  $\text{CDCl}_3$ *S,R*-10d,  $^1\text{H}$ ,  $\text{CDCl}_3$ 

VIII Appendix

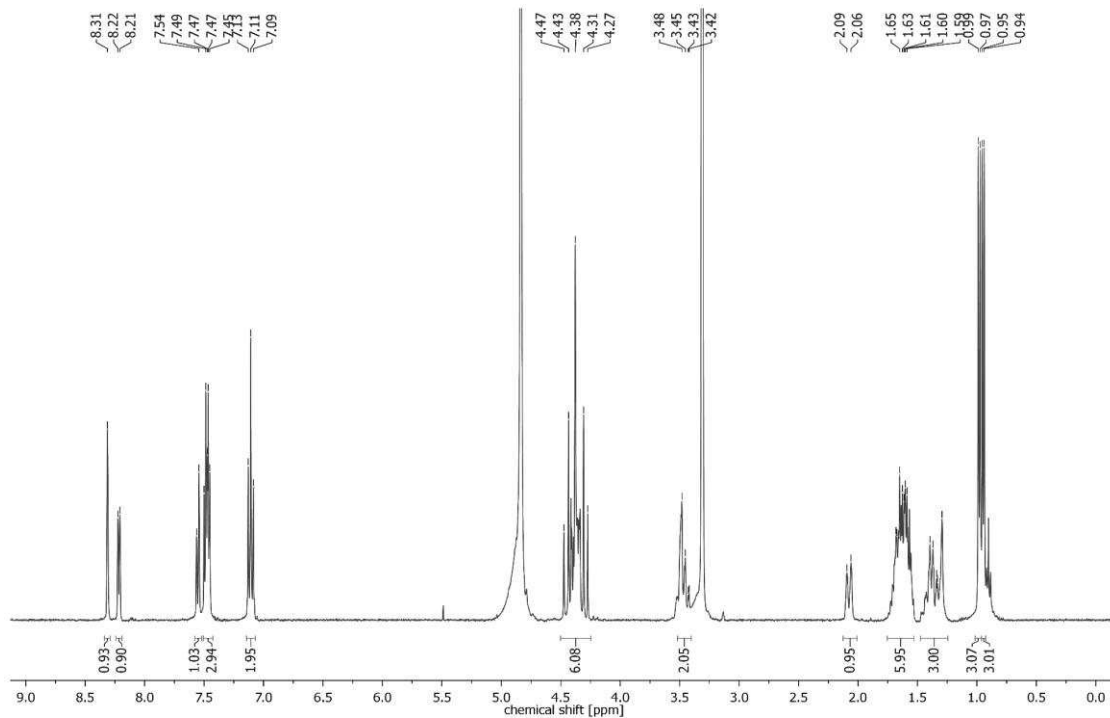
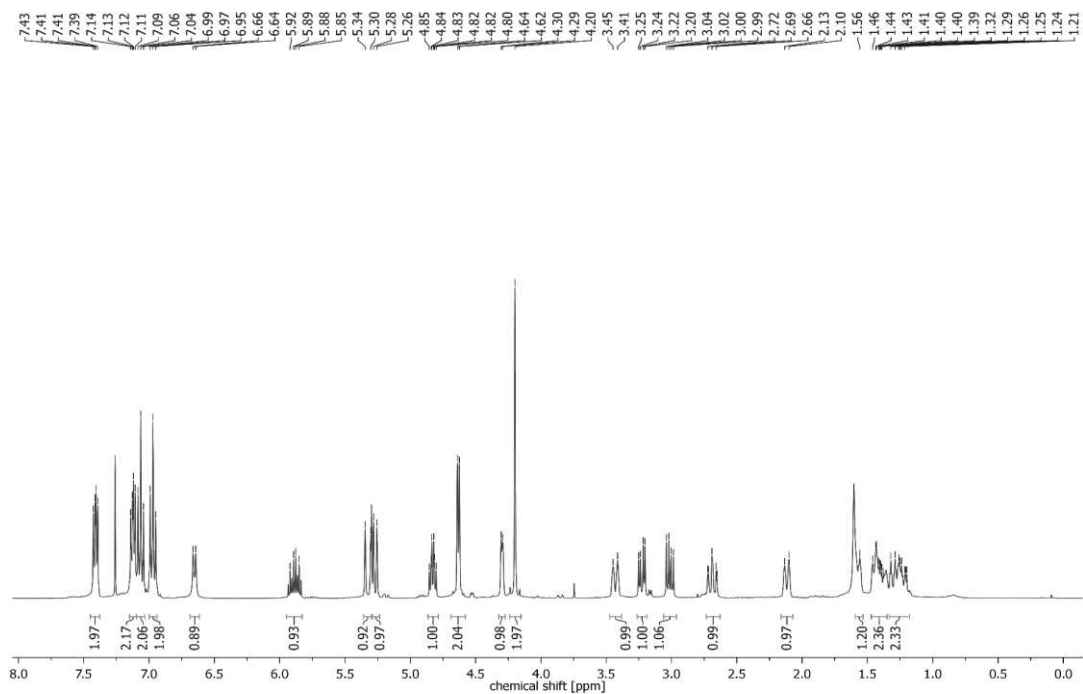
*S,S*-21g, <sup>1</sup>H, CDCl<sub>3</sub>



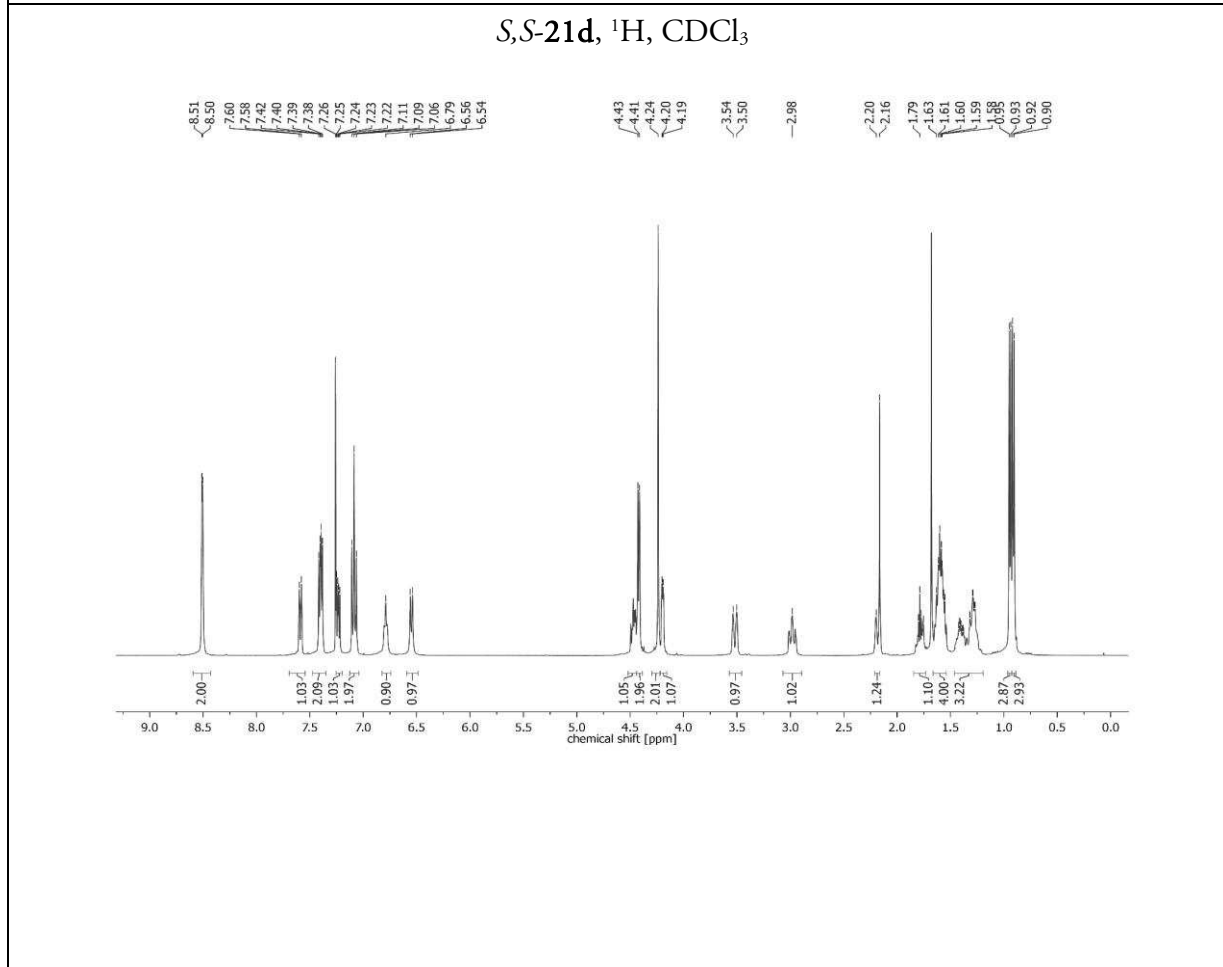
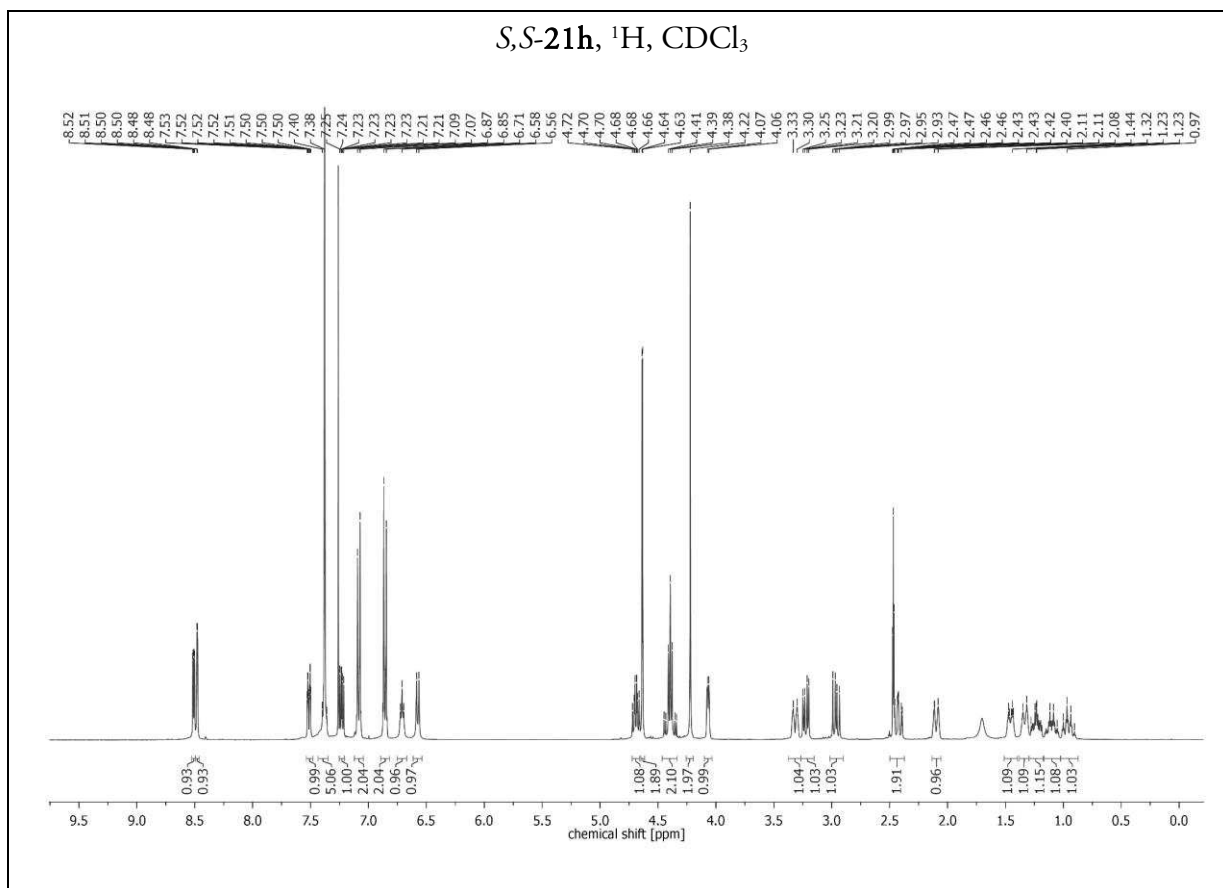
*S,S*-22g, <sup>1</sup>H, CD<sub>3</sub>OD

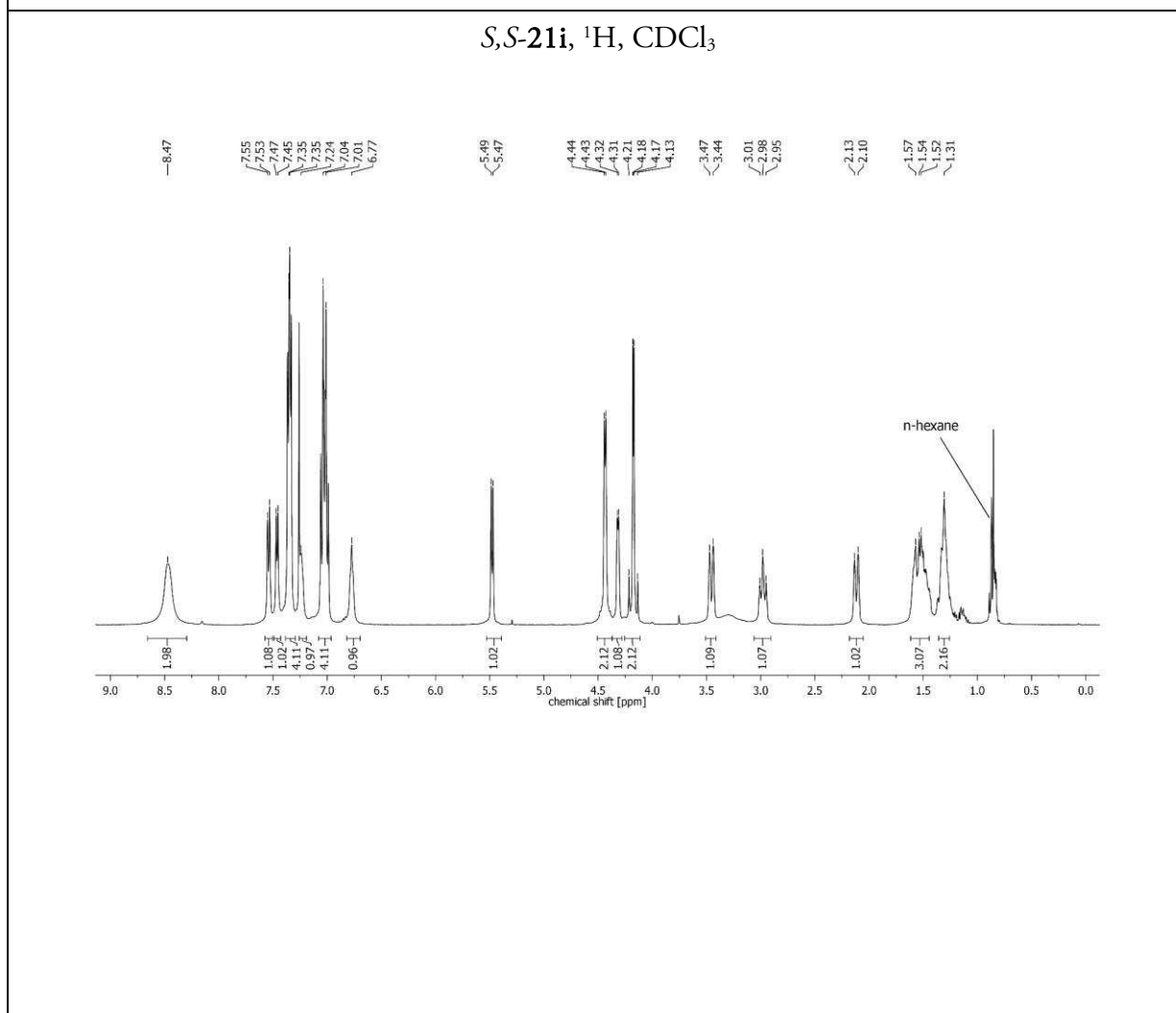
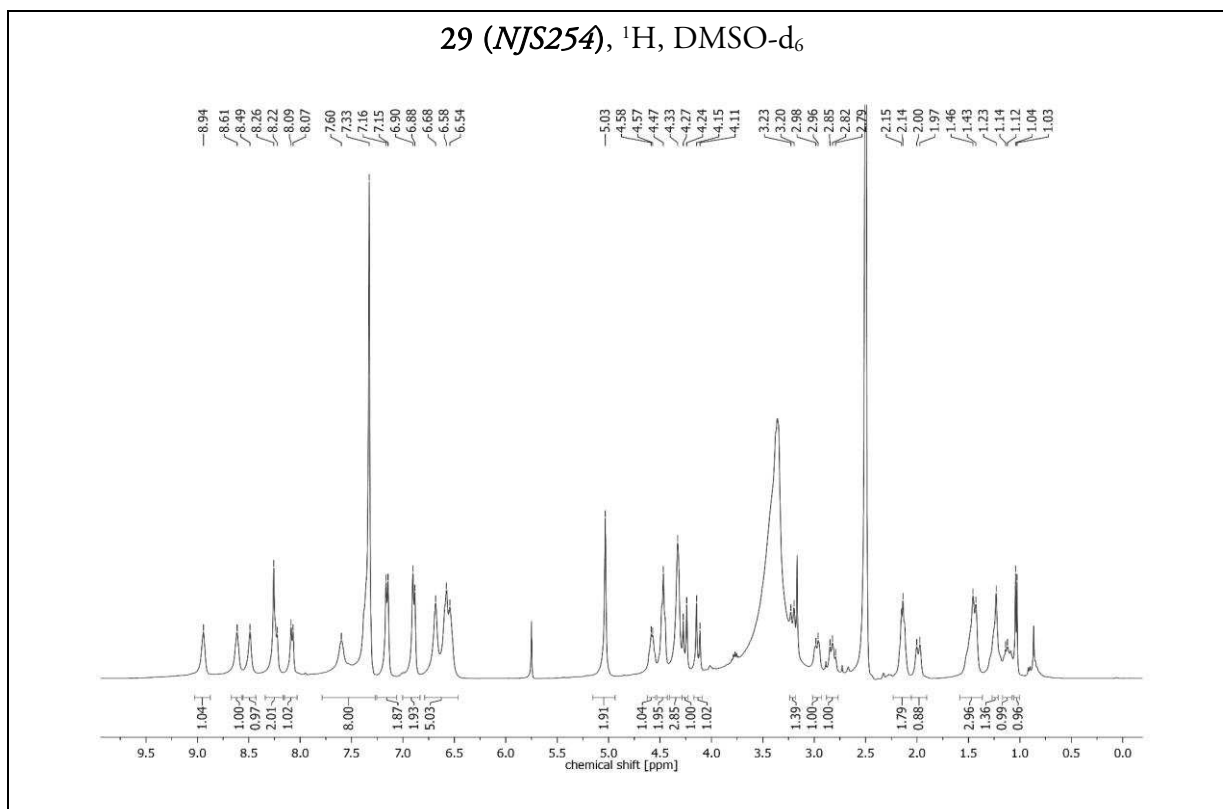


## VIII Appendix

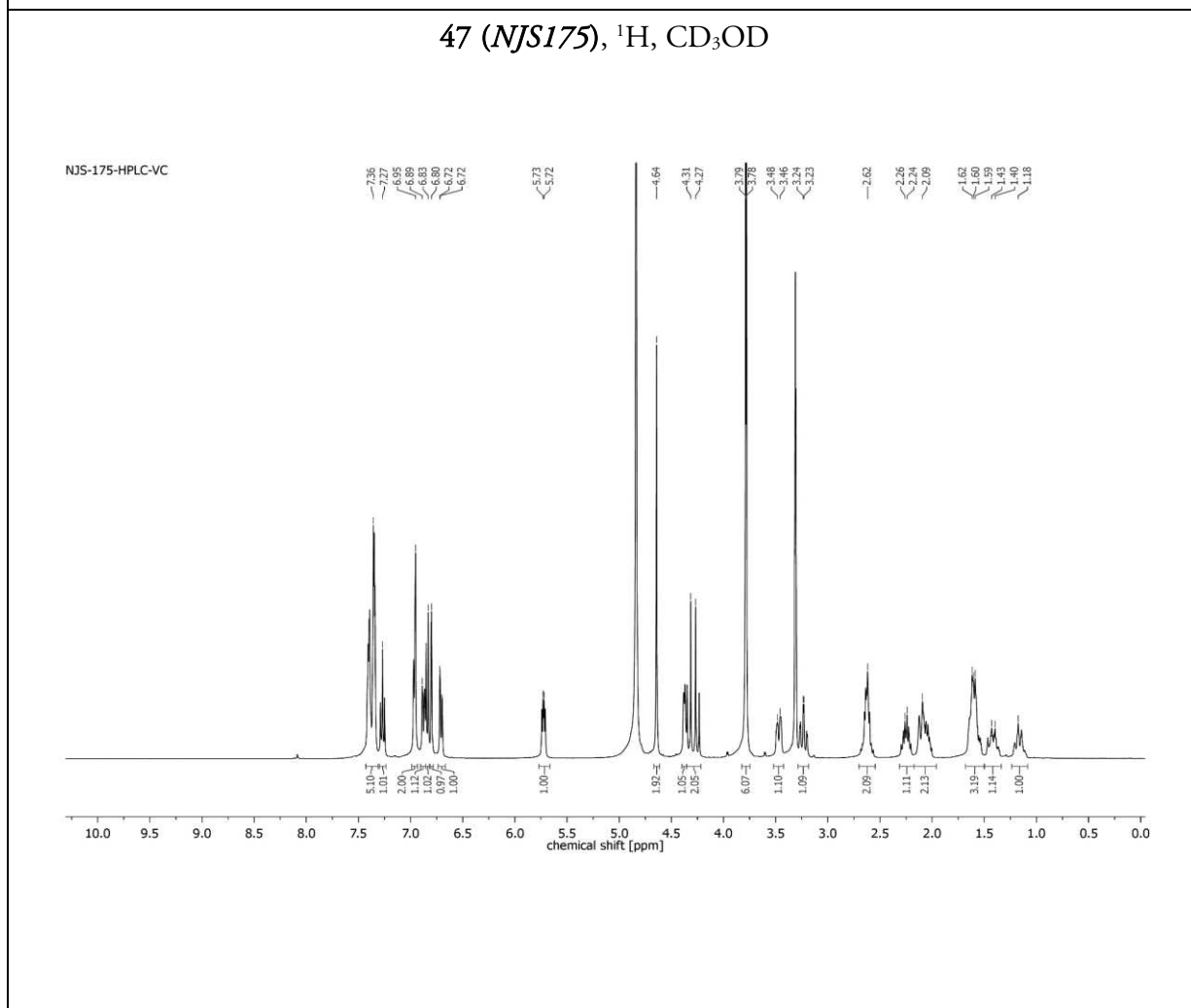
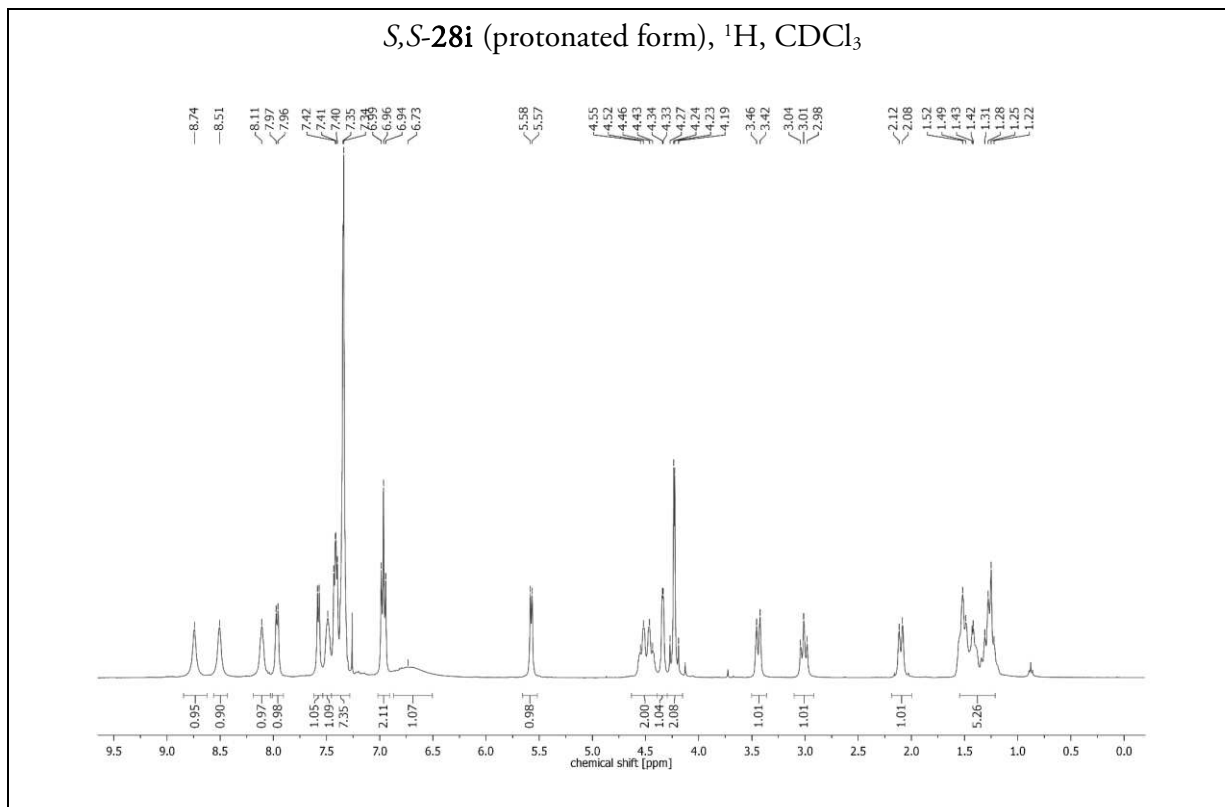
*S,S*-22d,  $^1\text{H}$ ,  $\text{CD}_3\text{OD}$ *S,S*-25g,  $^1\text{H}$ ,  $\text{CDCl}_3$ 

VIII Appendix

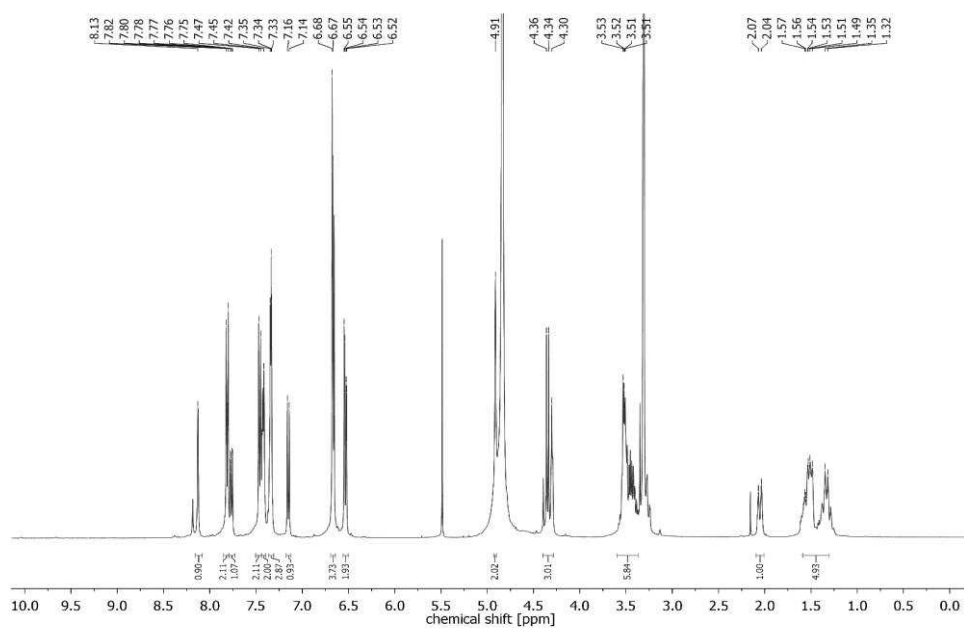
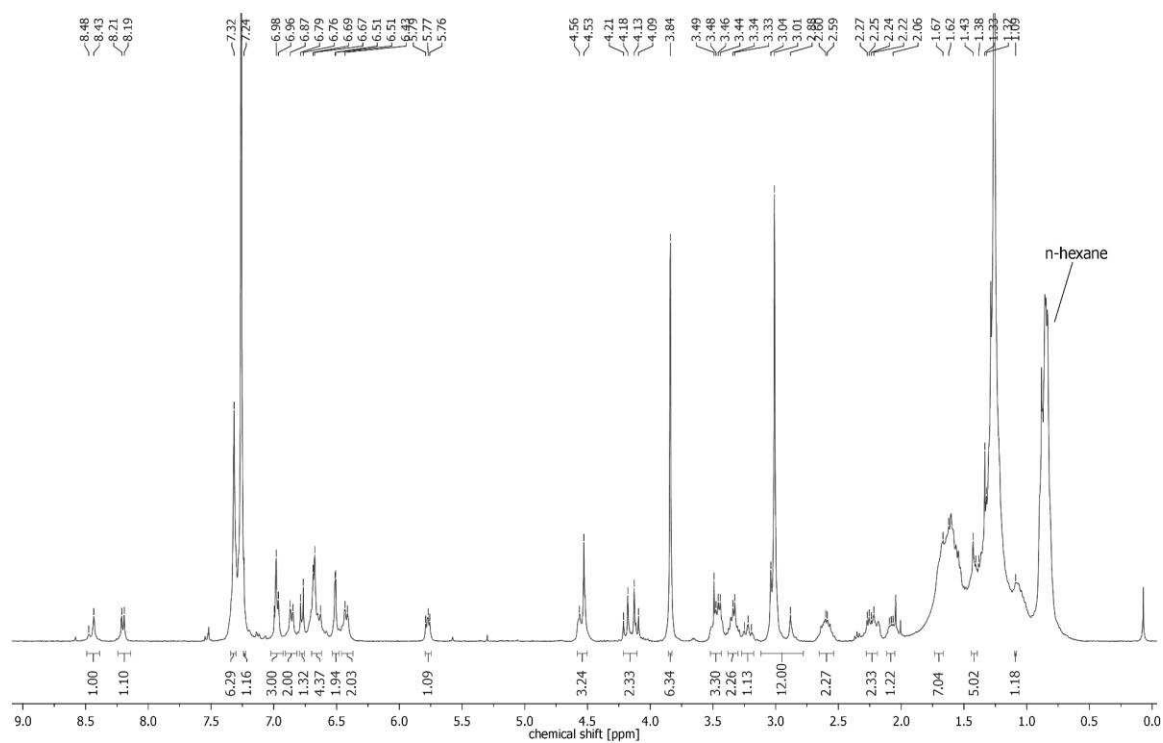




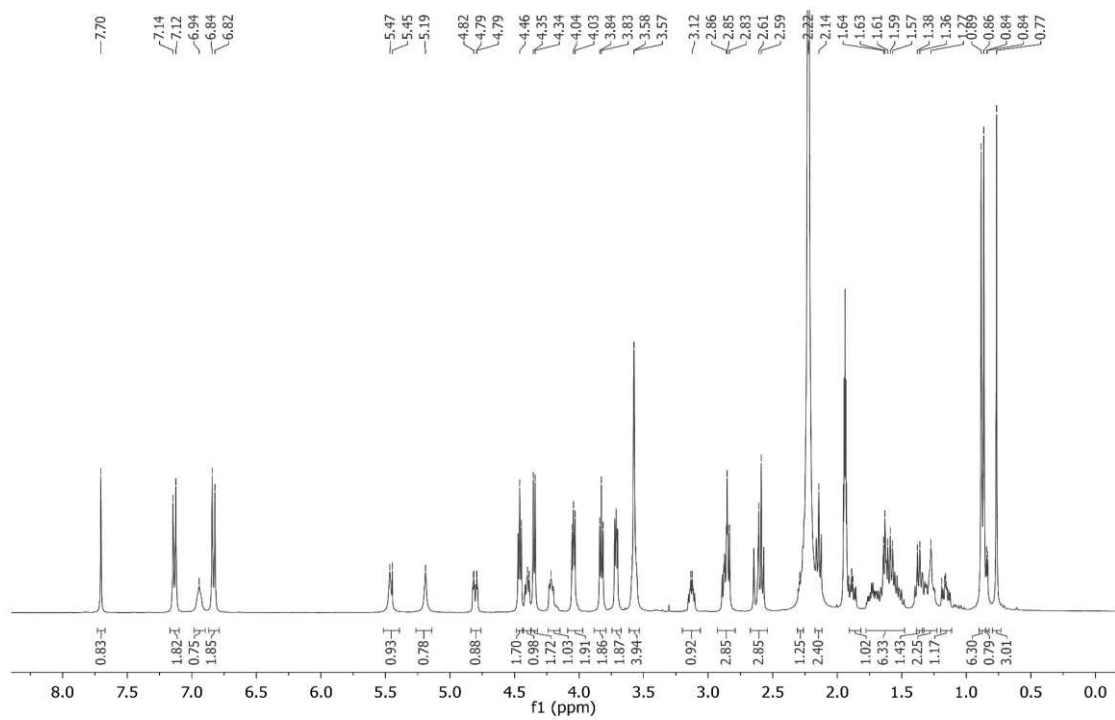
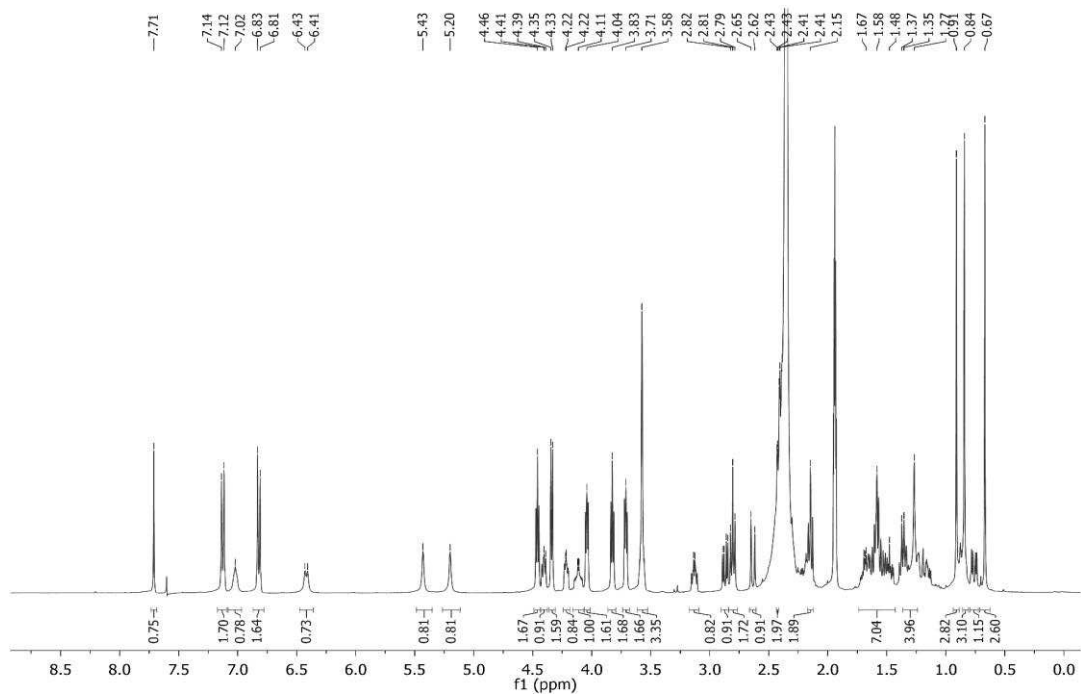
VIII Appendix





31 (*NJS166*),  $^1\text{H}$ ,  $\text{CD}_3\text{OD}$ 32 (*NJS205*),  $^1\text{H}$ ,  $\text{CDCl}_3$ 

## VIII Appendix

11 (*NJS25*),  $^1\text{H}$ ,  $\text{CD}_3\text{CN}$ 12 (*NJS28*),  $^1\text{H}$ ,  $\text{CD}_3\text{CN}$ 



### 3 Authorship Statement

Synthesis and Characterization of Antimicrobial Inhibitors of the "Macrophage Infectivity Potentiator" Protein and Fluorescent Probes, Fluorescent probe for the identification of potent inhibitors of the macrophage infectivity potentiator (Mip) protein of Burkholderia pseudomallei; Scheuplein, N. J.; Lohr, T.; Vivoli Vega, M.; Ankrett, D.; Seufert, F.; Kirchner, L.; Harmer, N.J.; Holzgrabe, Ulrike; SLAS Discovery, 2023, 12 pages; DOI: 10.1016/j.slasd.2023.03.004.

detailed description of published percentages (in %)

disclosure of authorship (if applicable: main author, co-author, corresponding author) with first/last name (initial letters)

Author 1 (N.J.S.), Author 2 (T.L.), Author 3 (M.V.V.), Author 4 (D.A.), Author 5 (F.S.), Author 6 (L.K.), Author 7 (N.J.H.), Author 8 (U.H.)									
Task	N.J.S.	T.L.	M.V.V.	D.A.	F.S.	L.K.	N.J.H.	U.H.	Σ in percent
Investigation – (Re-)Synthesis of the FP Probe and Inhibitors	8%				3%				11%
Investigation – FP Assay and Preparation		8%	3%	3%			6%		20%
Investigation – ITC		2%							2%
Investigation – HRMS						3%			3%
Writing – original draft	11%	5%							16%
Writing – review & editing	2.5%	2.5%					2.5%	2.5%	10%
Formal analysis	2%	2%					2%		6%
Conceptualization and Study design							4%	4%	8%
Methodology		3.33%	3.33%		3.33%				10%
Funding acquisition							2%	2%	4%
Project Administration								4%	4%
Supervision and Validation							3%	3%	6%
<b>AMOUNT</b>	23.5%	22.83%	6.33%	3%	6.33%	3%	19.5%	15.5%	100%

N.J.S. and T.L. are equal first authors. N.J.H. and U.H. are shared corresponding authors.

## AUTHORSHIP STATEMENT

Synthesis and Characterization of Antimicrobial Inhibitors of the "Macrophage Infectivity Potentiator" Protein and Fluorescent Probes, Targeting Protein Folding: A Novel Approach for the Treatment of Pathogenic Bacteria. Scheuplein, N. J.; Bzdyl, N. M.; Kibble, E. A.; Lohr, T.; Holzgrabe, U.; Sarkar-Tyson, M. *J. Med. Chem.* **2020**, 63 (22), 13355-13388. DOI: 10.1021/acs.jmedchem.0c00911

detailed description of published percentages (in %)

disclosure of authorship (if applicable: main author, co-author, corresponding author) with first/last name (initial letters)

Author 1 (N.J.S.), Author 2 (N.M.B.), Author 3 (E.A.K.), Author 4 (T.L.), Author 5 (U.H.), Author 6 (M.S.T.)							
Task	N.J.S.	N.M.B.	E.A.K.	T.L.	U.H.	M.S.T.	Σ in percent
Writing - original draft - Cyclophilins and parvulins in bacteria		15%					15%
Writing - original draft - Chemistry component	15%			15%			30%
Writing - original draft - FKBP in bacteria			10%				10%
Review and edit manuscript	2%	4%			4%	4%	14%
Chemical numbering, graphical abstract	1%						1%
Referencing, Reviewer Comments, Journal Guidelines		3%					3%
Collate sections						3%	3%
Comment on manuscript prior to publication	2%	2%	2%	2%	2%	2%	12%
Funding acquisition					2%	2%	4%
Project Administration					2%	2%	4%
Supervision and Validation					2%	2%	4%
<b>Amount</b>	20%	24%	12%	17%	12%	15%	100%

N.J.S. and N.M.B. are equal first authors. M.S.T. and U.H. are shared corresponding authors.

## AUTHORSHIP STATEMENT

Synthesis and Characterization of Antimicrobial Inhibitors of the "Macrophage Infectivity Potentiator" Protein and Fluorescent Probes, Analysis of Structure–Activity-Relationships of Novel Inhibitors of the Macrophage Infectivity Potentiator (Mip) Proteins of *Neisseria meningitidis*, *Neisseria gonorrhoeae*, and *Burkholderia pseudomallei*; Scheuplein, N. J.; Bzdyl, N. M.; Lohr, T.; Kibble, E. A.; Hasenkopf, A.; Sarkar-Tyson, M.; Holzgrabe, Ulrike. Submitted manuscript (J. Med. Chem.), ~67 pages, 2023.

detailed description of published percentages (in %)

disclosure of authorship (if applicable: main author, co-author, corresponding author) with first/last name (initial letters)

Author 1 (N.J.S.), Author 2 (N.M.B.), Author 3 (T.L.), Author 4 (E.A.K.), Author 5 (A.H.), Author 6 (M.S.-T.), Author 7 (U.H.)								
Task	N.J.S.	N.M.B.	T.L.	E.A.K.	A.H.	M.S.-T.	U.H.	Σ in percent
(Re-)Synthesis and Purification of Inhibitors	12%		2%		12%			26%
Synthesis of FP Probe	4%							4%
Fluorescence Polarization Assay			5%					5%
Solubility, Purity, Cytotoxicity (NIH, HEK)	4%		2%		4%			10%
Protein Purification, PPIase Assay, and Cell-based Assay		10%		5%				15%
Writing and SAR Analysis – original draft	12%	2%	2%		2%			18%
Writing – internal review & editing	2%	2%	2%			2%	2%	10%
Conceptualization and Study design						2%	2%	4%
Funding acquisition						2%	2%	4%
Supervision and Validation						2%	2%	4%
<b>AMOUNT</b>	34%	14%	13%	5%	18%	8%	8%	100%

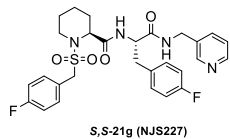
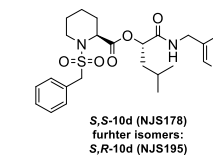
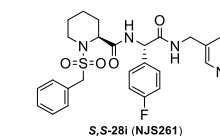
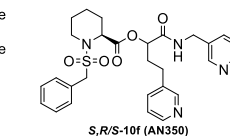
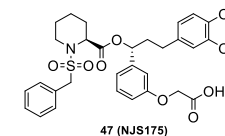
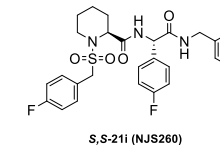
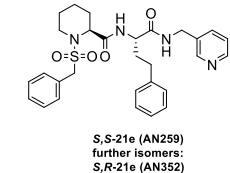
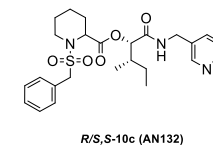
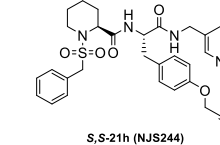
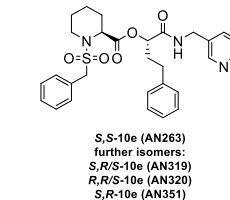
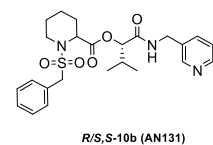
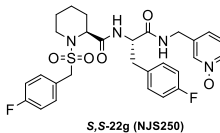
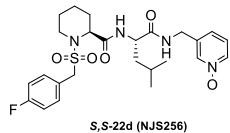
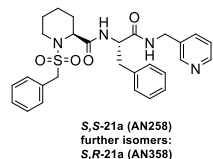
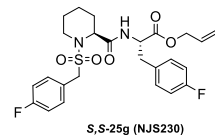
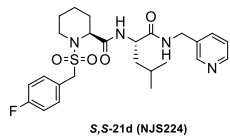
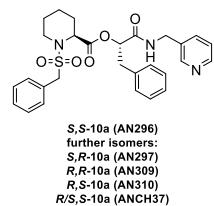
N.J.S. is the first author. M.S.-T. and U.H. are shared corresponding authors.

All compounds in Chapter III\_4 labeled with a LabID starting with "AN" were originally synthesized by Anja Hasenkopf. Among them are the following final stages. At this point, reference is made again to the contribution of Anja Hasenkopf. R/S,S-10a (ANCH37), S,R-10a (AN297), S,S-10a (AN296), R,R-10a (AN309), R,S-10a (AN310), S,S-21a (AN258), S,R-21a (AN358), R/S,S-10b (AN131), R/S, S-10c (AN132), R/S,S-10d (AN133), S,R/S-10e (AN319), R,R/S-10e (AN320), S,S-10e (AN263), S,R-10e (AN351), S,S-21e (AN259), S,R-21e (AN352), S,R/S-10f (AN350).

Synthesized by Theresa Lohr: R/S,S-22a (TL75). Synthesized by Florian Seufert: 9 (SF235), 11 (SF354).

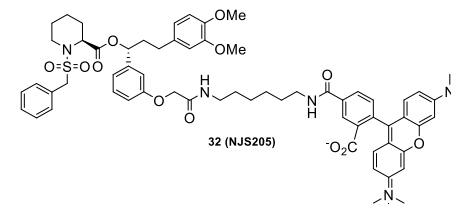
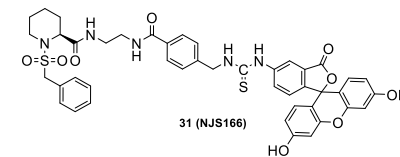
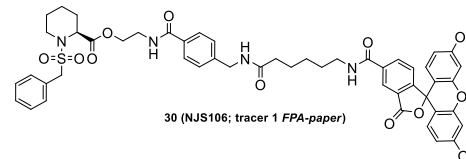
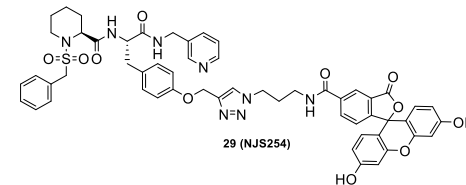
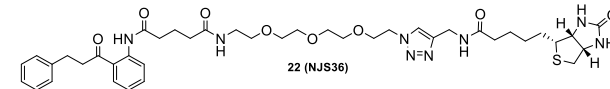
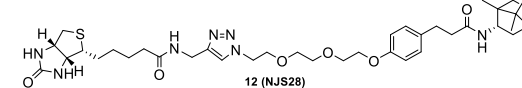
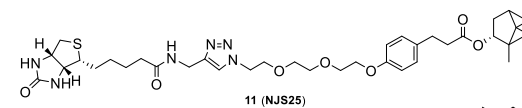
The substance code is taken from the side chain paper.

4 Compounds



All "ANxy" substances were first synthesized by Anja Hasenkopf and are illustrated here for a more straightforward comprehension of the side chain paper (III\_4).

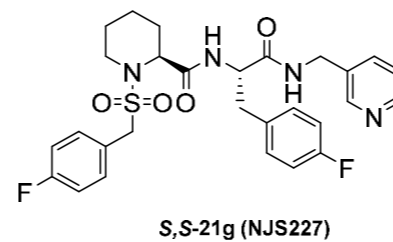
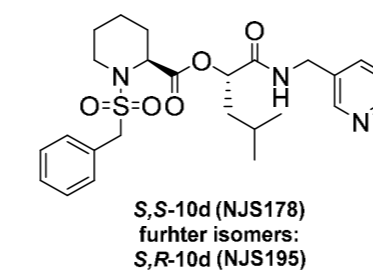
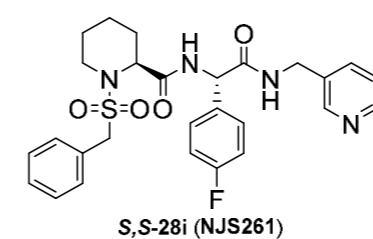
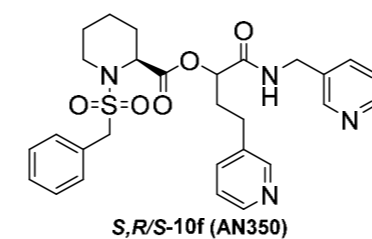
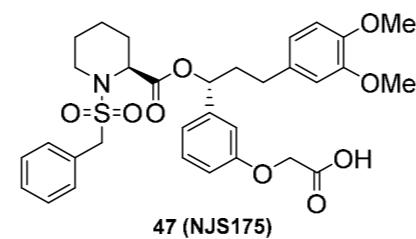
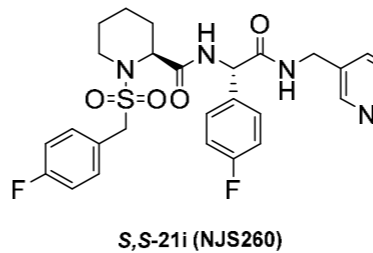
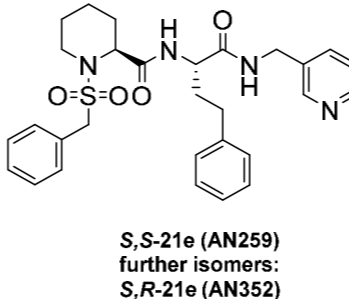
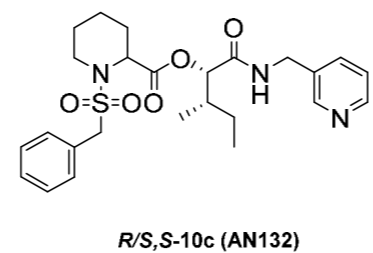
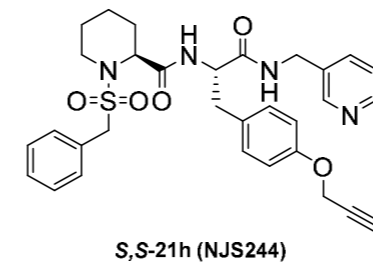
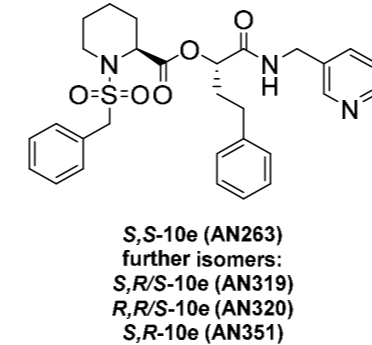
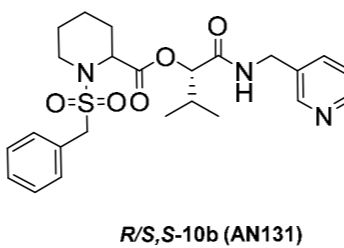
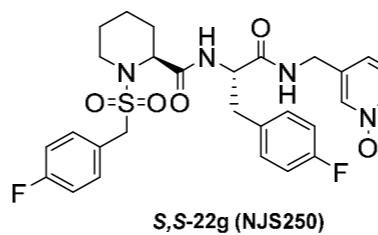
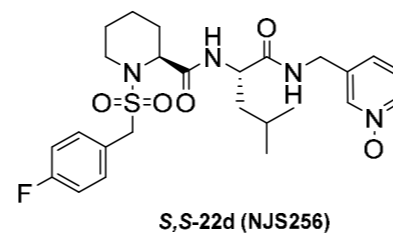
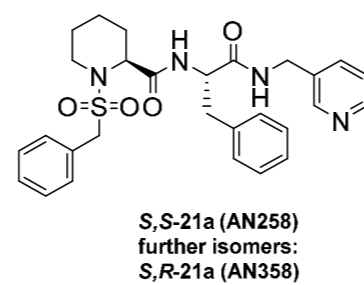
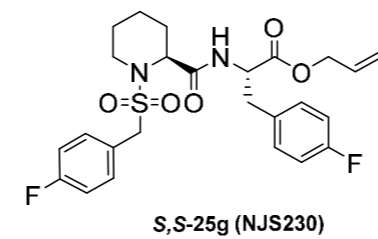
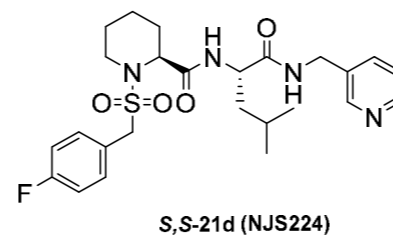
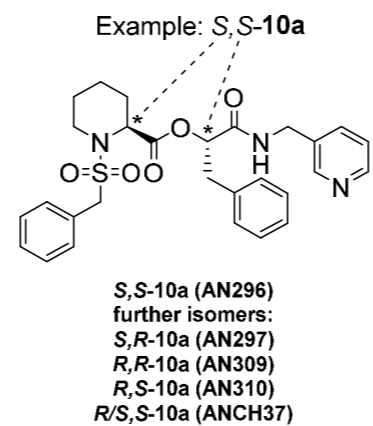
Molecules from the FPA paper (SLAS Discovery) are depicted in Chapter III\_2.3.4. The numbers here correspond to those in the Side Chain Paper (III\_4), as well as the chapters III\_1, and III\_3.



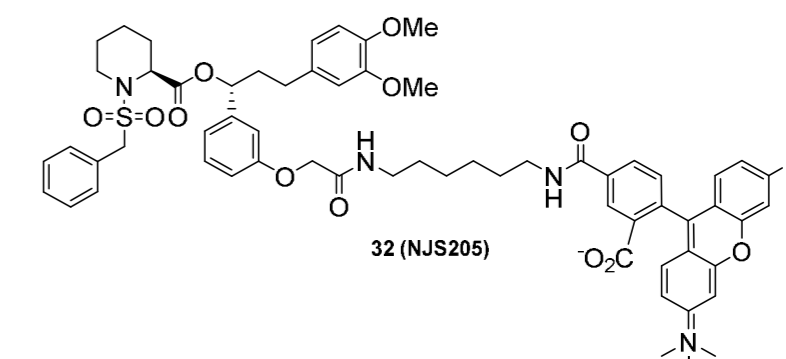
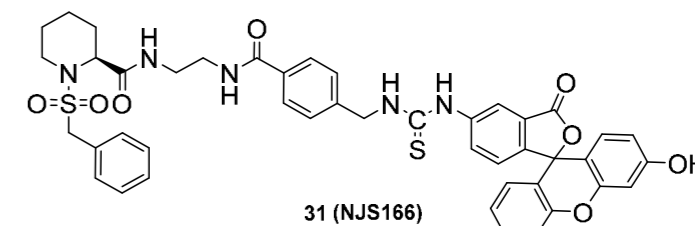
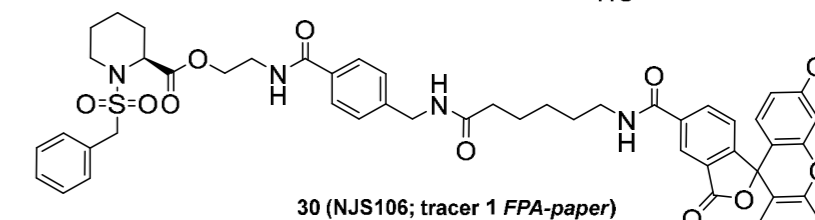
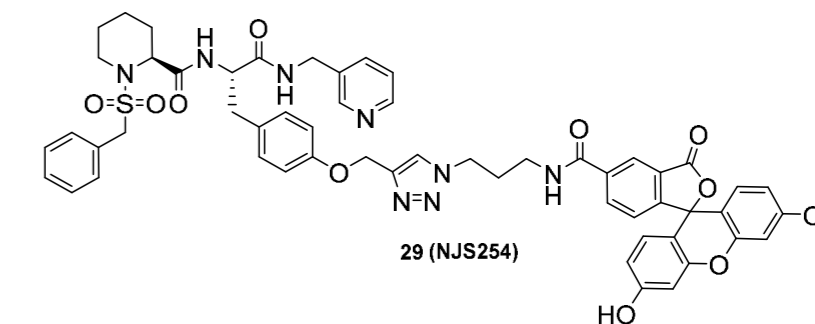
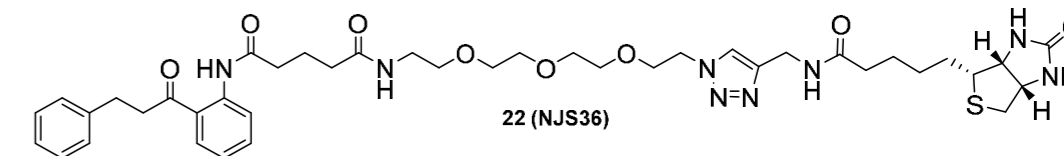
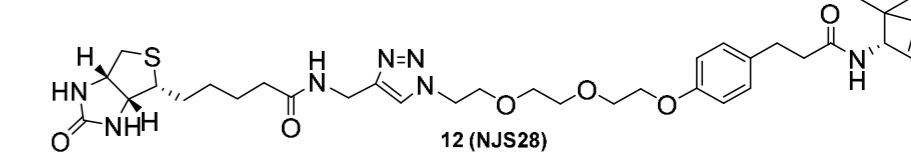
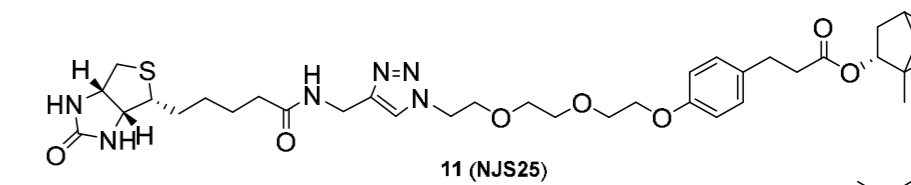


## FINAL COMPOUNDS

Unfold this page to reveal structures.



Molecules from the FPA paper (SLAS Discovery) are depicted in Chapter III\_2.3.4. The numbers here correspond to those in the Side Chain Paper (III\_4), as well as the chapters III\_1, and III\_3.



All "ANxy" substances were first synthesized by Anja Hasenkopf and are illustrated here for a more straightforward comprehension of the side chain paper (III\_4).

### Conference Contributions and Patent

Poster presentation at the 2019 GDCh annual meeting "Frontiers in medicinal chemistry", Nicolas Scheuplein, *Development and synthesis of modified and labeled inhibitors of the macrophage infectivity potentiator (Mip) protein*, University of Würzburg, 24.–27. Mar. 2019.

Poster presentation at the networking meeting on the National Drug Initiative at the Federal Ministry of Education and Research, Nicolas Scheuplein, Theresa Lohr, *Synthesis of Pipecolate-based compounds against Trypanosoma cruzi - Mip*, BMBF, Berlin, 08. Oct. 2019.

Online Poster presentation at the 2021 DPhG annual meeting, Nicolas Scheuplein, Theresa Lohr, *Assay and inhibitor development for Macrophage Infectivity Potentiator proteins against Gram-negative bacteria and parasites*, University of Leipzig, 29. Sep. 2021.

Patent, *MIP inhibitors*, Application-Number: 2022900706, Australia; Inventors: Ulrike Holzgrabe, Nicolas Scheuplein, Theresa Lohr, Anja Hasenkopf, Assignor: University of Würzburg, Assignee: DMTC Limited, Australia; Filing Date: 21 Mar. 2022.